INFLUENCE OF CROSS-FRAME DETAILING ON CURVED AND SKEWED STEEL I-GIRDER BRIDGES

A Dissertation
Presented to
The Academic Faculty

by

Cagri Ozgur

In Partial Fulfillment
of the Requirements for the Degree
Doctor of Philosophy in the
School of Civil and Environmental Engineering

Georgia Institute of Technology

December 2011

INFLUENCE OF CROSS-FRAME DETAILING ON CURVED AND SKEWED STEEL I-GIRDER BRIDGES

Approved by:

Dr. Donald W. White, Advisor
School of Civil and Environmental Engineering
Georgia Institute of Technology

Dr. Roberto T. Leon, Advisor
School of Civil and Environmental Engineering
Georgia Institute of Technology

Dr. Kenneth M. Will
School of Civil and Environmental Engineering
Georgia Institute of Technology

Dr. Bruce R. Ellingwood
School of Civil and Environmental Engineering
Georgia Institute of Technology

Dr. George Kardomateas
School of Aerospace Engineering
Georgia Institute of Technology

Date Approved: August 9, 2011

To my parents, Huri and Guner Kemal Ozgur

ACKNOWLEDGEMENTS

I would like to use this opportunity to thank all those who have contributed to my doctoral studies and supported me during this journey.

I would like to express my deepest gratitude to my advisor, Dr. Donald W. White, for his guidance, patience, and encouragement from the beginning to the end of this study. He was more than an advisor, and it was a great honor to work with him.

Heartfelt appreciation is also extended to my other advisor, Dr. Roberto T. Leon, for his incessant support, assistance, and insight throughout the preparation and completion of this research.

My gratitude also goes to my thesis committee members, Dr. Bruce R. Ellingwood, Dr. Kenneth M. Will, and Dr. George Kardomateas, for their valuable comments and revisions. I would also like to thank Prof. Ted Galambos for offering his wisdom and input during this work.

This research was funded by the National Cooperative Highway Research Program and is a part of the efforts under Project NCHRP 12-79, Guidelines for Analytical Methods and Erection Engineering of Curved and Skewed Steel Deck-Girder Bridges. The financial support from the National Cooperative Highway Research Program (NCHRP) is gratefully acknowledged.

Special thanks are extended to Domenic Coletti of HDR Engineering, Brandon Chavel of HDR Engineering, John Yadlosky of HDR Engineering, Bob Cisneros of High Steel Structures, Inc., and Ronnie Medlock of High Steel Structures, Inc. for providing detailed information, data, and comments.

Special thanks to my colleagues, Yoon Duk Kim, Telmo Andres Sanchez, Yavuz Mentes, Juan M. Jimenez Chong, and Cliff Bishop for their input and understanding. They made the office a positive, collaborative work environment. I am also grateful to Kristy Snedden for her spiritual support, and to my friend Cannoli for helping me through the most demanding days.

Greatest thanks to my parents, Huri and Guner Kemal Ozgur, for dedicating their lives to their children. I will forever be indebted to my parents for their belief in me and for encouraging me to go after my dreams. I am very proud and fortunate to be their child. I would like also to thank to my sister, Ayca Eminoglu, for her encouragement and for raising two wonderful daughters, Melisa and Cagla.

Last but not least, I owe my loving thanks to my girlfriend, Margaret Ann Greaves. Without her unwavering support, understanding, lovely smile, and generous heart, this journey would have been more difficult. She made the hard days bearable and good days unforgettable.

TABLE OF CONTENTS

LIST OF TABLES

LIST OF FIGURES

SUMMARY

Curved and skewed I-girder bridges exhibit torsional displacements of the individual girders and of the overall bridge cross-section under dead loads. As a result, the girder webs can be plumb in only one configuration. If the structure is built such that the webs are plumb in the ideal no-load position, they generally cannot be plumb under the action of the structure's steel or total dead load; hence, twisting of the girders is unavoidable under dead loads. The deflected geometry resulting from these torsional displacements can impact the fit-up of the members, the erection requirements (crane positions and capacities, the number of temporary supports, tie down requirements, etc.), the bearing cost and type, and the overall strength of the structure. Furthermore, significant layover may be visually objectionable, particularly at piers and abutments.

If the torsional deflections are large enough, then the cross-frames are typically detailed to compensate for them, either partially or fully. As specified in Article C6.7.2 of the AASHTO LRFD Specifications, different types of cross-frame detailing methods are used to achieve theoretically plumb webs under the no-load, steel dead load, or total dead load conditions. Each of the cross-frame detailing methods has ramifications on the behavior and constructability of a bridge. Currently, there is much confusion and divergence of opinion in the bridge industry regarding the stage at which steel I-girder webs should be ideally plumb and the consequences of out-of-plumbness at other stages. Furthermore, concerns are often raised about potential fit-up problems during steel erection as well as the control of the final deck geometry (e.g., cross-slopes and joint alignment). These influences and ramifications of cross-frame detailing need to be investigated and explained so that resulting field problems leading to needless construction delays and legal claims can be avoided.

This dissertation addresses the influence of cross-frame detailing on curved and/or skewed steel I-girder bridges during steel erection and concrete deck placement by conducting comprehensive analytical studies. Procedures to determine the lack-of-fit forces due to dead-load-fit (DLF) detailing are developed to assess the impact of different types of cross-frame detailing. The studies include benchmarking of refined analytical models against selected full-scale experimental tests and field measurements. These analytical models are then utilized to study a variety of practical combinations and permutations of bridge parameters pertaining

to horizontal curvature and skew effects. This research develops and clarifies procedures and provides new knowledge with respect to the impact of cross-frame detailing methods on: 1) constructed bridge geometries, 2) cross-frame forces, 3) girder stresses, 4) system strengths, 5) potential uplift at bearings, and 6) fit-up during erection. These developments provide the basis for the development of refined guidelines for: 1) practices to alleviate fit-up difficulties during erection, 2) selection of cross-frame detailing methods as a function of I-girder bridge geometry characteristics, and 3) procedures to calculate the locked-in forces due to DLF cross-frame detailing.

CHAPTER I.

INTRODUCTION

1.1. Introduction and Background

Curved and skewed I-girder bridges exhibit torsional displacements of the individual girders and of the overall bridge cross-section under dead loads. As a result, the girder webs can be plumb only in one configuration. If the structure is built such that the webs are plumb in the ideal no-load position, they generally cannot be plumb under the action of the structure's steel or total dead load; hence, twisting of the girders is unavoidable under dead loads. The deflected geometry resulting from these torsional displacements can impact the fit-up of the members (i.e., come-along and jacking forces), the erection requirements (crane positions and capacities, the number of temporary supports, tie down requirements, etc.), the bearing cost and type, and the overall strength of the structure. Furthermore, significant layover may be visually objectionable, particularly at piers and abutments.

If the torsional deflections are large enough, then the cross-frames are typically detailed to compensate for them, either partially or fully. Different types of cross-frame detailing methods are used to achieve theoretically plumb webs under the no-load, steel dead load, or total dead load conditions (AASHTO (2010) Section C6.7.2). These methods are referred to as:

1. No-Load Fit (NLF): The cross-frames are fabricated to fit the girders in their cambered no-load (fully supported) geometry without inducing any locked-in forces.
2. Steel Dead Load Fit (SDLF): The cross-frames are fabricated to fit the girders in their theoretical final plumb position under steel dead load (that is plumb webs but with the steel dead load vertical deflections subtracted from the initial girder camber).
3. Total Dead Load Fit (TDLF): The cross-frames are fabricated to fit the girders in their theoretical final plumb position under total dead load (that is plumb webs but with the total dead load vertical deflections subtracted from the initial girder camber).

In the vast majority of cases, I-girders are fabricated with plumb webs prior to assembly into the structure (the only exception would be the use of twist camber, which is discussed in AASHTO (2010) Article C6.7.2 but is rarely used in practice). However, for SDLF and TDLF

detailing, the cross-frames are detailed to connect to the girders in their steel or total dead load position, with the steel or total dead-load vertical camber removed from the girders. Therefore, there is a lack-of-fit between the cross-frame work points and the work point positions on the girders in the initial no-load geometry. As a result, the individual girders must be twisted in the direction opposite to their dead load torsional rotations to make the connections to the cross-frames. (Usually, this does not present any problem since the girders are relatively flexible with respect to twisting and lateral bending.) Subsequently, the girders deflect and rotate approximately into their final plumb positions under the steel or total dead load. The initial lack-of-fit between the cross-frame and girders induces internal stresses and deformations within the structure. These stresses and deformation can impact the constructed geometry of the bridge, and the component and system strengths in unintended ways.

Each of the above methods of detailing the cross-frames results in different deformed geometries during the erection of the structure. Moreover, the lack-of-fit between the cross-frames and girders in the no-load geometry is non-zero for DLF (Dead Load Fit, i.e., TDLF or SDLF) detailing. Therefore, the displacement incompatibilities between the bridge components during the steel erection are different for each cross-frame detailing method, requiring different practices to alleviate fit-up problems.

Currently, there is much confusion and divergence of opinion in the bridge industry regarding the stage at which steel I-girder webs should be ideally plumb and the consequences of out-of-plumbness at other stages. Furthermore, concerns are often raised about potential fit-up problems and/or corresponding locked-in stresses in the steel during erection as well as the control of the final deck geometry (e.g., cross-slopes and joint alignment) in bridges with large skew and/or curvature.

1.2. Problem Statement and Research Objectives

Each of the cross-frame detailing methods discussed in the previous section has ramifications on the behavior and constructability of a bridge. There are various subtle influences for different bridge geometries that are not well known or understood. These ramifications and influences need to be investigated and explained so that resulting field problems leading to needless construction delays and legal claims can be avoided.

In this research, various attributes of cross-frame detailing methods are investigated using refined finite element analysis solutions. The developed finite element analysis techniques are

benchmarked against selected experimental data and field measurements to verify that the physical behavior of I-girder bridges can be reproduced realistically and reliably. The core objectives of this research are as follows:

- **Develop effective analysis procedures for the calculation of lack-of-fit effects due to DLF detailing**

For DLF detailing, the system behavior and component responses can be captured accurately by including the corresponding locked-in stress effects in the analysis. Currently there is little information about how to best implement the spatial lack-of-fit between cross-frames and girders in analysis models. In this research, procedures are developed to include these lack-of-fit effects in the analysis.

- **Evaluate the influence of locked-in stress effects due to DLF detailing on the bridge geometry and the component and system strengths**

The internal stresses in the physical structure due to locked-in stress effects associated with DLF detailing can be very different from the internal stresses in the physical structure for NLF detailing, which is commonly assumed in practice for bridge design.

Locked-in stresses can influence the constructed geometry of the bridge in ways that are typically unexpected in current practice. This is because they can produce deflections that are not predicted by common analysis models that do not include locked-in stress effects. For instance, engineers commonly calculate girder camber diagrams without considering locked-in stress effects. However, the physical bridge may exhibit different vertical deflections than assumed in setting the cambers, which can lead to deviations from the predicted final girder elevations and final deck profiles. As a result, the deck thickness can be over-run or under-run or the bridge cross-slopes can differ from the intended values.

DLF detailing causes locked-in stresses that can increase or decrease the component and system strength of the structure. In some cases, these stresses offset the dead load stresses; however, in other cases they are additive with the dead load stresses. Chang and White (2006) showed that TDLF detailing causes a slight decrease in the structural capacity of a full-scale radially-supported bridge tested at the FHWA Turner Fairbank Highway Research Center. The decrease in strength is due to the resulting locked-in stresses. This research expands on the previous work by Chang and White (2006) to assess the impact of detailing methods on bridge system strength for a broad range of bridge geometries and configurations.

A common practice for many curved, radially-supported bridges is NLF detailing. However, constructing the bridge with NLF detailing may result in a measurable amplification of second-order effects due to layover of the girders or the development of overall flange lateral bending of the bridge in some cases. There are limited studies published to date that investigate the global behavior due to the type of cross-frame detailing. This research aims to address the impact of cross-frame detailing on second-order effects and overall flange lateral bending effects in curved I-girder bridges.

Locked-in stress effects can affect the bridge geometry (deck profile, girder cambers, layovers, etc.), component strength (cross-frame forces, girder major-axis bending, and flange lateral bending stresses), and system strength. The general impact of these types of stresses is not well known. Prior studies mainly focus on the girder responses. This research addresses the distribution of the cross-frame forces in the system due to DLF detailing as well as the system strength during construction. One of the core objectives of this study is to evaluate the impact of locked-in stresses on the bridge constructed geometry, as well as component and system strengths via refined finite element analysis solutions.

- **Evaluate the impact of cross-frame detailing on fit-up during steel erection**

Bridges with certain geometric characteristics are more prone to fit-up difficulty. In addition, site constraints, type of the cross-frame detailing, and availability of equipment can have significant influence on the constructability of bridges. Chavel (2008), Chang and White (2006), and Bell and Linzell (2007) have addressed problems encountered in the field in specific bridges constructed with specific cross-frame detailing methods.

In this research, the influence of cross-frame detailing is investigated on a broad range of bridges to address when fit-up problems may occur and when cross-frames detailing methods must be modified to avoid exacerbation of fit-up problems. Moreover, potential uplift at bearings is investigated for curved systems with or without skewed bearing lines since they experience torsional overturning forces under dead loads. Different erection practices are investigated to provide recommendations and guidance to alleviate fit-up problems and improve the bridge performance with respect to different types of cross-frame detailing.

- **Identify conditions when locked-in stress effects need to be included in the design-analysis and when they can be neglected**

Engineers almost never include the inherent lack-of-fit in their structural analysis. AASHTO (2010) Article C6.7.2 states that engineers may need to consider the potential for any

problematic locked-in stresses. However, the decision of when these locked-in stresses should be evaluated is left to engineering judgement, since there is little detailed quantitative information available to gauge when these stresses need to be included in the design analysis. This research provides guidelines and recommendations for when engineers need to include locked-in stress effects in their models and when it is sufficient to neglect locked-in stress effects in the analysis predictions for structures built with DLF detailing.

- **Provide recommendations for selecting the type of cross-frame detailing method for different bridge geometries**

There is no common agreement on how to choose the most suitable type of cross-frame detailing method for a given bridge. This causes problems and confusion among consultants, erectors, contractors, fabricators, and owners, which can result in construction delays and economic losses due to fit-up problems, or just a simple lack of understanding of the highly complex bridge behavior associated with these relatively simple cross-frame detailing practices.

This research demonstrates both simple and comprehensive explanations of how DLF detailing works. The goal is to improve the broad understanding of cross-frame detailing methods in the steel bridge profession. The research draws on findings from parametric studies to provide recommendations for selecting the type of detailing for different categories of bridges by considering the overall bridge performance and constructability.

- **Identify conditions where simple analysis solutions provide accurate results for the bridges constructed with DLF detailing**

For straight and skewed bridges constructed with TDLF detailing, it is typically understood that the lack-of-fit between the girders and cross-frames develops girder twists opposite to the ones due to dead loads. Furthermore, it is often assumed that girder twist due to locked-in stress effects perfectly cancels out the twist due to dead loads. If such is the case, a basic line-girder analysis can provide accurate predictions of a given load state for the bridges constructed with DLF detailing. Other less basic line-girder analysis solutions such as the V-load method for curved radially supported bridges are also based on simple assumptions. Engineers need guidelines to determine when simple analysis procedures are sufficient to capture the behavior due to detailing and when they should employ more complex analysis methods that include the influence of lack-of-fit.

This research uses refined finite element analysis models to simulate the physical behavior of a number of bridges designed with line-girder analysis and constructed with DLF detailing. By

evaluating detailed bridge responses using refined finite element analysis (FEA) solutions, the research identifies conditions when simple analysis methods such as line-girder analysis are sufficient to capture the behavior due to DLF detailing.

1.3. Summary of Key Contributions

This research aims to make the following key contributions:

- Provide simple and comprehensive explanations of how DLF detailing works, as well as demonstrate the impact and consequences of different methods of cross-frame detailing.
- Develop effective procedures for calculating lack-of-fit effects in design-analysis methods, in cases where they need to be included.
- Evaluate the impact of locked-in stress effects due to DLF detailing on
    - Bridge constructed geometry (Girder layovers and vertical displacements).
    - Component strength (Girders and cross-frames), and
    - System strength.
- Assess the impact of cross-frame detailing on second-order amplification of the responses and overall (global) flange lateral bending effects.
- Determine the impact of cross-frame detailing on fit-up considerations during erection.
- Identify cases where fit-up problems may occur and when cross-frame detailing methods must be modified to avoid exacerbation of fit-up problems.
- Provide procedures for the estimation of fit-up forces to predict fit-up difficulties.
- Provide recommendations for steel erection practices to alleviate fit-up problems and improve the bridge performance for different cross-frame detailing methods.
- Provide estimates of tendency for uplift during construction.
- Provide guidance for selection of bearings based on the bridge geometry.
- Provide recommendations for selecting the type of cross-frame detailing method for different bridge geometries.
- Identify conditions where stresses due to lack-of-fit should be included in design analysis and when they can be neglected.
- Identify conditions where simple solutions provide sufficient predictions for bridges constructed with DLF detailing.
- Demonstrate the correct calculation of locked-in vertical displacements when setting girder cambers, where these displacements are important.

- Evaluate the impact of bolt slip on component responses.

1.4. Organization

This dissertation is subdivided into eight main chapters. Chapter 2 provides an overview of cross-frame detailing methods and the typical deflections at the cross-frame locations. It also discusses specific hand calculation equations commonly used with 1D and 2D methods regarding the deflections at the cross-frame locations. Assumptions about and current practices utilizing the common cross-frame detailing methods are then discussed. This chapter closes with a description of several key bridge attributes.

Chapter 3 provides an overview of common structural analysis tools available in current practice for analysis of curved and/or skewed steel girder bridges. This chapter proposes refined finite element analysis procedures for simulation studies and provides information about the validation of the analytical procedures used in this research. Additionally, specific analysis procedures for determining locked-in force effects due to cross-frame detailing methods are presented. This chapter continues with a discussion of the development of a model generator for rapid creation and modification of refined finite element analysis models. The chapter closes with a description of methods for post-processing of analysis results to demonstrate the research findings.

Chapter 4 provides an overview of the analytical studies leading to the conclusions of this study. The emphasis is on the development and design of a large parametric study of curved and skewed I-girder bridge systems conducted in this research. Chapter 5 explains the kinematics of torsional rotations due to dead loads through a series of examples. The coupling between different I-girder bridge displacements and rotations is laid out. Chapter 5 goes on to evaluate the impact of locked-in force effects due to cross-frame detailing on the bridge geometry, as well as on the component and system strengths. The highly complex bridge behavior associated with the relatively simple cross-frame detailing methods is evaluated through analytical studies. It is emphasized that these locked-in forces often are beneficial in that they provide a simple and cost-effective means of achieving plumb webs under a given dead load condition. However, in certain cases, locked-in forces need to be considered in determining vertical deflections and setting cambers, and in evaluating structural resistances. Particular attention is given to the impact of DLF detailing on bridge deflections, cross-frame forces, and girder stresses. Estimation of the locked-in layovers is also presented in Chapter 5. The impact of cross-frame detailing

methods on the system strength is the evaluated by full-nonlinear finite element analysis solutions. Lastly, the impact of bolt slip in the cross-frame connections on the component responses is investigated using selected case studies.

Chapter 6 discusses a number of considerations that can alleviate fit-up problems and improve the structural behavior during erection. First, the influence of the type of cross-frame detailing on fit-up is discussed. Next, basic guidelines are provided for engineers to eliminate problems during the erection of the bridges. These guidelines include checking the tendency for uplift and admissible bearing torsional rotation limits. Additionally, a way of estimating the required fit-up forces at different stages of steel erection is proposed. Recommended practices to alleviate the fit-up problems for different types of cross-frame detailing methods are presented with several examples. These practices include using the weight of the steel structure to help resolve displacement incompatibilities for certain types of cross-frame detailing methods, using temporary X-bracing and struts, providing a minimum ratio relative to the adjacent unbraced lengths at the first cross-frame offset from a bearing line, using X-type cross-frames without top chords, and finally using temporary supports.

Chapter 7 addresses design considerations regarding the method of cross-frame detailing. First, the selection of the most effective type of cross-frame detailing with respect to constructability and improved overall behavior is discussed for different bridge geometries. Conditions are defined for when the locked-in forces from cross-frame detailing should be considered in the design. In certain cases, these forces need to be considered in setting cambers and/or in evaluating the structural resistance. The proper ways of setting the cambers by considering the locked-in vertical displacements are demonstrated by analytical studies. Chapter 7 goes on to discuss when an accurate structural analysis, not including locked-in force effects, can potentially be used to estimate the maximum cross-frame forces and girder lateral bending stresses in an I-girder bridge where DLF detailing is employed. Also, design recommendations are provided regarding DLF detailing to reduce or eliminate the need for a more sophisticated type of analysis. Finally, Chapter 7 gives the conditions necessary to identify when simple analysis solutions provide sufficient predictions for bridges constructed with DLF detailing.

Finally, Chapter 8 provides a summary and conclusions from this research as well as directions for future work.

Appendix A provides a sample of benchmark solutions to validate the analytical procedures used in this study. The simulation capabilities are validated against full-scale, straight and

curved bridge I-girders which are tested to failure. Furthermore, the FEA techniques are validated against the field measurements on a straight and skewed bridge studied in University of Houston and TXDOT research as well as experimental measurements from a full-scale radially-supported bridge tested at the FHWA Turner Fairbank Highway Research Center.

Appendix B provides the overall characteristics of the collected existing I-girder bridges for NCHRP (2011). Sketches of the collected existing I-bridges are provided. These sketches succinctly convey a great deal of useful information about the bridge geometric parameters handled in recent practice.

Appendix C provides detailed descriptions of selected case study bridges used to present and demonstrate the findings of this research. This appendix also gives in depth information about the bridges used for benchmarking and validation purposes.

Appendix D presents detailed steel and total dead load finite element analysis results for selected bridges constructed with different types of cross-frame detailing methods.

CHAPTER II.

BACKGROUND INFORMATION

2.1. Estimation of Layovers

The cross-frames at skewed bearing lines tend to rotate about their own skewed axis and warp (twist) out of their plane due to the girder rotations. However, typically they are relatively rigid compared to the girders in their own plane. Figure 2.1.1 shows the representative I-girder top flange deflections and rotations at a hypothetical fixed bearing location on a skewed bearing line, where θ is the skew angle (taken as the angle between the normal to the girders at their ends and the tangent to the skewed bearing line, thus $\theta = 0$ for no skew), ϕ_z is the girder torsional rotation at the skewed bearing line, ϕ_x is the major-axis bending rotation at the skewed bearing line, Δ_z is the longitudinal deflection of the top flange due to the major-axis bending rotation, Δ_x is the girder layover due to the torsional rotation, and *h* may be approximated as the distance between the centroids of the flanges.

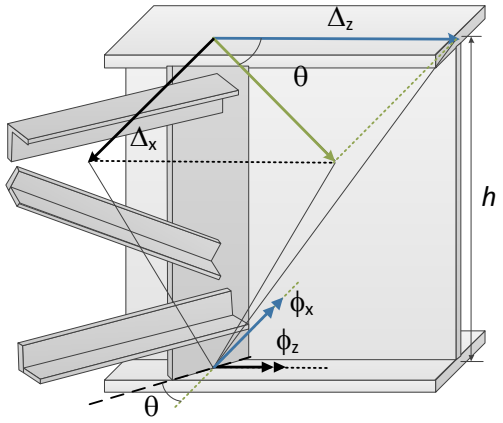

Figure 2.1.1. Girder top flange deflections and girder rotations at a fixed bearing location on a skewed bearing line.

The skewed orientation of the cross-frame forces the major-axis bending rotation and the torsional rotation of the girder to be coupled together at the bearing, since the in-plane cross-frame deformations are relatively small compared to the other displacements. As shown in Ozgur and White (2007), assuming small rotations such that $\tan(\phi) \cong \sin(\phi) \cong \phi$, the deflection of the top flange due to the major-axis bending rotation can be derived from the geometry as

$$\Delta_z = h\,\phi_x \tag{2.1.1}$$

Also, the layover of the girders at the skewed bearing due to the torsional rotations can be expressed as

$$\Delta_x = h\,\phi_z \tag{2.1.2}$$

Furthermore, because of the kinematic constraint induced by the in-plane rigidity of the cross-frame, the coupling relationship between the twist and the major-axis bending rotations is

$$\phi_z = \phi_x \tan(\theta) \tag{2.1.3}$$

Therefore, the layover of the girder at the skewed bearing line is forced to be

$$\Delta_x = \Delta_z \tan(\theta) = h\,\phi_x \tan(\theta) \tag{2.1.4}$$

In the case of a non-fixed bearing, Eq. 2.1.4 still gives the girder layover at the bearing, i.e., the relative lateral displacement of the top and bottom flanges, but the bottom flange is allowed to translate according to the degrees of freedom at the bearing. Similarly, Eq. 2.1.3 gives the torsional rotation of the girder at the bearing.

It is emphasized that properly designed cross-frames typically are relatively rigid compared to the girders in I-girder bridges. Taking advantage of this assumption, the layovers of the girders within the spans also may be estimated. Figure 2.1.2 shows representative girder deflections and rotations at an intermediate cross-frame location where Δ_y is the differential vertical displacement between the girders due to dead loads and *s* is the girder spacing.

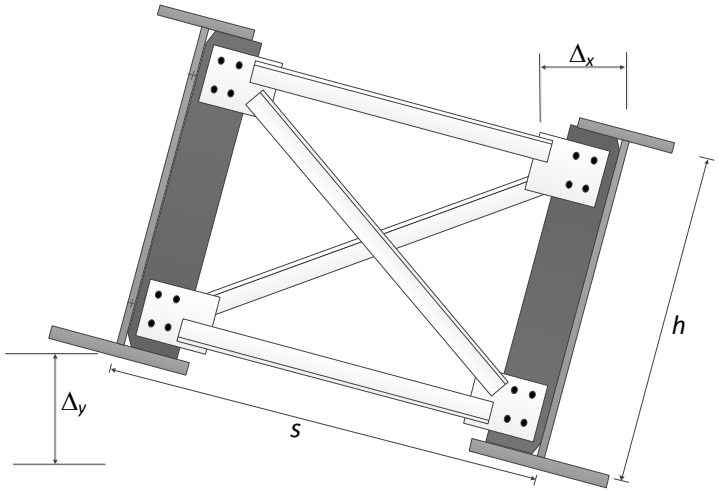

Figure 2.1.2. Girder deflections and rotations for an interior cross-frame location.

The layovers within the span can be estimated from the differential vertical displacements, assuming negligible cross-frame in-plane deformations, and cross-frames framed normal to the girders, as

$$\Delta_x = h\,\Delta_y / s \tag{2.1.5}$$

where *s* is the spacing between adjacent girders (Sanchez, 2011), and the girder twists are

$$\phi_z = \Delta_y / s \tag{2.1.6}$$

If the intermediate cross-frames are skewed relative to the girders, the girder twists at the cross-frame locations can be estimated by adding the results from Eqs. 2.1.6 and 2.1.3, where θ is the skew angle of the cross-frame and ϕ_x is the girder major-axis bending rotation at the cross-frame.

2.2. Cross-Frame Detailing Methods

Curved and skewed I-girder bridges exhibit significant torsional displacements of the individual girders and of the overall bridge cross-section. As a result, the girder webs can be plumb in only one configuration. If the structure is built such that the webs are plumb in the ideal no-load position, they generally cannot be plumb under the action of the structure's steel or total dead load. The deflected geometry resulting from these torsional displacements can impact the fit-up of the members (i.e. come-along and jacking forces), the erection requirements (crane position and capacities, number of temporary supports and tie downs), and the bearing cost and type. Furthermore, significant layover can be visually objectionable. This is particularly the case at piers and abutments.

If the torsional deflections are large enough, then the cross-frames are typically detailed with a lack-of-fit that induces opposing torsional displacements to offset the dead load torsional rotations. As explained in the AASHTO LRFD Specifications Article C6.7.2 (AASHTO, 2010), different types of cross-frame detailing are used to achieve approximately plumb webs in the theoretically no-load, steel dead load, or total dead load conditions. These methods are summarized below.

No-Load Fit (NLF): The cross-frames are fabricated to fit the girders in their cambered, plumb, no-load geometry without inducing any locked-in forces (i.e., there is no lack-of-fit). Figure 2.2.1 illustrates the behavior associated with NLF detailing at a representative intermediate cross-frame in the no-load geometry (girders supported on blocking) and under the action of the dead loads. The cross-frame is assumed to be normal to the girders for purposes of the discussion here. The girders deflect from their plumb no-load geometry into an out-of-plumb position under the action of the dead loads. In Fig. 2.2.1, this twisting of the girders is driven primarily by the larger vertical deflection of the girder on the right compared to the one on the left. Since the cross-frame deformation is relatively small within its plane, the cross-frame induces a twist into the girders due to the differential vertical displacements.

In addition, as explained in Section 2.1, the cross-frames at skewed bearing lines tend to rotate about their own skewed axis and warp (twist) out of their plane. However, the cross-frames are again relatively stiff within their own plane. Therefore, the girders lay over at any skewed bearing line to maintain compatibility between the girders and the cross-frames under the dead load rotations at the bearing line. This is illustrated by Fig. 2.1.1.

The above two sources of girder layover work both jointly and independently. That is, if the bearing line cross-frames were theoretically taken out, the layovers at the bearing lines, caused by the intermediate cross-frames, would be different. Similarly, if the bearing line cross-frames were left in and the intermediate cross-frames taken out, the girder layovers would be different at the intermediate cross-frame locations.

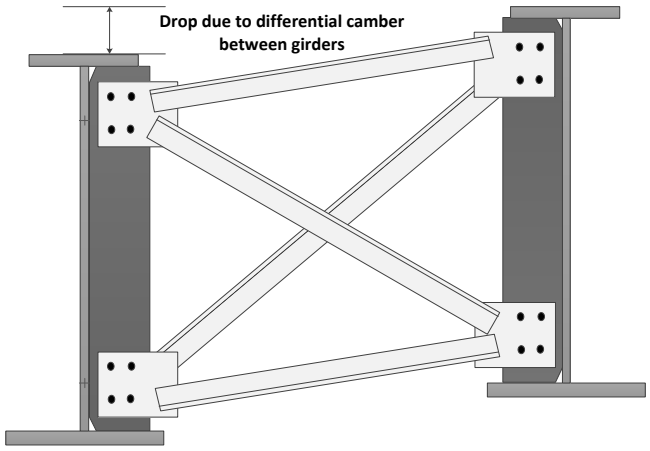

(i) no-load geometry

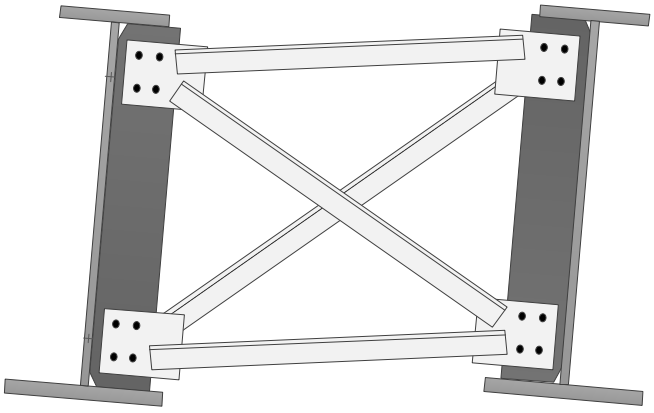

(ii) under the action of dead loads

Figure 2.2.1. Illustration of the behavior associated with No-Load Fit (NLF) detailing at intermediate cross-frames

Total Dead Load Fit (TDLF): The cross-frames are fabricated to fit the girders in their ideal final plumb position under total dead load (that is plumb webs but with the total dead load vertical deflections subtracted from the initial girder camber). Figure 2.2.2 illustrates the behavior associated with TDLF detailing at an intermediate cross-frame (assumed normal to the girders) before it is connected to girders in the no-load geometry, after it is connected to girders in the theoretical no-load position (if the cross-frames could be connected to the girders without any dead load on the structure), and under the total dead load. The intermediate cross-frame does not fit to the girders in the no-load geometry since it is fabricated for the final plumb geometry. Also, as noted above, the cross-frame is relatively stiff in its own plane. Therefore, the girders, which are relatively flexible, must be twisted in a direction opposite to their dead load torsional rotations to make the connections to the cross-frame. However, under the action of the total dead loads, the girder webs rotate back to an approximately plumb position. The lack-of-fit between the girders and cross-frame, due to the differential vertical camber, induces additional locked-in internal stresses and corresponding deformations in the structure when the girders and cross-frames are forced together to make their connections.

All of the illustrations of the deflections, rotations and deformations in Fig. 2.2.2 correspond to a generic location within the span. To achieve a web plumb condition under the total dead load at a skewed bearing line, the opposite of the layover under the total dead load needs to be applied at this location initially (i.e., due to the lack-of-fit). Based on the assumption that the in-plane cross-frame deformations are relatively small, this is achieved by fabricating the end cross-frames to fit the final geometry of the girders, but attaching the cross-frames to the girders in their initial cambered geometry. Assume that the girder end connection plates, which are also the bearing stiffeners, are vertical in the reference geometry shown in Fig. 2.1.1. Due to the total dead load camber, the girder end connection plates are rotated by the negative of the total dead load major-axis bending rotations shown in Fig. 2.1.1 ($-\phi_x$) to achieve the initial cambered geometry. Correspondingly, if the cross-frames at the bearing line are to be connected to the girders in the theoretical no-load geometry, the girder top flange must be laid over by the negative of the dead load layover shown in Fig. 2.1.1 ($-\Delta_x$). The girders typically are fabricated with plumb webs in their initial no-load geometry. Therefore, the girder top flange in Fig. 2.1.1 must be forced over by $-\Delta_x$ to make the connection to the bearing line cross-frame in the ideal no-load condition.

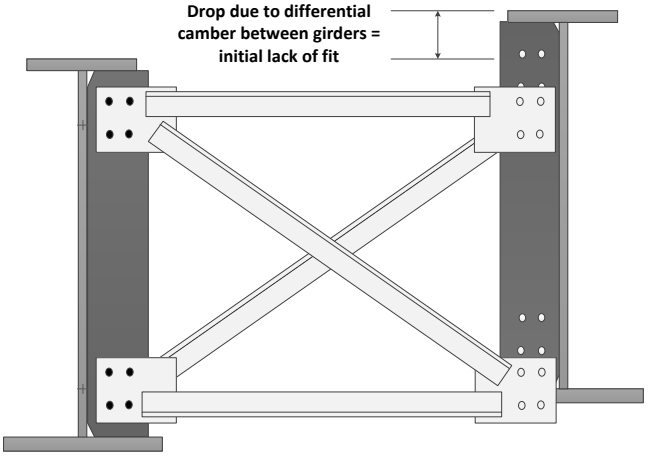

(i) no-load geometry before connecting the cross-frames

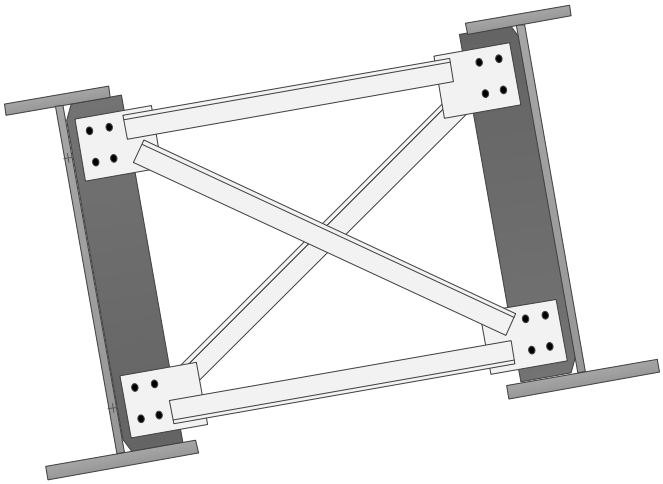

(ii) no-load geometry after connecting the cross-frames

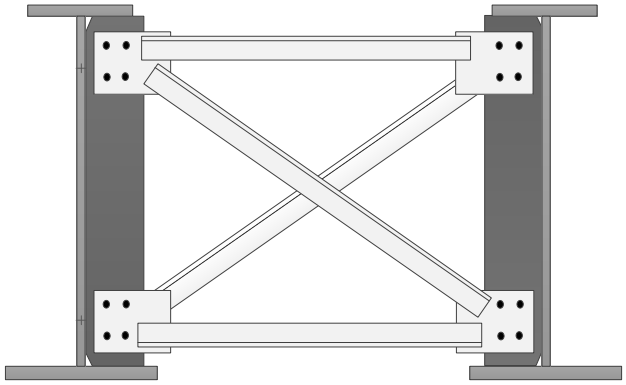

(iii) under the total dead load

Figure 2.2.2. Illustration of the behavior associated with Total Dead Load Fit (TDLF) detailing at intermediate cross-frames.

When the total dead load has been applied to the structure, the girders "unwind" under the application of the load such that they come back to an approximately plumb position in the final constructed configuration. The girders deflect into the approximately plumb position shown in Fig. 2.2.2 (iii) at the intermediate cross-frame locations, the girders rotate approximately back to the plumb reference geometry in Fig. 2.1.1 at the bearings, and the end connection plates (i.e., the bearing stiffeners) rotate approximately back to the vertical position shown in Fig. 2.1.1.

Steel Dead Load Fit (SDLF): The cross-frames are fabricated to fit the girders in their idealized final plumb position under the steel dead load (that is plumb webs but with the steel dead load vertical deflections subtracted from the initial girder camber). SDLF detailing is similar to TDLF detailing in that locked-in stresses and deformations are developed due to a lack-of-fit. However, the lack-of-fit between the cross-frames and girders in the no-load geometry for SDLF is typically much smaller than that due to TDLF. When SDLF is used, the webs rotate back to an approximately plumb position under the action of the steel dead loads.

The type of the detailing generally should be specified by the designer since it may impact the construction requirements, the girder layovers and vertical deflections, and the overall performance of the bridge.

2.3. Current Practice Regarding Cross-Frame Detailing Methods

For the bridges constructed with NLF detailing, fabricators can use one of two options for the fabrication of the intermediate cross-frames:

- Detail the cross-frames such that the drop of cross-frames changes along the length of the bridge (see Fig. 2.2.1(i)).
- Fabricate the cross-frames all as the same dimensions and detail the connection plates based on the differential camber between the girders (See Fig. 2.3.1).

It should be noted that the drops of the cross-frames often vary along the lengths due to the cross-slopes and changes in superelevation of the bridge. Furthermore, the preferred practice for fabricating the cross-frames typically is to vary the drops in by moving one side of a jig (AASHTO/NSBA, 2006). Therefore, the first of the above options is the more common one.

Skewed end cross-frames are fabricated similarly but based on the major-axis bending rotations due to initial dead load cambers. The shop assembly of the bridge components constructed with NLF detailing is possible since the cross-frames are detailed to fit the girders in the no-load geometry.

For bridges constructed with DLF detailing, fabricators make the cross-frames based on the theoretical final plumb geometry. The final geometry typically corresponds to the stage where plumb webs are targeted but where the differential vertical displacements and rotations associated with the dead loads are taken out. Therefore, shop assembly of bridges constructed with DLF detailing is difficult since the girders need to be rotated as well as displaced vertically to overcome the lack-of-fit between the cross-frames and girders.

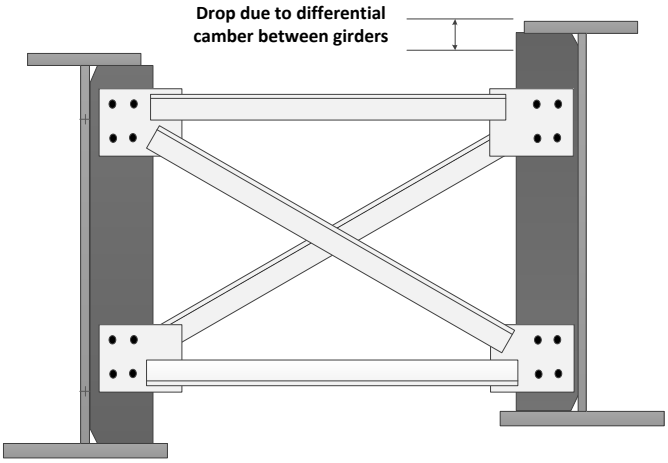

Figure 2.3.1. Illustration of the detailing the connection plates differently based on the differential cambers between the girders for No-Load Fit (NLF) detailing

Although AASHTO (2010) Article C6.7.2 states that engineers may need to consider the potential for any problematic locked-in stresses for horizontally curved I-girder bridges, with or without any skewed supports, engineers practically never include the inherent lack-of-fit in their structural analysis. For a straight and skewed bridge constructed with DLF detailing, engineers typically assume

- exactly plumb girders,
- zero flange lateral bending stresses, and
- zero cross-frame forces

under the targeted plumb load level. Furthermore, it is very common to assume that girders provide no lateral restraint compared to the cross-frames so the girders can be twisted without any resistance to make the connections. In some cases erectors are not informed or aware that the cross-frames may require large fit-up forces or special erection schemes to overcome the corresponding lack-of-fit.

Chavel and Earls (2001, 2006a) studied the erection procedures for a specific long-span curved steel I-girder bridge constructed with TDLF detailing and showed that the girder

displacements and stresses as well as support reactions are significantly affected due to locked-in stresses associated with the DLF detailing. Therefore, for certain bridges constructed with DLF detailing, the final elevation of the girders and the deck profile can deviate significantly from the predictions due to the locked-in stress effects. Moreover, the above misconceptions can lead to overstressing of the members or fit-up problems during construction.

2.4. Key Bridge Attributes

2.4.1. *Nuisance stiffness*

"Nuisance stiffness" is characterized as unwanted stiffness in secondary members, other primary members, or connections, producing undesirable load paths in a structural system (Krupicka and Poellot 1993). Nuisance stiffness can lead to difficulties during erection due to 3D deflections of the bridge; handling of large displacement incompatibilities at nuisance stiffness locations can require large applied forces. Unwanted stiffness often can occur near skewed supports. Krupicka and Poellot (1993) provide an extensive discussion of various design and detailing options to reduce the effects of nuisance stiffness in highly skewed bridge structures. They point out that these problems are particularly severe in wide bridges with heavy skew. They discuss the following options to control nuisance stiffness:

- Interrupt the load path by eliminating selected cross-frames from a given line,
- Provide slotted holes in selected cross-frames and tighten the bolts after deck placement, a method often effective for staged construction of the bridge cross-section (use of slotted holes generally must be very limited such that the corresponding deflections are very localized; otherwise, the engineer is giving up the ability to control of the geometry of the bridge),
- Remove diagonal members from selected cross-frames to eliminate their ability to transfer shear, and
- Shift the cross-frames slightly (i.e., offset them) to eliminate framing directly into a bearing location.

These options must be considered with particular care on significantly curved bridges, where it is also important to develop the full width of the bridge cross-section via the interconnection of the girders by the cross-frames.

For highly skewed bridges, engineers typically find it advantageous to reduce the transverse stiffness of the bridge by staggering the cross-frames particularly in the vicinity of the supports. This layout of cross-frames reduces the magnitude of the cross-frame forces at the expense of increased lateral bending stresses in the girder flanges. When a staggered cross-frame pattern is used, AASHTO (2010) Section C.6.7.4.2 advises that flange lateral bending stresses are determined best by direct structural analysis.

Figure 2.4.1 shows a case in which a staggered cross-frame layout is applied to eliminate the nuisance stiffness in the vicinity of the skewed bearings. Framing the cross-frames directly into or close to the bearing locations can introduce large nuisance stiffness problems (see Fig. 2.4.1(i)). Figure 2.4.1(ii) provides an improved layout to avoid this problem. The load path is interrupted by eliminating selected cross-frames from a given line. Shifting the cross-frames slightly to eliminate framing directly into a bearing location can also reduce nuisance stiffness.

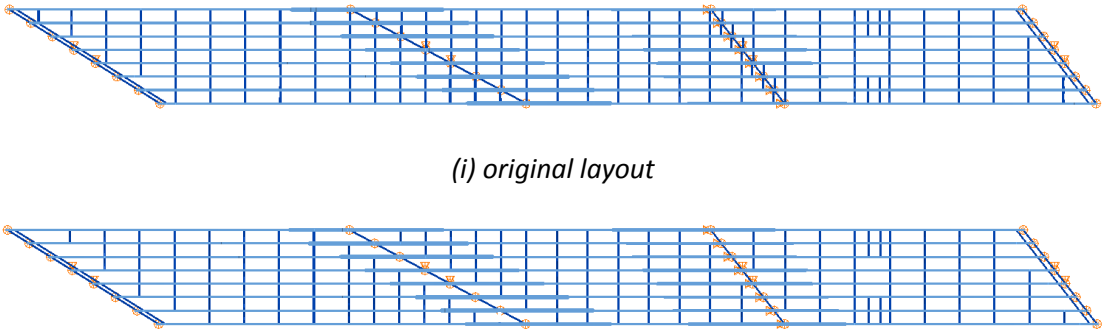

(i) original layout

(ii) improved layout

Figure 2.4.1. Illustration of the options to avoid nuisance stiffness.

Sanchez (2011) also introduces a new innovative way of alleviating the nuisance stiffness effects by fanning the cross-frames to follow the orientation of the skewed bearings, as shown in Fig. 2.4.2. In this scheme, the key concept is to frame the intermediate cross-frames into the girders at the points having similar layovers prior to the installation of the cross-frames. Sanchez (2011) finds that a fanned cross-frame layout reduces the flange lateral bending stresses and cross-frame forces by minimizing the additional deformations forced into the girders by the intermediate cross-frames. Sanchez (2011) indicates that the fanned cross-frame layout performs better than the staggered cross-frame layout at mitigating the skew effects. It should be noted that cross-frames along the length of the bridge require different member lengths for the fanned configuration.

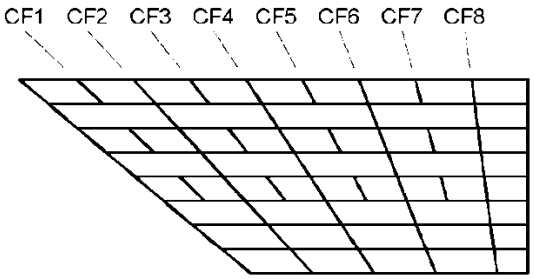

Figure 2.4.2.Fanned cross-frame configuration with girders grouped in pairs to diminish the skew effects.

2.4.2. *Characterizing the level of skew effects*

The skewed bearing lines subject the bridge cross-section to torsion by developing transverse load paths between the girders through the cross-frames (see Figure 2.4.3). Vertical displacements, girder major-axis bending stresses, and girder flange lateral bending stresses can be influenced significantly if the transverse load transfer is large (large skew effects).

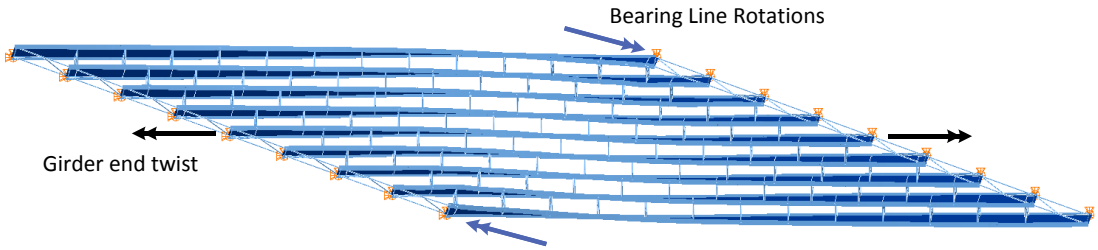

Figure 2.4.3.Twist of the bridge cross-section due to skewed bearing lines.

Sanchez (2011) introduces the skew index which characterizes the level of skew effects. This index is defined as

$$I_S = (no\ of\ girders - 1)\ s\ \tan(\theta)\ /L_S \qquad (2.4.1)$$

where; L_S is the span length of the bridge centerline. This index characterizes the level of skew effects by considering the skew angle, span length and the width of the steel structure. It should be noted that the skew effects are also influenced by the cross-frame layout, which is not addressed by Eq. 2.4.1. Sanchez (2011) observes that as the index increases the influence of skew effects on the bridge responses increases as well. Sanchez (2011) proposes three limits to identify the level of skew effects:

- $I_S < 0.30$

  The skew effects are minor for the bridges in this category.

- $0.30 \leq I_s \leq 0.65$

The largest flange lateral bending stresses for bridges in this category tend to be more than 30% of the major-axis bending stresses, which may be considered as large flange lateral bending effects based on the limit suggested in the Commentary to Article 6.7.4.2 of AASHTO (2010), which states that for curved bridges, "A maximum value of 0.3 may be used for the bending stress ratio" (i.e., f_ℓ / f_b).

- $I_S > 0.65$

  For the bridges in this category, the girder major-axis bending stresses and vertical displacements can be significantly affected by the skew effects.

CHAPTER III.

ANALYTICAL REPRESENTATION OF CROSS-FRAME DETAILING METHODS

3.1. Overview of Analysis Methods

Various analysis methods are available for engineering of bridges. It is important to understand the applicability of these methods so that the right tool is selected for a bridge in the most effective ways. This understanding will save engineers time and give them confidence when evaluating a bridge response.

The deflections of the structure at the completion of the steel erection and during the deck placement are often of key importance. Prior studies such as Chang et al. (2005) and Coletti and Yadlosky (2007), NCHRP (2011) and Sanchez (2011) have shown clearly that 1D and 2D analysis idealizations can often err substantially in the prediction of bridge 3D system deflections. There are numerous reasons for these errors, including:

- Lack of consideration of the influence of fixed bearing restraints or off-axis restraints from guided bearings. The actual height of the bearings must be included in the analysis for accurate prediction of these effects.
- Lack of representation of the location of cross-frames through the depth of the bridge cross-section and/or the combined shear and bending flexibility of the cross-frames.
- Assuming the centroidal axes of all the girders, cross-frames, etc. are located at a single depth, and neglecting all the displacements in a horizontal plane at this depth, as well as the rotations about an axis normal to this plane.
- Lack of consideration of the warping torsion response of the I-girders (e.g., the flange lateral bending response due to horizontal curvature) on the overall deflections of the structure.
- Lack of representation of cross-frame general stiffness.

Guidelines for analytical methods and erection engineering of curved and skewed bridges are provided by NCHRP (2011).

The most basic analysis method for engineering of bridges is line-girder analysis (1D) in which individual girders are modeled disregarding the structural steel framing of the bridge.

There are different variations of line-girder analysis such as the V-Load method introduced by Richardson et al. (1963), where the interaction between the girders and cross-frames are accounted in a coarse fashion. In the V-Load method, curved I-girders are modeled as straight girders with the same length, but vertical loads are applied at the cross-frame locations to represent the torsional effects in the girder system.

The next level of analysis is 2D grid analysis methods in which girders and cross-frames are modeled as line elements that have three degrees-of-freedom (dofs) per node, two rotational (major axis bending and torsional rotations) and one translational (vertical displacement). The vertical depth of the superstructure is not considered in the model. The girders and their cross-frames are theoretically connected together at a common elevation which is taken as the centroidal or shear center axis of girders. All the bearing supports theoretically are located at this same elevation in the model. There are also 2D-Frame analysis methods which line elements have 6 dof per node (three rotational and three translations). The modeling features of 2D-Frame analysis methods are essentially same with 2D-Grid analysis methods. 2D-Frame analysis methods are extended as Plate and Eccentric Beam analysis methods in which composite bridge deck is modeled using flat shell (or plate) finite elements and the girders are modeled using 6 dof per node frame elements with an offset relative to the slab. The Plate and Eccentric beam analysis model is used typically for modeling of the composite bridge structure in its final constructed configuration.

The next level of analysis is conventional 3D-Frame analysis methods where the capabilities of the 2D-frame elements are used but girders are modeled at their actual spatial locations. Moreover, cross-fames are modeled through the depth but single frame element is used to represent the entire cross-frame. There are also refined 3D-Frame analysis methods where the frame element has 7 dof per node. The additional dof corresponds to warping dof. This type of element can be utilized to provide a highly accurate characterization of bridge I-girder torsional stiffnesses. This type of element is also often used with comprehensive modeling of the information through the depth of the structure. Chang (2006) and Chang and White (2006) showed by their 3D-Frame analysis software (GT-Sabre) that including the modeling of all the individual cross-frame components (i.e., separate modeling of the cross-frame chords and diagonals) with the additional warping dof is capable of matching the results of 3D FEA quite closely, with the exception that it is not able to capture the influence of I-girder web distortion on the physical responses.

The most refined level of analysis is 3D FEA, which has the potential to predict the system behavior accurately. Generally speaking, any matrix analysis software where the structure is modeled in three dimensions may be referred to as a three-dimensional finite element analysis (3D FEA). This research adopts a more restrictive definition of 3D FEA provided by AASHTO/NSBA G13.1 (2011). According to G13.1, an analysis method is classified as 3D FEA if:

1) The superstructure is modeled fully in three dimensions,
2) The individual girder flanges are modeled using beam, shell or solid type elements,
3) The girder webs are modeled using shell or solid type elements,
4) The cross-frames or diaphragms are modeled using truss, beam, shell or solid type elements as appropriate, and
5) The concrete deck is modeled using shell or solid elements (when considering the response of the composite structure).

Section 3.2 discusses the 3D finite element analysis modeling strategies that are used for the analytical studies in this research.

3.2. Simulation Modeling (3D FEA) of I-Girder Bridges

In recent years, the capabilities for simulation of physical tests using advanced 3D finite element analysis (FEA) has progressed to the point that, in numerous areas, the results from physical experiments can be reproduced quite realistically and quite reliably. However, similar to quality experimental testing, the execution of test simulations requires great care. This is particularly the case where advanced simulation capabilities are not facilitated well by software user interfaces. It should be noted that the results from an FEA test simulation are only as good as the accuracy of:

- The detailed geometry (e.g., plate thicknesses, deck-slab thicknesses, haunch depths, girder web depths, bearing heights, bearing plan locations, etc.),
- The load and displacement boundary conditions,
- The assumed (or nominal) initial conditions (e.g., initial internal residual stresses, geometric imperfections, any lack-of-fit between components in their unloaded condition, etc.),
- The constitutive relationships for the various constituent materials,
- The kinematic assumptions and/or constraints imposed by the structural theories.

The consideration of above the attributes should not detract from the usage of advanced 3D FEA test simulations. In many respects, the above attributes are more easily specified, controlled and quantified in sophisticated 3D FEA models. In this research, the 3D FEA test simulations are conducted using ABAQUS (Simulia, 2010). The following sections explain the modeling procedures to capture the elastic and inelastic behavior of the bridges during construction. For the FEA studies conducted in the research, the simulation models amount to highly refined 3D FEA design analysis solutions representing all of the important nominal behavioral characteristics of curved and skewed steel I-girder bridges.

3.2.1. *Elastic modeling of I-girder bridges*

Figure 3.2.1 shows an example 3D FEA representation of a portion of an I-girder bridge for elastic geometrically linear (linear elastic) or geometrically nonlinear (second-order elastic) analysis solutions. The webs are modeled using 12 S4R elements through their depth. The number of elements along the girder length is selected such that each shell element has an aspect ratio close to one. The S4R element is a 4-node quadrilateral displacement-based shell element with reduced integration and a large-strain formulation. Five integration points for the webs of the steel I-girders are used through the thickness of the shell elements. The flanges of the girders, and the transverse stiffeners (bearing stiffeners, intermediate transverse stiffeners, and cross-frame connection plates) are modeled using the B31 element, which is a two-node beam element compatible with the S4R shell elements.

All of the bridge components are modeled at their nominal physical geometric locations using their nominal physical dimensions, with the exception that the webs are modeled between the centerlines of the flanges. Therefore, the flanges are at the correct physical depth in all cases, and the model of the web has an overlap of t_f /2 with the flange areas. This is comparable to the manner in which joint size is neglected in the modeling of frame structures; the resulting additional web area is on the order of the steel area from web-flange fillet welds, which otherwise is not included in the model. At flange section transitions, the reference axis of the beam elements is shifted to follow the shift in the flange centroid, and prismatic beam elements with a thickness and width equal to the average of the flange thickness and width are used for single element length. Figure 3.2.2 shows a representative FEA model at a flange thickness transition. Therefore, the depth of the girder web also shifts with changes in the flange thickness in the FEA model. The average of the two flange thicknesses is used within the one-element transition length.

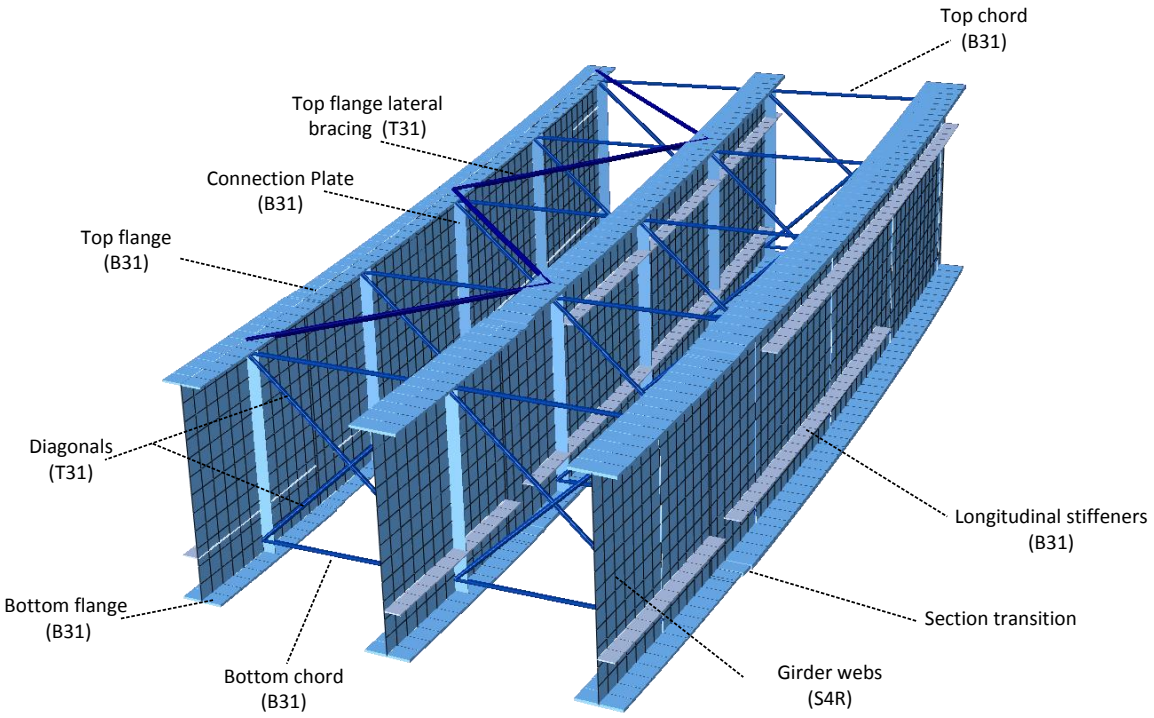

Figure 3.2.1. Example 3D FEA representation of the I-girder bridge components for elastic linear/geometric nonlinear analysis solutions.

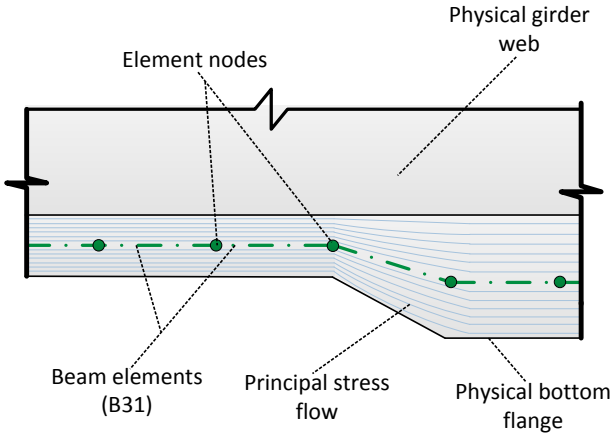

Figure 3.2.2. Representative FEA model at a flange thickness transition.

Cross-frame diagonals are modeled with T31 truss elements while the top and bottom chords are represented by B31 beam elements to maintain the stability of the cross-frames in the direction normal to their plane. The cross-frame elements are connected to girder webs at the intersection of the centerline of the cross-frame member and the girder web. If this work point does not coincide with a girder web node, a new node is introduced at that location and a "linear" multi-point constraint is used. This constrains each degree of freedom at the newly

created node to be interpolated linearly from the corresponding degrees of freedom at the adjacent web nodes along the depth of the web. Longitudinal stiffeners are modeled by using the B31 element. If the elevation of the longitudinal stiffener does not coincide with the web nodes, the “linear” multi-point constraint is used to introduce a new node to define these elements. Lastly, if a flange-level lateral bracing system is used, these members are modeled with T31 truss elements. These truss elements, which represent the flange lateral bracing members, are connected to the girder flanges at the web-flange juncture, which is typically the designed workpoint used in practice. For the elastic analyses the modulus of elasticity of the steel is taken as 29000 ksi.

Bearings are modeled as a point vertical support at the web-flange juncture since beam elements are used to model the flanges (the beam element kinematics enforces a linearly varying displacement across the width of the flange). The girder model is generally free to rotate about the point support location, and horizontal displacement constraints representing guided bearings are placed at the point support location. The substructure is modeled as a rigid support, including any temporary towers for construction.

In this study, all bridges are analyzed for the dead load due to the self-weight of the steel, as well as the concrete deck and other loads acting on the non-composite bridge since the behavior during the construction is in interest. The steel sections alone are assumed to resist the wet concrete dead load in addition to the weight of the steel components, the slab reinforcing steel, forms and construction equipment. The GRAV command is used in the FEA model to include the steel self-weight as distributed body loads. The steel density is taken as 490 pcf. The weight of the formwork (10 psf), the concrete slab including the reinforcing steel (150 psf) is applied to the top flanges as uniformly distributed line loads based on the tributary width of each girder across the cross-section of the bridge. In addition, the overhang brackets used to resist the weight of wet concrete and formwork at the fascia girders is considered in the model, subjecting the fascia girders to torsion. The overhang brackets are assumed to frame into the webs at web-flange junctures. To simulate this loading, the overhang bracket loads are modeled as two equal and opposite radial forces that create a uniformly distributed torque on the fascia girders. The weight of the construction equipment is neglected in this study.

The specified dead load camber is applied to the girder models by using the IMPERFECTION command. The girder cambers are set so that the slab is ideally flat under the total non-composite dead load. The initial camber profile is obtained from the negative of the total dead

load vertical deflections. Superelevation, grade, and vertical curves are neglected in this research to simplify the modeling and behavior. The sequence of application of the loads to the bridge FEA model of the bridge is as follows:

1. *Generation of the complete model:* The FEA model of the bridge is generated assuming that the girder webs are plumb in the initial no-load configuration. An initial camber of the girders is applied by using the IMPERFECTION command.
2. *Applying the steel dead load:* The self weight of the steel members is "turned on" by using the GRAV command.
3. *Application of the weight of the forms and the concrete dead weight:* The steel section alone must resist the dead and construction loads that are applied before the concrete deck is hardened. Therefore, the dead load from the wet concrete and forms is assumed to be carried by the non-composite steel sections alone. Eccentric bracket loads on exterior girders are applied as two equal and opposite radial forces which create a uniformly distributed torque on the exterior girders.

3.2.2. *Inelastic modeling of I-girder bridges*

For the strength evaluation of the bridges, the internal stresses can go beyond the yielding limit and elastic models cannot capture the true corresponding physical response. In these cases, inelastic (geometric and material nonlinear) models are used to capture the plastic deformations that may occur in the system. Residual stresses and imperfections generally can influence significantly the maximum load capacity of structures. Therefore, for the inelastic analyses, residual stresses and geometric imperfections due to fabrication of the girders are considered to represent the physical behavior more accurately.

Figure 3.2.3 shows an example 3D FEA representation of a portion of an I-girder bridge for full-nonlinear analysis solutions. The webs are modeled using 20 S4R elements through their depth for full-nonlinear analysis solutions. Flanges are modeled using 12 S4R elements along the width of the flanges which enables one to include the residual stresses.

The nominal residual stress pattern is shown in Fig. 3.2.4. The residual stress pattern is taken from Kim (2010), which is referred as best-fit Prawel residual stress pattern. It is found by Kim (2010) that the best-fit Prawel residual stress pattern provides a reasonable lower bound compared to the experimental test results that are done by Prawel et al. (1974) for the welded I-section members. The residual stress pattern is self-equilibrating for each cross-section where

the maximum compressive residual stress in the flanges is 0.25 F_y at the tips of the flanges and decreases linearly to 0.1 F_y at the one third of the flange width from the tips of the flange. The maximum tensile stress is constant as 0.5 F_y at the vicinity of the web flange juncture for the length of $b_f/12$ at each side of the web flange juncture. The maximum tensile residual stress for the web is F_y within the $D/20$ from the web flange juncture. Maximum compressive residual stress of 0.176 F_y is provided in the middle of the web for a length of 0.8 D. For the cases of slender web, compressive residual stress of 0.176 F_y decreased to the web plate buckling stress since 0.176 F_y is larger than the web plate buckling stress assuming singly-supported boundary conditions. Figure 3.2.5 provides a representative residual stress distribution applied to an example FEA simulation.

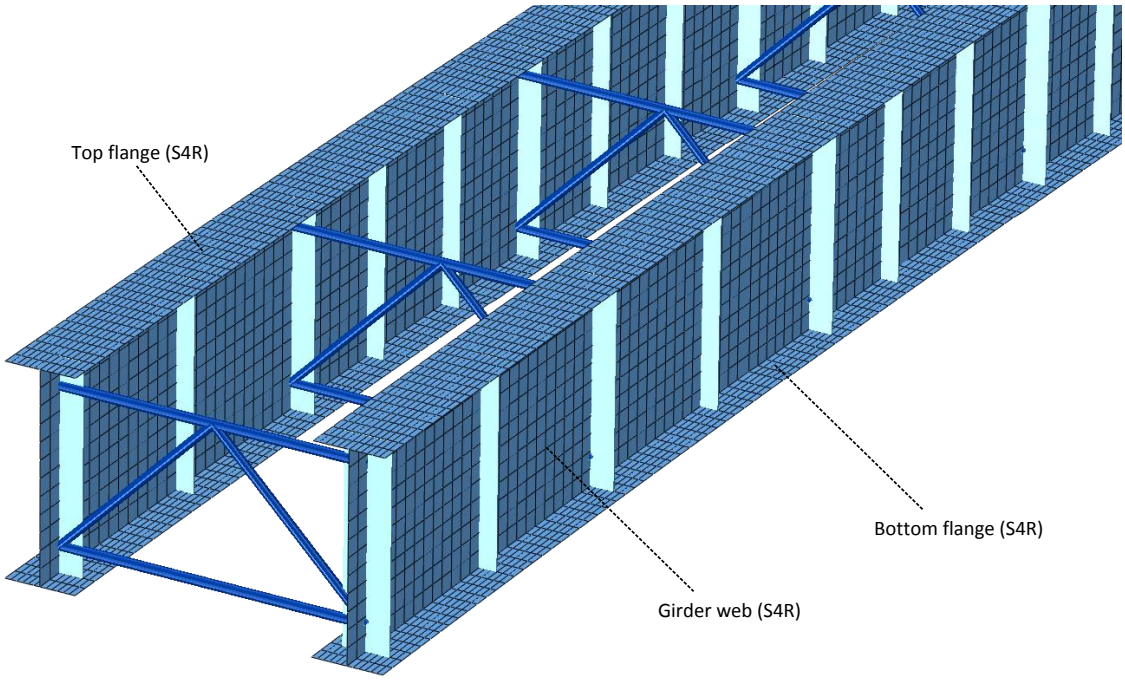

Figure 3.2.3. Example 3D FEA representation of the I-girder bridge components for full-nonlinear analysis solutions.

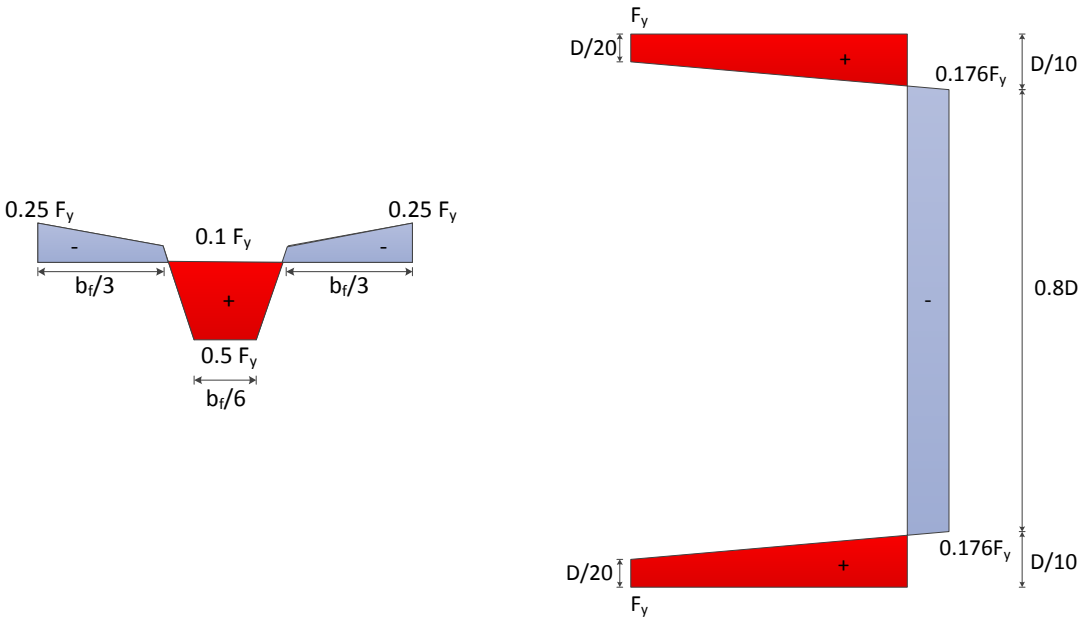

(i) girder flange *(ii) girder web*

Figure 3.2.4. Residual stress pattern for (i) girder flanges and (ii) girder web.

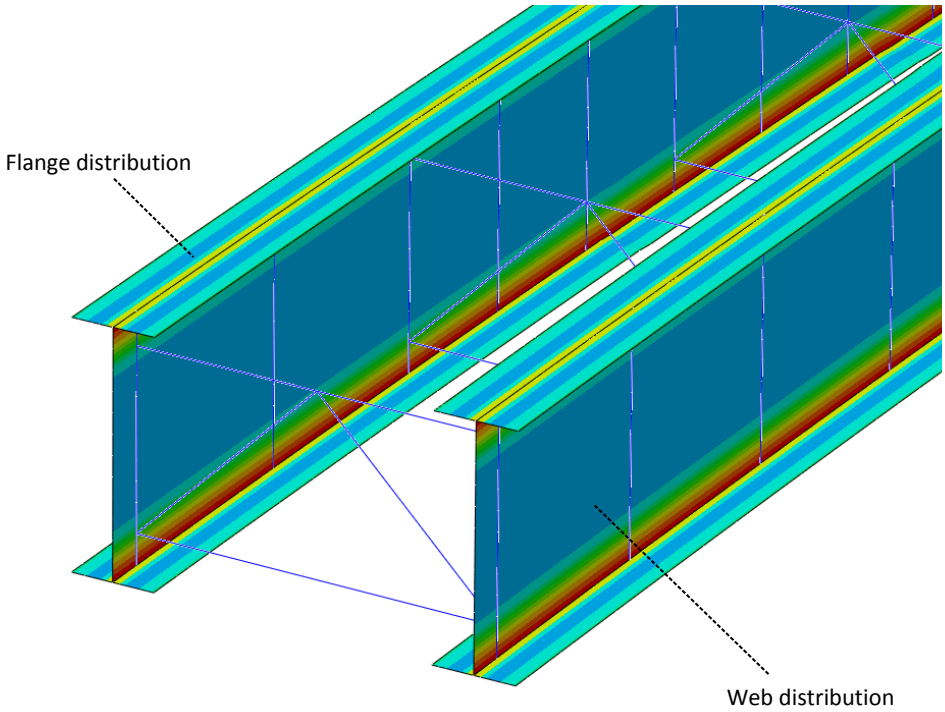

Figure 3.2.5. Representative residual stress distribution applied to an example FEA simulation.

At flange section transitions, the reference axis of the shell elements is shifted to follow the shift in the flange centroid, and prismatic shell elements with a thickness and width equal to the average of the flange thickness and width are used for two element lengths. Flange nodes that are along the width of the flange at the stiffener locations are tied to the node at the web flange juncture by the ABAQUS beam-type multi-point constraint since the beam elements are used for the transverse stiffeners (bearing stiffeners, intermediate transverse stiffeners, and cross-frame connection plates). This constraint provides a rigid beam between specified nodes to constrain the displacement and rotation at the flange nodes that are at the stiffener location to the displacement and rotation at the node at the web flange juncture. The beam-type multi-point constraint is only applied to one side of the flange at that location, if the stiffener is at the one side of the girder.

For inelastic models, flange nodes that are across the width of the flange at bearing locations are tied to the node at the web flange juncture by ABAQUS beam-type multi-point constraint to allow flanges rotate and twist at the bearing locations. This provides linear displacements across the width of the flanges.

Grade 50 material is used for most of the bridges. A representative stress-strain curve for AASHTO M270 Grade 50W steel and a multilinear fit to averaged results from a suite of coupon tests are shown in Fig. 3.2.6. Results of the stress-strain data from tension coupon tests obtained from Beshah (2008) are used as a base for the description of the material yield and strain hardening characteristics in this work. The test results are summarized in Table 3.2.1 in terms of the average engineering stress and strain. Since the finite elements used in this research are formulated for large strain, the true stress and true strain must be used when defining the material stress-strain response. Therefore, the engineering stress-strain data is converted to true stress-strain data using the following formulas (Simulia 2010):

$$\sigma = \sigma_{nom}(1 + \varepsilon_{nom}) \tag{3.2.1}$$

$$\varepsilon = \ln(1 + \varepsilon_{nom}) \tag{3.2.2}$$

where, σ, σ_{nom}, ε, and ε_{nom} are true stress, engineering stress, true strain, and engineering strain respectively.

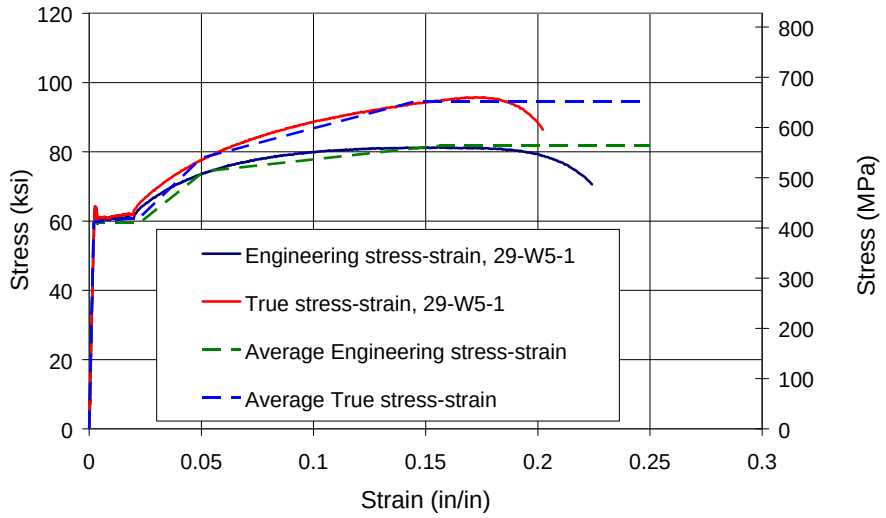

Figure 3.2.6. Representative stress-strain curve for AASHTO M270 Grade 50W steel.

Table 3.2.1. Average engineering stress-strain data from the tension coupon tests (Beshah, 2008).

N	E (ksi)	Static F_y (ksi)	E_{st} (ksi)	ε_{st} (%)	F_u (ksi)	ε_u (%)
6	29650	57.56	592	1.18	81.850	12.3

A multi-linear stress-strain curve is fit to the above true stress-strain results by defining four anchor points (Zureick et al. 2002). The first anchor point is the initial yield point of the material where the plastic strain is zero. The second point is defined at the onset of strain hardening (ε_{st}, F_y). The third point is arbitrarily selected at a total engineering stress of $F_y + 2/3\ (F_u - F_y)$. The engineering strain corresponding to this point is determined as $\varepsilon_{st} + 2/3\ (F_u - F_y) / E_{st}$. The fourth point is defined at the ultimate tensile stress on the engineering stress-strain curve. Lastly, the true stress is assumed to be constant for strains larger than those associated with the fourth point. The static yield of the test result is scaled such that the yield is exactly equal to 50 ksi for this research. Figure 3.2.7 shows multi-linear stress-strain curve used in this study for Grade 50 material which is scaled from the multi-linear stress-strain curve in Fig. 3.2.6. Table 3.2.2 gives the specific stress-strain data. For the slab reinforcing steel, an elastic-perfectly plastic stress-strain response with a nominal yield strength of 60 ksi is assumed.

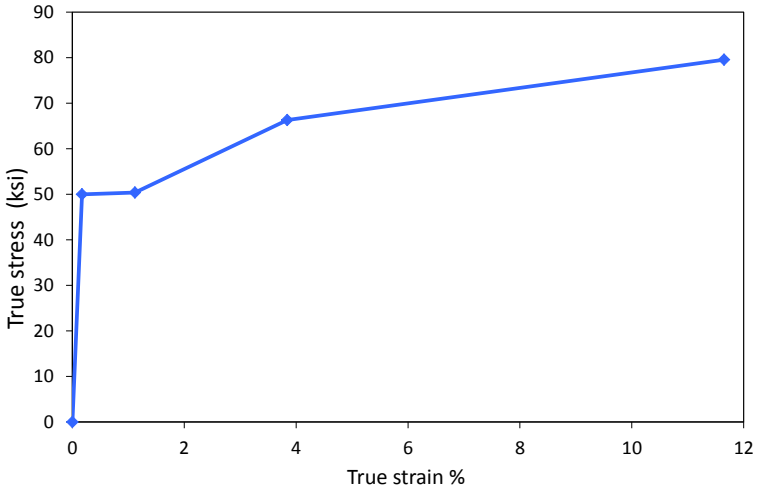

Figure 3.2.7. *True stress-strain responses for the structural steel (Grade50).*

Table 3.2.2. Data points for multi-linear stress-strain response for steel members.

Point	*True Strain (%)*	*True Stress (ksi)*
Yielding	*0.17*	*50*
Onset of strain hardening	*1.12*	*50.38*
Intermediate strain hardening	*3.84*	*66.31*
Ultimate strength	*11.65*	*79.56*

3.3. Validation of Analytical Procedures

The FEA modeling techniques are extended from the previous research by Jung (2006), which was validated against a full scale horizontally-curved I-girder bridge test conducted at the FHWA Turner-Fairbank Highway Research Center. In the current research, these FEA modeling techniques are validated further with respect to simulation of the elastic and inelastic behavior of I-girder bridges. Appendix A provides a sample of validations for different cases including full-scale straight and curved I-girders tested to failure, a straight and skewed bridge where field measurements are available, and the curved bridge tested at the FHWA Turner-Fairbank Highway Research Center.

3.4. Model Generator for Test Simulations

This study aims to achieve its objectives by conducting numerous test simulations. Therefore, the amount of time and effort for creating these sophisticated 3D FEA models must be reduced. This is accomplished by the development of a model generator which is written by using MATLAB (2010). The model generator reads span data sheets of the bridge (excel file) which contains the bridge information and then creates an ABAQUS input file of the bridge. This

program is capable of generating the models needed for elastic (beam-shell model) and inelastic (shell model) solutions with desired mesh density. Figure 3.4.1 shows the flow of steps to generate 3D ABAQUS FEA model.

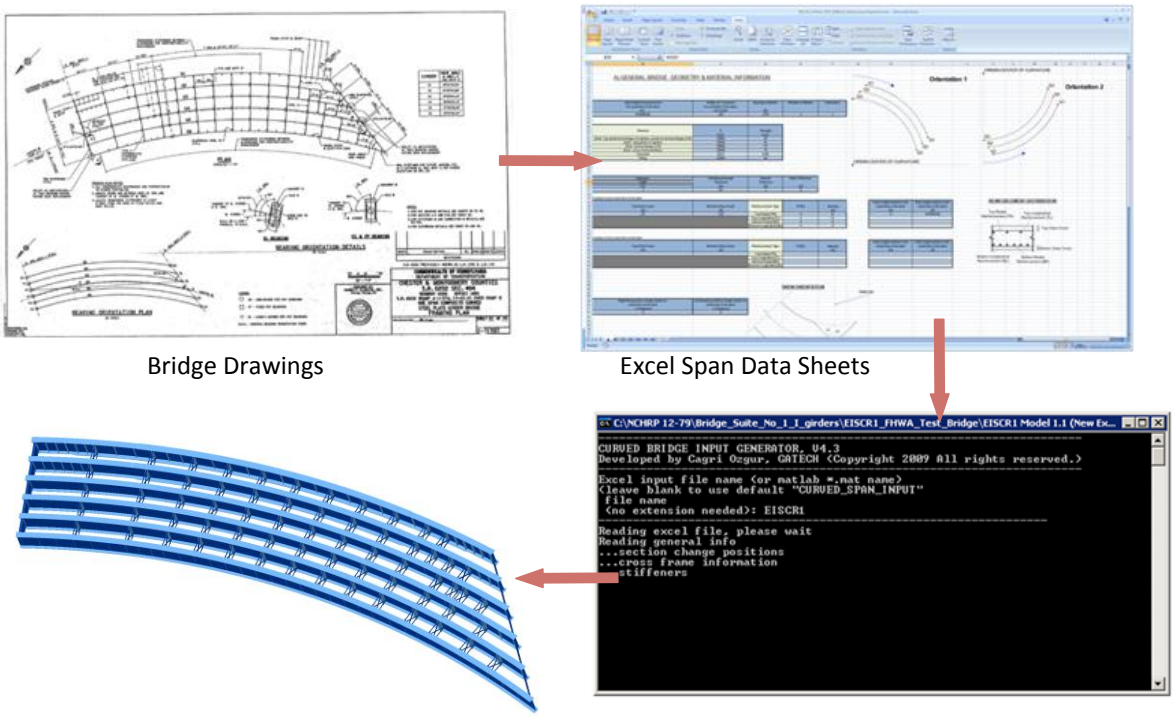

Figure 3.4.1. Flow of steps to generate 3D ABAQUS FEA model.

3.5. Procedures for Determining Locked-In Force Effects due to Cross-Frame Detailing

There are significant complexities associated with the detailing options; however, once broken down into manageable steps, the behavior is rather straightforward. Analysis solutions for the lack-of-fit associated with DLF detailing are fundamentally no different than typical lack-of-fit problems students first solve in undergraduate Strength of Materials; however, the lack-of-fit due to DLF detailing is generally a 3D geometry problem. The analysis for capturing the influence of cross-frame detailing may be obtained using either of two procedures:

1) Construct a model of the bridge in which all of the components are initially unconnected represented in their true no-load geometry under zero load. Then perform a sequential geometric nonlinear analysis in which the various components are assembled together according to the erection plans, forcing fit-up between the components where they do

not fit. It is important to use a software that calculates the strains necessary to insert a component into the current deformed structure by step-by-step simulation (Chang, 2006; Chang and White, 2006). To the knowledge of the authors, only a few current commercial analysis or analysis and design programs do this correctly. Other software packages will likely add these calculations once the issues are made more clear.

2) Construct a full model of any intermediate erection stage of the bridge with the girders in their initial no-load cambered and plumb positions, with the cross-frames connected to the girders, and with initial strains introduced into the cross-frames corresponding to the lack-of-fit caused by the type of cross-frame detailing. Perform a geometric nonlinear analysis of this specific stage by simply "turning gravity on," and including the cross-frame member initial strains in the analysis.

Both of these procedures give identical results. The first- or second-order bridge responses (displacements, reactions internal stresses etc.) for a given geometry and loading are independent of the order of the component assembly or load application (unique), given that:

- The structure stays elastic during any stages prior to and including the stage under consideration,
- The loading on the system is conservative,
- The incidental restraint from the supports is negligible (e.g. unreleased friction at bearings, etc.),
- The tolerances at bolt holes, bearing elevations, etc. are small enough to have a negligible effect on the behavior.

This fact has been discussed and demonstrated previously by Chang and White (2006) and by Chang (2006). Note that the above statements do not apply to staged deck placement in unshored bridge construction. In this case, the slab concrete sets up on the deflected geometry of the structure. Hence, the structure deflections depend on the sequence of the slab placement, as well as the concrete material properties at a given stage. Also, the forces required to assemble the structure during erection can depend significantly on the erection procedures (e.g., selection of temporary shoring towers, etc.) and the sequence of erection, as well as the type of cross-frame detailing. However, the final steel dead load geometry is unique within the context of the above assumptions.

In this work, the second option is used to obtain the research objectives. The initial strains corresponding to the lack-of-fit are introduced to each cross-frame member. These strains are calculated by using the cross-frame member length in the final targeted dead load position, which is also the fabricated (no-load) length of the cross-frame members, (Configuration 1) and the length between the work points on the girders in the initially-plumb cambered geometry of the girders (i.e., the no-load geometry of the girders, Configuration 2).

The differential cambers between the girders often correspond to large initial strains in the cross-frame members. Therefore, it is important that these initial strains are calculated based on the element formulation. If the element formulation is based on engineering strain, then the initial strains can be expressed as

$$\varepsilon_{\text{initial strain}} = \frac{\text{L}_{\text{Configuration.2}} - \text{L}_{\text{Configuration.1}}}{\text{L}_{\text{Configuration.1}}} \tag{3.5.1}$$

On the other hand, if the element formulation is based on true strain, then the initial strains should be calculated as the log strain to account for large strain attributes. Initial strains that are based on the log strain formulation can be expressed in an incremental form as:

$$\delta\varepsilon_{initial\ strain} = \frac{\delta L}{L} \tag{3.5.2}$$

where *L* is the final configuration. Hence, when Eq. 3.5.2 is integrated, one obtains

$$\varepsilon_{initial\ strain} = \int_{L_{Configuration.1}}^{L_{Configuration.2}} \delta\varepsilon_{initial\ strain} = \ln\left[\frac{L_{Configuration.2}}{L_{Configuration.1}}\right] \tag{3.5.3}$$

Equation 3.5.3 can be expressed in terms of engineering strain as:

$$\varepsilon_{initial\ strain} = \ln\left(1 + \frac{L_{Configuration.2} - L_{Configuration.1}}{L_{Configuration.1}}\right) \tag{3.5.4}$$

If one wants to apply initial forces instead of initial strains or stresses, then the effects of area change should be included as:

$$A_{Configuration.1} + dA = A_{Configuration.1}(1 - \upsilon\, d\varepsilon)^2 \approx A_{Configuration.1}(1 - 2\upsilon\, d\varepsilon) \tag{3.5.5}$$

where υ is Poison's ratio. If both sides of Eq. 3.5.2 are divided by $A_{Configuration.1}$ and substituted into Eq. 3.5.5 then one obtains,

$$\frac{dA}{A_{Configuration.1}} = -2\upsilon\frac{\delta L}{L} \tag{3.5.6}$$

If the both sides are integrated then Eq. 3.5.6 becomes,

$$\int_{A_{Configuration.1}}^{A_{Configuration.2}} \left(\frac{dA}{A_{Configuration.1}}\right) = -2\upsilon \ln\left[\frac{L_{Configuration.2}}{L_{Configuration.1}}\right] \tag{3.5.7}$$

and

$$\ln\left[\frac{A_{Configuration.2}}{A_{Configuration.1}}\right] = -2\upsilon \ln\left[\frac{L_{Configuration.2}}{L_{Configuration.1}}\right] \tag{3.5.8}$$

If the exponential of both sides are taken Eq. 3.5.8 becomes

$$\frac{A_{Configuration.2}}{A_{Configuration.1}} = \left[\frac{L_{Configuration.2}}{L_{Configuration.1}}\right]^{2\upsilon} \tag{3.5.9}$$

If the volume is assumed constant in the cross-frame element formulation, which is strictly valid only in the case of υ = 0.5, then Eq. 3.3.9 can be written as:

$$A_{Configuration.2} = A_{Configuration.1}\left[\frac{L_{Configuration.2}}{L_{Configuration.1}}\right] \tag{3.5.10}$$

In this research, the initial strains are calculated from the log strain since the element formulation is based on true strain.

If the initial strains/stresses (or forces) due to lack-of-fit of the members are applied to an isolated statically determinate cross-frame subassembly that is connected into the initially-plumb cambered geometry (Configuration 2), then when the structure is released, the cross-frame "springs back" to its no-load rectangular configuration and the final internal stresses in the cross-frame members is zero. Figure 3.5.1 shows two possible final conditions for two different statically determinate cases. It should be noted that in both cases the cross-frames must spring back to the rectangular position which corresponds to the un-stressed member lengths for Configuration 1. However, the lack-of-fit due to DLF detailing is generally a 3D geometry problem and the cross-frames and the surrounding structure are typically statically indeterminate.

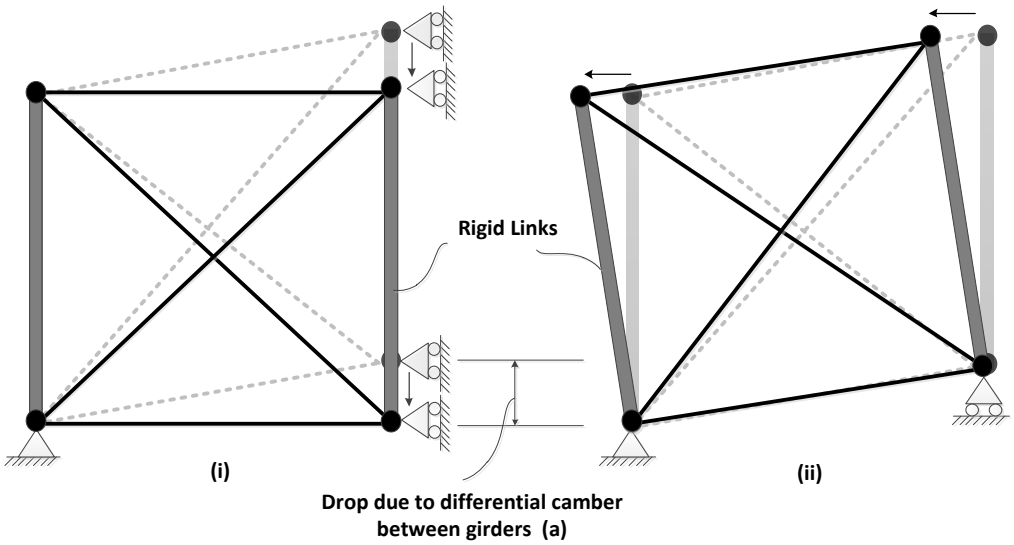

Figure 3.5.1. The final configuration of an example intermediate cross-frame due to lack-of-fit forces.

Figure 3.5.2 provides an example perspective representation of an intermediate cross-frame location. As noted above, the work points on the two girders are connected in the no-load geometry of the cross-frames (Configuration 1) as well as in the initially-plumb cambered geometry of the girders (Configuration 2). The approach described above can be applied to calculate the initial strains by calculating the lengths at Configuration 1 and Configuration 2 using the spatial coordinates of the work points in the two configurations.

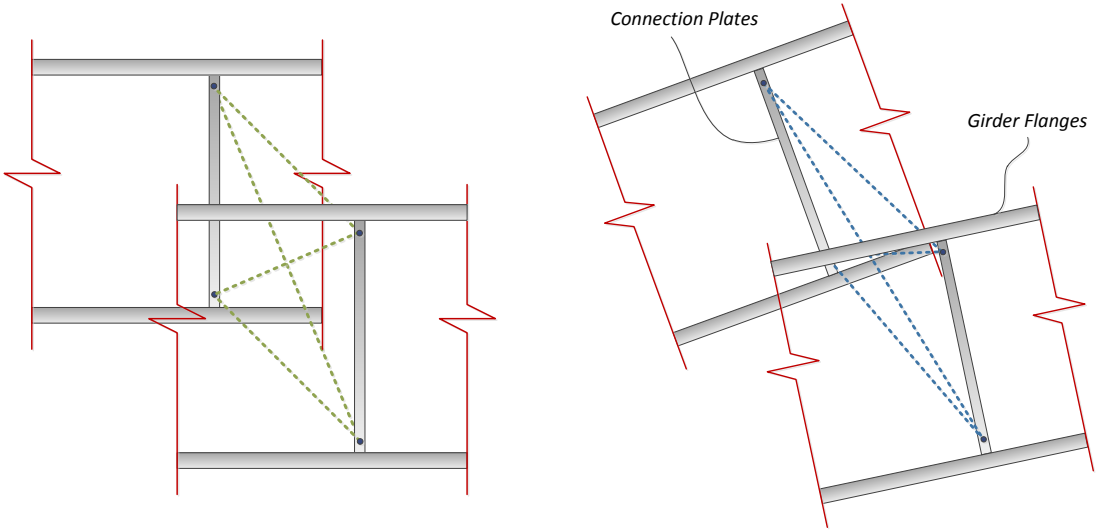

(i) Girders in the final geometry (Configuration 1)

(ii) Girders in initially plumb cambered geometry (Configuration 2)

Figure 3.5.2. Example of an intermediate cross-frame at its initial plumb geometry and final plumb geometry.

Alternatively, these strains can be obtained via the software by imposing the vertical deflections associated with the girder dead load cambers, specifically running an imposed displacement pre-analysis that starts at Configuration 1 with the cross-frames attached to the girders in the final idealized geometry (with the girders plumb, but with the steel or total dead load girder camber removed) and ends at Configuration 2, which is the initially-plumb no-load girder geometry. Figure 3.5.3 shows the Configuration 1 and Configuration 2 geometries from the displacement analysis of a two girder unit.

The imposed displacements can be obtained from the girder camber diagrams or the negative of the steel or total dead load displacements. For the bridges constructed with SDLF detailing, the imposed displacements correspond to the steel dead load cambers. On the other hand, for the bridges constructed with TDLF detailing, the imposed displacements correspond to

the total dead load cambers. It should be noted that all the radial or lateral displacements of the girders must be restrained in the above imposed displacement analysis in order to achieve the theoretical cambered geometry (otherwise, the girders will tend to deflect out-of-plane when the camber displacements are imposed on the model). The resulting cross-frame member strains are the same lack-of-fit strains calculated by the previously discussed procedure using the work point coordinates. In the subsequent analyses, cross-frame strains that are obtained from the imposed displacement pre-analysis are included as initial strains to account for the lack-of-fit forces associated with the cross-frame detailing.

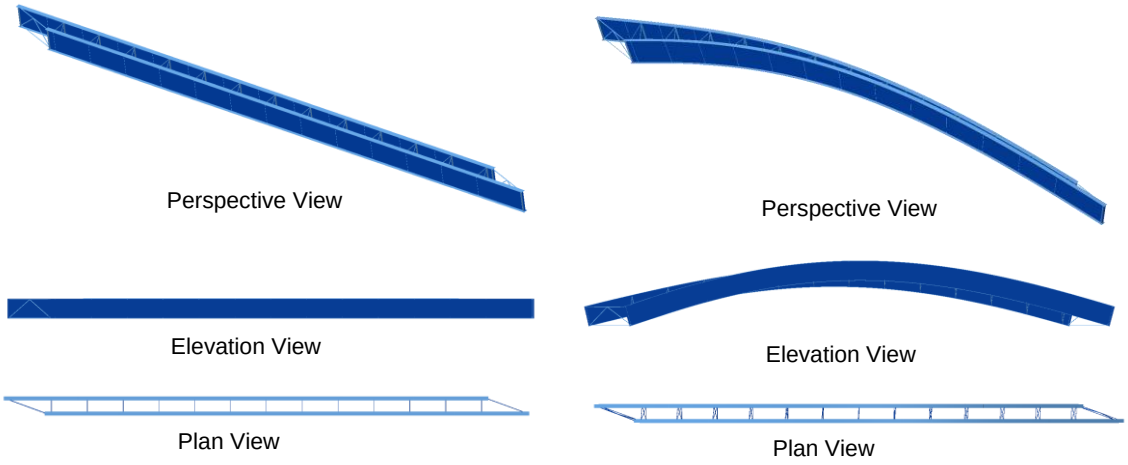

(i) Girders in the final geometry (Configuration 1)

(ii) Girders in initially plumb cambered geometry (Configuration 2)

Figure 3.5.3. Configurations 1 and 2 from the displacement analysis (Displacements are amplified by 20x).

In 2D-grid analysis models, each cross-frame is typically represented with a single beam element. The cross-frames are modeled traditionally using beam elements that are formulated based on the classical Euler-Bernoulli or Timoshenko beam theory. These representations generally do not capture the structural behavior of these components accurately. Sanchez (2011) shows the development of two-node elements (having the same dofs as beam elements) that properly capture the kinematics of X-type, V-type, and inverted V-type cross-frames. It is possible to include locked-in stress effects in the analysis with the elements presented in Sanchez (2011) as well as with conventional beam elements. For this purpose, the initial nodal forces associated with the lack-of-fit between the girders and cross-frames can be calculated by direct usage of the element stiffness matrices.

For intermediate cross-frames that are normal to the girders, the only significant initial lack-of-fit forces (i.e., the forces associated with the initial strains) are those due to the differential vertical displacement between the girders (see Fig. 3.5.4), whereas for skewed end cross-frames the primary initial lack-of-fit forces are due to the compatibility between the girders and the cross-frames at the skewed bearing lines (see Fig. 3.5.5). For intermediate cross-frames that are normal to the girders, the initial nodal forces can be calculated by supporting the cross-frame element rigidly at one of the vertical dofs, then imposing the differential vertical camber to the "free" vertical degree of freedom (see Fig. 3.5.6).

For the skewed end cross-frames, a similar approach can be used, but the cross-frame is rigidly supported in the vertical direction and subjected to the bending rotations within its plane obtained from the corresponding components of the girder camber end rotations tied to the compatibility between the girders and the cross-frames (see Fig. 3.5.7). It should be noted that the twisting of the cross-frames has a negligible effect on initial lack-of-fit forces; therefore, the initial internal forces or stresses due to twisting of the cross-frames can be neglected when calculating the initial lack-of-fit forces. For skewed intermediate cross-frames, both the girder major-axis bending rotations due to the vertical camber as well as the differential vertical cambers should be considered to calculate the initial nodal forces associated with the lack-of-fit. The calculated initial nodal forces associated with the lack-of-fit are then included in the analysis to obtain the internal stresses and deformations associated with DLF detailing.

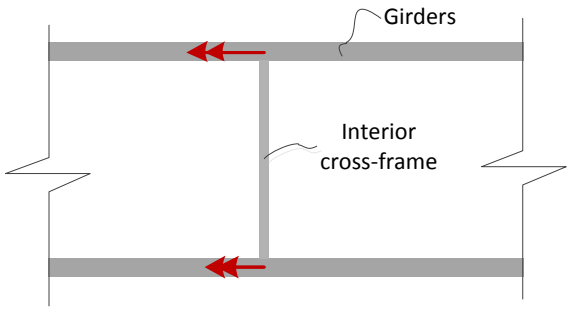

Figure 3.5.4. Illustration of the differential bending rotations for intermediate cross-frame locations.

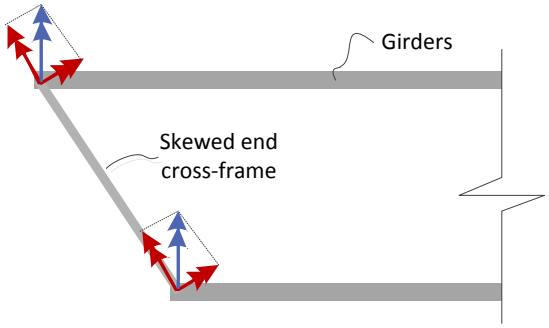

Figure 3.5.5. Illustration of the differential bending rotations for skewed end cross-frame.

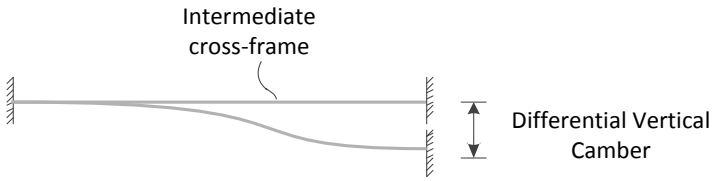

Figure 3.5.6. Imposed differential vertical camber for intermediate cross-frame, used to calculate initial lack-of-fit forces.

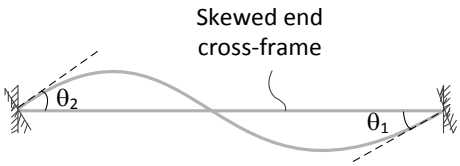

Figure 3.5.7. Imposed rotations on bearing-line cross-frames, used to calculate initial lack-of-fit forces.

3.6. Post-Processing Analysis Results

The sensitivity studies done in the subsequent chapters are conducted using refined 3D FEA solutions. Girder layovers, girder vertical displacements, girder major-axis bending rotations, flange lateral bending stresses and cross-frame forces are considered to evaluate the bridge responses. These responses are calculated under steel and total dead loads, and generally considering either NLF detailing as well as lack-of-fit due to SDLF and TDLF detailing. These responses are obtained as follows:

- Girder layovers are obtained along the length of the girder by calculating the relative lateral/radial movement of the top flanges with respect to bottom flanges.
- Vertical displacements are reported at the web-flange juncture of the bottom flange nodes.

- Major-axis bending stresses are obtained at top and bottom flanges by extrapolation of the axial stresses at the top and bottom web flange juncture to the extreme fiber of the flanges.
- Flange lateral bending stresses are obtained by taking the difference of element stresses between the tip of the flange and the web-flange juncture.
- Cross-frame forces are obtained by taking axial stress or axial force of the top and bottom chords, and diagonals.

CHAPTER IV.

DESIGN OF ANALYTICAL STUDIES

This chapter provides a concise overview of the design and execution of the analytical studies, which supply the fundamental basis for the recommendations of this research. The analytical studies developed here are also used by NCHRP Project 12-79 (NCHRP, 2011) to evaluate the accuracy of different analysis methods on the erection engineering of curved and skewed steel I-girder bridges. This chapter also provides information about the selected case study bridges that are used in the subsequent chapters.

4.1. Introduction

Curved and/or skewed bridge structures with different geometries can respond in dramatically different ways during their various stages of construction; therefore, extensive studies of a wide range of bridge structures are necessary to gain a true understanding of the accuracy of different analysis methods and the effect of this accuracy on structural performance.

It should be emphasized that both over-prediction and under-prediction of displacements can be equally problematic in cases where certain relative deflections are critical. Furthermore, one should not specify a simple blanket accuracy requirement on all analysis deflections. Specific relative deflections need to be considered, and in cases where the deflections are sufficiently small, larger inaccuracies can be tolerated.

It is important that the accuracy of simplified analysis methods be evaluated using actual bridge designs that satisfy either prior and/or current AASHTO design criteria. The results of simply varying bridge parameters without checking Specification requirements can be misleading. The AASHTO requirements must be satisfied for the parametric study bridges to allow the research to establish appropriate relationships between bridge design variables and recommended levels of analysis and construction engineering effort.

One of the early tasks of this research and NCHRP Project 12-79 (NCHRP, 2011) was to identify existing bridges representing a spectrum of various combinations of span arrangement, span length, curvature, bridge widths and skew. It was decided to consider both simple and continuous-spans, and that preference would be given to bridges that had:

- Good instrumented field data or at least good field observations, particularly data and observations during intermediate stages of construction and
- Detailed construction plans,

and in which

- The design and construction satisfied prior and/or current AASHTO Specifications and established recommendations, yet in which construction challenges were encountered or certain attributes resulted in concerns about the final state of stress in the girders.

Bridges where technical challenges were addressed very successfully as well as cases where there were some significant problems were sought. However bridges involving generally acknowledged poor practices, (e.g., inappropriate use of oversize or slotted holes, inadequate attachment of cross-frames during construction, etc.), were not considered. The focus of this research and of NCHRP Project 12-79 (NCHRP, 2011) was on analysis and design using appropriate practices. Analysis requirements for forensic investigation of bridges with faulty details were not addressed. However, it was hoped that the studies would shed light on the ability of analysis methods to highlight faulty erection schemes, etc., given appropriate design details.

Once the above existing bridge collection effort was completed, then the geometric factors influencing the analysis, design and construction of the bridges were identified. Finally, a range and number of levels of these factors were selected for subsequent analytical study.

The following sections provide a detailed description of each of the above steps.

4.2. Identification of Existing Bridges

A total of 85 I-girder units of existing bridges have been collected from various owners and consultants who contributed to NCHRP (2011). Appendix B provides the overall characteristics of the collected existing I-girder bridges. Summary sketches of the deck plan and bearing line geometries are shown for all of these units. These summary sketches offer a useful way of understanding the various attributes of the bridge geometries handled in recent practice. The collected existing I-girder bridges are subdivided into the following categories:

- I-girder bridges, Simple-span, Straight, with Skewed supports (ISSS),
- I-girder bridges, Continuous-span, Straight, with Skewed supports (ICSS),
- I-girder bridges, Simple-span, Curved, with Radial supports (ISCR),

- I-girder bridges, Continuous-span, Curved, with Radial supports (ICCR),
- I-girder bridges, Simple-span, Curved, with Skewed supports (ISCS), and
- I-girder bridges, Continuous-span, Curved, with Skewed supports (ICCS).

A sample of the collected curved and skewed I-girder bridges is shown in Fig. 4.2.1. Each bridge shows an assigned bridge code based on the main geometric characteristics of its deck, and information about the bridge location is included. The general geometric information is displayed for each span including length, radius of curvature, deck width, and support skew angles. In addition the source of the bridge is indicated. Notes describing the number of girders and other important information regarding the bridge design and construction are included. The various collected existing bridges served two purposes:

1. The composite of all the existing bridges was an aid to the NCHRP (2011) project team in gauging the range and level of geometries that should be considered within the main parametric studies of the research.
2. A number of the existing bridges that best fit the research and NCHRP (2011) criteria for the analytical studies discussed in Section 4.1 were selected and inserted into the complete parametric study matrix, discussed subsequently in this chapter.

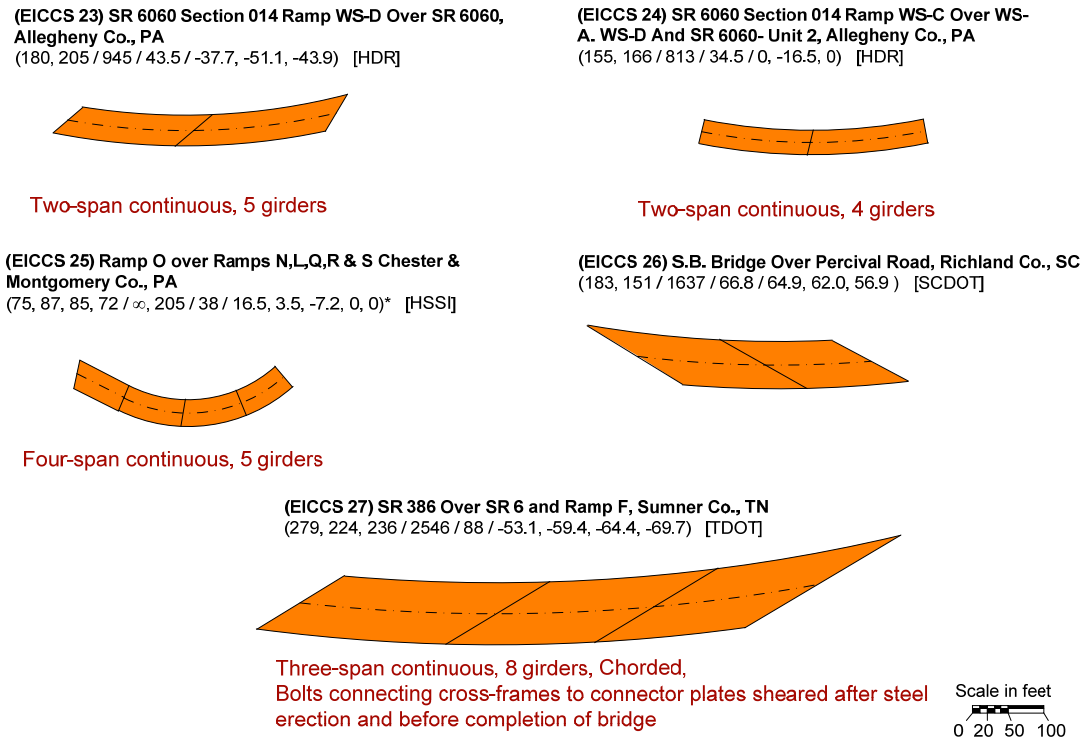

Figure 4.2.1. *Sample of the collected Existing I-girder bridges, Continuous span, Curved with Skewed supports, (EICCS #.)*

Only twelve of the I-girder bridges had both (1) measurements or field observations of some type during construction as well as (2) detailed construction plans. Furthermore, the extent of the field measurements was generally limited. Detailed field measurements and observations were taken for the bridge EICCR22a by the NCHRP (2011) during the course of NCHRP 12-79 (Leon et al., 2011). A number of the bridges were indicated as being very successful projects, with the bridge responding as predicted with respect to aspects such as initial layover of the webs but with the girders approaching a plumb condition under total dead load. A number of cases were cited as having a range of field problems including difficulty of fit-up, or unexpected final geometries.

In addition to the existing bridges, a number of useful detailed LRFD example bridge designs have been published in the recent literature. Figure 4.2.2 summarizes the plan geometries of several of these hypothetical bridges. The straight, non-skewed bridges in these examples were selected to serve as useful base-line problems. The analysis accuracy results for these cases can serve as useful indicators or benchmarks for decisions about the levels of accuracy sufficient for bridges with more complex geometries.

The selection of the existing and example bridges for inclusion in the overall parametric study is addressed subsequently in the discussion of the main analytical studies.

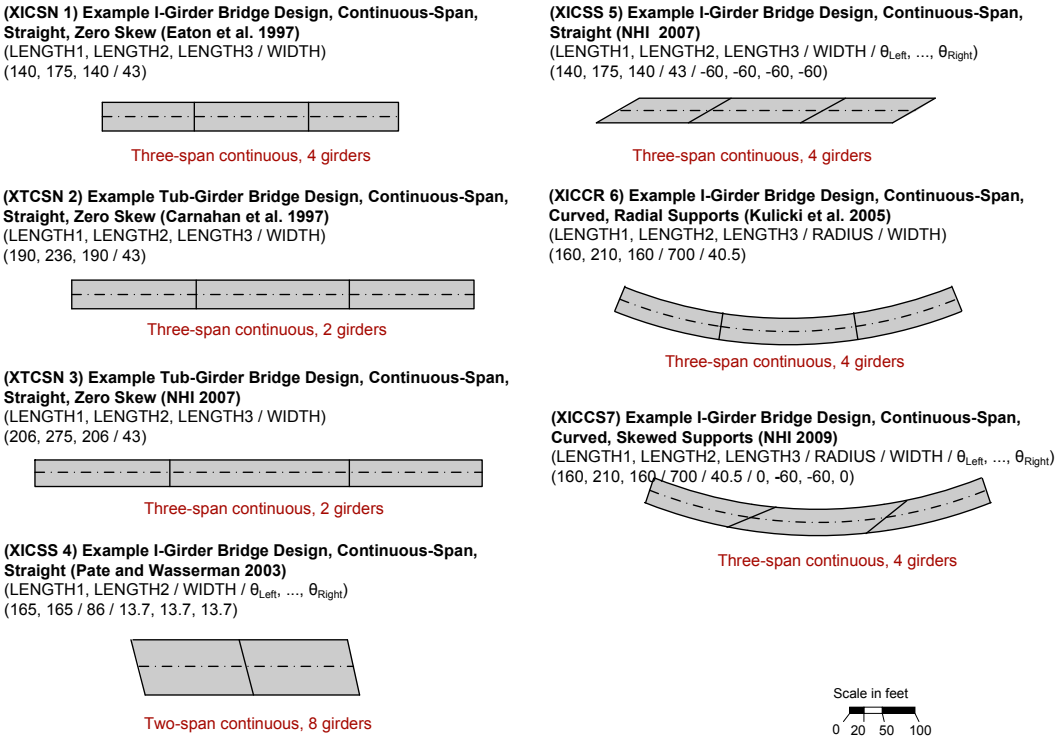

Figure 4.2.2. *AASHTO LRFD example bridge designs.*

4.3. Selection of Geometric Factors

4.3.1. *Identification of primary geometric factors*

It is clear that if the research is to consider methods of cross-frame detailing and analysis accuracy for curved and/or skewed steel I-girder bridges, then it must consider the following factors in the experimental design of its parametric studies:

- Some measure of the horizontal curvature and
- Some quantification of the magnitude and pattern of skew.

Furthermore, it is apparent that the bridge responses, and hence the analysis accuracy, can be affected significantly by the magnitude of the span lengths as well as the span length-to-width ratios. Longer span bridges tend to be affected more substantially by dead load effects, potentially resulting in more significant stability considerations during construction. In addition, beyond a certain span length, I-girder bridges are more likely to need partial or full-span horizontal flange-level bracing systems to ensure adequate stability and sufficient resistance to lateral loads during construction. Flange lateral bracing systems cause portions of the structure to act as "pseudo-box girders," fundamentally changing the behavior of the structural system. Furthermore, longer bridges generally exhibit larger overall deflections. These larger overall deflections can lead to larger relative deflections at certain locations in the structural system, which can sometimes be problematic during construction. Longer span bridges often have a smaller ratio of the girder spacing relative to the girder depths, and typically have larger girder depth-to-flange-width ratios. These attributes can fundamentally affect various relative deflections in the structure as well as local and overall behavior and analysis accuracy at the different stages of construction.

In addition, the bridge span length-to-width ratios can significantly impact the influence of skew. Skewed bridges with smaller span length-to-width ratios tend to have more significant load transfer to the bearing lines across the width of the structure, and hence more significant "nuisance stiffness" effects that need to be addressed in the design. Furthermore, relatively narrow horizontally curved bridges experience a greater torsional "overturning component" of the reactions, which tends to increase the vertical reactions on the girders further from the center of curvature and decrease the vertical reactions on the girders closer to the center of curvature. In addition, relatively wide horizontally-curved bridges can have more substantial concerns related to overturning at intermediate stages of the steel erection, prior to assembly

of the girders across the full width of the bridge cross-section. These spans become more stable as additional girders are erected and connected by cross-frames across the width of the bridge. Wide horizontally-curved bridges also can have greater concerns associated with overturning forces during deck placement.

Lastly, it is apparent that the bridge responses (and the analysis accuracy) can be significantly affected by whether the spans are simply-supported or continuous. Simple-span bridges tend to have larger deflections for a given geometry, and potentially can be more difficult to handle during construction. Although simple-span girders can see negative bending during erection (due to lifting or temporary support from holding cranes, etc.), continuous-spans have more significant negative bending considerations. Furthermore, particularly in I-girder bridges, continuous-span bridges can have significant interactions between adjacent spans with respect to both major-axis bending as well as the overall torsional response.

All of the above factors can have a substantial influence on the many detailed structural attributes of steel I-girder bridges. Also, there can be significant interactions between these factors in terms of their influence on the bridge responses, as well as the accuracy of different bridge analysis methods.

If one considers the many detailed attributes of steel I-girder bridge structural systems and their members and components addressed subsequently, the combinations and permutations of potential bridge designs become endless. Hence, in this research and in the NCHRP Project 12-79 studies, it was decided that the most practical way of covering the design space of curved and/or skewed I-girder bridges was to consider a range of practical combinations and permutations of the following primary factors:

- Arc span length of the bridge centerline, L_{as},
- Deck width normal to the girders, w, (in phased construction projects, w is determined separately for each bridge unit)
- Horizontal curvature, of which the most appropriate characterization is discussed below,
- Skew angle of the bearing lines relative to the bridge centerline, θ,
- Skew pattern of the bearing lines, of which the most appropriate characterization is discussed below, and
- Span type, simple and various types of continuous spans.

4.3.2. *Characterization of horizontal curvature*

Regarding the most appropriate characterization of horizontal curvature effects on the bridge behavior and the analysis accuracy, the non-dimensional factor L_{as}/R, which is the subtended angle of a span's centerline expressed in radians, is important (see Fig. 4.3.1). However, the maximum practical values of L_{as}/R can vary substantially with the width of the structural system. The maximum L_{as}/R is limited in relatively narrow bridges because of overall overturning of the structure (or structural unit). This characteristic of the behavior is best illustrated by considering the plan sketches of the two hypothetical simple-span bridges shown in Fig. 4.3.2. Both bridges have arc-span lengths of L_{as} = 300 ft and a constant horizontal radius of curvature R. However, one bridge has a 30 ft wide deck while the other has an 80 ft wide deck. If one considers a representative uniformly distributed deck weight loading on these two structures, the subtended angle between the supports L_{as}/R needs to be much smaller for the narrower structure to avoid uplift at the girder supports closer to the center of curvature.

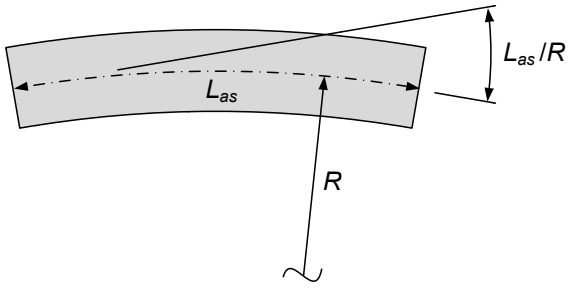

Figure 4.3.1. Subtended angle of a span's centerline, L_{as}/R.

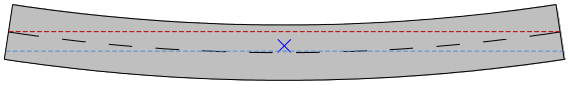

L_{as} = 300, w = 30, R = 1000, L_{as}/R = 0.30

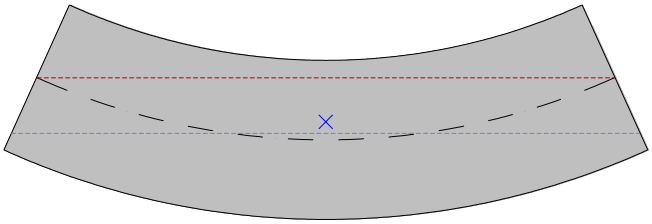

L_{as} = 300, w = 80, R = 353, L_{as}/R = 0.85

Figure 4.3.2. Plan geometries of two representative simple-span horizontally-curved bridges with L_{as} = 350 ft (all dimensions in ft unless noted otherwise).

Two dashed lines are drawn along the length direction of the plan sketches in Fig. 4.3.2. One of the dashed lines is the chord between the girder bearings on the outside of the curve. The other is the chord between the points of intersection of the bridge centerline with the end bearing lines. Also shown on the plan sketches is the symbol "*x*", which indicates the centroid of the deck area (and hence the centroid of the above hypothetical loading). For bridges that are more highly curved (smaller *R*), the centroid (*x*) is closer to the outside chord line. If the curvature is such that the centroid (*x*) is positioned directly over the outside chord line, then all the bridge reactions have to be zero except for the reactions at the outside bearings, assuming that none of the bearings are capable of resisting uplift. That is, the bridge unit is at the verge of tipping about its outside bearings (assuming a single span and simply-supported ends). This is obviously an extreme condition. Even a bridge with a much smaller radius of curvature would require hold downs at bearings closer to the center of curvature to equilibrate (or balance) the uniform deck weight.

The following "torsion index" is an indicator of the overall torsion within a bridge (or bridge unit) span, as well as the tendency for uplift at the bearings:

$$I_T = s_c/(s_c + b) \tag{4.3.1}$$

The terms in this equation, illustrated in Fig. 4.3.3, are:

- s_c, the perpendicular distance between location of the centroid of the deck and the chord between the inside bearing locations, and
- *b*, the perpendicular distance from the centroid (x) to the chord between the bearing locations on the outside fascia girders.

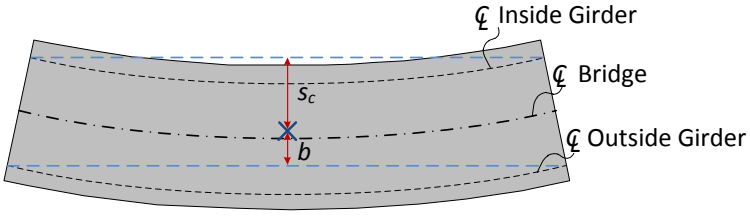

Figure 4.3.3. Illustration of terms for expressing I_T.

A value of I_T = 0.5 means that the centroid of the deck area is mid-way between the chords intersecting the outside and inside end bearings. This is the ideal case where the radius of curvature is equal to infinity and the skew is zero, i.e., a straight tangent bridge. A value of I_T = 1.0 means that the centroid of the deck area is located at the chord line between the

outside bearings. This implies that the bridge is at incipient overturning instability, by rocking about its outside bearings under uniform self-weight.

As noted above, the torsion index is related the magnitude of the overall torsion that exists in the bridge (or bridge unit) span, due to the eccentricity of its self-weight.

For curved simple-span radially supported I-girder bridges, the horizontal curvature values for the parametric studies were selected by first conducting basic estimates to determine the largest curvature (smallest *R*) without having uplift at the most critical bearing location(s) under nominal dead plus live loads. This value of *R* was used as the most extreme value for the horizontal curvature. This radius of curvature then was increased 1.5 times to obtain cases with smaller curvature (larger *R*). This approach produced lower- and upper-bound values of I_T equal to 0.58 and 0.71 respectively. Continuous-span bridges can tolerate higher indices due to continuity with the adjacent spans. Therefore, for curved continuous-span radially supported I-girder bridges, lower and upper bound values of I_T were obtained as 0.66 and 0.88 respectively.

4.3.3. *Characterization of skew pattern*

There are a number of factors related to the representation of the skew pattern for practical designs. Figure 4.3.4 shows a number of possible combinations of θ values and skew patterns on individual straight I-girder bridge spans with *w* = 80 ft and *L* = 250 ft. In general, various combinations of these arrangements are practical for continuous-span bridges. The first four cases in the figure have parallel bearing lines, that is, equal skew of the end supports. The four values of skew shown are 20, 35, 50 and 70°. The 20° skew case is significant since the AASHTO LRFD Specifications permit the cross-frames to be oriented parallel to the bearing lines up to this limit. The 70° skew case is the maximum skew angle considered in prior NCHRP studies on deck effective widths (Shah, 2007). In addition, as summarized subsequently, this is the maximum value of the skew encountered in the existing I-girder bridges shown in the previous section. The 35° skew is considered as a practical median skew value between zero and 70°, and 50° was selected as an appropriate large skew angle between 35° and the relatively extreme value of 70°.

The other sketches in Fig. 4.3.4 show a number of representative unequal skew arrangements on individual straight spans in I-girder bridges. Cases 5 and 6 in the figure entail a situation where, due to a site geometry constraint existing at only one position, only one of the bearing lines is skewed. Case 7 shows a possible case where the bearing lines are skewed equally but in opposite directions. This case is considered to be more unusual, or exceptional.

However, interestingly, the bearing line orientations for this case are exactly what one would encounter with a curved radially-supported span and L_{as}/R = 0.70. The outline of the deck is dashed in this case to highlight the fact that this geometry is considered exceptional. Case 8 is similar to Cases 5 and 6, but with a 70° skew. This case illustrates a situation where, due to the extreme skew of the left-hand bearing line, the span length on one side of the deck is more than two times that on the other side of the deck, i.e., $L_2/L_1 > 2$. A value of $L_2/L_1 = 2$ was considered to be a practical maximum limit by this research. It should be noted that if the span length of the centerline were larger, or if the deck width *w* were smaller for this case, this L_2/L_1 limit would not be exceeded. The outline of the deck geometry for Case 8 is shown in light grey to emphasize that this deck geometry is considered impractical. The above L_2/L_1 limit can be satisfied with θ = 70° if the bearing lines are parallel as in Case 4, or if the bearing lines are unequally skewed such as in Case 9. Lastly, Case 10 shows an extreme situation of unequal skew in opposite directions for the two bearing lines. In this case, the bearing lines are oriented at 90° relative to one another. It was decided by NCHRP (2011) project team that one would practically never encounter a relative angle between adjacent bearing lines of more than 90°. This type of bearing arrangement could occur for example if the span were crossing the corner of a rectangular lot and the bearing lines had to be placed parallel to the sides of the lot. Note that $L_2/L_1 > 2$ for Case 10; however, if the span is larger or the deck width is smaller, the $L_2/L_1 \leq 2$ limit could be satisfied.

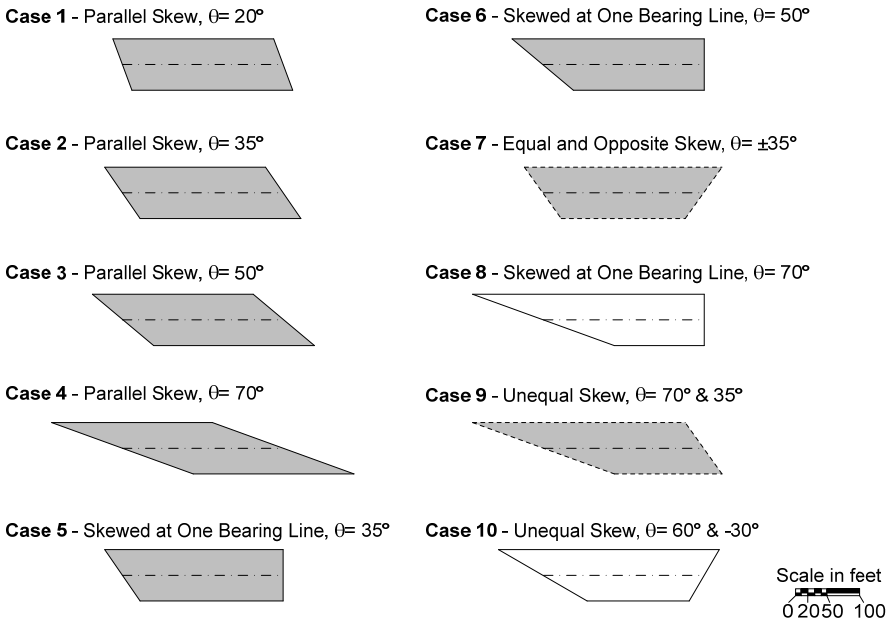

Figure 4.3.4. Potential skew combinations for straight I-girder bridge spans with w = 80 ft and L = 250 ft.

Figure 4.3.5 shows the various possible combinations of horizontal curvature and approximately $\pm$ 15 and 30^o skew on individual I-girder bridge spans with L_{as} = 150 ft, w = 30 ft and R = 400 ft. Again, various combinations of these arrangements are possible for continuous-span bridges. The skew and horizontal curvature combinations in Fig. 4.3.5 are similar to those shown for the straight bridge spans in Fig. 4.3.4. However, whereas a number of patterns with positive and negative skew produce the same net geometry in straight bridges, these positive and negative skew values do not produce the same geometry in similar curved bridges, due to the horizontal curvature. It should be noted that the skew pattern and curvature can create more exceptional cases in I-girder bridges since the skew angles are typically larger for I-girder bridges. Therefore, small skew angle value is selected to illustrate the possible combinations of horizontal curvature and skew angle. Fourteen total combinations are shown in Fig. 4.3.5 that need to be considered in general. A large number of these combinations may be considered as exceptional cases and are drawn with dashed lines. Note that for Cases 2, 5 and 9 in Fig. 4.3.5, the magnitudes of the skew angles are modified slightly to make the bearing lines parallel.

The possible combinations of skew and horizontal curvature for I-girder bridges are similar to those shown in Fig. 4.3.5, except that as noted previously, somewhat larger skew values can be accommodated generally in I-girder bridges. The extent of these patterns was taken as being limited predominantly by:

- A maximum limit on the ratio of the arc-span lengths of the outside and inside edges of the deck, L_{aso}/L_{asi}, of 2, and
- A maximum limit on the orientation of adjacent bearing lines of 90^o

similar to the limits discussed previously for the straight skewed bridges. Lastly, for highly curved spans, it was recognized that the skew angle at the inside edge of the deck can be substantially larger than that at the deck centerline. This is illustrated in Fig. 4.3.6. It was decided that it is not practical for the skew angle at the inside edge of the deck to be greater than 70^o in these types of cases.

All of the above factors can have a substantial influence on the many detailed structural attributes of steel I-girder bridges. Also, there can be significant interactions between these factors in terms of their effects on the bridge responses, as well as the accuracy of different bridge analysis methods.

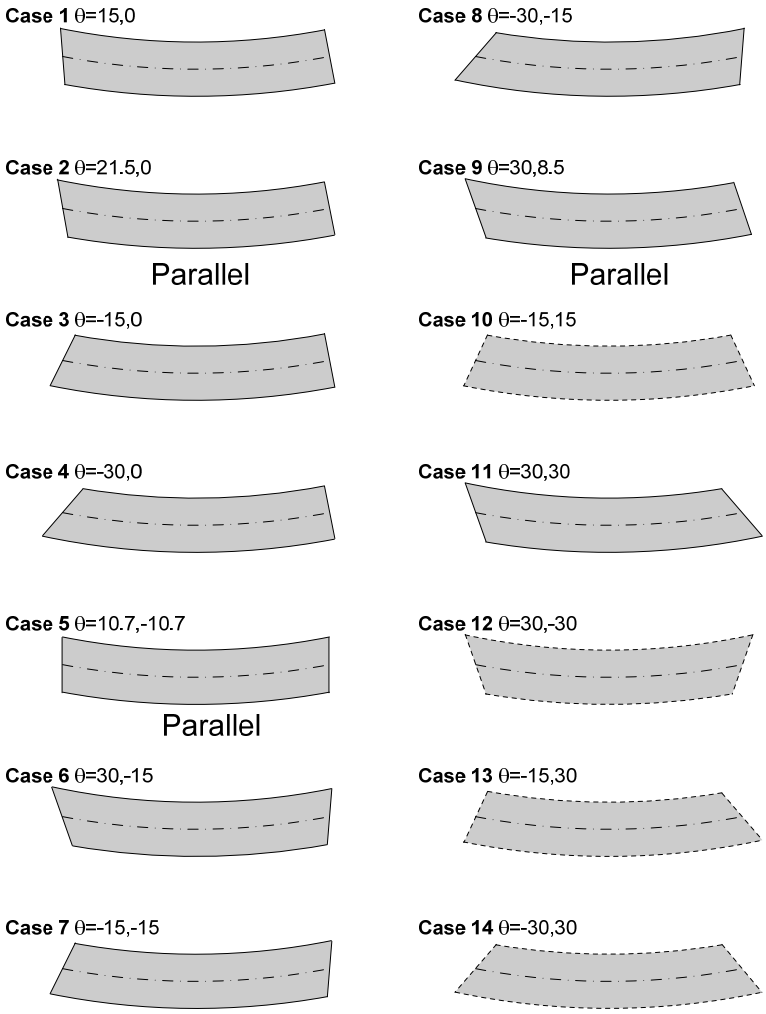

Figure 4.3.5. Example potential skew and horizontal curvature combinations for curved I-girder bridge spans with w = 30 ft, L_{as} = 150 ft and R = 400 ft.

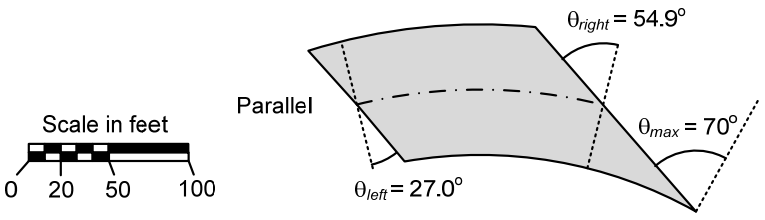

Figure 4.3.6. Highly-curved span with a skew angle of 70° at the inside edge of the deck and 54.9° at the centerline of the deck, w *= 80 ft,* L_{as} *= 150 ft,* R *= 308 ft.*

4.4. Synthesis of Primary Factor Ranges from the Collected Bridges

Upon perusing the distribution of the above primary factors among the existing bridges collected in this research, the following ranges of these factors can be observed:

- Arc-span length, L_{as}
  - 120 to 254 ft (straight simple spans with skewed supports)
  - 90 ft (curved simple spans with radial supports)
    - Only one bridge was identified as curved simple span with radial supports; this was the FHWA Test bridge, EISCR1.
  - 106 to 252 ft (curved simple spans with skewed supports)
  - 119 to 445 ft (straight continuous spans with zero skew)
  - 73 to 257 ft (straight continuous spans with skewed supports)
  - 101 to 334 ft (curved continuous spans with radial supports)
  - 50 to 279 ft (curved continuous spans with skewed supports)
- Deck width, w
  - 24 to 87.5 ft (spans with skew)
  - 30 to 71 ft (spans with radial supports, with the exception of the EISCR1 FHWA test bridge, which was 23.5 ft)
- Torsion Index, I_T
  - 0.48 to 0.87
- Skew angle of the bearing lines relative to a tangent to the bridge centerline, θ
  - 0 to 69.5^o (straight bridges)
  - 0 to 64.3^o (curved bridges)
- Skew pattern
  - The bearing lines are parallel in most of the collected I-girder bridges.
  - One straight bridge (EICSS2) has $\theta = 61.8^o$ & 38^o in one span.
  - One curved bridge (EICCS15) has $\theta = 0^o$ & 49.5^o resulting in a 19.8^o difference in orientation between the bearing lines in one span.
  - One curved bridge (EICCS5) has $\theta = 0^o$ & 60.2^o resulting in a 72^o difference in orientation between the bearing lines in one span.
- Type-of-span
  - Most of the collected I-girder bridges are continuous-span.
  - Ratio of exterior-to-interior span lengths: 0.56 to 1.25
  - Ratio of adjacent interior span lengths: 0.63 to 1.0
  - Ratio of span lengths, 2-span continuous: 0.77 to 1.0

The values for several additional "secondary" parameters discussed in the above, but not selected as primary factors in the design of the parametric studies, are:

- Arc-span length to deck width ratio, L_{as}/w
  - 0.55 to 14.77 (spans with skew)
  - 1.67 to 8.83 (curved spans with radial supports)
- Subtended angle of the span's centerline, L_{as}/R
  - 0.0 to 0.57 radians

4.5. Selection of Primary Factor Ranges and Levels

Table 4.5.1 shows the ranges and levels of the primary factors that were selected for the main analytical study of this research and NCHRP (2011). These primary factors are discussed in detail in the preceding sections.

Table 4.5.1. Primary factor ranges and levels for the main parametric study.

Factor	Ranges and Levels
Type of span	Simple, 2-span continuous, and 3-span continuous with one balanced end span and one end span equal in length to the main center span. Use the above 3-span continuous bridges as base ICCR cases. Consider both 2- and 3-span continuous bridges for the ICSS, and ICCS cases. Consider at least one 2-span continuous bridge with a significant unbalance between the span lengths.
Maximum arc-span length of bridge centerline, L_{as}	150, 225 & 300 ft for simple-spans 150, 250 & 350 ft for continuous-spans
Deck width, w	30 ft (1 to 2 traffic lanes +shoulders & barriers) 80 ft (4 to 5 traffic lanes + shoulders & barriers
Torsion Index, I_T	0.58 to 0.71 for ISCR bridges 0.66 to 0.88 for ICCR bridges
Skew angle relative to the bridge centerline, θ	20^o, 35^o, 50^o & 70^0 but with θ at the inside edge of the deck $\leq 70^o$ in curved spans
Skew pattern	Consider the $\pm$ combinations of skew angles shown in Fig. 4.3.4 (for straight bridges) and Fig. 4.3.5 (for curved bridges), but using $\theta = 35$ & 70^o for I-girder bridges. Limit the ratio of the arc-span lengths along the edges of the deck, L_2/L_1, to a maximum value of 2.0 in all cases Limit the difference in orientation of adjacent bearing lines to a maximum of 90^o in all cases Give preference to typical (i.e., non-exceptional) bridge geometries

The first row of Table 4.5.1 addresses the type of span. Three-span continuous designs with one balanced end span and one end span of equal length to the main span capture both the behavior associated with drop-in spans as well as the interactions between balanced and unbalanced continuous-spans. However, two-span continuous bridges are apt to be more sensitive to skew effects. Also, the potential combinations of skew arrangements become large

as the number of spans is increased. Many of these combinations, however, would have a minor effect on the final analysis accuracy assessments, due to the fact that the influence of the skew at a particular bearing line tends to die out as one moves several spans away from this bearing line. Furthermore, long multi-span curved bridges often may have only a few skewed bearing lines because of geometry constraints at a particular location, whereas it may be possible to orient other bearing lines radially. This can be understood by considering cases such as EICCS1 and EICCS5 in Figure B.1.6. In these structures, one would quickly reach the maximum practical θ value of approximately 70^o if, for instance, all the bearing lines were parallel.

It was desired to study several continuous-span bridges that had significant unbalanced span lengths. This consideration was addressed by inserting selected existing bridges into the matrix of parametric study bridges. Also, a few bridges with more than three spans were considered by insertion of a number of existing bridges in the overall parametric study matrix.

The second row of Table 4.5.1 shows the values selected for the arc-span length. The selected lengths for simple-spans were taken as 150, 225 and 300 ft and the selected lengths for continuous-spans were taken as 150, 250 and 350 ft. The maximum span length of L_{as} = 350 ft. was selected to match the maximum value targeted by the AASHTO (2010) Specifications. All but one span of one of the existing I-girder bridges had arc-span lengths smaller than 350 ft., although three of the existing I-girder bridge units had spans larger than 300 ft. The span larger than 350 ft is one of the straight spans of the Ford City bridge (bridge EICCR 11). In current practice, horizontal flange lateral bracing systems often are considered even for arc-span lengths of 250 ft. An arc-span length of L_{as} = 150 ft is a rough lower-bound value at which welded girders are generally required.

The third row of Table 4.5.1 shows the selected deck widths for the parametric study bridges. For the I-girder bridges, deck widths of 30 ft and 80 ft were selected. The smaller 30 ft width is representative of one- to two-lane bridges, whereas the larger 80 ft width is representative of structures with four to five lanes.

The combinations of L_{as} from 150 to 350 ft with w from 30 to 80 ft give a range for the arc-span length to the bridge width L_{as}/w from 150 /80 = 1.88 to 11.7. The maximum value for this range is slightly larger than the maximum L_{as}/w of 7.90 and 8.29 for the existing I-girder bridges. It was believed that these larger values should be studied to fully address the bridge responses and analysis accuracies for these practical but more extreme geometry conditions.

The fourth row of Table 4.5.1 gives the selected ranges and levels for the torsion index I_T. The implications of I_T ranging from 0.5 to 1.0 have been discussed in Section 4.3.2. This parameter was used in establishing the horizontal radius of curvature R for the ISCR and ICCR designs, given the arc-span length L_{as} and the deck width w. The horizontal radius of curvature obtained for the ISCR designs was then employed for other new curved ISCS parametric bridge designs. Similarly, the horizontal radius of curvature obtained for the ICCR designs was employed for the other new curved ICCS parametric bridge designs. A maximum limit on L_{as}/R of 1.0 was imposed on the parametric designs. This limit can govern for shorter spans with wide decks and is somewhat larger than the maximum L_{as}/R of 0.57 and 0.68 radians for the collected existing I-girder bridges. Nevertheless, it was believed that $L_{as}/R = 1.0$ is a practical extreme that should be addressed in the parametric study design. Wide bridges with these larger L_{as}/R values may require special handling during the steel erection and/or deck placement.

The fifth row of Table 4.5.1 shows the selected ranges and levels of the skew angle θ. As noted previously, AASHTO (2010) allows the cross-frames to be framed parallel to the bearing lines in cases with $\theta \leq 20^o$. Furthermore, it is expected that the effects of skew may be sufficiently small that a line-girder analysis may work quite adequately for certain cases at this skew level. A value of 70^o is a reasonable maximum limit for θ. This value was the maximum considered in studies of deck effective widths by (Shah, 2007), and represents roughly the largest skew angle encountered in the existing bridges.

Lastly, the sixth row of Table 4.5.1 explains the recommended variations of the skew pattern considered. These variations are more easily understood by showing the actual deck plan geometries for various hypothetical new bridge designs. The reader is referred to Section 4.6 for these illustrations.

4.6. Selection of the Analytical Study Bridges

The following sub-sections summarize the key characteristics of the I-girder bridges selected for the analytical studies given the ranges and levels of the primary factors identified in Section 4.5. To arrive at the analytical study design, first a full factorial design matrix involving all the above factors and levels was developed. This led to more than 500 I-girder bridges that would need to be studied. Fortunately, a number of these combinations and permutations could be considered impractical or unbuildable. However, even after the impractical and unbuildable cases were eliminated, the total number of bridges arrived at in the study design was relatively

large. Therefore, some prioritization of the bridges was necessary within the full range of practical designs. As noted by Montgomery (2004), "If the experimenter can reasonably assume that certain high-order interactions are negligible, information on the main effects and low-order interactions may be obtained by running only a fraction of the complete factorial experiment. These fractional factorial designs are among the most widely used types of designs for product and process design and for process improvement." In the context of the analytical study design, this involved the elimination of individual bridges or groups of bridges where the interaction between the primary factor effects was expected to be relatively small. Furthermore, a number of bridges in which the combination of factors led to:

- Exceptional (i.e., particularly unusual) structures, and
- Designs that were very similar in one or more characteristics to other designs

were eliminated.

Once these selections were completed, the library of existing bridges summarized in Appendix B was searched for bridges that:

- Matched closely with the analytical study design selections, and
- Satisfied the criteria described in Section 4.1.

In a few cases, modifications were made to the analytical study design to include existing bridges that were particularly good candidates based on the criteria in Section 4.1. In addition, several of the Example bridges from Fig. 4.2.2 that matched closely with the analytical study design selections were selected for inclusion in the analytical study. The remaining bridges in the study design were targeted as "New" bridges, indicating that they were to be fully designed by the NCHRP 12-79 project team using the AASHTO LRFD Specifications and current common standards of care.

The initial design of the suite of bridges arrived at, based on the above process, involved approximately 100 bridges. The bridges were then subdivided into smaller suites for execution of the analytical studies. Various milestones were identified at which the study bridge selections were reevaluated based on what was learned from the completed studies. The resulting final study targeted 58 total I-girder bridges.

The following sections first discuss several base straight, non-skewed study bridges, followed by straight skewed simple and continuous-span cases, then simple and continuous-span curved bridges with radial supports, and finally curved and skewed simple- and continuous-span bridges. Each of these sections includes simple summary sketches of the bridge deck plan

and bearing-line geometries corresponding to the designs along with a title block for each of the bridges containing:

1) An identification label, composed of the letter "X" for "eXample" bridge designs followed by the symbols explained at the beginning of Section 4.2, indicating the bridge category (e.g., ISSS, ICSS, etc), and ending with the bridge number for that category. An additional category, ICSN is introduced in Fig. 4.6.1. The "CSN" designation stands for Continuous-span, Straight, with Non-skewed supports. For example, the first eXample bridge in Fig. 4.6.1 is labeled "XICSN1."
2) An identification label, composed of the letter "E" for "Existing" followed by the above symbols indicating the bridge category, and ending with the bridge number for that category, e.g., bridge "EISSS3" in Fig. 4.6.2.
3) An identification label, composed of the letter "N" for "New" bridge designs followed by the above symbols indicating the bridge category, and ending with the bridge number for that category, e.g., bridge "NISSS1" in Fig. 4.6.2.
4) A summary of the basic geometry information about the bridge, enclosed in parentheses. For instance, in Fig. 4.6.2, the basic geometry information includes:
   - The span length of the bridge centerline,
   - The out-to-out width of the bridge deck perpendicular to the bridge centerline, and
   - The skew angle with respect to centerline of the bridge for both bearing lines.

   This information is conveyed symbolically in the figure caption as "(LENGTH/WIDTH/θ_1, θ_2)." The other categories have similar but different basic geometry information. This information is summarized symbolically in each of the figure captions. The skew angle of the bearing lines is represented by the symbol θ. This angle is taken as zero when a bearing line is perpendicular to the centerline of the structure, that is, when the bearing line does not have any skew.

All of the figures referenced in the following sub-sections adopt the following conventions:

- Typical or common geometries are sketched using a solid black outline,
- Geometries considered unusual or exceptional are sketched using a black dashed outline,
- A few bridge geometries that are considered impractical or unbuildable are sketched using a solid light-grey outline. (The only cases shown that are impractical or

unbuildable are a few bridges with high skew and relatively small length-to-width ratios, where if the spans were longer or the deck were more narrow, the geometry would indeed be possible.)

- The deck plans for the eXample bridges are shaded and cross-hatched,
- The deck plans for the Existing bridges are shaded with a textured background,
- The deck plans for selected New bridges are shaded with a solid background,
- The bridge unit centerlines are indicated by a "dot-dash" line, and
- The different phases in phased construction bridges (i.e., bridges constructed as a number of separate longitudinal units) are delineated by dashed lines.

4.6.1. *Straight Non-Skewed base comparison cases (ICSN)*

The straight non-skewed base comparison bridge case is illustrated in Fig. 4.6.1. The analysis accuracy results for these cases serve as useful indicators or benchmarks for decisions about the levels of accuracy sufficient for bridges with more complex geometries.

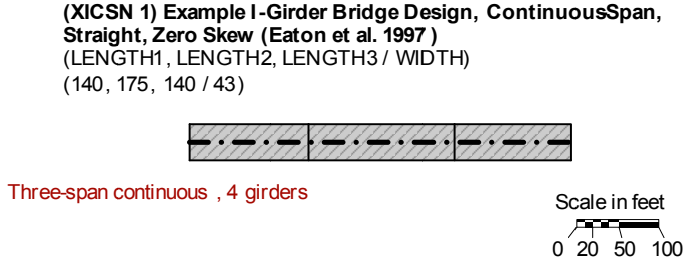

Figure 4.6.1. *eXample Straight Non-skewed bridges used as base comparison cases, (LENGTH1, LENGTH2, LENGTH3 / WIDTH).*

4.6.2. *Simple-span bridges, Straight, with Skewed supports (ISSS)*

Figure 4.6.2 shows the 60 total combinations and permutations for the ISSS bridges obtained considering:

- The ten combinations of skew magnitude and pattern for the straight bridges illustrated previously in Fig. 4.3.4 as {(θ_{Left}, θ_{Right})= (20^o,20^o), (35^o,35^o), (50^o,50^o), (70^o,70^o), (35^o,0^o), (50^o,0^o), (35^o,-35^o), (70^o,0^o), (70^o,35^o), (60^o,-30^o)},
- The three values for the length, L_{as} =150, 225, 300 ft, and
- The two values for the deck width, w = 30 and 80 ft.

Figure 4.6.2. Existing, eXample and New I-girder bridges, Continuous-span, Straight with Skewed supports, EICSS, XICSS or NICSS (LENGTH1, LENGTH2, ... / WIDTH / θ_{Left}, ..., θ_{Right}). The columns in the matrix for (L = 250 ft , w = 30 ft) and (L = 350 ft , w = 30 ft) are not shown.

In Fig. 4.6.2, one can observe that the ISSS bridges selected for study emphasize the bridges with smaller L_{as}/w and larger θ. The influence of the skew is expected to be significant for the bridges in the 3rd and 4th rows. The selection of unequal skew cases in the 6th row parallels the selections in the 3rd row, except for NISSS33 and NISSS36. Bridge NISSS37, in the 7th row, is an interesting case in that the orientation of its bearing lines is the same as in the curved design NISCR10 (shown subsequently). The inclusion of this bridge allows for a comparison of the effects of the bearing orientation alone in NISSS37 versus the effects of the horizontal curvature in NISCR10. In addition, several parallel skew cases are considered in Fig. 4.6.2, with an emphasis on the bridges with larger L_{as}/w and moderate skew angle (e.g. NISSS2), as well as a wider bridge with a 20 degrees of skew (NISSS11).

EISSS3 is one of two adjacent simple-spans on a highly-skewed grade separation structure, on SR 10003 (Chicken Road) over US 74 between SR 1155 and SR 1161 in Robeson County, NC. This bridge was closely monitored during construction, and field data relating to undesirable girder layover and bowing of the girder webs has been collected by Morera (2010). The availability of the field data and the successful construction, which nonetheless resulted in some concerns about the state of the girders, made this bridge a worthwhile candidate for study. Figure 4.6.3 shows several photos of the Chicken Road bridge.

Figure 4.6.3. EISSS3, Bridge on SR 1003 (Chicken Road) over US74 between SR 1155 and SR 1161, Robeson Co., NC, (Morera, 2010)

EISSS5 is selected due to its large skew angle and short span length. Moreover, EISSS6 is selected since this bridge is constructed with TDLF detailing and provides extensive information about the erection practices to eliminate the fit-up problems. The bridge was provided by High Steel Structures, Inc. Figure 4.6.4 shows a photo of EISSS6 during steel erection.

Figure 4.6.4. EISSS6, Bridge on Westchester Co., NY (courtesy of R. Cisneros, High Steel Structures Inc.).

4.6.3. *Continuous-span bridges, Straight, with Skewed supports (ICSS)*

Figure 4.6.5 shows four of six groups of ICSS bridges. The six groups correspond to the combinations of three span lengths and the two deck widths. Two different widths of 30 and 80 ft were considered for L =150 ft in Fig. 4.6.5, but only 80 ft wide bridges were considered for L = 250 and 350 ft. This is because the effect of skew was expected to be smaller for the narrower longer-span bridges. Furthermore, the bridges with L = 250 and 350 ft and w = 30 ft are not shown since these combinations and permutations were found to be exceptional due to their large length-to-width ratios.

In Fig. 4.6.5, the top four rows of the matrix include four two-span continuous bridges with unequal skew and one case with parallel skew. Only values of $\theta = 35^{o}$ were considered for these selected cases.

Figure 4.6.5. Existing, eXample and New I-girder bridges, Continuous-span, Straight with Skewed supports, EICSS, XICSS or NICSS (LENGTH1, LENGTH2, ... / WIDTH / θ_{Left}, ..., θ_{Right}). The columns in the matrix for (L = 250 ft , w = 30 ft) and (L = 350 ft , w = 30 ft) are not shown.

The case with the parallel skew (EICSS1) is a steel overpass on Sunnyside Road Interchange, (I-15B) over I-15, in Bonneville County, ID. This bridge represents a successful implementation of total dead load fit detailing, which aims to ensure that the webs are plumb under the total steel plus concrete dead load. Both field observations and field data are available for this bridge. Figure 4.6.6 shows the gap at the sole plate at one of the bearings of this bridge under the steel dead load. Although daylight is apparent between the sole plate and the elastomeric bearing pad on one side under the steel dead load condition, the girders rotated as expected during the deck placement such that full contact was established with the elastomeric pads. Figure 4.6.7 shows the lack-of-fit between one of the girder connection plates and the bolt holes in a cross-frame on this bridge, during the steel erection. This was expected and intentional due in part to the total dead load fit of the cross-frames. That is, the holes in the girder connection plates and in the cross-frame plates had to be aligned. This hole alignment was achieved on the Sunnyside Road job using drift pins without any other mechanical aid.

Figure 4.6.6. EICSS1, Steel Overpass Sunnyside Road I.C. (I-15B) over I-15, Bonneville Co. ID, gap at sole plate under steel dead load; the girders rotated during the deck placement such that full contact was established with the elastomeric pads (courtesy of Matt Farrar, ITD).

Figure 4.6.7. EICSS1, Steel Overpass Sunnyside Road I.C. (I-15B) over I-15, Bonneville Co. ID, bolt hole alignment during erection; for this job, drift pins were used to align the holes without mechanical aid (courtesy of Matt Farrar, ITD).

Trends in the behavior for other skews were targeted by the ISSS and ICCS cases in Figs. 4.6.2 and 4.6.18 discussed subsequently. The last four rows are three-span continuous designs with parallel skew. Two cases with unequal skew and a narrower deck, NICSS1 and 3, were selected for L = 150 ft and two comparable cases but with the wider deck, NICSS25 and 27, were selected for L = 350 ft. Parallel skews with the extreme skew angles were considered by selecting bridges XICSS5 and NICSS16, with L = 150 ft and w = 30 ft and 80 ft for the 3-span continuous designs.

The bridge XICSS5 is taken from the NHI Course No.130081A-D (NHI/FHWA, 2007), which is an LRFD eXample design developed by Grubb et al. (2007) for the National Highway Institute. Since detailed design calculations are shown for this structure, it was selected to serve as an excellent example for the benchmarking.

In addition, several cases involving 3-span continuous designs with parallel skews were selected due to the availability of similar Existing bridges in the literature:

- EICSS2 is located at I-235 EB over E. University Ave., Polk County, IA. This bridge, recommended by Iowa DOT, had difficulty with the installation of cross-frames during the steel erection. According to Iowa DOT, the fabricator detailed and fabricated the cross-frames for the final dead load condition, i.e., total dead load fit. The problem was resolved by requiring the fabricator to supply new cross-frames that were detailed for steel dead load fit. The bridge has an interesting combination of a relatively wide deck,

and substantial unequal skew of the bearing lines. Therefore, it represents a potentially useful case where total dead load fit detailing may be problematic.

- EICSS12 is located at US 82 main lane underpass at 19th stress west bound, Lubbock County, TX. This bridge is one of several suggested by TxDOT. This bridge involves a field implementation and evaluation of the use of lean-on cross-frames to alleviate issues of nuisance stiffness in significantly skewed bridges and to eliminate cross-frame diagonals within a large portion of the bridge framing. The design and construction of this bridge are discussed by Helwig et al. (2003). Field data are reported by Romage (2008). This bridge provided an outstanding potential opportunity for validation or verification of the refined analysis methods utilized in this research versus available experimental and analytical results.

4.6.4. *Simple-span bridges, Curved, with Radial supports (ISCR)*

Figure 4.6.8 shows the 12 total combinations including three values for the arc-span length (L_{as}=150, 225, 300 ft), the two values for the deck width (w=30, 80 ft), and the two values for the radius of curvature. One corresponds to the largest curvature (smallest R) without having uplift at the most critical bearing location(s) under nominal dead plus live loads, and the other corresponds to the smaller curvature (larger R) for the ISCR bridge designs. Seven of the 12 ISCR bridges in Fig. 4.6.8 are selected. These designs are intended to establish the main trends regarding the structural behavior as a function of horizontal curvature and deck width for the different span lengths.

EISCR1 was inserted into the parametric study, which was a very useful case for initial benchmarking and verification of various analysis methods, including simplified 1D I-girder bridge analysis methods coupled with V-load calculations, as well as virtual test simulations procedures. This is due to the following characteristics of this test bridge:

- There were a very large number of channels of instrumentation collected and reduced at various stages of the steel erection, deck placement, and loading of this bridge in its final composite condition. This is one of the largest bridge structures ever tested indoors, under carefully controlled conditions.
- The geometry of this structure is relatively basic, and should be one of the cases most amenable to simplified analysis.

- This test bridge was designed at or slightly above a number of maximum limits in the AASHTO LRFD Specifications. Hence a number of its characteristics are likely to accentuate the effect of certain analysis and/or design approximations.

Jung (2006) and Jung and White (2008) provide a detailed discussion of the characteristics and the behavior of this test bridge. These references also provide substantial prior results from FEA simulation models similar to the types of simulation models that are employed in this research. Figure 4.6.9 shows a view of the FHWA test bridge at an intermediate stage of the steel erection, when the first two of the three girders in this bridge had been placed on their support bearings and connected together by cross-frames.

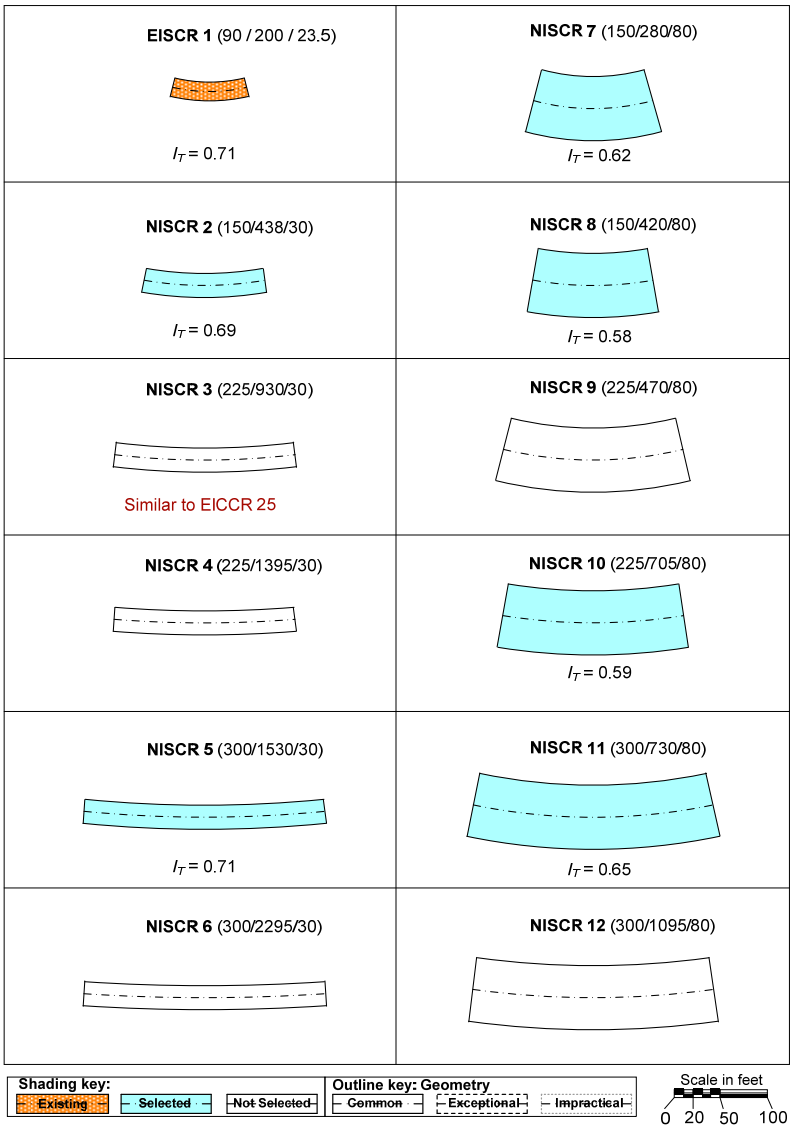

Figure 4.6.8. Existing and New I-girder bridges, Simple-span, Curved with Radial supports, EISCR or NISCR (LENGTH / RADIUS / WIDTH).

Figure 4.6.9. EISCR1, FHWA Test Bridge (Jung 2006, Jung and White 2008).

4.6.5. *Continuous-span bridges, Curved, with Radial supports (ICCR)*

Figure 4.6.10 shows 12 total combinations of L_{as} (=150, 250, 350 ft), *w* (=30, 80 ft) and the two values for the radius of curvature, one corresponding to the largest curvature (smallest *R*) without having uplift at the most critical bearing location(s) under nominal dead plus live loads and other one corresponding to the smaller curvature (larger *R*) for the ICCR bridges.

In Figure 4.6.10, all of the cases with the narrower deck are selected as shown in the first column of this experimental design matrix except NICCR5. The selection is mainly driven by the Existing bridge designs. EICCR22a was selected since it has extensive field observations and measurements, which is reported by Leon et al. (2011). Figure 4.6.11 shows several photos of EICCR22a during steel erection.

EICCR11, which is the Ford City Bridge, in Ford City, PA, was inserted into the analytical study since it represents an important model case where due to combinations of long spans, deep girders with relatively close spacing compared to the girder depths, and relatively tight curvature, substantial erection challenges had to be addressed in the erection engineering of the structure. This bridge has been studied thoroughly in prior work by Chavel and Earls (2006a & b & 2001) and by Chang (2006). Hence, it represented another valuable case that can be used to validate the analysis and design methods. Figure 4.6.12 shows an overall photo of the Ford

City bridge during its steel erection. Figure 4.6.13 emphasizes the overall depth of the girders relative to their horizontal spacing. Figure 4.6.14 provides several snapshots during the installation of a key drop-in segment on this bridge.

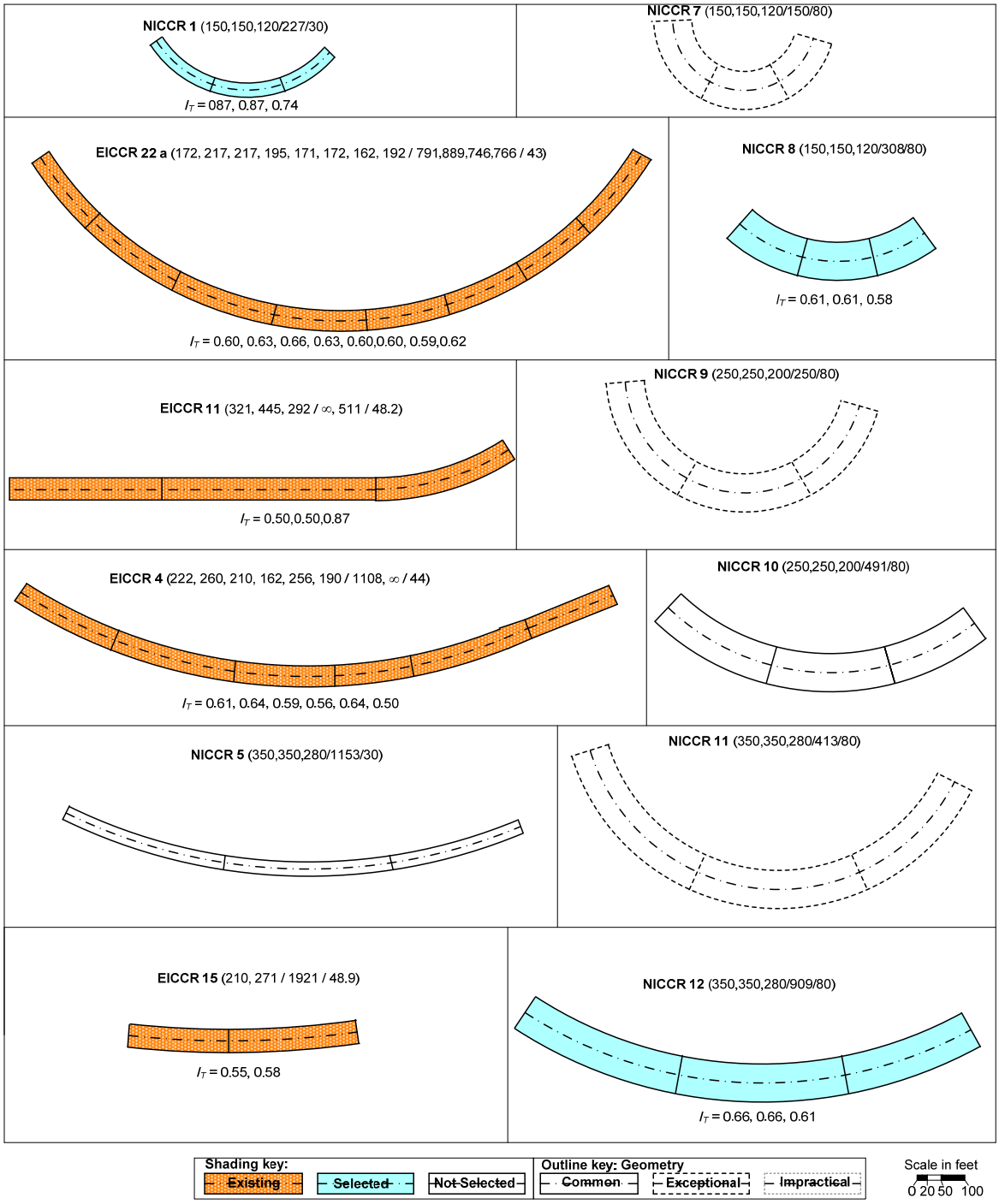

Figure 4.6.10. Existing, eXample and New I-girder bridges, Continuous-span, Curved with Radial supports, EICCR, XICCR or NICCR (LENGTH1, LENGTH2, ... / RADIUS / WIDTH).

Figure 4.6.11. EICCR22a, Bridge No. 12 Ramp B over I-40, Robertson Avenue Project, Davidson Co., TN.

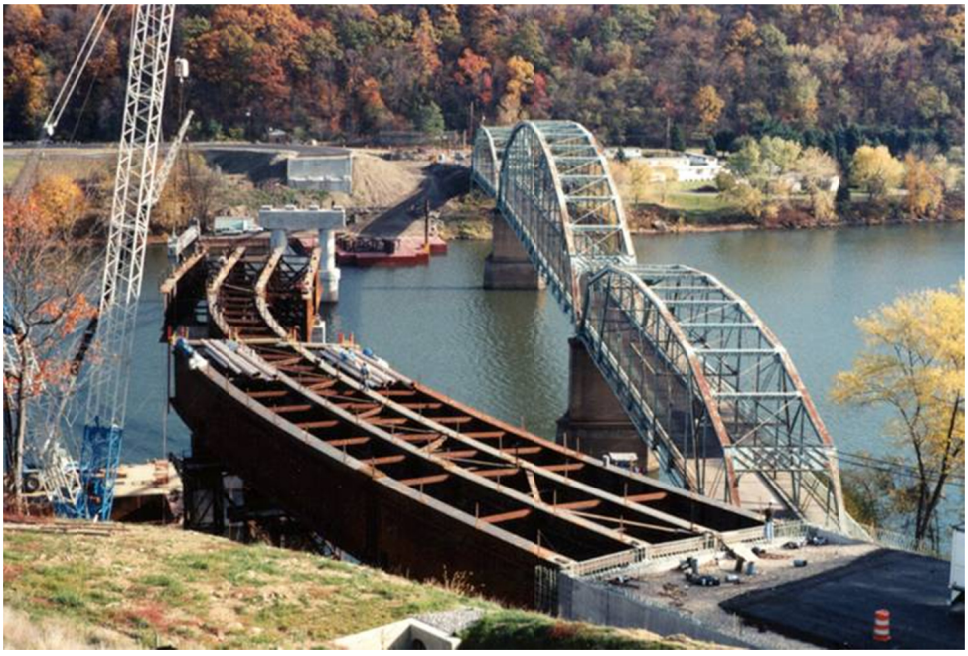

Figure 4.6.12. EICCR11, Ford City Bridge, Ford City, PA (Chavel, 2008).

Figure 4.6.13. EICCR11, Ford City Bridge, Ford City, PA, girder depth and spacing (Chavel, 2008).

Figure 4.6.14. EICCR11, Ford City Bridge, Ford City, PA, installation of drop-in segment (Chavel, 2008).

EICCR4 is located at Ramp GG, John F. Kennedy Memorial Highway, I-95 Express Toll Lanes and I-695 Interchange, Baltimore County, MD. High Steel Structures, Inc. did the fabrication and the steel erection for this bridge. Members of the NCHRP (2011) project team visited the job site to observe the erection of a drop-in segment on the second span from the right hand end of this bridge in the sketch during August 2007. Figure 4.6.15 is a photo of the bridge just prior to installation of this drop-in segment.

EICCR15 is located at SR 6220 A11 over SR 6220 NB and SB, Centre County, PA. This bridge was studied experimentally and analytically by Shura (2004) and is discussed by Domalik et al. (2005). Due to its unequal span lengths (ratio of the arc-span lengths of 0.77), this bridge exhibits important torsional interactions between its two spans. The shorter span actually twists in the direction opposite from the torsional deformation of the longer span. As a result, this bridge was selected to serve as an important case for assessment of the sufficiency or limitations of various simplified analysis methods.

In addition, two of the three cases with wider decks and smaller curvature (larger *R*) were considered in the second column of the matrix except NICCR10. The wider-deck cases with tighter curvature in Fig. 4.6.10 were considered to be exceptional designs. The influence of

these wide decks with tight curvatures was expected to be captured sufficiently via the combo of ISCR and ISCS bridges.

Figure 4.6.15. EICCR4, Ramp GG John F. Kennedy Memorial Highway, I-95 Express Toll Lanes and I-695 Interchange, Baltimore Co., MD, August 2007.

4.6.6. *Simple-span bridges, Curved, with Skewed supports (ISCS)*

Figure 4.6.16 displays four of twelve groups of I-girder bridges considering:

- The twelve combinations of skew magnitude,
- The two values for length, L_{as} =150 and 300 ft,
- The two values for the deck width w =30 and 80ft, and
- The four values of radius of curvature R = 438, 280, 420 and 730 ft which were selected from ISCR bridges.

Since the effects of skew are generally larger in wider bridges for a given arc span length, emphasis was placed on bridges with the wider decks in the design of the ISCS studies.

In addition, none of the bridges with 225 ft arc-span length are considered in Fig. 4.6.16. This is because it was expected that the interactions between the effects of the curvature and skew on I-girder bridges could be captured sufficiently by studying the ISSS, ICSS, ISCR, ICCR, ISCS and ICCS bridges with L_{as} = 150 ft.

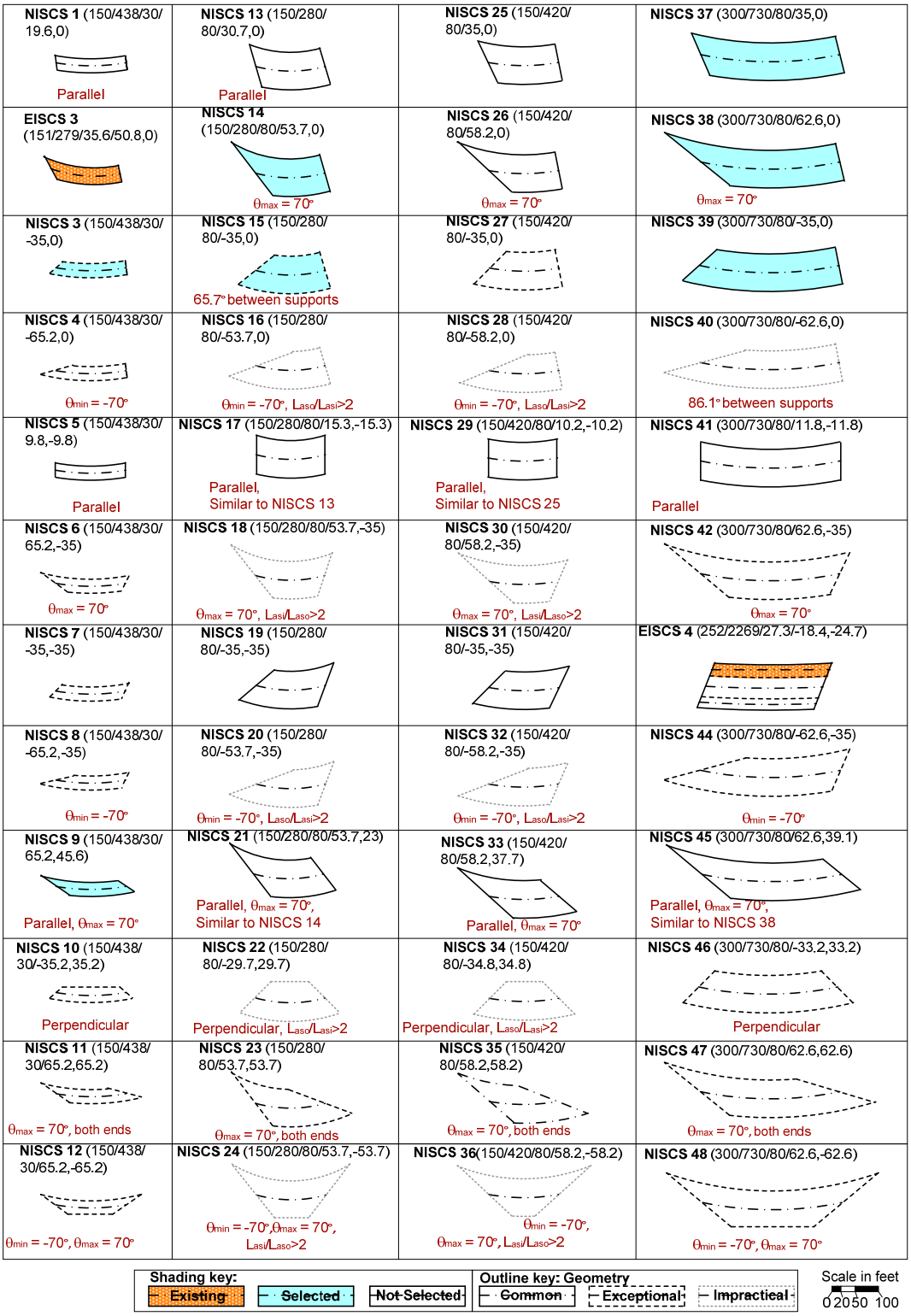

Figure 4.6.16. Existing and New I-girder bridges, Simple-span, Curved with Skewed supports, EISCS or NISCS (LENGTH / RADIUS / WIDTH / θ_{Left}, θ_{Right}). The columns in the matrix for (L = 150 ft , w =30 ft, R = 292 ft), (L = 225 ft , w =30 ft, R = 930 and 1395 ft), (L = 225 ft , w =80 ft, R = 470 and 705 ft), (L = 300 ft , w =30 ft, R = 1530 and 2295 ft) and (L = 300 ft , w =80 ft, R = 1095 ft) are not shown.

One case with L_{as} = 300 ft, the case with the wider deck and tighter curvature, was included to investigate the interaction effect on a longer-span design where some type of flange-level lateral bracing system is likely.

In Fig. 4.6.16 one can observe that the bridges in the 2nd and 3rd rows of 1st, 2nd and 3rd columns were selected except NSCS1 and NSCS3 for analytical studies. These bridges were selected to capture the behavior with respect to the variation in the L_{as} /w and L_{as} /R ratios. NISCS9 was selected to capture the effect of parallel skewed bearings along with curvature effects.

EISCS3 was inserted into the design matrix. This bridge is SR 8002 Ramp A-1, in King of Prussia, PA, studied extensively by Chavel and Earls (2003) and Chavel (2008) in their prior research (see Fig. 4.6.17). Moreover, the third phase of EISCS4 was inserted into the study matrix since this phase experienced large differential displacements with respect to the adjacent units due to its large length-to-width ratio.

Figure 4.6.17. EISCS3, SR 8002 Ramp A-1, King of Prussia, PA (Chavel and Earls, 2003).

4.6.7. *Continuous-span bridges, Curved, with Skewed supports (ICCS)*

Figure 4.6.18 shows six of the twelve possible groups of ICCS bridges. Note that the R values selected for the ICCR bridges (Fig. 4.6.10) were used also for the subsequent ICCS designs in Fig. 4.6.18. Rows 1 through 3 of the experimental design matrix shown in this figure correspond to different orientations of the bearing lines relative to the curved geometry, but with the bearing lines parallel (or near parallel in cases where the skew angle is limited by $\theta = +70^{o}$ at the inside edge of the deck). The bridges in the fourth row are similar to those in row 1, but with

zero skew at the bearing line at the right hand end of the bridge. Three of the four combinations of deck width and horizontal curvature for *L* = 150 ft are considered in columns 1 through 3 of this matrix. Narrow 250 ft continuous-spans with the tighter curvature are considered in the fourth column. This case was included because ramp type structures with roughly 250 ft span lengths are very common. The last two columns of Fig. 4.6.18 show 350 ft two-span continuous bridges with 80 ft wide decks and each of the values of horizontal curvature determined previously. The narrower bridges were not considered for these span lengths, since it was expected that the influence of skew will be more minor for these bridges. Lastly, all of the 150 ft span bridges in column 1 of the Fig. 4.6.18 test matrix were selected. In addition, all the of 250 and 350 ft span bridges in columns 4 and 6 were selected except the ones with perfect symmetry about the center pier (NICCS15 and 23) and NICCS22, since this bridge is similar to the ones in the ICCR bridges. The case with perfect symmetry about the center pier was believed to be less common for these types of bridge geometry. The two non-exceptional cases with the wider decks were considered in the third column of this experimental design matrix. NICCS11 was also not selected since this bridge is similar to NICCR8 in Fig. 4.6.10.

EICCS 10 was inserted into the design matrix, which is MN DOT Bridge No. 27998, TH94 between 27th Avenue and Huron Boulevard in Minneapolis, MN. This bridge has been studied extensively, both experimentally and analytically, by Galambos et al. (1996). Also, it has been used by Nowak et al. (2006) as part of the calibration of the AASHTO LRFD Specifications for curved steel bridges. Therefore, this bridge was selected to be of particular value in relating the implications of analysis accuracy in the context of structural reliability calibration and assessment of strengths.

EICCS1 was also inserted into the design matrix, which is located at I-459 / US31 Interchange Flyover A, Jefferson County, AL. The construction of this bridge was observed and thoroughly documented by Osborne (2002). The bridge represents a successful implementation of total dead load fit detailing on a significantly curved span with one pier location that is substantially skewed relative to a radial line. Figure 4.6.19 shows a photo looking along the length of the bridge at the skewed bearing line during construction. Figure 4.6.20 shows another snapshot of the steel erection.

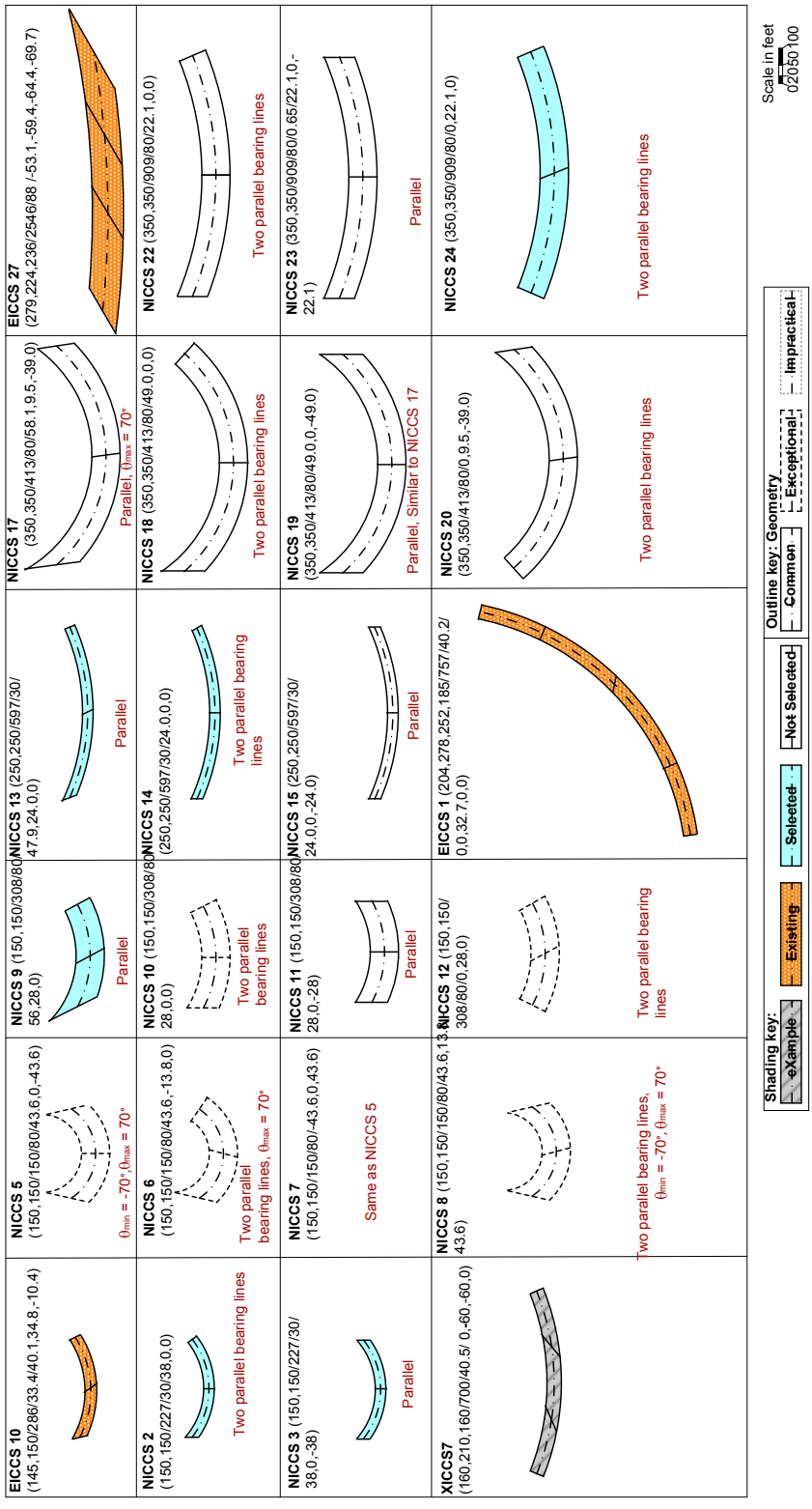

Figure 4.6.18. Existing and New I-girder bridges, Continuous-span, Curved with Skewed supports, EICCS or NICCS (LENGTH1, LENGTH2, ... / RADIUS / WIDTH / θ_{Left}, ..., θ_{Right}). The columns in the matrix for (L = 150 ft , w =30 ft, R = 438 ft), (L = 250 ft , w =30 ft, R = 1179 ft), (L = 250 ft , w =80 ft, R = 250 and 491 ft), (L = 350 ft , w =30 ft, R = 1153 and 2291 ft) are not shown.

Figure 4.6.19. EICCS1, I-459 / US31 Interchange Flyover A, Jefferson Co. AL (Osborne 2002).

Figure 4.6.20. EICCS1, I-459 / US31 Interchange Flyover A, Jefferson Co. AL (Osborne 2002).

4.7. Summary of New, Existing and Example Bridges

Table 4.7.1 provides an overall summary of the number of New, Exisiting and eXample bridges for each of the major groups of bridges. Fifty-eight bridges were selected in total for the analytical studies, including 16 existing bridges and 42 parametric study designs.

Table 4.7.1. Overall summary of New, Existing and eXample I-girder bridges.

Description		**Cases**
eXample I-girder, Continuous-span, Straight, No skew (Base comparison case)		**1**
ISSS	(EISSS) Existing, I-girder, Simple-span, Straight, Skewed supports	3
	(XISSS) eXample, I-girder, Simple-span, Straight, Skewed supports	0
	(NISSS) New, I-girder, Simple-span, Straight, Skewed supports	12
	Total: ISSS	**15**
ICSS	(EICSS) Existing, I-girder, Continuous-span, Straight, Skewed supports	3
	(XICSS) eXample, I-girder, Continuous-span, Straight, Skewed supports	1
	(NICSS) New, I-girder, Continuous-span, Straight, Skewed supports	5
	Total: ICSS	**9**
ISCR	(EISCR) Existing, I-girder, Simple-span, Curved, Radial supports	1
	(XISCR) eXample, I-girder Simple-span, Curved, Radial supports	0
	(NISCR) New, I-girder Simple-span, Curved, Radial supports	6
	Total: ISCR	**7**
ICCR	(EICCR) Existing, I-girder, Continuous-span, Curved, Radial supports	4
	(XICCR) eXample, I-girder, Continuous-span, Curved Radial supports	0
	(NICCR) New, I-girder, Continuous-span, Curved Radial supports	3
	Total: ICCR	**7**
ISCS	(EISCS) Existing, I-girder, Simple-span, Curved, Skewed supports	2
	(XISCS) eXample, I-girder, Simple-span, Curved, Skewed supports	0
	(NISCS) New, I-girder, Simple-span, Curved, Skewed supports	7
	Total: ISCS	**9**
ICCS	(EICCS) Existing, I-girder, Continuous-span, Curved, Skewed supports	3
	(XICCS) eXample, I-girder, Continuous-span, Curved, Skewed supports	1
	(NICCS) New, I-girder, Continuous-span, Curved, Skewed supports	6
	Total: ICCS	**10**
Total: Existing I-girder bridges		16
Total: eXample I-girder bridges		3
Total: New I-girder bridges		39
Total: I-girder bridges		58

4.8. Case Study Bridges

For the studies conducted here and in NCHRP Project 12-79 (NCHRP, 2011), the complete analytical matrix (58 I-girder bridges) discussed in Sections 4.6 and 4.7 was investigated for NLF detailing. Additionally, approximately 45 I-girder bridges were investigated for SDLF and TDLF detailing. However, several case study bridges are selected and documented from the overall analytical study for the subsequent studies presented in this dissertation. These case study bridges are selected to demonstrate the research findings pertaining to horizontal curvature and skew effects in the clearest fashion. Therefore, the selected case study bridges generally correspond to the more extreme bridge geometries from the broader study. The selected case study bridges are EISSS6, NISSS54, XICSSS5, NICSR2, NISCR5, NISCS14, NISCS15, NISCS37 and EICCCR11. Detailed descriptions of these bridges, which are used to present and demonstrate the findings of this research, are provided in Appendix C.

CHAPTER V.

EVALUATION OF DEAD LOAD FIT CROSS-FRAME DETAILING ON SYSTEM AND COMPONENT RESPONSES

Although AASHTO (2010) Article C6.7.2 states that engineers may need to consider potential problematic locked-in stress effects due to DLF detailing for horizontally curved I-girder bridges, with or without skewed supports, engineers practically never include the inherent lack-of-fit in their structural analysis in current practice. However, in certain cases, the locked-in forces may significantly influence the girder layovers, the girder vertical displacements, the cross-frame forces, and the girder major-axis bending and/or flange lateral bending stresses. This chapter evaluates the impact of locked-in force effects due to cross-frame detailing on the component and system responses and bridge strength during construction. The kinematics of the dead load torsional rotations in I-girder bridges constructed with NLF detailing are explained in Section 5.1. Sections 5.2 through 5.5 evaluate the impact of locked-in stresses on the bridge geometry (layovers and vertical displacements), cross-frame forces, girder stresses and strength respectively by using refined FEA solutions. The detailed analysis results are presented for different types of detailing for several bridges in Appendix D. Lastly, Section 5.6 investigates the impact of cross-frame connection bolt slip on component responses via several case studies.

5.1. Torsional Rotations in I-Girder Bridges due to Dead Loads

Twist of the girders and the bridge cross-section under load is unavoidable due to various couplings between the bridge components. The primary sources of girder twist can be due to skewed bearings, curvature, differential vertical displacements at the intermediate cross-frame locations, unbalanced loadings, and different girder sizes. Figure 5.1.1 illustrates total dead load girder layovers of several representative bridges constructed with NLF detailing.

For straight and skewed bridges, the end layovers are mainly driven by the coupling between major-axis bending rotations and torsional rotations at the skewed bearing lines. Figure 5.1.1(i) provides the total dead load layovers of a representative straight skewed bridge with parallel skewed bearing lines (NISSS54) constructed with NLF detailing. It can be observed from Fig. 5.1.1(i) that the girder top flanges twist upwards at the left bearing line, whereas they twist downwards at the right bearing line under dead loads due to the coupling at the skewed bearing line. This effect creates a twist in the opposite direction at the bearing lines.

Layovers are developed at the intermediate cross-frame locations. Perpendicular intermediate cross-frames are provided between adjacent girders at locations having differential vertical displacements. However, the cross-frames are relatively stiff within their planes compared to the torsional stiffness of the I-girders. Therefore, the intermediate cross-frames enforce the same layovers between the adjacent girders.

The layovers typically vary in a nonlinear fashion along the length of the girders due to the interaction between different couplings as in Fig. 5.1.2. Figure 5.1.2 provides the girder layovers versus the distance *z* measured from the left-hand acute corner of the bridge NISSS54. This figure demonstrates that the interior cross-frames enforce the same layovers between the adjacent girders at the cross-frame locations. The cross-frames push the girders back-and-forth to enforce the same girder layover within the span since a staggered cross-frame pattern is utilized for the bridge NISSS54. Enforcement of the same girder layovers at the intermediate cross-frame locations creates a "zig-zag" pattern in the girder layovers. Further, intermediate cross-frames that are close to the skewed bearing lines develop a sudden change in the girder layovers to enforce the same layover between adjacent girders. High local deformations of the flanges can be observed at these locations due to the close interaction between different couplings. This behavior can be observed in Fig. 5.1.2 at the first intermediate cross-frame, adjacent to the obtuse corners of the bridge.

For curved bridges with radial supports, there is a coupling between major-axis bending deflections and torsional rotations due to curvature. Therefore, in curved radially-supported bridges, the top flange of the girders layover toward the outside of the curve and the bottom flanges layover toward the inside due to curvature effects under dead loads, as shown in Fig. 5.1.1(ii). For curved I-girder bridges, the coupling can be understood by considering a basic simply-supported curved I-girder with torsionally simply-supported end conditions subjected to transverse loads as shown in Fig. 5.1.3. The girder torsional deformations near the end supports have a substantial impact on the mid-span vertical displacements. Overhang bracket loadings also develop layovers on the fascia girders, which tends to increase the outside girder layovers and decrease the inside girder layovers in curved bridges.

For curved bridges with skewed bearings, girder layovers occur due to the combination of the couplings stated above. Girder end layovers are observed due to coupling with major-axis bending deformations at the skewed bearings, as shown in Figs. 5.1.1(iii) and 5.1.1(iv). The girder layovers within the span are mainly due to coupling with the major-axis bending rotations

(curvature effects) and the enforcement of the same layovers between adjacent girders at the intermediate cross-frame locations. Bridges with positive skewed bearing lines (counter clockwise direction) decrease the girder layovers within the span under dead loads since the twist direction of the girder layovers due to curvature effects is opposite to that due to the skew (see Fig. 5.1.1(iii)). On the other hand, curved bridges with negative skewed bearing lines (clockwise direction) increase the girder layovers within the span as the twist direction of the girders at the skewed bearings is the same as that within the span (see Fig. 5.1.1(iv)).

Continuous-span bridges generally experience an interaction between the layovers in adjacent spans. For instance, in Fig. 5.1.1(v), girder layovers are developed in the third span due to curvature effects, causing layovers in the straight second span due to continuity effects.

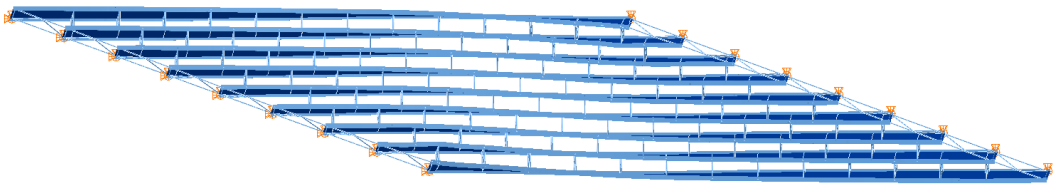

(i) NISSS54, Straight and Skewed supports (magnified by 10x)

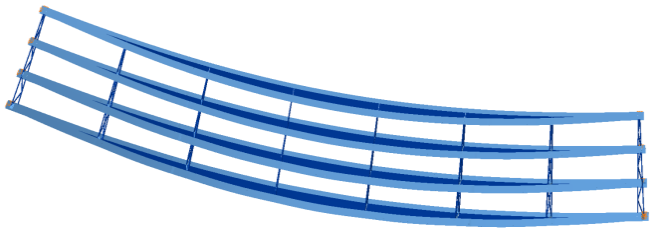

(ii) NISCR2, Curved with radial supports (magnified by 20x)

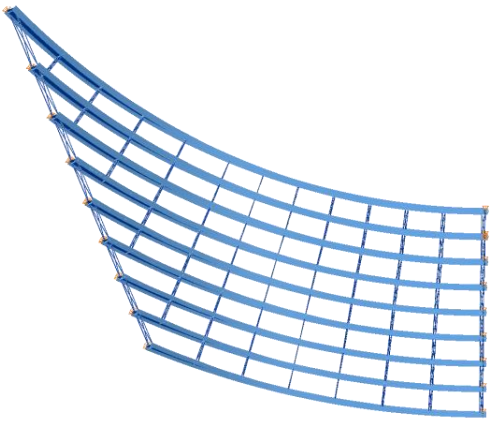

(iii) NISCS14, Curved with positive skew angle (magnified by 30x)

Figure 5.1.1. Girder layovers for different bridge geometries.

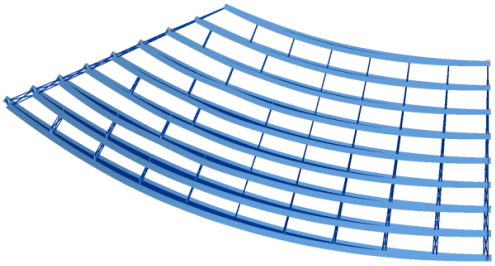

(iv) NISCS15, Curved with negative skew angle (magnified by 20x)

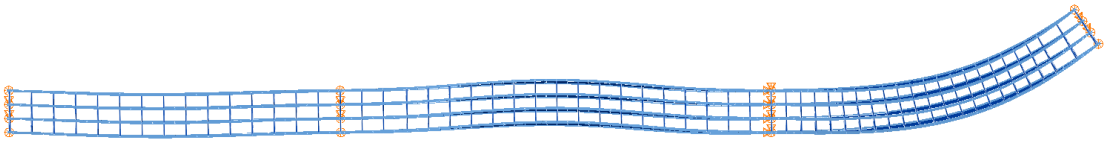

(v) EICCR11, Continuous bridges (magnified by 10x)

Figure 5.1.1. (continued). Girder layovers for different bridge geometries.

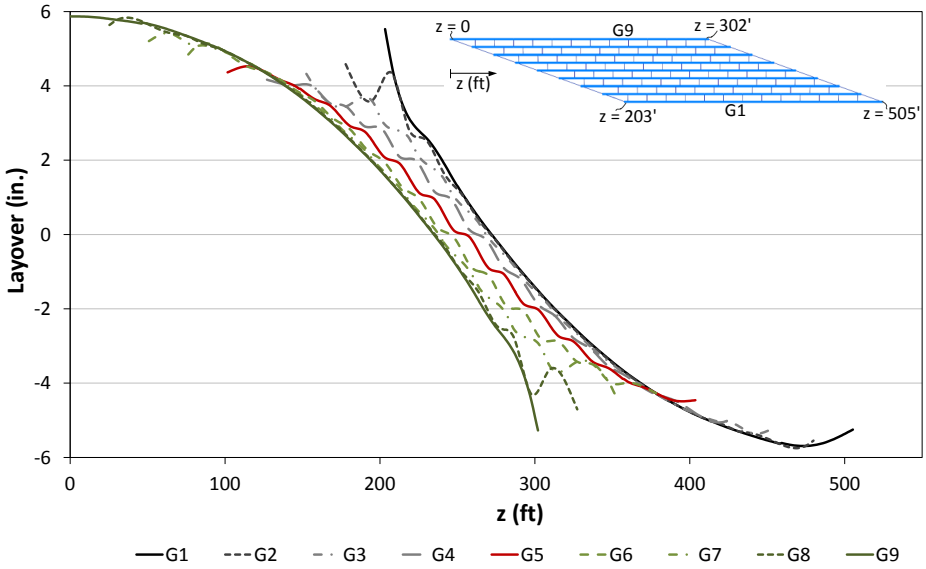

Figure 5.1.2. NISSS54, Girder layovers under total dead load for NLF detailing.

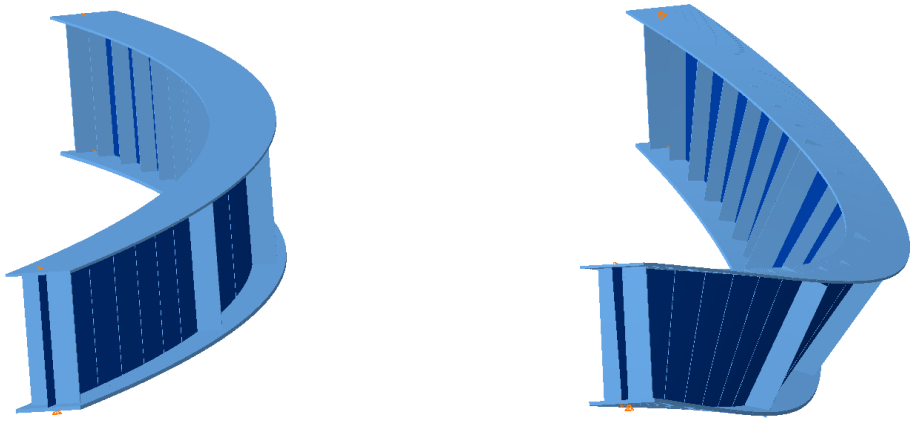

(i) Undeformed shape *(ii) Deflected shape (Magnified by 2x)*

Figure 5.1.3. *Coupling between girder vertical displacements and girder twist for curved bridges.*

5.2. Impact of Dead Load Fit Cross-Frame Detailing on Constructed Bridge Geometry

5.2.1. *Girder layovers*

As noted previously, bridge I-girders in curved and/or skewed bridges generally can be plumb only in one load condition. The cross-frames are relatively stiff within their planes compared to the torsional stiffness of the I-girders. Therefore, a common assumption is that the girders can be twisted and forced to fit the cross-frames under any lack-of-fit. However, twisting of the girders can be difficult in cases where the twist is coupled significantly with major-axis bending rotations and vertical deflections. This is often the case for curved girders. The ultimate goal with any DLF (Dead Load Fit, i.e., TDLF or SDLF) detailing is to obtain plumb webs at the targeted load level by using the rigidity of the cross-frames to impose girder torsional rotations opposite to the dead load torsional rotations. The direction of the torsional rotations is mainly driven by the differential vertical camber within the span (assuming that the cross-frames are normal to the girders) and by the rotational compatibility with the bearing line cross-frames and the direction of the girder end rotations due to the camber at the bearing lines. The differential vertical camber between the girders and the rotational compatibility at the bearing lines associated with the girder camber rotations are the primary sources of the lack-of-fit for SDLF and TDLF detailing.

Figures 5.2.1 and 5.2.2 show a representative set of total dead load girder camber profiles and the corresponding differential camber between the girders for a straight I-girder bridge with parallel skew and a curved I-girder bridge with radial supports, respectively. In these figures, the sign of the differential camber is positive when the girder with the larger number has the larger camber. For instance, the differential camber between girders G2 and G1 at the bottom left corner of the bridge in Fig. 5.2.1(ii) is +3.4, meaning that the camber is 3.4 inches higher in girder G2 at the first intermediate cross-frame from the bearing line. Conversely, the differential camber between girders G8 and G9 at the upper right corner of the bridge is -3.4 inches, indicating that the camber in G8 is 3.4 inches higher than in G9 at the first intermediate cross-frame at that location. The differential camber between the girders can be either positive or negative depending on the difference between the girder camber profiles at the cross-frame locations, as illustrated in Fig. 5.2.3.

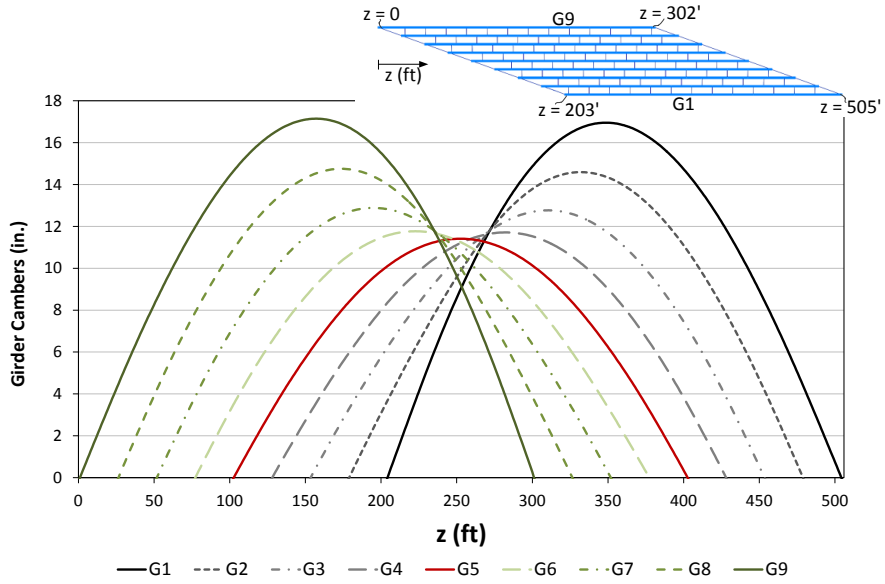

(i) Girder cambers under total dead load

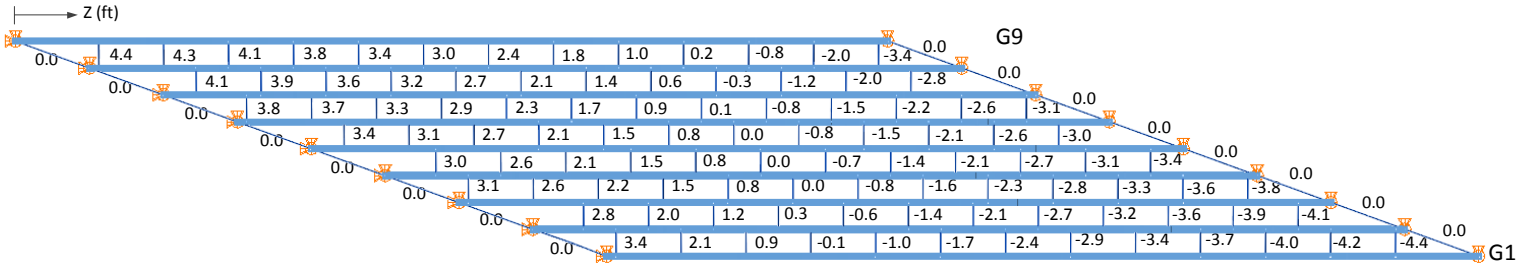

(ii) Differential camber between girders

Figure 5.2.1. NISSS54, Girder cambers and the differential camber between the girders obtained from FEA vertical deflections.

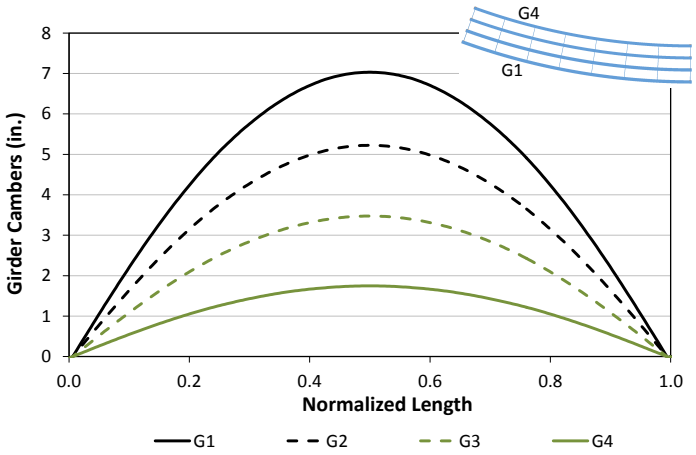

(i) Girder cambers under total dead load

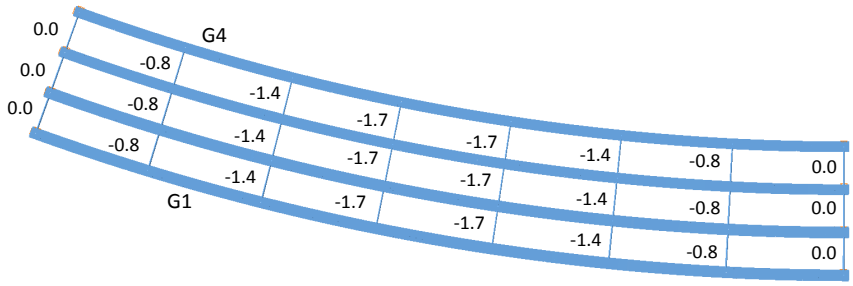

(ii) Differential camber between girders

Figure 5.2.2. NISCR2, Girder cambers and the differential camber between the girders obtained from FEA vertical deflections

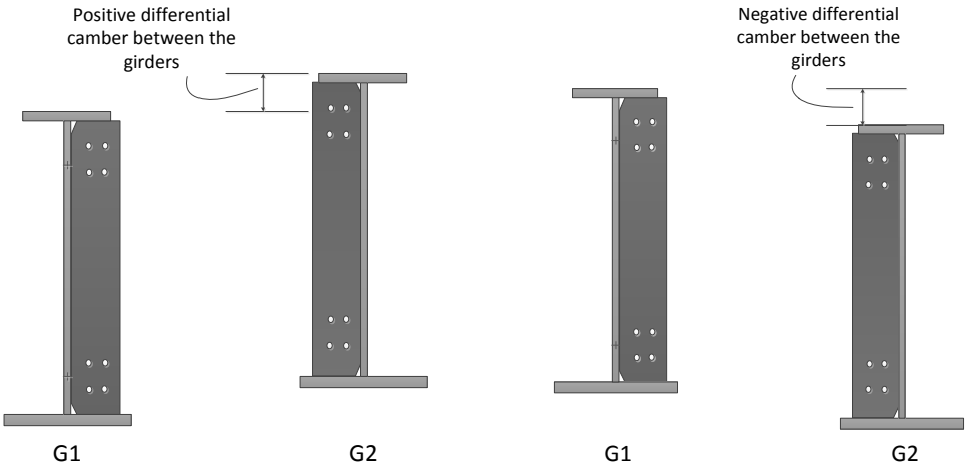

(i) Positive differential camber between girders

(ii) Negative differential camber between girders

Figure 5.2.3. Representative sketch of positive and negative differential camber between the girders.

For DLF (Dead Load Fit, i.e., TDLF or SDLF) detailing of the intermediate cross-frames, the girders need to be twisted to connect the cross-frames between them. The movements at the intermediate cross-frame locations are illustrated in Fig. 5.2.4 for locations with positive and negative differential camber between the girders in the no-load geometry. In the case of straight bridges with parallel skew orientations, both positive and negative differential cambers are obtained between the girders since the parallel skew orientation of the bearing lines offsets the camber profiles of the girders as shown in Fig. 5.2.1(i). For instance, the camber profiles for the fascia girders G1 and G9 are the same; however, the left-hand bearing location for G1 is located at a *z* coordinate of 203 ft., i.e., G1 starts at 203 ft. into the span of G9. The opposite sign of the differential cambers at each of the bridge results in a twisting of the girders, due to the lack-of-fit of the cross-frames, that is in opposite directions at the two ends. These lack-of-fit twist rotations are in turn opposite in sign relative to the twist rotations of the girders under dead load.

Figure 5.2.5 shows the girder G1 layovers of NISSS54 due to the lack-of-fit associated with TDLF detailing at three different erection stages. In the first stage, only the end cross-frames are installed. In the second stage, the first intermediate cross-frame from the left bearing is installed. Lastly, in the third stage, all the interior cross-frames are installed. In stage one of Fig. 5.2.5, the lack-of-fit of the end cross-frames due to major-axis camber rotations develops girder layovers that are opposite to the layovers caused by dead loads. It is clear from Fig. 5.2.5 that the girder layovers within the span are different for each of the erection stages. Figure 5.2.6 shows the deflected shape at erection stage three. It should be noted from the erection stage three (Figs. 5.2.5 and 5.2.6) that the twist of the cross-frames due to locked-in force effects are observed even at the locations with zero differential camber (e.g. cross-frames at the mid-span). The twisting occurs due to coupling between the twist rotations and other rotations and between the twist rotations and other displacements.

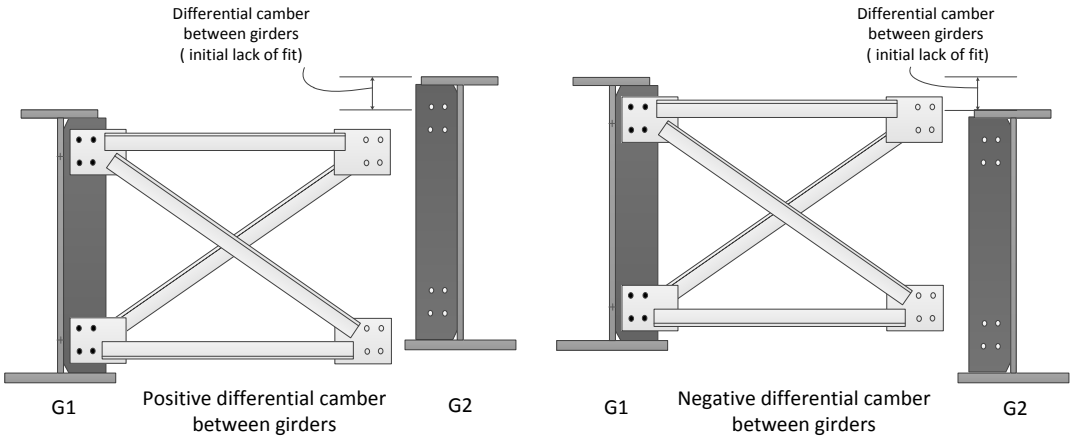

(i) Initially plumb no-load geometry of girders

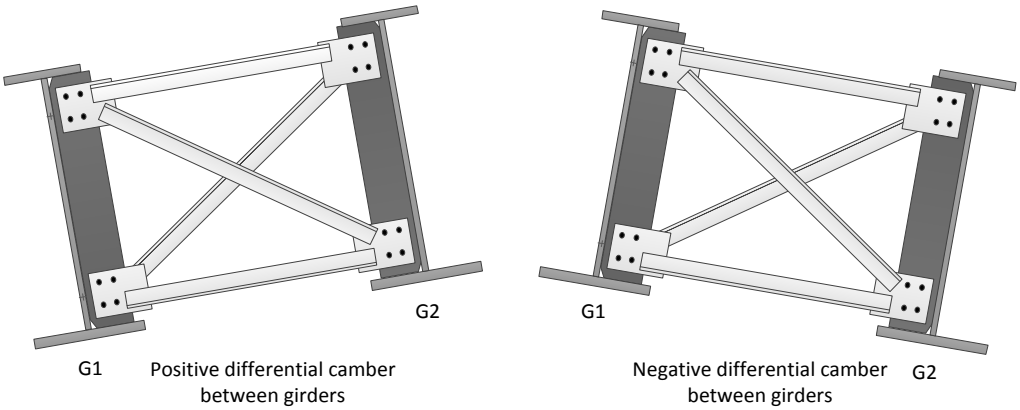

(ii) Cross-frames connected in ideal initial no-load geometry

Figure 5.2.4. Induced girder twist at intermediate cross-frame locations for positive and negative differential camber between girders in ideal no-load geometry.

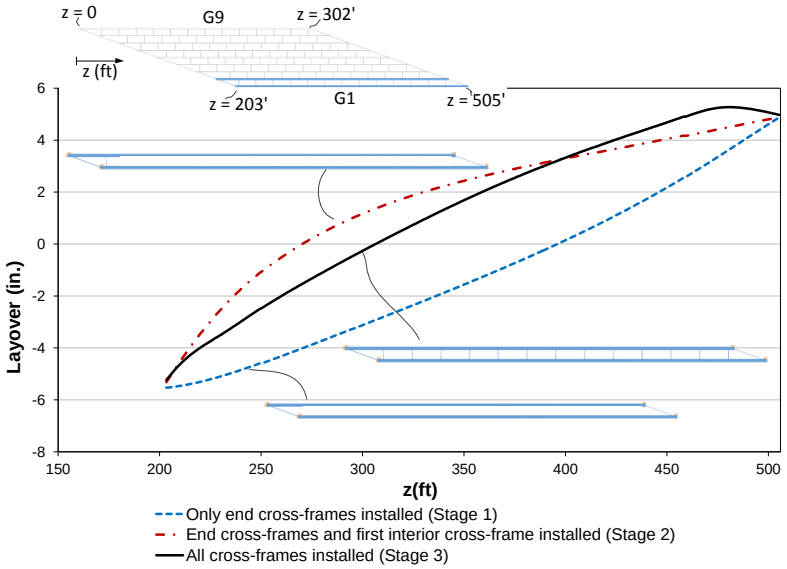

Figure 5.2.5. NISSS54, Girder 1 layovers under lack-of-fit due to TDLF detailing at different stages.

Figure 5.2.6. NISSS54, Deflected shape of Girders 1 and 2 under lack-of-fit due to TDLF detailing (magnified by 10x)

The intermediate cross-frames usually have high in-plane stiffness so they enforce the same layovers between the adjacent girders at the cross-frame locations. Fig.5.2.7 shows the layovers for both girders G1 and G2 due to the lack-of-fit associated with TDLF detailing. It should be noted from Fig 5.2.7 that the girder layovers are almost linear (except in the vicinity of the skewed bearing lines due to close interaction between layovers due to coupling at the skewed bearing lines and the coupling at the intermediate cross-frame locations). However, when the bridge is completed, the girder layovers within the span can be different since the transverse and torsional stiffness of the bridge increases. For instance, Fig. 5.2.8 demonstrates the deflected shape of the completed bridge due to lack-of-fit forces for TDLF detailing. Figure 5.2.9 provides the magnitudes of girder layovers due to lack-of-fit for TDLF detailing plotted along the length of the bridge starting from the left acute corner. It should be noted from Figs. 5.2.8 and 5.2.9 that the girder layovers are not as smooth as the ones in Figs. 5.2.6 and 5.2.7 due to interaction between various couplings that are mentioned in Section 5.1. It should be noted that it is harder to enforce the same layover at the intermediate cross-frame locations that are located at a stiff transverse load path. These are the locations where there is a substantial second derivative of the layovers in Figs. 5.2.8 and 5.2.9.

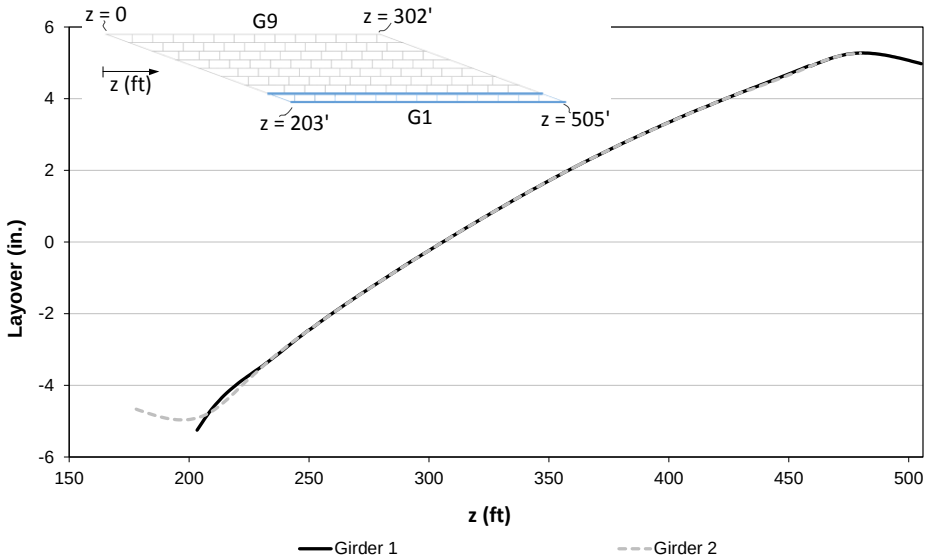

Figure 5.2.7. NISSS54,Girder 1 and 2 layovers under lack-of-fit due to TDLF detailing.

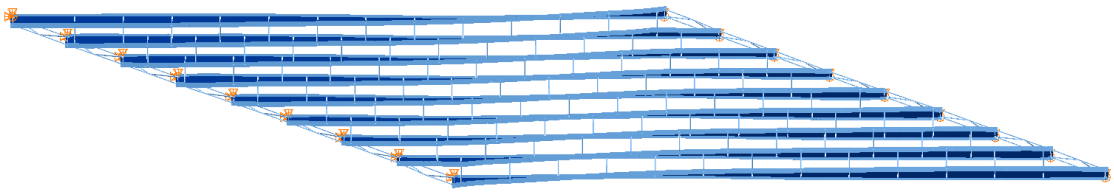

Figure 5.2.8. NISSS54, Deflected shape under lack-of-fit due to TDLF detailing (magnified by 10x).

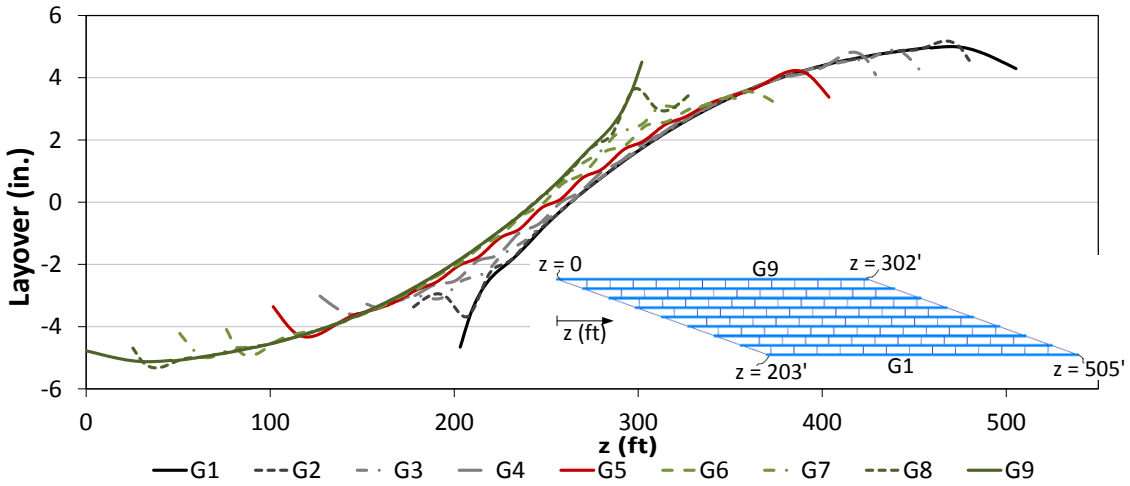

Figure 5.2.9. NISSS54, Girder layovers under lack-of-fit due to TDLF detailing.

Figures 5.2.10 and 5.2.11 illustrate the deflected shape of the bridge NISSS54 under steel and total dead loads, respectively. Each of these figures shows the magnified deflections associated with each of the three main types of cross-frame detailing. Similarly, Figs. 5.2.12 and 5.2.13 illustrate the magnitudes of girder layovers of this straight-skewed bridge under steel and total dead load respectively for each of the types of cross-frame detailing. The girder layovers are plotted along the length of bridge starting from the left acute corner. The NISSS54 bridge has a large skew index (I_S = 0.68, a la Eq. 2.5.1), indicating that the influence of skew is large on the response of the structure. The torsional rotations at the bearings due to the total dead load are more than 0.04 radians in this structure which is typically the maximum rotation limit considered for a steel reinforced elastomeric bearing, as discussed in subsequently in Section 6.2.1 in detail.

Approximately plumb girders are obtained under the steel dead load if the bridge is constructed with SDLF detailing as shown in Figs. 5.2.10(ii) and 5.2.12(ii). For TDLF detailing, the cross-frames are detailed such that they approximately compensate the total dead load deflections. Therefore, layovers in the opposite direction from those due to the total dead load

are obtained under the *steel dead load* when TDLF detailing is used, as shown in Figs. 5.2.10(iii) and 5.2.12(iii). However, approximately plumb girders are obtained for the bridge where the cross-frames are detailed for TDLF, once the total dead load is placed on the bridge, as illustrated in in Figs. 5.2.11(iii) and 5.2.13(iii). The differences between the locked-in layovers and dead load layovers cause the deviation from the theoretical plumb position of the web. These two sources of layovers do not offset each other completely. Figure 5.2.14 shows the superposition of layovers from Figs. 5.2.13(i) and 5.2.9. It is clear from Fig.5.2.14 that the superposed layovers are very similar to the ones in Fig. 5.2.13(iii).

The compensating girder layovers generated by DLF detailing are never exactly equal and opposite to the dead load layovers. This is mainly due to:

- The stress state due to the torsional effects of the distributed dead loads cannot possibly be matched exactly by the concentrated internal forces from the cross-frames induced by DLF detailing. The difference between the girder stress state induced by the lack-of-fit forces and the girder stress state associated with the dead load torsion causes additional deformations within the structure.
- The girder camber profiles may have been obtained from an analysis that does not fully capture the true interactions between the girders associated with the three-dimensional response of the bridge. These approximate cambers tend to increase the differences between the stress states due to the torsional effects of the dead load and the stress states due to lack-of-fit of the cross-frames.

As a result, slight deviations from the plumb configuration are observed generally at the targeted dead load conditions.

The girders tend to be closer to the theoretical plumb conditions when contiguous intermediate cross-frame lines are utilized since the “back-and-forth” load transfer effects are eliminated. Fig. 5.2.15 provides the layovers of XICSS5; i) constructed with SDLF detailing under steel dead load, and ii) constructed with TDLF detailing under total dead load. The girder layovers associated with the SDLF detailing are found to be very close to the theoretical plumb position of the webs (see Fig. 5.2.15(i)).

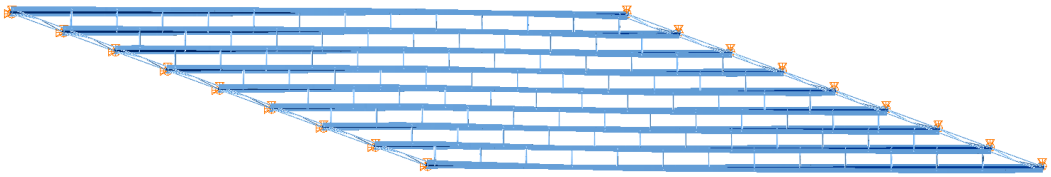

(i) NLF

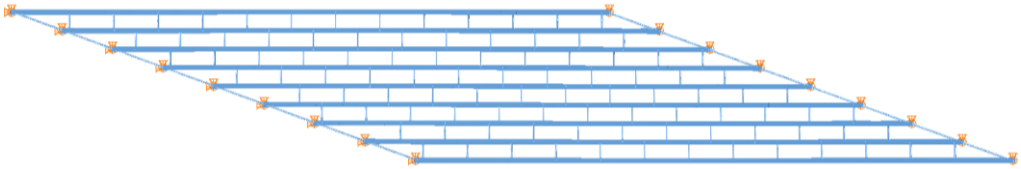

(ii) SDLF

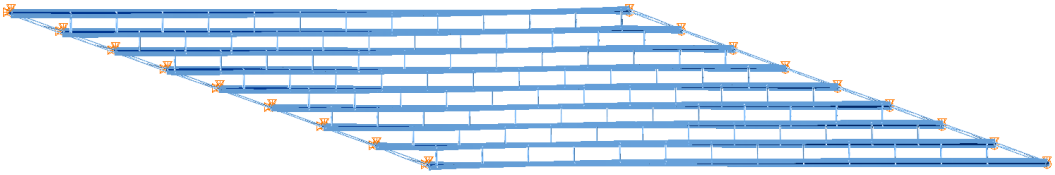

(iii) TDLF

Figure 5.2.10. NISSS54, Deflected shape under steel dead load for different types of detailing methods (magnified by 10x).

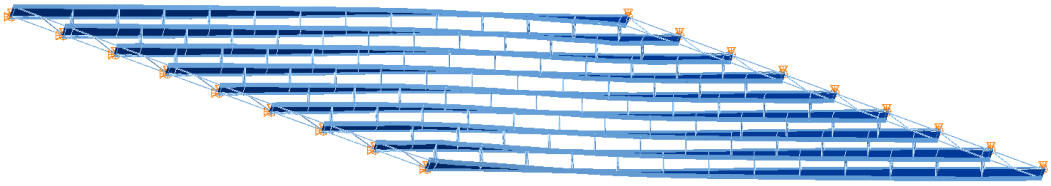

(i) NLF

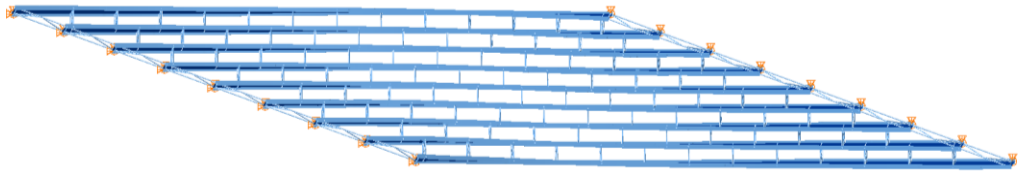

(ii) SDLF

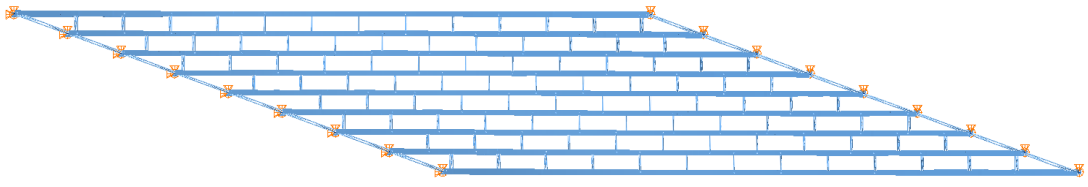

(iii) TDLF

Figure 5.2.11. NISSS54, Deflected shape under total dead load for different types of detailing methods (magnified by 10x).

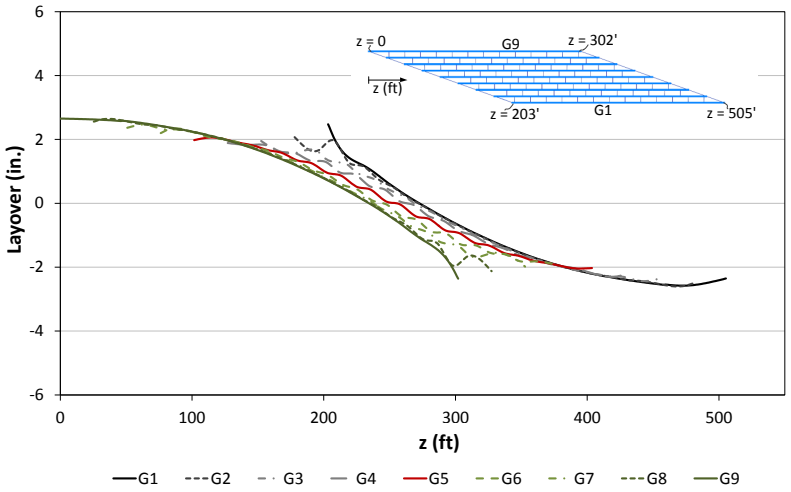

(i) NLF

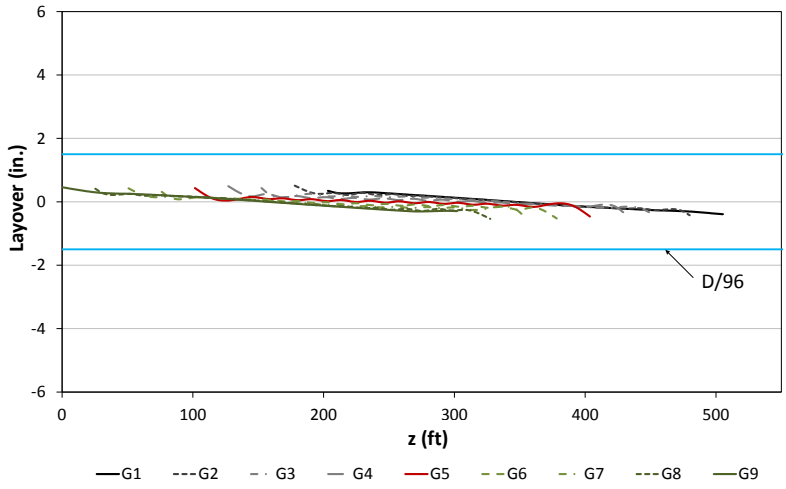

(ii) SDLF

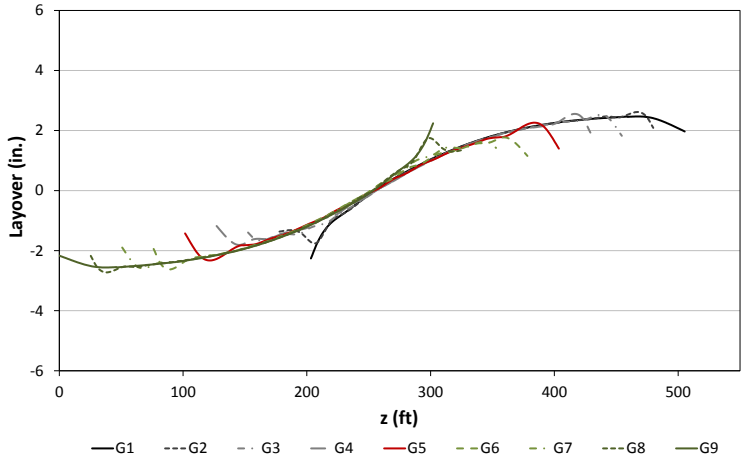

(iii) TDLF

Figure 5.2.12. NISSS54, Layover of girders under steel dead load for different types of detailing methods.

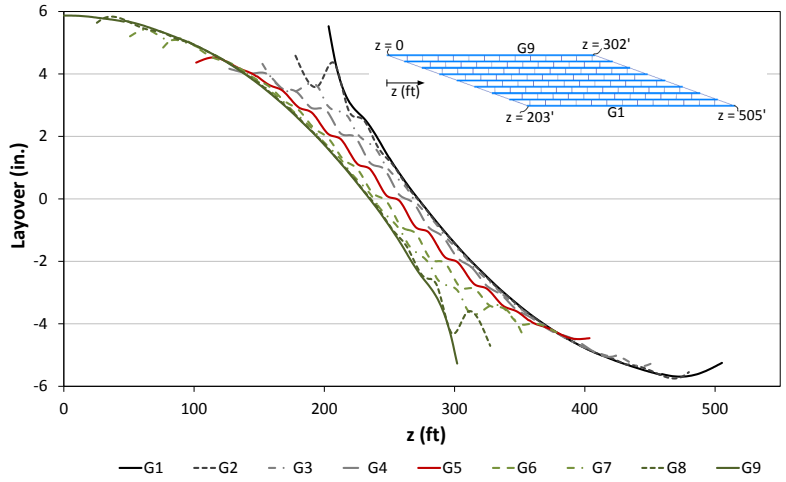

(i) NLF

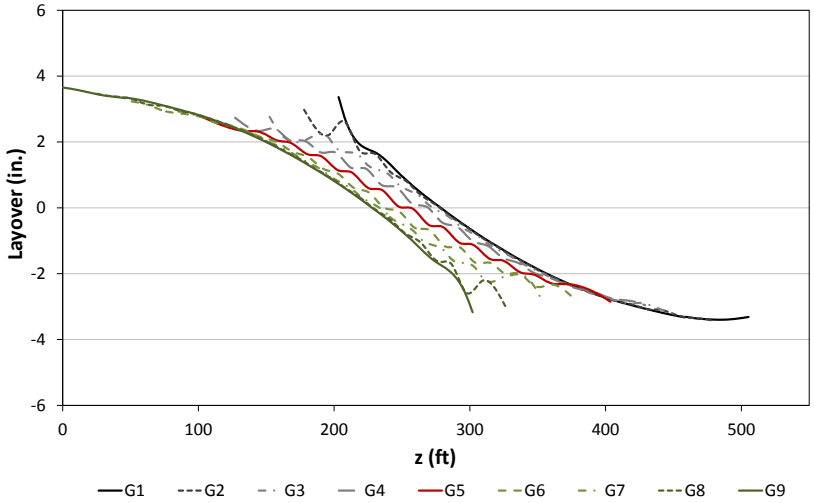

(ii) SDLF

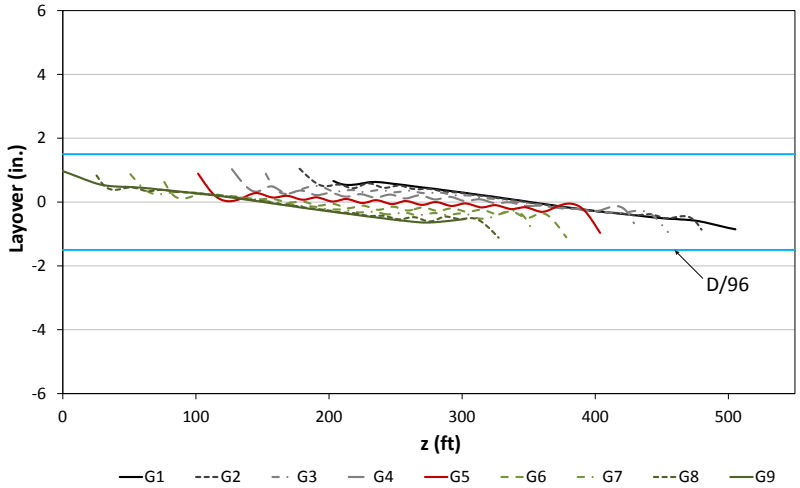

(iii) TDLF

Figure 5.2.13. NISSS54, Layover of girders under total dead load for types of different detailing methods.

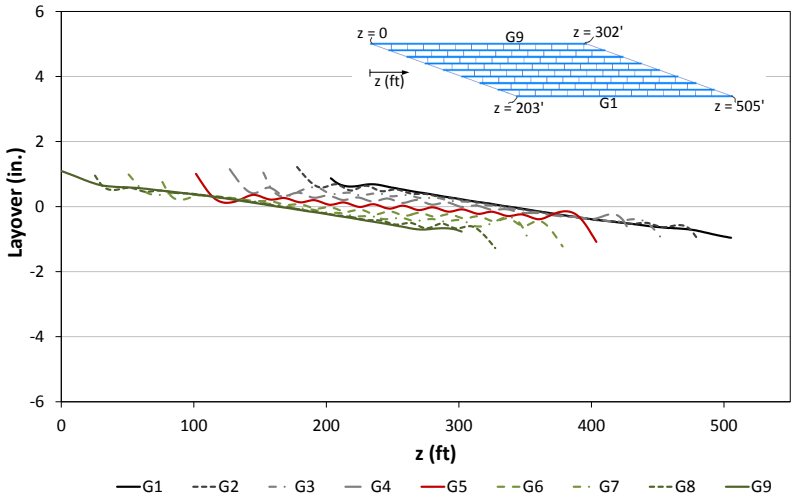

Figure 5.2.14. NISSS54, Superposition of NLF detailing girder layovers and locked-in layovers due to TDLF detailing.

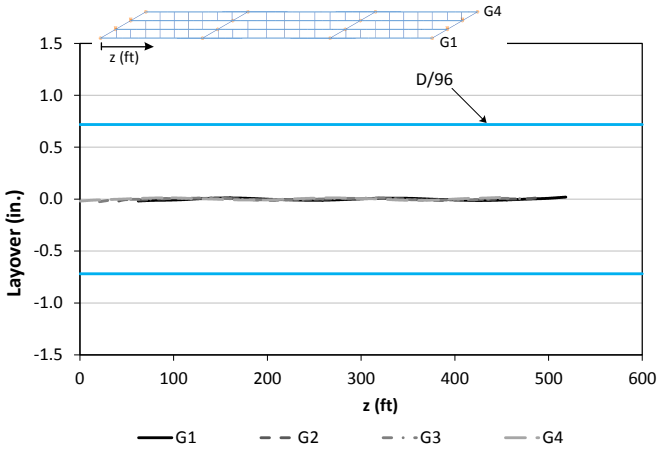

(i) constructed with SDLF under steel dead load

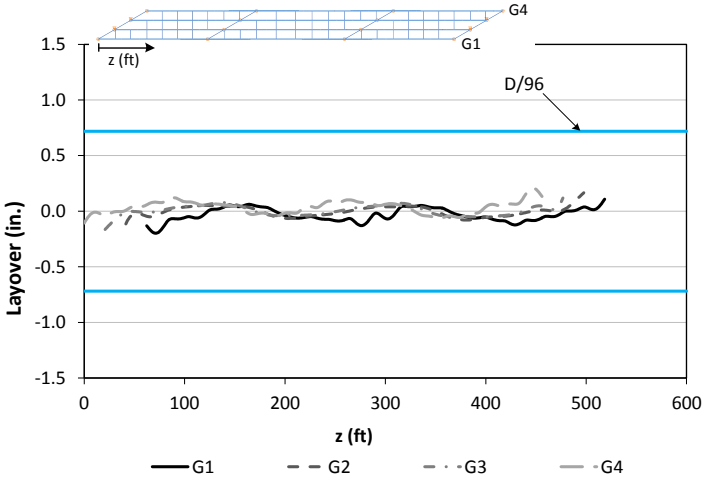

(ii) constructed with TDLF under total dead load

Figure 5.2.15. XICSS5, Layover of girders; (i) constructed with SDLF detailing under steel dead load, (ii) constructed with TDLF detailing under total dead load.

For curved radially-supported bridges, the differential camber between the girders is always negative, moving from the girders that are farther from the center of curvature toward the center of curvature, due to larger deflection of the "outside" girders compared to the "inside" girders. This enforces a twist opposite to the layovers caused by the dead loads. Figures 5.2.16 and 5.2.17 demonstrate the girder layovers due to lack-of-fit forces associated with TDLF detailing for the bridge NISCR2. Figure 5.2.18 illustrates the magnitudes of girder layovers of the bridge NISCR2 under lack-of-fit forces for TDLF detailing. It should be noted from Fig. 5.2.17(ii) that reverse twisting of the curved girders causes cross-section distortion due to the coupling between major-axis bending and torsional rotations. These deformations are largest for the outside girders since they are exposed to larger vertical displacements which are coupled with twisting of the section. It should be noted that one-sided connection plates are used at the fascia girders which are relatively less stiff compared to the interior girders. Also, larger deformations due to locked-in forces associated with DLF detailing are expected for tightly curved girders. For curved and skewed I-bridges combinations of nuisance stiffness effects and curvature effects have to be overcome by reverse twisting. Detailed girder results are shown for curved and skewed bridges in Appendix D.

To sum up, slight deviations from the theoretical plumb configurations are generally observed at the targeted load conditions since the torsional rotations due to locked-in stress effects do not offset the rotations due to dead loads completely. However, it is found from the analytical studies that the deviations from the plumb configurations tend to be less than the commonly used tolerance of ±(web depth, in inches) /96 regardless of the bridge type and geometry. This tolerance is adapted from AASHTO/NSBA (2007) which is used to quantify the deviation from theoretical erected web position for inspection purposes. Figures 5.2.19 and 5.2.20 illustrate two of the extreme cases where significant girder layovers are observed in the bridges if constructed with NLF detailing. However, in both cases these layovers are reduced below the limit of ±(web depth, in inch) /96 with the application of TDLF detailing.

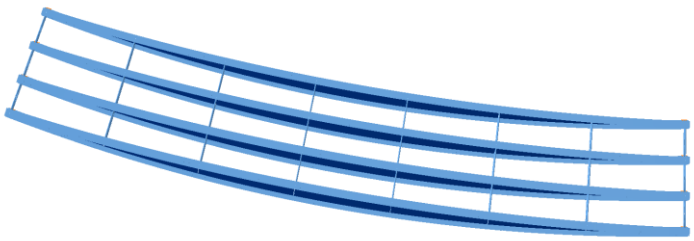

Figure 5.2.16. NISCR2, Deflected shape due to lack-of-fit for to TDLF detailing (magnified by 20x).

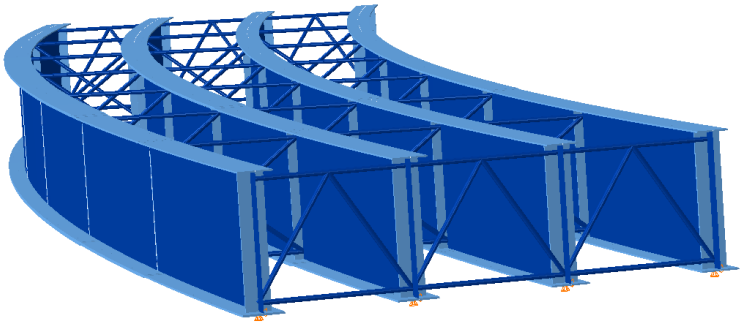

(i) Undeformed shape

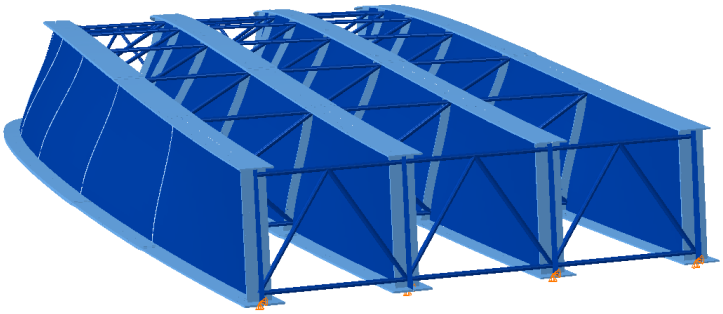

(ii) Deflected shape (Magnified by 30x)

Figure 5.2.17. NISCR2, Deflected shape due to lack-of-fit for TDLF detailing (magnified by 30x).

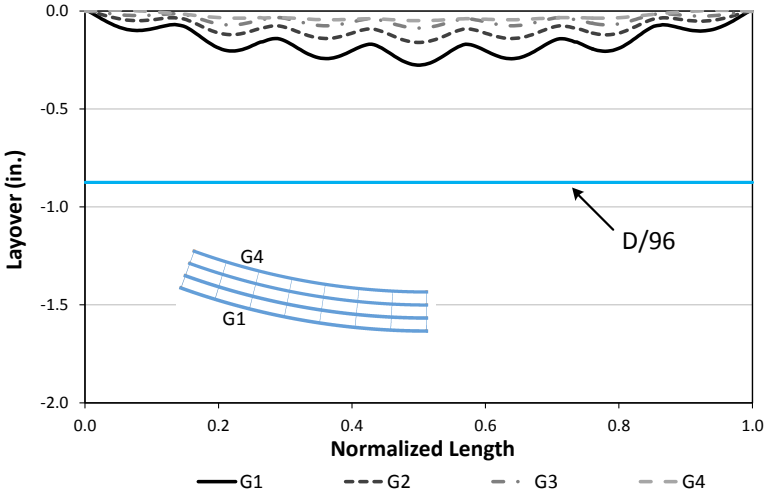

Figure 5.2.18. NISCR2, Layover of girders constructed with TDLF detailing under total dead load.

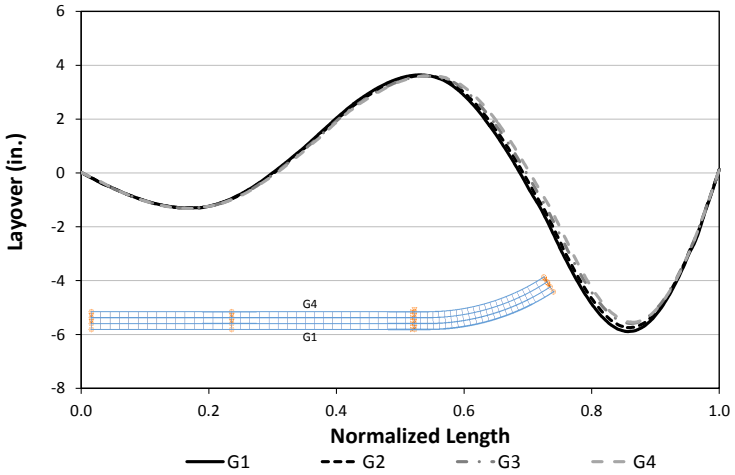

(i) NLF

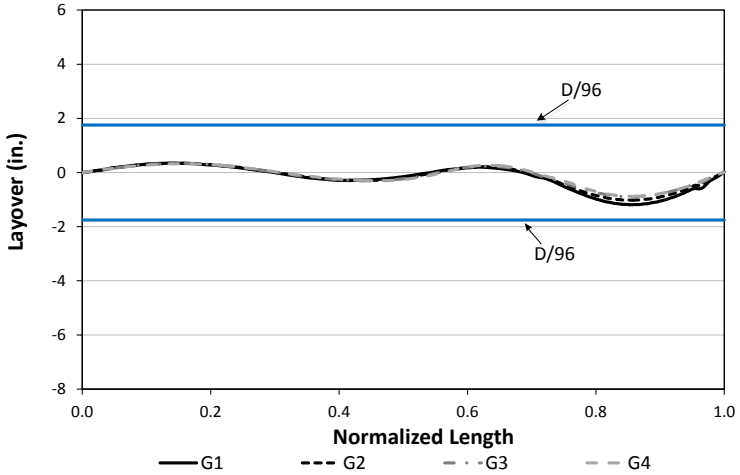

(ii) TDLF

Figure 5.2.19. EICCR11, Girder layovers under total dead load for NLF and TDLF detailing.

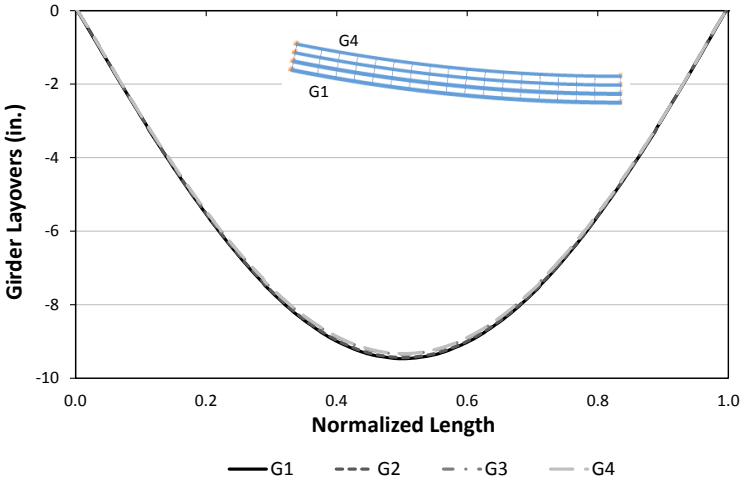

(i) NLF

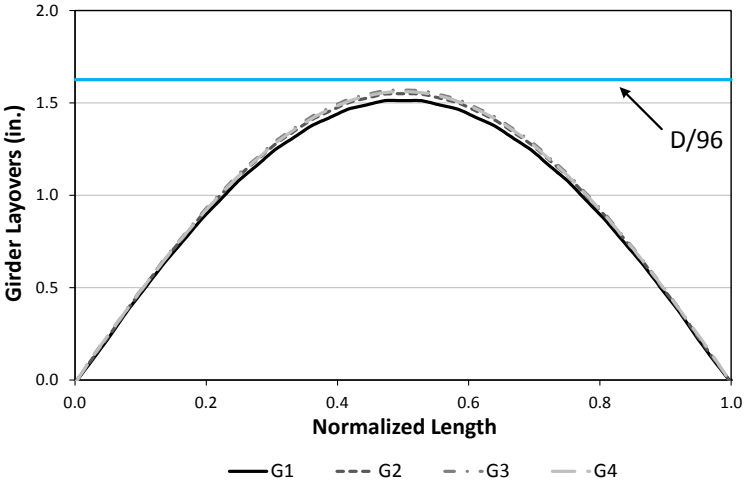

(ii) TDLF

Figure 5.2.20. NISCR5, Girder layovers under total dead load for NLF and TDLF detailing.

5.2.2. *Vertical displacements*

In current practice, the girder camber diagrams are practically always determined without considering the locked-in force effects. However, locked-in forces due to DLF detailing potentially can have a significant influence on the vertical deflections. Hence, the physical bridge may exhibit different vertical deflections than assumed in setting the cambers. This can lead to deviations from the predicted final deck profile and final girder elevations. It is stated in AASHTO/NSBA (2007) that the deviation from the theoretical vertical alignment (elevation) cannot exceed -0, +1/4 inch x (total length, in feet from nearest support)/10. Also, maximum deviation is ¾ inch in cantilever sections or 1.5 inches between supports.

For straight and skewed bridges, the locked-in forces from DLF detailing tend to have a small effect on the vertical displacements. This is because there is little to no coupling between the individual girder vertical displacements and the individual girder twisting for straight I-girders. Additionally, girders are stiff to resist major-axis bending rotations due to lack-of-fit associated with DLF detailing thus the additional vertical deformations are minor. Figure 5.2.21 shows the locked-in vertical displacements of a bridge (NISSS54), constructed with TDLF detailing. For girder G5, the maximum deflection is obtained as -1.32 inches whereas it is -0.77 inches for the girder G1. The deviation tolerance is calculated as 3.75 inches which is larger than the vertical displacements due to locked-in stress effects.

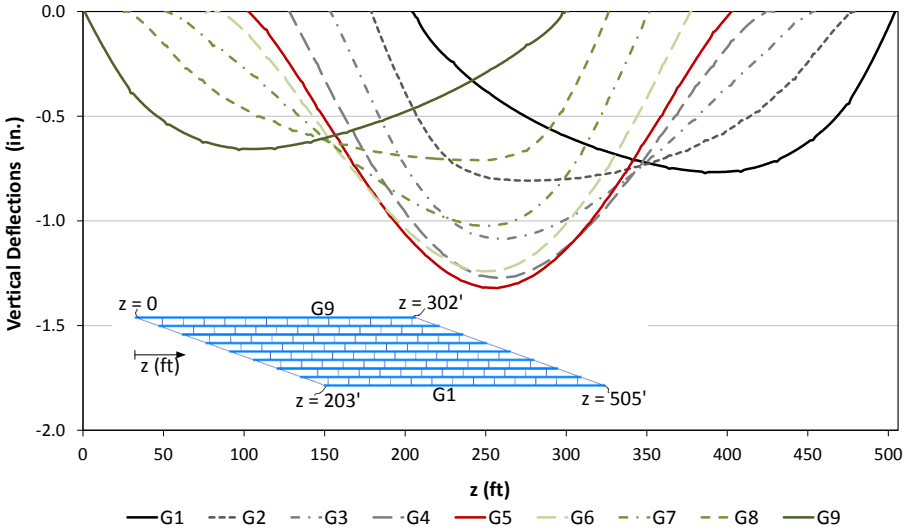

Figure 5.2.21. NISSS54, Vertical deflections under lack-of-fit due to TDLF detailing.

Figure 5.2.22 shows total dead load vertical deflections for the straight-skewed bridge NISSS54 considering each of the types of cross-frame detailing. It can be observed from Fig. 5.2.22 that there is essentially no difference in the vertical deflections of the fascia girders

due to the type of cross-frame detailing in this bridge. Both of these girders exhibit 17 inches of vertical deflection at their mid-span under the total dead load. However, the middle girder (Girder 5) has slightly more than 12 inches of vertical deflection under the total dead load if TDLF detailing is used, whereas it has slightly more than 11 inches of vertical deflection if NLF detailing is used. These small differences in the vertical deflections are due to the restraint provided by the stiff transverse load path. That is, part of the total dead load tributary to girder G5 is distributed transversely to the bearing lines by the staggered cross-frames framing between the obtuse corners of the bridge, combined with the lateral bending resistance of the girder flanges.

The total load vertical deflections are generally offset by the total vertical camber in the girders. In current practice, the above differences in the NLF and TDLF vertical deflections due to lack-of-fit between the girders and cross-frames are practically never accounted for. One can conclude that the 1 inch difference in the vertical deflection of Girder 5 is relatively minor. It can be accommodated in the girder haunch depths when setting the forms for the concrete deck; however, this can occur only if the contractor anticipates the above behavior.

The difference in the vertical displacements due to DLF detailing tends to be minor for the continuous straight and skewed bridges due to continuity effects. Also, the use of continuous cross-frames tends to reduce the back-and-forth behavior of the flanges which lead to relatively smaller locked-in vertical displacements. These cases are illustrated in Fig. 5.2.23, which shows the total dead load vertical displacements of XICSS5, constructed with different types of cross-frame detailing. The differences in the vertical displacements are minor for DLF detailing compared to the case with NLF detailing.

Conversely, for curved radially-supported bridges, the locked-in forces due to DLF detailing generally have a significant effect on the vertical displacements of the girders. This is due to the significant coupling between the major-axis bending and torsion in curved I-girders. Figures 5.2.24 and 5.2.25 show representative examples from the bridges NISCR5 and EICCR11 where excessive locked-in vertical deformations are observed. In these cases, bridges can exhibit different vertical deflections than the ones assumed in setting the cambers (based on NLF detailing) which can result in deviation in the bridge cross-slopes from the intended values or under or over prediction of the deck profile.

The deviation in the total vertical deflections due to DLF detailing can be minor for the bridges with minor overall torsional effects, as shown in Fig. 5.2.26. Also, relatively smaller

locked-in vertical displacements due to DLF detailing are expected for the curved bridges with positive skew angles (counter clockwise direction) compared to the ones with negative skew angles (clockwise direction) since the girder layovers due to curvature effects tend to be reduced by the layovers due to skewed bearing (as illustrated in Fig. 5.2.27 for two representative curved and skewed bridges). The absolute variation in the vertical displacements is found as 0.51 inches for NISCS14 whereas it is 1.57 inches for NISCS15.

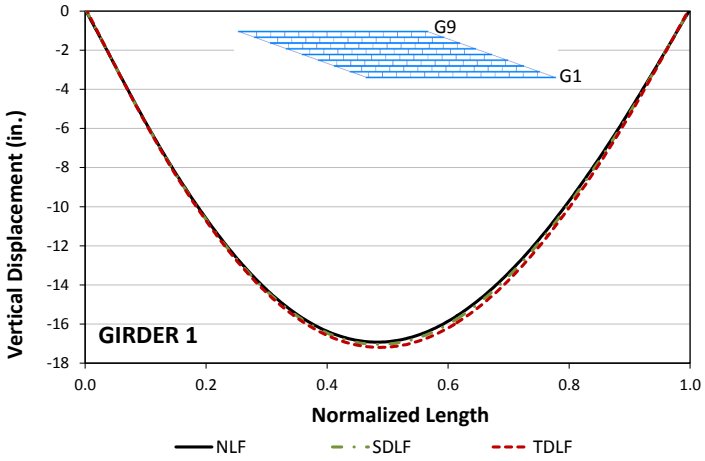

(i) Girder 1

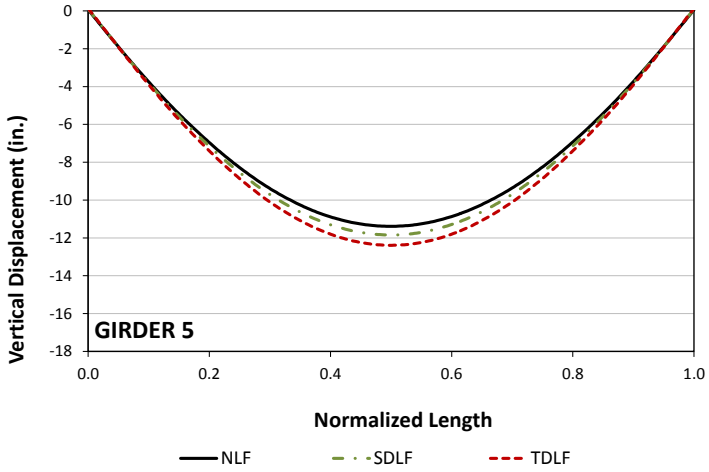

(ii) Girder 5

Figure 5.2.22. NISSS54, Vertical deflections under total dead load for different detailing methods.

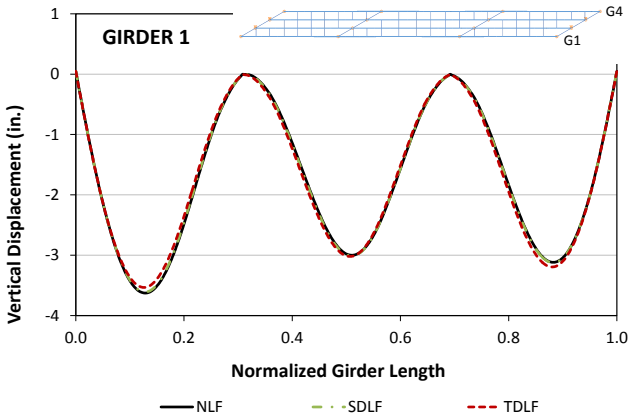

(i) Girder 1

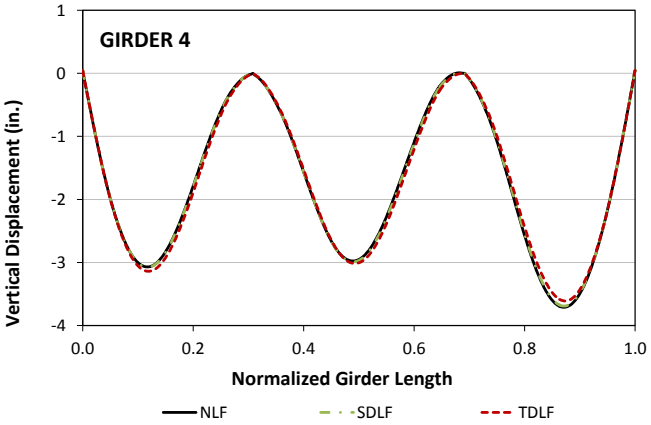

(ii) Girder 4

Figure 5.2.23. XICSS5, Vertical deflections under total dead load for different detailing methods.

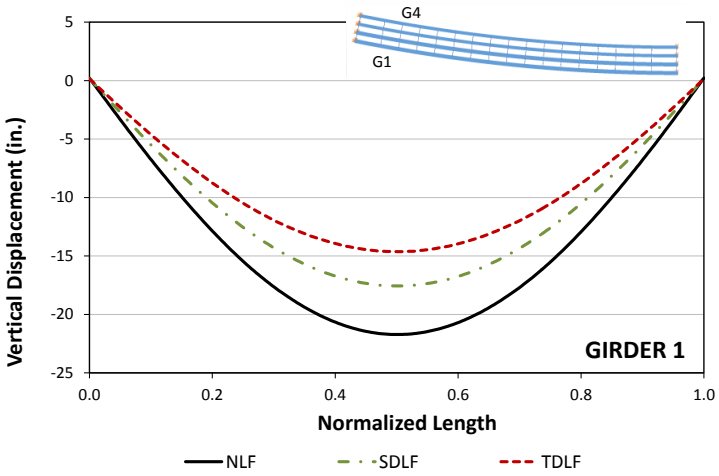

(i) Girder 1

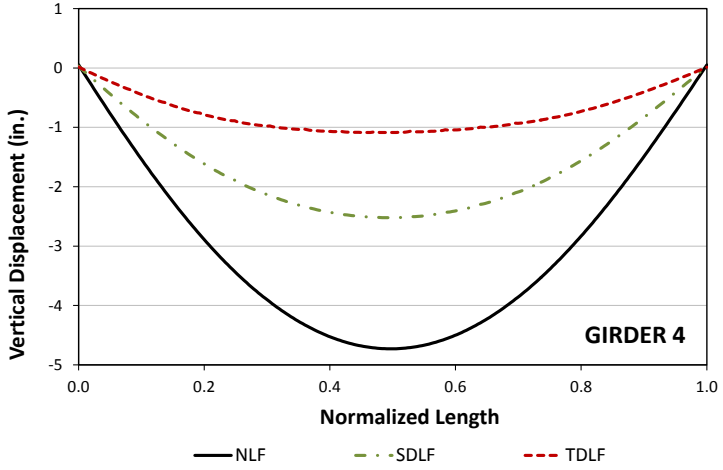

(ii) Girder 4

Figure 5.2.24. NISCR5, Vertical deflections under total dead load for different detailing methods.

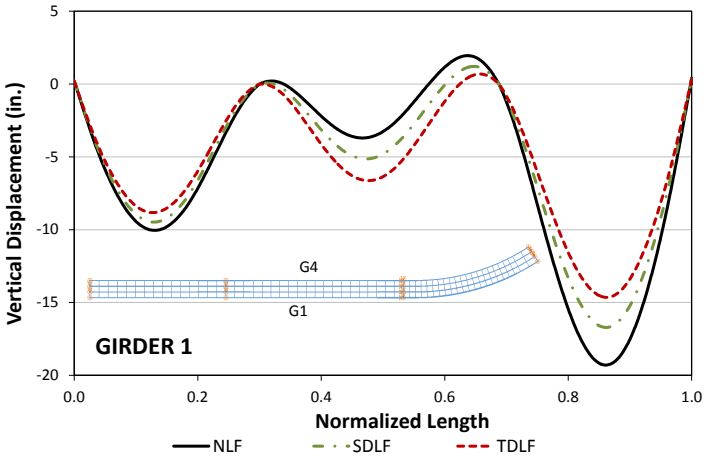

(i) Girder 1

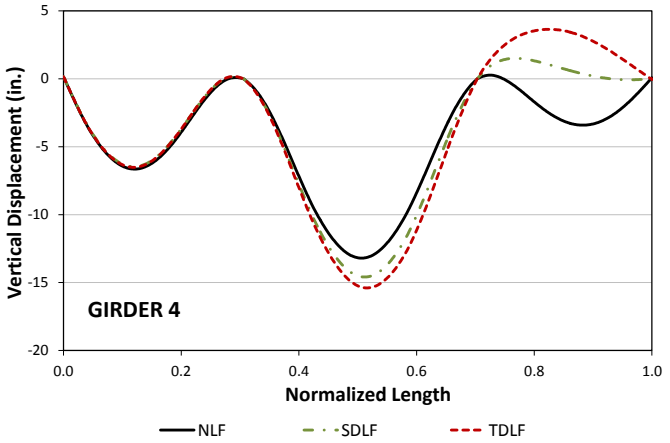

(ii) Girder 4

Figure 5.2.25. EICCR11, Vertical deflections under total dead load for different detailing methods

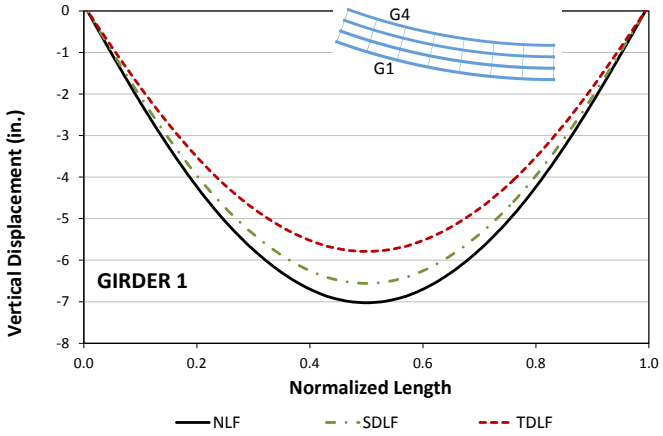

(i) Girder 1

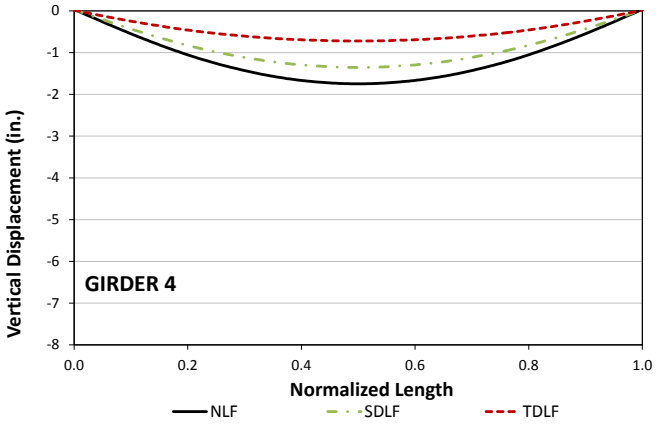

(ii) Girder 4

Figure 5.2.26. NISCR2, Vertical deflections under total dead load for different detailing methods.

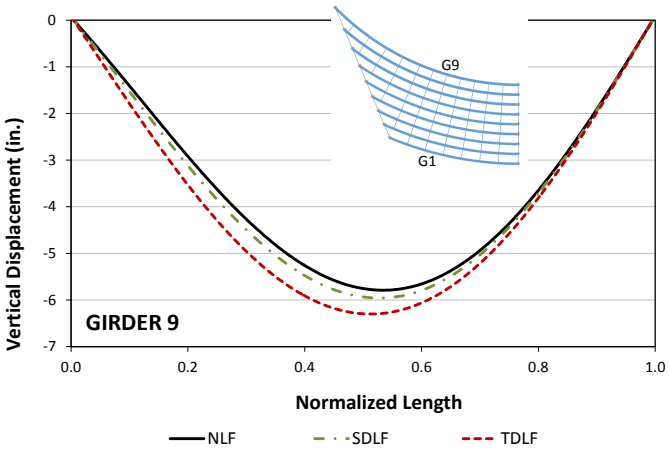

(i) NISCS14, Girder 9

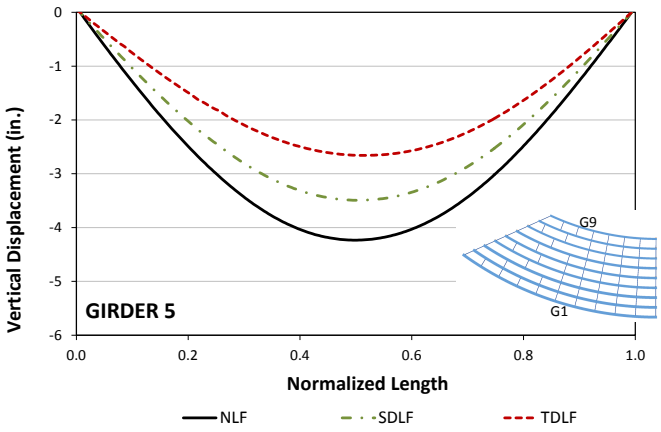

(i) NISCS15, Girder 5

Figure 5.2.27. Selected girder vertical deflections of NISCS14 and NISCS15 under total dead load for different detailing methods

5.2.3. *Estimation of layovers due to locked-in stress effects*

It is shown in the previous sections that the locked-in layovers are approximately opposite to the dead load girder layovers. Skewed end cross-frames are typically relatively rigid compared to the girders within their own plane. The skewed orientation of the cross-frame forces a coupling between the major-axis bending rotation and the torsional rotation of the girder at the bearing, since the in-plane cross-frame deformations are relatively small compared to the other displacements (see Fig. 2.1.1). This compatibility also holds under deflections due to locked-in force effects. Skewed cross-frames tend to rotate about their own skewed axis and warp (twist)

out of their plane to close the lack-of-fit due to DLF detailing. As a result, girder layovers at the skewed bearing line due to lack-of-fit forces can be estimated from

$$\Delta_{x\,LOF} = \Delta_{z.C}\ \tan(\theta) \tag{5.2.1}$$

by using the compatibility between the girders and cross-frames, assuming negligible cross-frame in-plane deformations. $\Delta_{x\,LOF}$ is the girder layover due to locked-in force effects, $\Delta_{z.C}$, is the longitudinal movement due to camber, and θ is the skew angle. The intermediate cross-frame does not fit to the girders in the no-load geometry since it is fabricated for the final plumb geometry. Again, it is emphasized that interior cross-frames typically are relatively rigid compared to the girders in I-girder bridges. For bridges constructed with DLF detailing, the girders, which are relatively flexible, must be twisted in a direction opposite to their dead load torsional rotations to make the connections to the cross-frame. Therefore, the layovers within the span can be estimated from the differential vertical camber between the girders, assuming negligible cross-frame in-plane deformation, as

$$\Delta_{x\,LOF} = h\left(\Delta_{y.C}/s\right) \tag{5.2.2}$$

where , *h* may be approximated as the distance between the centroids of the flanges, $\Delta_{y.C}$ is the differential vertical camber between girders at the intermediate cross-frame location, and s is the spacing between the girders.

Equations 5.2.1 and 5.2.2 tend to provide better estimates for the cases where the locked-in major-axis bending rotation of the girders is minor. Figure 5.2.28 provides locked-in layovers of girders G1 and G5 of NISSS54, constructed with TDLF detailing. Figure 5.2.28 also provides locked-in layover estimations of the girders by using Eqs. 5.2.1 and 5.2.2. It should be noted that the estimated values are close to the finite element analysis predictions. Minor differences are observed due to additional deflections and rotations from locked-in force effects. In the cases with large locked-in vertical displacements (e.g. curved bridges), the induced locked-in longitudinal and vertical displacements should be included in Eqs. 5.2.1 and 5.2.2 to obtain more accurate predictions. Figure 5.2.29 provides the locked-in layover estimations by considering the additional locked-in vertical and longitudinal displacements in Eqs. 5.2.1 and 5.2.2.

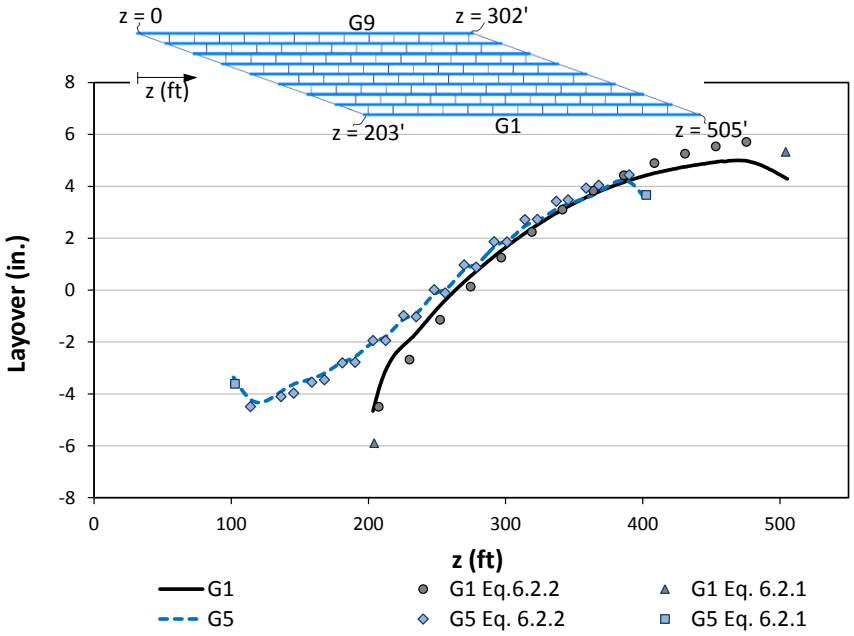

Figure 5.2.28. NISSS54, Estimated locked-in layovers from Eqs. 5.2.1 and 5.2.2.

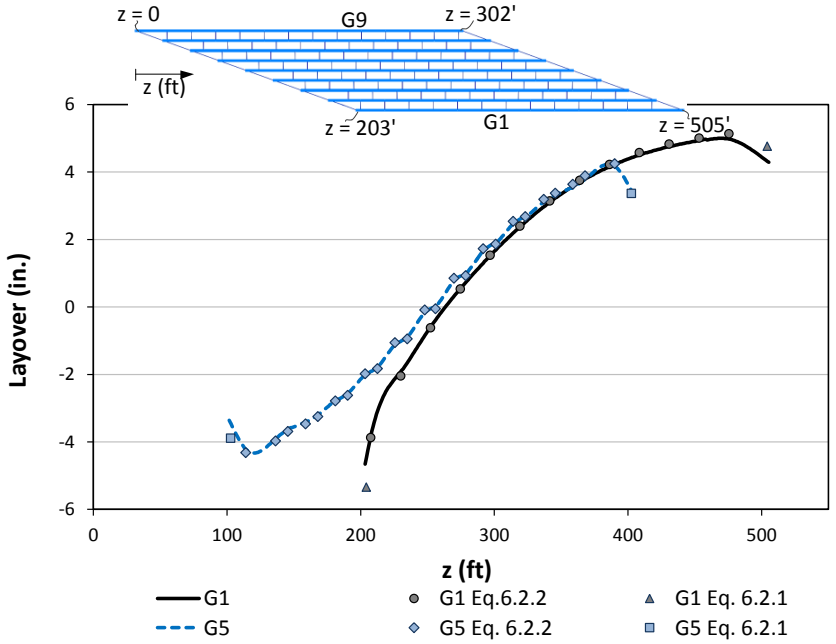

Figure 5.2.29. NISSS54, Estimated locked-in layovers from Eqs. 5.2.1 and 5.2.2 by considering locked-in longitudinal and vertical displacements.

5.3. Impact of Dead Load Fit Cross-Frame Detailing on Cross-Frame Forces

In straight skewed bridges constructed with NLF detailing, relatively large forces tend to be developed in the cross-frames along the shorter (and stiffer) diagonal direction between the corners of the structure. For instance, Fig. 5.3.1 shows the distribution of the largest total dead load cross-frame component axial forces in each of the cross-frames throughout the bridge NISSS54 for NLF detailing. The most highly loaded cross-frame members are colored dark red, while the more lightly loaded cross-frame members are shaded light grey. The largest magnitude cross-frame component axial force is labeled next to each of the cross-frames in the picture. In addition, the total sum of the absolute value of all the cross-frame component axial forces is shown in the upper right corner of the figure. Additionally, the mean of the diagonal, top and bottom chord forces and maximum and minimum of the diagonal, top and bottom chord axial stresses are reported at the left bottom corner.

For NLF detailing (see Fig. 5.3.1), the cross-frames along the short direction between the obtuse corners of the bridge are the ones that are most highly stressed. In Fig. 5.3.1, the top and bottom chords of the cross-frames are the most highly loaded in all the cross-frames except for a few cross-frames close to the obtuse corners, where the diagonals are more heavily loaded. These patterns are consistent with the concept that the above cross-frames are predominantly developing internal bending moments and shear forces associated with a “simply-supported” load transfer in the short direction between the obtuse corners of the bridge. The diagonals in the bearing line cross-frames near the obtuse corners experience particularly large forces (475 kips).

Figure 5.3.2 illustrates this transverse load path in the bridge NISSS54 by indicating the magnitude of the largest component force in each of the intermediate cross-frames, normalized by the largest cross-frame component force. The cross-frames with ratios larger than 0.5, located between the obtuse corners of the bridge, are shaded in red.

Additionally, Fig. 5.3.3 provides the contour of total dead load cross-frame forces of the bridge NISSS54 for NLF detailing. Tension forces are shown in red contours whereas compressional forces are shown in blue contours. The maximums of the diagonal, top and bottom chord forces are also shown in Fig. 5.3.1.

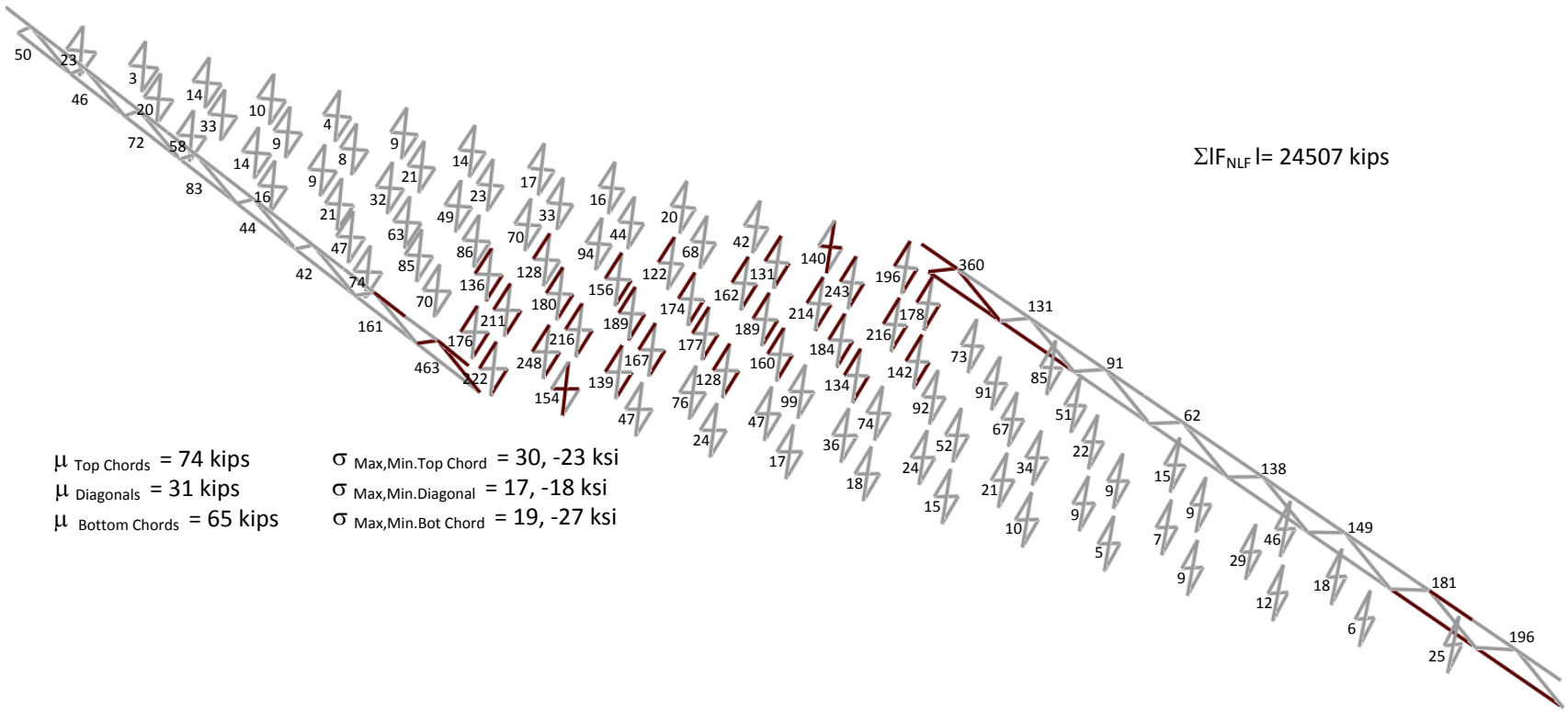

Figure 5.3.1. NISSS54, maximum amplitude of the component axial forces in each of the cross-frames under total dead load (NLF detailing).

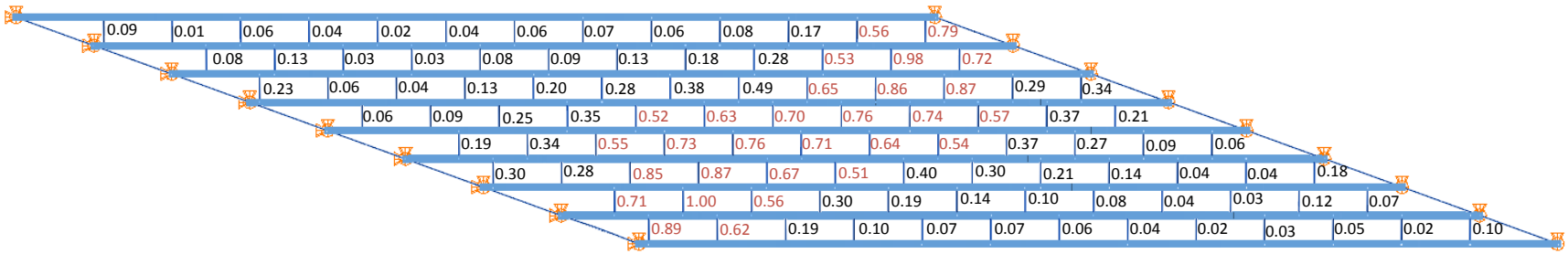

Figure 5.3.2. NISSS54, Normalized maximum amplitude of the component axial forces in each of the cross-frames under total dead load (NLF detailing).

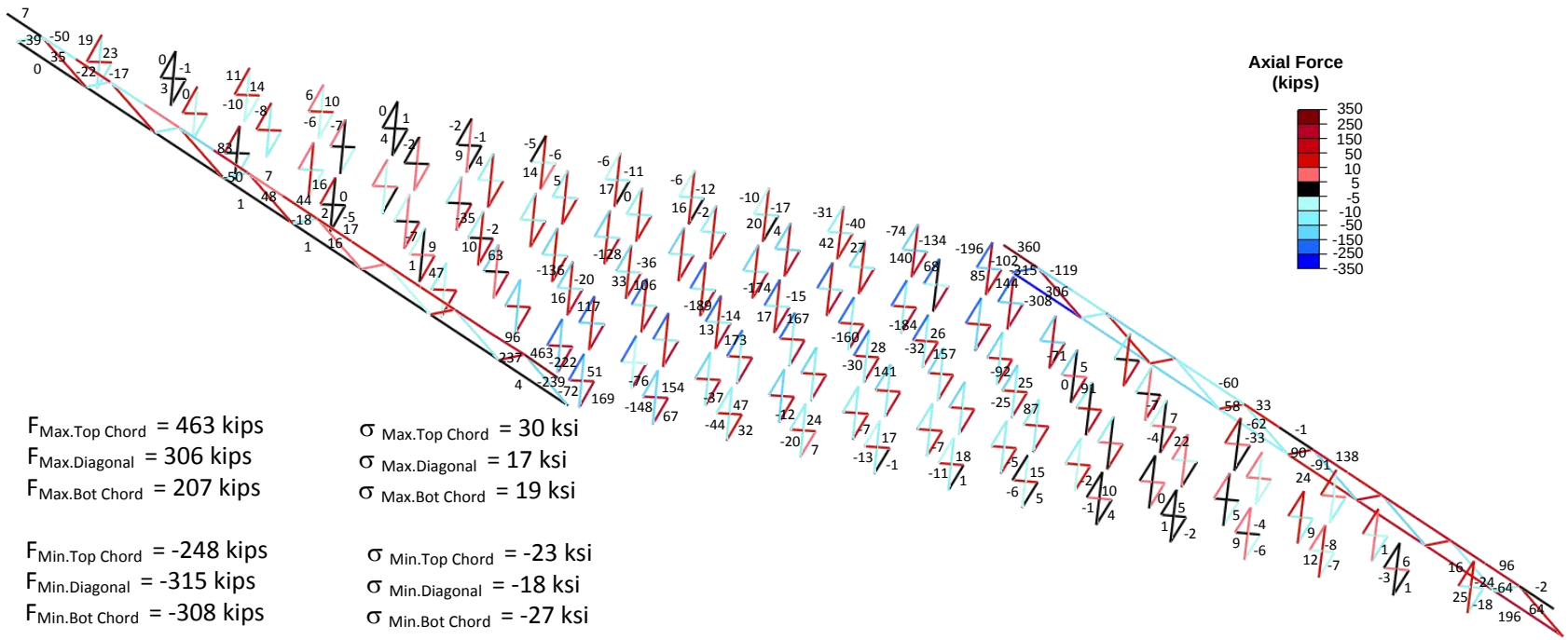

Figure 5.3.3. NISSS54, Cross-frame force contours under total dead load (NLF detailing).

For the bridges constructed with DLF detailing, large locked-in cross-frame forces develop on the stiff transverse load paths, at the places with relatively large lateral stiffness of the adjacent girders and at the locations with large differential camber. Figure 5.3.4 demonstrates the locked-in cross-frames of two girder system that are constructed with TDLF detailing. It is clear from Fig. 5.3.4 that induced diagonal forces are larger than the forces in the top and bottom chords. These cross-frame forces are induced from the torsional movements due to lack-of-fit. Also, relatively larger cross-frame forces tend to develop for the interior cross-frames at the places where the girder needs to be twisted the most (see Fig.5.3.4). This is typically the cross-frame locations with relatively large differential vertical cambers since the girder needs to be twisted further to connect the cross-frames. Differential camber between the girders is shown for the bridge NISSS54 in Fig. 5.2.1. This behavior is found to be typical for the bridges that are studied.

Figure 5.3.5 illustrates the typical induced diagonal forces due to lack-of-fit for the cross-frame locations with positive and negative differential camber between the girders. Again, these forces are induced from the torsional movements due to lack-of-fit associated with DLF detailing. For cross-frame locations with a positive differential camber between the girders, compressive forces are generated for bottom diagonals where tensile forces are generated for top diagonals. Top and bottom diagonals are illustrated in Fig. 5.3.5. This behavior is opposite for the cross-frame locations with a negative differential camber between the girders. It should be noted that top and bottom chord forces due to lack-of-fit forces are not zero but relatively lower than the diagonal forces associated with lack-of-fit forces.

The stiffness of the overall system changes during the construction of the bridges which can influence the cross-frame froces. Figure 5.3.6 demonstrates the locked-in cross-frame forces of the completed bridge NISSS54. If cross-frame forces from Figs. 5.3.4 and 5.3.6 are compared, the forces increased along the stiff transverse load path by the addition of the adjacent girders. For instance, diagonal locked-in forces increase from 41 kips to 129 kips for the cross-frame close to the left skewed cross-frame location at the acute corner. It is also clear from Figs. 5.3.4 and 5.3.6 that top and bottom chord forces increase significantly along the stiff transverse load path. For instance, top chord forces increase from 19 kips to 173 kips and bottom chord forces increase from -33 kips to -124 kips for the cross-frame close to the left skewed cross-frame

location at the acute corner. It should be note that locked-in cross-frame diagonal forces are still relatively large at the places with the large differential vertical camber between the girders.

For straight bridges constructed with TDLF detailing, the locked-in cross-frame forces are approximately equal and opposite to the total dead load forces in the regions having the largest transverse stiffness, i.e., in the highlighted region of Fig. 5.3.2. However, the locked-in forces in the cross-frames tend to be substantially different than the dead load forces outside of this region (see Figs. 5.3.3 and 5.3.6).

Large locked-in forces can be developed outside the stiff transverse load paths depending on the relative lateral stiffness of the adjacent girders and the differential camber. These cross-frame locations are typically observed at intermediate cross-frames locations that are at framed close to the skewed bearings.

It should be emphasized that the dead load cross-frame forces from a NLF analysis are not the opposite of the lack-of-fit forces from a lack-of-fit analysis or vice-versa. These two sets of forces can be close to being equal and opposite in the regions of the bridge having the largest transverse stiffness, but in other regions, they can be substantially different. This is because stresses and deformations induced by DLF detailing are not the same as the stresses and deformations induced by the dead loads.

In the case of the bridge shown in Fig. 5.3.1, the cross-frames in the vicinity of the short direction between the obtuse corners of the bridge tend to have their total dead load forces mostly relieved by the effects of the TDLF detailing, while the cross-frames in the vicinity of the acute corners tend to have their total dead load forces increased relative to the NLF case. Figure 5.3.7 shows the distribution of the largest total dead load cross-frame component axial forces in each of the cross-frames throughout the bridge NISSS54 associated with TDLF detailing. The most highly loaded cross-frame members are shown in the darker color, while the more lightly loaded cross-frame members are shaded light grey. One can observe that the cross-frame forces along the stiff diagonal direction are significantly reduced by the TDLF detailing, but they are not zero. In addition, the forces in several of the cross-frame diagonals near the acute corners are significantly increased. For instance, maximum amplitude of the total dead load component axial force for the end cross-frame at the left obtuse corner is decreased to 55 kips from 460 kips due TDLF detailing, whereas the ones for the intermediate cross-frames at the obtuse corners is increased from 23 kips to 133 kips due to TDLF detailing. Similarly, the

maximum amplitude of the total dead load component axial force for the first intermediate cross-frame at the obtuse corner of the left bearing line is decreased to 52 kips from 222 kips due to TDLF detailing.

In straight-skewed bridges constructed with TDLF detailing, cross-frames located along the stiff transverse load paths may see their largest forces during the steel erection since the locked-in cross-frame forces are not yet relieved by the dead load forces from the deck weight. Figures 5.3.8 and 5.3.9 provide the distribution of the largest steel dead load cross-frame component axial forces in each of the cross-frames throughout the bridge NISSS54 associated with NLF and TDLF detailing cases respectively. The total absolute sum of the largest steel dead load cross-frame component axial forces associated with the TDLF detailing is 1.95 times the ones associated with the NLF detailing case. Conversely, straight bridges constructed with SDLF detailing tend to see the lowest cross-frame forces under the steel dead load. Figure 5.3.10 demonstrates the distribution of the largest steel dead load cross-frame component axial forces in each of the cross-frames throughout the bridge NISSS54 for SDLF detailing case. The total absolute sum of the largest steel dead load cross-frame component axial forces associated with the SDLF detailing is 0.71 times the ones associated with the NLF detailing case.

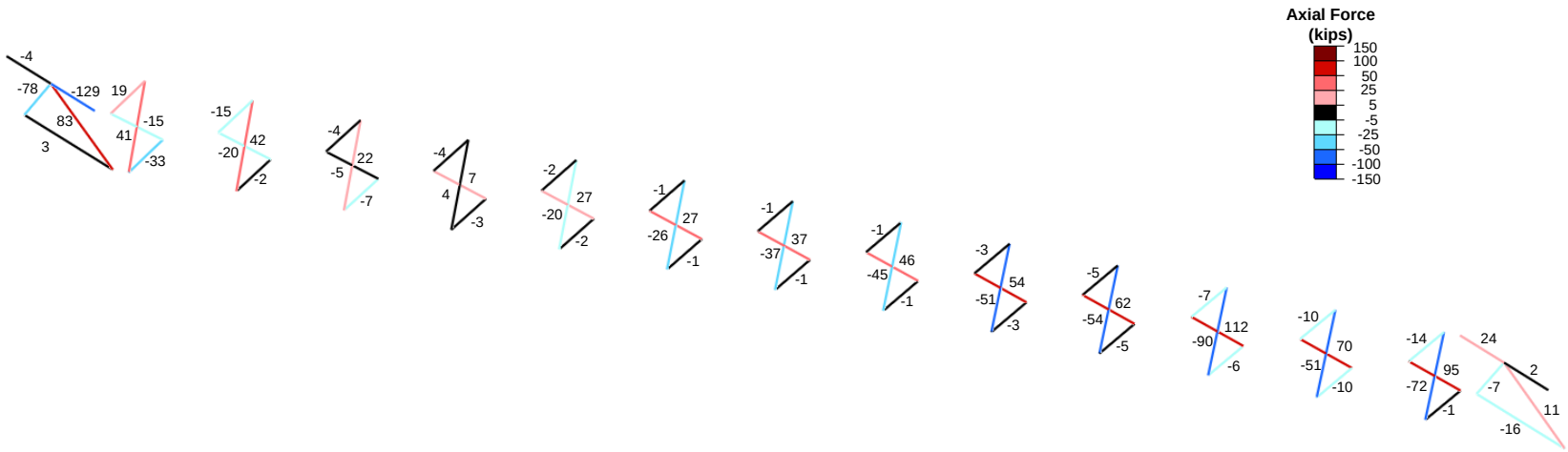

Figure 5.3.4. NISSS54, Cross-frame forces between Girder 1 and 2 under lack-of-fit due to TDLF detailing.

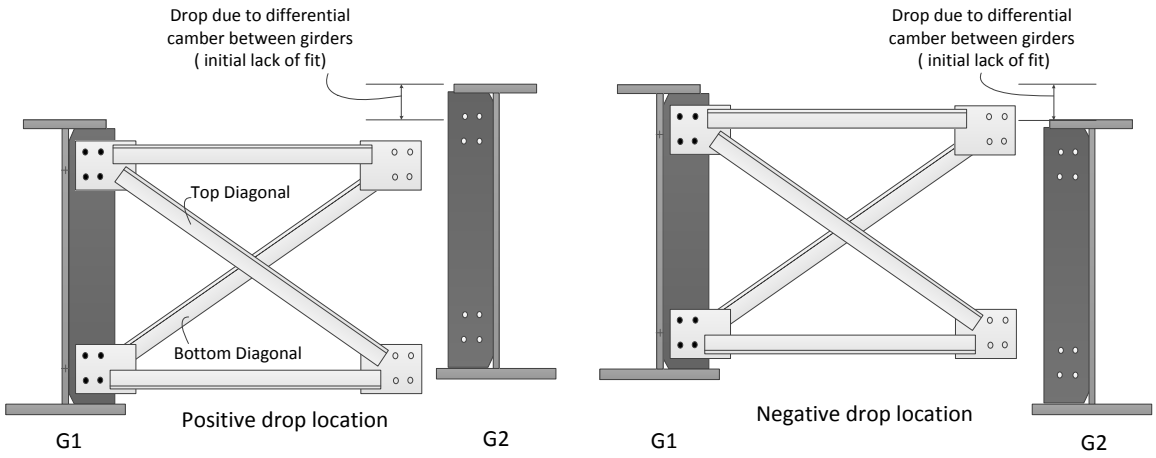

(i) Initially plumb no-load geometry of girders

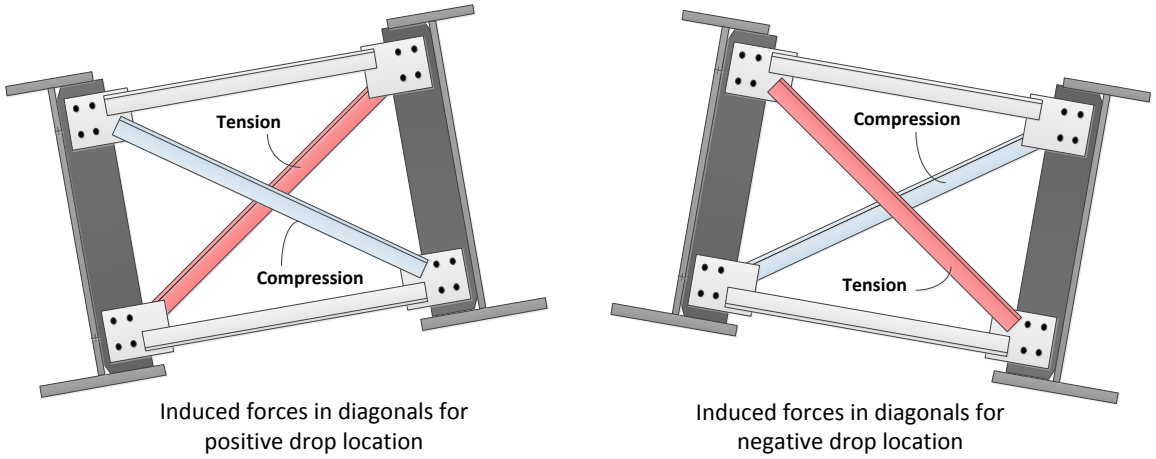

(ii) Cross-frames connected in ideal initial no-load geometry

Figure 5.3.5. Induced diagonal forces due to lack-of-fit for opposite differential deflection locations.

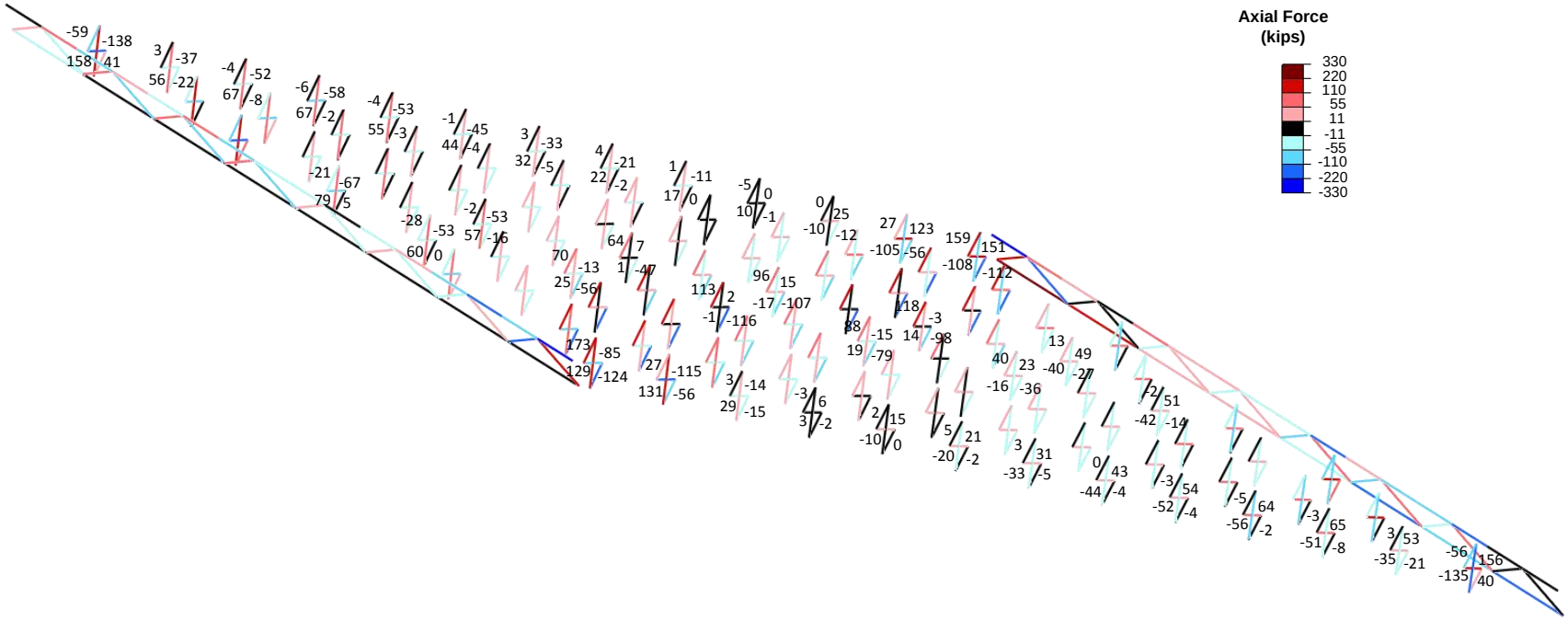

Figure 5.3.6. NISSS54, Cross-frame forces under lack-of-fit due to TDLF detailing.

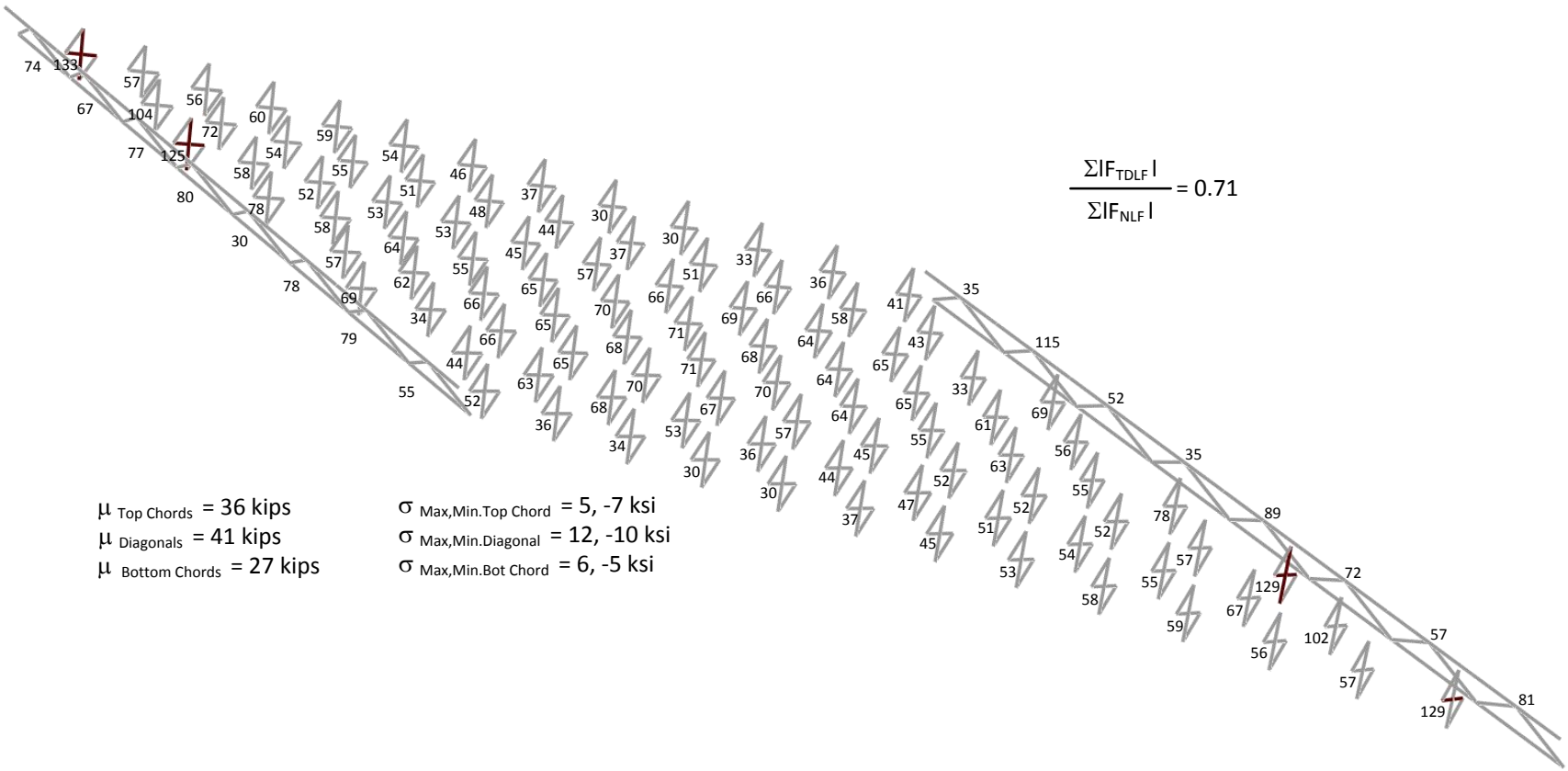

Figure 5.3.7. NISSS54, maximum amplitude of the component axial forces in each of the cross-frames under total dead load (TDLF detailing).

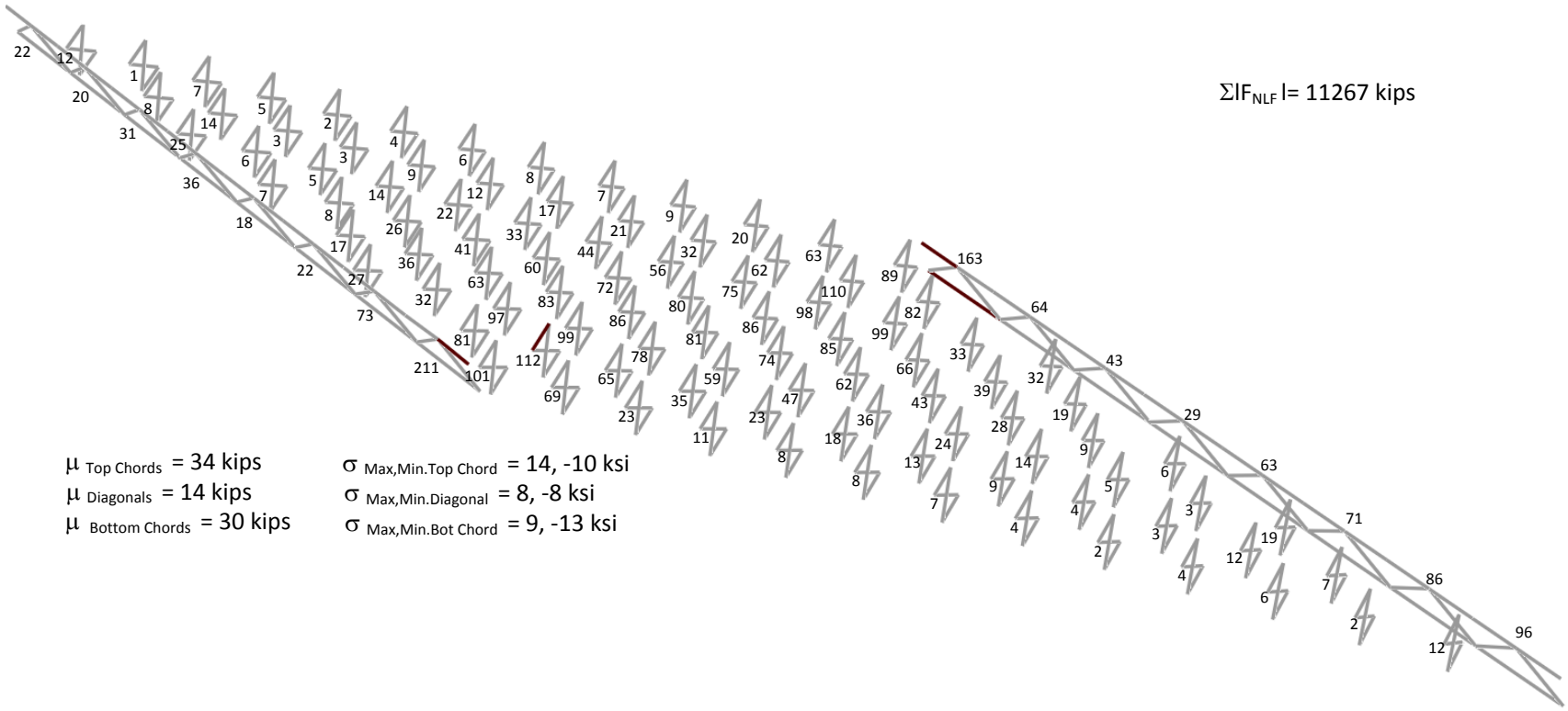

Figure 5.3.8. NISSS54, maximum amplitude of the component axial forces in each of the cross-frames under steel dead load (NLF detailing).

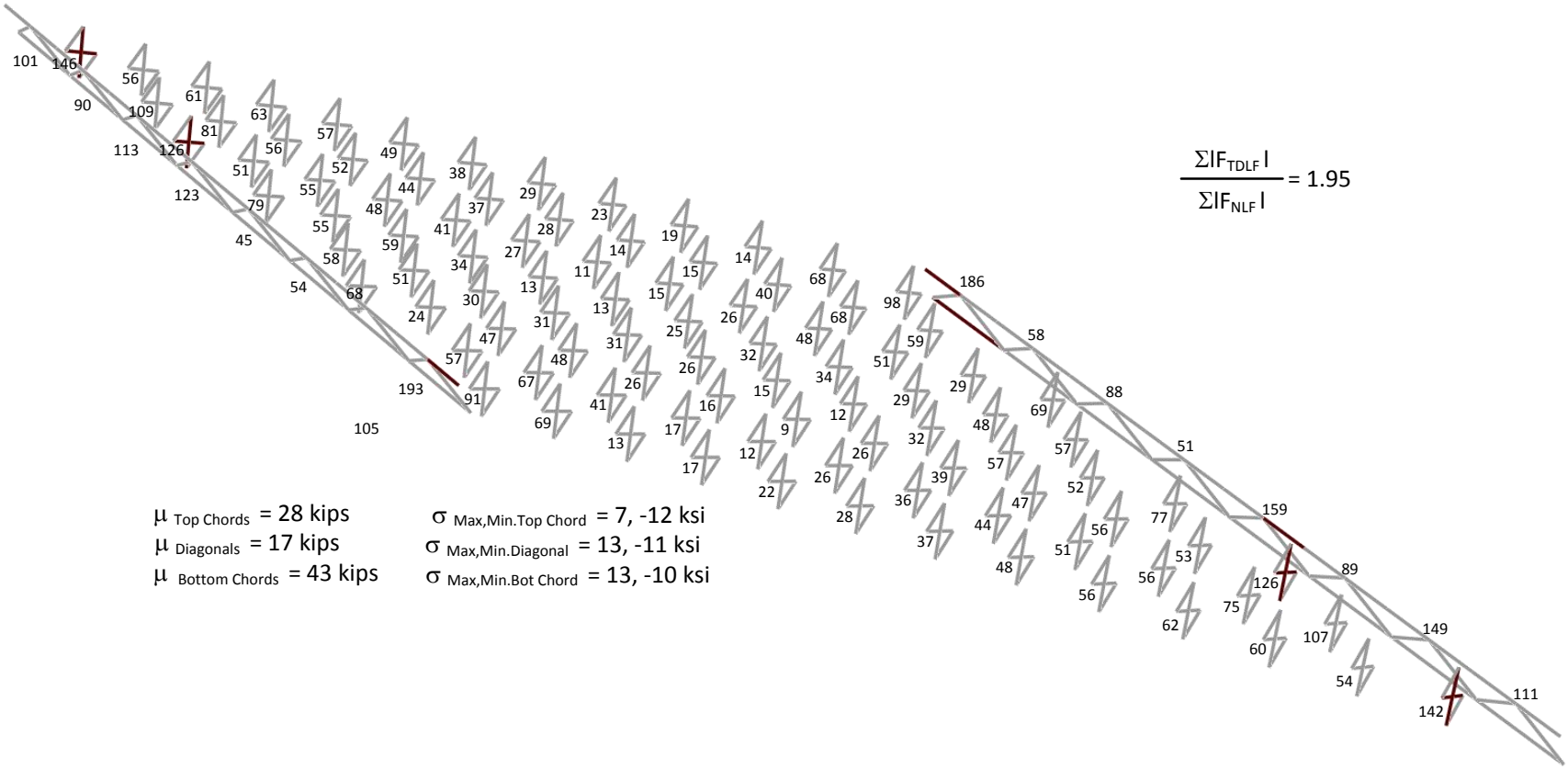

Figure 5.3.9. NISSS54, maximum amplitude of the component axial forces in each of the cross-frames under steel dead load (TDLF detailing).

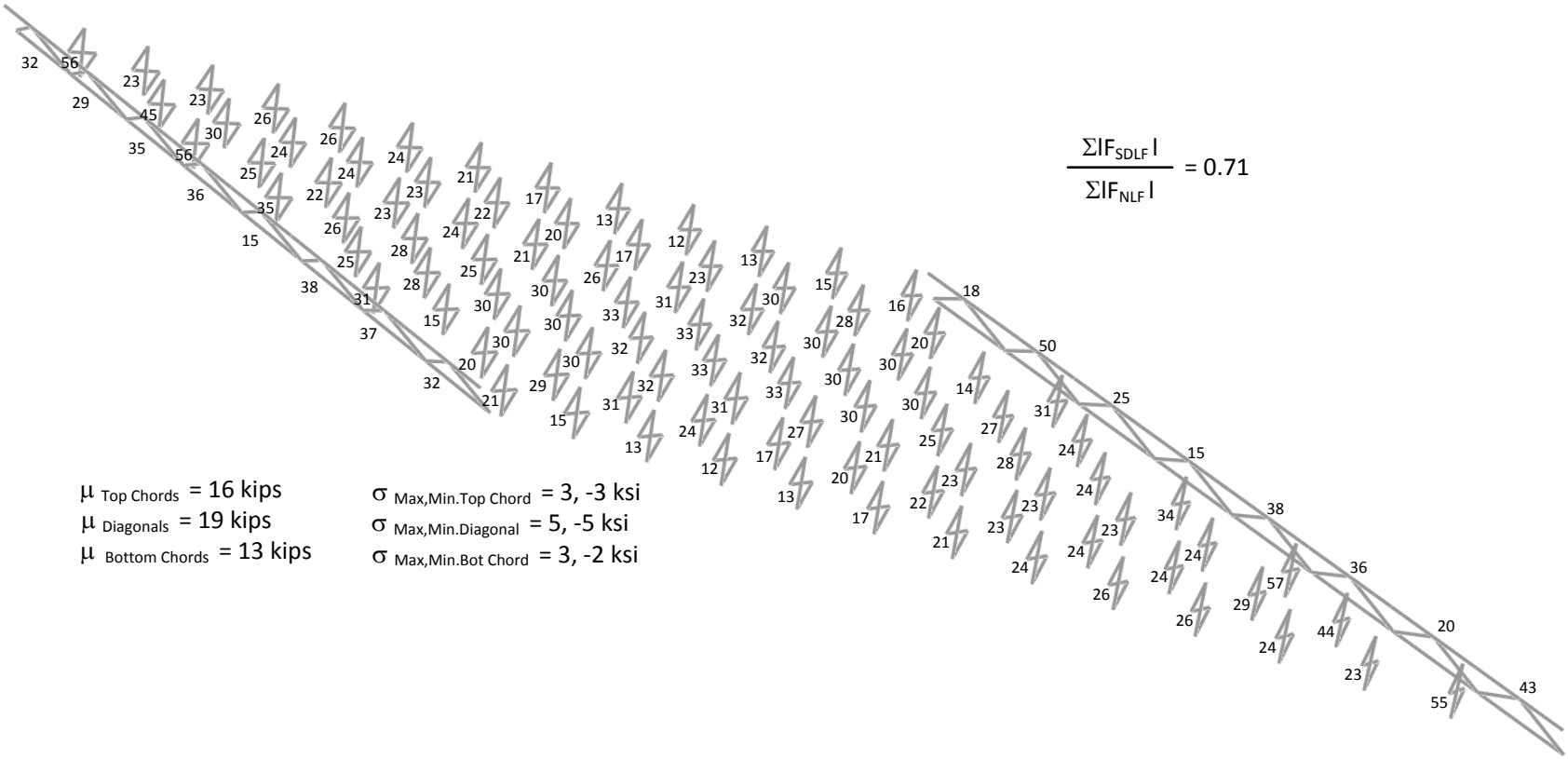

Figure 5.3.10. NISSS54, maximum amplitude of the component axial forces in each of the cross-frames under steel dead load (SDLF detailing).

The cross-frames are primary load carrying members in curved bridges. Figure 5.3.11 provides a total dead load cross-frame axial force contour schematic for a representative curved radially-supported bridge NISCR2 constructed with NLF detailing. It is clear from Fig. 5.3.11 that the top and bottom chords are the most stressed members. Moreover, tensile forces are generated on the top diagonals whereas compressive forces are generated on the bottom diagonals. This behavior can be understood on a simplified model by assuming the girders resist the bending moment entirely by axial forces in the flanges. This force can be approximated by distributing the girder major-axis bending stress (*M*) at a cross-section to the flanges as

$$P_{flange} = M/D \tag{5.3.1}$$

where *D* is the distance between the centroid of top and bottom flange. However, these forces are not collinear due to the curved geometry; thus, lateral forces (*H*) have to be developed on the girders to satisfy the force equilibrium, as shown in Fig. 5.3.12. If these lateral forces (*H*) are carried to the cross-frames (assuming cross-frames frame directly to the girder flanges), shear forces (*V*) are needed to satisfy the moment equilibrium at the cross-frame, as illustrated in Fig. 5.3.13. The illustrated forces can only be generated by having the tensile forces on bottom diagonals and compressive forces on the second diagonals. Moreover, top chords develop tensile forces while bottom chords develop compression forces.

It should be noted from Fig. 5.3.11 that diagonal forces due to the dead loads are in the same direction with the forces corresponding to locked-in diagonal forces at the cross-frame locations with negative differential camber between the girders. Figure 5.3.14 illustrates the locked-in cross-frame force contour of the bridge NISCR2, constructed with TDLF. It can be observed from Fig. 5.3.14 that locked-in cross-frame diagonal forces are relatively larger for the locations with larger differential camber between the girders. Differential camber between the girders is shown for bridge NISCR2 in Fig. 5.2.2.

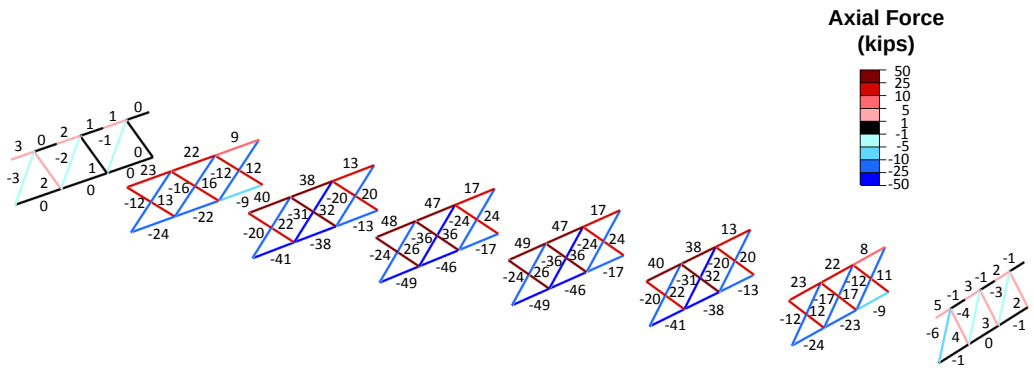

Figure 5.3.11. NISCR2, Cross-frame forces under total dead load (NLF detailing).

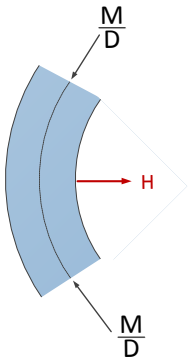

Figure 5.3.12. Simplified free-body diagram at cross-frame location.

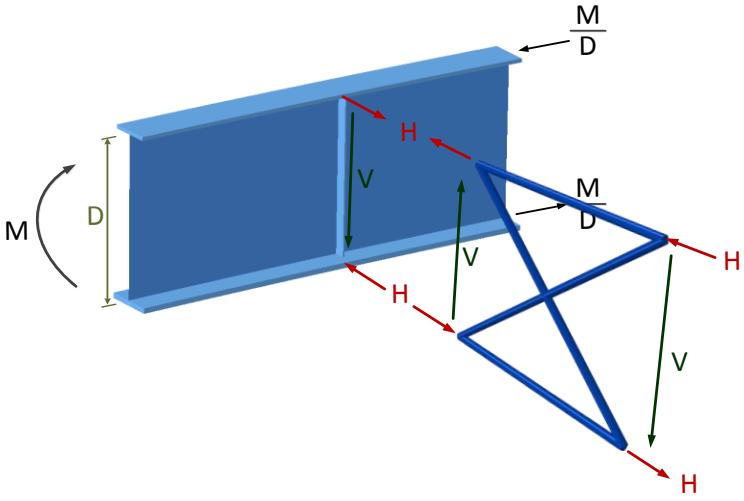

Figure 5.3.13. Simplified free-body diagram of top flange at cross-frame location.

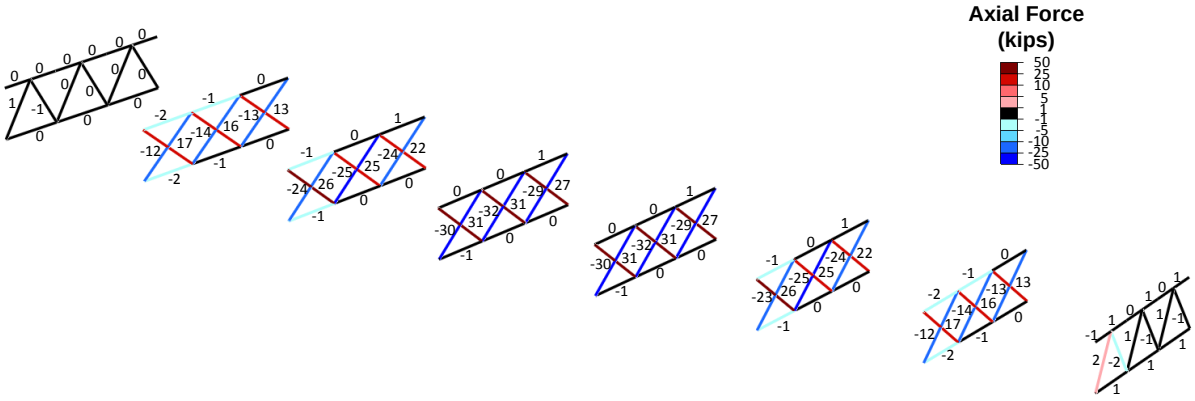

Figure 5.3.14. NISCR2, Cross-frame forces due to lack-of-fit (TDLF detailing).

In curved radially-supported bridges, locked-in cross-frame forces due to DLF detailing tend to add with the dead load forces in all the cross-frames. It should be noted that SDLF detailing

generally results in smaller locked-in forces compared to TDLF detailing. Figures 5.3.15 and 5.3.16 illustrate the maximum amplitude of the total dead load component axial forces in each of the cross-frames for the curved radially-supported bridge considered previously in Section 5.2.1 (NISCR2). Figure 5.3.15 shows the results for NLF detailing, whereas Fig. 5.3.16 shows the results for TDLF detailing. The maximum locked-in cross-frame forces occur in the cross-frames closest to the mid-span. This is because the lack-of-fit between the girders and cross-frames is largest at these locations.

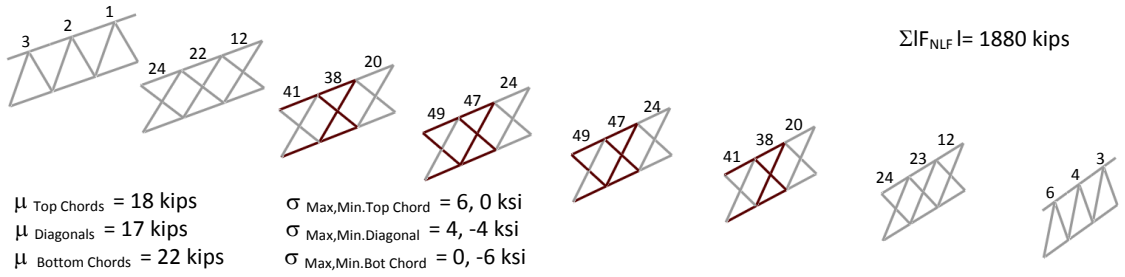

Figure 5.3.15. NISCR2, maximum amplitude of the component axial forces in each of the cross-frames under total dead load (NLF detailing).

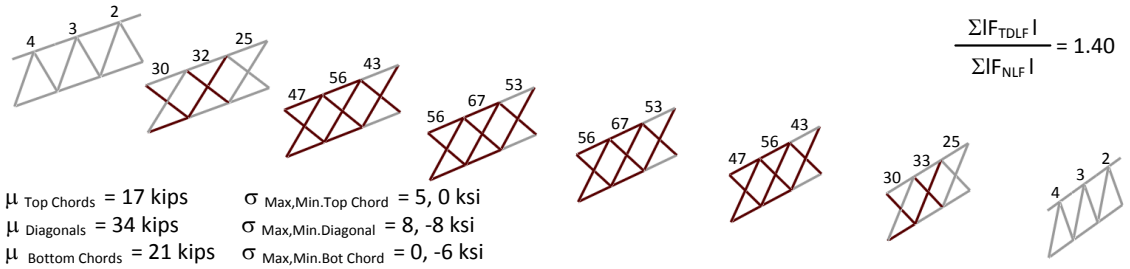

Figure 5.3.16. NISCR2, maximum amplitude of the component axial forces in each of the cross-frames under total dead load (TDLF detailing).

For curved bridges with negative skew angle (clockwise direction) the pattern of locked-in diagonal forces are similar to the ones in curved bridges with radial supports due to the negative differential camber between the girders. Therefore, the total diagonal forces tend to increase due to DLF detailing of the bridge in the curved bridges with negative skew angles, as illustrated in Figs. 5.3.17 and 5.3.18.

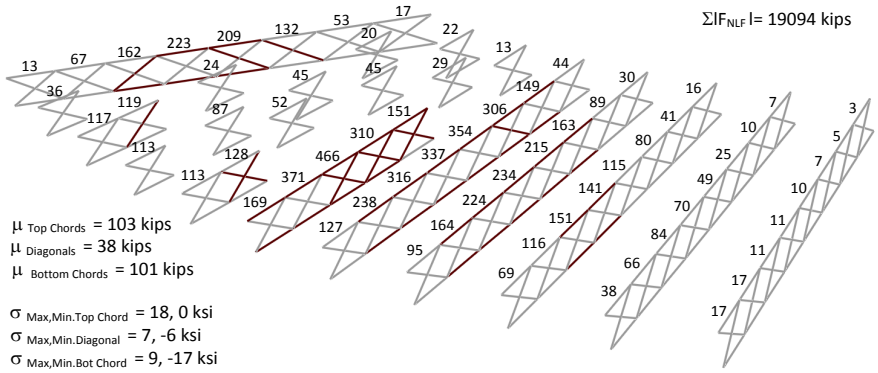

Figure 5.3.17. NISCS15, maximum amplitude of the component axial forces in each of the cross-frames under total dead load (NLF detailing).

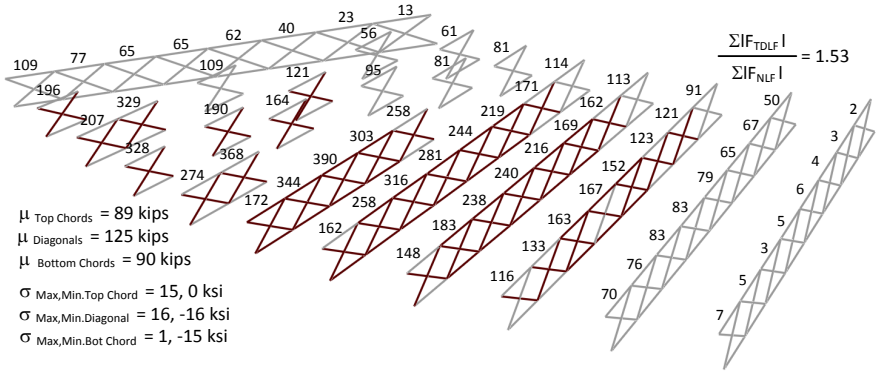

Figure 5.3.18. NISCS15, maximum amplitude of the component axial forces in each of the cross-frames under total dead load (TDLF detailing).

For curved bridges with positive skew angles (counter clockwise direction), the differential camber between the girders can be positive, moving from the girders that are farther from the center of curvature toward the center of curvature, due to larger deflection of the "inside" girders compared to the "outside" girders in the vicinity of the skewed bearing lines. Cross-frame diagonal forces tend to reduce at these locations due to the locked-in stress effects. However this relaxation of the system can be only observed in the vicinity of the skewed supports. Figures 5.3.19 and 5.3.20 provides a comparison of the maximum amplitude of the component axial forces in each of the cross-frames on an example bridge (NISCS14), constructed with NLF and TDLF detailing. For the bridges with longer span lengths, positive differential camber between the girders is typically developed in the vicinity of the positively skewed bearings. However, negative differential camber between the girders is expected farther in the span due to the large span lengths. Total cross-frame forces at the vicinity of the skewed bearings tend to be reduced by the locked-in cross-frame forces due to DLF detailing. For the

locations with negative differential camber, the cross-frame forces tend to increase since the locked-in diagonal forces add up with the dead load responses.

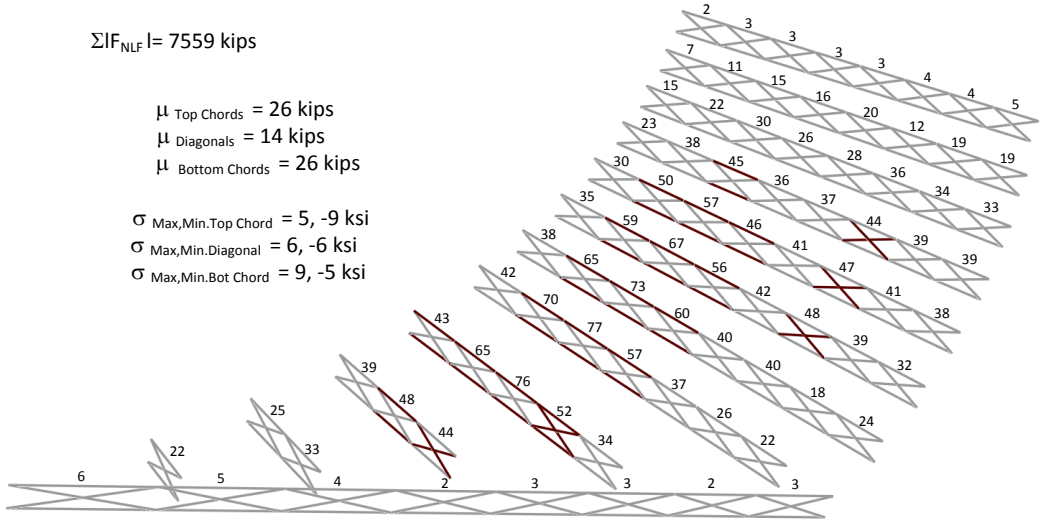

Figure 5.3.19. NISCS14, maximum amplitude of the component axial forces in each of the cross-frames under total dead load (NLF detailing).

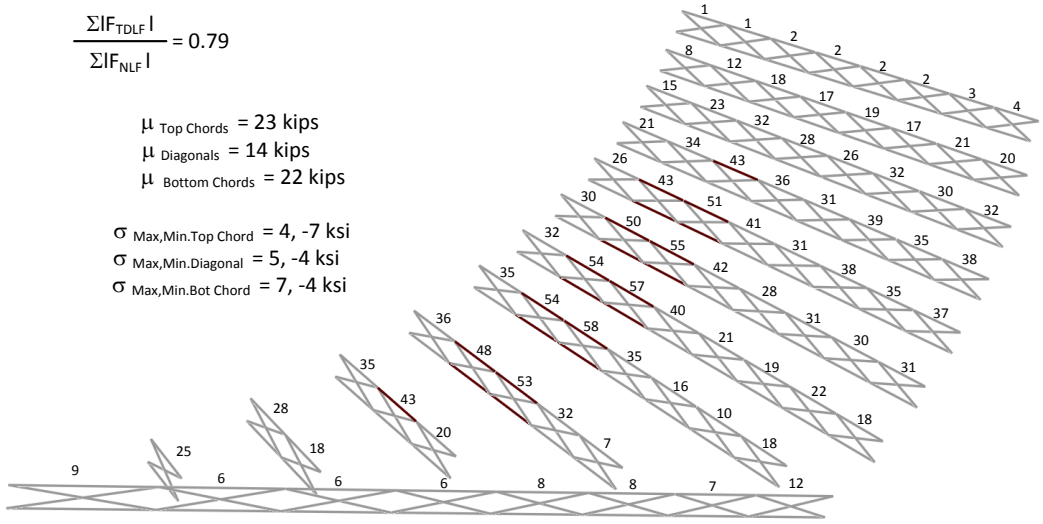

Figure 5.3.20. NISCS14, maximum amplitude of the component axial forces in each of the cross-frames under total dead load (TDLF detailing).

5.4. Impact of Dead Load Fit Cross-Frame Detailing on Girder Stresses

DLF detailing of the bridges develop twist in the no-load geometry that is opposite to the ones due to dead loads. The torsional effects due to DLF detailing induce stresses in the system as the girders resist the vertical and lateral movements. Figures 5.4.1 and 5.4.2 demonstrates the induced locked-in stresses due to TDLF detailing of the bridge NISSS54 and the curved radially-supported bridge NISCR2 that is shown in the previous sections.

Locked-in major-axis bending stresses due to DLF detailing are minor for both straight-skewed and curved radially-supported bridges. For straight I-girder bridges, this can be understood by observing the general lack of coupling between torsion and major-axis bending in straight I-girders. For curved I-girder bridges, this can be understood by considering a basic simply-supported curved I-girder with torsionally simply-supported end conditions subjected to transverse loads as shown in Fig. 5.1.2. The girder torsional deformations near the end supports have a substantial impact on the mid-span vertical displacements. However, the girder internal major-axis bending moments and the corresponding major-axis bending stresses at the mid-span are not affected significantly by the horizontal curvature. It should be noted from Figs. 5.4.1(i) and 5.4.2(i) that the local peaks in the locked-in major-axis bending stresses are due to the cross-section distortions at the cross-frame connections. For example, in the bridge NISSS54, the largest major-axis bending stresses are obtained at the corners of the bridge for girders G1 and G9 whereas major-axis bending stresses are largest towards the middle of the span for girder G5. This kind of behavior is similar to that obtained with locked-in vertical displacements since there is no coupling between torsional rotations and major-axis bending rotations for straight-skewed bridges. Similarly, locked-in major-axis bending stresses for curved bridges are minor, as shown in Figure 5.4.2(i).

Opposite twisting of the flanges in the no-load geometry due to DLF detailing induces flange lateral bending stresses. For straight and skewed bridges, locked-in flange lateral bending stresses are developed:

- at intermediate cross-frames that are located too close to skewed bearing lines which causes local peaks in the locked-in girder flange lateral bending stresses, as well as cross-frame forces can be observed due to “nuisance stiffness effects”, and
- at the interior girders due to the transverse load transfer effects.

In curved girders, locked-in flange lateral bending stresses are also induced due to overall global lateral bending in the girder flanges. The locked-in flange lateral bending stresses due to overall global lateral bending in the girder flanges are usually minor, as shown in Fig. 5.4.3 with several curved bridges. However, local peaks for the locked-in flange lateral bending stresses can be observed in the vicinity of the skewed bearings due to nuisance stiffness effects (see Fig. 5.4.3(iii)).

The girder flange lateral bending stresses are reduced significantly in straight-skewed bridges due to DLF detailing. The smallest total flange lateral bending stresses tend to occur under steel dead load, if SDLF detailing is used and under total dead load if TDLF detailing is used for these bridges. In these cases the girders largely unwind into their approximately plumb positions under the corresponding dead load effects. However, engineers often incorrectly conclude that since the girders were plumb in their no-load condition, and since they are also plumb in the targeted dead load condition the girder flange lateral bending stresses are zero, the cross-frame forces are zero, and the girders respond essentially in the manner assumed in a line-girder analysis when the bridge is in the targeted dead load condition.

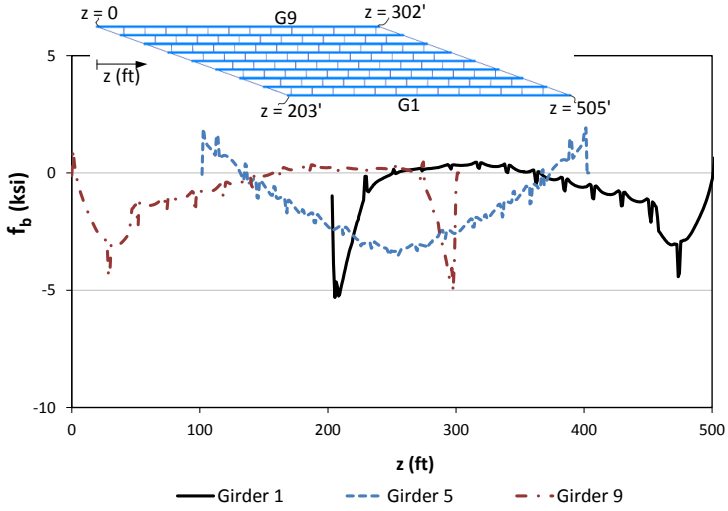

(i) f_b, Major-axis bending stresses

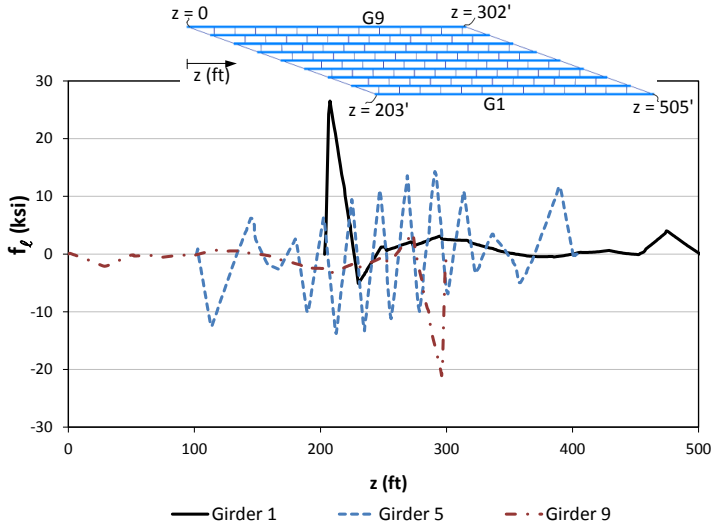

(ii) f_ℓ, flange lateral bending stresses

Figure 5.4.1. NISSS54, Top flange major-axis and minor-axis bending stresses due lack-of-fit for TDLF detailing.

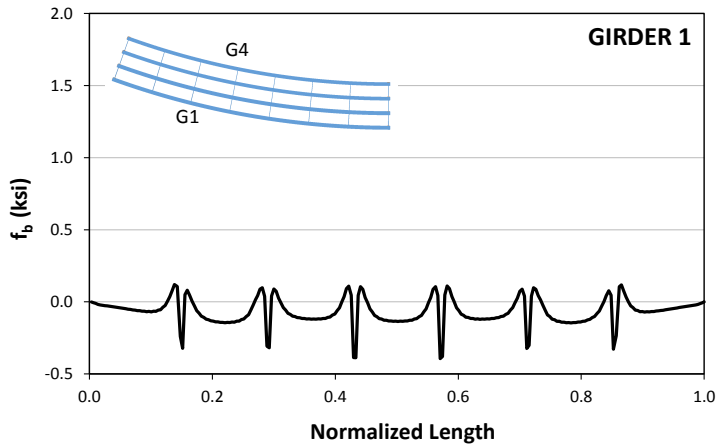

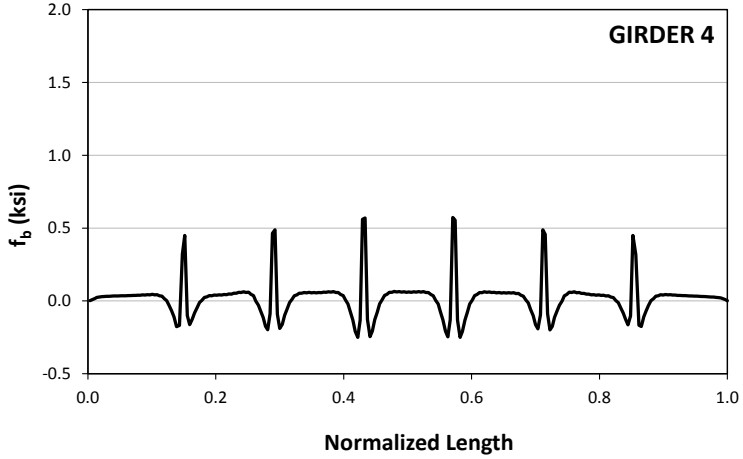

(i) f_b, Major-axis bending stresses

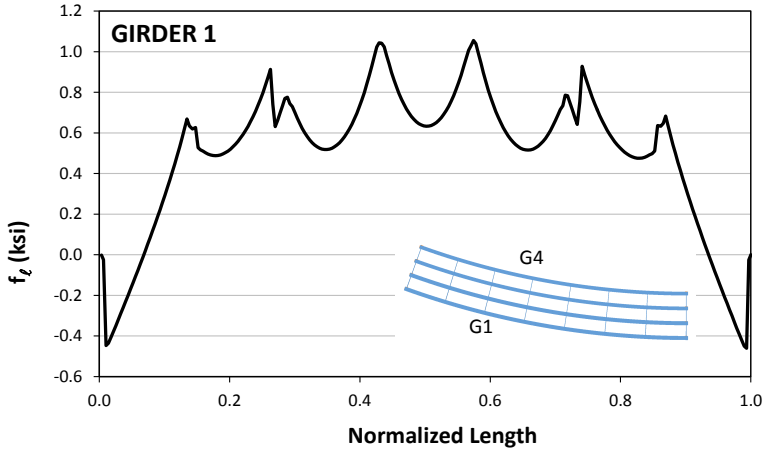

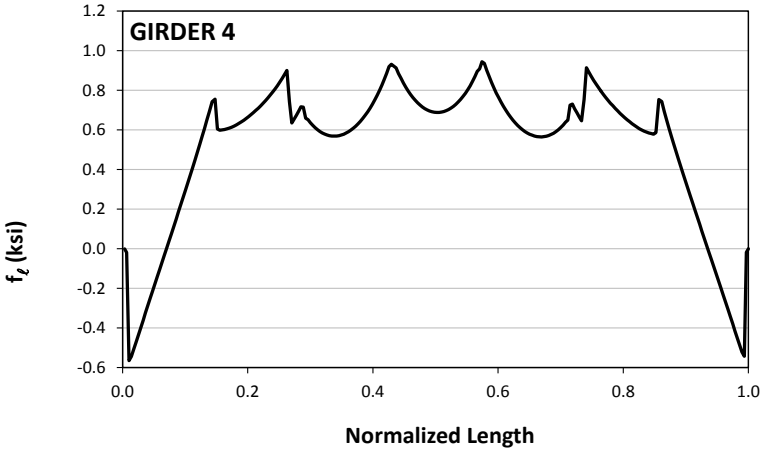

(ii) f_ℓ, flange lateral bending stress

Figure 5.4.2. NISCR2, Top flange major-axis and minor-axis bending stresses due lack-of-fit for TDLF detailing.

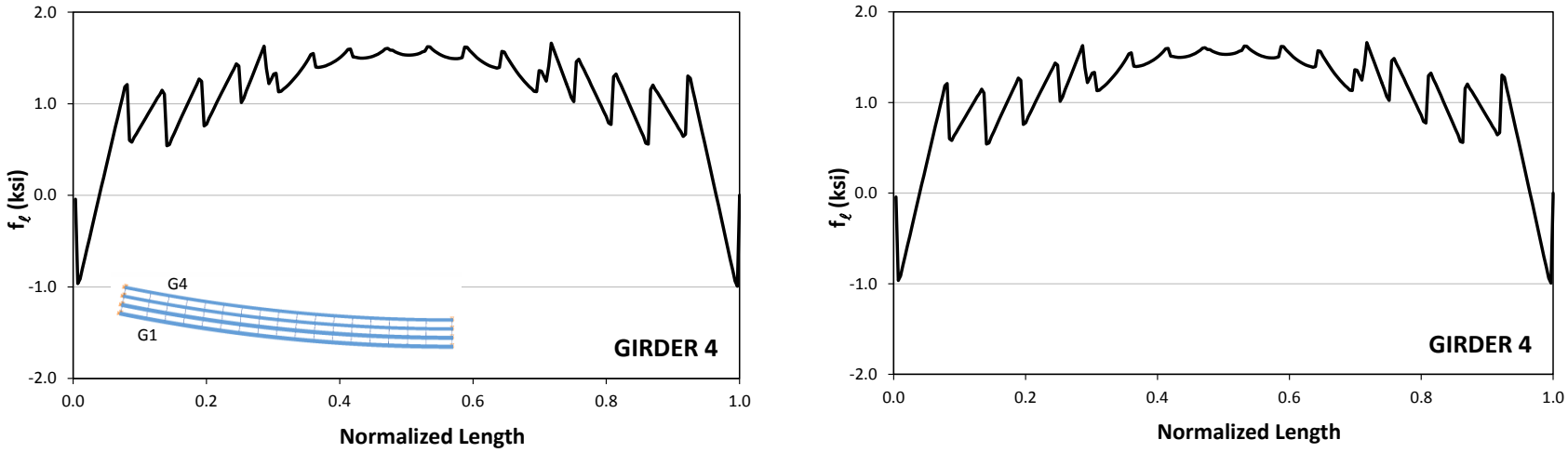

(i) NISCR5

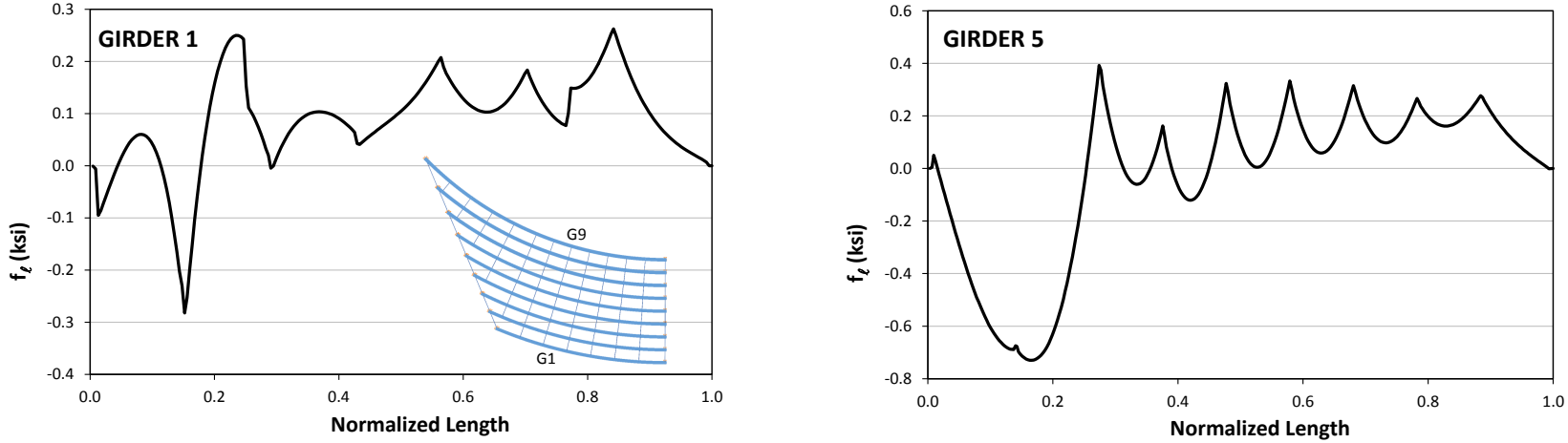

(ii) NISCS14

Figure 5.4.3. Top flange lateral bending stresses due lack-of-fit for TDLF detailing.

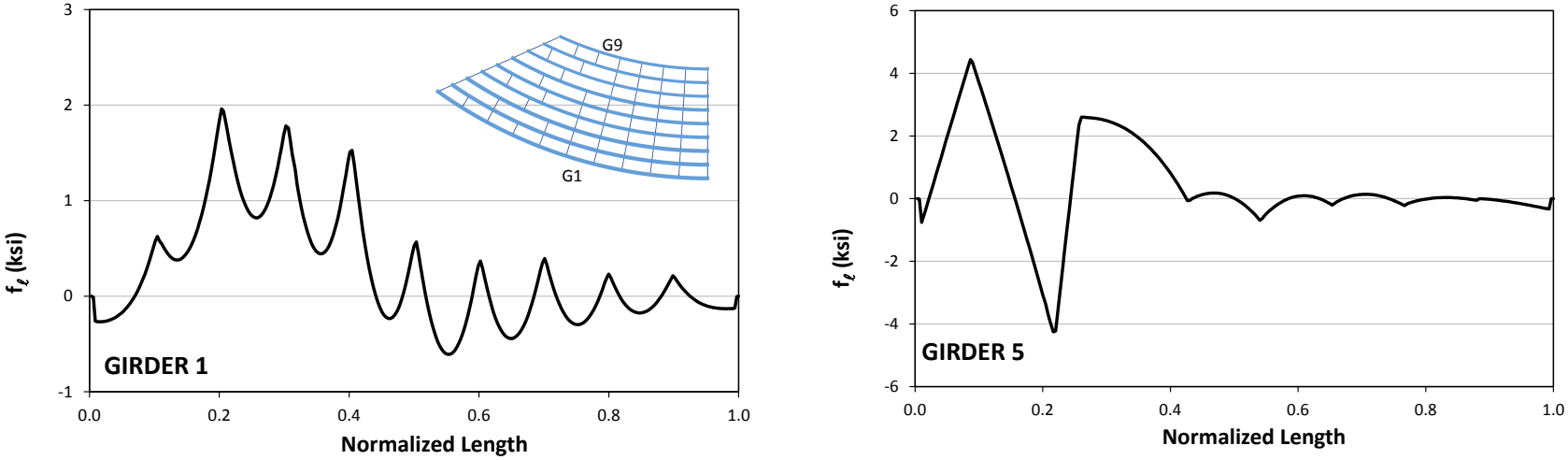

(iii) NISCS15

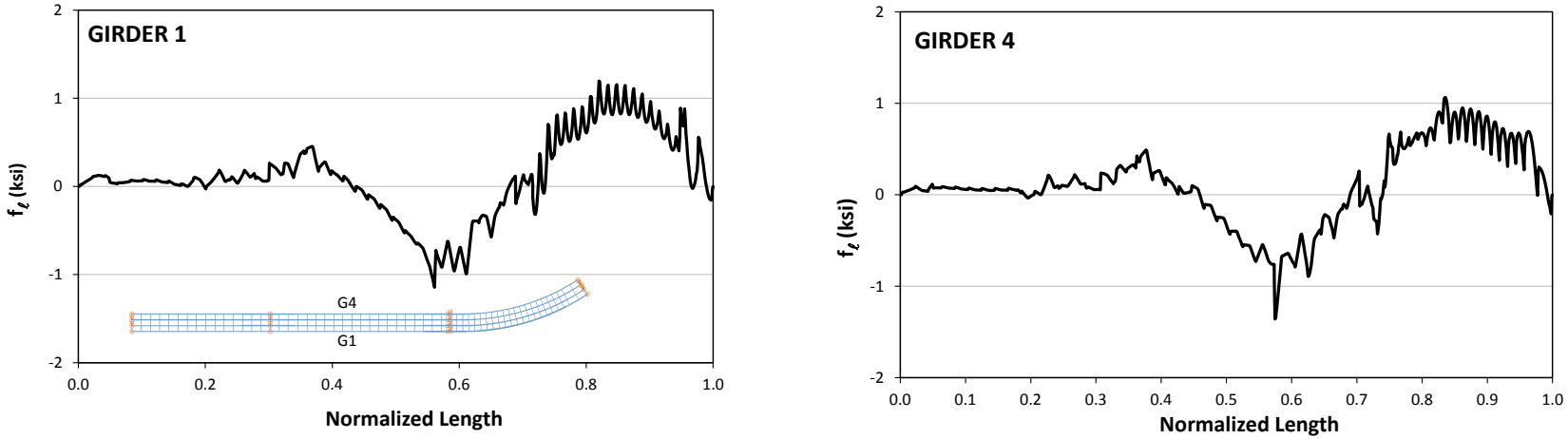

(iv) EICCR11

Figure 5.4.3. (continued). Top flange lateral bending stresses due lack-of-fit for TDLF detailing.

However, it is important to note that the girder flange lateral bending stresses do not completely vanish due to the differences between the locked-in stresses from the DLF detailing and the stresses related to the torsion of the girders under the targeted dead load. There are several reasons for this behavior:

- In particular, local peaks in girder flange lateral bending stresses, as well as cross-frame forces, can be observed due to "nuisance stiffness effects" at locations such as intermediate cross-frames that are located too close to skewed bearing lines. Also, the stresses in the girders due to locked-in force effects do not tend to match the torsional stresses due to the three-dimensional loading effects in these regions.
- In addition, when staggered cross-frames are utilized such as in the bridge NISSS54, there is substantial flange lateral bending in the interior girders due to the transverse load transfer effects. The interior girder flanges are loaded "back-and-forth" in opposing directions by the cross-frames. The corresponding flange lateral bending in these girders is generally reduced, but is not completely nullified by the locked-in force effects.
- Lastly, in the fascia girders, significant flange lateral bending can occur in some cases due to eccentric overhang bracket loads. These bending effects are of course not nullified by the lack-of-fit forces from DLF detailing.

Figure 5.4.1 shows selected girder major-axis bending and flange lateral bending stresses under total dead load for the different types of detailing methods in the bridge NISSS54. In this structure, the major-axis bending stresses in the fascia girders are essentially unaffected by the type of cross-frame detailing. The maximum total dead load flexural stress in the top flange of these girders is 30 ksi. The total dead load major-axis bending stresses in the middle girder (Girder 5) are slightly increased for the TDLF detailing case, yet are consistent with the larger vertical displacements in Girder 5 for TDLF detailing. However, the differences in the stresses for the major-axis bending of Girder 5 are relatively minor. The maximum f_b in Girder 5 is approximately 20 ksi under the total dead load.

The flange lateral bending stresses are relatively small in the fascia girders for all the methods of detailing in the bridge NISSS54, and are predominantly due to eccentric overhang bracket loads with the exception of the locations near the obtuse corners of the bridge. At the obtuse corners, relatively large lateral forces are introduced into the fascia girders from the

chords of the first two intermediate cross-frames near the bearing lines. This causes a "spike" in the flange lateral bending stresses near the ends of the fascia girders. This spike in f_ℓ is largest for the NLF detailing case, and it is reduced by the lack-of-fit stresses introduced into the girders in the cases of SDLF and TDLF detailing.

The total dead load lateral bending stresses are significant in Girder 5 regardless of the method of cross-frame detailing. They are largest for the NLF detailing case, reaching peak values of nearly 22 ksi near the mid-span. These flange lateral bending stresses are reduced by the lack-of-fit effects introduced into the girders by SDLF or TDLF detailing. The resulting maximum total dead load f_ℓ values are approximately 15 ksi for SDLF detailing and 8 ksi for TDLF detailing. These significant flange lateral bending stresses in Girder 5 are due to the use of the staggered cross-frames in this bridge and the "back-and-forth" load transfer effects mentioned previously. Staggered cross-frames generally are expected to reduce the magnitude of the cross-frame forces that need to be resisted due to the skew effects, but they introduce "back-and-forth" lateral loads on the girder flanges in the middle regions of the bridge. These forces are highest near the mid-span of the middle girders because these locations are in the middle of the stiff transverse load path first discussed in Section 5.3.

There is no "spike" in the flange lateral bending stresses in Girder 5 near its ends. This is because the forces coming into the girder from the intermediate cross-frames near the support are not as large in Girder 5 as in the exterior fascia girders. The predominant lateral bending action on Girder 5 is near the middle of the span. Unfortunately, this is also where the girder major-axis bending stresses are the highest.

In cases with contiguous intermediate cross-frame lines, the total flange lateral bending stresses associated with DLF detailing are found to be very close to zero except in the fascia girders and at cross-frame locations with nuisance stiffness effects. This behavior is demonstrated in Fig. 5.4.5 with a representative bridge XICSS5 by comparing the steel dead load girder stresses for each type of cross-frame detailing methods. It can be observed from Fig. 5.4.5 that the total flange lateral bending stresses are almost zero for the case with SDLF detailing since the locked-in stresses are close to being equal and opposite to the ones due to dead loads. Figure 5.4.6 provides the total dead load girder stresses for each type of cross-frame detailing. It should be noted from Fig. 5.4.6 that the flange lateral bending stresses in the fascia girders are predominantly due to eccentric overhang bracket loads and cannot be reduced by

any of the detailing methods. It is also clear from the above cases that the major-axis bending stresses are essentially unaffected from the DLF detailing

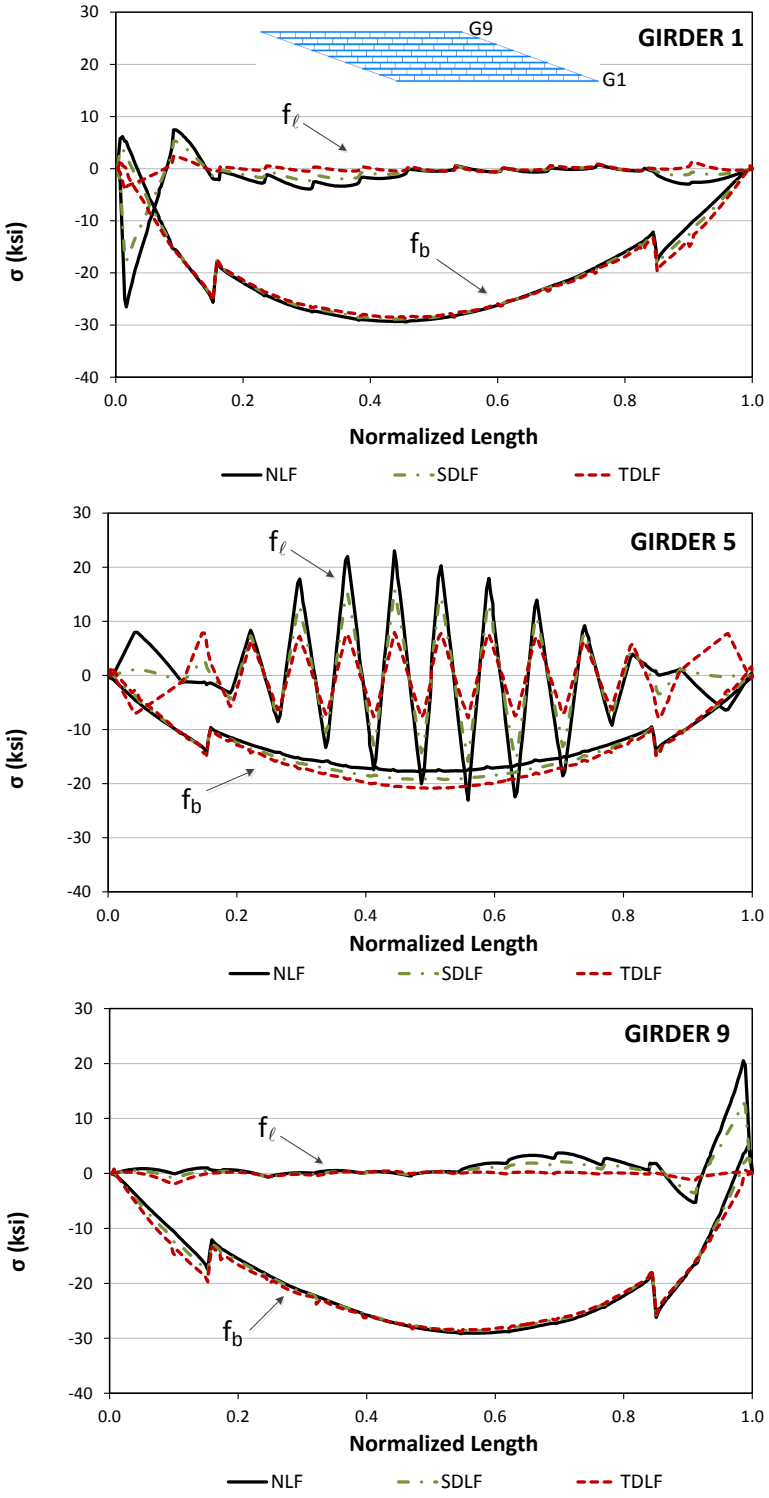

Figure 5.4.4. NISSS54, Top flange stresses under total dead load for different detailing methods.

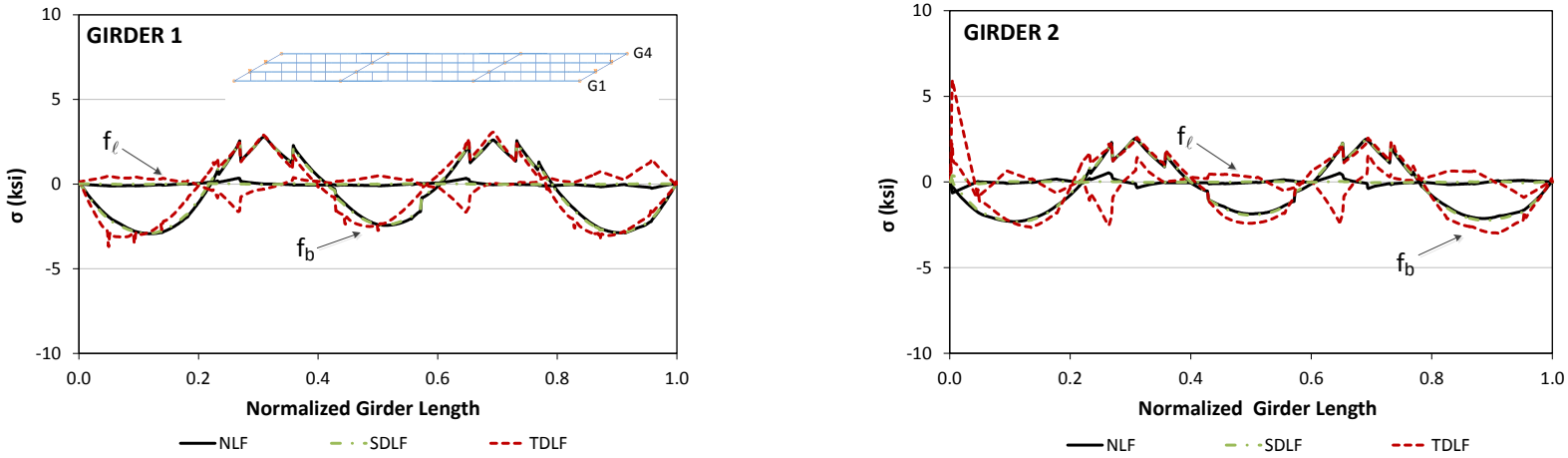

Figure 5.4.5. XICSS5, Top flange stresses under steel dead load for different detailing methods.

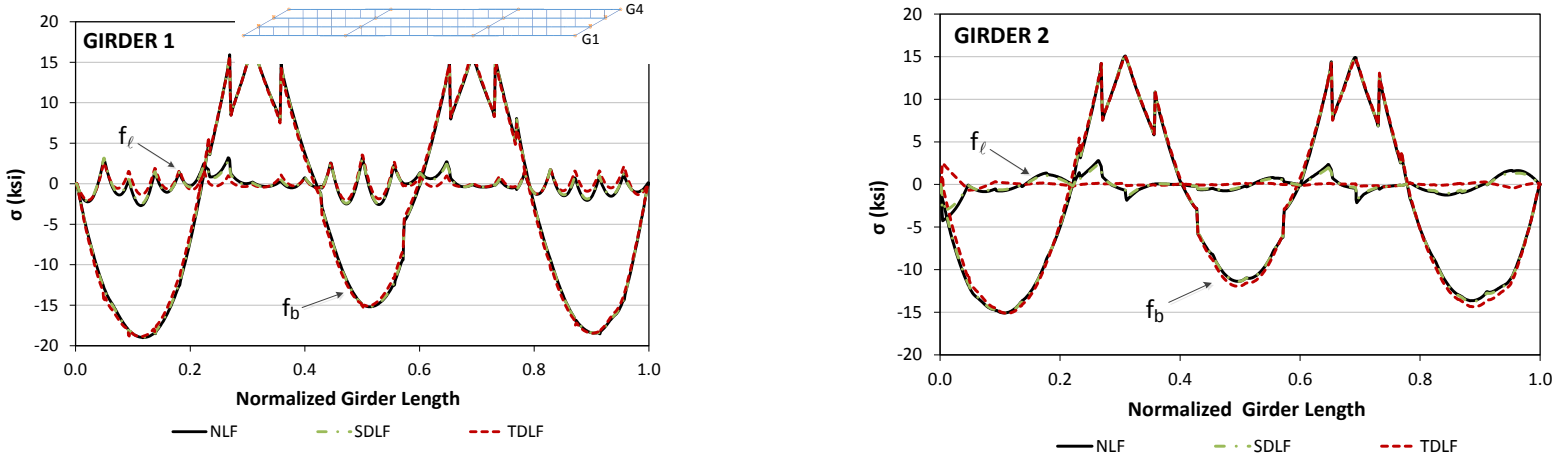

Figure 5.4.6. XICSS5, Top flange stresses under total dead load for different detailing methods.

For curved radially-supported bridges, the “local” flange lateral bending effects between the cross-frames due to the horizontal curvature are not influenced by the DLF detailing. However, DLF detailing of curved bridges induces an overall global lateral bending in the girder flanges in the direction:

- opposite to the lateral bending of the girders due to the torsional rotation of the bridge cross-section,
- opposite to the bending within the girder unbraced lengths between the cross-frames, and
- in the same direction as the “negative” flange lateral bending stresses due to the continuity of the curved flanges across the cross-frame locations.

That is, the locked-in forces due to DLF detailing tend to reduce the overall “global” girder flange lateral bending stresses in curved bridges. Figure 5.4.7 illustrates this effect in the bridge NISCR2. In shorter and/or wider curved bridge structures, this overall flange lateral bending effect is relatively minor. However, in some cases, such as narrow curved bridge units, this effect can be substantial. These effects are relatively minor in the bridge NISCR2, although the percentage change in the flange lateral bending stresses on the inside girder is somewhat large.

For curved bridges with high overturning effects, dead load flange lateral bending stresses tend to be amplified due to the second order effects. This is especially the case for the curved bridges with large length-to-width ratios. However, DLF detailing of these bridges eliminate the amplification of the flange lateral bending stresses since the overall section is twisted due to DLF detailing. Figure 5.4.8 provides example bridges with larger overturning effects that cause second order amplification of the flange lateral bending stresses under total dead load. Figure 5.4.8 also provides the reduction of the second order amplification of the flange lateral bending stresses due to DLF detailing of the bridges.

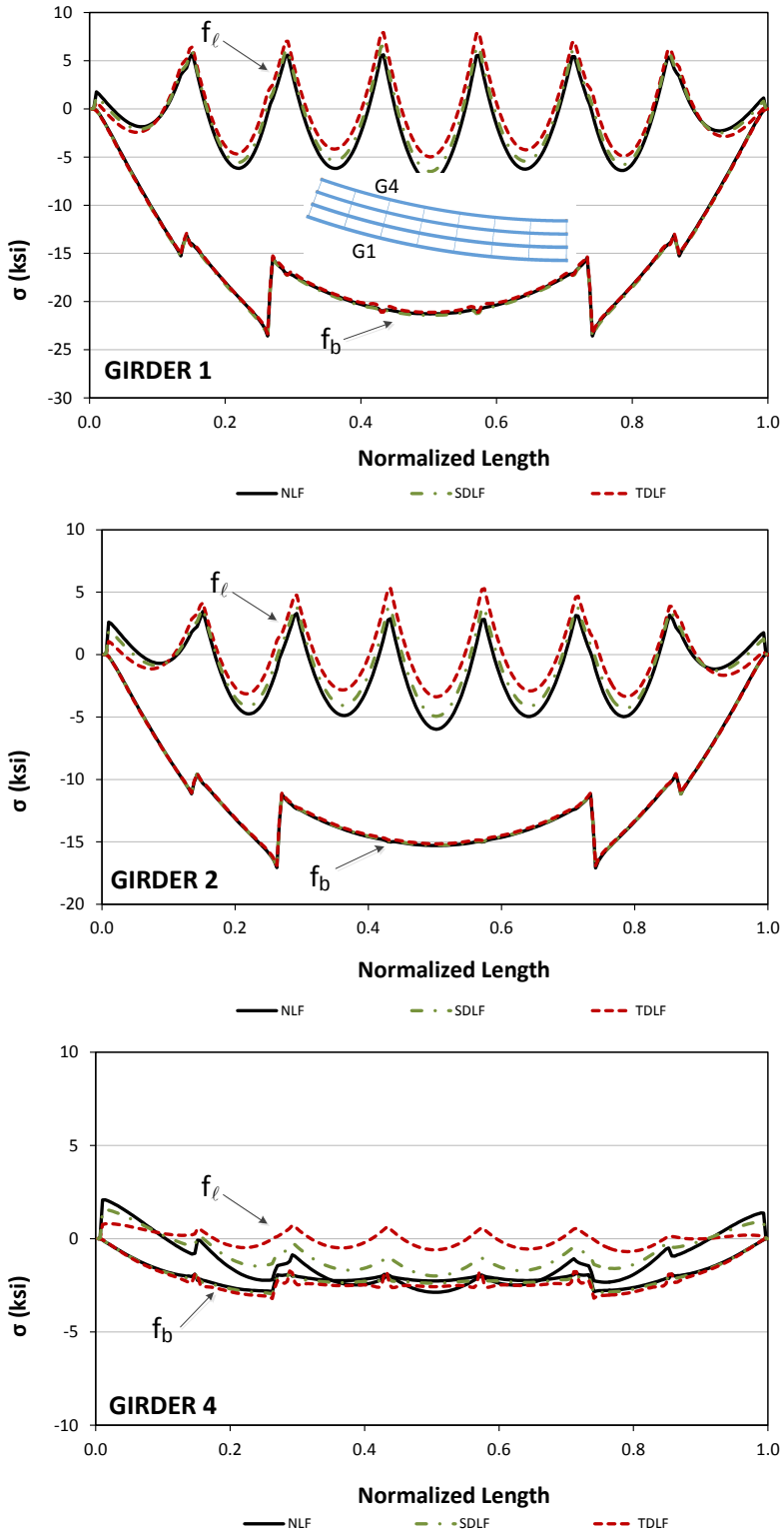

Figure 5.4.7. NISCR2, Top flange stresses under total dead load for different detailing methods.

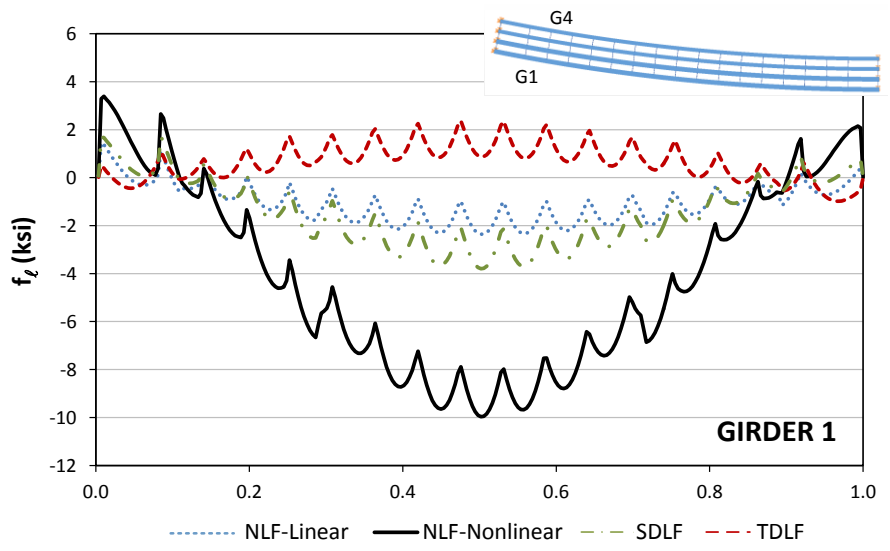

(i) NISCR5

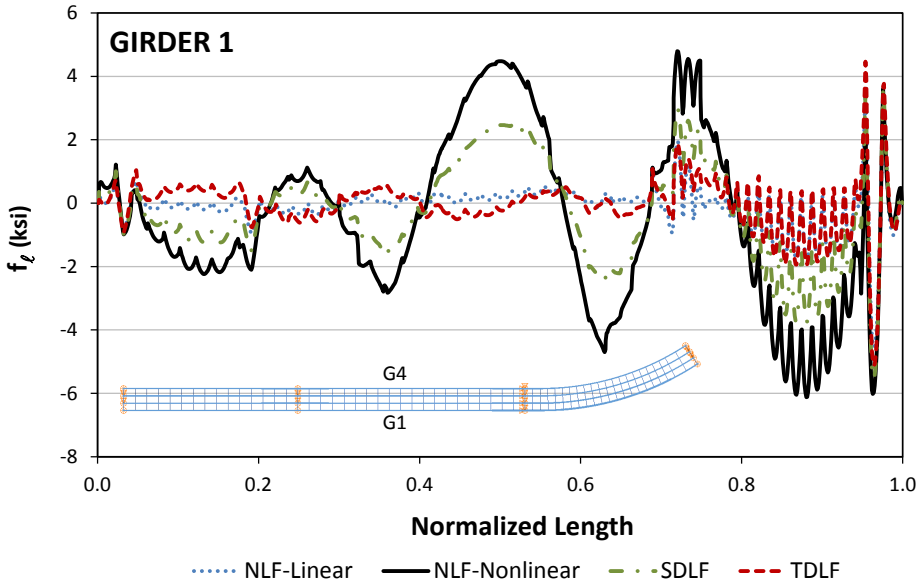

(ii) EICCR11

Figure 5.4.8. Total dead load top flange lateral bending stresses for representative bridges with large overturning effects

5.5. Impact of Dead Load Fit Cross-Frame Detailing on Strength

Girders can be plumb only in one condition. Cross-frame detailing methods are used commonly as effective ways of achieving plumb girder webs within acceptable tolerances in I-girder bridge construction. It was found by Chavel (2008) that the ultimate load capacity of the individual girders are reduced slightly compared to the plumb girders. It was also reported that the reduction is mainly due to the reduction in the cross-sectional properties of girders in the rotated configuration. The impact of the girder layover on the load capacity and on the lateral position of the roadway is likely to be inconsequential in many of these cases. The AASHTO LRFD Specifications provide explicit provisions for checking of strength during construction

It is shown in the previous sections that DLF detailing of the straight and skewed bridges does not increase the overall girder stresses significantly. Moreover, it is shown that maximum cross-frame forces observed in a straight-skewed bridge constructed with DLF detailing are unlikely to exceed the ones that are observed with NLF detailing unless cross-frames are framed very close to the skewed bearings. Therefore, additional locked-in force effects due to DLF detailing do not affect the bridge system strength significantly, assuming that the cross-frames are sized adequately and that the critical components are the girders.

Locked-in force effects can be additive to some of the dead load responses, such as the cross-frame forces in curved and radially-supported bridges. Therefore, the impact of locked-in stress effects on strength of curved bridges is investigated.

It is illustrated in Sections 5.2 and 5.4 that bridges with curved girders are susceptible to overall (global) flange lateral bending which can cause failures due to stability related reasons. Furthermore, it was shown by Yura et al. (2008) and Sanchez (2011) that curved bridges with large span-to-width ratios can develop significant second-order amplification due to global deflections. Figure 5.5.1 provides a bridge with the characteristics discussed above where significant second-order effects are observed due to its large span length-to-width ratio (L/w = 100). The bridge that is shown in Fig. 5.5.1 is designated with the name NISCR5 in the design matrix. Figures 5.5.2 and 5.5.3 provide typical top girder stresses and radial displacements of girder G1 under total dead load for NLF detailing from geometric nonlinear analyses. It is observed from Fig. 5.5.2 that the total flange lateral bending stresses are amplified due to global movement of the bridge (see Fig. 5.5.3)

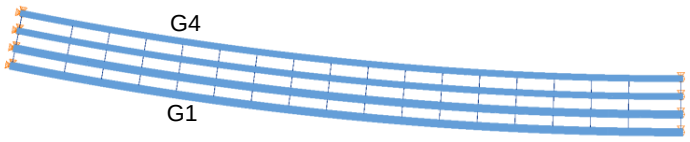

Figure 5.5.1. Example of a curved bridge with large span-to-width ratio (NISCR5).

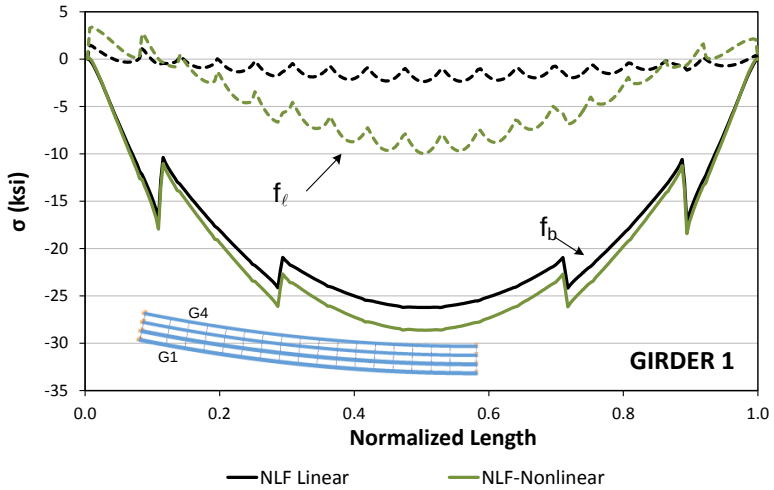

Figure 5.5.2. NISCR5, Top flange stresses under total dead load for NLF detailing method from linear and geometric nonlinear analyses.

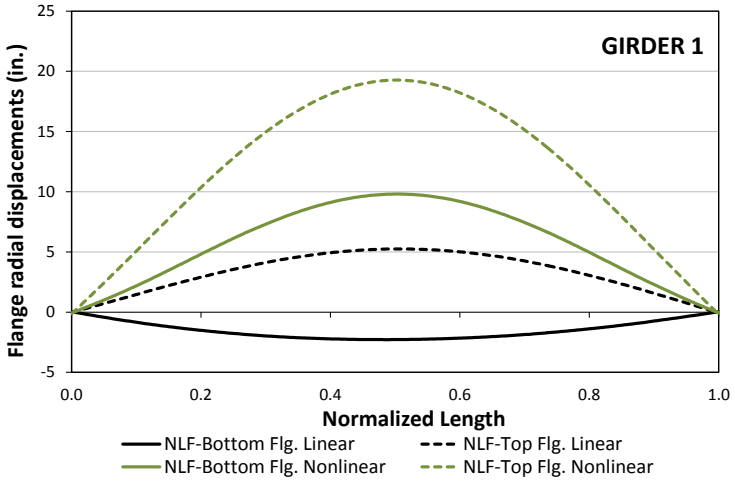

Figure 5.5.3. NISCR5, flange radial displacements under total dead load for NLF detailing method from linear and geometric nonlinear analyses.

It is also shown in Sections 5.2 and 5.4 that locked-in forces due to DLF detailing of the cross-frames tend to reduce global flange lateral bending of the curved bridges, as illustrated in Figs. 5.5.4 and 5.5.5 for NISCR5. Figures 5.5.4 and 5.5.5 show the girder G1 total dead load stresses and radial displacements for each type of cross-frame detailing.

It should be noted from Fig. 5.5.4 that the DLF detailing of the bridge tends to reduce the second-order amplification effects on the flange lateral bending stresses since DLF detailing of curved bridges generally induces overall lateral bending in the girder flanges that is opposite to the lateral bending of the girders due to torsional rotation of the bridge cross-section. The reduction is higher for TDLF detailing since approximately plumb webs under total dead load is targeted. It is emphasized that these locked-in forces are beneficial, but they may come with a "price." In the case of curved bridges with radial supports, the DLF detailing increases the diagonal cross-frame forces. Minimum and maximum cross-frame member stresses due to lack-of-fit are determined as -11.4 ksi and 11.13 ksi for TDLF detailing and -6.29 ksi and 6.19 ksi for SDLF detailing of NISCR5, whereas the minimum and maximum cross-frame stresses under total dead load for NLF detailing is determined as 4.20 ksi and 4.5 ksi.

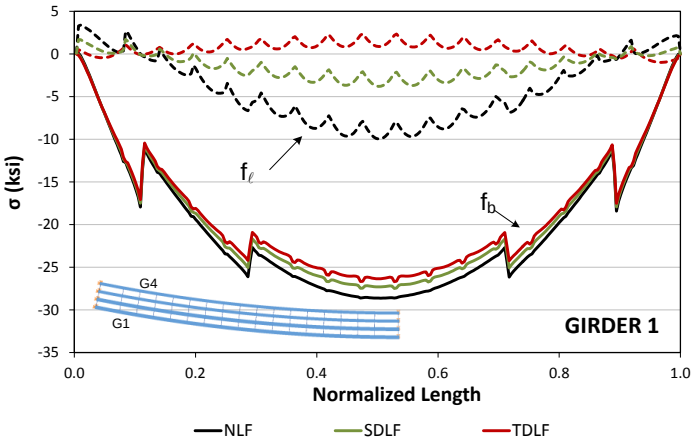

Figure 5.5.4. NISCR5, Top flange stresses under total dead load for different detailing methods.

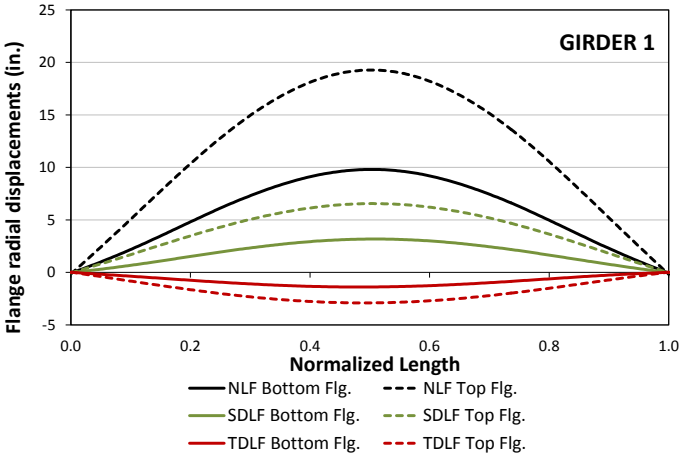

Figure 5.5.5. NISCR5, Flange radial displacements under total dead load for different detailing methods.

The reduction in the overall torsional effects can also impact the strength of the bridge since the strength of these types of bridges is usually governed by global stability type failures. Therefore, the influence of the method of detailing on the bridge system strength of the curved bridges, are investigated assuming that the cross-frames are sized adequately and that the critical components are the girders.

Full-nonlinear FEA solutions are conducted for the assessment of the different types of cross-frame detailing during construction. Analyses are conducted for the bridges NISCR2 and NISCR5. NISCR2 is a shorter bridge (150 ft span) with a 30 ft deck width that shows relatively minor global flange lateral bending effects. However, NISCR5 is a more extreme 300 ft simple-span bridge with a 30 ft deck width and no flange-level lateral bracing system. This bridge experiences significant second-order effects under the total dead load. Modeling strategies that are discussed in Chapter 3 are used for the finite element evaluation, including the application of residual stresses and grade 50 material properties. Cross-frames are assumed to be elastic in the full-nonlinear FEA simulations and load deflection curves are generated for different types of detailing by monitoring the vertical and lateral deflections in the mid-span of the outside girder (Girder 1) with respect to the applied load fraction (ALF). The applied load fraction (ALF) is the multiple of the nominal total dead load applied to the bridge.

Figures 5.5.6 through 5.5.9 provide the load deflection curves of NISCR5 for each type of cross-frame detailing method. The sum of the nominal total dead load is calculated as 2796.2 kips. Displacements values are reported at the mid-span of the outside girder (Girder 1). In Figs. 5.5.6 through 5.5.9, girder vertical displacements, top and bottom radial displacements and girder layover at the mid-span of girder G1 are reported, respectively. NISCR5 is only able to develop 1.34 times the total dead load for the case with NLF detailing and 1.36 times the total dead load for the case with SDLF detailing. However, with TDLF detailing, the overall torsional rotations are reduced, thus reducing the second-order amplification and resulting in a load capacity of 1.54 times the nominal total dead load. It should be noted for the case with SDLF detailing that the structure starts unloading when the maximum load is reached. The unloading part is not shown in Figs. 5.5.6 through 5.5.9.

Also, it should be noted from Figs. 5.5.7 and 5.5.9 that reversed layovers are obtained with DLF detailing for the lower load fractions (ALF < 1). Reversed layovers indicate the opposite direction of the natural behavior when load is applied. This is due to locked-in stresses effects. It

should be also noted that the girders are approximately plumb only under nominal steel dead load for SDLF detailing (ALF=0.57). Figures 5.5.10 and 5.5.11 provide FEA deflections and mid-thickness equivalent plastic strain of NISCR5 at the maximum load fraction and failure, respectively.

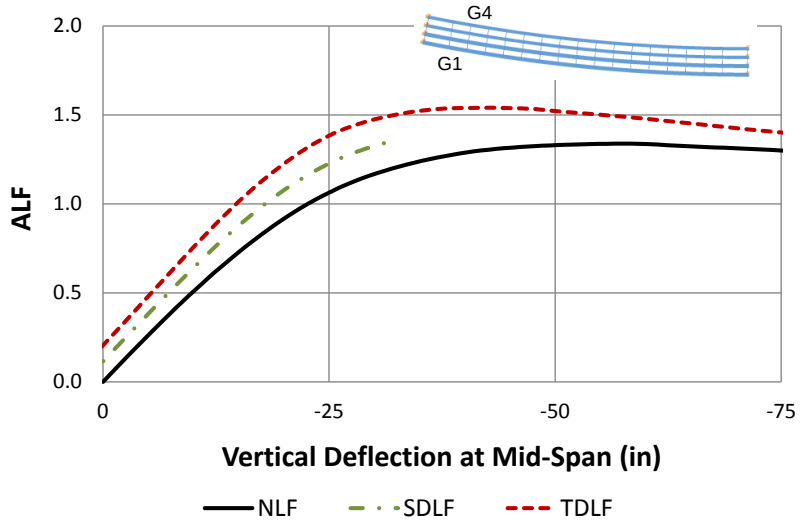

Figure 5.5.6. NISCR5, vertical displacements at the mid-span of girder G1 under applied load fraction of the total dead load for different detailing methods.

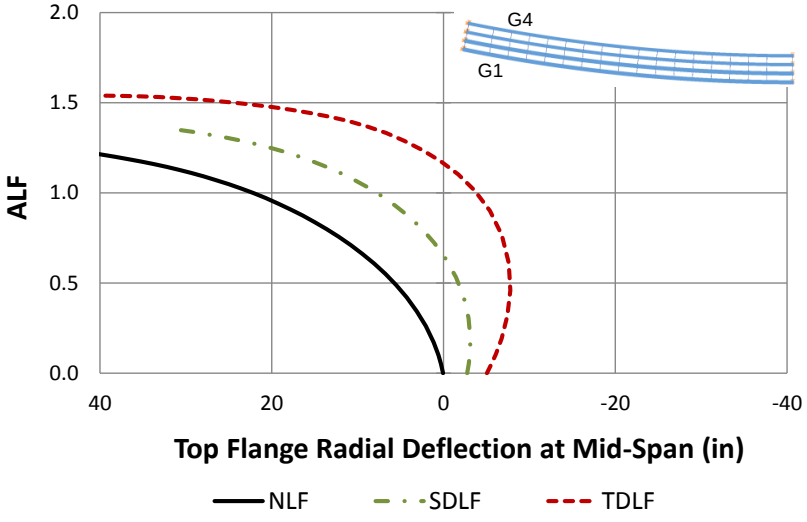

Figure 5.5.7. NISCR5, top flange displacements at the mid-span of girder G1 under applied load fraction of the total dead load for different detailing methods.

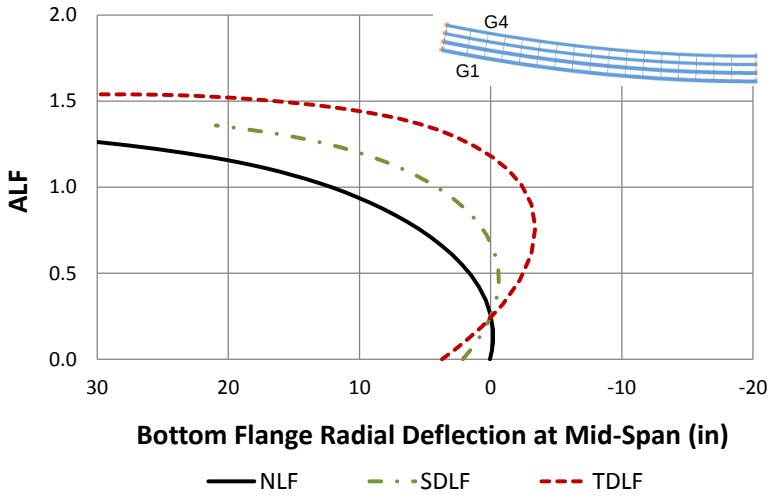

Figure 5.5.8. NISCR5, bottom flange displacements at the mid-span of girder G1 under applied load fraction of the total dead load for different detailing methods.

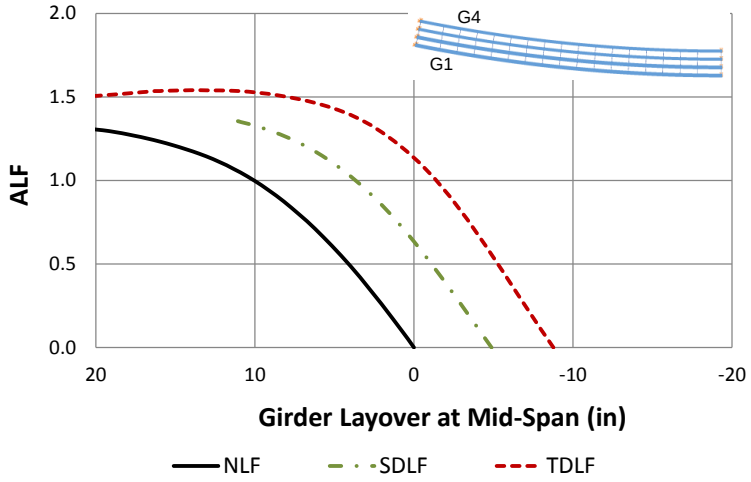

Figure 5.5.9. NISCR5, girder layover at the mid-span of girder G1 under applied load fraction of the total dead load for different detailing methods.

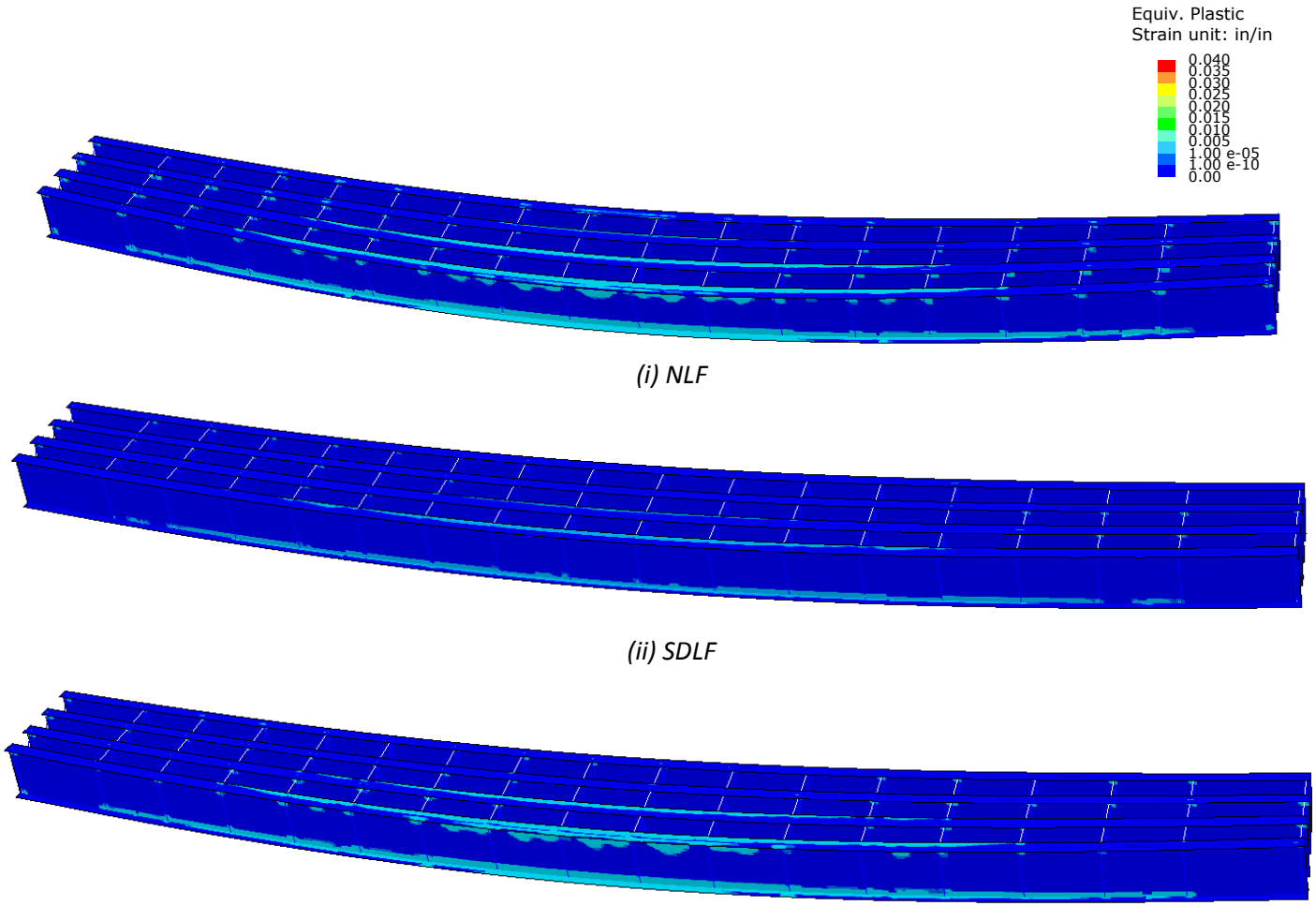

(i) NLF

(ii) SDLF

(iii) TDLF

Figure 5.5.10. NISCR5, Perspective view of mid-thickness equivalent plastic strains and deflected shape at maximum applied load of total dead load.

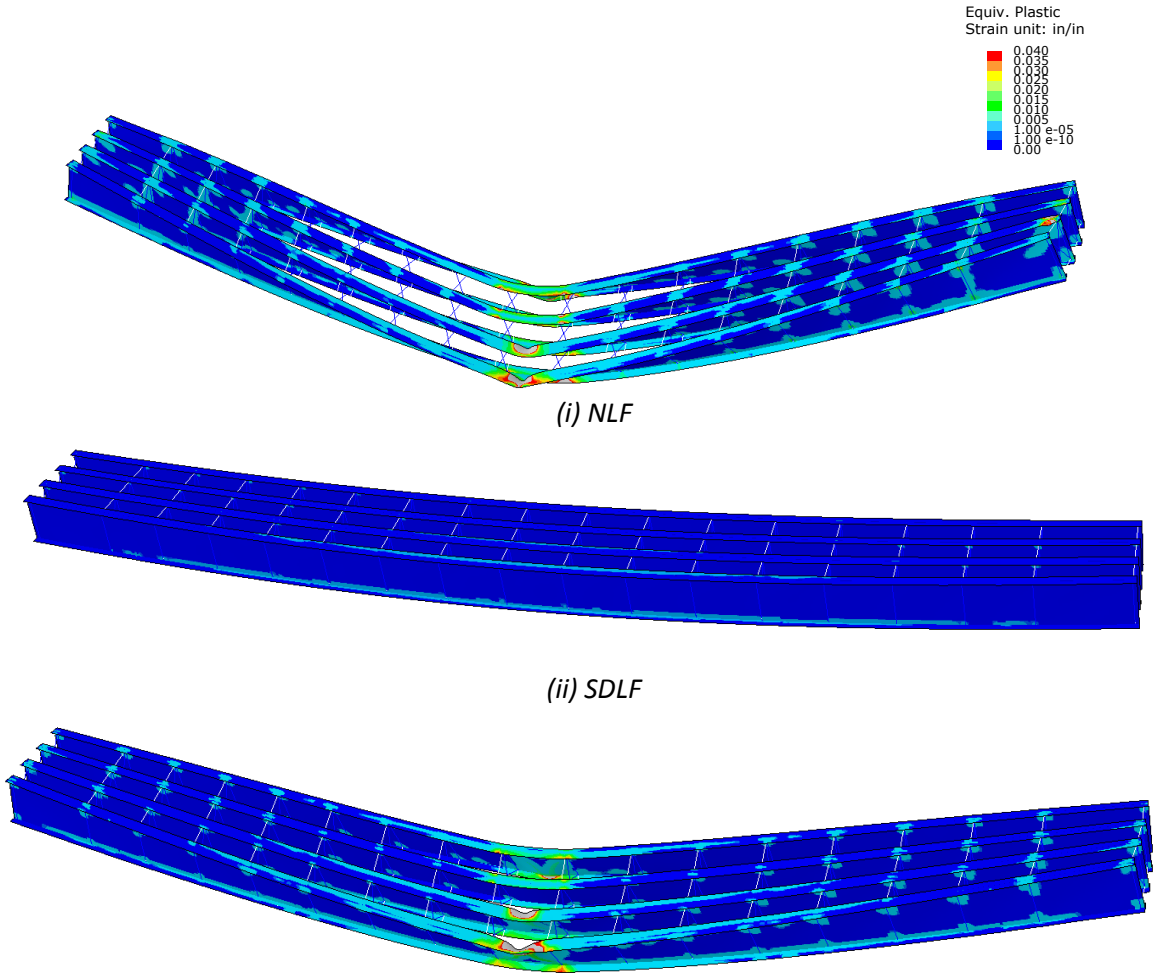

(i) NLF

(ii) SDLF

(iii) TDLF

Figure 5.5.11. NISCR5, Perspective view of mid-thickness equivalent plastic strains and deflected shape at the end of the analysis.

Figures 5.5.12 through 5.5.15 provide the load deflection curves of NISCR2 for different types of detailing methods. The applied load fraction (ALF) is the multiple of the nominal total dead load applied to the bridge. The sum of the nominal total dead load is calculated as 956 kips. Displacements values are reported at the mid-span of the outside girder (Girder 1). In Figs. 5.5.12 through 5.5.15, girder vertical displacements, top and bottom radial displacements and girder layover at the mid-span of Girder 1 are reported, respectively. The maximum applied load fraction observed is 1.98, 2.01 and 2.05 for NLF, SDLF and TDLF detailing respectively. The maximum applied load level is essentially the same for each type of cross-frame detailing methods. Figures 5.5.12 through 5.5.15 demonstrates that there is relatively little on the overall bridge capacity due to the type of the detailing. This is because in shorter and/or wider curved bridges, overall (global) lateral bending effects tend to be small. Figures 5.5.16 and 5.5.17 provide FEA deflections and mid-thickness equivalent plastic strain of NISCR5 at the maximum load fraction and failure, respectively.

In summary, additional locked-in force effects due to DLF detailing do not affect the bridge system strength significantly, assuming that the cross-frames are sized adequately and that the critical components are the girders. In fact, it is demonstrated that locked-in force effects can increase the strength of the curved bridges that are susceptible to overall second-order effects or significant overall (global) flange lateral bending. Unfortunately, DLF detailing of horizontally curved bridges increases the cross-frame diagonal forces.

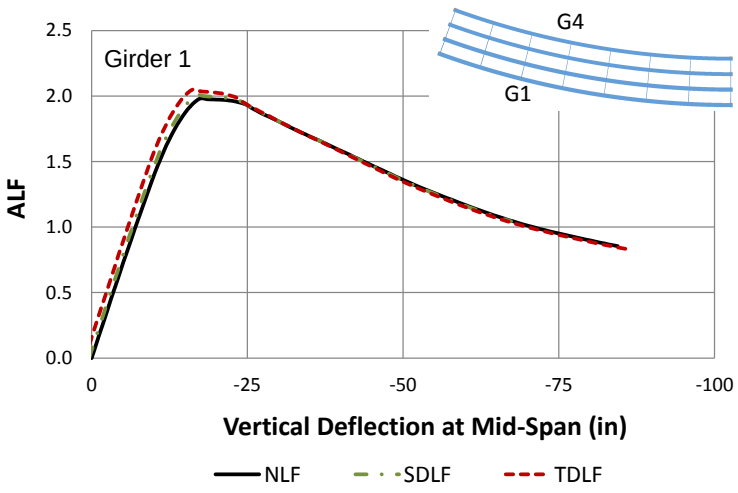

Figure 5.5.12. NISCR2, vertical displacements at the mid-span of girder 1 under applied load fraction of the total dead load for different detailing methods.

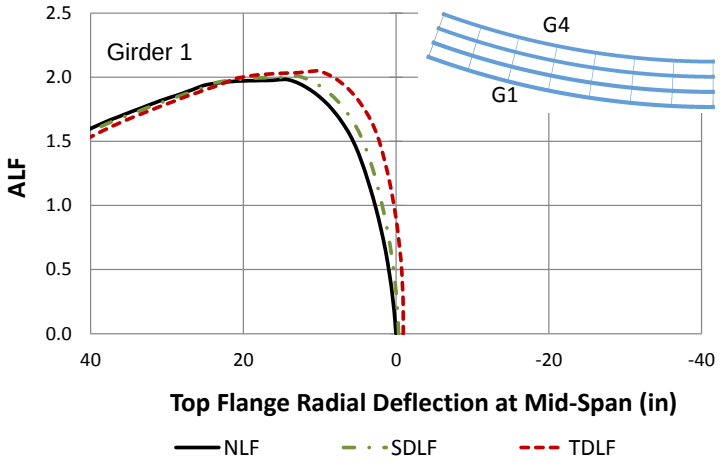

Figure 5.5.13. NISCR2, top flange displacements at the mid-span of girder G1 under applied load fraction of the total dead load for different detailing methods.

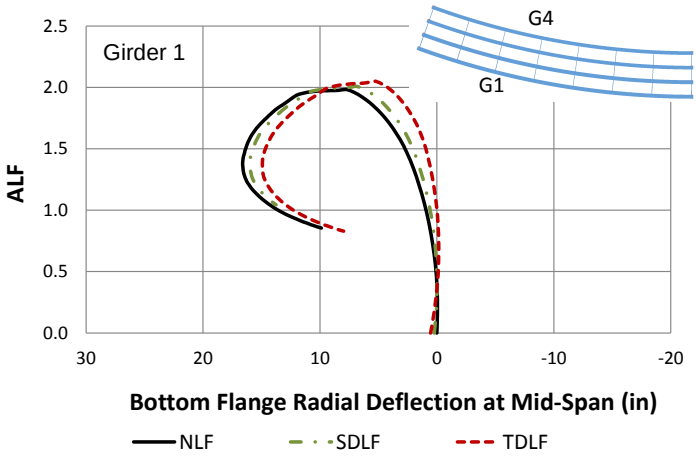

Figure 5.5.14. NISCR2, bottom flange displacements at the mid-span of girder G1under applied load fraction of the total dead load for different detailing methods.

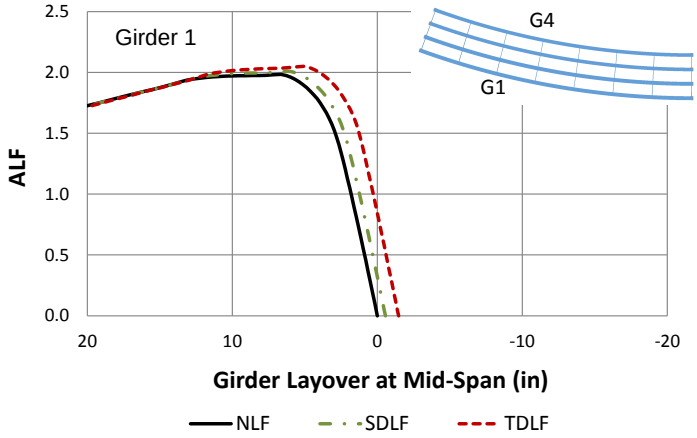

Figure 5.5.15. NISCR2, girder layover at the mid-span of girder G1 under applied load fraction of the total dead load for different detailing methods.

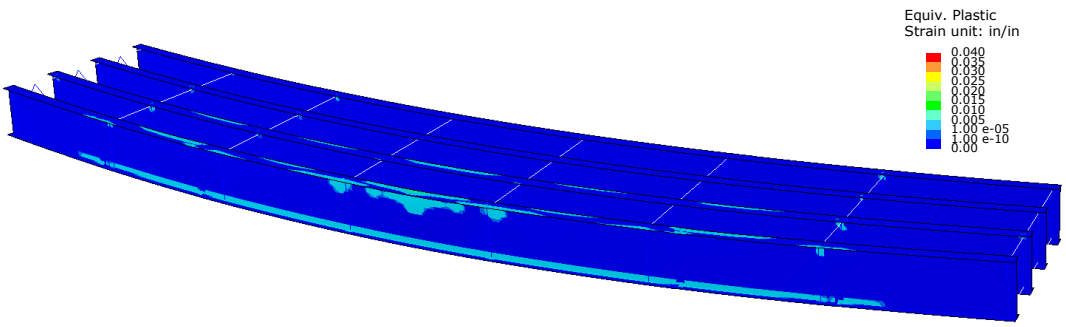

(i) NLF

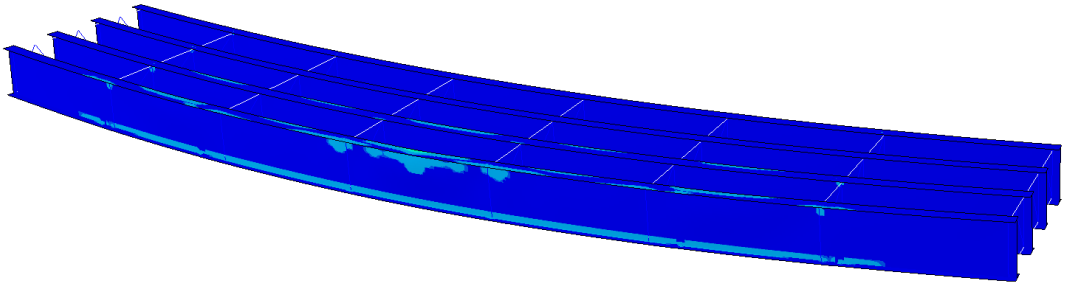

(ii) SDLF

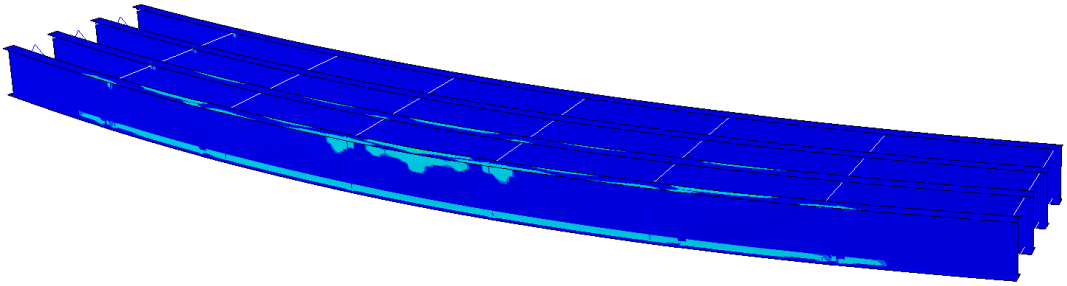

(iii) TDLF

Figure 5.5.16. NISCR2, Perspective view of mid-thickness equivalent plastic strains and deflected shape at maximum applied load of total dead load.

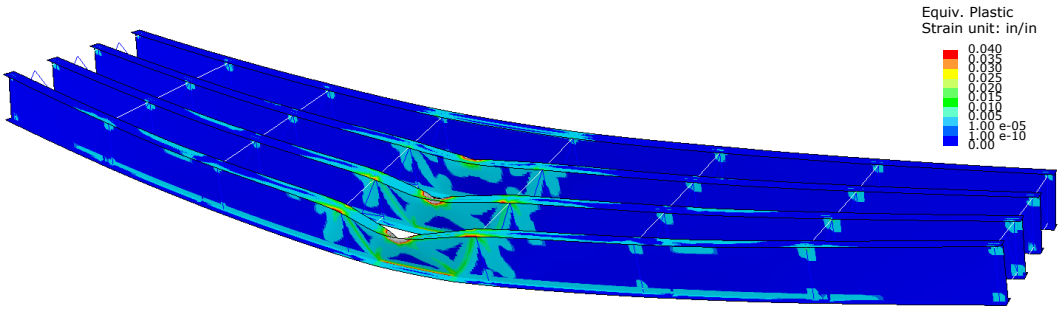

(i) NLF

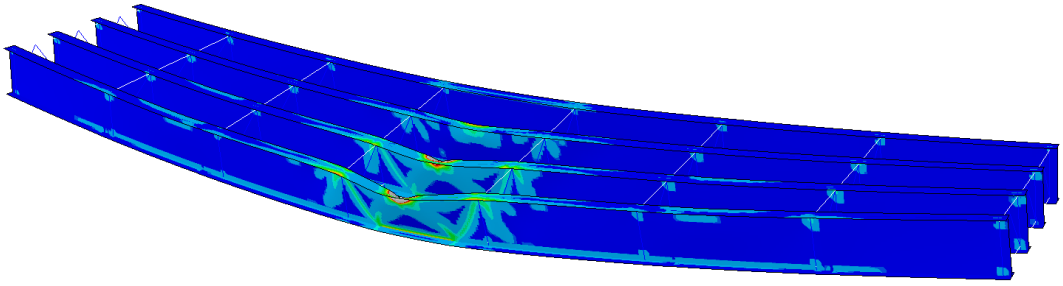

(ii) SDLF

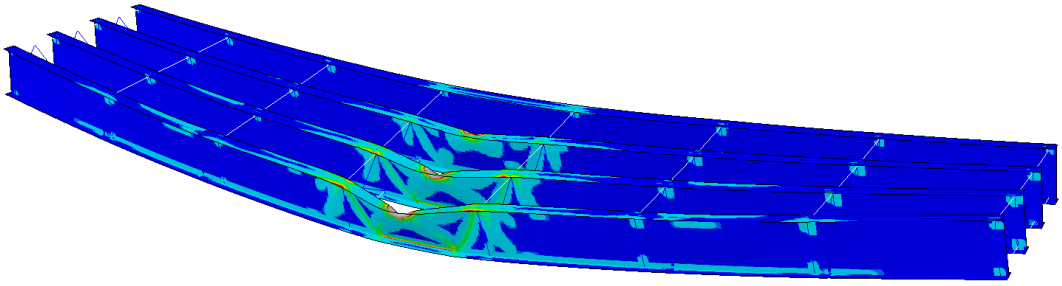

(iii) TDLF

Figure 5.5.17. NISCR2, Perspective view of mid-thickness equivalent plastic strains and deflected shape at the end of the analysis.

5.6. Impact of Bolt Slip on Component Responses

Cross-frame members are often connected to the girders by bolted connections. Induced cross-frame forces due to dead load or locked-in stress effects due to DLF detailing may be reduced due to the bolt slip. Moreover, bolt slip can influence the girder displacements and stresses.

In this section, the impact of bolt slip on cross-frame forces, girder stresses, and girder displacements are investigated by using the example bridge, NISSS54. Three cross-frames are selected from this bridge to evaluate the influence of bolt slip on the component responses. Figure 5.6.1 shows the selected cross-frames. Cross-frames CF-1 and CF-2 are selected since these cross-frames are located at the stiff transverse load path and large cross-frame forces are induced in these cross-frames due to dead loads. Additionally cross-frame CF-3 is selected since large locked-in cross-frame forces are induced in this cross-frame due to DLF detailing.

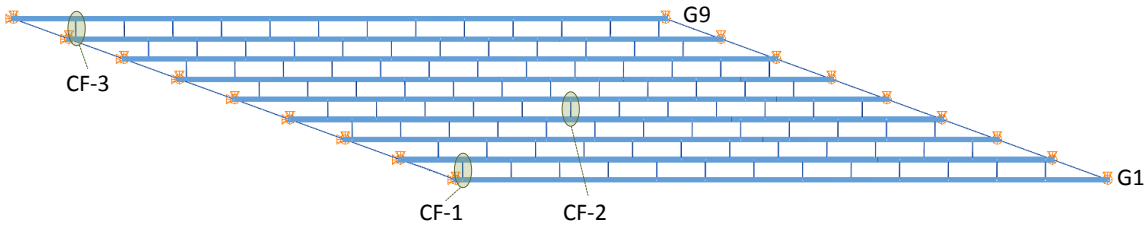

Figure 5.6.1. NISSS54, selected cross-frames for evaluating the influence of bolt slip.

For each of the cross-frames, 1/8 inches of bolt slip is introduced in both diagonal members by using an initial stress approach. It should be noted that the bolt slip is introduced only to the diagonals. Separate analyses are conducted to investigate the impact of bolt slip in each of the diagonals of the selected cross-frames on the component responses.

Table 5.6.1 shows the cross-frame forces for each of the cross-frames solely due to bolt slip. It should be noted that the maximum change in the diagonal force is 35.2, 34.0 and 32.1 kips due to bolt slip. The diagonal forces are also the maximum forces that are observed in the bridge NISSS54. For cross-frame CF-3, the locked-in cross-frame diagonal forces due to TDLF detailing are -137.54 and 158 kips. Although the diagonal forces due to locked-in stresses may be reduced by 35 kips due to bolt slip for the bridge NISSS54, the locked-in cross-frame forces cannot be relieved completely.

Table 5.6.1. Cross-frame forces due to bolt slip at cross-frames 1 through 3.

Cross-frame #	Bottom Chord (kips)	Top Chord (kips)	Diagonals (kips)	
1	0.1	3.3	25.4	-35.2
2	0.4	-0.3	33.7	-34.0
3	-9.1	-28.0	19.9	-32.1

Figure 5.6.2 shows the magnitude of the girder layovers due to bolt slip at cross-frames CF-1 through CF-3, plotted with respect to *z* axis for each girder. The maximum girder layover due to slip is less than 0.2 inches for each of the cases. The largest girder layovers are observed at the cross-frame locations where bolt slip occurs. For instance, relatively larger layovers are observed for girders G1 and G2 in the vicinity of the cross-frame CF-1. Similarly, relatively larger layovers are observed in the vicinity of the CF-2, if the bolt slip occurs at CF-2.

Figure 5.6.3 provides the vertical displacements of girders G1, G5 and G9 due to bolt slip at cross-frames CF-1 through CF-3. The maximum vertical displacement due to slip is less than 0.03 inches for all cases. Figure 5.6.4 shows the girder major-axis bending stresses of girders G1, G5, and G9 due to bolt slip at cross-frames CF-1 through CF-3. The maximum girder major-axis bending stress is observed to be less than 1 ksi for all of the cases. Figure 5.6.5 illustrates the girder flange lateral bending stresses due to bolt slip at cross-frames CF-1 through CF-3. The maximum girder flange lateral bending stress is less than 4 ksi for all of the cases.

In summary, a 1/8 inch bolt slip within a single cross-frame diagonal tends to have negligible influence on girder responses. Although bolt slip can relieve some of the diagonal locked-in cross-frame forces associated with DLF detailing, or other large dead load forces, the induced forces due to bolt slip are not large enough to have a significant impact on the cross-frame forces.

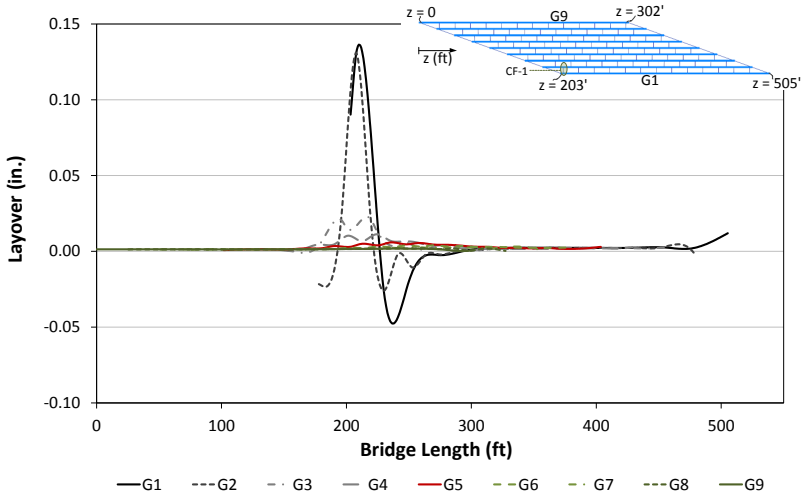

(i) Slip at cross-frame 1

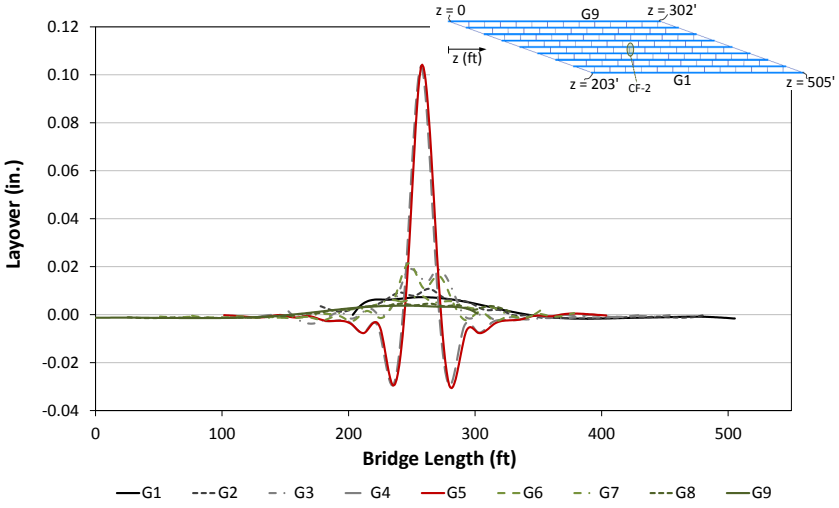

(ii) Slip at cross-frame 2

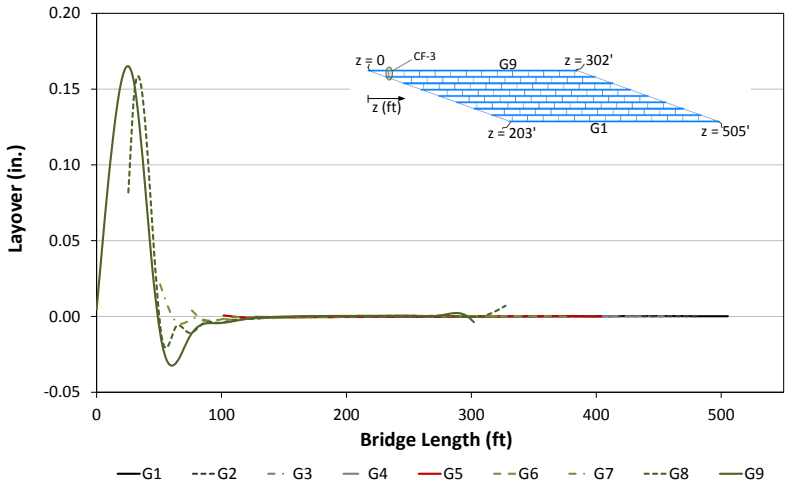

(iii) Slip at cross-frame 3

Figure 5.6.2. NISSS54, Girder layovers due to bolt slip at cross-frames CF-1 through CF-3.

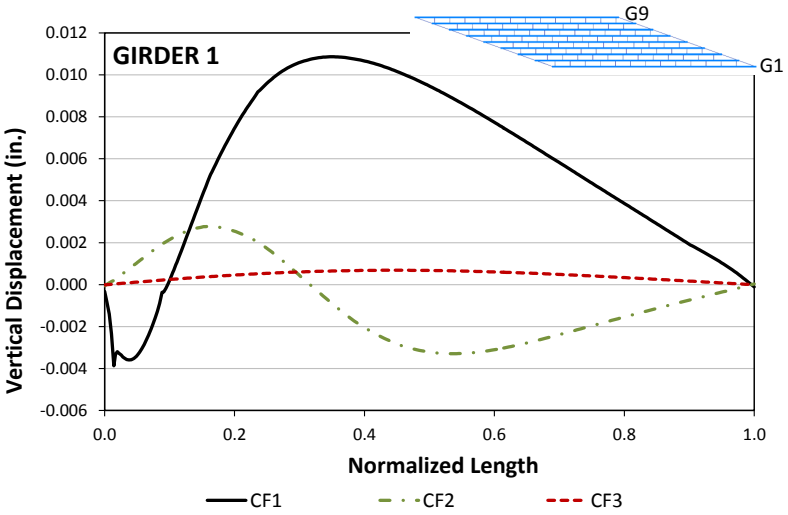

(i) Girder 1

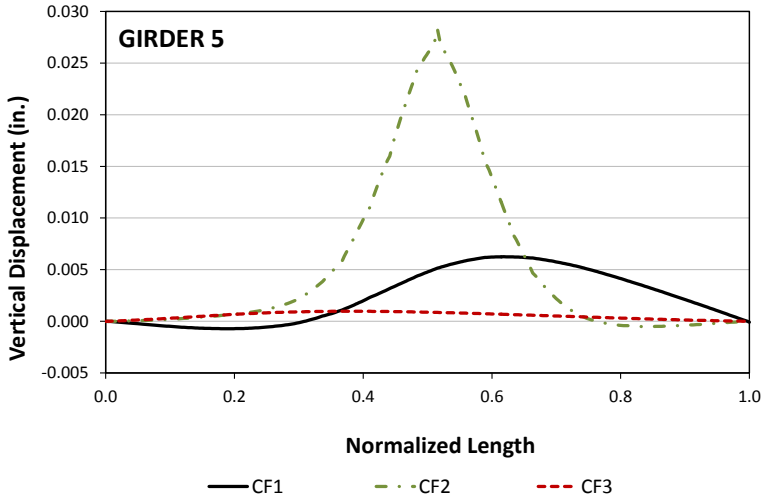

(ii) Girder 5

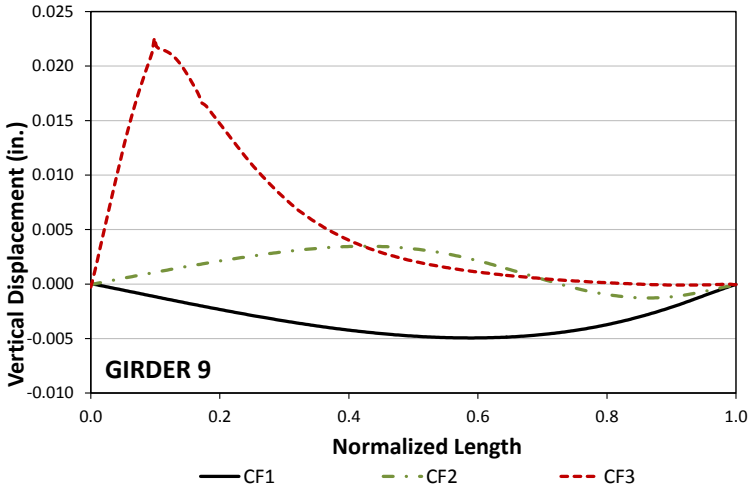

(iii) Girder 9

Figure 5.6.3. NISSS54, Vertical displacements due to bolt slip at cross-frames CF-1 through CF-3.

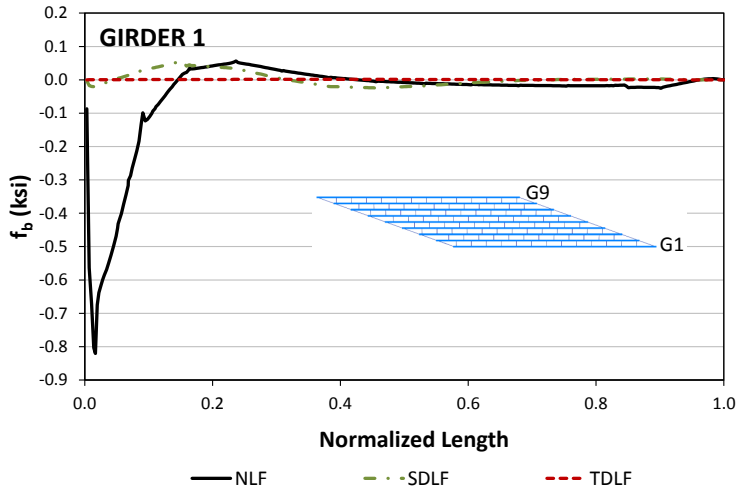

(i) Girder 1

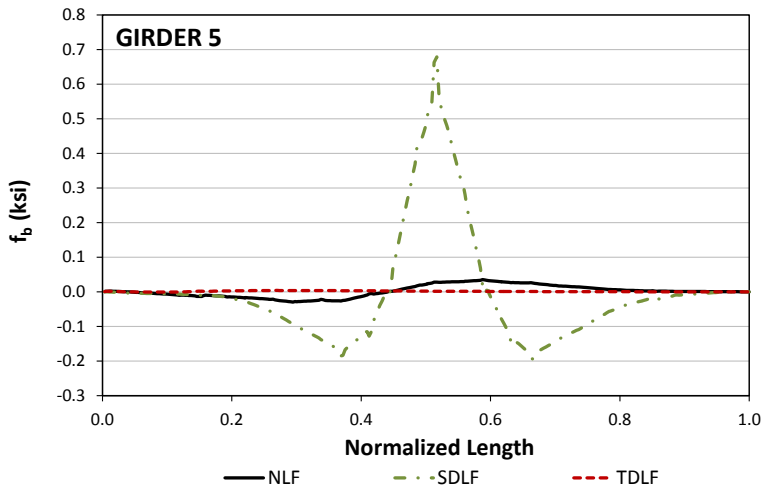

(ii) Girder 5

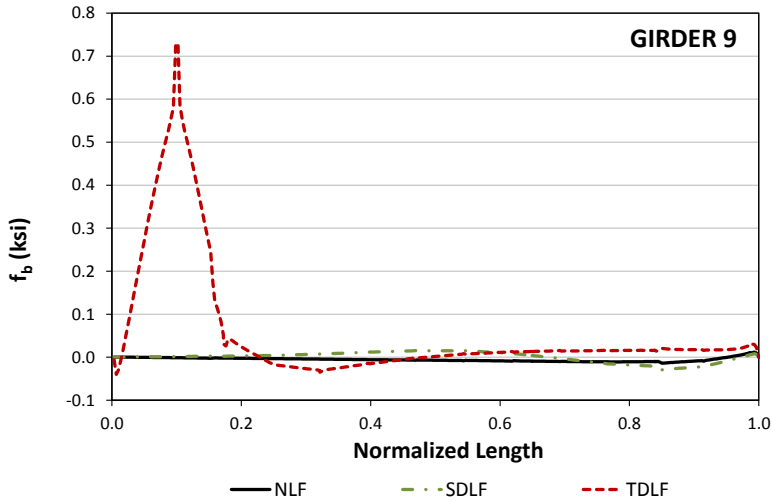

(iii) Girder 9

Figure 5.6.4. NISSS54, Girder major-axis bending stresses due to bolt slip at cross-frames CF-1 through CF-3.

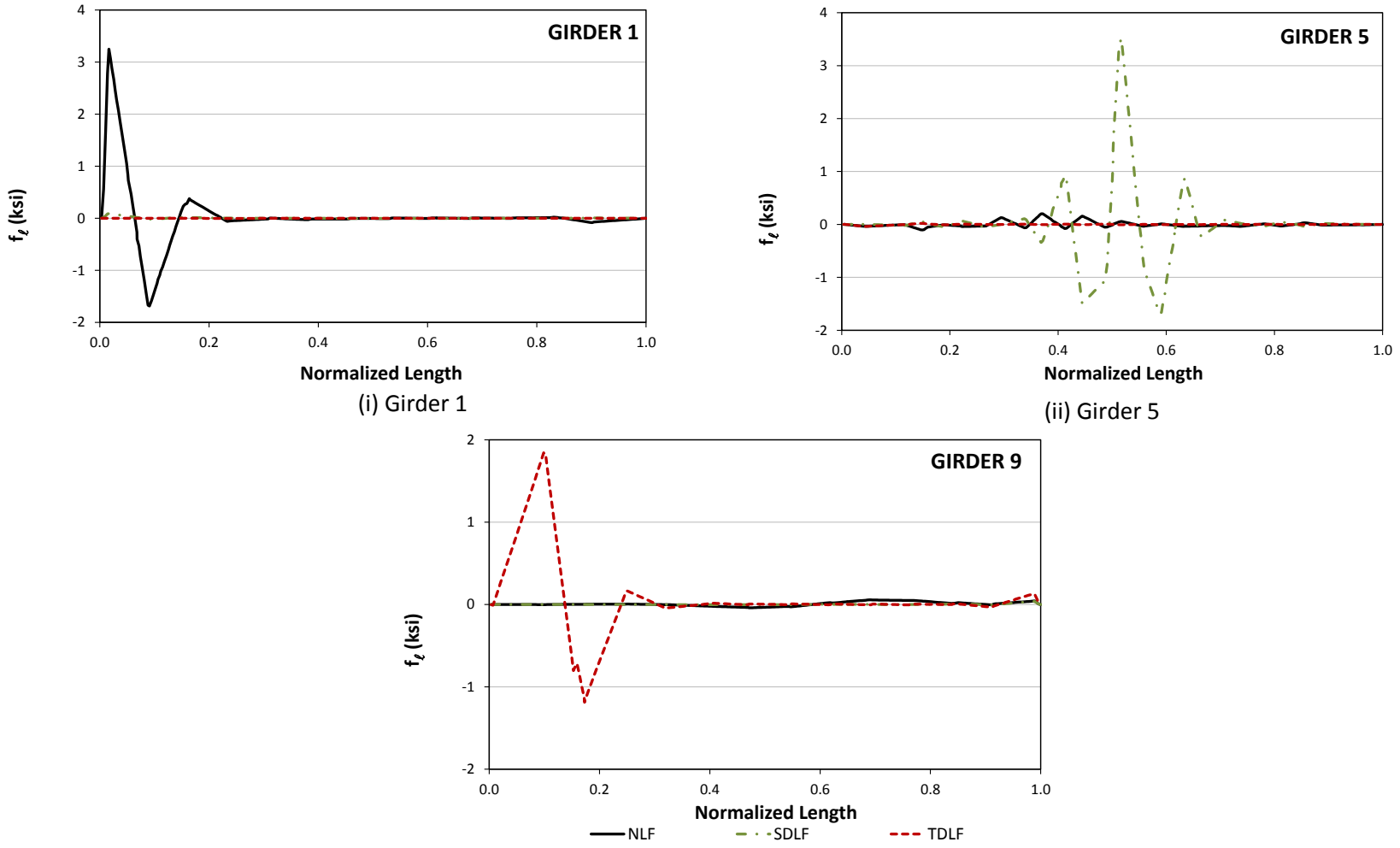

Figure 5.6.5. NISSS54, Girder flange lateral bending stresses due to bolt slip at cross-frames CF-1 through CF-3.

CHAPTER VI.

EVALUATION OF CROSS-FRAME DETAILING ON FIT-UP

Forces required to assemble the structure during erection can depend significantly on the erection procedures (e.g., selection of temporary shoring towers and, selection of holding cranes), the sequence of erection, and the type of cross-frame detailing used, although the final steel dead load geometry is unique. This chapter details the evaluations and provides guidance and recommendations to alleviate fit-up problems in I-girder bridges by using several bridge examples. Basic guidelines are provided to eliminate problems regarding staying within the admissible bearing rotation limits and checking the tendency of the bridge or bridge units for uplift during construction. Additionally, a way of estimating the required fit-up forces at different stages of steel erection is proposed in this Chapter.

6.1. Influence of Type of Cross-Frame Detailing on Fit-Up

Bridges generally experience 3D deflections during erection which can reduce or increase the displacement incompatibilities between the connection points of the bridge components. The displacement incompatibilities between connections can be different for different types of cross-frame detailing under the same construction stage. In bridges with NLF detailing, cross-frames are detailed to fit the girders under their theoretical no-load geometry. Any variation from the no-load geometry requires fit-up forces to assemble the cross-frames since the deflected geometry creates displacement incompatibilities. In the bridges with SDLF detailing, the lack-of-fit between the cross-frames and girders tends to be close to zero once the steel dead load camber is completely taken out of the girders by steel dead loads. However, this is rarely the case for partially erected structures as their rotational deflections can be different from those of the fully assembled bridge. In the bridges with TDLF detailing, lack-of-fit between the cross-frames and girders tend to be close to zero once total dead load camber is taken out of the girders by total dead load. Zero lack-of-fit for TDLF detailing is impossible to achieve since a steel structure has to be fully erected before pouring the concrete.

Displacement incompatibilities can be reduced by the selected erection scheme. For instance, SDLF detailing tends to minimize the fit-up forces (and stresses) during the steel erection unless the bridge is essentially supported in its no-load condition during the erection.

This is because the steel dead load deflections (and deformations) in the various partially erected units are closer to the final steel dead load deflections (and deformations) than to the total dead load or zero-load ones. Of course, if one provides sufficient temporary supports, holding cranes, etc. such that the partially erected structure is essentially in a no-load condition, NLF detailing minimizes the fit-up forces. TDLF detailing generally leads to larger fit-up forces since the steel structure is absent from the concrete dead load, but the cross-frames are detailed to fit-up with the girders once the total dead load cambers are taken out of the girders by the steel + concrete dead load. However, in most cases, the decision about which erection procedure to use is usually driven by site constraints.

There are different ways of controlling the deflected shape of the bridge during erection. Temporary supports and holding cranes can be used to release the steel dead load cambers of the girders during construction by letting the structure to displace due to dead loads. These practices are particularly beneficial when the girders need to be displaced vertically to reduce the displacement incompatibility to connect the cross-frames.

In the case of curved girders, it is more efficient to erect the girders from outside to inside for curved systems. This method is preferred since the top flanges of curved girders tend to lay-over in the direction away from the center of curvature under their dead load. By erecting subsequent girders from the outside (girders further away from the center of curvature) to the inside (girders closer to the center of curvature), the self-weight of the components being assembled into the partially erected structure helps to rotate the previously erected girders back into the desired geometry. If the girders are erected from inside to outside, large forces may be required in certain cases to lift the outside girder of the partially erected structure to achieve fit-up with a new outside girder.

6.2. Basic Guidelines for Erection

6.2.1. *Estimation of the bearing rotations for bridges, constructed with NLF detailing*

As mentioned in Chapter 2, for the bridges constructed with NLF detailing, girder layovers at the skewed bearings are unavoidable under dead loads. The torsional rotation capacity of the bearings can be insufficient if the layovers are excessive. The most commonly used bearing types are plain elastomeric bearings and steel reinforced elastomeric bearings. The maximum rotational capacities of the above bearing types are typically considered as 0.01 radians for

elastomeric bearings and 0.04 radians for steel reinforced elastomeric bearings (NHI/FHWA, 2011).

Given the major-axis bending rotation at the bearings and the skew angle it is possible to estimate the torsional rotation at the skewed bearings as discussed in Chapter 2. The twist angle or web out-of-plumbness of the member at the cross-frame location is expressed as

$$\phi_z = \phi_x \tan(\theta) \tag{6.2.1}$$

in Chapter 2. The admissible bearing rotation limits can be expressed as a function of the skew angle and major-axis bending rotation at the bearing by using Eq. 6.2.1 as shown in Figs. 6.2.1 and 6.2.2 for the given bearing types. Figure 6.2.1 is developed for plain elastomeric bearings while Fig. 6.2.2 is developed for steel reinforced elastomeric bearings. For the plain elastomeric bearing, ϕ_x in Eq. 6.2.1 is set to 0.01 radians which is the maximum torsional rotation limit. For steel reinforced elastomeric bearing, ϕ_x in Eq. 6.2.1 is set to 0.04 radians which is the maximum torsional rotational limit. Percentages of the maximum rotational capacity of the bearing are provided to accommodate the fact that part of the rotation is taken up by live loads. The curves in Figs. 6.2.1 and 6.2.2 can be generated for other bearing types by using the same approach.

These plots can be used to check targeted bearing rotation level, given the major-axis bending rotation and the skew angle. If the intersection point of the skew angle and ϕ_x of a bridge falls below the targeted bearing rotation level, the bridge does not violate the targeted bearing rotation level. Otherwise, the bridge should be constructed with either SDLF of TDLF detailing to reduce the layovers.

Table 6.2.1 summarizes the maximum girder layovers of the study bridges at the skewed supports under steel and total dead loads (third and fourth columns, respectively). The layover values in Table 6.2.1 are obtained from finite element analysis solutions of the bridges, constructed with NLF detailing. Additionally, girder depth of the each bridge is provided in the second column of Table 6.2.1. Girder torsional rotations under steel and total dead loads are tabulated in the fifth and sixth columns of Table 6.2.1. Table 6.2.1 demonstrates that if plain elastomeric bearings are used, five bridges exceed the maximum torsional rotation capacity of the bearings under steel dead load and twenty five of the bridges exceed the maximum torsional rotation capacity of the bearings under total dead load (highlighted with blue shading). In contrast, if steel elastomeric bearings are used only two of the bridges (NISSS14 and NISSS54) exceed the maximum torsional rotation capacity of the bearings under total dead load

(highlighted with red shading). The layovers at the bearings can be reduced by DLF detailing for the cases in which the bearing rotation capacities are exceeded.

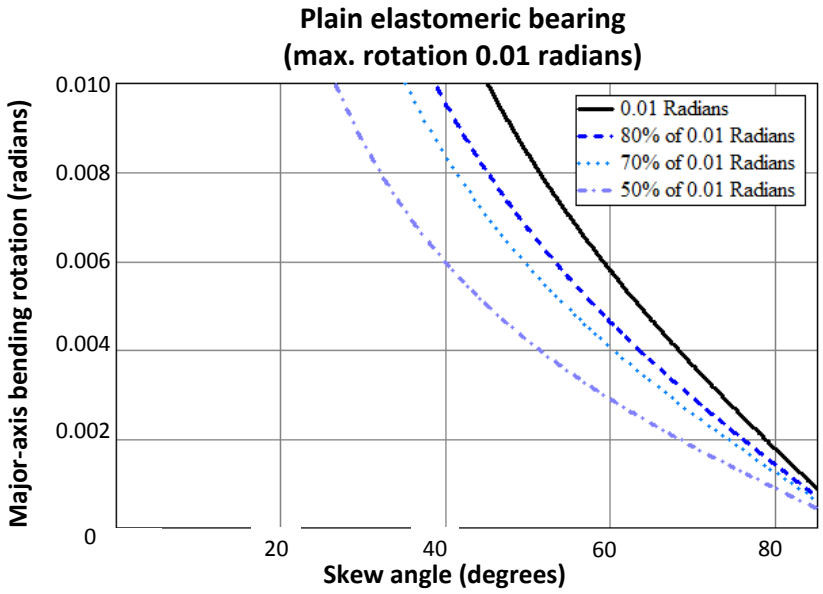

Figure 6.2.1.Torsional rotation levels for plain elastomeric bearings for given major-axis bending rotation and skew angle of the bearing.

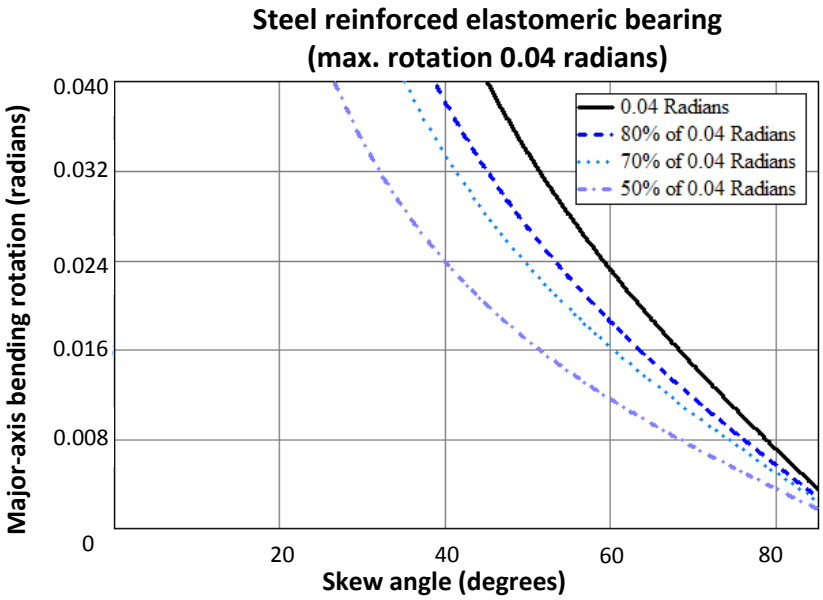

Figure 6.2.2. Torsional rotation levels for steel reinforced elastomeric bearings for given major-axis bending rotation and skew angle of the bearing.

Table 6.2.1. FEA girder layovers and torsional rotations at the bearings under steel and total dead load for the studied skewed bridges.

Bridge Name	Girder Depth (in)	Δ_{x_SDL} (in) FEA	Δ_{x_TDL} (in) FEA	ϕ_{z_SDL} (rad) Eq. 2.1.2	ϕ_{z_TDL} (rad) Eq. 2.1.2
NISSS2	72	0.2	0.6	0.002	0.008
EISSS3	57	0.2	1.3	0.003	0.023
NISSS4	72	0.7	2.7	0.009	0.038
NISSS6	72	0.3	1.2	0.004	0.016
NISSS11	72	0.1	0.4	0.001	0.005
NISSS13	72	0.3	1.2	0.004	0.017
NISSS14	72	0.7	3.3	0.010	0.046
EISSS5	49	0.3	1.5	0.006	0.030
NISSS16	72	0.4	1.5	0.005	0.021
EISSS6	120	1.8	4.4	0.015	0.036
NISSS36	108	0.8	2.3	0.008	0.021
NISSS37	120	0.4	0.9	0.003	0.007
NISSS53	150	1.1	2.6	0.008	0.018
NISSS54	144	2.7	5.9	0.018	0.041
NISSS56	162	1.4	3.0	0.008	0.018
NICSS1	72	0.0	0.0	0.000	0.000
NICSS3	72	0.1	0.3	0.001	0.005
XICSS5	69	0.2	1.0	0.002	0.015
EICSS1	51	0.1	0.6	0.002	0.011
ECSS12	54	0.2	1.0	0.004	0.018
NICSS16	72	0.3	1.7	0.004	0.023
EICSS2	98	0.8	2.5	0.008	0.026
NICSS25	168	0.0	0.0	0.000	0.000
NICSS27	168	0.5	1.1	0.003	0.006
EISCS3	68	0.4	1.0	0.006	0.015
NISCS3	78	0.3	0.8	0.004	0.011
NISCS9	78	0.5	1.4	0.006	0.018
NISCS14	72	0.3	1.1	0.005	0.015
NISCS15	90	0.4	0.9	0.004	0.010
NISCS37	174	0.8	1.3	0.004	0.008
NISCS38	156	1.5	3.3	0.010	0.021
NISCS39	180	1.4	2.4	0.008	0.013
EICCS10	50	0.1	0.3	0.002	0.006
NICCS2	84	0.1	0.2	0.001	0.002
NICCS3	72	0.1	0.4	0.002	0.005
XICCS7	92	0.0	0.0	0.000	0.000
NICCS9	72	0.3	1.0	0.003	0.014
NICCS13	114	0.3	0.9	0.003	0.008
NICCS14	114	0.2	0.4	0.002	0.004
EICCS1	96	0.0	0.0	0.000	0.000
EICCS27	90	1.0	3.6	0.011	0.040
NICCS24	168	0.0	0.0	0.000	0.000

6.2.2. *Estimation of tendency to uplift at bearings*

Horizontally curved systems experience torsional overturning forces under applied loads since there is an offset between the line between the bearings of the girder and applied loads. Overturning effects can lead to uplift problems during construction. An approximate indicator of the overall torsion within the bridge span (or bridge unit), and the tendency for uplift at the bearings, is introduced in Chapter 4 by a "torsion index" (I_T). As noted in Chapter 4, the torsion index is related to the magnitude of the overall torsion that exists within the bridge (or bridge unit) span due to eccentricity of its self-weight. Furthermore, the torsion index gives some indication of the potential for uplift at the bearings locations. Table 6.2.2 provides the calculated overturning parameters for the study bridges. For continuous bridges, the I_T index is calculated for each span individually. For the straight bridges with parallel skewed or no skewed bearings, I_T = 0.5 means that the centroid of the deck area is mid-way between the chords intersecting the end bearing lines.

The bridges summarized in Table 6.2.2 are checked for uplift under total dead loads for NLF detailing. No uplift is observed for the ISSN, ISSS, and ICSS bridge categories from the FEA predictions. Torsion indices are calculated between 0.50 and 0.58 for these bridge categories. For the curved I-girder bridges (ISCR, ISCS, ICCR, and ICCS), torsion indices are calculated between 0.48 and 0.88. Most of the higher indices correspond to ICCR and ICCS bridge categories. For the ISCS bridge category, torsion indices are calculated between 0.55 and 0.71. Uplift of the bearings is observed for several bridges of this category. These bridges are NISCS3 (I_T =0.71), NISCS15 (I_T =0.67), and NISCS39 (I_T = 0.68). Significantly, none of the bridges with I_T < 0.65 have experienced uplift. For ISCR and ISCS bridge categories, there are several cases with I_T > 0.65 but uplift does not occur. These cases are EISCR1 (I_T = 0.71), NISCR2 (I_T = 0.69), NISCR5 (I_T = 0.71), NISCR11 (I_T = 0.65), and EISCS3 (I_T = 0.68). However, the ratio of the inside to outside bearing reactions is found to be very small for these cases. Table 6.2.3 summaries the ratio of the sum inside to outside girder reactions under steel and total dead load for these bridges. It should be noted that the ratios are slightly higher under total dead load due to the restoring effect of the overhang bracket loadings for inside girders.

As noted above, the torsion index is related the magnitude of the overall torsion that exists in the bridge span (or bridge unit), due to the eccentricity of its self-weight. Furthermore, it provides some indication of the potential for uplift at bearings. In this research, it has been observed that simple-span I-girder bridges with a torsion index of 0.65 and higher are

susceptible to uplift at the bearings. Continuous span bridges can tolerate higher indices due to the stabilizing effect of the continuity with the adjacent spans. However, the continuity with the adjacent spans generally varies during the steel erection, and therefore, $I_T > 0.65$ serves as a rough indicator of when the engineer should check carefully for uplift in continuous-span I-girder bridges.

It should be noted for straight and skewed bridges that TDLF detailing tends to make the bearings, which are on the shorter (and stiffer) diagonal direction between the corners of the deck, see uplift until the total dead load is on the bridge.

Table 6.2.2. Calculated torsion indices for studied bridges.

Bridge Category	Bridge Name	I_T
ICSN	XICSN1	0.50, 0.50, 0.50
ISSS	NISSS2	0.50
	EISSS3	0.50
	NISSS4	0.50
	NISSS6	0.53
	NISSS11	0.50
	NISSS13	0.50
	NISSS14	0.50
	EISSS5	0.50
	NISSS16	0.58
	EISSS6	0.50
	NISSS36	0.55
	NISSS37	0.54
	NISSS53	0.50
	NISSS54	0.50
	NISSS56	0.53
ICSS	NICSS1	0.48, 0.52
	NICSS3	0.50, 0.52
	XICSS5	0.50, 0.50, 0.50
	EICSS1	0.50, 0.50
	ECSS12	0.50, 0.50
	NICSS16	0.50, 0.50, 0.50
	EICSS2	0.48, 0.55, 0.50
	NICSS25	0.48, 0.52
	NICSS27	0.50, 0.52
ISCR	EISCR1	0.71
	NISCR2	0.69
	NISCR5	0.71
	NISCR7	0.62
	NISCR8	0.58
	NISCR10	0.59
	NISCR11	0.65

Table 6.2.2. (continued). Calculated torsion indices for studied bridges.

Bridge Category	Bridge Name	I_T			
ISCS	EISCS3	0.68			
	NISCS3	0.71			
	NISCS9	0.63			
	NISCS14	0.55			
	NISCS15	0.67			
	NISCS37	0.62			
	NISCS38	0.59			
	NISCS39	0.68			
	EISCS4	0.64			
ICCR	NICCR1	0.87,	0.87,	0.74	
	EICCR22a	0.60,	0.63,	0.66,	0.63,
		0.60,	0.60,	0.59,	0.62
	EICCR11	0.50,	0.50,	0.87	
	EICCR4	0.61,	0.64,	0.59,	0.56,
		0.64,	0.50		
	EICCR15	0.55,	0.58		
	NICCR8	0.61,	0.61,	0.58	
	NICCR12	0.66,	0.66,	0.61	
ICCS	EICCS10	0.73,	0.72		
	NICCS2	0.81,	0.87		
	NICCS3	0.81,	0.81		
	XICCS7	0.55,	0.64,	0.65	
	NICCS9	0.53,	0.58		
	NICCS13	0.84,	0.85		
	NICCS14	0.85,	0.88		
	EICCS1	0.65,	0.80,	0.70,	0.62
	EICCS27	0.51,	0.49,	0.47	
	NICCS24	0.68,	0.65		

Table 6.2.3. Ratio of the sum of outside bearing reactions to the sum of inside girder reactions for selected bridges.

Bridge	SDL	TDL
	$\Sigma R_{in} / \Sigma R_{out}$	$\Sigma R_{in} / \Sigma R_{out}$
EISCR1	0.12	0.23
NISCR2	0.10	0.17
NISCR5	0.06	0.06
NISCR11	0.05	0.11
EISCS3	0.17	0.21

6.3. Estimation of Fit-up Forces

For DLF detailing, cross-frames do not fit to the girders in the no-load geometry due to the lack-of-fit between the girders. Similarly, for NLF detailing, cross-frames may not fit-up with girders during steel erection due to dead load deflections. In both cases, girders have to be twisted and forced to connect to the cross-frames. Come-along or jacking screws are used to twist the girders to fit in to position. Figure 6.3.1 is a representative sketch of the use of a come-along at the interior cross-frame location.

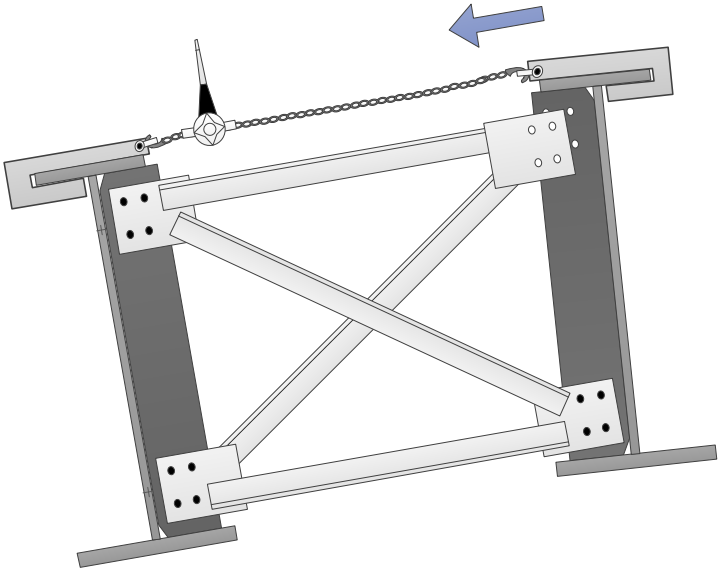

Figure 6.3.1. Intermediate cross-frame location during assemble of the cross-frame.

Spatial displacements can develop during erection of the bridges due to dead load deflections, assemble of the end cross-frames, temporary supports, and blocked profile of the girders, and other related problems. The deflected geometry can influence the come-along forces significantly. Large forces can be required to accommodate the large displacement incompatibilities due to dead load deflections or DLF detailing of the cross-frames which can lead to fit-up problems. However, come-along forces can be estimated by calculating the stiffness of the girder at the intermediate cross-frame location and the required additional layover of the girder to connect the cross-frame to the girder. Figure 6.3.2 illustrates the girder that needs to be pulled to make the connection. Δ_{xR} in Fig. 6.3.2 is the required additional layover of the girder to make the connection with the cross-frame, y_{st} is the distance to the shear center from the top flange. Come along force on the top flange is denoted as $F_{come.along}$. The come-along devices typically are used between the top flanges of adjacent girders; thus, these forces are assumed to act only at the top flanges (See Fig. 6.3.1).

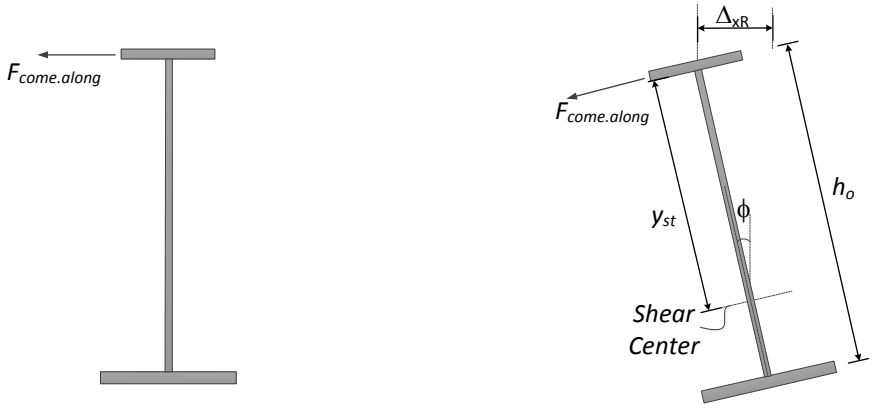

(i) initial geometry *(ii) rotated geometry*

Figure 6.3.2. Representative rotation of the section at the cross-frame location.

6.3.1. *Estimation of girder layovers during erection*

Equation 2.1.5 is introduced in Chapter 2 to estimate the layovers within the span by using the differential vertical displacements, and assuming negligible cross-frame in-plane deformations. The use of this equation can be extended to estimate the girder layovers at different steel erection stages by considering the dead load deflections and the differential camber between the girders. The girder layover (Δ_x) can be expressed as

$$\Delta_x = \Delta_{x.Const} + \Delta_{xR} \tag{6.3.1}$$

where, $\Delta_{x.Const}$, is the layover due to dead load deflections in the current constructed configuration, and Δ_{xR} is the additional required layover to make the connection of the cross-frame. The layovers in Eq. 6.3.1 are illustrated in Fig. 6.3.3. Similarly, differential vertical displacements between girders can be reduced due to dead load deflections during construction. Hence, the current differential vertical displacement can be written as

$$\Delta_{yR} = \Delta_{y.C} - \Delta_{y.Const} \tag{6.3.2}$$

where $\Delta_{y.Const}$ is the differential vertical displacement due to dead loads in the current constructed configuration, Δ_{yR} is the remaining differential vertical displacement between the girders, and $\Delta_{y.C}$ is the initial differential vertical camber between the girders. As a summary, Eq. 2.1.5 can be expresses as

$$\Delta_{xR} = h\left(\frac{\Delta_{y.C} - \Delta_{y.Const}}{s}\right) - \Delta_{xConst} \tag{6.3.3}$$

$\Delta_{x.Const}$ can be conservatively estimated from Eq. 2.1.5 by using $\Delta_{y.Const}$. Therefore, Eq. 6.3.3 can also be expressed as

$$\Delta_{xR} = h\left[\left(\frac{\Delta_{y} - \Delta_{y.Const}}{s}\right) - \left(\frac{\Delta_{y.Const}}{s}\right)\right] \tag{6.3.4}$$

for the cases where $\Delta_{x.Const}$ is unknown.

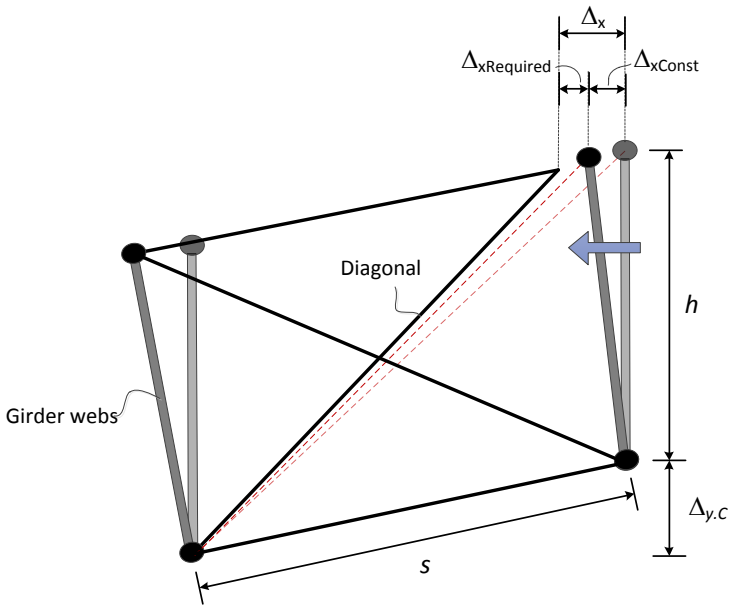

Figure 6.3.3. Required layover to make the connection and layovers due to construction for an intermediate cross-frame location.

6.3.2. *Estimation of girder stiffness at the intermediate cross-frame locations*

Come-along forces can be significantly different depending on the magnitude of the required layovers to make the connection and transverse stiffness of the erected unit. The stiffness of the girder at the intermediate cross-frame location can be approximated by either the torsional stiffness of the girder or the lateral stiffness of the flange.

Torsional stiffness of the girders can be estimated using the unit load concept. Since the girder webs are stiffened at the cross-frame locations from connection plates, it can be assumed that the girder webs remain plane during rotation. Total torsional moment on the I-section members is composed from Saint-Venant's torsion and the warping torsion. The total torsional moment is expressed as:

$$M_{total} = M_{St.Venant} + M_{Warping} = GJ\frac{d\phi}{dz} - EC_w\frac{d^3\phi}{dz^3} \tag{6.3.5}$$

where E and G are the elastic and the shear moduli, J and C_w are the St.-Venant torsional constant and warping constant, ϕ is the angle of twist, and z is the rotation axis.

C_w can be calculated for singly-symmetric sections as

$$C_w = {h_o}^2\,{b_{f.Bot}}^3\,t_{f.Bot}\,\frac{1}{12\left[1+\left(\frac{b_{f.Bot}}{b_{f.Top}}\right)^3\left(\frac{t_{f.Bot}}{t_{f.Top}}\right)\right]} \tag{6.3.6}$$

where $b_{f.Bot}$ and $b_{f.Top}$ are the bottom and top flange width, $t_{f.Bot}$ and $t_{f.Top}$ are the bottom and top flange thickness, and h_o is the distance between the flange centroids.

The differential equation expressed in Eq. 6.3.5 can be solved by combining the homogenous solution and the particular solution. The angle of twist can be expressed as

$$\phi = \phi_h + \phi_p = A_1 \sinh(\lambda\, z) + A_2 \cosh(\lambda\, z) + A_3\, z + A_4 \tag{6.3.7}$$

for constant torsional moment along a portion of the member where

$$\lambda = \sqrt{\frac{G\,J}{E\,C_w}} \tag{6.3.8}$$

Assuming torsionally simple supports at the end cross-frames and torsionally fixed supports at the next available cross-frame location, torsional stiffness of the girder can be estimated at the intermediate cross-frame location by introducing a unit torsional moment at the targeted cross-frame location. Figure 6.3.4 illustrates the simplified model.

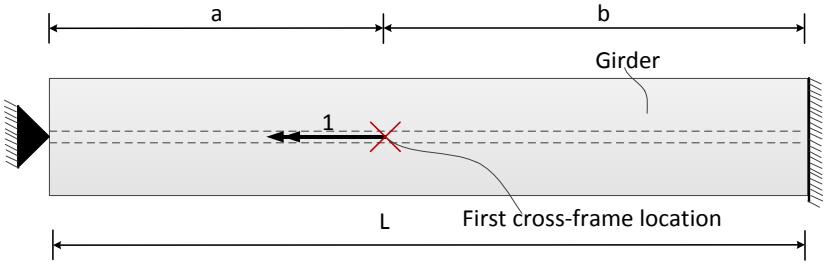

Figure 6.3.4. Torsionally fixed and simple support model with unit torsion.

Figure 6.3.5 provides the total distribution of the moment along the girder due to the applied unit torsional moment. Torsional moment at the simple support can be calculated as

$$R_{simple\ support} = \frac{b^2\,(a+2\,L)}{2\,L^3} \tag{6.3.9}$$

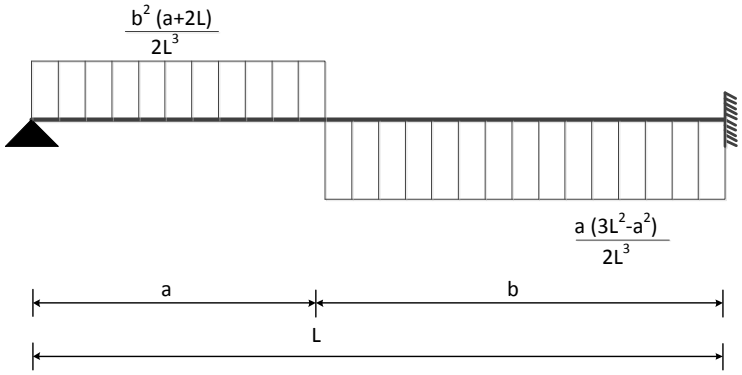

Figure 6.3.5.Total torsional moment for the applied unit torsion.

Torsional moment is constant for $x < a$. Therefore, A_3 can be calculated from the particular solution of the differential equation by using Eq. 6.3.5 as

$$\frac{b^2\,(a+2\,L)}{2\,L^3} = GJ\frac{d\phi_p}{dz} - EC_w\frac{d^3\phi_p}{dz^3} \tag{6.3.10}$$

The third derivative of the particular solution is zero so Eq. 6.3.10 becomes

$$\frac{b^2\,(a+2\,L)}{2\,L^3} = GJA_3 \tag{6.3.11}$$

If one collects the terms, A_3 can be obtained as

$$A_3 = \frac{b^2\,(a+2\,L)}{2GJ\,L^3} \tag{6.3.12}$$

If Eq. 6.3.12 is plugged into Eq. 6.3.7 and the local axis is moved to the application of the torsional moment then Eq. 6.3.7 becomes,

$$\phi = A_1 \sinh\big(\lambda\,(z-a)\big) + A_2 \cosh\big(\lambda\,(z-a)\big) + \frac{b^2\,(a+2\,L)}{2GJ\,L^3}(z-a) + A_4 \tag{6.3.13}$$

Figure 6.3.6 illustrates the assumed boundary conditions for the simplified model. Since there is no rotation at the supports, $\phi = 0$ at the point of the applied torsional moment, $\phi' = 0$ because the fixed end cross-section cannot warp, and $\phi'' = 0$ because the pinned support cross-section can warp freely.

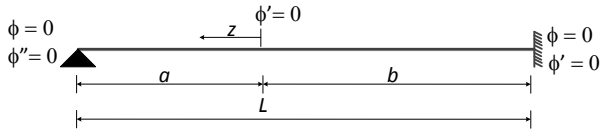

Figure 6.3.6.Boundary conditions for the simplified model.

Eq. 6.3.13 is discontinuous at $z = 0$. For calculating the torsional stiffness of the system, it is sufficient to obtain only one part of the differential equation. If Eq. 6.3.13 is evaluated for $a \le z < 0$ and by using the boundary condition $z = a$, $\phi = 0$ and $\phi'' = 0$

$$A_2 = A_3 = 0 \tag{6.3.14}$$

and from $z = 0$, $\phi' = 0$,

$$A_1 = \frac{2\,L\,b^2 + a\,b^2}{2\,G\,J\,L^3\lambda\cosh(a\,\lambda)} \tag{6.3.15}$$

Finally, Eq. 6.3.14 becomes for $a \le z < 0$,

$$\phi = \frac{2\,L\,b^2 + a\,b^2}{2\,G\,J\,L^3\lambda\cosh(a\,\lambda)} \sinh\big(\lambda\,(z-a)\big) + \frac{b^2\,(a+2\,L)}{2GJ\,L^3}(z-a) \tag{6.3.16}$$

The torsional stiffness at z = 0 can be estimated by taking the inverse of Eq.6.3.16.

$$k_\phi = \frac{1}{\frac{2\,L\,b^2 + a\,b^2}{2\,G\,J\,L^3\lambda\cosh(a\,\lambda)} \sinh\big(\lambda\,(-a)\big) + \frac{b^2\,(a+2\,L)}{2GJ\,L^3}(-a)} \tag{6.3.17}$$

Similarly, the lateral stiffness of the top flange can be estimated by introducing a unit lateral load at the cross-frame location of a prop cantilever beam (see Fig. 6.3.7) and taking the inverse of the resulting displacement represented by

$$k_{Lateral} = \frac{1}{\frac{a^2\,b^3}{12\;E\;I_{y.TopFlange}\;L^3}(3\,L+a)} \tag{6.3.18}$$

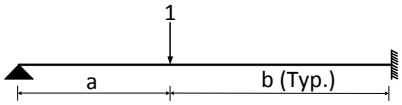

Figure 6.3.7. Simplified model for the calculation of the lateral stiffness of the flange at the first cross-frame location.

6.3.3. *Estimation of come-along forces*

Approximating the girder rotation at the shear center and assuming that the girder is rotated by pulling the top flange with a come-along, the come-along force ($F_{come.along}$) can be estimated by using the torsional stiffness derived in Eq. 6.3.17 and the moment equilibrium on the section, shown as

$$F_{come.along} = \frac{k_\phi}{y_{st}}\left(\frac{\Delta_{x\ Required}}{h_o}\right) \tag{6.3.19}$$

For small unbraced lengths, the lateral stiffness of the top flange provides better estimates for the come-along forces since distortion of the section is likely which invalidate the approximation of the girder torsional stiffness. Conversely, for longer unbraced lengths, the contributions from the Saint-Venant's torsion can be significant which cannot be captured by the lateral stiffness of the flange. Therefore the required force can be conservatively estimated as

$$F_{come.along} = max\left[\frac{k_\phi}{y_{st}}\left(\frac{\Delta_{x\ Required}}{h_o}\right), k_{Lateral}\Delta_{x\ Required}\right] \tag{6.3.20}$$

Equation 6.3.20 is evaluated with four cases where different scenarios are targeted for connecting an intermediate cross-frame. Girder dimensions and bridge properties of EISSS6 are provided in Appendix C. Table 6.3.1 provides the different erection scenarios of EISSS6 for connecting the first intermediate cross-frame that is closest to the end of the bridge. Come-along forces are estimated for the erection stages shown in Table 6.3.1 by using Eq. 6.3.20. In the FEA models, a temporary bottom strut is placed at the targeted cross-frame location and 10 kips is applied to the top flange of the targeted cross-frame assuming that girder G8 is pulled towards the rest of the system by using a come-along. Resulting girder layovers at the targeted cross-frame for each scenario is reported in Table 6.3.2. Then come-along forces are estimated by using the layovers at the cross-frame locations and compared with the initial applied load. The estimates of these forces are reported in Table 6.3.2 for each scenario. It is clear that the come-along forces used to assemble the cross-frames are predicted conservatively for all cases. Therefore, Eq. 6.3.20 can be used to estimate the come-along forces for a particular erection stage of a bridge. Erection procedure can be revised if the estimated forces are large ($F_{come.along}$> 12 kips). Typical load for single come-along is 12 kips.

Table 6.3.1. Different erection scenarios of EISS6 for assembling the cross-frame at the extreme end of the bridge.

Scenario	Plan View	Description
1	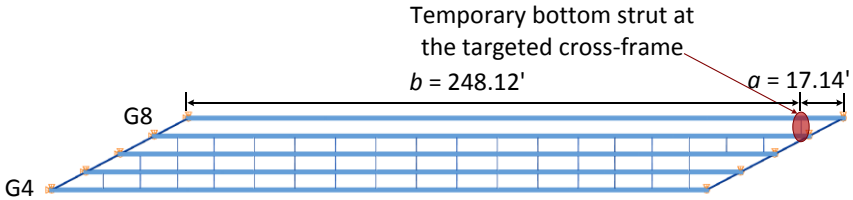	Only end cross-frames are installed between girder lines G7 and G8. Targeted cross-frame is initially connected by temporary bottom strut.
2		End cross-frames are installed between girder lines G7 and G8. All interior cross-frames are installed except two cross-frames that are closest to the targeted cross-frame. Targeted cross-frame is initially connected by temporary bottom strut.
3		End cross-frames are installed between girder lines G7 and G8. All interior cross-frames are installed except one cross-frame that is closest to the targeted cross-frame. Targeted cross-frame is initially connected by temporary bottom strut.
4		End cross-frames are installed between girder lines G7 and G8. All interior cross-frames are installed except the targeted cross-frame. Targeted cross-frame is initially connected by temporary bottom strut.

Table 6.3.2. Comparison of the come-along forces for the required layovers.

Scenario	$\Delta_{x\,R}$(inch) FEA	$F_{come.along}$ (kips) FEA	$F_{come.along}$ (kips) EQ.6.2.20
1	2.09	10.0	15.4
2	1.14	10.0	12.7
3	0.81	10.0	11.3
4	0.36	10.0	12.6

6.4. Recommended Practices to Alleviate Fit-up Problems for Different Methods of Detailing

Selected erection practices and cross-frame detailing methods can significantly impact the fit-up of the members. In this section, steel erection practices are recommended to alleviate the fit-up difficulties for particular situations. These practices include the following:

- Taking advantage of the steel dead load deflections during erection
- Using temporary X-bracings and temporary struts
- Providing a minimum offset distance from the skewed bearing line for framing the first intermediate cross-frame or leaving certain cross-frames out
- Providing minimum ratio of adjacent unbraced lengths at first cross-frame offset from a bearing line
- Using cross-frames without top chords.
- Using temporary supports when necessary

The above practices are evaluated by analytical studies. The influence of cross-frame detailing methods on the above practices is also discussed for selected cases in the subsequent sections.

6.4.1. *Use of dead load deflections, temporary X-bracings, temporary struts*

Differential vertical cambers and the rotational compatibility at the bearing lines associated with girder camber rotations are the primary sources of lack-of-fit for DLF detailing. Pushing and pulling devices are usually used for connecting the cross-frame members. Representative sketches of the pulling and pushing devices are illustrated in Fig.6.4.1. The displacement incompatibilities are usually largest in the no-load geometry for the bridges constructed with DLF detailing. Figure 6.4.2 shows the differential vertical cambers of a representative bridge (EISSS6), constructed with TDLF detailing.

Large fit-up forces can be required if the girders need to be displaced vertically by the applied forces since the girders generally have large stiffness against major-axis bending deformations. These cases are more likely to occur at the locations with large differential vertical displacements between the girders and close interaction of the different displacement compatibilities (i.e. interior cross-frames that are framed close to the skewed bearings). It should be noted from Fig. 6.4.2 that erecting the bridge EISSS6 in the no-load geometry (i.e. with temporary supports) may require large fit-up forces. However, dead load deflections during steel erection can be used for reducing the displacement incompatibilities since girders displace laterally and vertically under dead loads. Therefore, fit-up forces that are required to connect the cross-frames can be reduced significantly by using dead load deflections. Furthermore, temporary X-bracings and temporary struts can be used to increase the lateral flexibility of the system during construction. Representative sketches of the temporary X-bracings and temporary struts are illustrated in Figure 6.4.3.

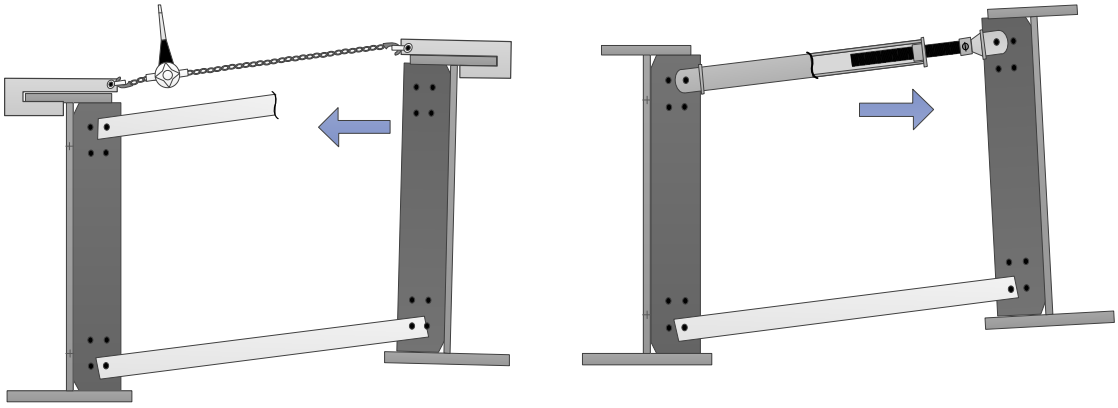

(i) Pulling Device (come-along) *(ii) Pushing Device (jacking screw)*

Figure 6.4.1. Representative pushing and pulling devices that are used during steel erection.

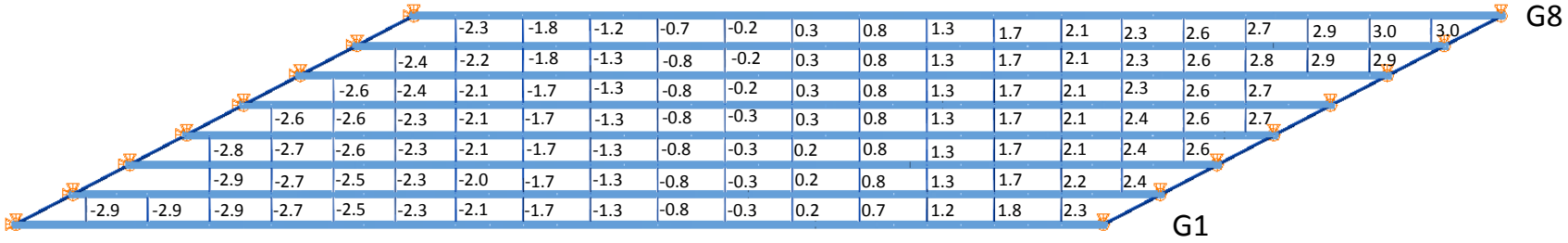

Figure 6.4.2. EISSS6, Differential camber between girders for TDLF detailing

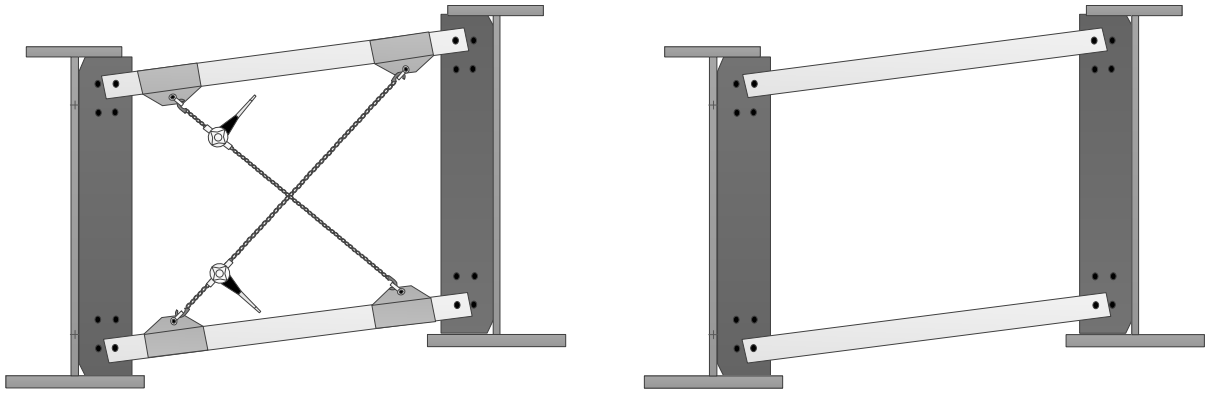

(i) Temporary X-Braces *(ii) Temporary Struts*

Figure 6.4.3. EISSS6, Representative sketch of temporary X-braces and temporary struts.

These practices are demonstrated by using the bridge EISSS6, constructed with TDLF detailing. The recommended erection scheme for the bridge EISSS6 to alleviate large fit-up forces is as follows:

Stage 1: Girder lines G4 and G5 are pre-assembled as a pair at no-load geometry by first installing the cross-frames in the middle of the span. Next, the remaining cross-frames are installed working from the middle of the span out toward the ends by jacking up or down at ends. Jacking up and down allows for adjustment of displacement incompatibilities. Additionally, connections can be made relatively easily since the structure is in pair which provides less transverse stiffness compared to the fully assembled structure.

After installing all cross-frames, the entire assembly is placed into position using cranes. The girder assembly is blocked to the steel dead load profile at the falsework tower by allowing the structure to deflect. Holding cranes are released after the girders are at their steel dead load profile, as shown in Fig. 6.4.4(i). Figure 6.4.5 shows the undeflected and deflected shapes of the girder assembly in the no-load profile and in the steel dead load profile when it is placed on the falsework. Deflections are magnified by 10 times. It should be noted from Fig 6.4.5(iii) that layovers in the opposite direction from those due to the total dead load are obtained under the *steel dead load* when TDLF detailing is used.

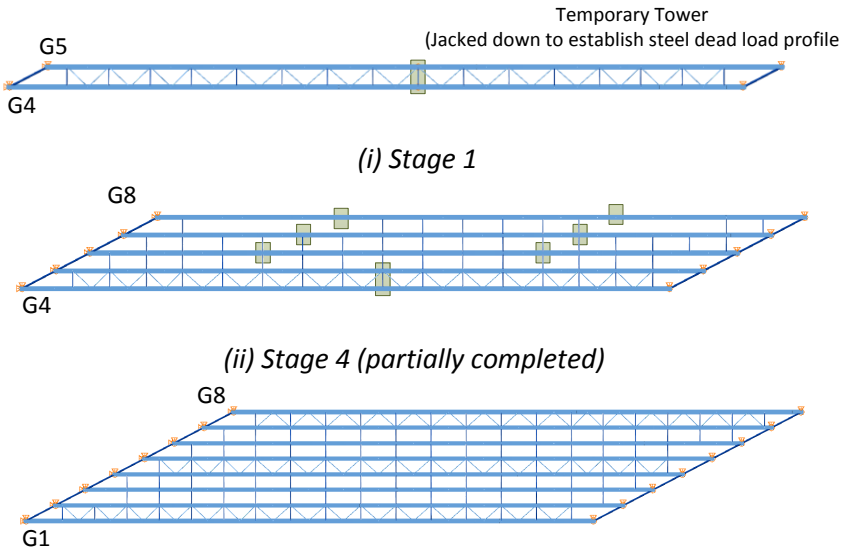

(i) Stage 1

(ii) Stage 4 (partially completed)

(iii) Stages 7 and 8

Figure 6.4.4. EISSS6, Selected erection stages.

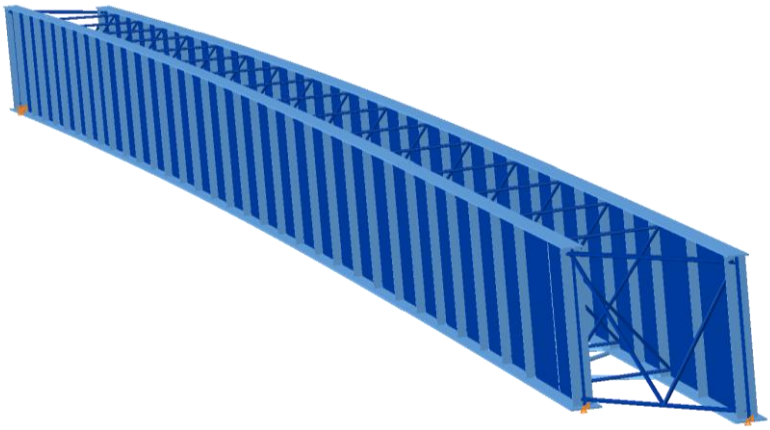

(i) Undeflected Geometry

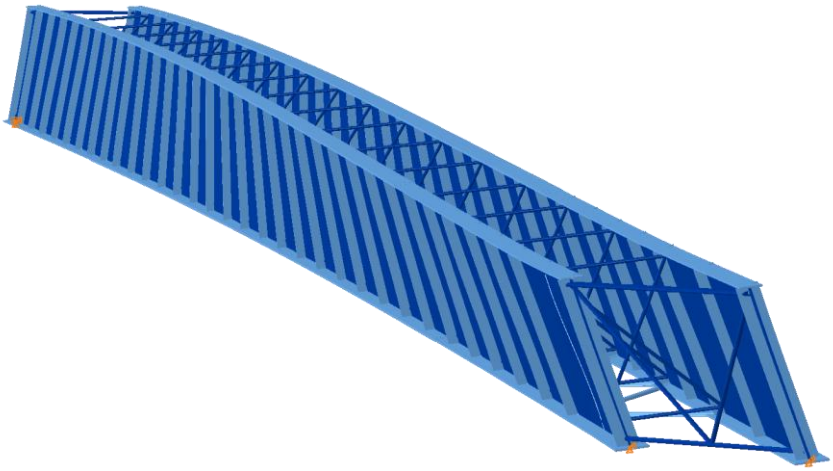

(ii) Deflected Geometry in the no-load profile

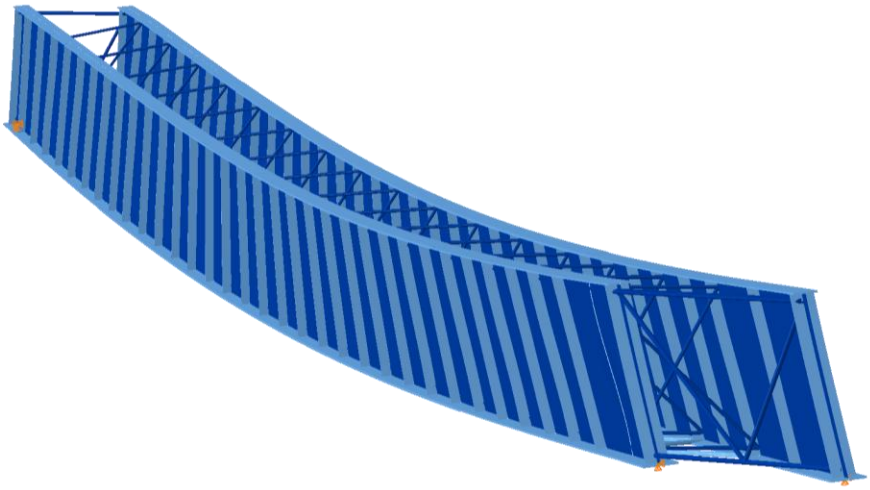

(iii) Deflected Geometry in the steel dead load profile

Figure 6.4.5. EISSS6, Stage 1, Undeflected and deflected geometries in the no-load and steel dead load profiles (magnified by 10x).

Stages 2 through 4: Erection procedures used for Stages 2 through 4 are similar to each other. Starting with girder line G6, the next girder line is erected for each subsequent erection stage. In Stages 2 through 4, the targeted girder line is brought to the steel dead load profile by using cranes and jacking down the falsework. This procedure is followed by installation of the cross-frames that are in the middle of the span (1/4 of the total cross-frames). These are the easiest cross-frames to install since the differential camber is lowest at these cross-frame locations and the girder line is relatively flexible at these locations. Temporary X-braces at each end of the bridge as well as temporary struts at the extreme ends of the girder are installed. Figure 6.4.6 provides the location of the temporary X-braces and struts for Stage 4. Temporary X-bracings are adjustable to allow the fit-up of other cross-frames while maintaining stability of the girder. The adjustable function of the temporary X-bracings enables the erector to handle the change in the differential displacements between the girders during the steel erection since the structure moves vertically and laterally. However, this operation is a very complex and may require coordinated effort of the erector. Additionally, temporary struts are used to keep the girder spacing constant. Top chords can be removed in the cases where the structure is stable or where it is hard to install them in the no-load geometry. This stage is followed by the installation of the remaining cross-frames from the middle of the span toward the abutments. In the subsequent sections, cross-frame fit-up forces are estimated for Stage 4, which is shown in Fig. 6.4.6. It should be noted that temporary supports are not shown in Fig. 6.4.6 since the structure is brought to the steel dead load geometry.

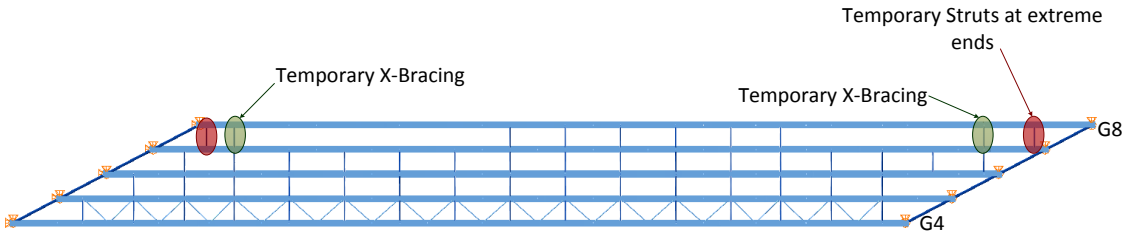

Figure 6.4.6. EISSS6, Stage 4 location of the temporary X-braces and temporary struts.

The lack-of-fit of the members, due to DLF detailing, is usually maximum in the no-load geometry. The differential camber between the girders for the selected cross frame locations (see Fig. 6.4.7 for selected cross-frames) at the no-load geometry is calculated from the differential vertical cambers as 2.98”, 2.96” and -2.32” for cross-frames CF-1 through CF-3 respectively. If the erector selects to install either of these cross-frames in the no-load

geometry, girders need to be twisted approximately as 3.78”, 3.75” and 2.94” at the selected cross-frame locations. The required girder twist is estimated from Eq. 5.2.2 by using the initial differential vertical camber between the girders at the selected cross-frame locations.

For the bridges constructed with DLF detailing, significant reduction in the displacement incompatibilities can be obtained by using the dead load vertical and lateral displacements. Figure 6.4.8 provides the undeflected and deflected geometry of Stage 4 under steel dead load for TDLF detailing where displacements are magnified by 10 times. The girder layovers are obtained from FEA solutions as 1.44”, 1.88” and 1.29” at the cross-frames CF-1 through CF-3. Moreover, the differential vertical displacements are reduced to 1.90”, 2.06” and 1.36” in the deflected position for cross-frames CF-1 through CF-3 respectively. Table 6.4.1 compares the required additional layovers to connect the either of the selected cross-frames for Stage 4 for the installation of the diagonal chords of the selected cross-frames. Required additional layovers to connect the either of the selected cross-frames are calculated by using Eqs.6.3.3 and 6.3.4.

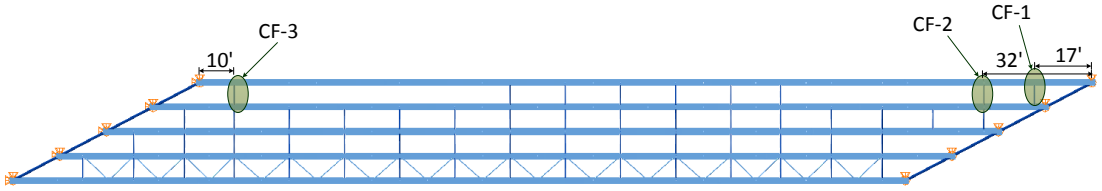

Figure 6.4.7. EISSS6, Selected cross-frame locations and the offset distances from the skewed bearing line.

Table 6.4.1. EISSS6, Required layovers to make install diagonals of the selected cross-frames in Stage 4.

Cross-Frame	Δ_R (inch) EQ. 6.3.3	Δ_R (inch) EQ. 6.3.4
1	0.97	1.05
2	0.73	1.48
3	-0.44	-0.52

Two different erection scenarios can provide very different displacement incompatibilities. For Stage 4 of EISSS6, if one wants the install the cross-frame CF-1 in the no-load geometry, the girder needs to be twisted by 3.78 inches whereas the twist reduces to 0.97 inches if the dead load deflections are used during construction. As mentioned before, large twist amounts can require large come-along and jacking forces. Table 6.4.2 compares the required additional layovers to install either of the cross-frames in the no-load geometry (second column) and in the deflected geometry (third and fourth columns). Come along-forces can be estimated form

Eq. 6.3.20 for either of these cases. Table 6.4.2 also provides the estimated come-along forces for cross-frames CF-1 through CF-3 to install either of the cross-frames at two different erection scenarios (columns 5th through 7th). It should be noted that come-along forces at 6th column are estimated by using Δ_R from 3rd column whereas, come along-forces in column 7th are estimated by using Δ_R from 4th columns. Table 6.4.2 illustrates that come-along and jacking forces can be reduced significantly by using the advantage of dead load deflections during construction. Typical maximum load for single come-along is 12 kips. It is clear for the installation of CF-1 and CF-3 in the no-load geometry that required come-along forces can be larger than the 12 kips (35 kips and 101 kips respectively). However, these forces can be reduced significantly if dead load deflections are used during steel erection (10kips and 18 kips respectively). It should be noted that the use of dead load deflections can increase the displacement incompatibilities if the bridge is constructed with NLF detailing.

Table 6.4.2. EISSS6, Estimated come-along forces for two different erection schemes for cross-frame locations 1 through 3.

Cross-Frame Location	Δ_R (inch) EQ. 5.2.2	Δ_R (inch) EQ. 6.3.3	Δ_R (inch) EQ. 6.3.4	$F_{come.along}$ (kips) No-Load Geometry	$F_{come.along}$ (kips) Stg.4	$F_{come.along}$ (kips) Stg.4
1	3.78	0.97	1.05	34.71	1.84	9.64
2	3.75	0.73	1.48	9.47	1.84	3.74
3	2.94	0.44	0.52	100.69	15.07	17.81

Stages 5 through 7: Stages 5 through 7 are similar to Stages 2 through 4. Girders are erected in a similar way, starting from girder line 3 and working towards girder line G1. Steel erection is completed at the end of Stage 7 (see Fig. 6.4.4(iii)).

Stage 8: The slab is poured in Stage 8. Approximately plumb girders are targeted at the end of Stage 8 since the bridge is constructed with TDLF detailing.

To sum up, the selected erection scheme can provide minimum fit-up forces. For the bridges constructed with DLF detailing, using the dead load deflections, temporary X-bracings, and temporary struts during erection can be beneficial to minimize the fit-up forces while maintaining the stability of the bridge geometry. Conversely, if the bridge is constructed with NLF detailing, using temporary supports to keep the structure close to the no-load geometry can provide less fit-up forces as shown in Section 6.4.4.

Perspective View

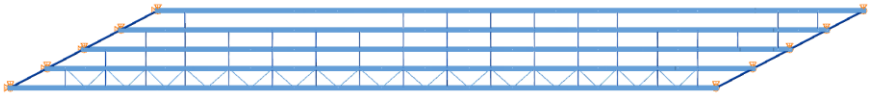

Plan View

(i) Undeflected Geometry

Perspective View

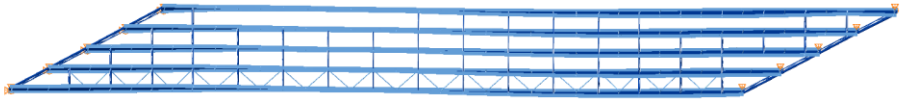

Plan View

(ii) Deflected Geometry

Figure 6.4.8. EISSS6, Stage 4 undeflected and Deflected geometry (magnified by 10x) under steel dead load for TDLF detailing.

6.4.2. *Minimum ratio of adjacent unbraced lengths at first cross-frame offset from a bearing line*

For bridges constructed with NLF detailing, large cross-frame forces can be induced in intermediate cross-frames framed close to the skewed supports due to nuisance stiffness effects. For bridges constructed with DLF detailing, large locked-in forces can be developed outside the stiff transverse load paths depending on the relative lateral stiffness of the adjacent girders and the magnitude of the differential vertical camber. These cross-frame locations are typically observed at intermediate cross-frames framed close to the skewed bearings. Figure 6.4.9 illustrates these locations in the bridge NISSS54 for different types of cross-frame detailing. For NLF detailing, total dead load cross-frame forces are largest at the obtuse corners of bridge NISSS54 (shaded with red in Fig. 6.4.9) due to nuisance stiffness effects. For DLF detailing, relatively large cross-frame forces are observed at the cross-frames located close to the skewed bearings lines (shaded with green in Fig. 6.4.9) due to large locked-in force effects from DLF detailing. The offset distances of the shaded cross-frames and the typical unbraced length within the span are also provided in Fig. 6.4.9.

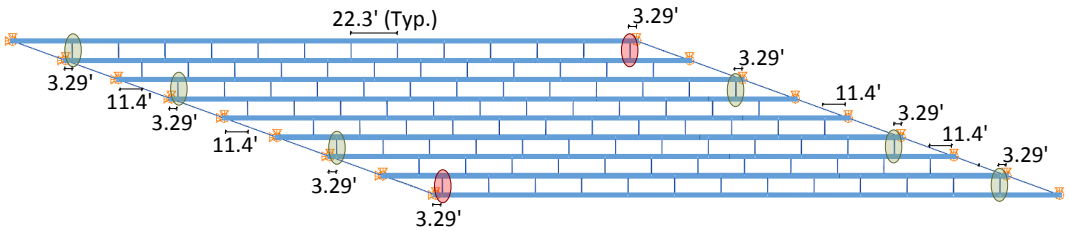

Figure 6.4.9. NISSS54, illustration of the close first intermediate cross-frame locations for methods of detailing.

Large cross-frame forces at the first intermediate cross-frames can be reduced by providing a certain offset distance from the skewed bearing line. Typically fabricators use at least 1.5 times the depth of the web to place the first cross-frame. However, for bridges with severe skew and short spans, this ratio provides offset distances that can cause large cross-frame forces at the first intermediate cross-frames. Therefore, the offset distance can be rationalized better by considering the differential stiffness of the unbraced lengths. Large cross-frame forces can be reduced as the cross-frames are connected farther away from the bearing lines such that the relative lateral stiffness is reasonable or these issues can be eliminated if the cross-frame is removed.

Lateral stiffness of the flange at the first cross-frame location can be estimated by isolating the girder flange and using a unit load concept, as in Fig. 6.4.10. The simple support represents

the bearing cross-frame, the distance *a* is the offset distance of the first cross-frame location and the fixed support is the next available intermediate cross-frame with the typical cross-frame spacing of the bridge. The typical cross-frame spacing within the span is denoted is as *b*.

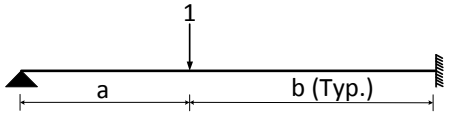

Figure 6.4.10. Simplified model for the calculation of the lateral stiffness of the flange at the first cross-frame location.

Lateral stiffness of the flange at the first cross-frame location can be expressed as the inverse of the deflection due to the unit load as

$$k_{Lateral} = \frac{12\ E\ I_{y.TopFlange}\ (a+b)^3}{a^2\ b^3\ (4a+3b)} \tag{6.4.1}$$

Similarly the lateral stiffness of the case where *a* = *b* can be calculated as

$$k_{Lateral} = \frac{96\ \mathrm{E}\ I_{y.TopFlange}}{7\ b^3} \tag{6.4.2}$$

The ratio of the lateral stiffness of the first cross-frame with respect to the lateral stiffness when *a* = *b* can be calculated by taking the ratios of Eqs. 6.3.1 to 6.3.2 as in

$$\chi_{Offset} = \frac{7\ (a+b)^3}{8\ a^2\ (4a+3b)} \tag{6.4.3}$$

Let $\alpha = a/b$ then Eq. 6.4.3 becomes

$$\chi_{Offset} = \frac{7\ (\alpha+1)^3}{8\ \alpha^2\ (4\alpha+3)} \tag{6.4.4}$$

As a result, Eq. 6.4.4 provides the change of ratio of the lateral stiffness of the first cross-frame in terms of the ratio of the unbraced lengths. Figure 6.4.11 shows the relative lateral stiffness versus the ratio α (which is the ratio of the offset length to the adjacent unbraced length) at the first interior cross-frame from a bearing line, α. Figure 6.4.11 demonstrates that the relative stiffness ratio increases significantly when $a \leq 0.4\ b$. For the cases when $a \leq 0.4\ b$, high cross-frame forces tend to develop at the first cross-frame locations.

For the bridge NISSS54, α ratios are calculated as 0.15 for those with an offset distance of 3.29 ft and 0.51 for those with an offset distance of 11.40 ft. Figure 6.4.12 provides the recommended cross-frame layout of bridge NISSS54 based on the recommended minimum offset ratio (*a >0.4 b).*

Figures 6.4.13 through 6.4.15 provide distribution of the largest total dead load cross-frame component axial forces in each of the cross-frames throughout the bridge NISSS54 for each type of cross-frame detailing. Figures 6.4.13 through 6.4.15 show that the magnitudes of the total

sum of the cross-frame forces are reduced compared to the forces observed from the original layout (See Figs. 5.3.1 and 5.3.7). Furthermore, Figs. 5.3.7 and 6.4.15 illustrate that large locked-in stresses are eliminated at the acute corners of the bridge due to the removal of the cross-frames that are close to the skewed bearing lines. It is also important the check the cross-frame forces under steel dead load for TDLF detailing since cross-frame forces tend to be larger under steel dead load due to locked-in stresses. Figure 6.4.16 provides the cross-frame forces under steel dead load for TDLF detailing. It should be noted from Figs. 6.4.13, 6.4.15 and 6.4.16 that cross-frame forces due to TDLF detailing do not exceed the cross-frame forces for NLF detailing. The locations with large locked-in forces are eliminated by removing the cross-frames that do not satisfy α >0.4. Figure 6.4.17 shows the girder major-axis and flange lateral bending stresses under total dead load for different cross-frame detailing methods. It is also clear from Fig. 6.4.17 that recommended offset of the first cross-frame leads to decrease in the flange lateral bending stresses when the results are compared with results of the original layout (See Figs. 6.4.17 and 5.4.4).

To sum up, the minimum ratio of the adjacent unbraced length at first cross-frame offset from a bearing line, α, should be taken as at least 0.4 since the relative lateral stiffness increases significantly for smaller ratios. This recommendation provides an offset distance of the first intermediate cross-frame, so that the forces in the cross-frame components are in acceptable levels. Furthermore, large locked-in cross-frame forces due to DLF detailing can be eliminated at the intermediate cross-frame locations with large relative lateral stiffness of the adjacent girders and large differential camber.

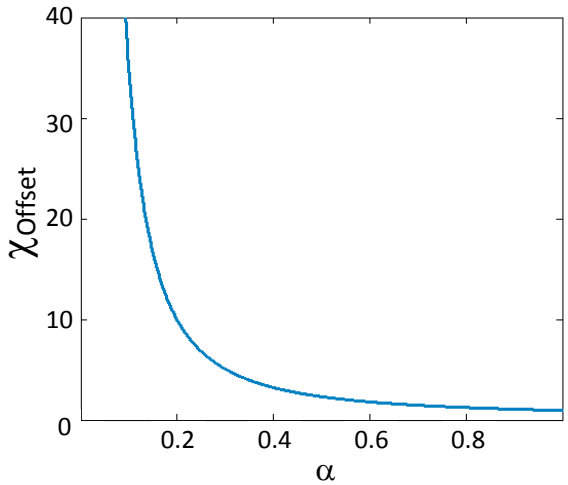

Figure 6.4.11. Ratio of the relative stiffness ratio for the first intermediate cross-frame.

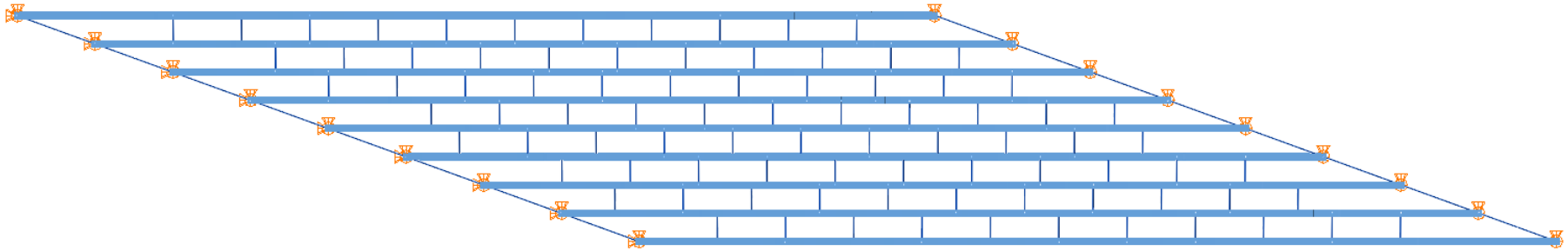

Figure 6.4.12. NISSS54, new layout of the cross-frames.

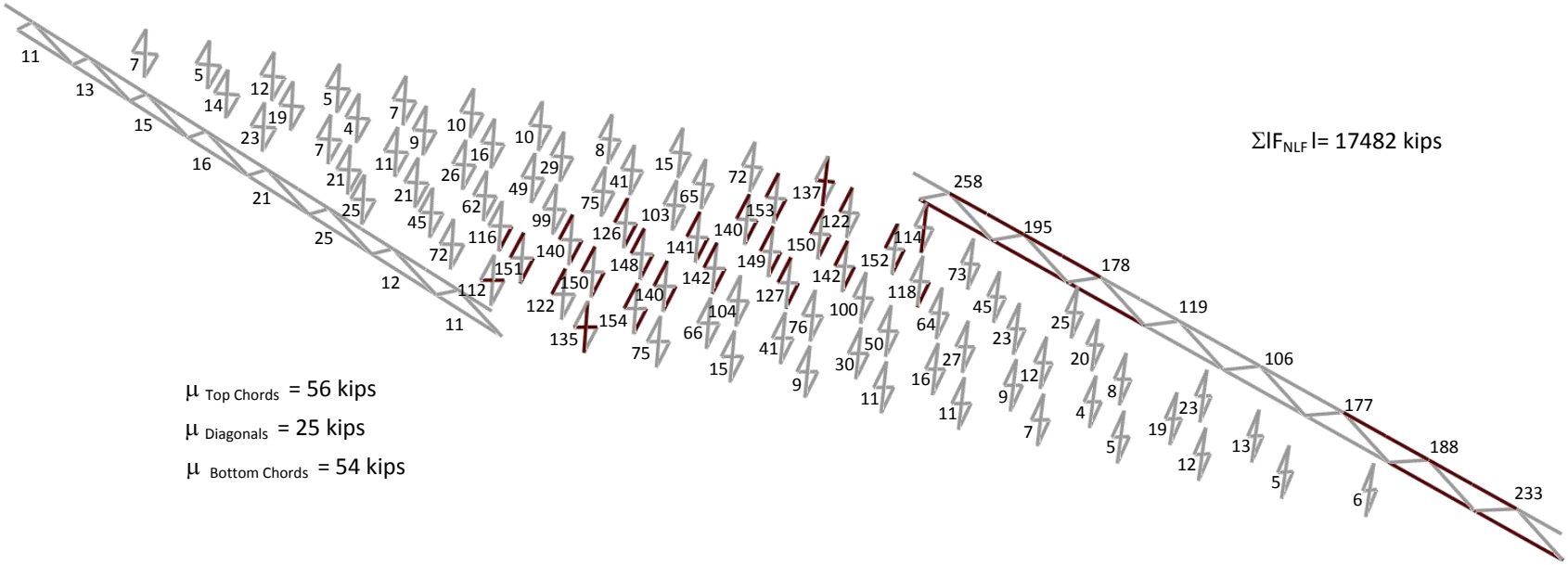

Figure 6.4.13. NISSS54, maximum amplitude of the component axial forces in each of the cross-frames under total dead load (NLF detailing).

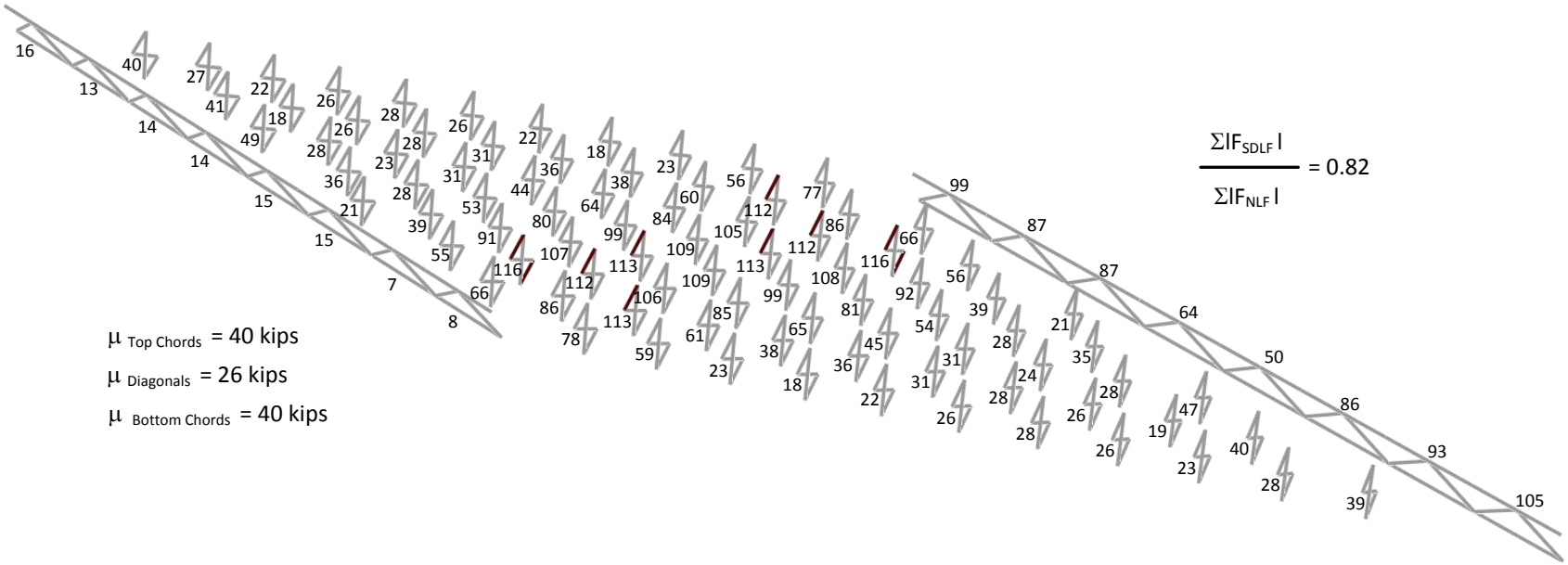

Figure 6.4.14. NISSS54, maximum amplitude of the component axial forces in each of the cross-frames under total dead load (SDLF detailing).

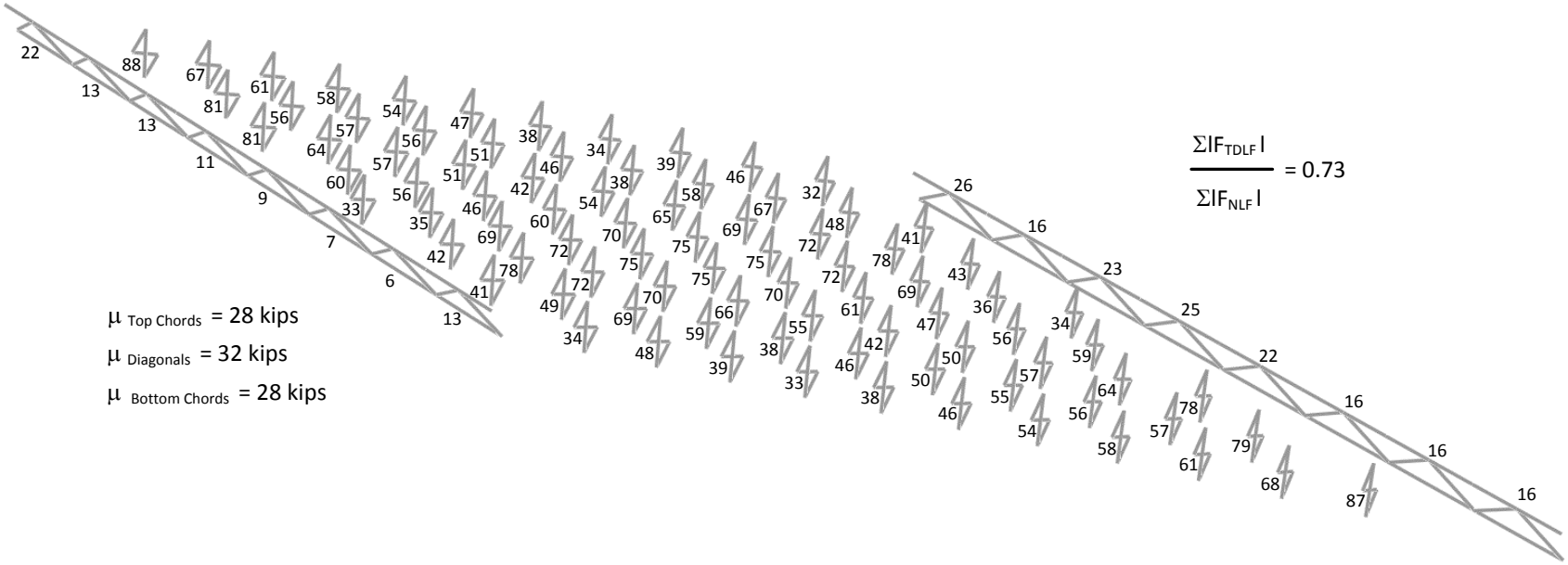

Figure 6.4.15. NISSS54, maximum amplitude of the component axial forces in each of the cross-frames under total dead load (TDLF detailing).

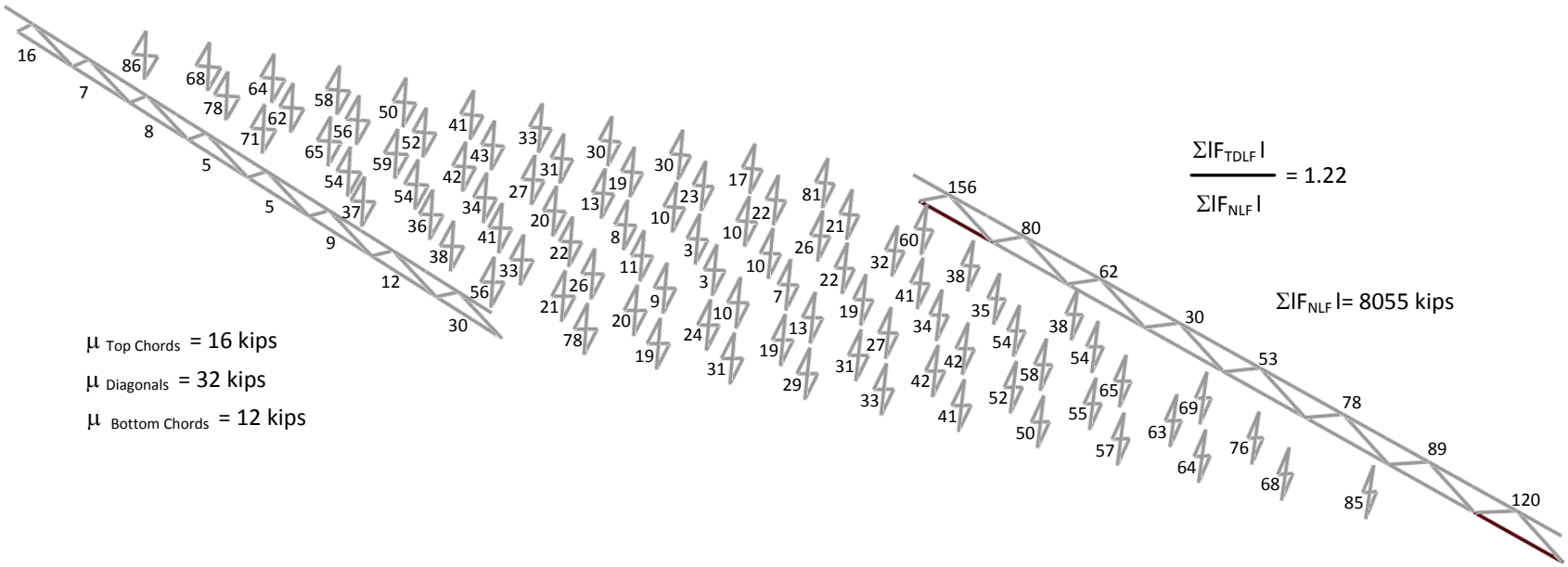

Figure 6.4.16. NISSS54, maximum amplitude of the component axial forces in each of the cross-frames under steel dead load (TDLF detailing).

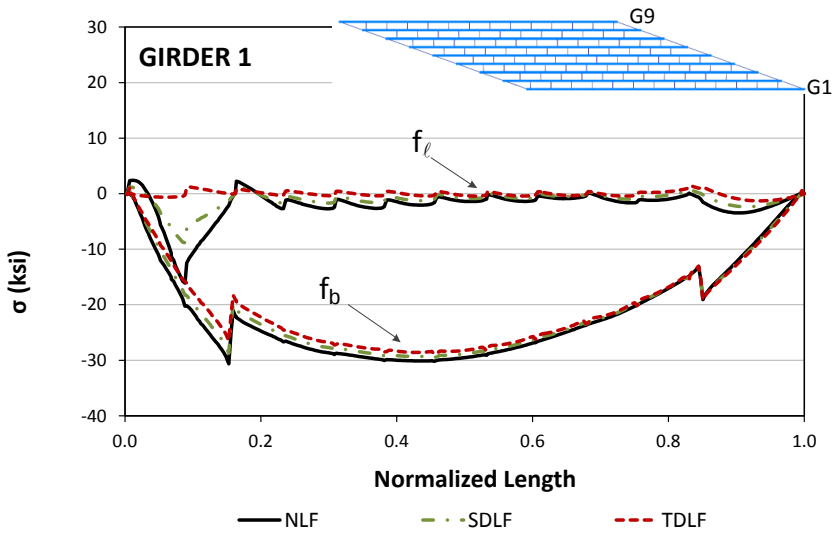

(i) NLF

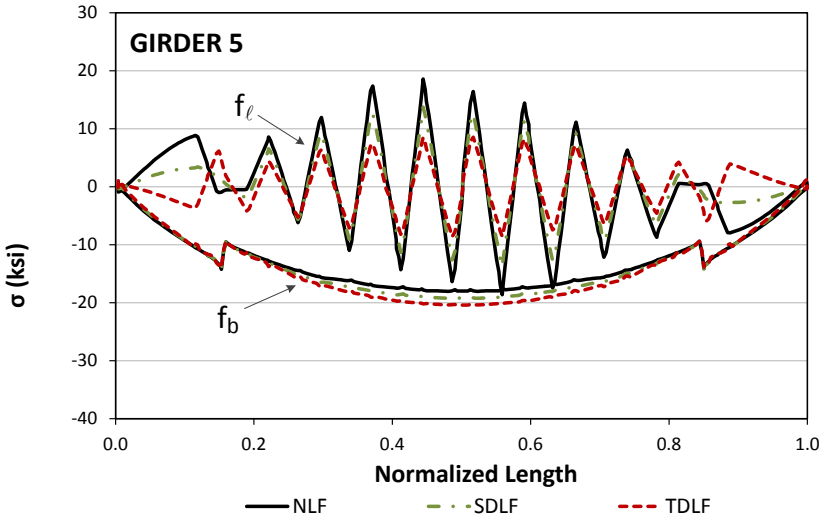

(ii) SDLF

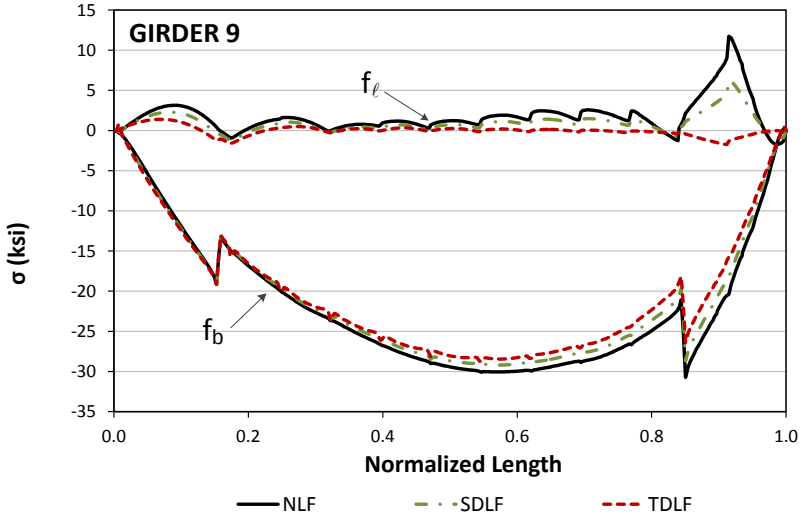

(iii) TDLF

Figure 6.4.17. NISSS54, Top flange stresses under total dead load for different detailing methods.

6.4.3. *X-type cross-frames without top chords*

X-type cross-frames without top chords are widely used by bridge engineers in straight and skewed bridges. X-type cross-frames are found to provide enough bracing to the girders due to their diagonals and are able to control the deck profile along the width of the bridge. Both the full X-type cross-frames and X-type cross-frames without top chords are found to provide the same bracing and vertical stiffness to control the deck profile (Sanchez, 2011).

For the bridges with significant skew effects, a staggered cross-frame pattern is usually unavoidable. As explained in Chapter 5, large cross-frame forces can be developed due to coupling between the twist rotations and other rotations and between the twist rotations and other displacements which can cause substantial flange lateral bending at the intermediate cross-frame locations. For instance, Fig. 6.4.18 shows girder layovers of the bridge NISSS54 with full X-type cross-frames under total dead load and Fig. 6.4.19 provides the major-axis bending and flange lateral bending stresses of girder G5 under total dead load for different types of detailing.

It should be observed from Figs. 6.4.18 and 6.4.19 that utilizing staggered cross-frame layout with full X-type configuration develops substantial flange lateral bending in the interior girders due to the transverse load transfer effects. The interior girder flanges are loaded "back-and-forth" in opposing directions by the cross-frames. Conversely, if the top chords are removed, the stiffness of the cross-frames in their own plane decreases. As a result, as the transverse stiffness of the bridge reduces so does the flange lateral bending of the system, as demonstrated in Fig. 6.4.20. Figure 6.4.20 shows the girder layovers of NISSS54 constructed with different types of detailing methods under total dead load. In Fig. 6.4.20 (i), girder layovers are smoother than the ones shown in Fig. 6.4.18.

Flange lateral bending stresses are also expected to reduce due to the reduction of the back-and-forth deformation of the girders, as shown in Fig. 6.4.20. Figure 6.4.21 shows the girder stresses of the bridge NISSS54 under total dead load for each type of detailing. It should be noted from Figs. 5.4.4 and 6.4.21 that the reduction in the flange lateral bending stresses is significant. The main reason for the reduction is that the cross-frame with top chords contributes mainly to the forces associated with the flange lateral bending stresses in the girders. Removal of the top chords provides smaller flange lateral bending stresses in girders. Figure 6.4.22 shows total dead load vertical displacements for different types of detailing. It should be noted from Figs. 5.3.15 and 6.4.22 that the vertical deflections are not influenced by

the removal of the top chords since they have negligible contribution to stiffness associated with major-axis bending rotations.

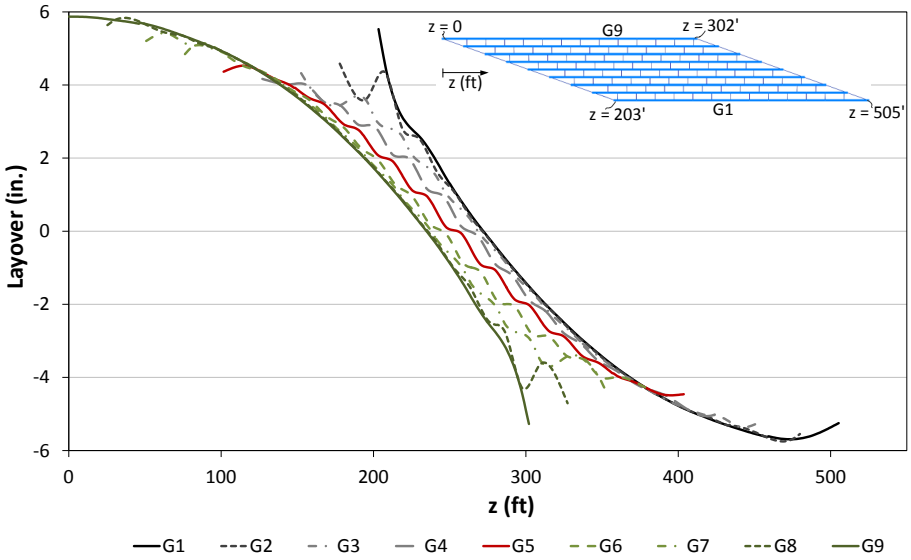

Figure 6.4.18. NISSS54 with top chords, Layover of girders under total dead load for NLF detailing.

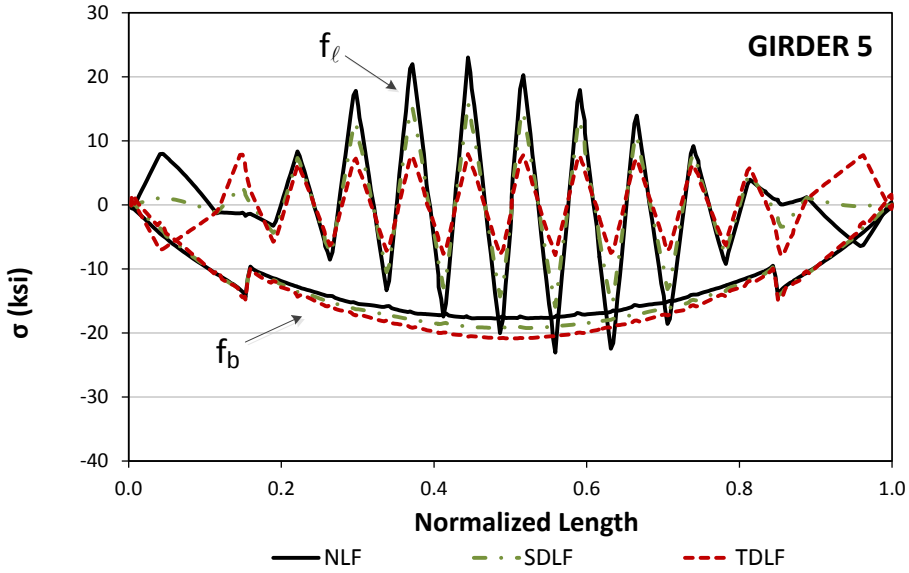

Figure 6.4.19. NISSS54 with top chords, Girder stresses under total dead load for different types of detailing.

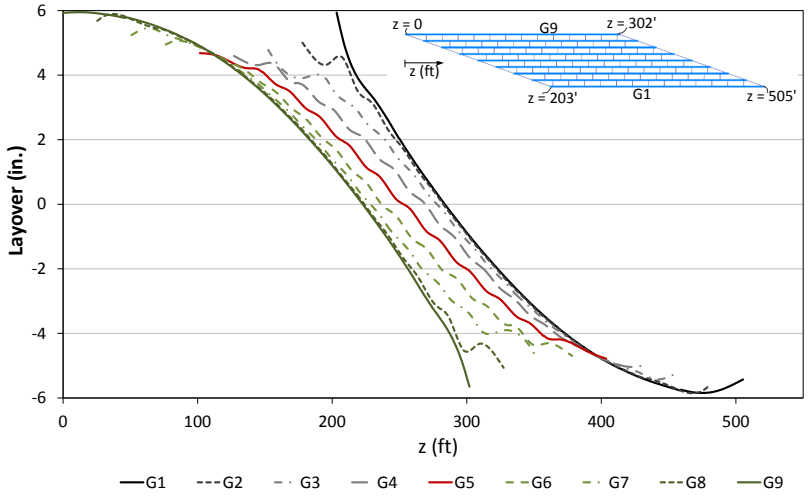

(i) NLF

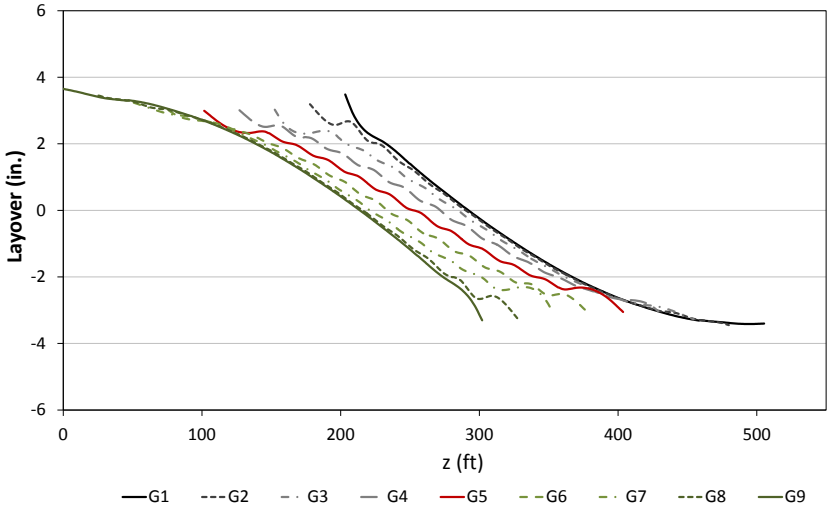

(ii) SDLF

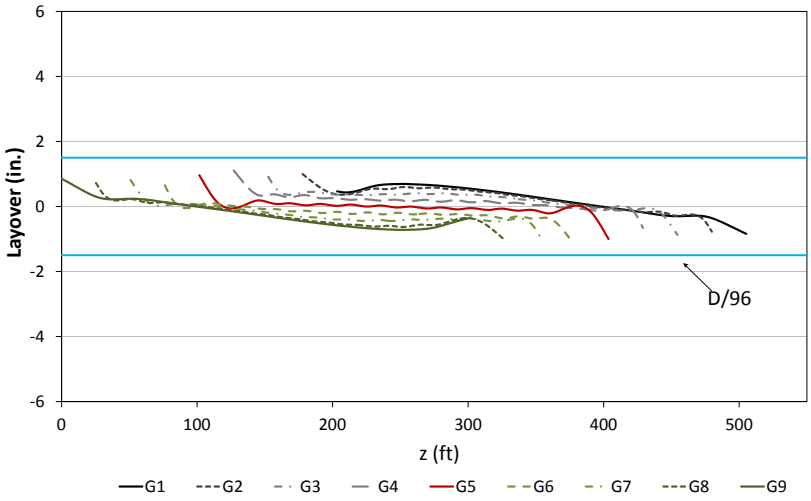

(iii) TDLF

Figure 6.4.20. NISSS54 without top chords, layover of girders under total dead load for different detailing methods.

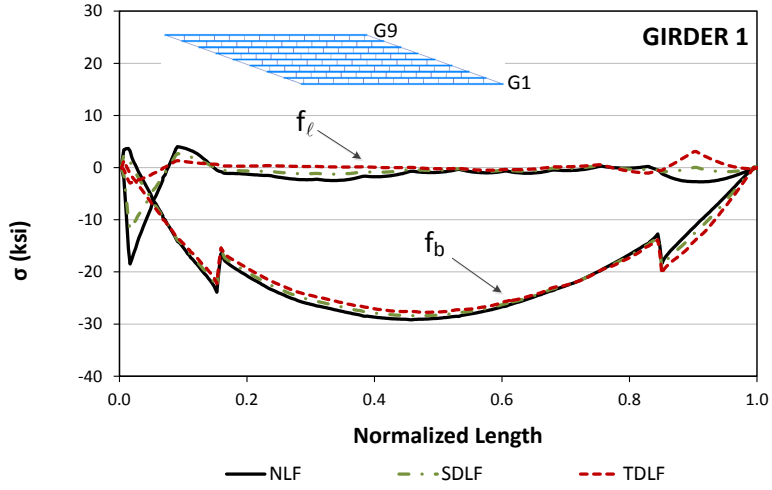

(i) NLF

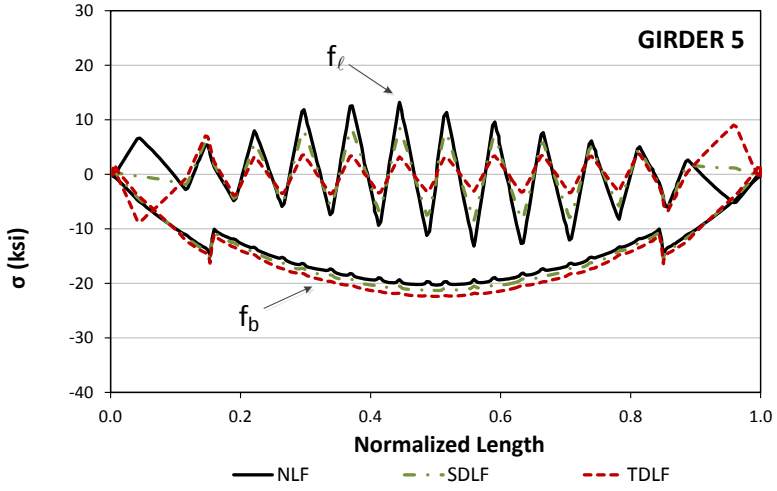

(ii) SDLF

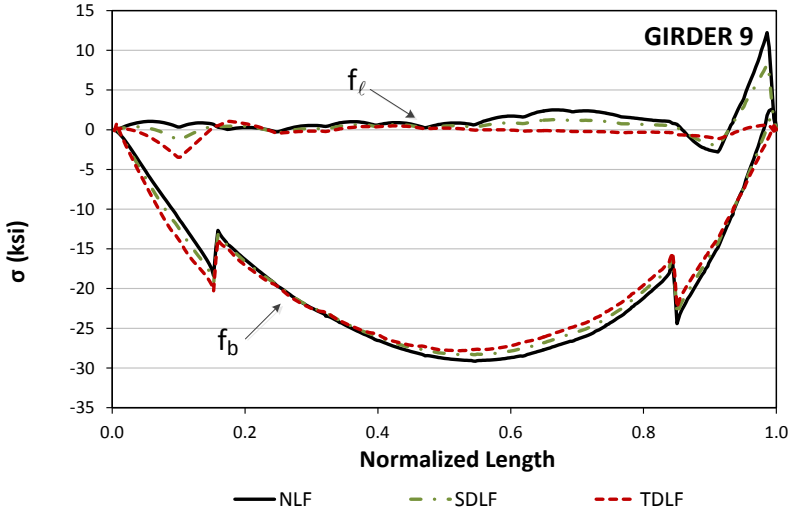

(iii) TDLF

Figure 6.4.21. NISSS54 without top chords, Girder stresses under total dead load for different detailing methods.

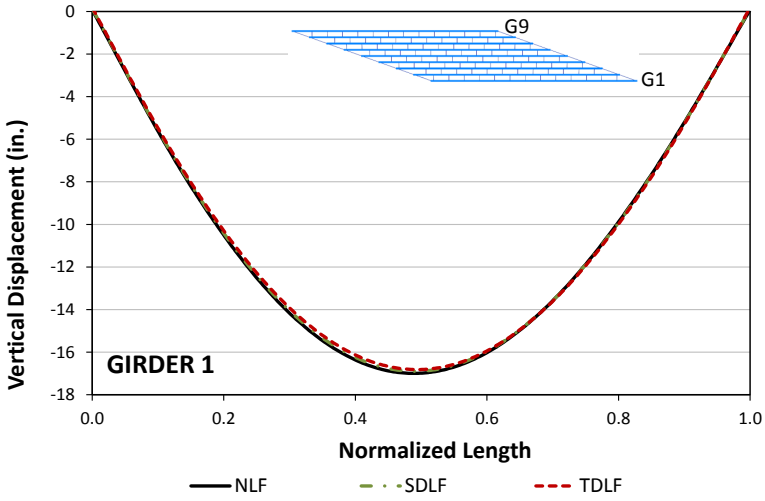

(i) NLF

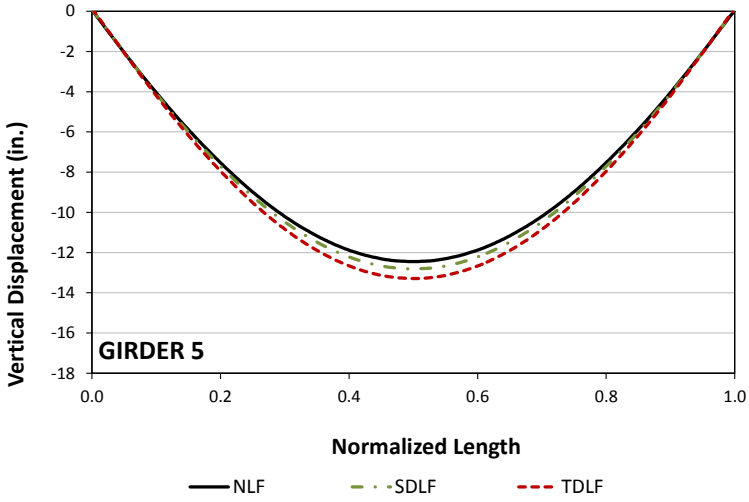

(ii) SDLF

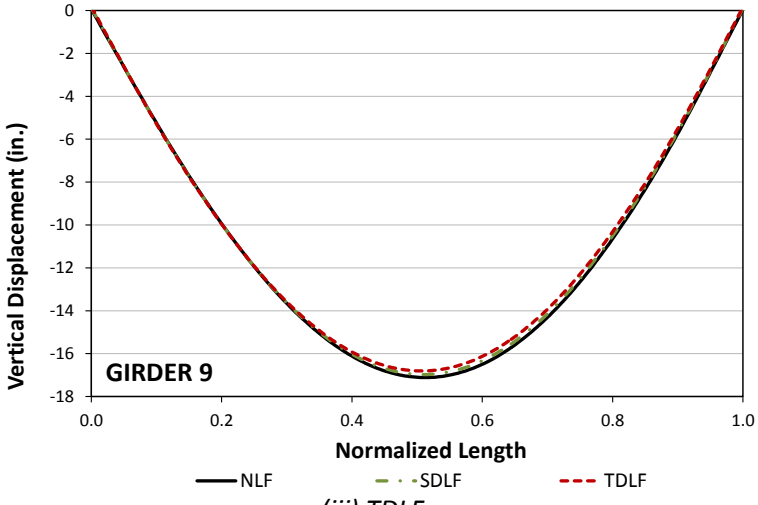

(iii) TDLF

Figure 6.4.22. NISSS54 without top chords, Girder vertical displacements under total dead load for different detailing methods.

Figures 6.4.23 through 6.4.25 show the distribution of the largest total dead load cross-frame component axial forces in each of the cross-frames throughout the bridge with no top chords for NLF, SDLF and TDLF detailing cases respectively. Also, Figures 6.4.26 through 6.4.28 show the distribution of the largest total dead load cross-frame component axial forces in each of the cross-frames throughout the bridge with no top chords for NLF, SDLF and TDLF detailing cases respectively under steel dead load. The most highly loaded cross-frame members are colored dark red, while the more lightly loaded cross-frame members are shaded light grey. The largest magnitude cross-frame component axial force is labeled next to each of the cross-frames in the picture. In addition, the total sum of the absolute value of all the cross-frame component axial forces is shown in the upper right corner of the figure. For the cases of DLF detailing, the sum of the total sum of the absolute value of all the cross-frame component axial forces is normalized with respect to values, obtained with NLF detailing, under the considered load level. Figures 6.4.23 through 6.4.27 demonstrate that the reduction in the cross-frame forces is higher compared to the configuration with top chords. However, large locked-in forces are observed at the intermediate cross-frames that are close to the skewed bearings. These forces can be eliminated by using the recommended ratio of adjacent unbraced lengths given in Section 6.4.2.

It should be noted that the increased transverse flexibility of the system can influence the fit-up forces since girders are easier to twist to make the connection. The fit-up forces are expected to be smaller than the ones with top chords since the transverse stiffness is reduced. In general, removing the top chords of the X-type cross-frames for straight and skewed I-girder bridges is recommended since they still provide enough bracing to girders, control the deck profile, reduce the flange lateral bending stresses and decrease the transverse stiffness. As the transverse flexibility of the system increases the girders require less force to fit-up with the cross-frames. It is also found that for the bridges constructed with DLF detailing, utilizing X-type cross-frames performs better than the ones with top chords in DLF detailing.

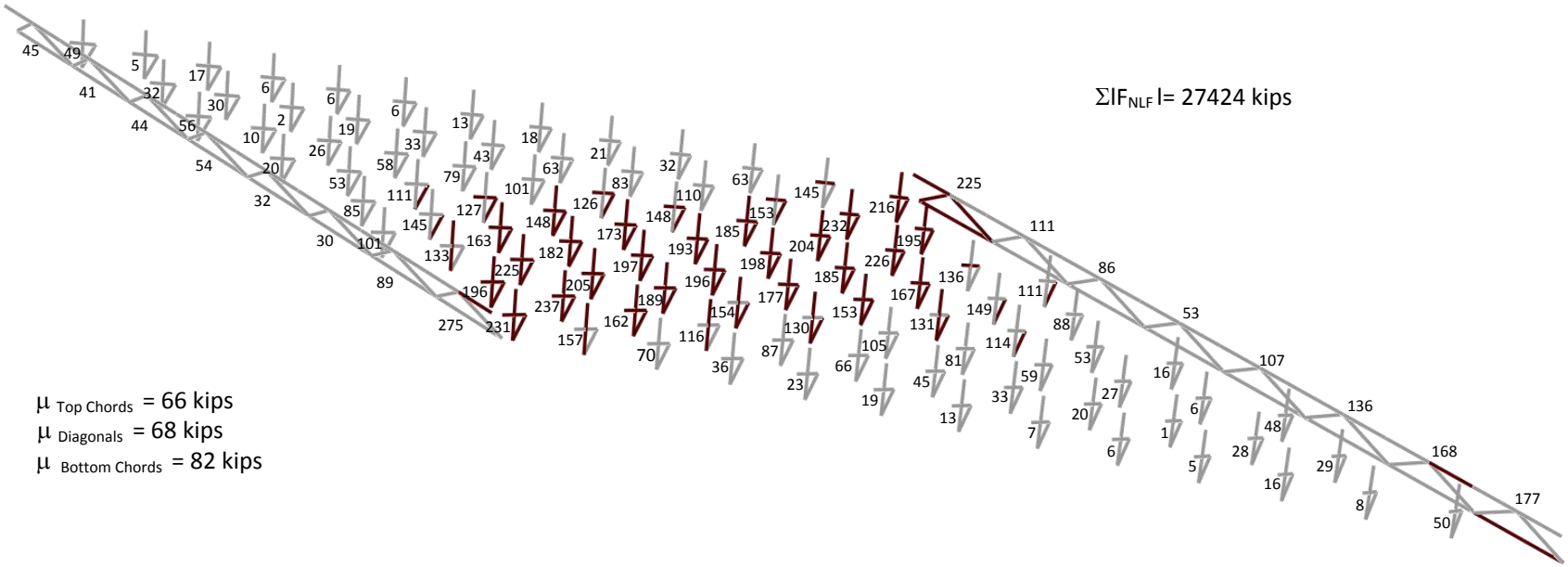

Figure 6.4.23. NISSS54 without top chords, maximum amplitude of the component axial forces in each of the cross-frames under total dead load (NLF detailing method).

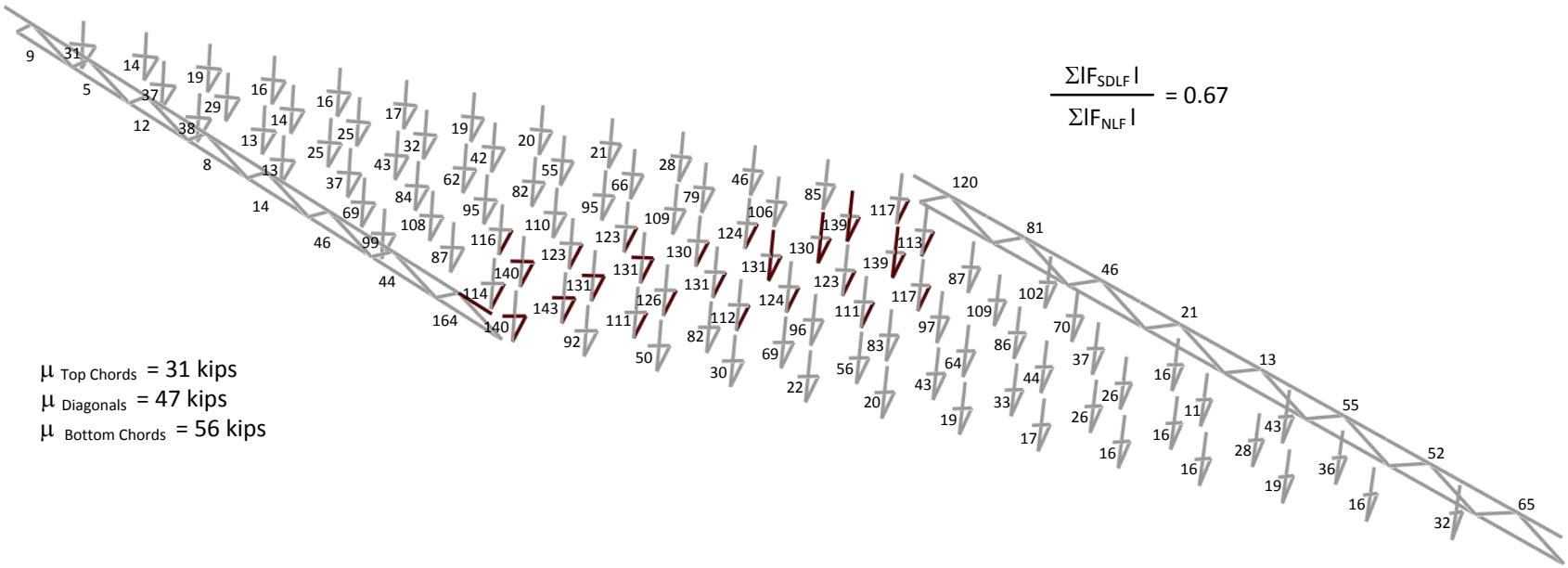

Figure 6.4.24. NISSS54 without top chords, maximum amplitude of the component axial forces in each of the cross-frames under total dead load (SDLF detailing).

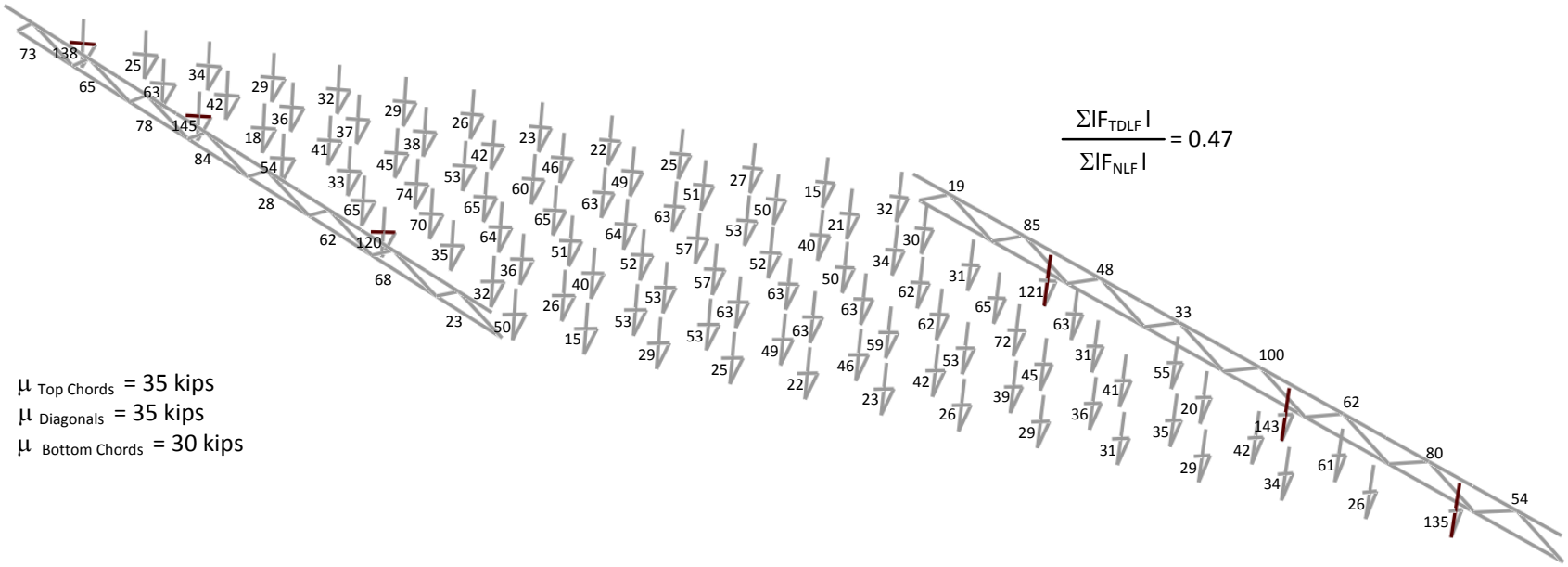

Figure 6.4.25. NISSS54 without top chords, maximum amplitude of the component axial forces in each of the cross-frames under total dead load (TDLF detailing).

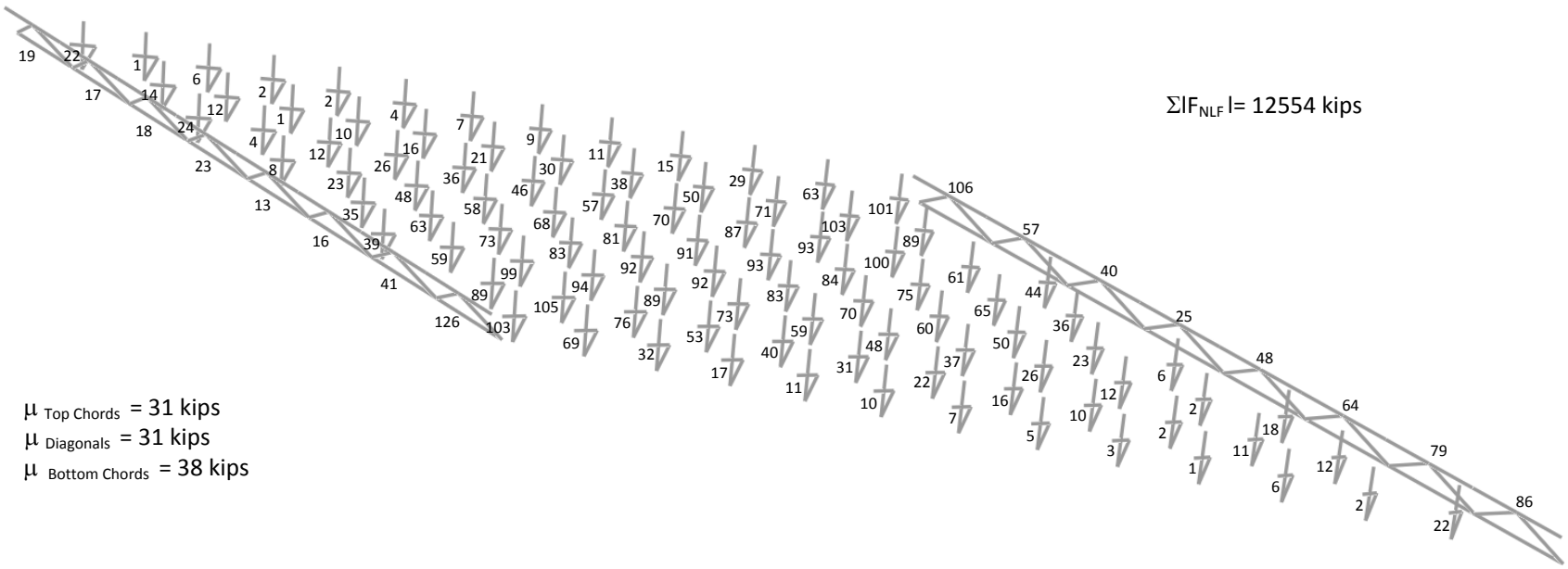

Figure 6.4.26. NISSS54 without top chords, maximum amplitude of the component axial forces in each of the cross-frames under steel dead load (NLF detailing).

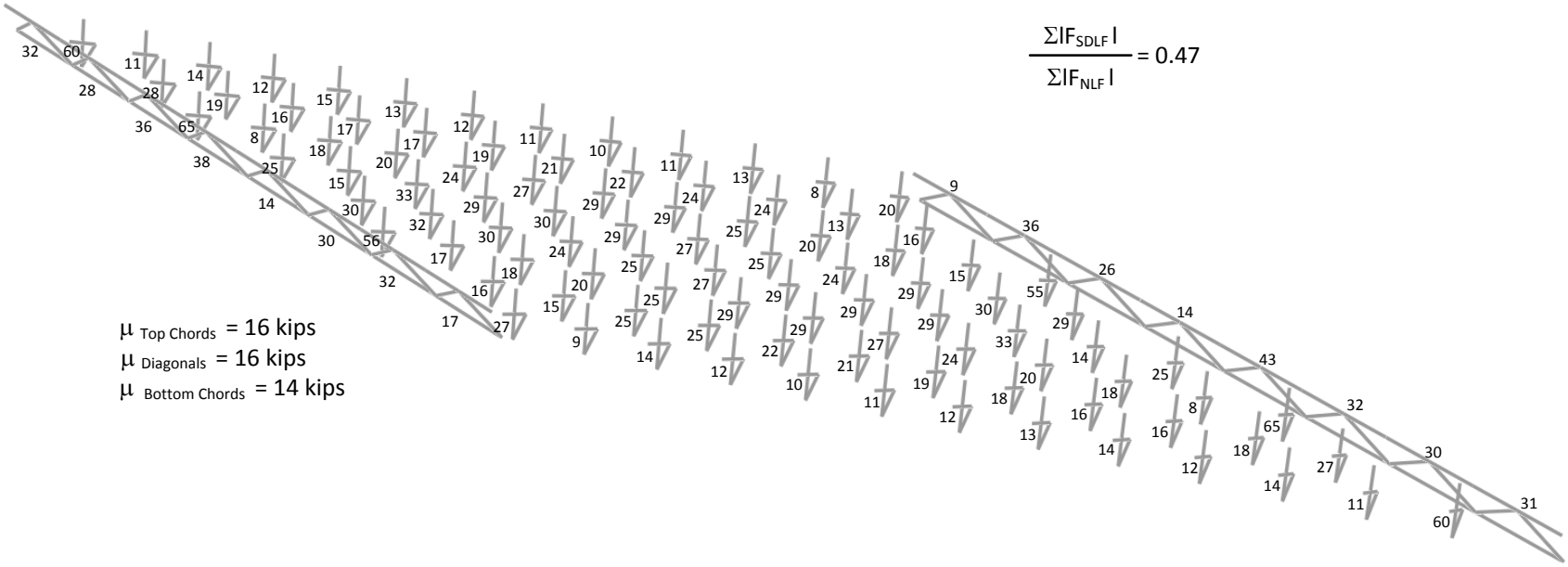

Figure 6.4.27. NISSS54 without top chords, maximum amplitude of the component axial forces in each of the cross-frames under steel dead load (SDLF detailing).

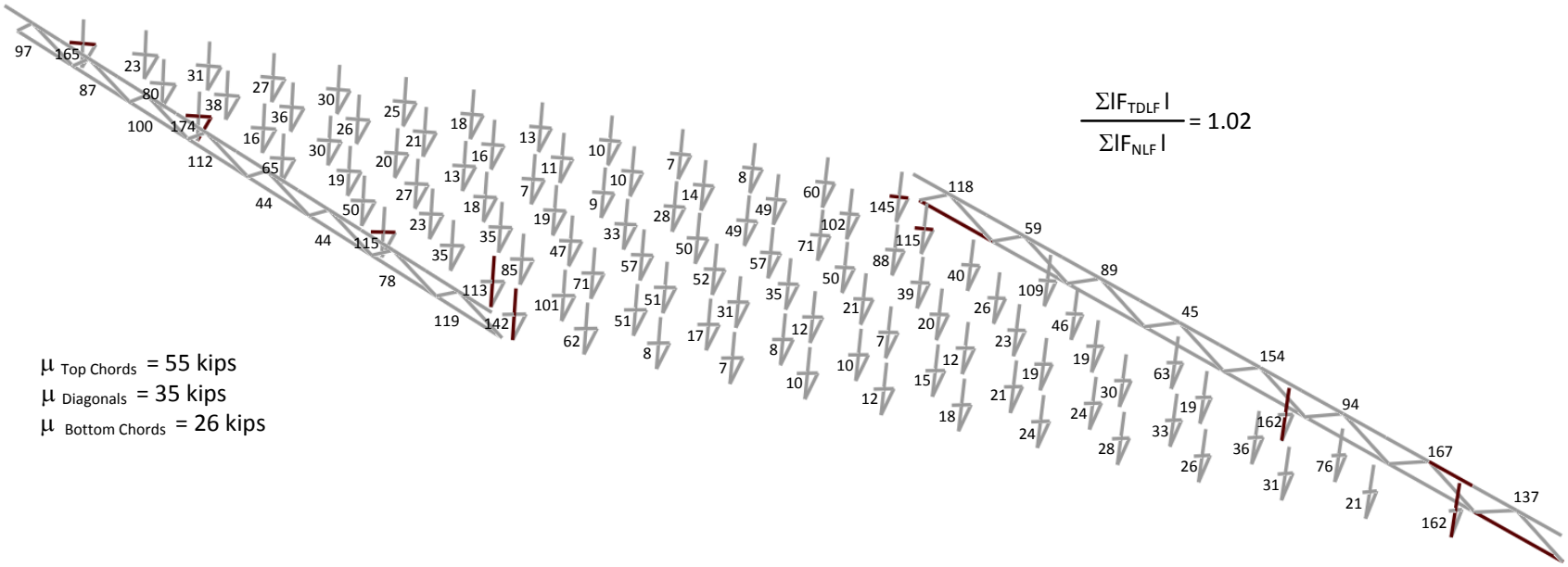

Figure 6.4.28. NISSS54 without top chords, maximum amplitude of the component axial forces in each of the cross-frames under steel dead load (TDLF detailing).

6.4.4. *Use of temporary supports*

For NLF detailing, cross-frames are detailed such that they connect to the girders in no-load geometry. As a result, any variation from the no-load geometry due to dead load deflections requires fit-up forces to assemble the cross-frames of the bridges constructed with NLF detailing. It is beneficial to minimize these displacement incompatibilities by using temporary supports. Typically, temporary supports (falsework) are used to control the differential vertical deflections between the bridge components and stabilize the bridge during erection. Using temporary supports during steel erection is especially important;

- For bridges or bridge units with large span lengths where relatively large differential deflections are likely between the girders due to dead load deflections. Large displacement incompatibilities can cause fit-up problems or large fit-up forces.
- For curved bridges or bridge units with large span-to-width ratios, the global deflections due to the overall torsion of the bridge can be problematic and cause failures resulting from stability issues (Yura et al, 2008 and Sanchez, 2011). Furthermore, these kinds of bridges are susceptible to second order amplification of the girder deflections and stresses. Large displacement amplifications can make it difficult to predict and control the structure's geometry during construction.

Figure 6.4.29 provides a bridge with the characteristics discussed above where global stability effects can be observed during erection. The bridge in Fig. 6.4.29 is designated with the name NISCR5 in the design matrix. Figure 6.4.30 illustrates the girder layovers under steel dead load from linear and nonlinear analyses. It can be observed from Fig. 6.4.30 that both flanges are shifting outward due to overall flange lateral bending and second-order effects.

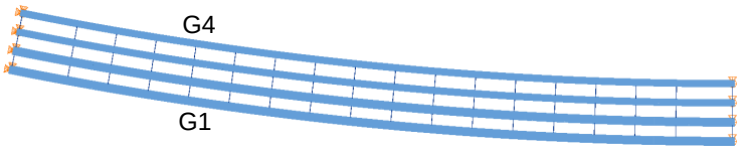

Figure 6.4.29. Example of a curved bridge with large span-to-width ratio (NISCR5).

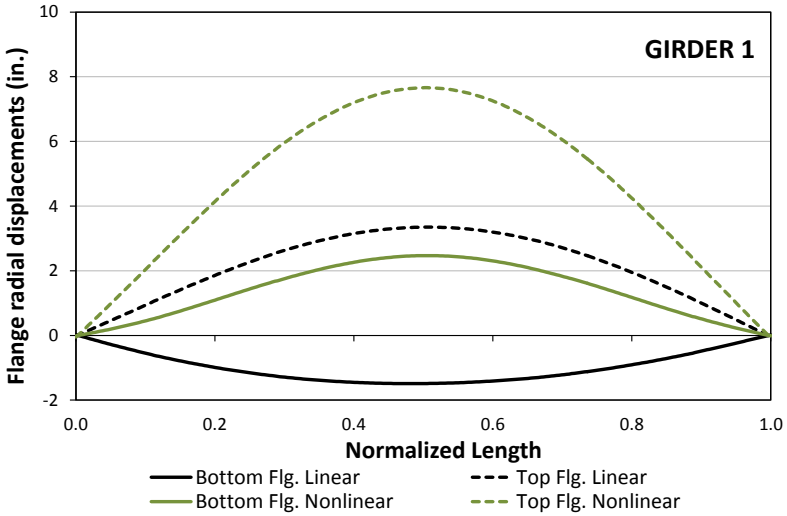

Figure 6.4.30. NISCR5, Girder layovers under steel dead load.

Excessive girder layovers can lead to fit-up problems or even a failure problem during erection. However, these problems can be eliminated by the use of temporary supports. Their use can limit vertical deflections of the girders during steel erection and prevent second-order amplifications. Figure 6.4.31 shows the erection stage 8 of NISCR5 where the steel structure is supported with a temporary support. Figures 6.4.32 and 6.4.33 provide girder layovers and deflections of NISCR5 under steel dead load. The displacements are obtained for cases with and without temporary supports from first- and second-order analyses. It should be noted from Figs. 6.4.32 and 6.4.33 that the amplified deflections are reduced by the use of the temporary supports. Figure 6.4.33 demonstrates that outside girder exhibits 12 inches of vertical displacement, whereas inside girder exhibits 2.5 inches of vertical displacement when temporary supports are not used. Large differences in the girder differential displacements can cause fit-up problems. Figure 6.4.33 further demonstrates that the structure tends to have fewer differential deflection incompatibilities when temporary supports are used since the girder deflections are minimized. As a result, very low fit-up forces can be needed to connect the cross-frames for the bridges that are constructed with NLF detailing. Additionally, girder major-axis and flange lateral bending stresses can be reduced by the use of temporary supports as shown in Fig. 6.4.34.

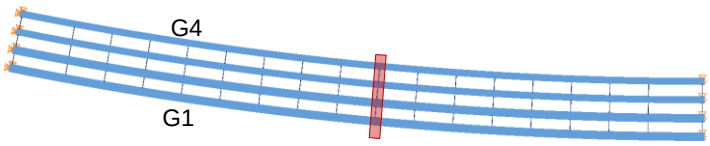

Figure 6.4.31. NISCR5, Consideration of Temporary supports.

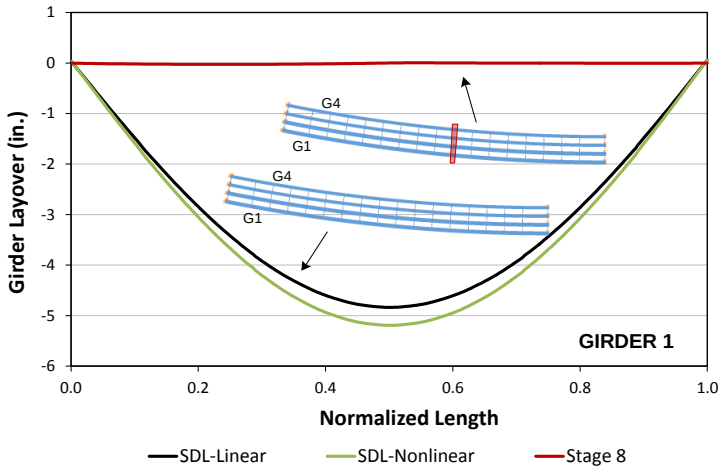

Figure 6.4.32. NISCR5, Girder layovers under steel dead load.

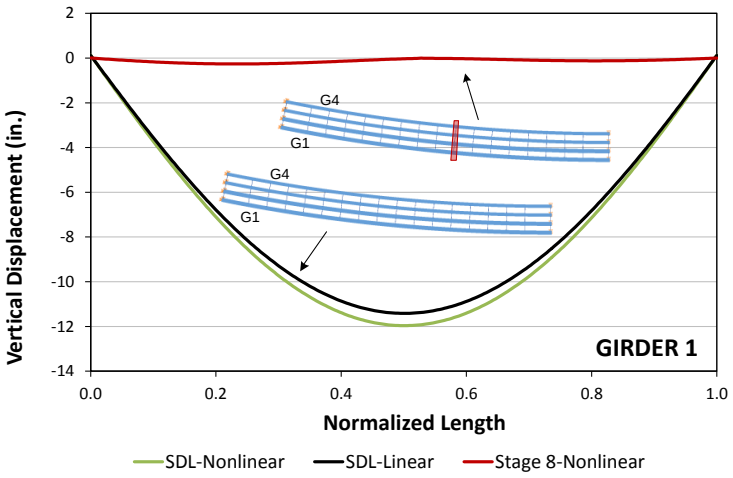

(i)Girder 1

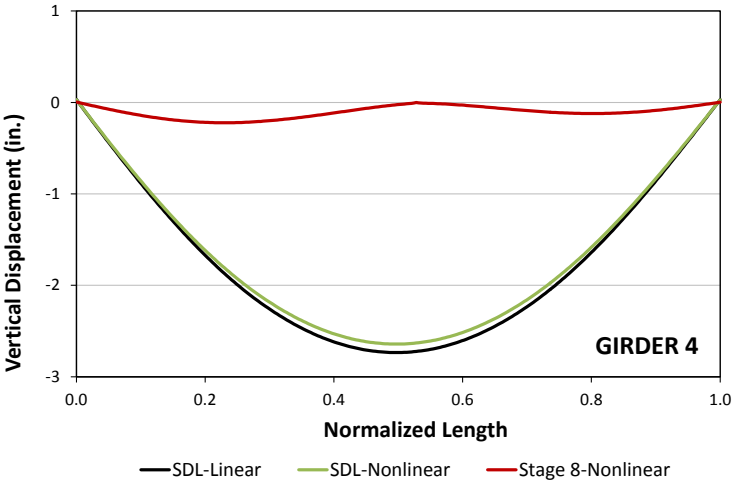

(ii)Girder 4

Figure 6.4.33. NISCR5, Girder vertical deflections under steel dead load with and without temporary supports.

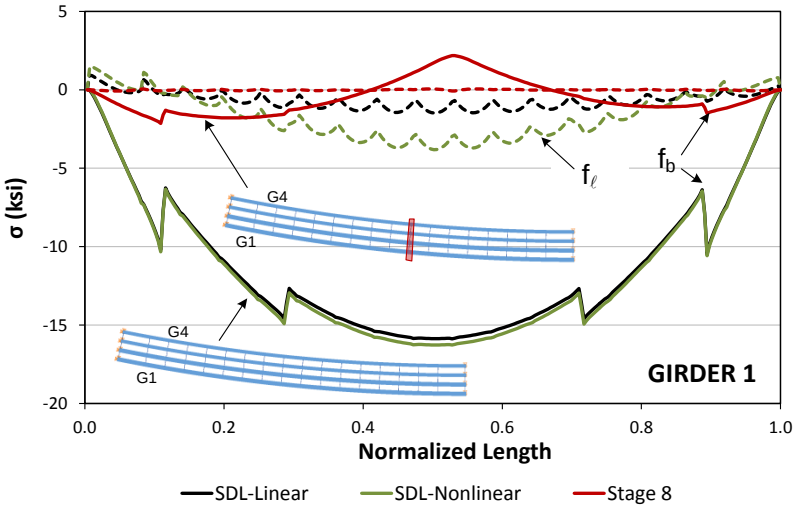

(i)Girder 1

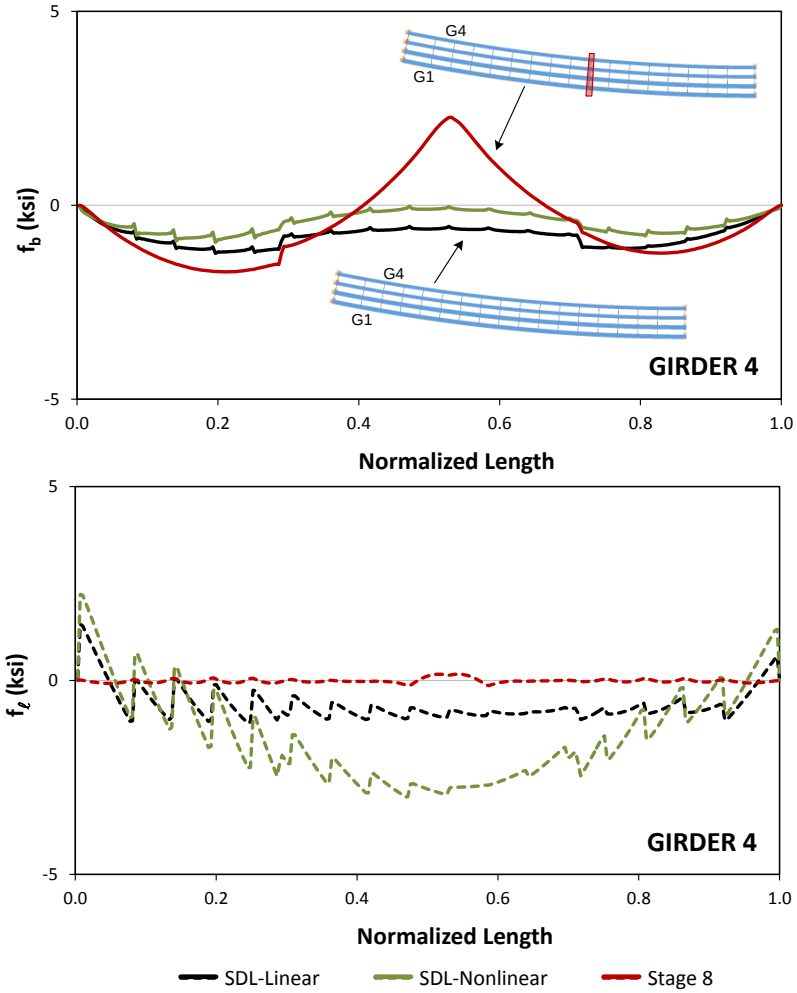

(ii)Girder 4

Figure 6.4.34. NISCR5, Fascia girder stresses under steel dead load with and without temporary supports.

Cross-frame forces are also reduced by using the temporary supports. The reduction is mainly due to keeping the structure close to its no-load geometry such that the bridge does not develop internal forces due to dead loads. Table 6.4.3 summaries the maximum tension and compression under steel dead load for each cross-frame member of NISCR5 with and without temporary supports. It is clear from Table 6.4.3 that the cross-frame forces are minimized with the use of a temporary support. This effect is mainly due to retaining the no-load geometry of the bridge. This is only true for the bridges constructed with NLF detailing. It is shown in Chapter 5 that use of DLF detailing tends to increase the cross-frame diagonal forces due to locked-in forces. Table 6.4.4 shows maximum tension and compression cross-frame forces under steel dead load for each cross-frame member of NISCR5 for different types of cross-frame detailing without any temporary supports. Figure 6.4.35 shows the outside girder stresses under steel dead load for different types of detailing. It should be noted that for the bridge constructed with SDLF detailing, the flange lateral bending stresses due to overturning effects are reduced at the expense of increasing the diagonal forces due to locked-in stresses.

Table 6.4.3. NISCR5, Cross-frame forces under steel dead load with and without temporary supports.

Cross-Frame Member	Load Case	Maximum Tension Force (kips)	Maximum Compression Force (kips)
Top Chord	SDL-Linear	20	-2
	SDL-Nonlinear	23	-1
	Stage 8-Nonlinear	7	-1
Diagonals	SDL-Linear	19	-24
	SDL-Nonlinear	21	-23
	Stage 8-Nonlinear	4	-18
Bottom Chord	SDL-Linear	1	-19
	SDL-Nonlinear	1	-22
	Stage 8-Nonlinear	4	-2

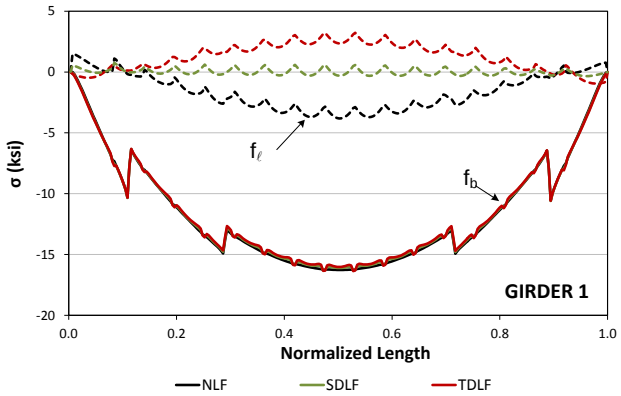

Figure 6.4.35. NISCR5, Outside girder stresses under steel dead load for different types of detailing.

Table 6.4.4. NISCR5, Cross-frame forces under steel dead load for different types of detailing.

Cross-Frame Member	Detailing Method	Maximum Tension Force (kips)	Maximum Compression Force (kips)
Top Chord	NLF	23	-1
	SDLF	18	0
	TDLF	12	-8
Diagonals	NLF	21	-23
	SDLF	88	-88
	TDLF	141	-143
Bottom Chord	NLF	1	-22
	SDLF	1	-23
	TDLF	3	-26

The long and narrow curved bridge cases can also be observed during the erection stages of a bridge, as in Fig. 6.4.36. In this particular example, NISCS37 is used where the last five girders are erected and first four girders are erected on temporary supports as two separate pieces. After assemblage of the first four girders is completed, two units are connected by cross-frames. Figure 6.4.37 shows the completed steel structure for NISCS37. Figure 6.4.38 provides the girder vertical deflections under steel dead load.

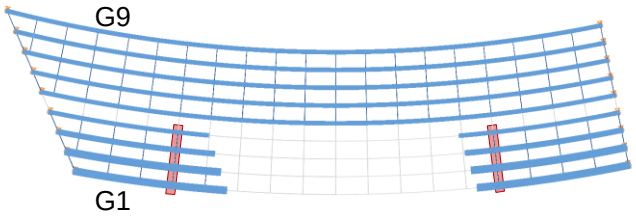

Figure 6.4.36. Possible example of an erection stage for NISCS37.

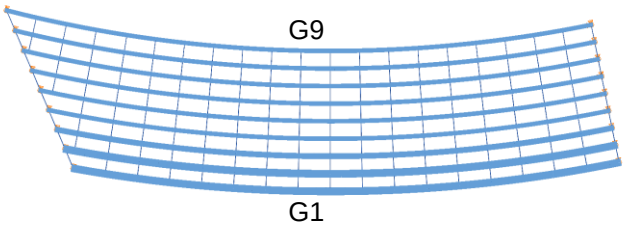

Figure 6.4.37. NISCS37,Completed steel structure.

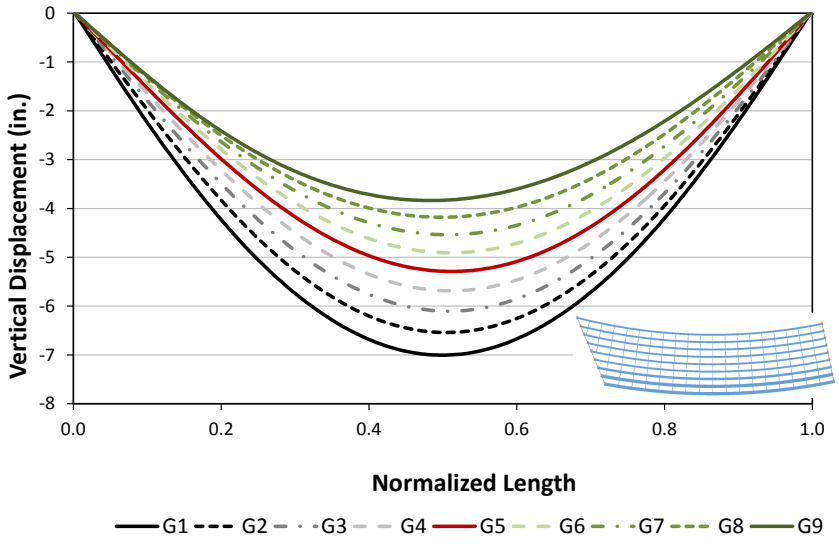

Figure 6.4.38. NISCS37, girder vertical deflections under steel dead load.

The final differential deflections between girders are less than 0.5 inches for the completed structure (see Fig. 6.4.38). Thus, after the first four girders are assembled, one can propose the erection scheme options shown in Fig. 6.4.39. The different cases can be summarized as follows:

- **case 1**: no temporary supports before connecting the cross-frames between girders G4 and G5
- **case 2:** two temporary supports under girders G1 through G4 before connecting the cross-frames between girders G4 and G5
- **case 3:** two temporary supports under girders G5 through G9 before connecting the cross-frames between girders G4 and G5
- **case 4**: two temporary supports under girders G1 through G9 before connecting the cross-frames between girders G4 and G5

Figure 6.4.40 shows girder deflections of girders G4 and G5 for cases 1 through 4 along the length of girder G5. Figure 6.4.40 shows that the differential deflections are significant for cases 1 and 2 due to the global effects mentioned above. On the other hand, cases 3 and 4 provide the smallest differential deflections between girders G4 and G5. Fewer fit-up problems should be expected for the cases where the differential deflections between the units are at a minimum. Figure 6.4.41 provides the girder layovers of girders G4 and G5 for cases 1 through 4 along the length of girder G5. It is also clear from Fig. 6.4.41 that providing continuous temporary supports gives the smallest layovers, which tends to provide the smallest fit-up forces for the erector.

In summary, temporary supports are essential for bridges constructed with NLF detailing where large differential deflection incompatibilities are expected during construction due to dead load deflections. Temporary supports can minimize these incompatibilities and provide stability during construction. Higher improvements are expected for bridges or units with large length-to-width ratio since these structures are more susceptible to overall flange lateral bending and second-order effects as illustrated earlier in this section and Section 5.5.

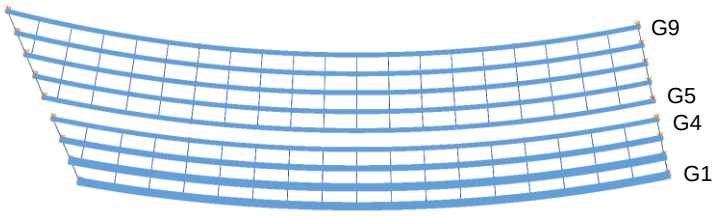

(i) Case 1

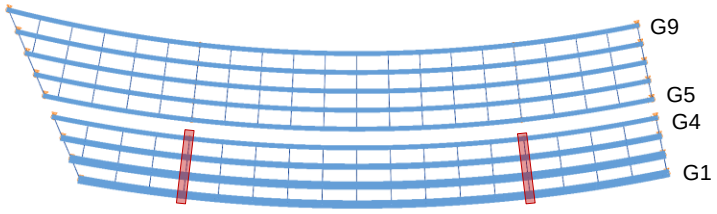

(ii) Case 2

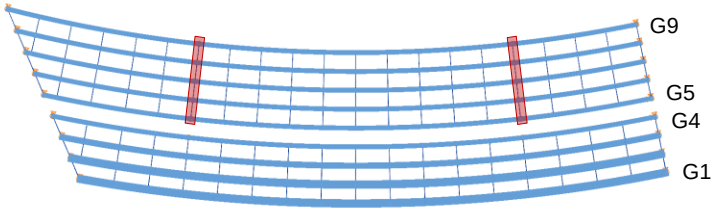

(iii) Case 3

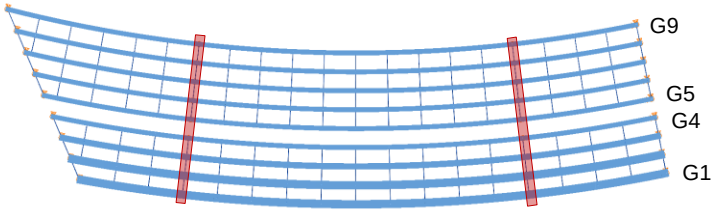

(iv) Case 4

Figure 6.4.39. NISCS37, Possible ways of using temporary supports for the selected erection scheme.

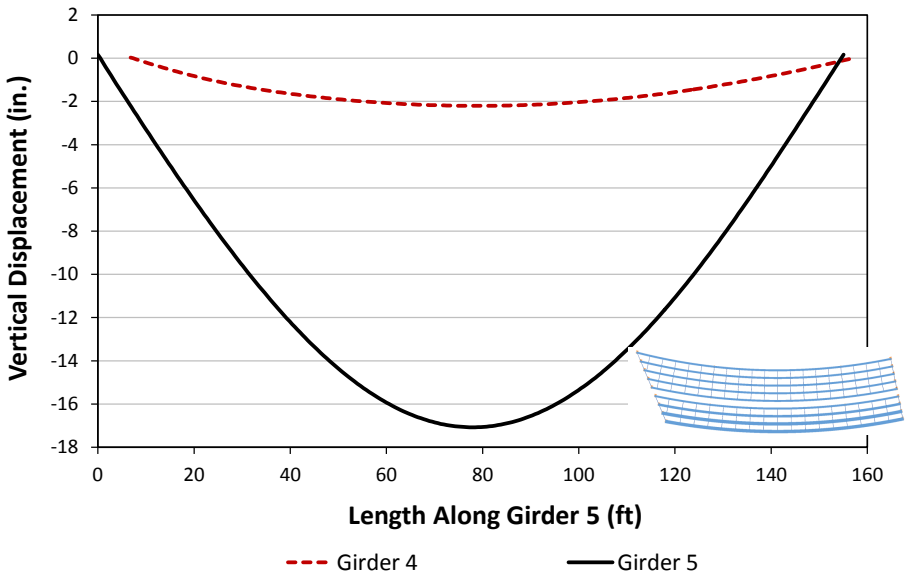

(i) Case 1

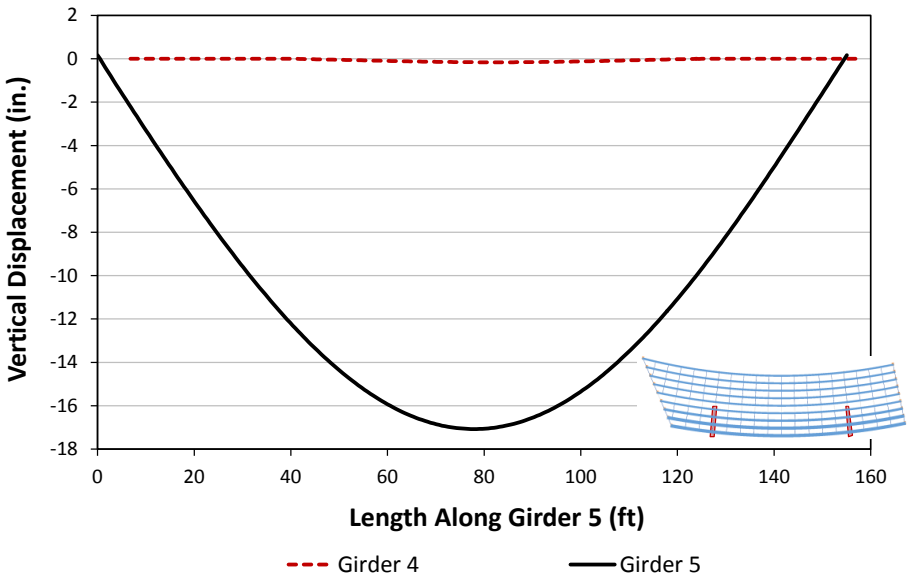

(ii) Case 2

Figure 6.4.40. NISCS37, Girder 4 and 5 vertical displacements for different scenarios.

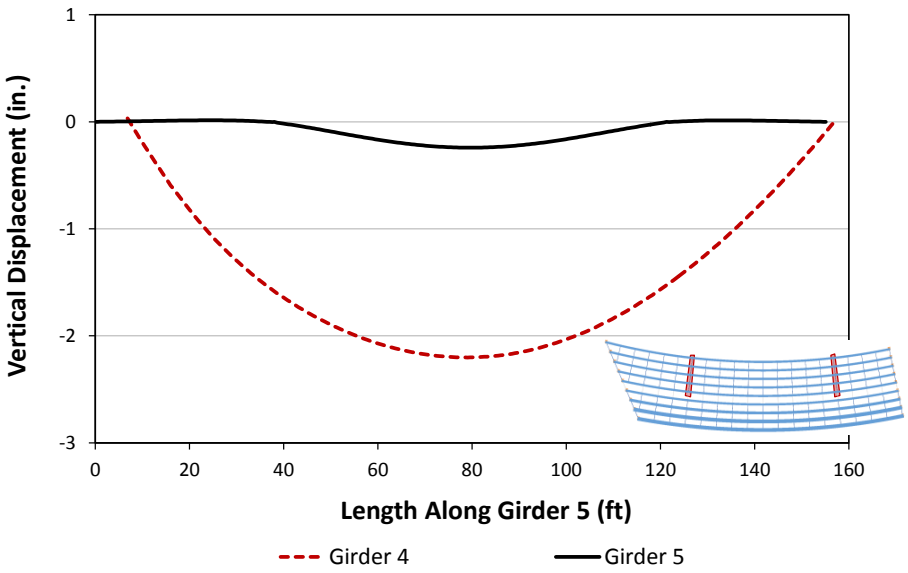

(iii) Case 3

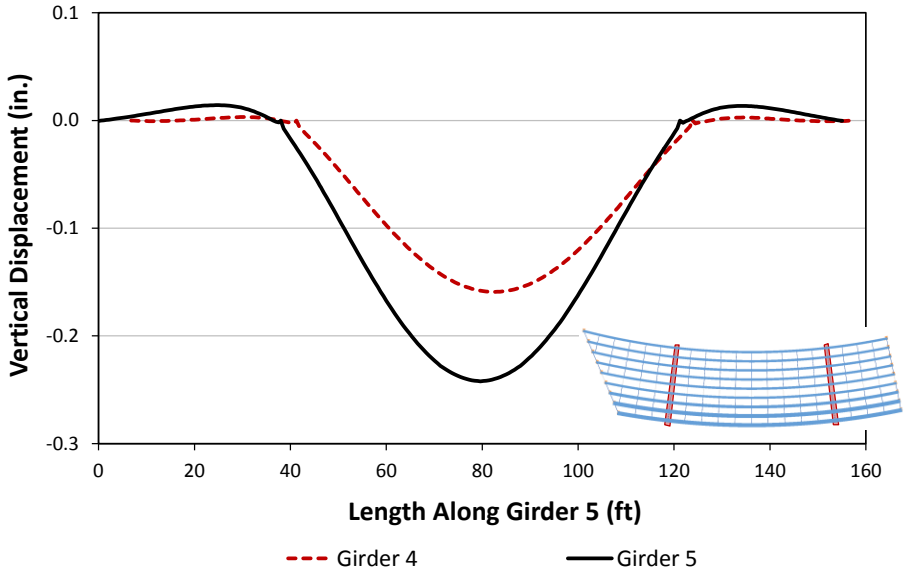

(iv) Case 4

Figure 6.4.40. (continued). NISCS37, Girder 4 and 5 vertical displacements for different scenarios.

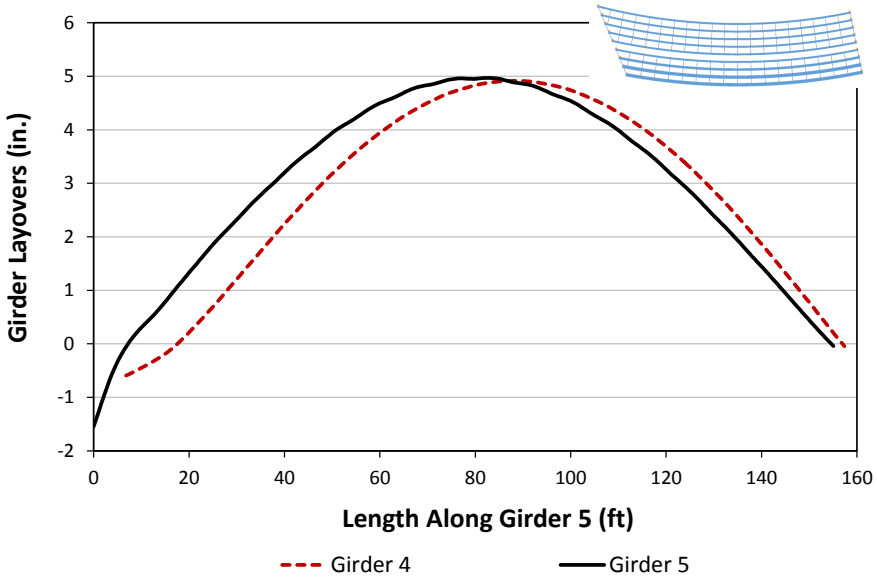

(i) Case 1

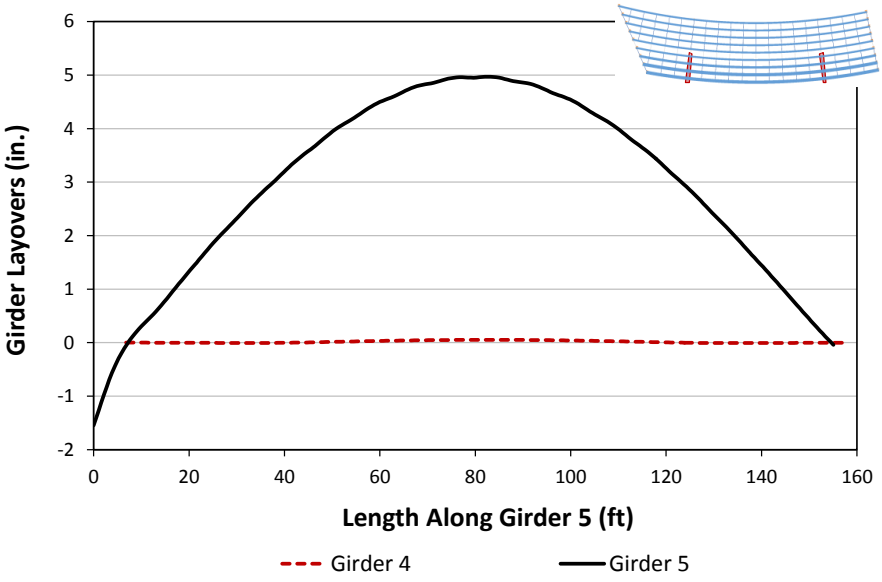

(ii) Case 2

Figure 6.4.41. NISCS37, Girder 4 and 5 layovers for different scenarios.

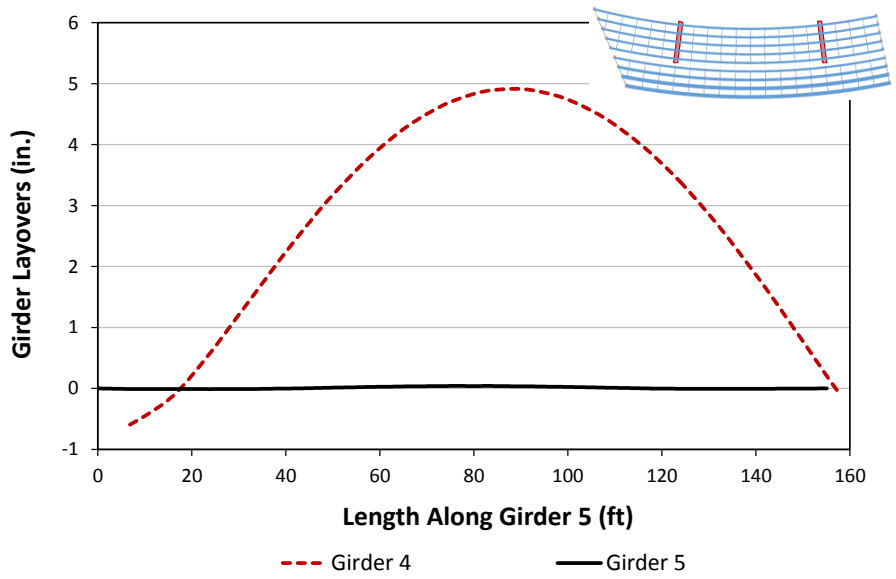

(iii) Case 3

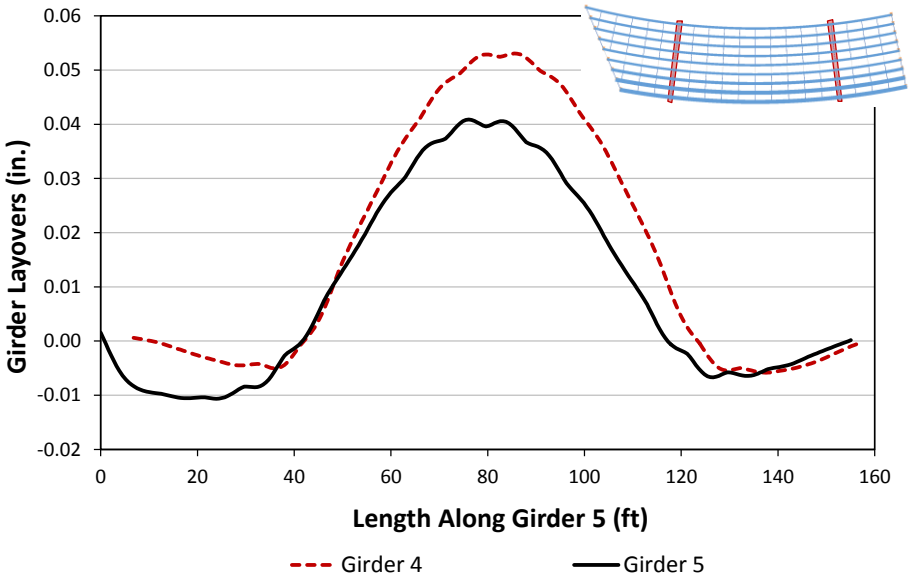

(iv) Case 4

Figure 6.4.41. (continued). NISCS37, Girder 4 and 5 layovers for different scenarios.

CHAPTER VII.

CONSIDERATION OF METHOD OF DETAILING IN DESIGN

The influence of locked-in stress effects on bridge geometry, component and bridge strength are evaluated in Chapter 5. Furthermore, it is also shown in Chapter 6 that particular cross-frame detailing method with a particular erection scheme can alleviate fit-up problems. Bridge characteristics and erection schemes of the bridge should be considered together when selecting particular cross-frame detailing method. This chapter focuses on when locked-in stress effects due to DLF detailing need to be included in design analysis and provides guidance for selecting the type of cross-frame detailing method for different bridge geometries for improved bridge behavior. Also, ways of considering locked-in vertical displacements when setting the cambers are demonstrated with examples. Moreover, capabilities of basic 1D analysis solutions to capture the bridge response associated with DLF detailing are evaluated. Recommendations and guidance are provided on when it is appropriate to use line-girder analysis solutions to capture the behavior associated with DLF detailing.

7.1. Selection of Cross-Frame Detailing Method

As mentioned in Chapter 2, girder layovers under dead load are unavoidable at skewed bearing lines when NLF detailing is used. The ultimate goal with the DLF detailing is to introduce a lack-of-fit that induces torsional displacements in the opposite direction from the dead load rotations to offset the dead load torsional rotations. Figures 7.1.1 and 7.1.2, from Chapter 6, show the admissible bearing rotation limits as function of the skew angle and major-axis bending rotation at the bearing. Figure 7.1.1 is developed for plain elastomeric bearings while Fig. 7.1.2 is developed for steel reinforced elastomeric bearings. Percentages of the maximum rotational capacity of the bearing are provided to accommodate the fact that part of the rotation is taken up by live loads. Similar curves can be generated for other types of bearings. If the intersection point of the skew angle and ϕ_x for a bridge falls below the targeted bearing rotation curve, the bridge can be detailed for NLF detailing. Otherwise, the bridge should be constructed with either SDLF or TDLF detailing to reduce the layovers. It should be noted that the layover of the girders at the targeted load conditions tend to not exceed the typical

tolerance of ±(web depth, in inch) /96 regardless of the bridge type and geometry if the bridge is to be constructed with DLF detailing.

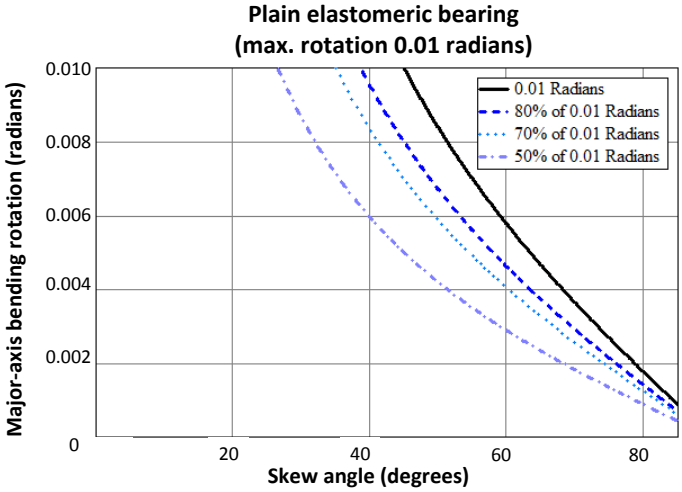

Figure 7.1.1. Torsional rotation levels for plain elastomeric bearings for given major-axis bending rotation and skew angle of the bearing.

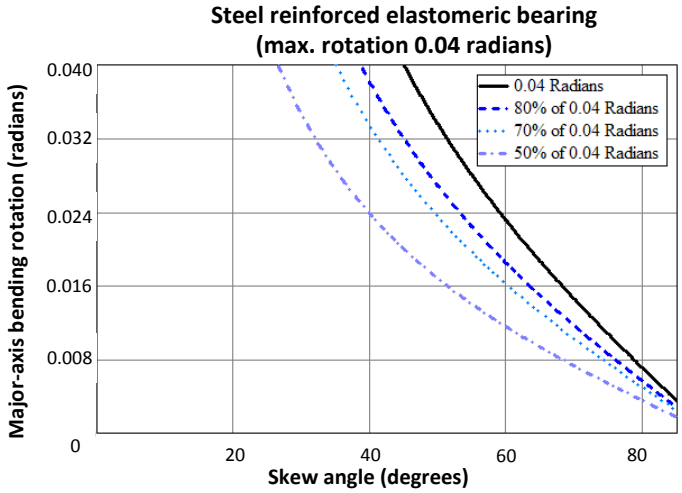

Figure 7.1.2. Torsional rotation levels for steel reinforced elastomeric bearings for given major-axis bending rotation and skew angle of the bearing.

However, one should be aware of the fact that the type of the detailing can impact the fit-up depending on the selected erection scheme as demonstrated in Chapter 6. There are various attributes that result in coupling between the twist rotations and other rotations and between the twist rotations and other displacements in curved and skewed I-girder bridges. These include:

- Skewed end cross-frames create a coupling between torsional rotations and major-axis bending rotations (see Fig. 2.1.1)

- Interior cross-frames enforce the same layovers between the adjacent girders at the cross-frame locations.
- Major-axis bending rotations are coupled with torsional rotations in curved girders.

For bridges constructed with NLF detailing, these compatibilities interact with each other under dead loads only whereas the interaction occurs both in the no-load geometry and under dead loads for the bridges constructed with DLF detailing. As a result, any variation from the no-load geometry due to dead load deflections requires fit-up forces to assemble the cross-frames of the bridges, constructed with NLF. For the bridges constructed with DLF detailing, fit-up forces are required at any stage due to lack-of-fit between the cross-frames and girders. Large fit-up forces can be required if the girders need to be displaced vertically by the applied forces since the girders generally have large stiffness against major-axis bending deformations. These cases are more likely to occur for curved girders, or at the locations with large differential vertical displacements between the girders and close interaction of the different displacement compatibilities (i.e. interior cross-frames that are framed close to the skewed bearings).

It should be noted that the forces required to assemble the structure during erection can depend significantly on the erection procedures. The selected erection procedure can have a considerable effect on the dead load deflections during erection. For instance, using temporary supports for bridges constructed with NLF detailing or using the dead load deflections during the erection for bridges constructed with DLF detailing can reduce any potential large differential vertical displacements. Therefore, fit-up forces can be reduced based on the selected erection scheme. For instance, fit-up forces are expected to be minimum for the bridges, constructed with SDLF detailing and erected using the dead load deflections. All these attributes are needed to be considered when selecting a particular detailing method.

The locked-in stress effects are currently not considered in the design analysis of I-girder bridges. Although the bridge is constructed with DLF detailing, bridge components are sized based on the predictions associated with NLF detailing. Similarly, girder cambers are set based on the predictions associated with NLF detailing. It is found in Chapter 5 that DLF detailing of the bridges has negligible effects on the dead load major-axis bending stresses. Therefore, locked-in major-axis bending stresses can be neglected in the design of I-girder bridges. However, it is found in Chapter 5 that locked-in stresses due to DLF detailing can have considerable effect on:

- *Vertical displacements*

  For bridges with curvature and/or skew and constructed with DLF detailing, physical bridge can develop vertical deflections significantly different than the ones predicted by NLF detailing of the bridge. This can lead to deviations in the deck profile and final elevations of the girder. If a curved and/or skewed bridge is constructed for DLF detailing, locked-in stress effects should be considered in the design analysis to obtain the correct deck elevation and girder camber requirements.

  For straight-skewed bridges, the locked-in effects have a minor or negligible influence on the final elevation of the girders. Therefore, for straight-skewed bridges, there is no need to include locked-in effects in the analysis unless more accurate predictions are desired.

- *Cross-frame forces*

  In curved bridges, constructed with DLF detailing, cross-frame forces can increase significantly (as shown in Section 5.3) due to locked-in stress effects. If a curved bridge with or without skew is constructed for DLF detailing, accurate cross-frame forces can only be captured by including the locked-in stress effects in design analysis.

  In current practice, cross-frame members of straight-skewed bridges are usually sized with respect to the NLF detailing predictions. However, the actual point-by-point cross-frame forces associated with DLF detailing can differ substantially from those obtained from the 3D FEA assuming NLF detailing. In the previous sections, it is shown that DLF detailing tends to develop cross-frame forces due to lack-of-fit that are approximately equal and opposite to the forces caused by dead load stresses in the regions having the largest transverse stiffness. However, locked-in stresses in cross-frames tend to be substantially different than the dead load stresses outside the transverse load paths. Particularly, large locked-in cross-frame forces are observed at the cross-frame locations that are placed closest to the skewed bearing lines with $\alpha \leq 0.4$, as shown in Chapters 5 and 6 where α is the ratio of the adjacent unbraced length at first cross-frame offset from a bearing line. This behavior is mainly observed since the relative lateral stiffness ratio, χ_{Offset} increases significantly as α gets smaller (see Fig. 7.4.11). Also, the magnitude of the differential vertical camber between girders tends to be largest at these locations, which causes relatively large locked-in forces.

However, it is found and demonstrated in Chapter 6, that large locked-in cross-frame forces can be eliminated by rearranging the cross-frame layout such that $\alpha > 0.4$ or removing the cross-frames where $\alpha \leq 0.4$. If this ratio is not satisfied, the maximum total dead load cross-frame force throughout the bridge under dead loads associated with TDLF detailing can be larger than the maximum total dead load cross-frame force associated with the NLF detailing. In the cases where $\alpha \leq 0.4$, locked-in force effects should be considered to size the cross-frames. On the other hand, if $\alpha > 0.4$, typically the maximum total dead load cross-frame force observed at any load case associated with DLF detailing tends to not exceed the maximum total dead load cross-frame force associated with NLF detailing. Therefore, for the bridges, constructed with DLF detailing, sizing the cross-frame members based on the predictions associated with NLF detailing can be used when $\alpha > 0.4$ is satisfied. The differences between the maximums is expected to be minor. Table 7.1.1 tabulates the maximum steel and total dead load cross-frame forces of selected bridges, constructed with different types of detailing. It should be noted that maximum cross-frame forces are obtained only considering intermediate cross-frames since these members usually have the same sizes.

Table 7.1.1. Maximum interior cross-frame forces under steel and total dead loads for selected bridges, constructed with different types of detailing.

Bridge	α_{min}	*NLF (kips)*		*SDLF (kips)*		*TDLF (kips)*	
		SDL	*TDL*	*SDL*	*TDL*	*SDL*	*TDL*
NISSS54	*0.1*	*112*	*248*	*57*	*162*	*146*	*133*
*NISSS54**	*0.5*	*71*	*154*	*36*	*116*	*86*	*88*
NISSS14	*0.2*	*37*	*158*	*17*	*137*	*96*	*75*
NISSS13	*0.3*	*4*	*15*	*5*	*13*	*23*	*25*
NISSS16	*0.5*	*22*	*62*	*14*	*58*	*46*	*45*
NISSS36	*0.3*	*56*	*122*	*20*	*84*	*48*	*46*
NISSS37	*0.3*	*14*	*27*	*11*	*24*	*18*	*28*
EISSS6	*0.2*	*44*	*99*	*30*	*72*	*86*	*81*
NICSS16	*0.2*	*18*	*93*	*7*	*81*	*38*	*37*
XICSS5	*0.1*	*7*	*45*	*5*	*42*	*34*	*32*
EICSS2	*0.2*	*39*	*118*	*13*	*89*	*62*	*39*

**Selected cross-frames are removed to have $\alpha_{min} > 0.4$.*

Table 7.1.1 shows that maximum total dead load cross-frame force associated with TDLF detailing of NISSS13 ($\alpha_{min} = 0.3$) is slightly larger than the ones associated with NLF detailing. However, in terms of stresses these forces are in the magnitude of 2.2 ksi and 3.4 ksi which the increase due to locked-in stresses is relatively minor. Additionally, for

straight and skewed bridges, maximum total dead load end cross-frame force is typically observed when the bridge is constructed with NLF detailing. Thus, sizing the members based on the predictions associated with NLF detailing tend to be conservative.

- *Flange lateral bending stresses*

  For straight and skewed bridges constructed with TDLF detailing, significant reduction of the flange lateral bending stresses are obtained due to the reverse torsional deformations that are developed due to lack-of-fit. However, flange lateral bending stresses do not completely vanish in the targeted load condition due to differences between locked-in stresses and the stresses due to the torsion of the girders under the targeted dead load. Additionally, it is found in Chapter 5 that for the bridges constructed with DLF detailing, fascia girders develop flange lateral bending stresses due to the overhang bracket loadings. As a result, if locked-in effects are not included in the analysis, flange lateral bending stress predictions associated with NLF detailing can be conservatively used in the design and the bridge will not be overstressed.

  For curved and skewed bridges constructed with DLF detailing, it is found that DLF detailing induces overall global lateral bending in the girder flanges which tends to reduce flange lateral bending stresses. The reduction is observed since the global flange lateral bending in the flanges due to locked-in force effects are opposite to the lateral bending of the girders due to torsional rotation of the bridge cross-section. Therefore, if locked-in effects are not included in the analysis, flange lateral bending stress prediction associated with NLF detailing can be conservatively used in the design. Unfortunately, for the predictions of the vertical displacements and cross-frame forces, locked-in stress effects should be included in the design of the bridges with curvature and skew.

- *Strength of the curved bridges during construction*

  The effect of the resulting girder layovers on the strength tends to be small (less than approximately 3%). For cases with three or more girders, the true system capacities tend to be larger than those implied by the AASHTO LRFD strength calculations, regardless of the method of cross-frame detailing. Locked-in effects increase the strength of the curved bridges during construction since the overall flange lateral bending effects are reduced due to DLF detailing.

For straight-skewed bridges, DLF detailing is found to be an effective way to control the plumbness of the girders. However, a minimum ratio of the offset length to the adjacent unbraced length at the first cross-frame from a bearing line should be taken to be at least 0.4 to avoid relatively large locked-in cross-frame forces. It should be noted that the fit-up forces can be minimal for SDLF detailing and reduced significantly for TDLF detailing if the dead load deflections are used during erection. There is no additional effort needed to include the locked-in stress effects for designing the straight and skewed bridges (when $\alpha > 0.4$ is satisfied) unless better prediction accuracy is needed. For the bridges constructed with DLF, bridge components can be sized based on the predictions associated with NLF detailing when $\alpha > 0.4$ is satisfied. This should provide an adequate design of the bridge such that girders and cross-frames are not overstressed, deviations on the bridge geometry are minor, and overall strength is not an issue.

For curved radially-supported bridges, NLF detailing is found to be the most effective approach. Girder layovers due to dead loads within the spans tend to be inconsequential but must be evaluated. Further, DLF detailing can have a significant effect on girder vertical deflections, cross-frame forces and girder flange lateral bending stresses. However, SDLF detailing is recommended for longer spans if large deflections during the steel erection are expected. In the case of SDLF detailing of curved radially-supported bridges, the engineer should consider locked-in force effects in the design to achieve the accurate bridge geometry and to size cross-frames adequately.

For I-girder bridges with combined curvature and skew, NLF detailing is found to be effective for the cases where the percentage of the maximum rotational capacity is not exceeded at the bearings. Example calculations of the percentages of the maximum rotational capacity with respect to the girder major-axis bending rotations and skew angle of the bridge are provided in Figs. 7.1.1 and 7.1.2 for plain elastomeric and steel reinforced elastomeric bearings. These curves can be generated for other types of bearings as well. Otherwise, SDLF detailing or an intermediate condition between SDLF and TDLF detailing is recommended for curved and skewed I-girder bridges. Also, for longer spans, if large differential deflections are expected SDLF detailing or NLF detailing and the use of beveled shim plates at the end bearing lines are recommended. In the case of DLF detailing of curved and skewed bridges, the engineer should consider the locked-in force effects in the design. It should be noted that all these recommendations can require a different erection scheme to minimize the fit-up forces.

7.2. Consideration of Locked-In Vertical Deflections when Setting Girder Cambers

Girder cambers are usually set to compensate the dead load vertical deflections. In this research, girder cambers are set so that the slab is ideally flat under the total non-composite dead load. Superelevation, grade, and vertical curves are neglected as mentioned in Chapter 3. Figure 7.2.1 provides the initial total dead load girder profiles of the NISSS54 and NISCR5. Girder cambers in Fig.7.2.1 are obtained from the negative of the total dead load vertical deflections of the bridges, constructed with NLF detailing. Thus, they do not account for any locked-in vertical displacements due to DLF detailing. It is concluded in Chapter 5 that locked-in vertical displacements due to DLF detailing is minor for straight-skewed bridges whereas they can be major for curved bridges. If locked-in vertical displacements are large enough, the physical bridge can develop different deflections compared with the analytical predictions such as the Ford City Bridge (EICCR11).

In current practice, girder camber diagrams are set without considering this effect. Hence, the physical bridge may exhibit different vertical deflections than the ones used for setting the cambers which can lead to deviations in the predicted final deck profile, and final girder elevation. Setting the girder cambers by considering locked-in vertical displacements due to DLF detailing can require an iterative process which the tolerance for the deviation from the predicted girder vertical deflections is based on engineering judgement.

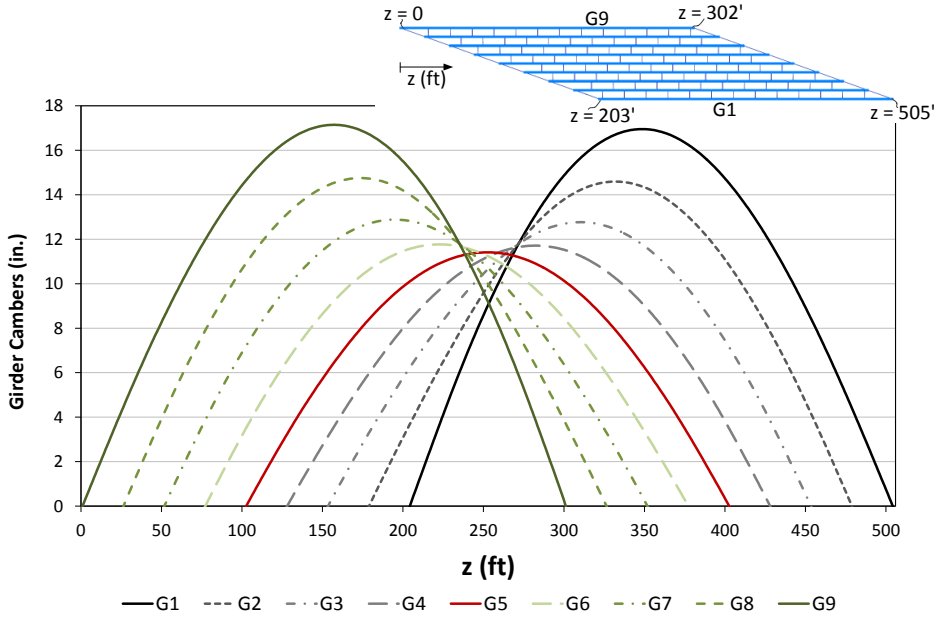

(i) NISSS54

Figure 7.2.1. Initial girder camber profile of NISSS54 and NISCR5

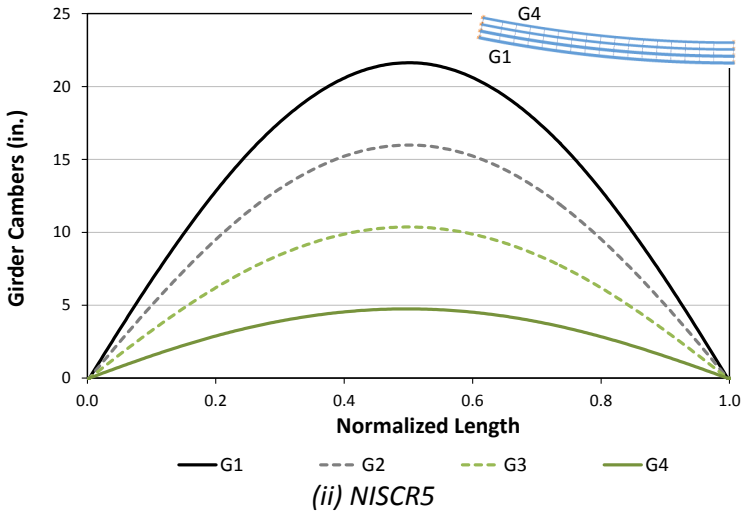

(ii) NISCR5

Figure 7.2.1. (continued). Initial girder camber profile of NISSS54 and NISCR5.

If locked-in vertical deflections associated with DLF detailing are considered in setting the cambers, the differential cambers between the girders change. This change can also influence the resulting locked-in vertical deflections associated with DLF detailing. However, in most cases, the deviation tends to be minor. However, if one continues the iteration, then one can obtain a unique girder camber profile where the differential camber between the girders induce the predicted locked-in vertical deflections. This is because only a unique distribution of differential camber between the girders can create the anticipated locked-in stress effects.

The iteration process can be described as follows:

1. Obtain the new girder camber profile for DLF detailing by considering the locked-in vertical displacements due to DLF detailing from the initial solution. This is basically the sum of the negative initial dead load deflections from NLF detailing of the bridge (Figure 7.2.1) and the negative of the locked-in vertical displacements due to DLF detailing (negative of the deflection in Figure 7.2.2). This camber profile is denoted as initial solution for DLF detailing of the bridge.
2. Analyze the bridge by using the procedures that are introduced in Chapter 3. If the vertical displacements from this step are same as the initial predicted displacements or the deviation tolerance is achieved stop iteration.
3. If different vertical displacements are obtained or the deviation is above the tolerance limit, the camber profile needed to be updated by considering the locked-in vertical displacements from the previous step. The iteration should continue until the girder

camber profiles are essentially the same with respect to the one in the previous solution or the deviation tolerance is achieved for the vertical displacements.

It should be noted that the iterative process does not require any additional level of engineering effort. The automation of the iteration can be easily implemented in the analysis software.

Figure 7.2.2 shows locked-in vertical displacements of two different representative bridges; NISSS54 and NISCR5 due to TDLF detailing. These two bridges represent the cases where one can consider the additional locked-in vertical deflections when setting the girder camber because the variations can be large (NISCR5) or one might want to capture the exact deck profile (NISSS54), although the deviations can be minor.

Figure 7.2.3 provides the converged camber profile for two representative bridges (NISSS54 and NISCR5). It should be noted from Fig. 7.2.3(i) that the camber profile is similar for the interior girders. This essentially indicates that the converged girder camber profile looks as if the interaction between the girders and cross-frames are minor. Additionally, Fig.7.2.4 shows differential vertical cambers between girders that are obtained from the initial and converged camber profiles of NISSS54. It should be noted from Fig. 7.3.4 that the magnitude of the differential vertical cambers between the girders is increased compared to the ones from the initial solution. It is expected that larger differential cambers between the girders can develop larger locked-in forces associated with TDLF detailing. Figure 7.2.5 shows the locked-in vertical displacements associated with TDLF detailing of the bridges NISSS54, and NISCR5 by using the converged girder camber profile. It is clear from Fig. 7.2.5(i) that the induced locked-in vertical displacements associated with TDLF detailing can be significantly different than the ones shown in Fig. 7.2.2(i) since the lack-of-fit between the girders are different in those two solutions. Figures 7.2.6 and 7.2.7 compare total dead load vertical displacements of the bridges NISSS54, and NISCR5 constructed with TDLF detailing by using initial and converged camber profiles. Total dead load vertical deflections of the bridges constructed with NLF detailing are also provided in Figs. 7.2.6 and 7.2.7.

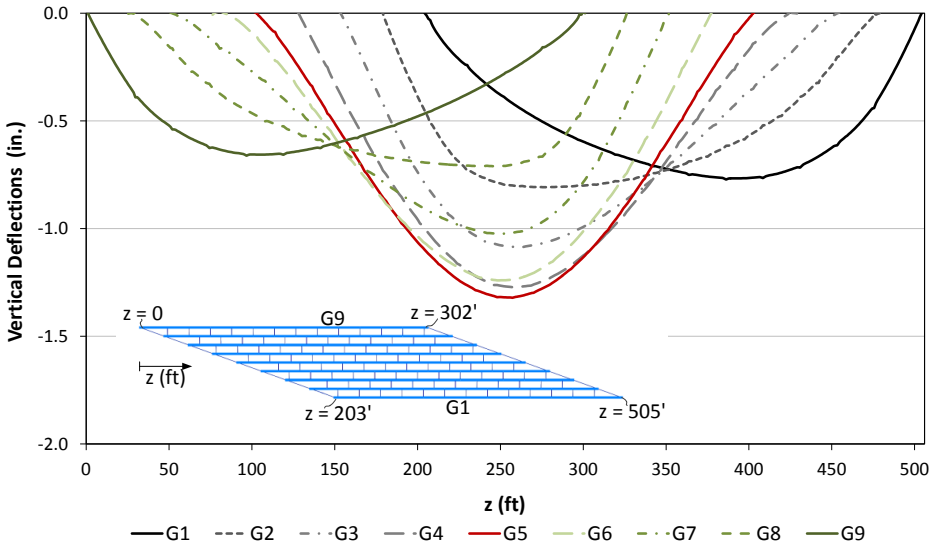

(i) NISSS54

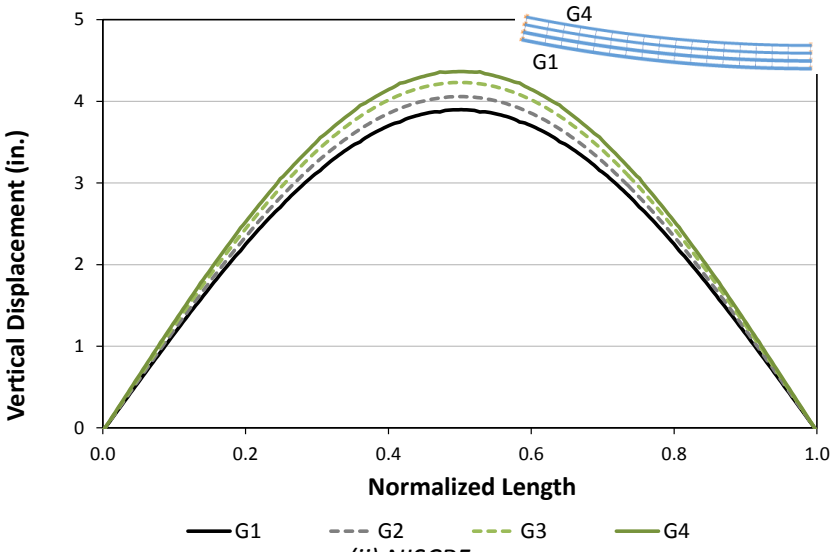

(ii) NISCR5

Figure 7.2.2. Locked-in vertical displacements due TDLF detailing of bridges NISSS54 and NISCR5 (initial solution).

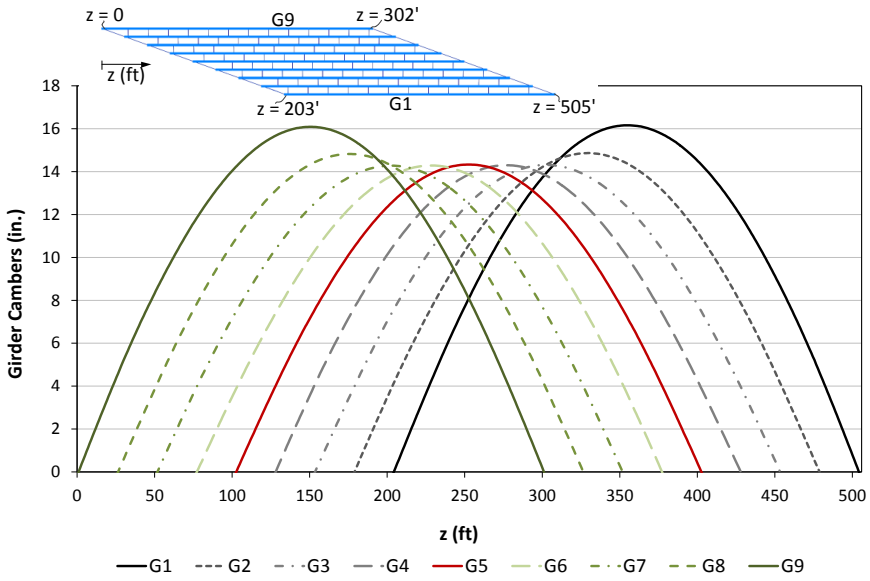

(i) NISSS54

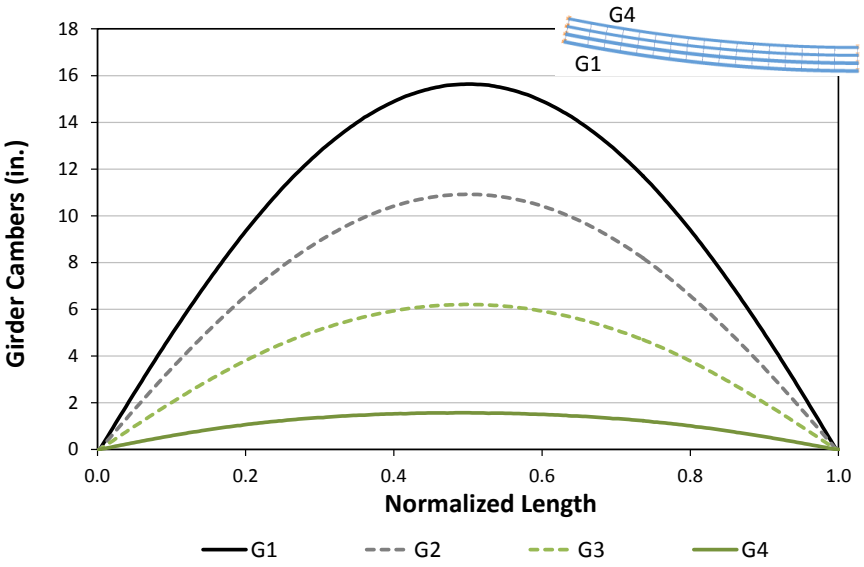

(ii) NISCR5

Figure 7.2.3. Converged camber profile for NISSS54 and NISCR5.

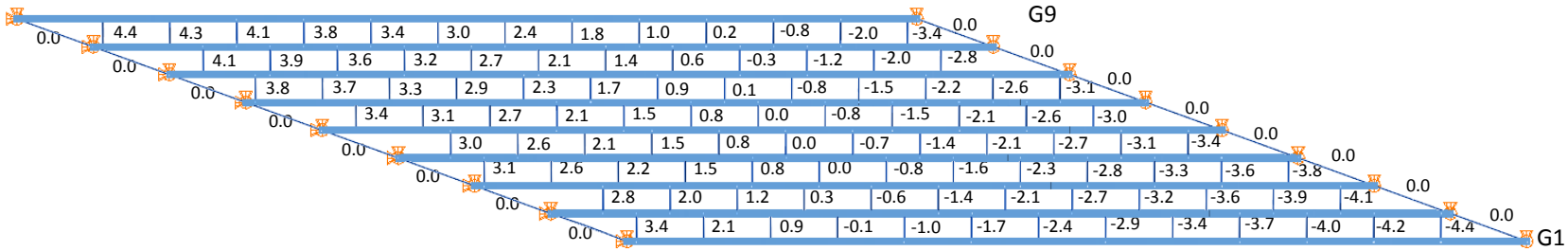

(i) Initial Solution

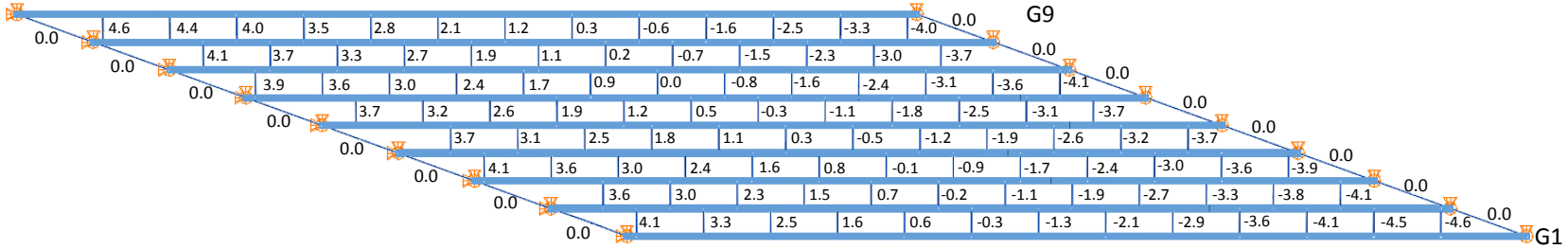

(ii) Converged Solution

Figure 7.2.4. NISSS54, Differential Camber between the girders obtained from initial and converged solutions under total dead loads.

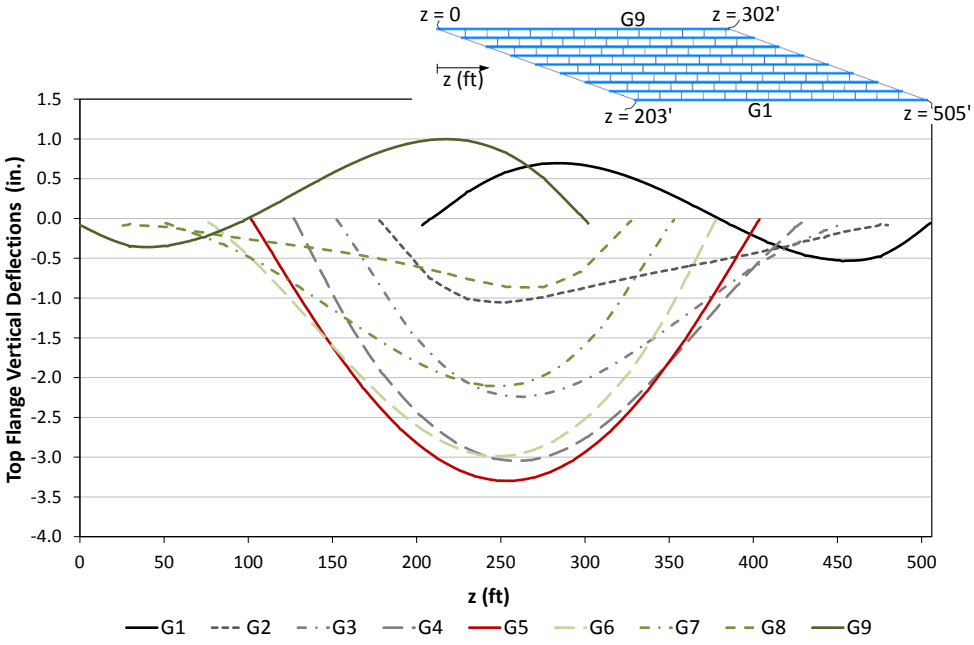

(ii) NISSS54

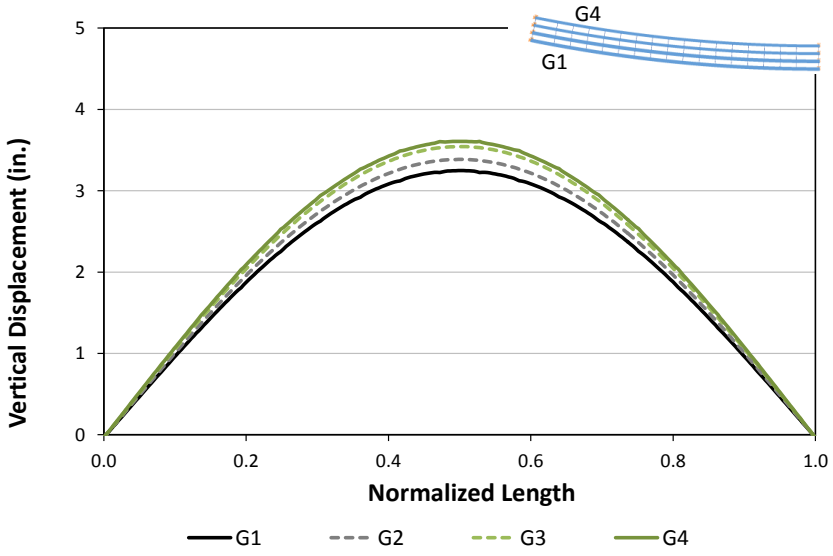

(ii) NISCR5

Figure 7.2.5. Locked-in vertical displacements due TDLF detailing of bridges NISSS54 and NISCR5 (converged solution).

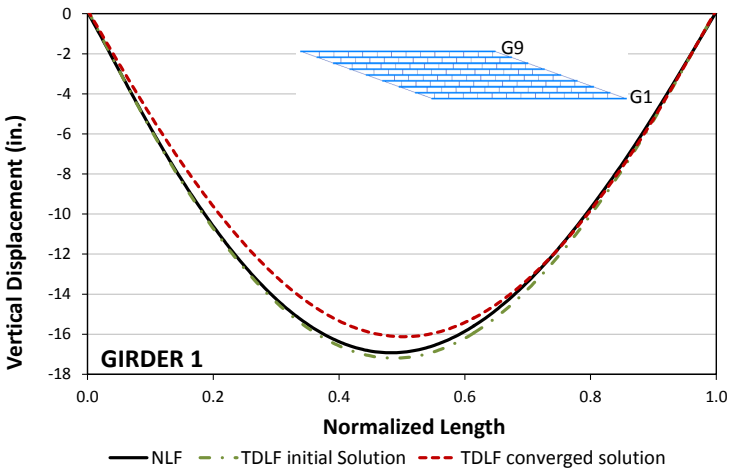

(i) Girder 1

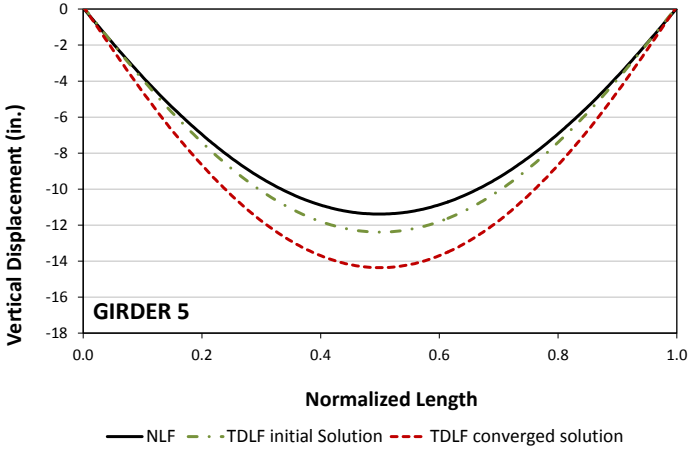

(ii) Girder 5

Figure 7.2.6. NISSS54, Vertical deflections under total dead load for different detailing methods.

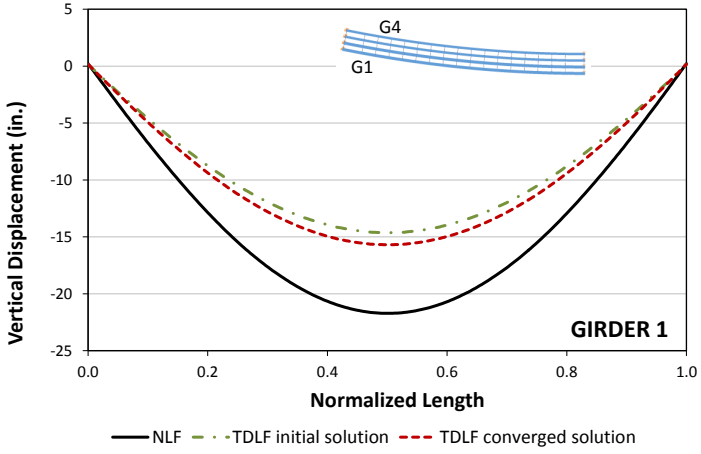

(i) Girder 1

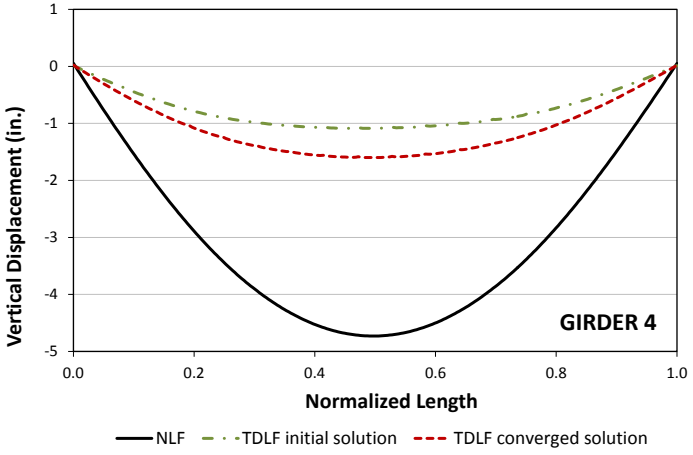

(ii) Girder 4

Figure 7.2.7. NISCR5, Vertical deflections under total dead load for different detailing methods.

The internal stresses and displacements that are developed in the system can be different from the initial solutions when the converged camber profile is used to construct the bridge with DLF detailing. It should be noted that the converged solution typically provides the girder layovers that are closest to theoretical plumb position under the targeted dead load since additional deformations due to locked-in stress effects are considered when setting the girder cambers. For instance, Fig. 7.2.8 shows the total dead load girder layovers of the NISSS54, constructed with TDLF detailing. Detailing the bridge for TDLF by using the converged camber profile provides plumb girders which are very close to the theoretical plumb positions. Also, Fig. 7.2.9 provides the total dead load girder layovers for NISCR5, constructed with NLF detailing and TDLF detailing by using the initial and converged camber profiles. It should be noted from Fig. 7.2.9 that the girders are closest to the plumb positions for the TDLF detailing of the bridge by using the converged camber profiles.

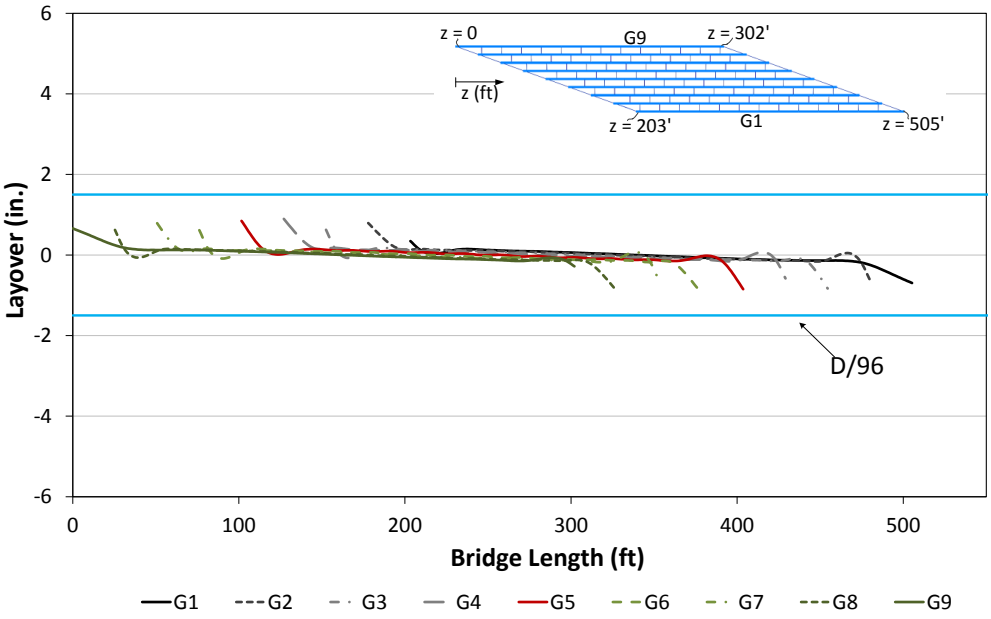

Figure 7.2.8. NISSS54, Girder layovers under total dead load for TDLF detailing by using the converged camber profile.

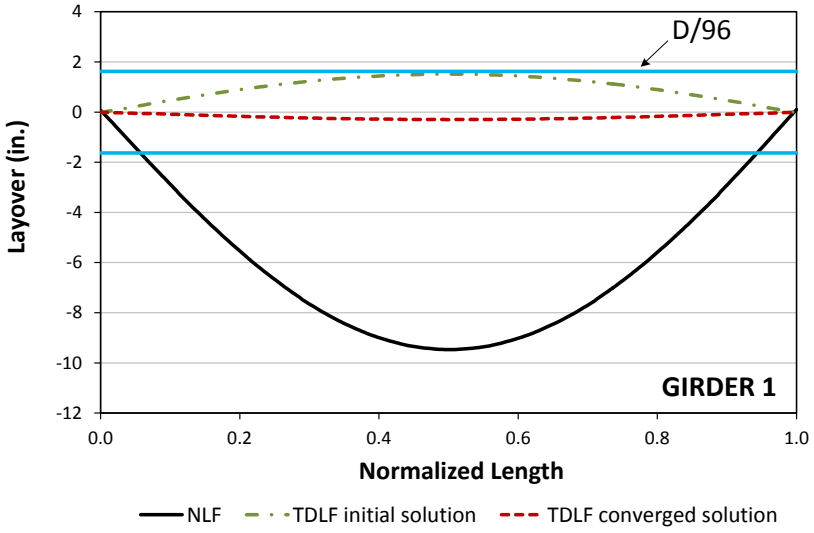

Figure 7.2.9. NISCR5, Girder layovers under total dead load.

Cross-frame forces are also expected to be different since the lack-of-fit between the cross-frames and girders is different than the initial solution. Different locked-in cross-frame forces can develop if there is a considerable change in the differential cambers between girders. For instance, Figs. 7.2.10 and 7.2.11 show the distribution of the largest total dead load cross-frame component axial forces in each of the cross-frames throughout the bridge for TDLF detailing under total and steel dead load, respectively. The most highly loaded cross-frame members are colored dark red, while the more lightly loaded cross-frame members are shaded light grey. The largest magnitude cross-frame component axial force is labeled next to each of the cross-frames in the picture. In addition, the total sum of the absolute value of all the cross-frame component axial forces are normalized with respect to NLF values and initial TDLF values under the considered load level. Additionally the mean of the diagonal, top and bottom chord forces are reported at the left bottom corner for each case. It should be noted from Fig. 7.2.10 that total sum of the absolute value of all the cross-frame component axial forces is reduced 61% and 17 % compared to NLF solution and the initial solution respectively. As mentioned in Chapter 5, the bulk part of the reduction is observed along the transverse load paths. Relatively larger cross-frame forces are observed at the cross-frames that are closest to the skewed bearings. This is mainly because the first cross-frames are placed close to the skewed bearings ($\alpha \leq 0.4$). It should be noted from Fig. 7.2.11 that total cross-frame forces under steel dead load are increased 90%, 37% compared to NLF solution and the initial solution respectively. Most of these induced forces cancel out with the dead load forces under total dead

load level. Fit-up problems can be observed unless steel deflections are not used during the steel erection. On the other hand, the total sum of the cross-frame forces can be reduced in the cases where the differential camber between the girders is reduced by the iteration process. For instance, the total sum of the absolute value of all the cross-frame component axial forces is obtained as 4916 kip for NISCR5 constructed with NLF detailing. TDLF detailing of NISCR5 increased the total sum of the absolute value of all the cross-frame component axial forces by 2.44 times due to the additive behavior of the locked-in effects. However, if the bridge is detailed for TDLF detailing by using the converged camber profile, the total sum of the absolute value of all the cross-frame component axial forces observed in NLF detailing is increased by 2.20 times.

It is found that the change in the major-axis bending stresses is relatively minor if the cambers are iterated. Figure 7.2.12 shows the girder major-axis bending and flange lateral bending stresses induced in the top flange of Girders G1, and G5 under the total dead load for the NLF and TDLF detailing of the bridge NISSS54 by using initial and converged camber profiles. It is observed from Fig. 7.2.12 that there is a minor change in the major-axis bending stresses due to the iteration process.

For straight-skewed bridges, similar to girder layovers, flange lateral bending stresses are expected to reduce with the iteration of the girder cambers. This can be also seen in Fig. 7.2.12. However, it should be noted from Fig. 7.2.12 that there are still some flange lateral bending stresses since locked-in flange lateral bending stresses do not offset dead load flange lateral bending stresses completely. Similarly at the obtuse corners, the spikes in the flange lateral bending stresses near the ends of the girders are still observed due to nuisance stiffness issues. Figure 7.2.13 provides the girder stresses for NISCR5 for different detailing scenarios. It should be noted that the second-order amplification of the flange lateral bending stresses due to overall twisting effects are minimized with the iteration process.

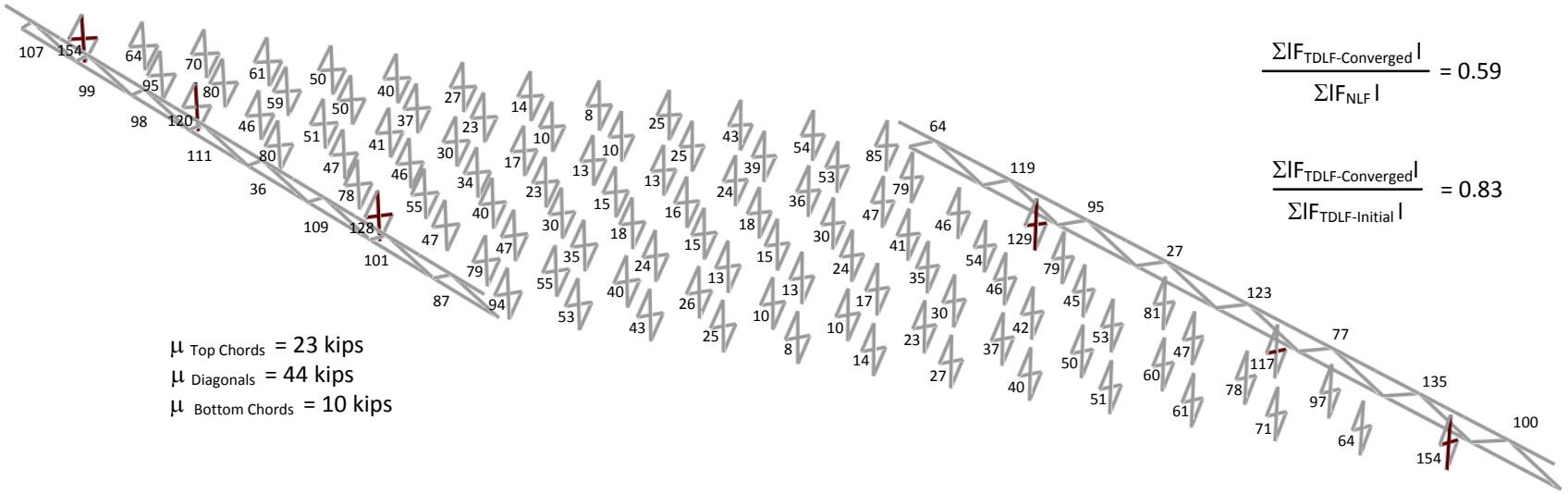

Figure 7.2.10. NISSS54, maximum amplitude of the component axial forces in each of the cross-frames under total dead load for TDLF detailing method.

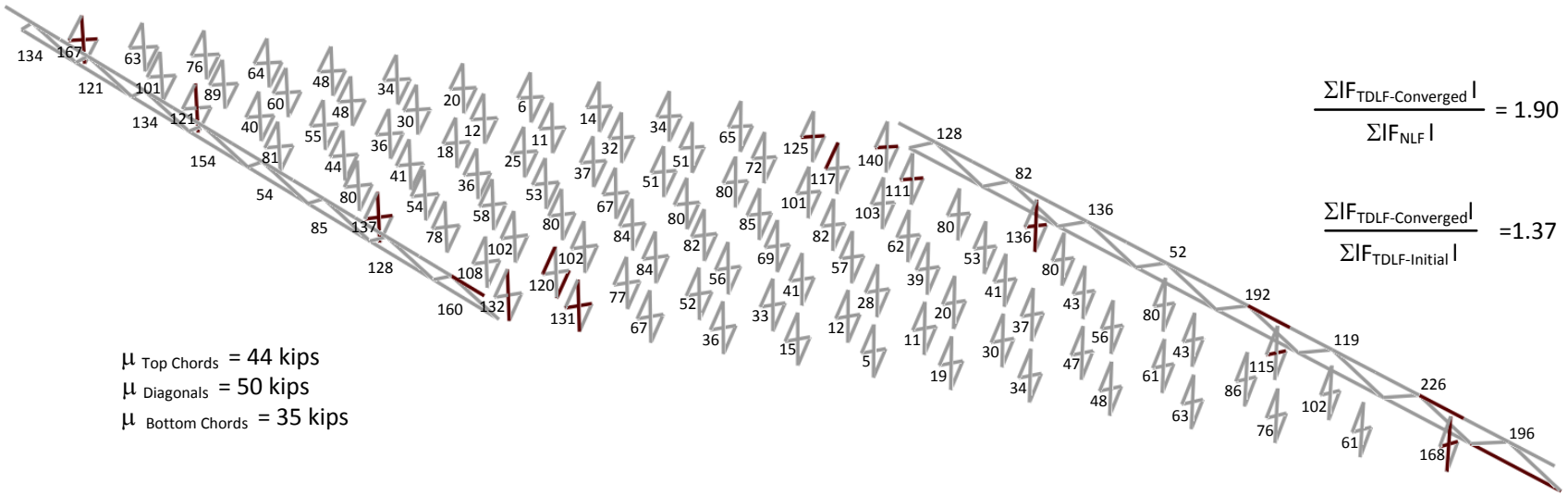

Figure 7.2.11. NISSS54, maximum amplitude of the component axial forces in each of the cross-frames under steel dead load for TDLF detailing methods.

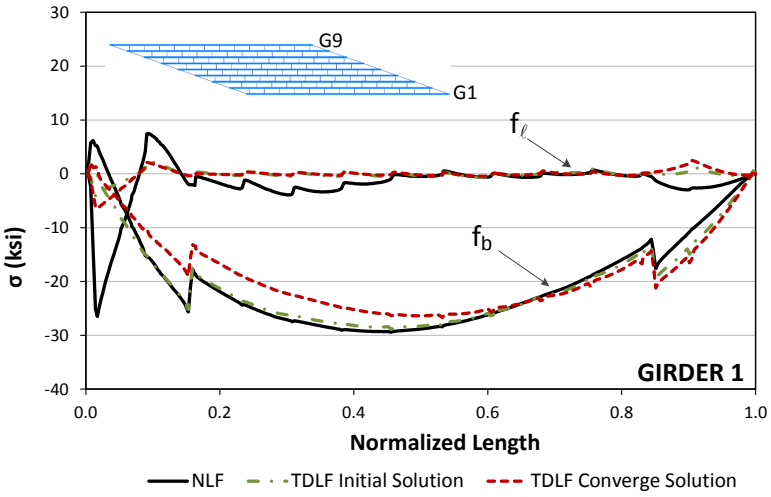

(i) Girder 1

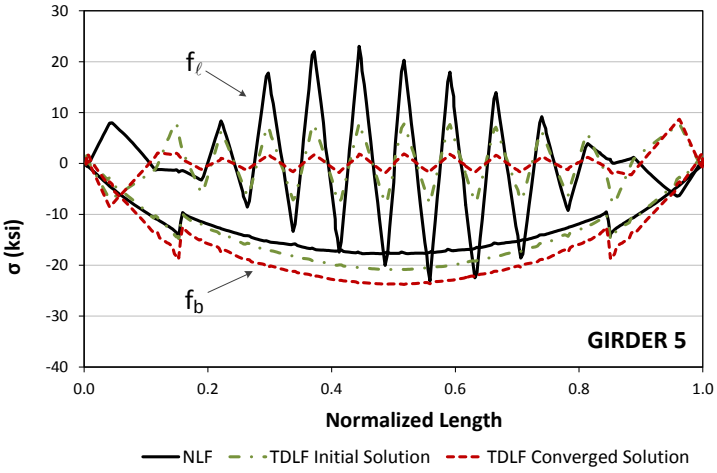

(ii) Girder 4

Figure 7.2.12. NISSS54, Top flange stresses under total dead load for different detailing methods.

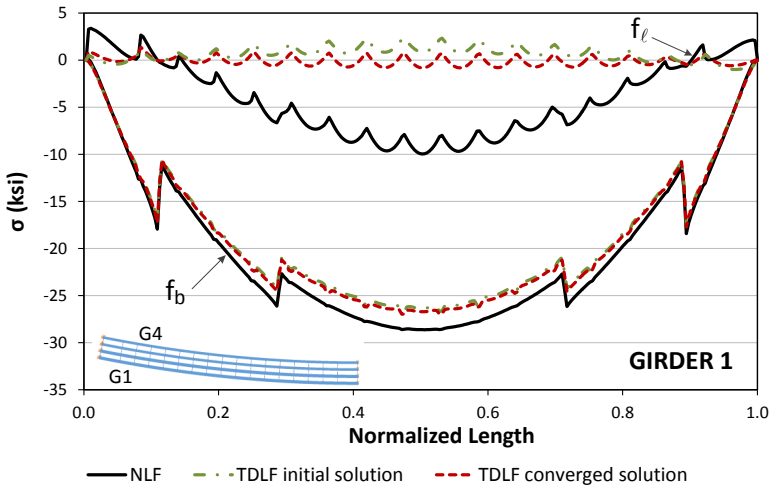

(i) Girder 1

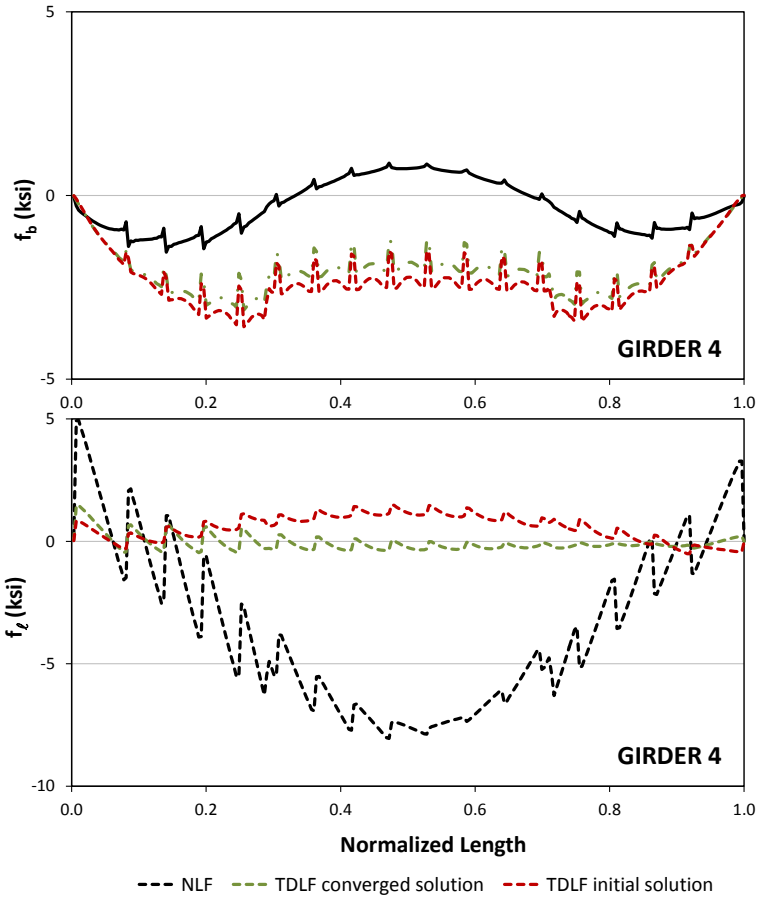

(ii) Girder 4

Figure 7.2.13. NISSS54, Top flange stresses under total dead load for different detailing methods.

7.3. Special Cases where Line-Girder Analysis Predicts Accurate Results for Straight-Skewed Bridges Constructed with DLF Detailing

Engineers widely use the line-girder analysis solutions to design straight skewed I-girder bridges. These methods work well given that the bridge behavior is similar with respect to the assumptions of the flexural model in the line-girder analysis. Analysis predictions are important in terms of detailing the cross-frames since camber profiles are set based on these predictions. Figure 7.3.1 demonstrates two sets of girder camber profiles based on a line-girder analysis versus a 3D FEA of the bridges, constructed with NLF detailing. It is obvious that the line-girder analysis solutions are not able to capture the behavior of the bridges due to large transverse load transfer between girders. Figures 7.3.2 and 7.3.3 provide the total dead load differential camber between girders for the bridges NISSS54 and XICSS5, respectively. The differential camber between the girders is obtained based on the line-girder analysis and 3D-FEA results. It should be noted from Figs. 7.3.2 and 7.3.3 that the magnitudes of the differential camber between the girders are different than the ones with 3D FEA results since vertical deflection predictions are different in both solutions.

It is showed in Section 7.2 that if Total Dead Load Fit (TDLF) detailing is used on straight skewed I-girder bridges (i.e., the bridges are detailed to have plumb webs in their final dead load condition), and if the girder cambers are set based on the results from converged girder camber profiles, the lack-of-fit stresses due to the cross-frame detailing come very close to canceling the stresses due to the torsion of the girders under the total dead load condition. As such, physical girder layovers are approximately zero only under total dead load.

For basic 1D line-girder analyses, individual girders are modeled disregarding the structural steel framing of the bridge. The dead loads applied to individual girders based on their tributary areas and the interaction between the cross-frames and girders are neglected; thus, no flange lateral bending are captured in basic 1D line-girder analysis solutions. As a result, the basic 1D line-girder analysis flexural model can be sufficient to capture the physical vertical displacement and major-axis bending stresses with good accuracy for the straight-skewed bridges, constructed with DLF detailing under the load level at which girder webs are theoretically plumb. However, the analysis solutions can be significantly off at the other load levels since flange lateral bending of the flanges are unavoidable at other load levels.

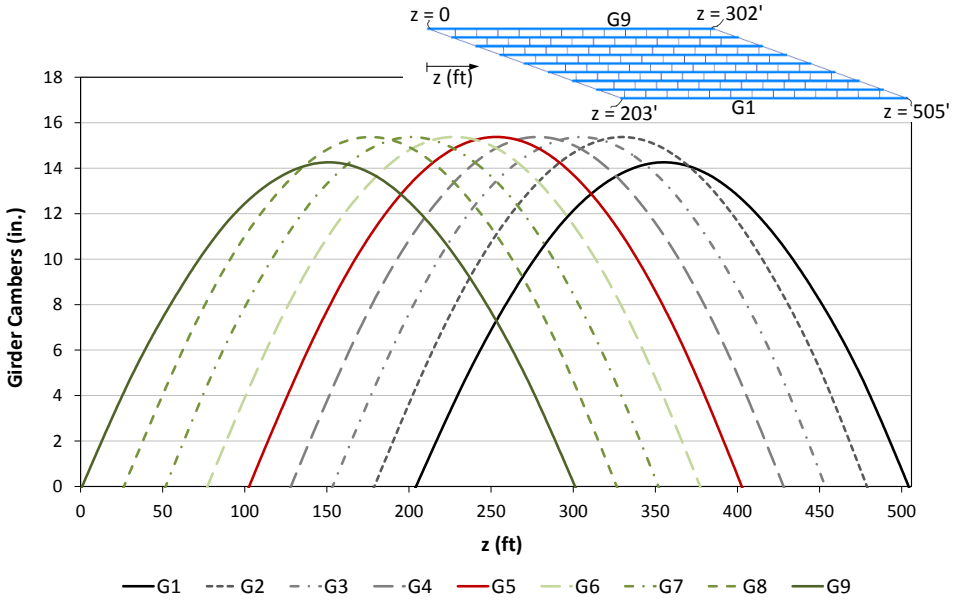

(i) Line-girder analysis

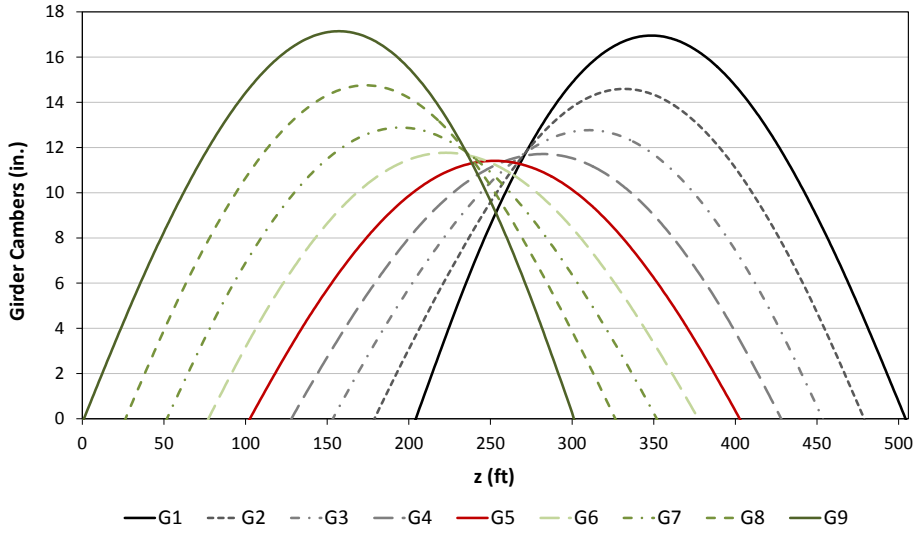

(ii) 3D FEA

Figure 7.3.1. NISSS54, Girder camber profiles, obtained from different analysis solutions.

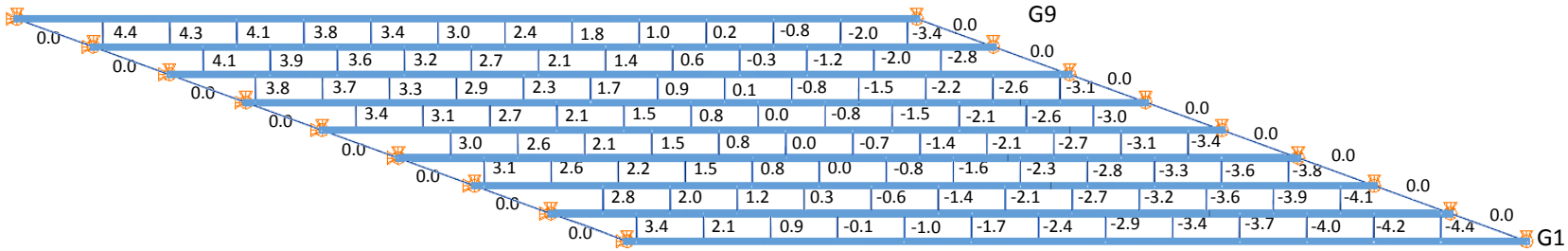

(i) 3D FEA solutions

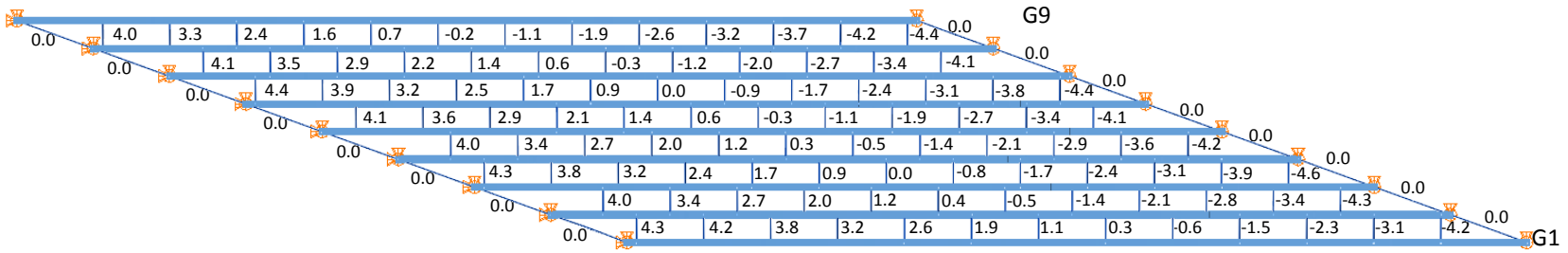

(ii) Basic 1D line-girder analysis solutions

Figure 7.3.2. NISSS54, Differential camber between girders from different analysis solutions.

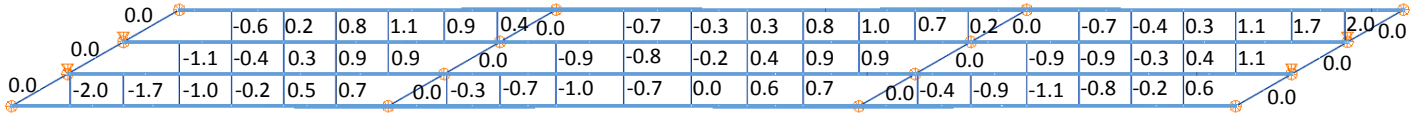

(i) 3D FEA solutions

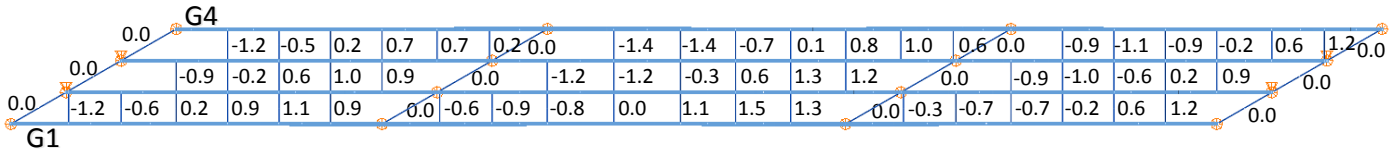

(ii) Basic 1D line-girder analysis solutions

Figure 7.3.3. XICSS5, Differential camber between girders from different analysis solutions.

Figures 7.3.4 and 7.3.5 show the total dead load girder layover of the bridges NISSS54 and XICSS5, constructed with TDLF detailing by using the camber profiles obtained from line-girder analysis solutions. NISSS54 and XICSS5 bridges are the two extreme examples of the design matrix where line-girder analysis is unable to capture the physical behavior of the bridge due to significant skew effects. It should be noted for both bridges that a web layover tolerance of ±(web depth, in inches) / 96 is checked under the targeted dead load level. It is important that the final web lateral position is not the same as the girder layovers that are shown in Figs. 5.2.13 and 5.2.16. This is because in all solutions, the lack-of-fit between the girders and cross-frames are different. Different differential camber between the girders develop different locked-in stress effects. Also, line-girder analysis solutions provide girder layovers that are closest to the theoretical plumb position under targeted dead loads.

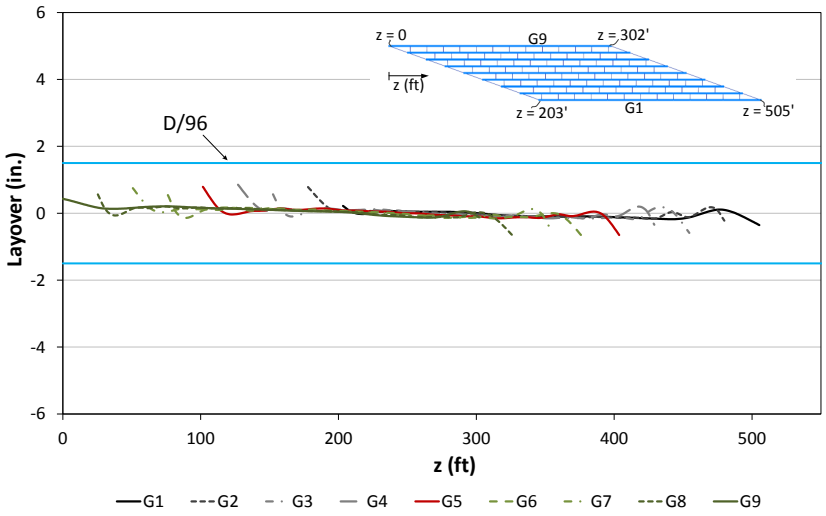

Figure 7.3.4. NISSS54, Girder layovers under total dead load for TDLF detailing.

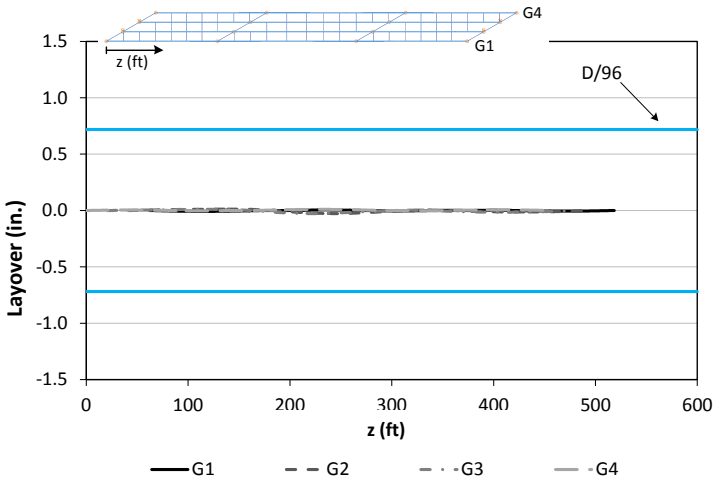

Figure 7.3.5. XICSS5, Girder layovers under total dead load for TDLF detailing.

Figure 7.3.6 provides the total dead load vertical deflections of the bridge NISSS54 along the normalized length of girders G1, G5 and G9. Vertical deflections are obtained from line-girder analysis solutions and test simulations, constructed with NLF detailing and TDLF detailing based on line-girder analysis camber profiles. Similarly, Fig. 7.3.7 provides the total dead load vertical deflections of the bridge XICSS5 along the normalized length of girders G1, G2, and G4. It is clear from Figs. 7.4.6 and 7.4.7 that line-girder analysis solutions differ significantly from finite element analysis predictions for NLF detailing of the bridges due to significant transverse load transfers. However, line-girder analysis vertical displacement predictions are essentially the same as the finite element analysis predictions of the bridge, constructed with TDLF detailing, where the cambers are set based on line-girder analysis.

Figures 7.3.8 and 7.3.9 show the total dead load major-axis bending and flange lateral bending stresses induced in the top flange of Girders G1, G5 and G9 of the bridges NISSS54 and XICSS5 for NLF and TDLF detailing where the cambers are set based on the line-girder analysis and line-girder analysis predictions. It should be noted that line-girder analysis solutions are not capable of providing any flange lateral bending of the girders.

It is obvious from Figs. 7.3.8 and 7.3.9 that line-girder analysis predictions cannot capture the major-axis bending stress predictions for NLF detailing. This is due to significant load paths along the transverse direction of the bridge. On the other hand, line-girder analysis solutions capture the physical girder major-axis bending stresses associated with TDLF detailing accurately. If the cambers are set based on line-girder analysis solutions, since there are almost no torsional deflections of the bridge under the total dead load, the basic flexural model is enough to capture the bridge behavior.

Unfortunately, line-girder analysis predictions do not necessarily produce accurate results for cases other than the total dead load condition if the bridge experiences torsional deformations and transverse load transfer effects.

Although there are no cross-frame predictions of line-girder analysis solutions, it is important to investigate the influence of setting the girder cambers based on line-girder analysis solutions on the cross-frame forces. Figures 7.3.10 and 7.3.11 show the distribution of the largest total dead load cross-frame component axial forces in each of the cross-frames throughout NISSS54 for TDLF detailing under total and steel dead load respectively. Figures 7.3.12 and 7.3.13 show the distribution of the largest cross-frame component axial forces in each of the cross-frames throughout the bridge XICSS5 for TDLF detailing under total

and steel dead load respectively. It is observed from Figs. 7.3.10 and 7.3.12 that cross-frame forces under total dead load are reduced by 40% for the bridge NISSS54 and 63% for the bridge XICSS5 with respect to NLF detailing when the cambers are set based on line-girder analysis solutions. The great reduction in the cross-frame forces can be explained by increased locked-in forces in the cross-frames. This can be better understood from Figs. 7.3.11 and 7.3.13 such that the increase in the cross-frame forces with respect to NLF detailing is 107% for the bridge NISSS54 and 546% for the bridge XICSS5. It should be also noted from Figs. 7.3.10 and 7.3.11 that the solutions are very similar to the ones that are obtained by setting the girder cambers based on converged solutions discussed in Section 7.2. However, they are not exactly same since there are slight differences in the total dead load girder cambers (See Figs. 7.3.1(i) and 7.2.3(i)).

If the girder cambers are set based on the results from 1D line-girder analyses and the bridge is detailed for TDLF, the lack-of-fit stresses due to the cross-frame detailing come very close to canceling the stresses due to the torsion of the girders under the total dead load condition. As such, physical girder layovers are approximately zero only under total dead load, and the basic 1D line-girder analysis flexural model is sufficient to capture the physical vertical displacement and major-axis bending stresses with good accuracy. This result is essentially independent of the magnitude and pattern of the support skews.

Unfortunately, line-girder analyses do not necessarily produce accurate results for cases other than the dead load condition under which the web is targeted to be plumb. This is because a line-girder analysis does not account for any transverse load transfer or girder torsional responses.

Similarly, if Steel Dead Load Fit (SDLF) detailing is used on straight skewed I-girder bridges (i.e., the bridges are detailed to have plumb webs in the completed steel dead load condition), and if the girder cambers are set based on the results from 1D line-girder analyses, a basic 1D line-girder analysis is sufficient to obtain accurate predictions of the girder major-axis bending and vertical displacements only under steel dead load condition. In this case however, physical flange lateral bending stresses are approximately zero since there are no overhang bracket loadings except the locations with large nuisance stiffness (i.e. intermediate cross-frames that are framed close to the skewed bearings). Also, cross-frame forces under steel dead loads are expected to be minimum along the transverse load paths.

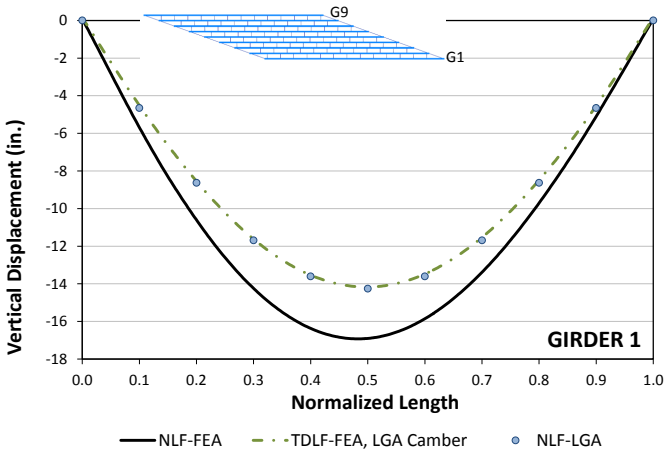

(i) Girder 1

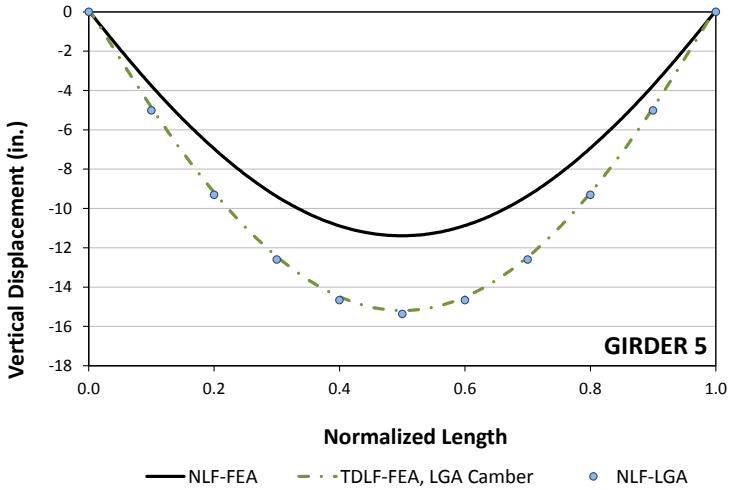

(ii) Girder 5

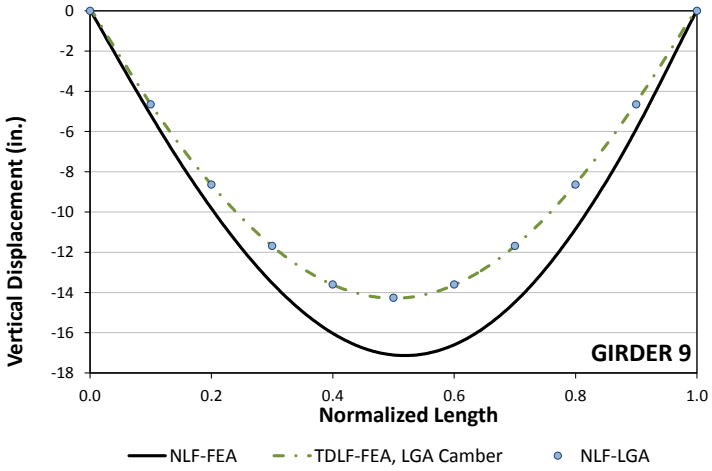

(iii) Girder 9

Figure 7.3.6. NISSS54, Vertical deflections under total dead load for different detailing methods.

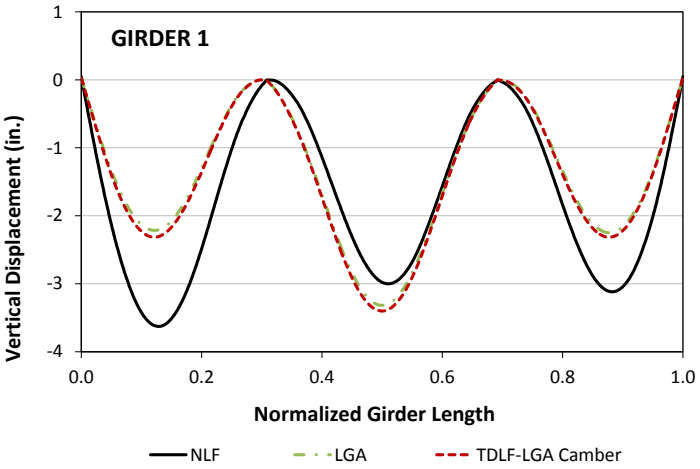

(i) Girder 1

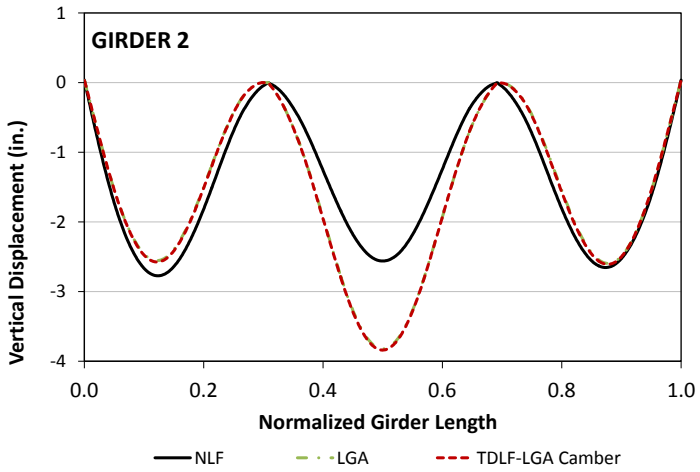

(ii) Girder 2

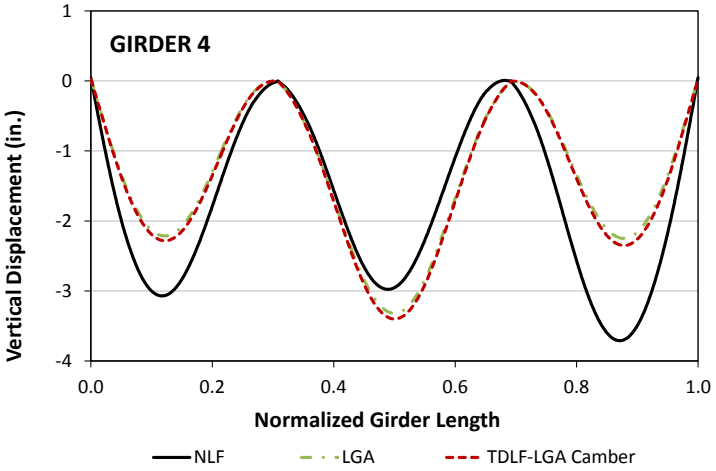

(iii) Girder 4

Figure 7.3.7. XICSS5, Vertical deflections under total dead load for different detailing methods.

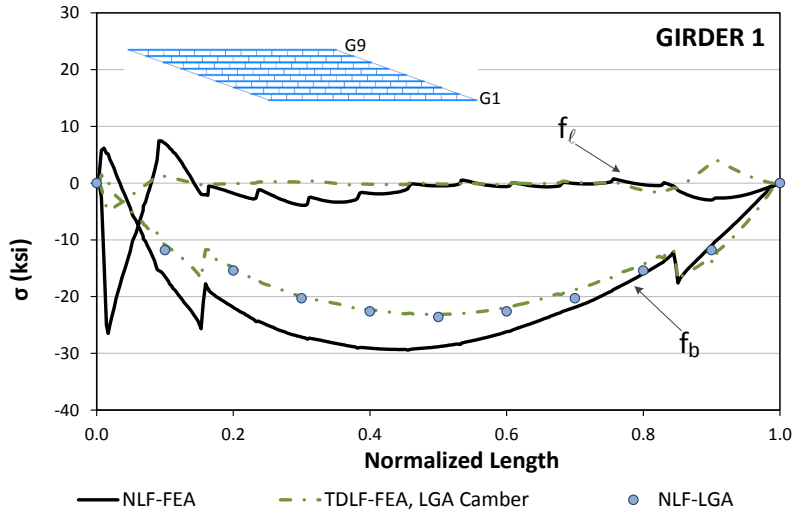

(i) Girder 1

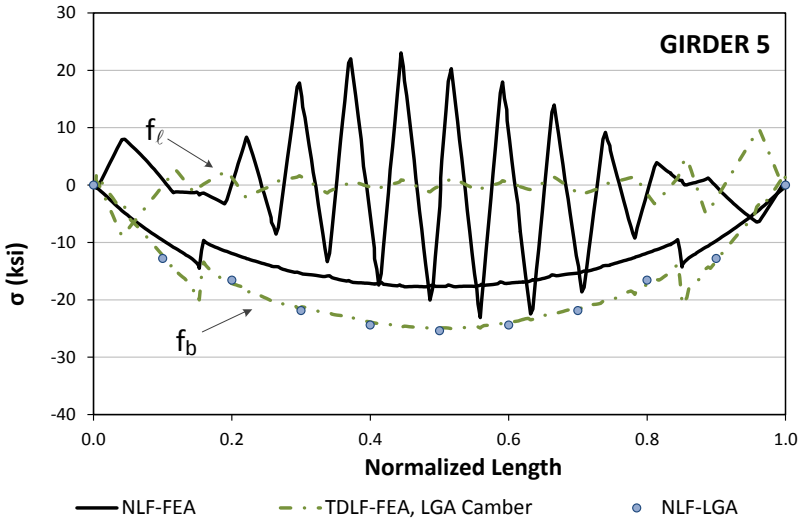

(ii) Girder 5

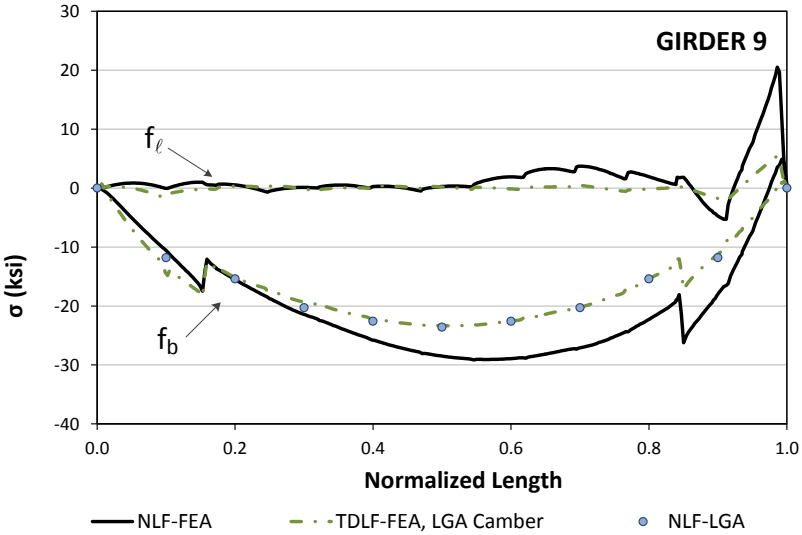

(iii) Girder 9

Figure 7.3.8. NISSS54, Top flange stresses under total dead load for different detailing methods.

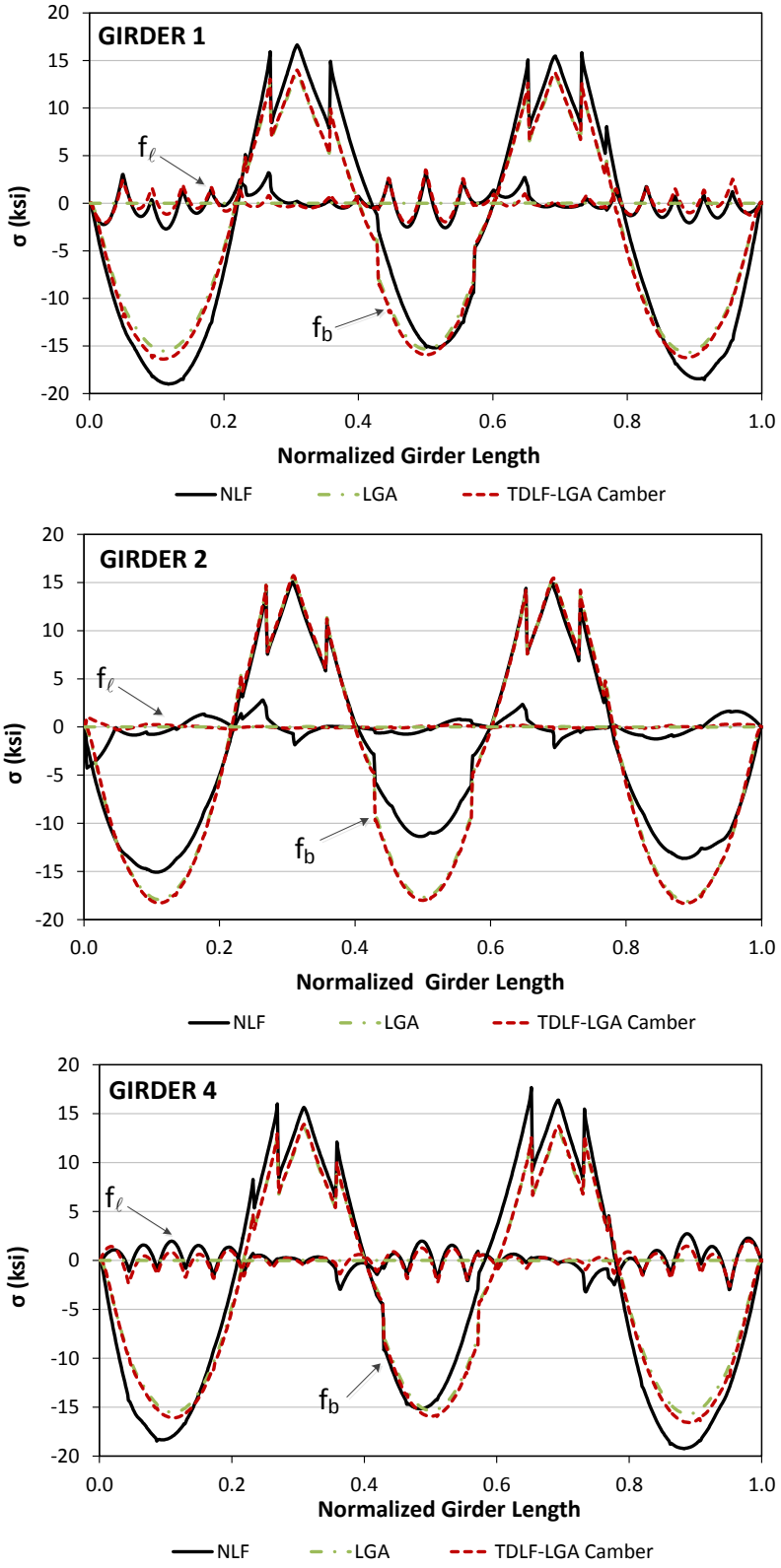

Figure 7.3.9. XICSS5, Top flange stresses under total dead load for different detailing methods.

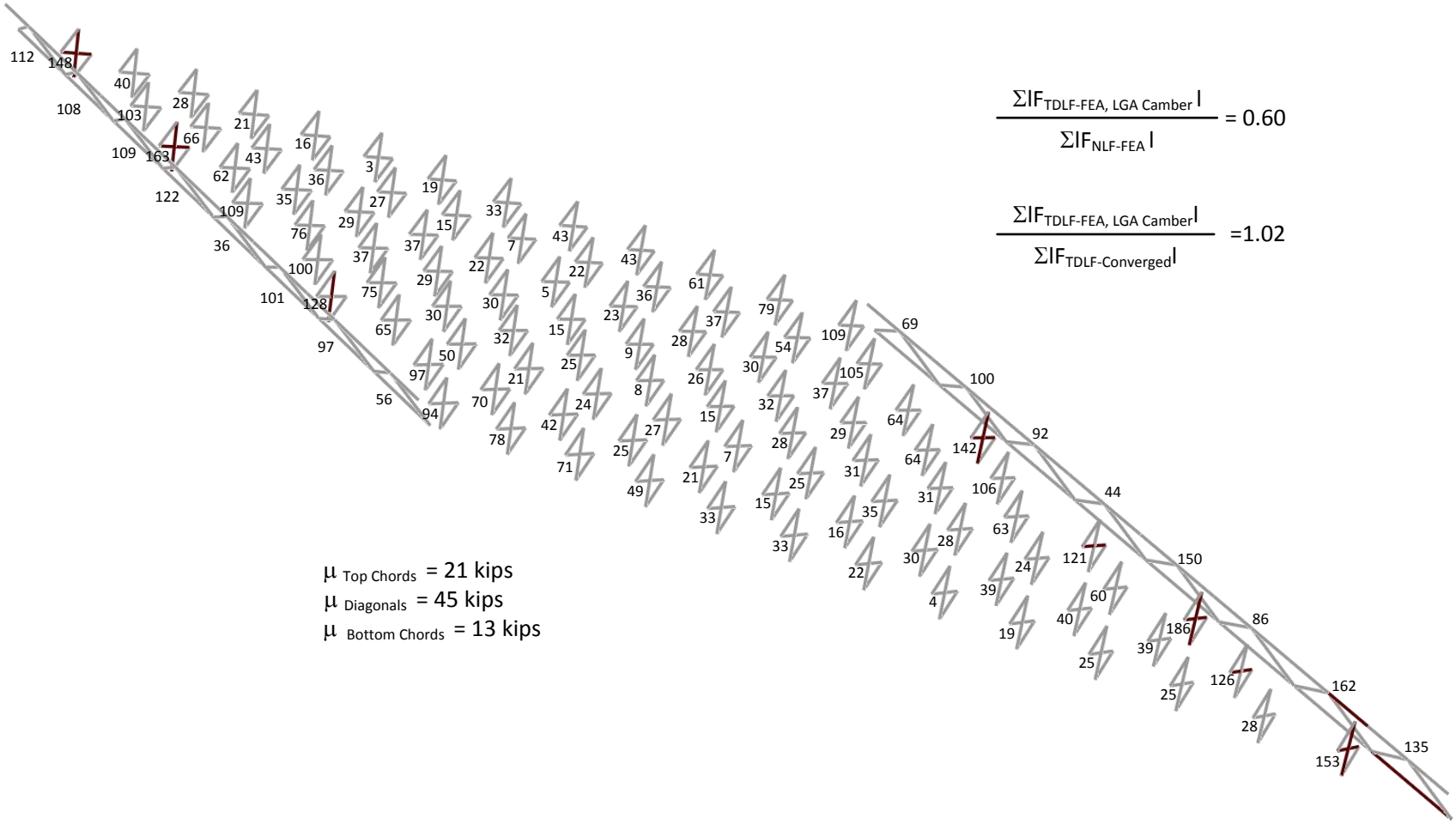

Figure 7.3.10. NISSS54, maximum amplitude of the component axial forces in each of the cross-frames under total dead load for TDLF detailing.

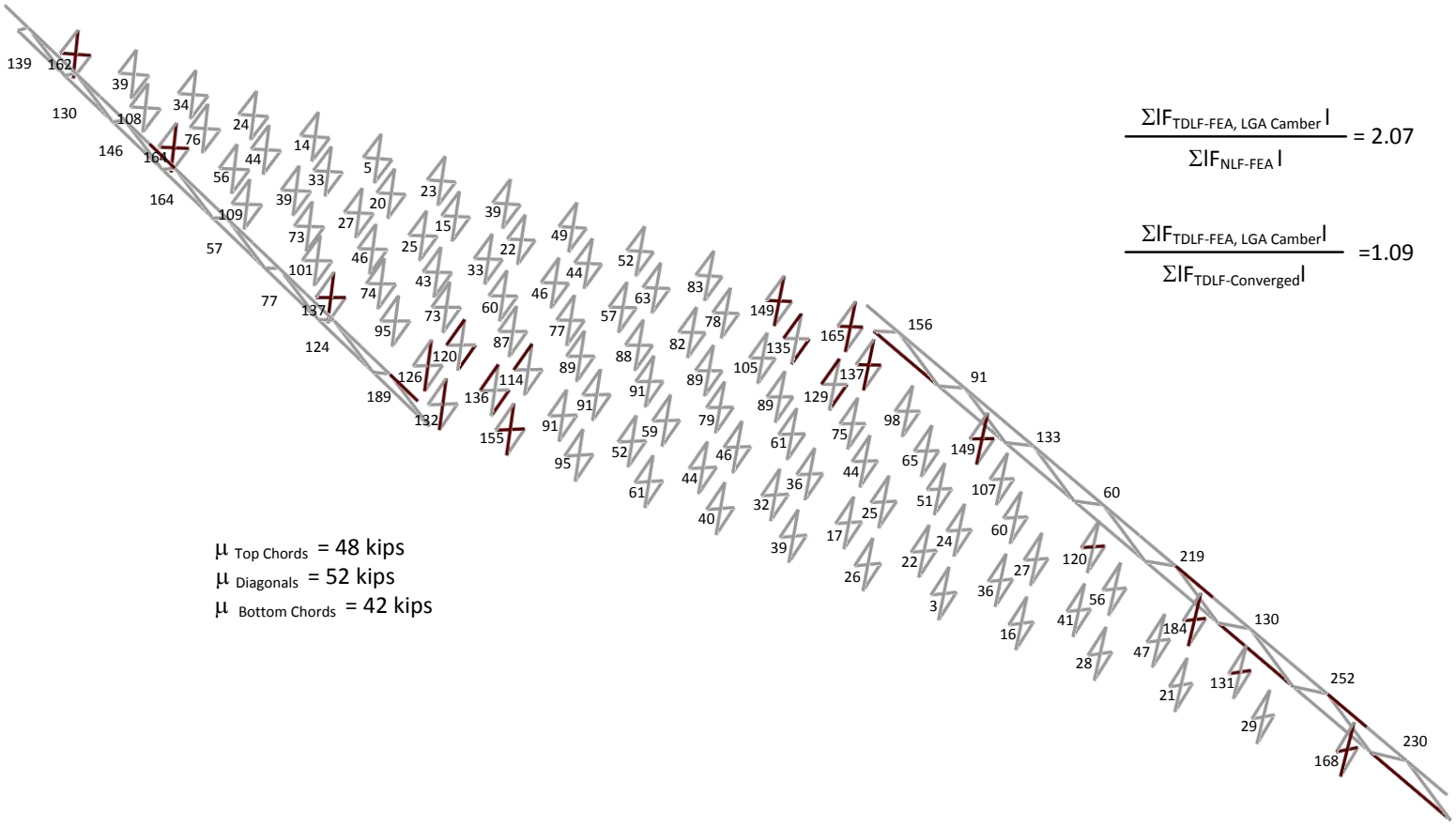

Figure 7.3.11. NISSS54, maximum amplitude of the component axial forces in each of the cross-frames under steel dead load for TDLF detailing methods.

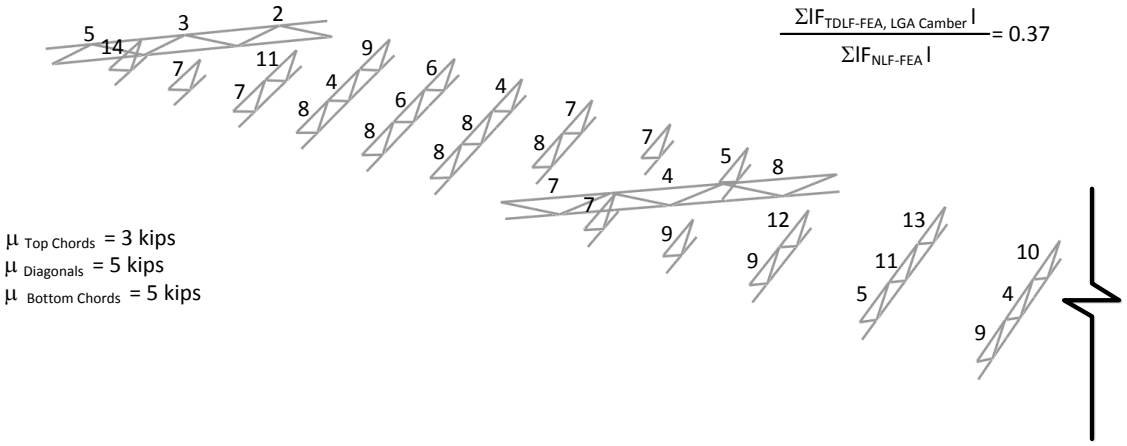

Figure 7.3.12. XICSS5, maximum amplitude of the component axial forces in each of the cross-frames under total dead load for TDLF detailing method.

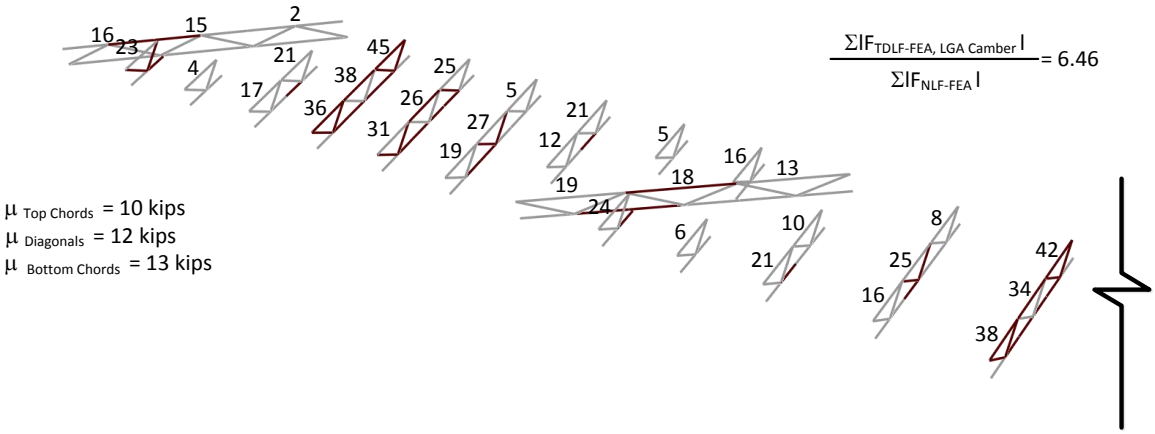

Figure 7.3.13. XICSS5, maximum amplitude of the component axial forces in each of the cross-frames under steel dead load for TDLF detailing methods.

7.4. Special Cases where a Line-Girder Analysis with V-load Approximation Predicts Accurate Results for Curved Radially-Supported Bridges Constructed with DLF Detailing

A line-girder analysis, with the V-load approximation for curvature effects, is used widely for the analysis and design of curved bridges with radial supports. In the V-Load analysis, curved girders are modeled as straight girders by using the same girder length of the considered girder. In addition to dead loads, which are based on the tributary area of the girders, vertical loads are applied along each span at connection points of cross-frames with girders, representing the torsional effects in the girder system. These assumptions can lead to poor predictions of the vertical displacements and flange lateral bending stresses in many cases for the bridges that are constructed with NLF detailing as demonstrated in Fig 7.4.1. Figure 7.4.1 shows the total dead load girder camber profiles of the bridge NISCR2, constructed with NLF detailing. Girder camber profiles are obtained from the negative of total dead load deflections by using V-load analysis and 3D FEA predictions, respectively. It is clear from Fig. 7.4.1 that V-load methods cannot capture the overall lateral bending of the girders due to torsional rotation of the girders.

However, it is shown in Chapter 5 and 6 that if Total Dead Load Fit (TDLF) detailing is used on curved I-girder bridges with radial supports (i.e., the bridges are detailed to have plumb webs in their final dead load condition), and if the girder cambers are set based on the results from 1D line-girder analyses, the lack-of-fit stresses due to the cross-frame detailing reduce the overall (global) flange lateral bending effects. As such, physical girders are approximately plumb under total dead load and flange lateral bending stresses are solely due to overhang bracket loadings and curvature effects.

Figure 7.4.2 show the physical girder layovers of a representative curved radially-supported bridge, constructed with TDLF detailing based on the girder cambers from V-load method. It should be noted from Fig. 7.4.2 that girders are approximately plumb under total dead load (smaller than ±(web depth, in inches) / 96). However, the deviation from the plumb position is different in Fig. 7.4.2 with respect to the results obtained by using the girder camber profile from a 3D FEA (see Fig. 5.2.19).

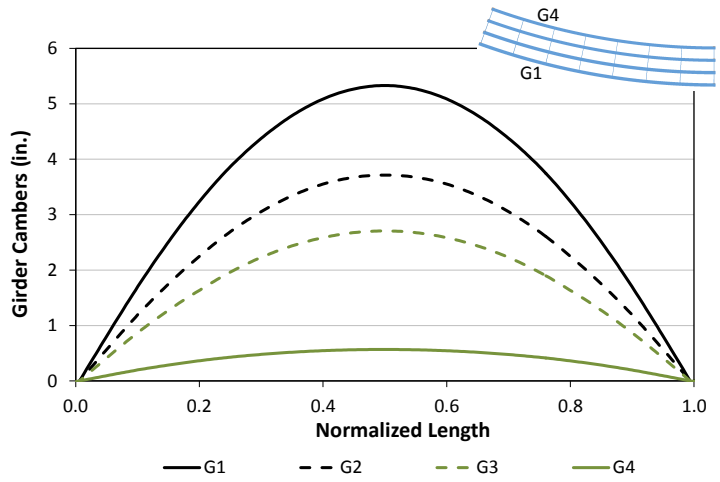

(i) Camber set based on line-girder analysis

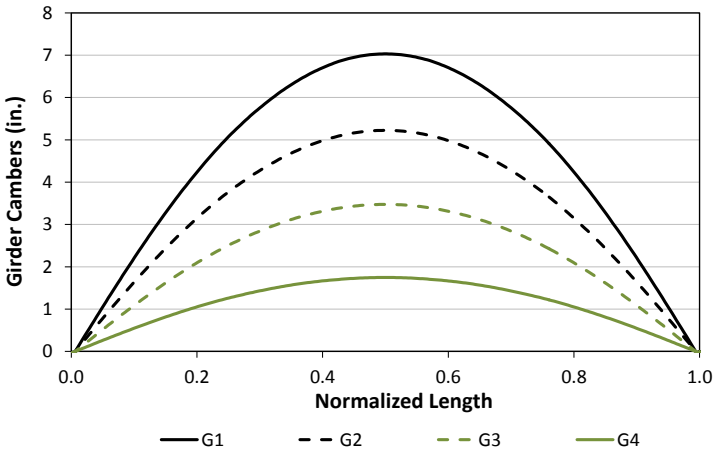

(ii) Camber set based on FEA deflections

Figure 7.4.1. NISCR2, Total dead load cambers obtained from line-girder and finite element analysis solutions.

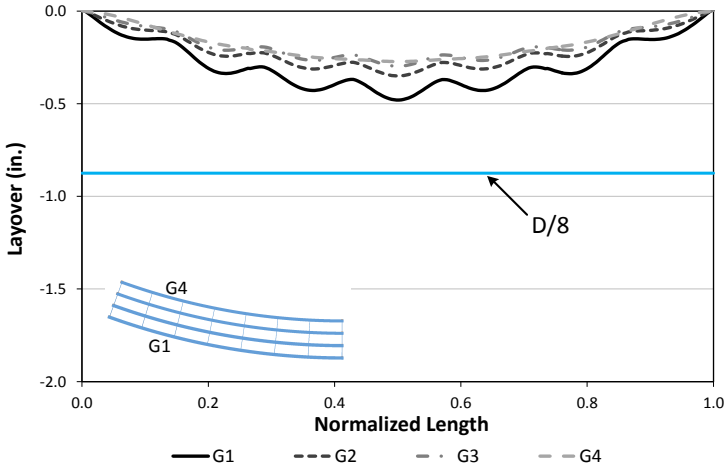

Figure 7.4.2. NISCR2, Relative lateral displacements under total dead load for TDLF detailing.

Figure 7.4.3 provides the vertical deflections of NISCR2 along the normalized length of girders G1, G2 and G4. The reported vertical displacements are obtained from the V-load method and test simulations, constructed with NLF detailing and TDLF detailing based on camber profiles from the V-load method. Physical vertical displacements associated with TDLF detailing are captured accurately by V-load analysis predictions if the girder cambers are set based on the V-load analysis solutions since the overall torsion of the bridge is reduced by constructing the bridge with DLF detailing.

Figure 7.4.4 shows the total dead load major-axis bending and flange lateral bending stresses induced in the top flange of girders G1, G2 and G4 for NLF and TDLF detailing where the cambers are set based on the line-girder analysis solutions. Line-girder analysis predictions correlate well with the solutions for NLF and TDLF since the locked-in major-axis bending stresses are minor for curved bridges. Flange lateral bending stresses can be predicted by V-load analysis at the cross-frame locations. The total dead load flange lateral bending stresses of the physical bridge, constructed with TDLF detailing, is captured with good accuracy by line-girder analysis solutions. This is again due to the reduction of the overall flange lateral bending effects due to DLF detailing. V-load assumptions do not account for this effect and once these effects are removed by DLF detailing, V-load analysis predictions provide accurate predictions of the girder major-axis bending stresses, flange lateral bending stresses and vertical displacements. It should be noted that the bridge experiences twisting under other loads. In those, cases, the V-load method may not provide good answers.

Figures 7.4.5 and 7.4.6 show the distribution of the largest total dead load cross-frame component axial forces in each of the cross-frames throughout the bridge NISCR2 for TDLF detailing under total and steel dead load respectively. As explained in Chapter 5, locked-in diagonal forces are additive with the dead load responses. It is observed from Fig. 7.4.5 that cross-frame forces under total dead load are increased by 37% for the bridge NISCR2 with respect to NLF detailing when the cambers are set based on line-girder analysis solutions. Moreover, the total sum of the absolute value of all the cross-frame component axial forces is 131% more than the sum for NLF detailing under steel dead load.

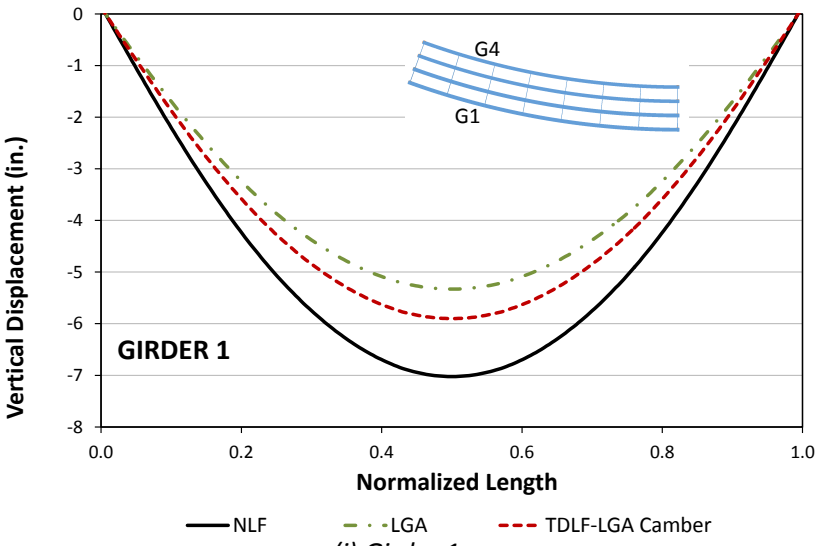

(i) Girder 1

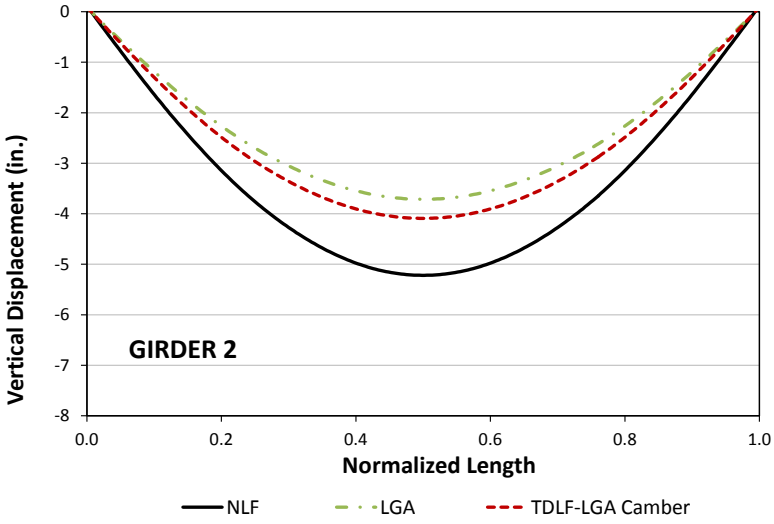

(ii) Girder 2

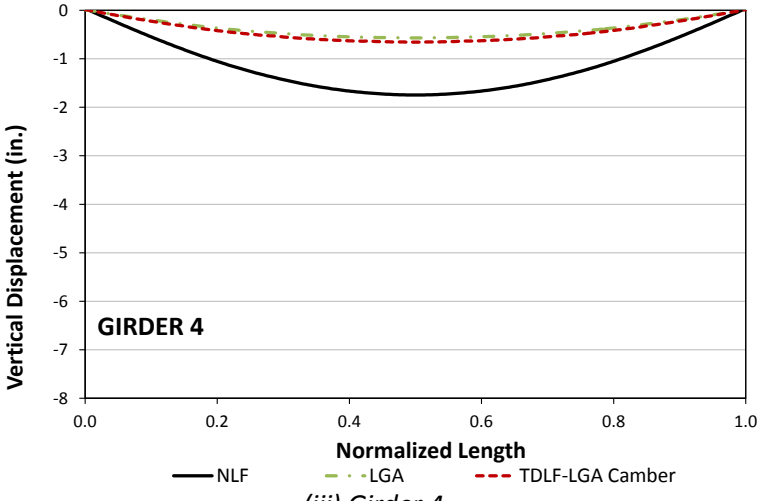

(iii) Girder 4

Figure 7.4.3. NISCR2, Vertical deflections under total dead load for different detailing methods.

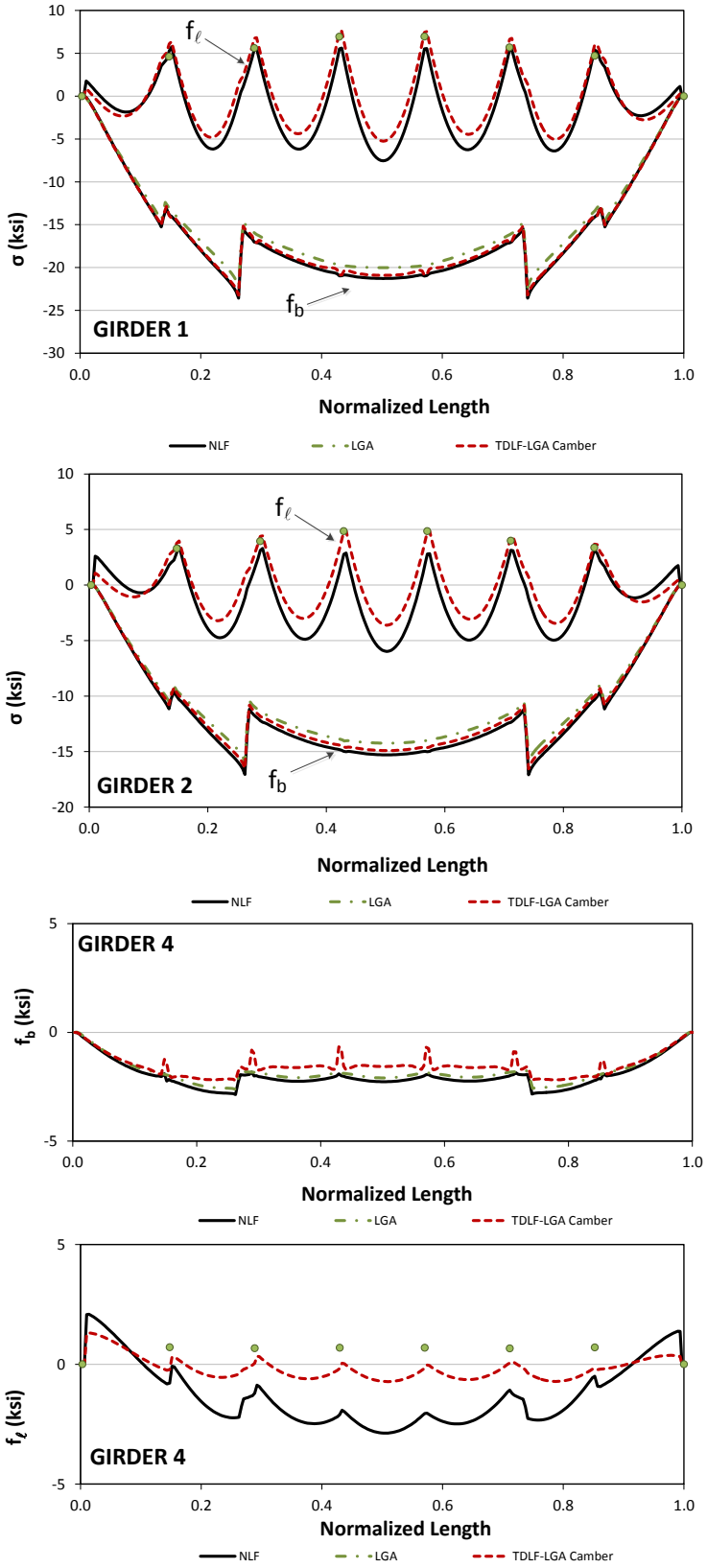

Figure 7.4.4. NISCR2, Top flange stresses under total dead load for different detailing methods.

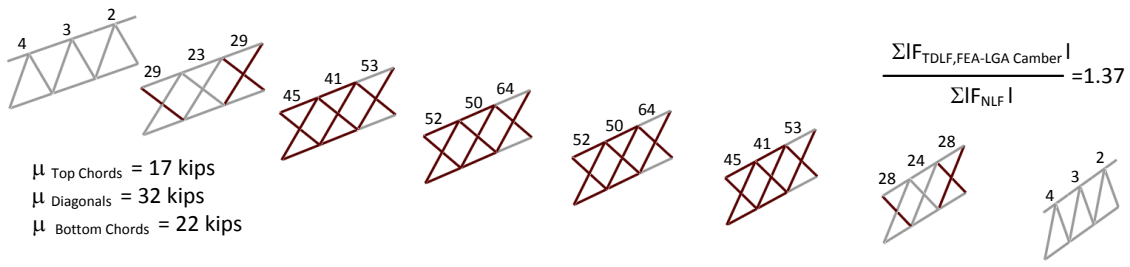

Figure 7.4.5. NISCR2, maximum amplitude of the component axial forces in each of the cross-frames under total dead load for TDLF detailing method (camber set based on line-girder analysis).

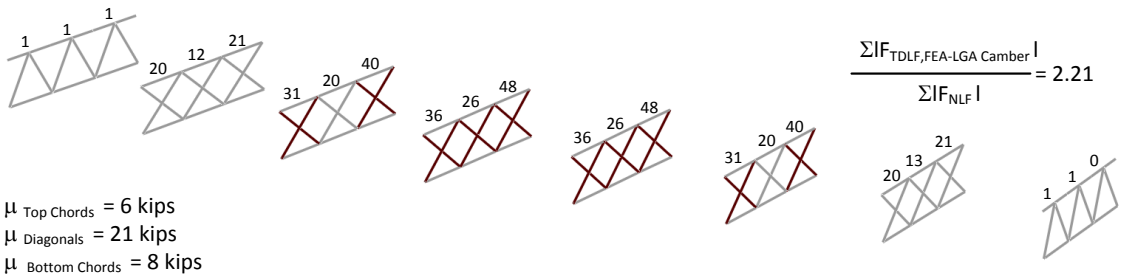

Figure 7.4.6. NISCR2, maximum amplitude of the component axial forces in each of the cross-frames under steel dead load for TDLF detailing methods.

Similarly, if Steel Dead Load Fit (SDLF) detailing is used on curved I-girder bridges with radial supports (i.e., the bridges are detailed to have plumb webs in the completed steel dead load condition) and, if the girder cambers are set based on the results from 1D line-girder analyses, a basic 1D line-girder analysis is sufficient to obtain accurate predictions of the girder stresses and vertical displacements in the steel dead load condition. Unfortunately, a V-load analysis does not necessarily produce accurate results with respect to the physical girder vertical displacements, major and minor axis bending stresses for other than the steel dead load condition.

CHAPTER VIII.

CONCLUSIONS

8.1. Summary and Impact of the Research

This dissertation addresses the influence of cross-frame detailing on curved and/or skewed steel I-girder bridges during steel erection and the concrete deck placement by conducting comprehensive analytical studies. Procedures to determine lack-of-fit forces due to dead load fit (DLF) detailing are developed to assess the impact of different types of cross-frame detailing. The studies include benchmarking of refined analytical models against selected full-scale experimental tests and field measurements. These analytical models are then utilized to study a variety of practical combinations and permutations of bridge parameters pertaining to horizontal curvature and skew effects. This research develops and clarifies procedures and provides new knowledge with respect to the impact of cross-frame detailing methods on:

(i) Constructed bridge geometries (girder layovers, bearing rotations, joint positions, deck elevations and deck cross-slopes),
(ii) Cross-frame forces,
(iii) Girder stresses,
(iv) System strengths,
(v) Potential uplift at bearings, and
(vi) Fit-up during erection.

These developments provide the basis for the development of refined guidelines for:

(i) Practices to alleviate fit-up difficulties during erection,
(ii) Selection of cross-frame detailing methods as a function of I-girder bridge geometry characteristics, and
(iii) Procedures to calculate the locked-in forces due to DLF cross-frame detailing.

8.2. Conclusions

The following subsections present the conclusions reached in this research.

8.2.1. *Impact of cross-frame detailing methods on constructed bridge geometry*

The key findings of this research pertaining to the impact of cross-frame detailing on the constructed bridge geometry are as follows:

- The direction of the torsional rotations due to dead load fit cross-frame detailing is driven by:
  1) The orientation of the differential vertical cambers between the girders at a given intermediate cross-frame (assuming that the intermediate cross-frames are normal to the girders),
  2) The rotational compatibility between the bearing line cross-frames and the girders, as well as the direction of the girder end rotations due to the camber at the bearing lines, and
  3) If the intermediate cross-frames are not normal to the girders, the combination of the orientation of the differential vertical cambers and the direction of the girder rotations due to the camber at the cross-frame connection plates.
- The locked-in layovers are different at the different stages of the construction since the stiffness of the system is changing. The girder twisting deformations tend to be larger in the vicinity of the stiff transverse load path.
- The compensating girder layovers generated by DLF detailing are never exactly equal and opposite to the dead load layovers. This is mainly because:
  1) The stress state due to the torsional effects of the dead load cannot possibly be matched exactly by the cross-frame forces induced by the DLF detailing. The difference between the girder stress state induced by the lack-of-fit forces and the girder stress state associated with the dead load torsion causes additional deformations within the structure.
  2) The girder camber profiles may have been obtained from an analysis that does not fully capture the true interactions between the girders associated with the three-dimensional response of the bridge. These approximate cambers tend to increase the differences between the stress states due to the torsional effects of the dead load and the stress states due to lack-of-fit of the cross-frames.

- If a bridge is constructed with DLF detailing, slight deviations from the plumb configuration are observed generally at the targeted load conditions. The deviations from the plumb configurations tend to be less than the commonly used tolerance of ±(web depth, in inches) /96, regardless of the bridge type and geometry.
- For straight and skewed bridges, the locked-in forces from DLF detailing tend to have a small effect on the vertical displacements.
- For curved radially-supported bridges, the locked-in forces due to DLF detailing generally have a significant effect on the vertical displacements of the girders. This is due to the significant coupling between the major-axis bending and torsion in curved I-girders.
- Locked-in layovers due to DLF detailing of can be estimated from,

$$\Delta_{x\,LOF} = \Delta_{z.C}\ \tan(\theta) \tag{8.2.1}$$

$$\Delta_{x\,LOF} = h\left(\Delta_{y.C}/s\right) \tag{8.2.2}$$

  These estimations can be useful to estimate the magnitude of the twist of the girder required to connect the cross-frame in no-load geometry.
- Equations 8.2.1 and 8.2.2 are found to provide better estimates once the locked-in vertical and longitudinal displacements are included in the calculations.

8.2.2. *Impact of cross-frame detailing methods on cross-frame forces*

The key findings of this research pertaining to the impact of cross-frame detailing on cross-frame forces are as follows:

- In straight skewed bridges constructed with NLF detailing, relatively large forces tend to be developed in the cross-frames along the shorter (and stiffer) diagonal direction between the corners of the deck.
- For bridges constructed with DLF detailing, large locked-in cross-frame forces develop on the stiff transverse load paths, at the places with relatively large lateral stiffness of the adjacent girders, and at the locations with large differential camber.
- The induced locked-in forces due to DLF detailing can be significantly different in the partially erected structure compared to the fully assembled structure.
- For straight bridges constructed with TDLF detailing, the locked-in cross-frame forces are approximately equal and opposite to the total dead load forces in the regions having

the largest transverse stiffness. However, the locked-in forces in the cross-frames tend to be substantially different from the total dead load forces outside of this region.

- For straight bridges constructed with SDLF detailing, the locked-in cross-frame forces are approximately equal and opposite to the steel dead load forces in the regions having the largest transverse stiffness. However, the locked-in forces in the cross-frames tend to be substantially different from the steel dead load forces outside of this region.
- In straight-skewed bridges constructed with TDLF detailing, cross-frames located along the stiff transverse load paths may see their largest forces during the steel erection since the locked-in cross-frame forces are not yet relieved by the dead load forces from the deck weight.
- For curved bridges, locked-in cross-frame forces due to DLF detailing tend to be additive with the dead load forces in all of the cross-frames. However, for curved bridges with positive skew angles, cross-frame forces can be reduced for the cross-frames that are located in the vicinity of the skewed bearings.

8.2.3. *Impact of cross-frame detailing methods on girder stresses*

The key findings of this research pertaining to the impact of cross-frame detailing on girder stresses are as follows:

- Changes in girder major-axis bending stress predictions are minor due to DLF detailing for both curved and/or skewed bridges. For example, in the Ford City bridge (EICCR11), which is a structure with a complex geometry, the maximum percentage change in girder major-axis bending stress due to TDLF detailing is only 11%. Of all the structures studied in this research, this bridge shows the largest change in girder major-axis bending stresses due to DLF detailing. In general, this response is insensitive to the use of a given detailing method.
- The twisting of the flanges in the no-load geometry due to DLF detailing, in the direction opposite to the deflections under load, induces flange lateral bending stresses. Locked-in flange lateral bending stresses develop:
  1) At intermediate cross-frames that are located close to skewed bearing lines. These local peaks in the locked-in girder flange lateral bending stresses, as well as correspondingly large cross-frame forces, are due to “nuisance stiffness” effects.
  2) At the interior girders in skewed bridges due to the transverse load transfer effects.

3) In curved girders, locked-in flange lateral bending stresses are also induced due to global lateral bending of the girder flanges.

- The girder flange lateral bending stresses are reduced significantly in straight-skewed bridges due to DLF detailing. The smallest net flange lateral bending stresses tend to occur under steel dead load if SDLF detailing is used and under total dead load if TDLF detailing is used for these bridges.
- In straight-skewed bridges, the girder flange lateral bending stresses do not completely vanish in the targeted dead load condition due to the differences between the locked-in stresses from DLF detailing and the stresses related to the torsion of the girders under the targeted dead load. There are several reasons for this behavior:
  1) In particular, local peaks in girder flange lateral bending stresses, as well as cross-frame forces, can be observed due to "nuisance stiffness" effects at locations such as intermediate cross-frames that are located close to skewed bearing lines. The stresses in the girders due to locked-in force effects generally do not match the torsional stresses due to the three-dimensional loading effects also in these regions.
  2) When staggered cross-frames are utilized in straight-skewed bridges, there is substantial flange lateral bending in the interior girders due to the transverse load transfer effects. The interior girder flanges are loaded "back-and-forth" in opposing directions by the cross-frames. The corresponding flange lateral bending in these girders is generally reduced, but is not completely nullified by the locked-in force effects.
  3) Lastly, in the fascia girders of the straight-skewed bridges, significant flange lateral bending can occur in some cases due to eccentric overhang bracket loads. These bending effects are of course not nullified by the lack-of-fit forces from DLF detailing.
- In cases with contiguous intermediate cross-frame lines, the total flange lateral bending stresses associated with DLF detailing are found to be very close to zero except in the fascia girders (due to overhang bracket loadings) and at cross-frame locations exhibiting "nuisance stiffness" effects.
- For curved radially-supported bridges, the "local" flange lateral bending effects between the cross-frames due to the horizontal curvature are not influenced by the DLF detailing.

However, DLF detailing of curved bridges induces an overall global lateral bending in the girder flanges in the direction:

1) Opposite to the lateral bending of the girders due to the torsional rotation of the bridge cross-section,
2) Opposite to the bending within the girder unbraced lengths between the cross-frames, and
3) In the same direction as the "negative" flange lateral bending stresses due to the continuity of the curved flanges across the cross-frame locations.

That is, the locked-in forces due to DLF detailing tend to reduce the overall "global" girder flange lateral bending stresses in curved bridges.

8.2.4. *Impact of cross-frame detailing methods on system strengths*

Additional locked-in force effects due to DLF detailing do not affect the bridge system strength significantly, assuming that the cross-frames are sized adequately for the total force effects and that the critical components are the girders. In fact, it is demonstrated that locked-in force effects can increase the strength of narrow curved bridges that are susceptible to overall second-order effects or significant overall (global) flange lateral bending as much as 13%. Unfortunately, DLF detailing of horizontally curved bridges tends to significantly increase the cross-frame diagonal forces. For instance, in the bridge NISCR5, the cross-frame forces increase by 268% due to TDLF detailing.

8.2.5. *Impact of bolt slip on component responses*

The impact of a small bolt slip (1/8 inch) at an individual cross-frame diagonal member is investigated through several case studies. The influence on the girder responses is found to be negligible. It is observed that the cross-frame forces due to dead load and/or locked-in force effects can be relieved by the bolt slip. This can be beneficial to relieve large cross-frame forces. However, it is observed for the cross-frame locations that have relatively large forces that a small bolt slip relieves a relatively small fraction of the cross-frame forces associated with DLF detailing or other large dead load forces.

8.2.6. *Estimation of tendency to uplift at bearings*

The key findings of this research pertaining to the impact of cross-frame detailing on uplift at bearings are as follows:

- A torsion index, I_T, is developed, which gives an indication of the magnitude of the overall torsion that exists in the bridge (or bridge unit) span due to the eccentricity of its self-weight. The torsion index, I_T, is a tool that can be used to detect potential girder uplift in the preliminary design of a curved and/or skewed bridge. A suggested limit on I_T to avoid uplift in simple-span I-girder bridge is 0.65. If the torsion index is above this limit in a given structure, then a refined 2D-grid analysis or 3D FEA should be conducted to evaluate the potential uplift condition. If uplift is then encountered, hold-downs or ballast should be provided at the uplift locations, or the bridge geometry should be revised to eliminate the uplift condition.
- Continuous span bridges can tolerate larger I_T due to the stabilizing effects of the continuity with the adjacent spans. However, the continuity with the adjacent spans generally varies during the steel erection, and therefore, $I_T > 0.65$ serves as a rough indicator of when the engineer should check carefully for uplift during construction in continuous-span I-girder bridges.

8.2.7. *Impact of cross-frame detailing on fit-up during erection*

Come-along forces for a particular erection stage of a bridge constructed with any type of cross-frame detailing can be estimated from

$$F_{come.along} = max\left[\frac{k_\Phi}{y_{st}}\left(\frac{\Delta_{x\ Required}}{h_o}\right), k_{Lateral}\Delta_{x\ Required}\right] \quad (8.2.3)$$

Come-along force estimates can be used as an indicator for fit-up problems. The typical maximum load for single come-along is 12 kips. Hence, if the estimated forces are larger than 12 kips, the erection scheme should be revisited to reduce the displacement incompatibilities between members (i.e., increasing the number of come-alongs, providing temporary supports for the bridges constructed with NLF detailing or using dead load deflections for the bridges constructed with DLF detailing).

8.2.8. *Recommended practices to alleviate fit-up problems*

The recommended practices to alleviate fit-up difficulties are as follows:

- For bridges constructed with DLF detailing, the use of the dead load deflections, temporary X-bracing, and temporary struts during erection are found to be beneficial to minimize the fit-up forces while maintaining the bridge stability.

- For bridges constructed with NLF detailing, use of temporary supports to keep the structure close to the no-load geometry can provide the smallest fit-up forces.
- Temporary supports are found to be essential for bridges constructed with NLF detailing where large differential deflection incompatibilities are expected during construction due to dead load deflections. Temporary supports can minimize the displacement incompatibilities between girders and units, help to control the bridge geometry, and provide stability during construction. Greater improvements are expected due to use of temporary supports for bridges or units with large length-to-width ratios where overall flange lateral bending and/or second-order effects are significant.
- It is found that the minimum ratio of the unbraced length to the adjacent unbraced length at the first cross-frame offset from a skewed bearing line, $\alpha = a/b$, should be taken as at least 0.4. This is because the relative lateral stiffness of the unbraced segments increases significantly for the smaller ratios. This recommendation helps maintain the forces in the cross-frame components at acceptable levels. That is, it helps reduce "nuisance stiffness" effects. In addition, this offset limit helps reduce large locked-in cross-frame forces due to DLF detailing at intermediate cross-frame locations with large relative lateral stiffness of the adjacent girders and large differential camber.
- Utilization of X-type cross-frames without top chords increases the bridge transverse flexibility. As the transverse flexibility of the system increases, the girders require less force to fit-up with the cross-frames. Therefore, the fit-up forces without top chords are expected to be smaller than the ones with top chords since the transverse stiffness is reduced.
- Removing the top chords of X-type cross-frames for straight and skewed I-girder bridges is recommended since the cross-frames are still able to provide enough bracing to girders to control the deck profile, reduce the flange lateral bending stresses, and decrease the transverse stiffness.

8.2.9. *Selection of bearings based on the bridge geometry*

Percentages of the maximum rotational capacity of the plain elastomeric and steel reinforced elastomeric bearings are expressed as a function of the skew angle and major-axis bending rotation by using the kinematic constraint induced by the in-plane rigidity of the cross-frame and the coupling relationship between the twist and the major-axis bending rotations.

Similar curves can be generated for other types of bearings. Guidance is provided for selecting the type of bearing given the skew angle and major-axis bending rotation of the girders at the bearings. Alternatively, maximum allowable major axis-bending rotation of the girder can be obtained given the desired bearing rotation limit and skew angle.

8.2.10. *Recommendations for selecting the type of the cross-frame detailing method*

For selecting the type of the cross-frame detailing method for a particular bridge, the following recommendations are developed from this research:

- For straight-skewed bridges, DLF detailing is found to be an effective way to control the plumbness of the girders. However, a minimum ratio of the offset length to the adjacent unbraced length at the first cross-frame from a bearing line should be taken to be at least 0.4 to avoid large locked-in cross-frame forces. TDLF detailing should be selected (or the cross-frames can be detailed for an intermediate condition between TDLF and SDLF) for cases where SDLF detailing does not limit the bearing rotations to less than the admissible bearing rotation values. It should be noted that the fit-up forces can be relatively small for SDLF detailing, and they can be reduced significantly for TDLF detailing if the dead load deflections are used during erection. That is if the girders are allowed to deflect to reduce the displacement incompatibilities between the girders. There is no additional effort needed to include the locked-in stress effects due to DLF detailing for designing the straight-skewed bridges (when $\alpha > 0.4$ is satisfied) unless a better prediction accuracy is needed. For the bridges constructed with DLF, the bridge components can be sized based on the predictions associated with NLF detailing when $\alpha > 0.4$ is satisfied. This should provide an adequate design of the bridge such that girders and cross-frames are not overstressed, deviations on the bridge geometry are minor, and overall strength is not an issue.
- For curved radially-supported bridges, NLF detailing is found to be the most effective approach since the locked-in stresses associated with DLF are additive with the dead load stresses, and girder layovers due to dead loads within the spans tend to be inconsequential. However, SDLF detailing is recommended for longer spans if large deflections during the steel erection are expected. If the bridge is constructed with DLF detailing, locked-in stress effects should be included in the design, to achieve accurate bridge geometry and to size cross-frames adequately.

- For I-girder bridges with combined curvature and skew, NLF detailing is found to be effective for the cases where the percentage of the maximum rotational capacity is not exceeded at the bearings. Example calculations of the percentages of the maximum rotational capacity with respect to the girder major-axis bending rotations and skew angle of the bridge are provided in Figs. 7.1.1 and 7.1.2 for plain elastomeric and steel reinforced elastomeric bearings. If the maximum rotational capacity is exceeded at the bearings, SDLF detailing or an intermediate condition between SDLF and TDLF detailing is recommended for curved and skewed I-girder bridges. Also, for longer spans, if large differential deflections are expected SDLF detailing or NLF detailing and the use of beveled shim plates at the end bearing lines are recommended. In the case of DLF detailing of curved and skewed bridges, the engineer should consider the locked-in force effects in the design.
- It should be noted that all of these recommendations can require a different erection scheme to minimize the fit-up forces. Displacement incompatibilities can be reduced by the selected erection scheme. For instance, SDLF detailing tends to minimize the fit-up forces (and stresses) during the steel erection unless the bridge is essentially supported in its no-load condition during the erection. This is because the steel dead load deflections (and deformations) in the various partially erected units are closer to the final steel dead load deflections (and deformations) than to the total dead load or zero-load ones. Of course, if sufficient temporary supports, holding cranes, etc. are provided such that the partially erected structure is essentially in a no-load condition, NLF detailing minimizes the fit-up forces. TDLF detailing generally leads to larger fit-up forces since the steel structure is absent from the concrete dead load, but the cross-frames are detailed to fit-up with the girders once the total dead load cambers are taken out of the girders by the steel + concrete dead load. However, in most cases, the decision about which erection procedure to use is usually driven by site constraints.

8.2.11. *Effective procedures for calculating lack-of-fit effects in design-analysis methods, in cases where they need to be included*

Influence of cross-frame detailing can be captured by constructing a full model of any intermediate erection stage of the bridge with the girders in their initial no-load cambered and plumb positions, with the cross-frames connected to the girders, and with initial strains

introduced into the cross-frames corresponding to the lack-of-fit caused by the type of cross-frame detailing.

The initial strains corresponding to the spatial lack-of-fit due to DLF detailing can be calculated by using the cross-frame member length in the final targeted dead load position, which is the fabrication length of the cross-frame members, and length between the work points of the girders in the initially-plumb cambered geometry. Alternatively, these strains can be obtained through the software by imposing the differential vertical deflections associated with the steel or total dead load cambers. Resulting cross-frame member strains correspond to the strains associated with the spatial lack-of-fit of the members due to DLF detailing.

8.2.12. *Consideration of locked-in vertical deflections when setting girder cambers*

In some cases such as the Ford City Bridge, DLF detailing can have a significant effect on the vertical displacements of the girders. In these cases, where locked-in vertical deflections lead to deviations in the predicted final deck profile and in the final girder elevation, the girder cambers should be set considering the locked-in stress effects. However, setting the girder cambers by considering locked-in vertical displacements due to DLF detailing can require an iterative process, in which the tolerance for the deviation from the predicted girder vertical deflections is based on engineering judgement. It is shown that the iterative process does not require any additional level of engineering effort. The automation of the iteration can be easily implemented in the analysis software.

The iterated girder cambers typically provide the girder layovers that are closest to theoretical plumb position under the targeted dead load since additional deformations due to locked-in stress effects are considered when setting the girder cambers.

Generally, it isn't essential to perform an iterative process to set the cambers for straight-skewed bridges constructed with DLF detailing since the locked-in forces from DLF detailing tend to have a small effect on the vertical displacements. However, if cambers are set based on the iterated results, the iterated girder cambers typically provide

- Lowest total dead load flange lateral bending stresses,
- Lowest total dead load cross-frame forces along the stiff transverse paths, and
- Largest locked-in cross-frame forces

under the targeted dead load level.

8.2.13. *Special cases where a line-girder analysis predicts accurate results for straight-skewed bridges constructed with DLF detailing*

If the girder cambers are set based on the results from 1D line-girder analyses and a straight-skewed bridge is detailed for TDLF, the lack-of-fit stresses due to the cross-frame detailing come very close to canceling the stresses due to the torsion of the girders under the total dead load condition. As such, the physical girder layovers are approximately zero only under total dead load, and the basic 1D line-girder analysis flexural model is sufficient to capture the physical vertical displacement and major-axis bending stresses with good accuracy. This result is essentially independent of the magnitude and pattern of the support skews.

Unfortunately, line-girder analysis does not necessarily produce accurate results for cases other than the dead load condition under which the web is targeted to be plumb. This is because a line-girder analysis does not account for any transverse load transfer or girder torsional responses.

Similarly, if Steel Dead Load Fit (SDLF) detailing is used on straight skewed I-girder bridges (i.e., the bridges are detailed to have plumb webs in the completed steel dead load condition), and if the girder cambers are set based on the results from a 1D line-girder analysis, a basic 1D line-girder analysis is sufficient to obtain accurate predictions of the girder major-axis bending and vertical displacements only under steel dead load condition.

8.2.14. *Special cases where line-girder analysis with V-Load Approximation predicts accurate results for curved radially-supported bridges constructed with DLF detailing*

If the girder cambers are set based on the results from 1D line-girder analyses with V-load approximations and a curved radially-supported bridge is detailed for TDLF, the lack-of-fit stresses reduce the overall flange lateral bending of the bridge. As such, the physical girder layovers are approximately zero only under the total dead load, and the 1D line-girder analysis with V-load approximation is sufficient to capture the physical vertical displacements, and major-axis bending stresses, and flange lateral bending stresses.

Similarly, if Steel Dead Load Fit (SDLF) detailing is used on a curved I-girder bridge with radial supports (i.e., the bridge is detailed to have plumb webs in the completed steel dead load condition), and if the girder cambers are set based on the results from 1D line-girder analyses, a basic 1D line-girder analysis is sufficient to obtain accurate predictions of the girder stresses and vertical displacements in the steel dead load condition. Unfortunately, a V-load analysis does

not generally produce accurate results with respect to the physical girder vertical displacements, or the girder major-axis and flange lateral bending stresses except the steel dead load condition.

8.3. Recommendations for Future Work

This study provides a comprehensive assessment of the influence of cross-frame detailing on curved and skewed I-girder bridges. Nevertheless, there are additional worthwhile areas for further study. These areas are as follows:

- There are plenty of basic observations and construction measurements for the bridges constructed with DLF detailing. However, currently there is no study where detailed measurements have been taken on bridges constructed with DLF detailing. Detailed measurement of the vertical displacements, girder layovers, girder stresses and cross-frame forces during steel erection can serve as a verification for the type of study conducted here.

- Cross-frames can be major load carrying elements in curved and/or skewed bridges. The present studies are conducted to evaluate the influence of the cross-frame detailing methods on girder strength, assuming cross-frames are sized properly. The influence of cross-frame component failure on the system limit state response should be investigated.

- In this research, staged deck placement is not considered. Different deck pouring sequences can develop different differential deflections between the girders, as well as impact the transverse stiffness of the system. The influence of staged deck placement on the behavior and performance of the bridges constructed with DLF detailing should be investigated.

- Live loads are not considered in this research since the emphasis is on the impact of cross-frame detailing methods on the strength, stability, and constructability of curved and/or skewed steel girder bridges under the action of their self-weight and various loads imposed during construction operations. However, cross-frames function under dead and live loads. Performance of the bridge constructed with DLF detailing should be quantified under dead and live load. The overall design of the cross-frames should be investigated more comprehensively.

APPENDIX A.

VALIDATION OF ANALYTICAL PROCEDURES

This appendix provides sample benchmark solutions that are used to validate the analytical procedures that are described in Chapter 3. Benchmark cases are selected from full-scale bridge girders where the girders are tested to failure. These cases involve an individual straight girder tested to failure by Schilling et al. (1988), an individual curved girder tested to failure by Shanmugam et al. (1995), straight-skewed I-girder bridge (EICSS12) monitored during deck pour by Romage (2008), and full-scale radially-supported bridge tested at the FHWA Turner Fairbank Highway Research Center and documented by Jung (2006).

A.1. Straight Girder Verification

Three full-scale bridge girders were tested to failure by Schilling et al. (1988). Specimen "S" is selected from these studies for validating the analytical capabilities. Specimen "S" has a length of 13ft with bearing stiffeners at the support locations and at the mid-span (loading point). There are also one-sided transverse stiffeners at several points as shown in Fig. A.1.1. Figure A.1.1 also shows the girder cross-sectional dimensions. Specimen "S" is simply supported, with girders supported laterally at the support locations and at the mid-span as shown in Fig. A.1.2. The average static yield stress is specified as 56.2ksi for web and 58.8 ksi for the flanges. For the full-nonlinear FEA solutions, the multi linear stress-strain curve, which is shown in Fig. 3.2.7, is scaled for specified web and flange yield stress. Additionally, an L /1000 imperfection is superimposed to each unbraced length of the compression flange in full-nonlinear FEA solutions. The direction of the geometric imperfection is associated with the first global buckling mode. The load deflection curves from experimental data and analytical solutions are compared in Fig. A.1.3. Mid-span vertical displacements are monitored at different applied load levels. It should be noted that there is a good correlation between the analysis predictions and experiment results.

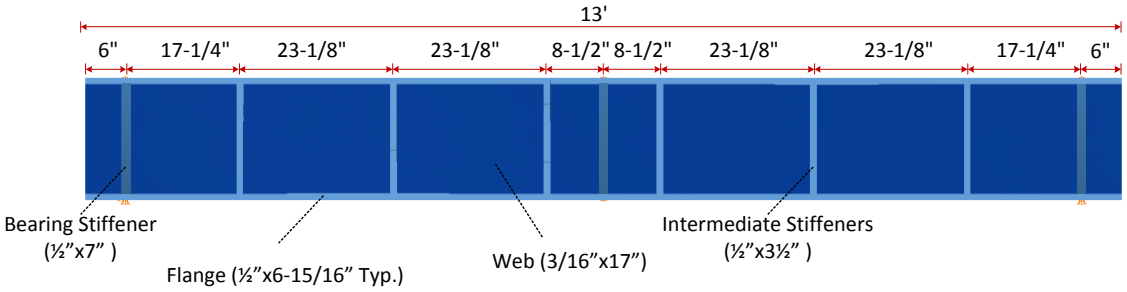

Figure A.1.1. Girder cross-section dimensions and lengths.

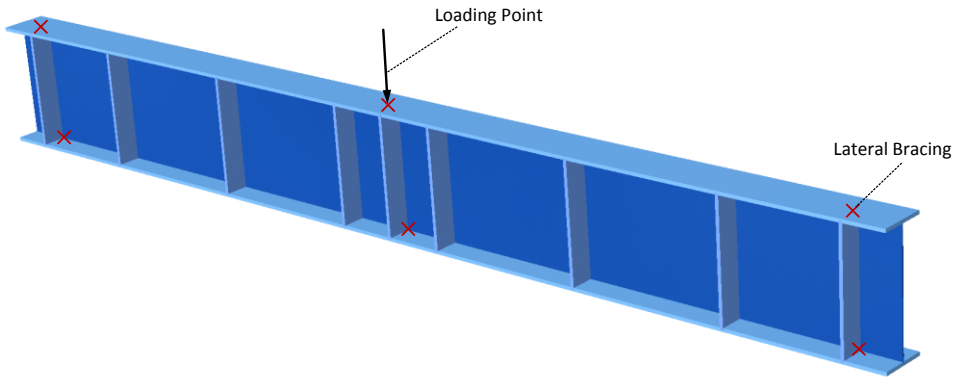

Figure A.1.2. Loading point and lateral bracing points.

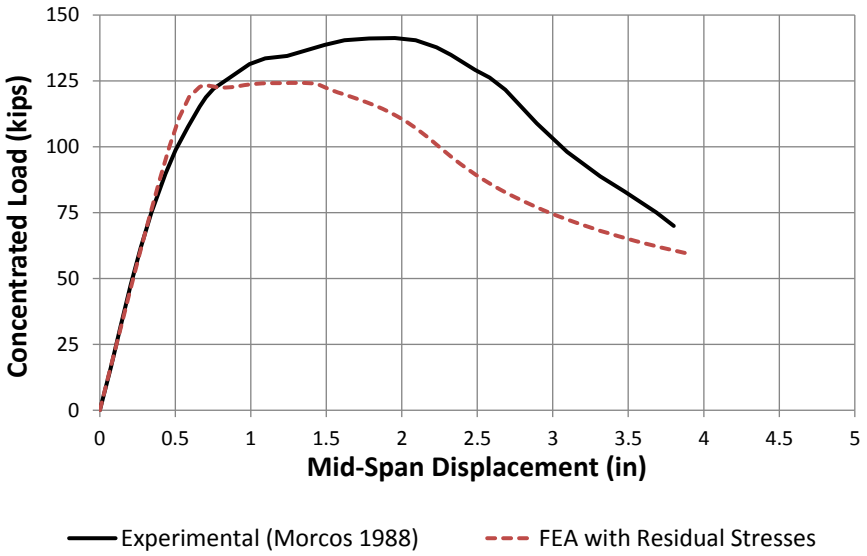

Figure A.1.3. Straight Girder FEA verification by load versus vertical deflections.

Figures A.1.4 and A.1.5 represent the sketches and pictures from Schilling et al. at the end of the test conducted on Specimen "S". Typical distortions after the testing are identified in Figs. A.1.4 and A.1.5. Figures A.1.6 through A.1.8 provide FEA deflections and the mid-thickness equivalent plastic strain of Specimen "S" at the end of the test. Figures A.1.4 through A.1.8 demonstrate

that the analytical procedures that are described in Chapter 3 are able to capture the complete behavior of the test specimen.

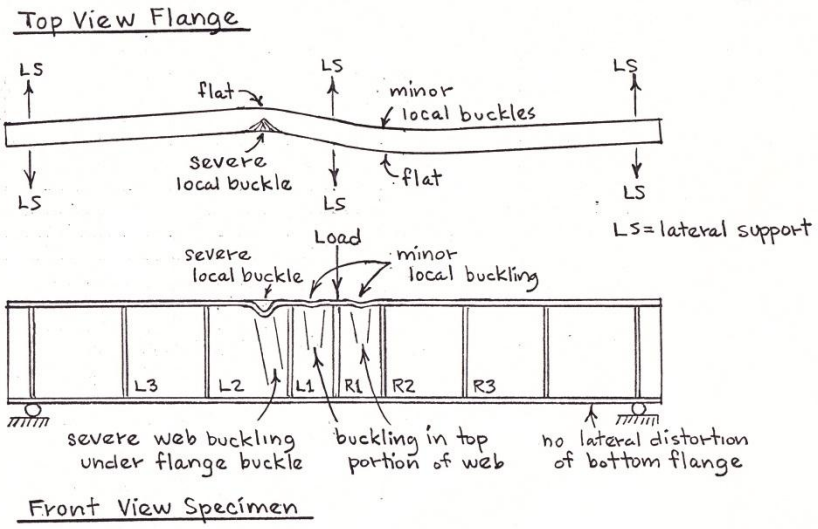

Figure A.1.4. Typical distortions after testing, Schilling et al (1988).

Figure A.1.5. Typical distortions after testing, Schilling et al (1988).

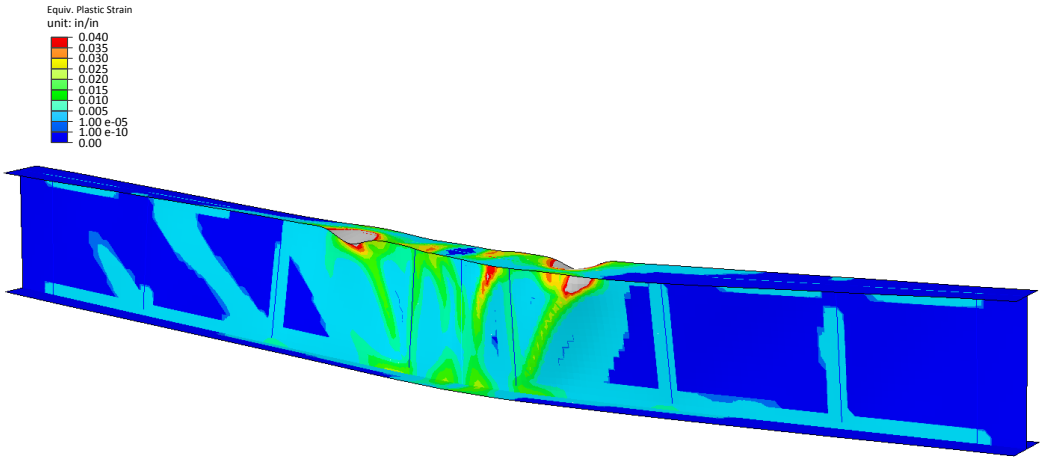

Figure A.1.6. Perspective view of mid-thickness equivalent plastic strains and deflected shape at the final applied test load.

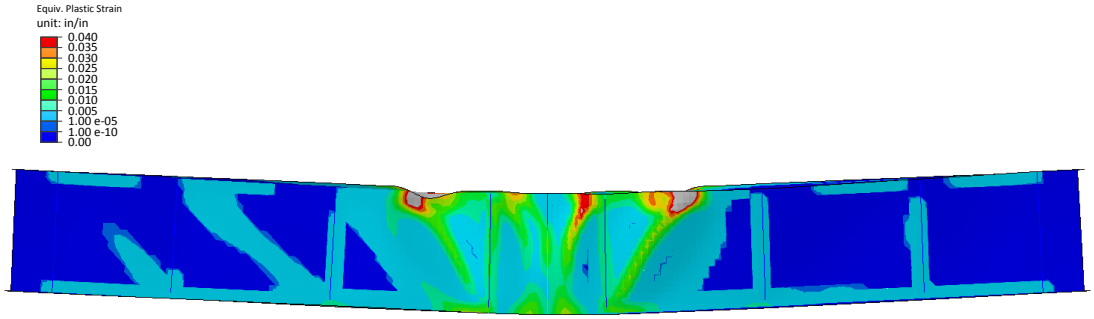

Figure A.1.7. Front view of mid-thickness equivalent plastic strains and deflected shape at the final applied test load.

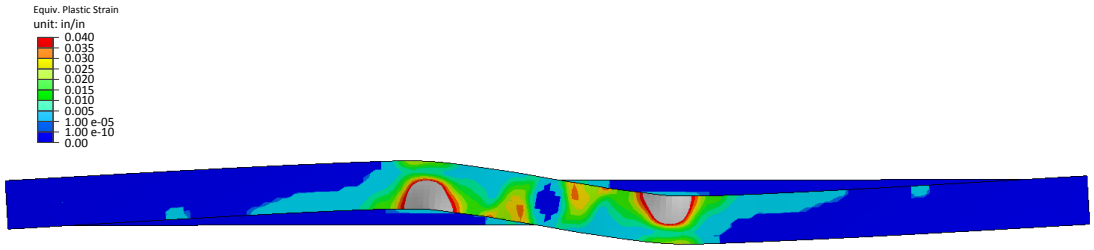

Figure A.1.8. Plan view of mid-thickness equivalent plastic strains and deflected shape at the final applied test load.

A.2. Curved Girder Verification

Ten full-scale curved girders were tested to failure by Shanmugam et al. (1995). Beam "CB1" is selected from the studies of Shanmugam et al. (1995) for benchmarking. Beam "CB1" is a simply supported curved beam with a radius of curvature of 65.62 ft and an arc length of 16.4 ft between its supports. Bearing stiffeners are provided at the support locations and at the loading point as shown in Figs. A.2.1 and A.2.2. Figure A.2.2 shows girder cross-sectional dimensions. Girders are supported laterally at the support locations and at the loading point as shown in Fig. A.2.1. The top flanges are restrained at the supports by a screw jack, preventing the girders from twisting. Beam "CB1" is a hot rolled section. As demonstrated by Shanmugam et al. (1995), that the material properties change due to cold bending during the curving process. The average static yield stress of is increased from 44.67 to 48.88 ksi for web and from 52.32 to 57.29 ksi for the flanges after the cold bending. For the full-nonlinear FEA solutions, the multi linear stress-strain curve, which is shown in Fig.3.2.7, is scaled for specified web and flange yield stress. The modulus of elasticity of the web and flanges are determined from the tensile test coupons as 29747 ksi and 32227 ksi respectively.

Load deflection curves from the experimental data and analytical solutions are compared in Figs. A.2.3 and A.2.4. The curves present the mid-span vertical and top flange radial displacements, respectively, at different applied loads. As in the case of Specimen "S", there is a good correlation between the analysis predictions and experimental results. There are minor differences in the predictions due to the top flange boundary conditions; it is believed that the test setup also caused warping restraint for the top flanges. Figures A.2.5 and A.2.6 provide FEA deflections and mid-thickness equivalent plastic strain of beam "CB1" at the load that the test is finished. As the comparisons demonstrate, full-nonlinear FEA solutions are in agreement with the test results.

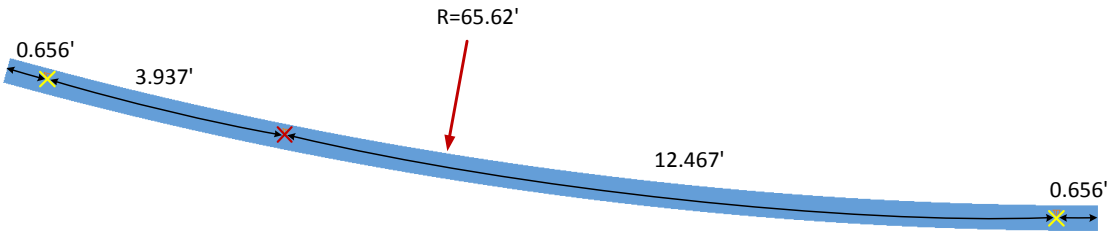

Figure A.2.1. Girder dimensions and boundary conditions

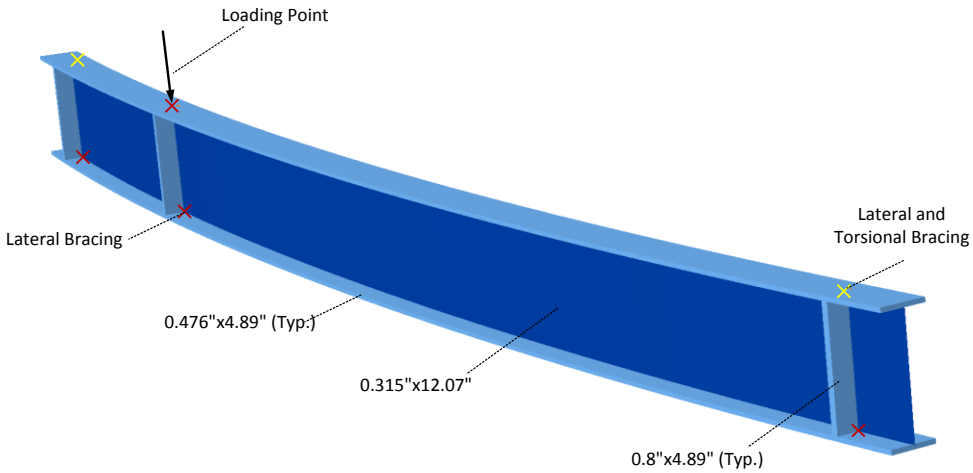

Figure A.2.2. Girder cross-section dimensions and boundary conditions.

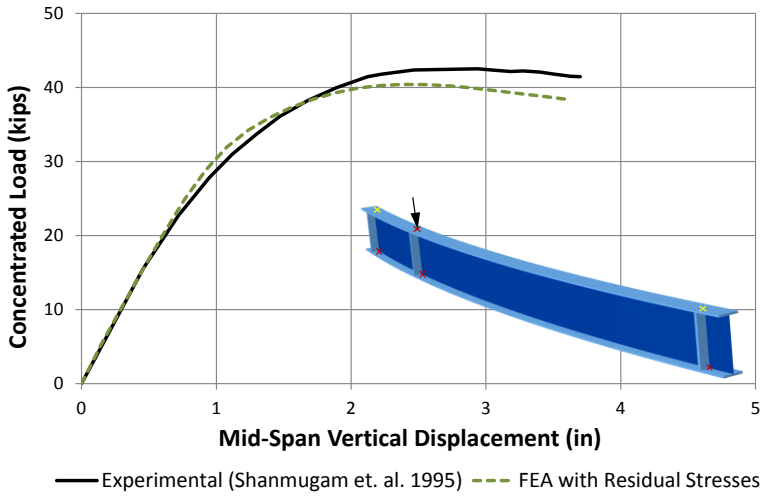

Figure A.2.3. Curved girder FEA verification by load versus vertical deflections at mid-span.

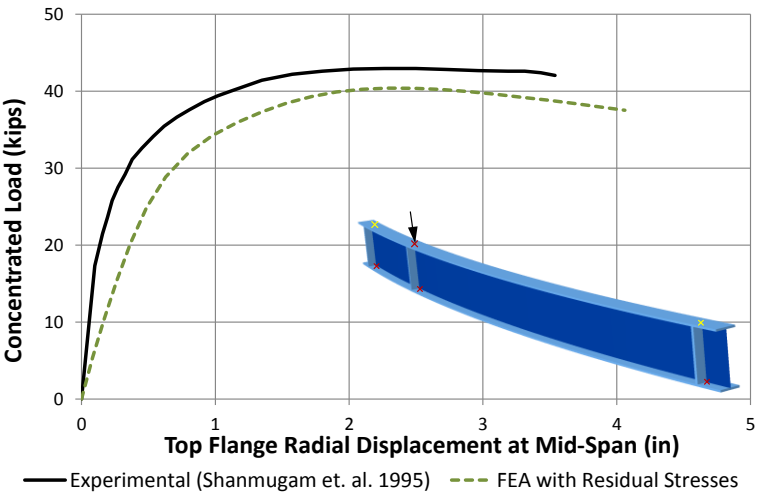

Figure A.2.4. Curved girder FEA verification by load versus radial deflections at mid-span.

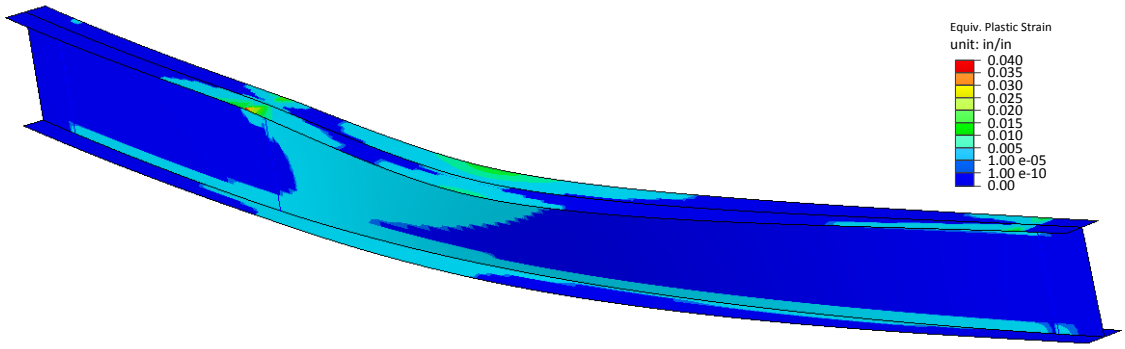

Figure A.2.5. Perspective view of mid-thickness equivalent plastic strains and deflected shape at the final applied test load.

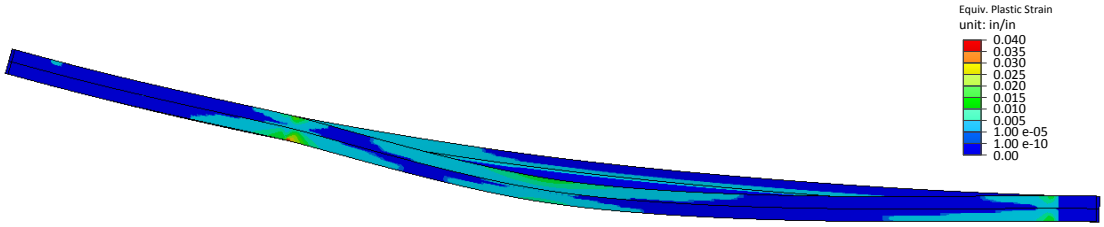

Figure A.2.6. Plan view of mid-thickness equivalent plastic strains and deflected shape at the final applied test load.

A.3. Field Data Comparisons, EICSS12, US 82 main lane underpass at 19th street west bound bridge

EICSS12, which is described in Appendix C.4, was instrumented and field measurements were taken during the deck pour by Romage (2008). The lean-on bracing system is implemented on 19th Street West Bound Bridge (EICSS12). Deflections are measured with laser distance meter and strain gages. This bridge is selected to benchmark the capabilities of the FEA solutions to predict the behavior of bridges during construction. For the FEA solutions, the construction loadings that are described in Section 3.2.1 are modified to match with actual values measured for EICSS12. The weight of the concrete is reported as 144 lbs/ft^3. Additionally, weight of the formworks is replaced with the weight of the stay-in-place forms for this bridge. AASHTO does not allow any yielding during the construction so there is no need for full-nonlinear analysis solutions. Therefore, analysis solutions only considering geometric nonlinearities are used to compare the results.

Vertical displacements under deck pour were reported at several points along the length of the bottom girder by Romage (2008). The displacement of the girders under deck pour is reported for each girder along the fifth brace point. Figure A.3.1 compares vertical displacements along the bottom girder (Girder 1) from the field measurements versus the FEA predictions. Figure A.3.2 compares the vertical displacements along the fifth brace line, which is illustrated by red shading in the inset. It should be noted from Figs. A.3.1 and A.3.2 that the finite element analysis solutions are in good agreement with field measurements. The modeling techniques provide results that are in agreement with field measurements.

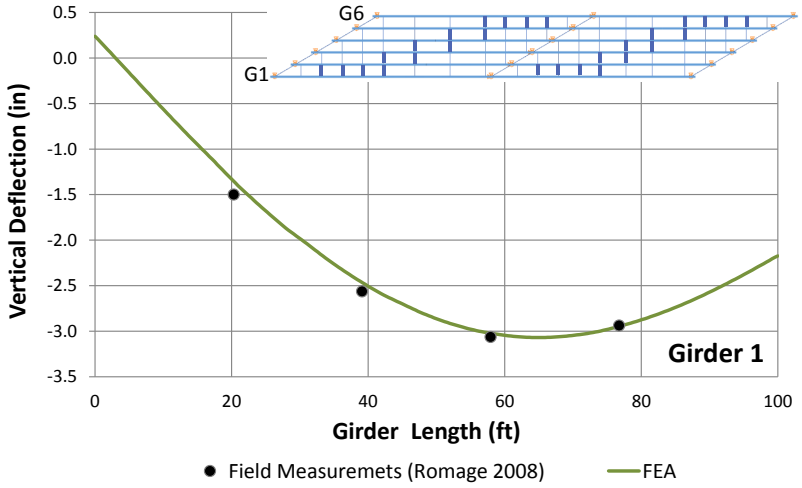

Figure A.3.1. EICSS12, FEA verification by comparing girder displacements along Girder 1.

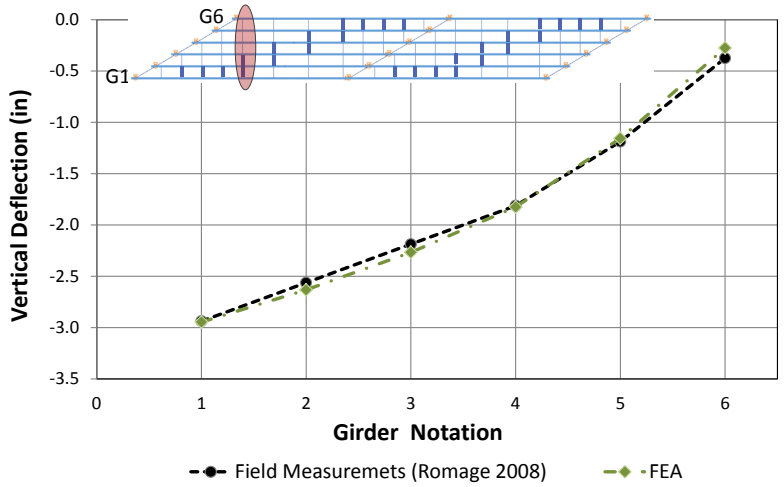

Figure A.3.2. EICSS12, FEA verification by comparing girder displacements at fifth bracing point.

A.4. Experimental Comparisons, ESCR1, FHWA Test Bridge

EISCR1, which is described in Appendix C.5, is full-scale radially-supported bridge tested at the FHWA Turner Fairbank Highway Research Center. Jung (2006) and Jung and White (2008) provide a detailed discussion of the characteristics and the behavior of this test bridge. Detailed monitoring of the girder responses are collected at various stages of the steel erection, deck placement, and loading of this bridge in its final composite condition. This one of the largest bridge structures ever tested indoors, under carefully controlled conditions.

Test measurements of girder major-axis bending and flange lateral bending stresses under steel and total dead loads are used to benchmark the FEA modeling techniques. AASHTO does not allow any yielding during the construction so there is no need for full-nonlinear analysis solutions. Therefore, analysis solutions only considering geometric nonlinearities are used to compare the results.

Figure A.4.1 compares steel dead load girder major-axis bending and flange lateral bending stresses of top and bottom flanges of the outside girder G1 from the test measurements versus the FEA predictions. Figure A.4.2 compares total dead load girder major-axis bending and flange lateral bending stresses of top and bottom flanges of the outside girder G1 from the test measurements versus the FEA predictions. It should be noted from Figs. A.4.1 and A.4.2 that the finite element analysis solutions are in good agreement with test measurements. The FEA techniques provide results that are in agreement with test measurements.

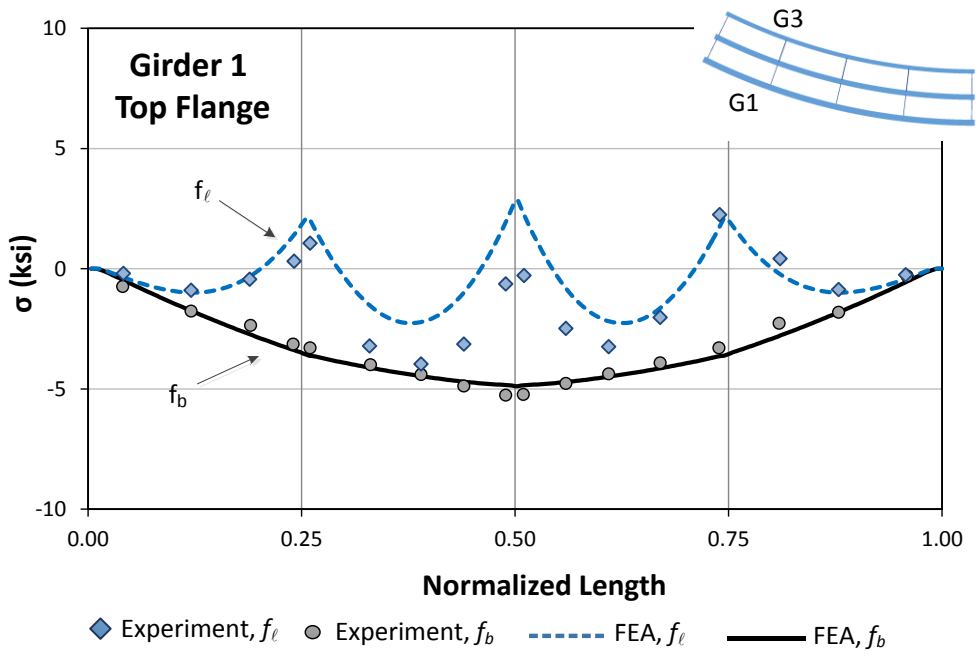

(i) Top flange

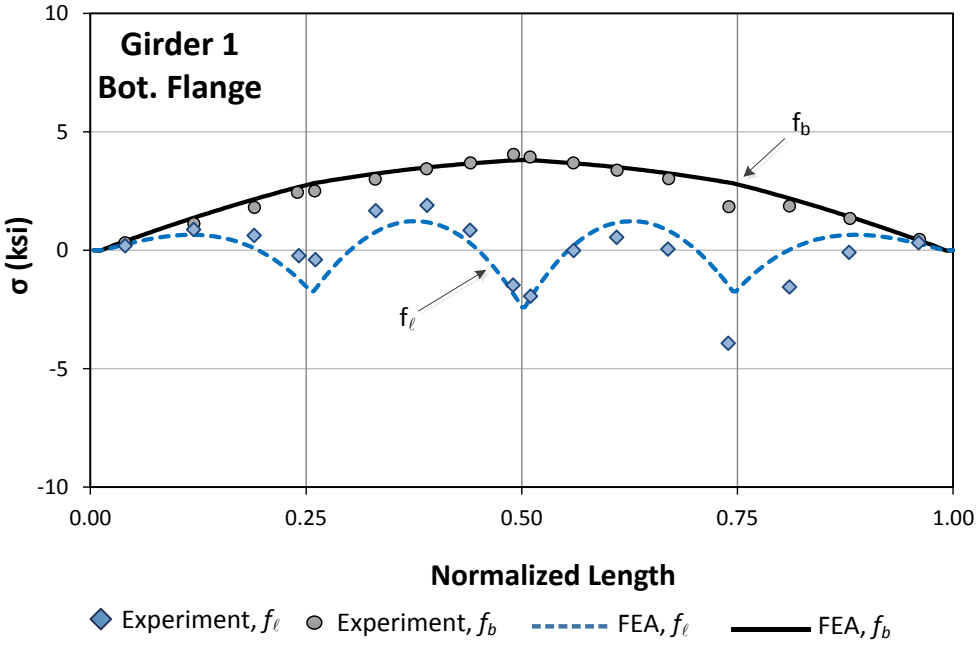

(ii) Bottom flange

Figure A.4.1. EISCR1, comparison of steel dead load girder major-axis bending and flange lateral bending stresses of top and bottom flanges for outside girder G1.

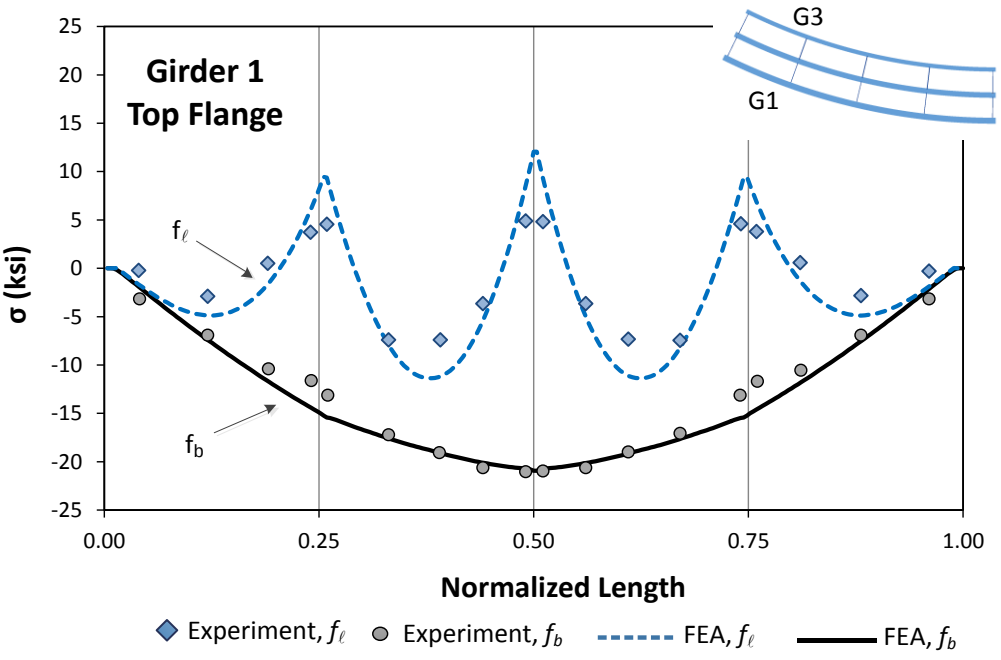

(i) Top flange

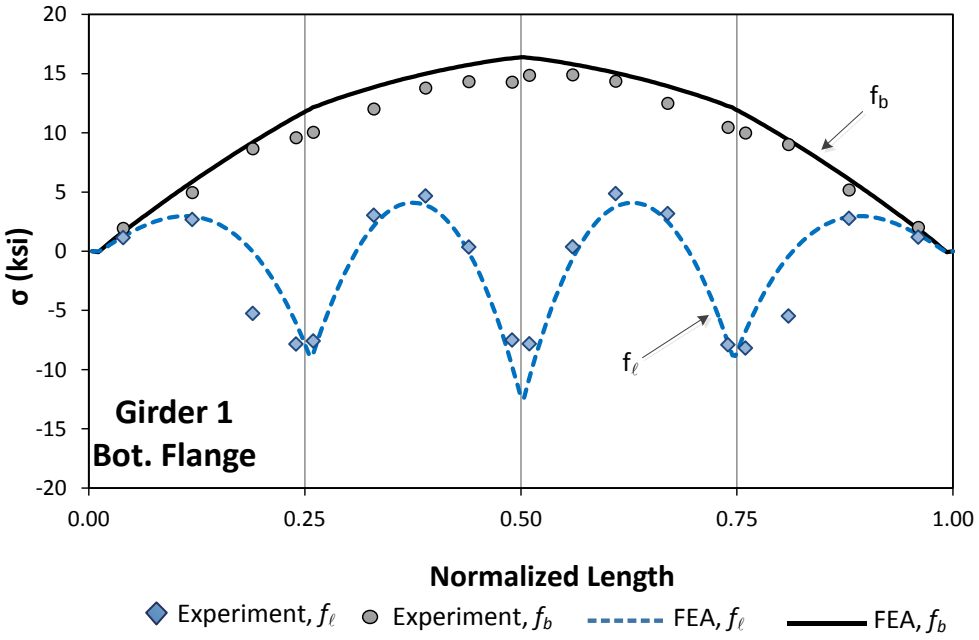

(ii) Bottom flange

Figure A.4.2. EISCR1, comparison of total dead load girder major-axis bending and flange lateral bending stresses of top and bottom flanges for outside girder G1.

APPENDIX B.

SUMMARY OF THE COLLECTED EXISTING I-GIRDER BRIDGES

This appendix summarizes the overall characteristics of the existing I-girder bridges collected from various owners and consultants who contributed to NCHRP (2011). The sketches of the collected existing I-bridges are provided Figs. B.1.1 through B.1.6.

Each of the bridge sketches in Figs. B.1.1 through B.1.6 has a title block containing the following information:

1. An identification label, composed of the letter "E" for "Existing" followed by the above symbols indicating the bridge category, and ending with the bridge number for that category, e.g., bridge "EISCR1" in Fig. B.1.3.
2. A description of the structure, composed of the bridge name and/or location.
3. A summary of the basic geometry information about the bridge, enclosed in parentheses. For instance, in Fig. B.1.3, the basic geometry information for the single EISCR bridge includes:
    - The arc-span length of the bridge centerline,
    - The horizontal radius of curvature of the bridge centerline, and
    - The out-to-out width of the bridge deck perpendicular to the bridge centerline.

    This information is conveyed symbolically in the figure caption as "(LENGTH/RADIUS/WIDTH)." The other categories have similar but different basic geometry information. This information is summarized symbolically in each of their figure captions. The skew angle of the bearing lines is represented by the symbol θ. This angle is taken as zero when a bearing line is perpendicular to the centerline of the structure, that is, when the bearing line does not have any skew.
4. The symbol "*", at the end of the parentheses delimiting the basic geometry information, if the bridge has erection plans. No symbol is shown if the bridge does not have erection plans.
5. The organization that provided the drawings for each bridge. This information is delimited by square brackets, i.e., "[FHWA]" in Fig. B.1.3.

Other pertinent information is provided underneath the plan sketch of each of the bridges. This information includes data such as the number of girders in the bridge cross-section, whether test or field data are available for the structure, references to papers or reports containing test data or documentation of previous research on the bridge, and brief notes regarding successes or difficulties for certain bridges. Note that one scale is utilized for all the simple-span bridges, whereas a slightly smaller scale is used for all the continuous-span bridges.

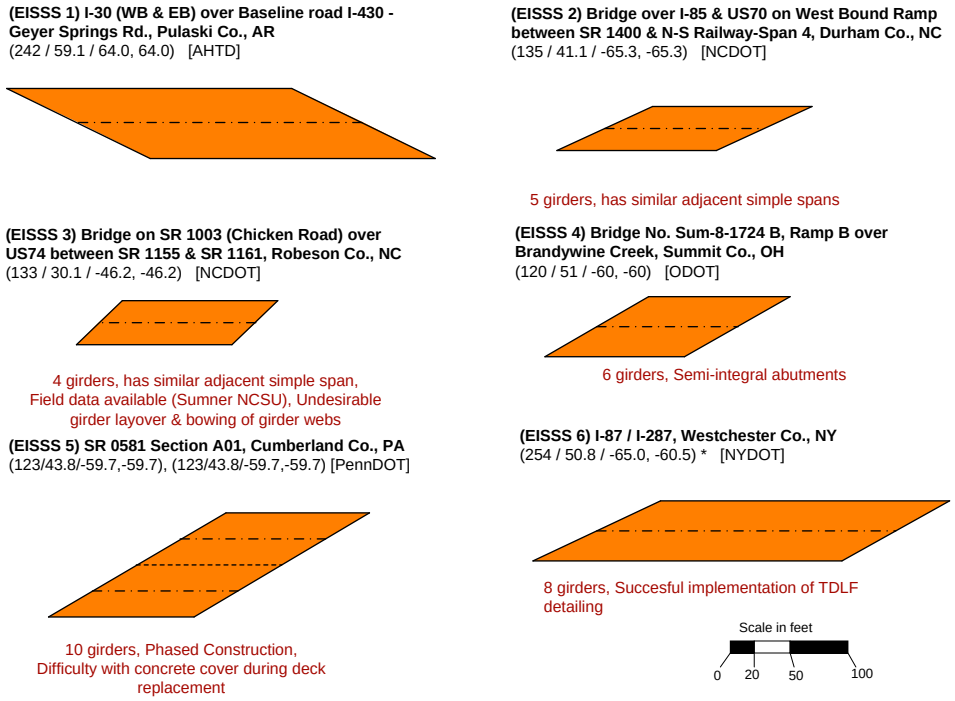

Figure B.1.1. Existing I-girder bridges, Simple-span, Straight with Skewed supports, (EISSS #) Description (LENGTH / WIDTH / θ_{Left}, θ_{Right}) [Source].

(EICSS 1) Steel Overpass Sunnyside Road I.C. (I-15B) Over I-15 , Bonneville Co., ID
(160, 160 / 95.2 / -35.2, -35.2, -35.2) [ITD]

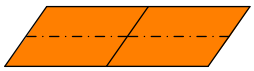

Two-span continuous, 9 girders,
Field data available,
Successful implementation of total dead load fit detailing

(EICSS 2) I-235 EB over E.University Ave., Polk Co., IA
(239, 257, 220 / 74.3 / 58, 61.8, 38, 38) [Iowa DOT]

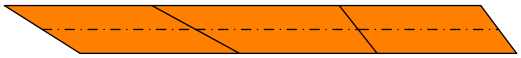

Three-span continuous, 8 girders,
Difficulty installing cross-frames during erection

(EICSS 3) Ramp C over EB I-80, IA
(80, 144, 80 / 26 / -15, -15, -15, -15) [Iowa DOT]

Three-span continuous, 5 girders,
Integral abutments

(EICSS 4) L40 over IA 60, Osceola Co., IA
(145, 148 / 33.2 / 41.0, 41.0, 41.0) [HDR]

Two-span continuous, 4 girders

(EICSS 5) W.BD. RTE. 350 Over I-435 state road from RTE. 40 to RTE. 350 about 2 miles NW of Raytown, Jackson Co., MO
(120, 170, 170, 120 / 40.7 / 56.0, 56.0, 56.0, 56.0, 56.0) [HDR]

Four-span continuous, 5 girders

(EICSS 6) E.BD. RTE. 350 over S.BD I-435 state road from RTE. 40 to RTE. 350 about 2 miles NW of Raytown, Jackson Co., MO
(190, 250, 190, 120 / 40.7 / 56.0, 56.0, 56.0, 56.0) [HDR]

Three-span continuous, 5 girders

(EICSS 7) Bridge over the Castor River, State Road from U.S. 67 to Route 51 about 8 miles S.E. of Frederick Town, Madison Co., MO
(143, 185, 143, 143 / 38.7 / -55.0, -55.0, -55.0, -55.0, -55.0) [HDR]

Four-span continuous, 5 girders

(EICSS 8) Milepost 63.83 Route 300 Bridge over NYS Thruway, NY
(120, 120 / 40.8 / 58.5, 58.5) [NYSDOT]

Two-span continuous, 8 girders,
Field data available (NYSDOT),
Very shallow plate girders (27 in deep).

(EICSS 9) Bridge No. Sum-27 I-1186 R, I-27 I NB & Ramp A Over SR 8, Summit Co., OH
(73, 120, 84, 52 / 91.8 to 95.1 / -48.5, -48.5, -48.5, -48.5, -48.5) [ODOT]

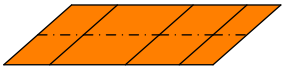

Four-span continuous, 11 girders, Semi-integral abutments

(EICSS 10) SR 0031 over Penn Turnpike, Somerset Co., PA
(161, 161 / 42.3 / -69.5, -69.5, -69.5) [HDR]

Two-span continuous, 5 girders

(EICSS 11) US 82 Mainlane Underpass at 9th Street, Lubbock Co., TX
(182, 172 / 70 / -53.7, -53.7, -53.7) [TxDOT]

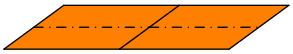

Two-span continuous, 9 girders,
Lean on cross-frame system,
Studied by Zhou (2006),
Field data is not published yet

(EICSS 12) US 82 Mainlane Underpass at 19th Street WB, Lubbock Co., TX
(150, 139 / 47 / -59.6, -59.6, -59.6) [TxDOT]

Two-span continuous, 6 girders,
Lean on cross-frame system

(EICSS 13) SR 90 Broadway Avenue Interchange, WA
(155, 177 / 87.7 / -56.8, -56.8, -56.8) [WSDOT]

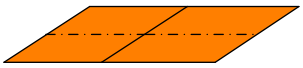

Two-span continuous, 9 girders,
Made use of partial slip of cross-frame bolts during erection

(EICSS 14) Bridge over BNSF Railroad Gillette-Moorcroft East BNSF RR Separation, Campbell Co., WY
(111, 163, 111 / 40.3 / 45, 45, 45, 45) [WYDOT]

Three-span continuous, 5 girders

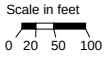

Figure B.1.2. Existing I-girder bridges, Continuous-span, Straight with Skewed supports, (EICSS #) Description (LENGTH1, LENGTH2, … / WIDTH / θ_{Left}, …, θ_{Right}) [Source].

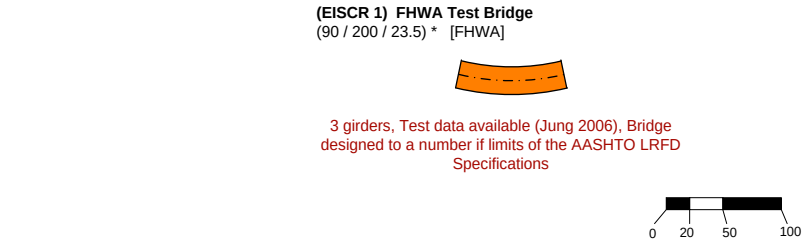

Figure B.1.3. Existing I-girder bridges, Simple-span, Curved with Radial supports, (EISCR #) Description (LENGTH / RADIUS / WIDTH) [Source].

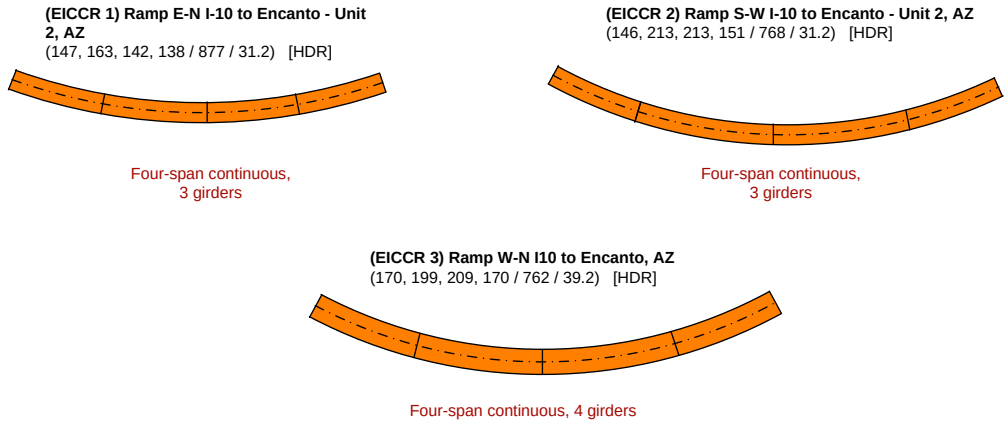

Figure B.1.4. Existing I-girder bridges, Continuous-span, Curved with Radial supports, (EICCR #) Description (LENGTH1, LENGTH2, ... / RADIUS1, RADIUS2, .../ WIDTH) [Source].

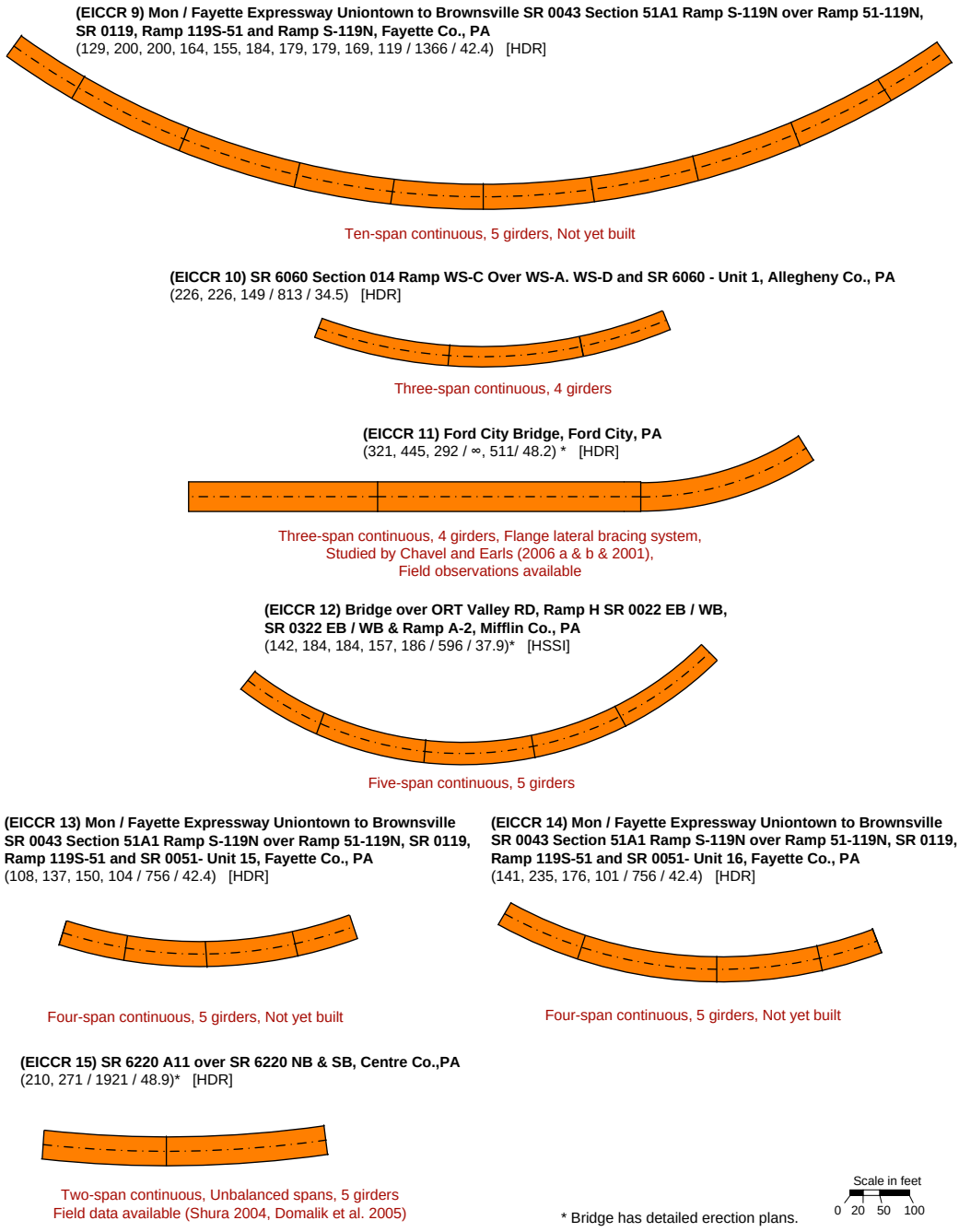

Figure B.1.4. (continued). Existing I-girder bridges, Continuous-span, Curved with Radial supports, (EICCR #) Description (LENGTH1, LENGTH2, … / RADIUS1, RADIUS2, .../ WIDTH) [Source].

(EICCR 16) SR 6026 Section CO2 over SR 0322 WB, Ramp N-W, SR 3007 & Ramp W-S- Unit 1, Centre Co., PA
(238, 334, 298 / 1940 / 46.9) [PennDOT]

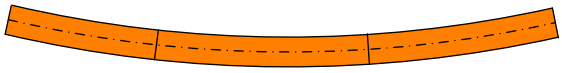

Three-span continuous, 5 girders,
Flange lateral bracing system, Study in progress (Linzell)

(EICCR 17) SR 6026 Section CO2 over SR 0322 WB, Ramp N-W, SR 3007 & Ramp W-S - Unit 2, Centre Co., PA
(298, 333, 266 / 1940 / 46.9) [PennDOT]

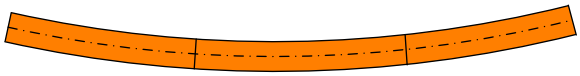

Three-span continuous, 5 girders,
Flange lateral bracing system, Study in Progress (Linzell)

(EICCR 18) Ramp G Over SR 0022, SR 0079, Campbells Run Road & Ramp F - Unit 1, Allegheny Co., PA
(182, 286, 236, 181 / 830 / 32.4)* [PennDOT]

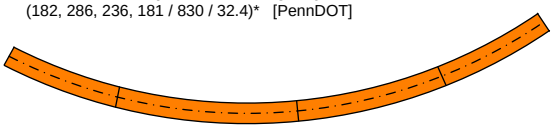

Four-span continuous, 5 girders,
Study in progress (Linzell)

(EICCR 19) Ramp G Over SR 0022, SR 0079, Campbells Run Road & Ramp F - Unit 2, Allegheny Co., PA
(206, 225, 208 / 830 / 32.4)* [PennDOT]

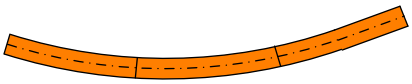

Three-span continuous, 5 girders,
Study in progress (Linzell)

(EICCR 20) PennDOT Structure #22737 (Structure #7A in construction documentation) at I-99 interchange, State College, PA
(296, 333, 266 / 1940 / 45.8)* [Linzell]

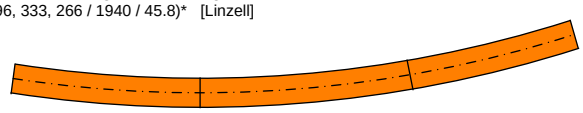

Three-span continuous, 5 girders,
Flange lateral bracing System, Field data available (Bell 2002)

(EICCR 21) SR 386 over Shute Lane, SR 6 and CSX Railroad, Sumner Co., TN
(237, 296, 237 / 1741 / 43.7) [TDOT]

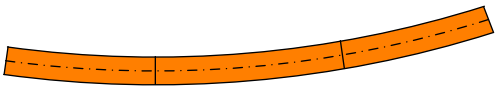

Three-span continuous, 5 girders

(EICCR 22) Ramp B over Briley Parkway and Ramp A, Davidson Co., TN
(141, 188, 188, 208, 157 / 449 / 44) [TDOT]

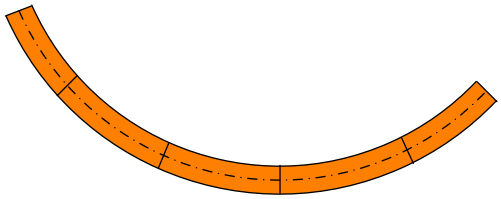

Five-span continuous, 5 girders,
Significantly curved

Scale in feet
0 20 50 100

* Bridge has detailed erection plans.

Figure B.1.4. (continued). Existing I-girder bridges, Continuous-span, Curved with Radial supports, (EICCR #) Description (LENGTH1, LENGTH2, … / RADIUS1, RADIUS2, …/ WIDTH) [Source].

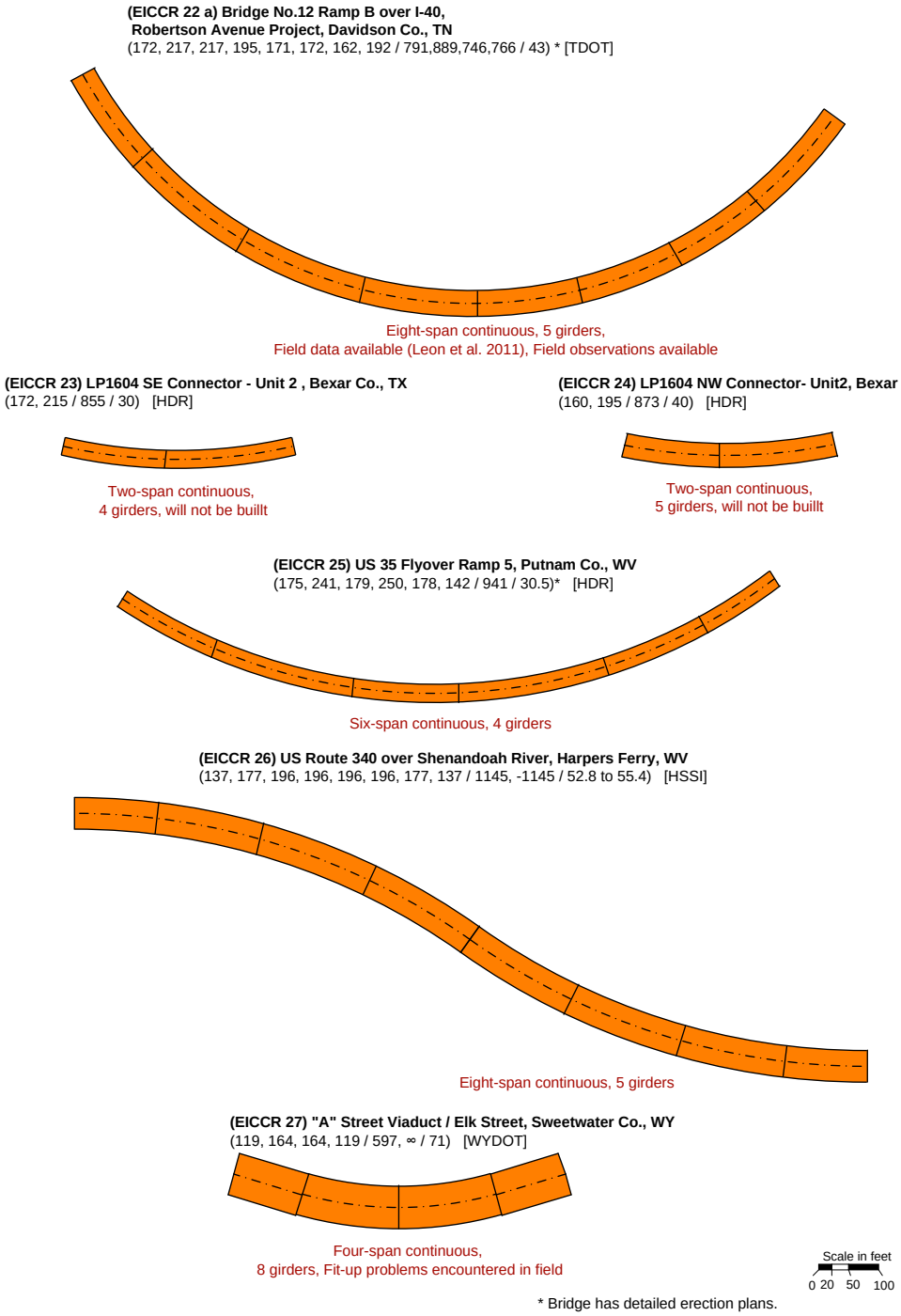

Figure B.1.4. (continued). Existing I-girder bridges, Continuous-span, Curved with Radial supports, (EICCR #) Description (LENGTH1, LENGTH2, ... / RADIUS1, RADIUS2, .../ WIDTH) [Source].

(EISCS 1) Relocated Route 44 Connector "B" over existing Cherry Street, Kingston & Plymouth, Plymouth Co., MA
(106 / 441 / 29.2 / 51.5, 37.7)* [HSSI]

4 girders

(EISCS 2) Bridge over US 401 SBL on US 1 NBL Between Raleigh & Wake Forest, Wake Co., NC
(201 / 2888 / 58.2 / 64.3, 58.9) [NCDOT]

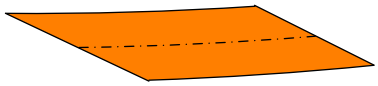

8 girders

(EISCS 3) SR 8002 Ramp A-1, King of Prussia, PA
(151 / 279 / 35.6 / 50.8, 0) * [HDR]

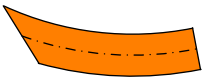

6 girders, Studied by Chavel and Earls (2003) & Chavel (2008), Field observations available

(EISCS 4) Long Shoals Road Overpass, Buncombe Co., NC
(252/2269/27.3/-18.4,-24.7), (251/2306/45.3/-18.1,-24.3), (250/2340/24/-17.8,-23.9) * [NCDOT]

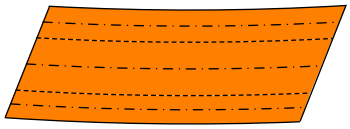

17 girders, Field observations available, Construction in 3 Phases

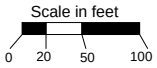

* Bridge has detailed erection plans.

Figure B.1.5. Existing I-girder bridges, Simple-span, Curved with Skewed supports, (EISCS #) Description (LENGTH / RADIUS / WIDTH / θ_{Left}, θ_{Right}) [Source].

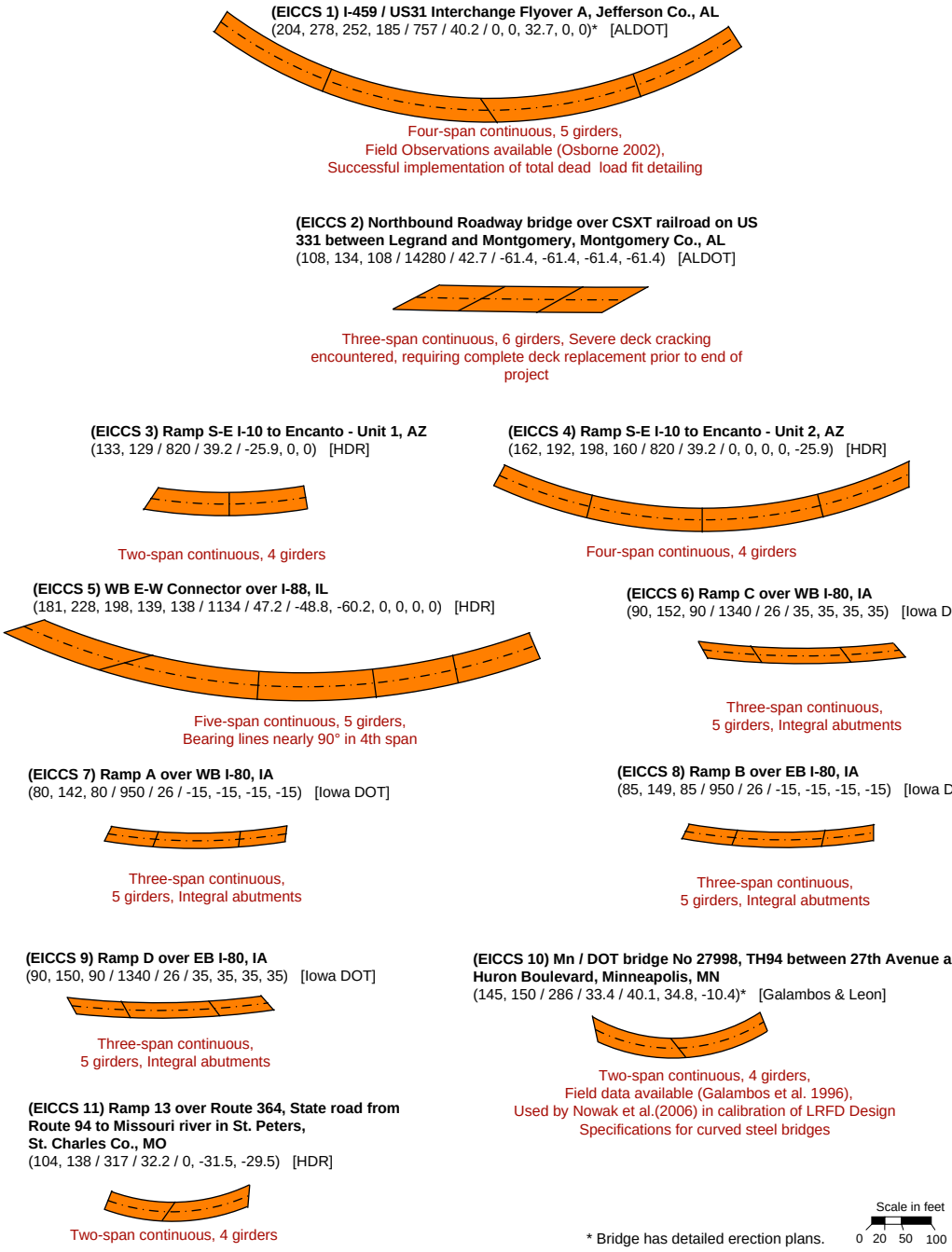

Figure B.1.6. Existing I-girder bridges, Continuous-span, Curved with Skewed supports, (EICCS #) Description (LENGTH1, LENGTH2, … / RADIUS / WIDTH / θ_{Left}, …, θ_{Right}) [Source].

(EICCS 12) SNI-A-BAR Rd. Over I-435 state road from RTE. 40 to RTE. 350 about 3.6 miles NW of Raytown, Jackson Co., MO
(60, 102, 92, 50 / 881 / 50.2 / -2.4, -6.4, -13.0, -18.9, -22.3) [HDR]

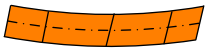

Four-span continuous, 5 girders

(EICCS 13) Bridge 5, West Dodge. 129th St. to I-680, Douglas Co., NE
(118, 128, 145 / 712, ∞, 699 / 32.7 / 0, 18.4, 18.8, 0) [HDR]

Three-span continuous, 4 girders

(EICCS 14) Abbott Drive Bridge, Abbott Drive over UPRR, Douglas Co., NE
(179, 168 / 1125, ∞ / 85.2 / -38, -42, -42) [HDR]

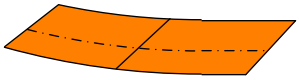

Two-span continuous, 8 girders,
Two different depths of cross-frames and girders

(EICCS 15) Suffern Interchange Ramp C, I-287 / Thruway / Route 17 Interchange - Unit 1, Rockland Co., NY
(148, 158 / 700 / 41.6 / 0, -49.5, -31.8) [NYSDOT]

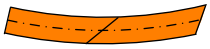

Two-span continuous, 5 girders,
Uplift issues encountered during erection

(EICCS 16) Bridge on Ramp BD over Greensboro Western Urban Loop, -RPCA-, and -CD- Between Bryan Blvd & US 220, Guilford Co., NC
(173, 171, 170 / 754 / 48.4 / 5.6, -2.6, 0, 0) [HDR]

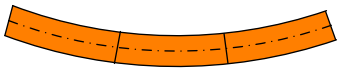

Three-span continuous, 5 girders

(EICCS 17) Bridge on Ramp BD over Bryan Blvd. and -RPD- between US 220 and Bryan Blvd, Guilford Co., NC
(117, 159 / 1574 / 48.4 / 0, 1.1, 0) [HDR]

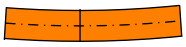

Two-span continuous, 5 girders

(EICCS 18) Bridge on Ramp CA over Bryan Blvd, and Ramp D between I-40 and Bryan Blvd, Guilford Co., NC
(107, 100, 110 / 754 / 48.4 / 0, -0.5, 0, 0) [HDR]

Three-span continuous, 5 girders

(EICCS 19) Bridge on Ramp CA over, Greensboro Western Urban loop, -RPD-, and -CD- BTN I-40 and Bryan Blvd, Guilford Co., NC
(100, 94, 82, 86 / 754 / 48.4 / 0, 0, 8.8, 2.6, 0) [HDR]

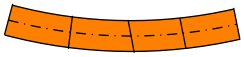

Four-span continuous, 5 girders

(EICCS 20) Bridge No. Sum-8-1757 B, Ramp B over Highland Road, Indian Creek & Ramp R3 & I-271, Summit Co., OH
(115, 170, 151, 182, 146 / 1347 / 49 / 0, 0, -20.7, 0, 0, 0)* [ODOT]

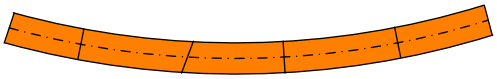

Five-span continuous, 6 girders

(EICCS 21) Grande Ronde River Bridge, Westbound Grande Ronde River Bridge Sec. Old Oregon Trail Hwy., Union Co., OR
(253, 177 / 951 / 50.9 / -31.1, -19.4, -27) [ODOT]

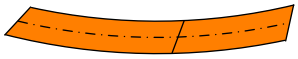

Two-span continuous,5 girders,
Stage 1, independent bridge structure in a phased construction

(EICCS 22) Grande Ronde River Bridge, Eastbound Grande Ronde River (Upper Perry) Bridge Sec. Old Oregon Trail Hwy., Union Co., OR
(240, 177 / 951 / 42.9 / -6.7, -20.4, -28.7) [ODOT]

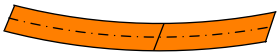

Two-span continuous, 4 girders

* Bridge has detailed erection plans.

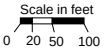

Figure B.1.6. (continued). Existing I-girder bridges, Continuous-span, Curved with Skewed supports, (EICCS #) Description (LENGTH1, LENGTH2, ... / RADIUS / WIDTH / θ_{Left}, ..., θ_{Right}) [Source].

(EICCS 23) SR 6060 Section 014 Ramp WS-D Over SR 6060, Allegheny Co., PA
(180, 205 / 945 / 43.5 / -37.7, -51.1, -43.9) [HDR]

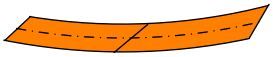

Two-span continuous, 5 girders

(EICCS 24) SR 6060 Section 014 Ramp WS-C Over WS-A. WS-D And SR 6060- Unit 2, Allegheny Co., PA
(155, 166 / 813 / 34.5 / 0, -16.5, 0) [HDR]

Two-span continuous, 4 girders

(EICCS 25) Ramp O over Ramps N,L,Q,R & S Chester & Montgomery Co., PA
(75, 87, 85, 72 / ∞, 205 / 38 / 16.5, 3.5, -7.2, 0, 0)* [HSSI]

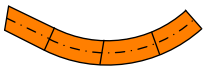

Four-span continuous, 5 girders

(EICCS 26) S.B. Bridge Over Percival Road, Richland Co., SC
(183, 151 / 1637 / 66.8 / 64.9, 62.0, 56.9) [SCDOT]

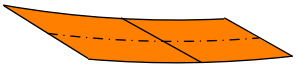

Two-span continuous, 6 girders

(EICCS 27) SR 386 Over SR 6 and Ramp F, Sumner Co., TN
(279, 224, 236 / 2546 / 88 / -53.1, -59.4, -64.4, -69.7) [TDOT]

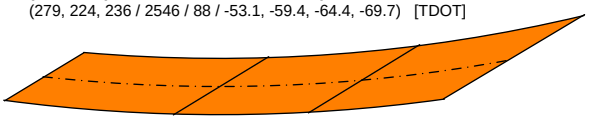

Three-span continuous, 8 girders, Chorded,
Bolts connecting cross-frames to connector plates sheared after steel erection and before completion of bridge

(EICCS 28) LP1604 SE Connector- Unit 1 , Bexar Co., TX
(169, 240, 168 / 855 / 30 / -11.3, 0, 0, 0) [HDR]

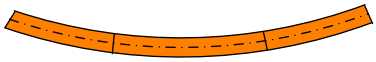

Three-span continuous, 4 girders, Will not be buillt

(EICCS 29) LP1604 NE Connector, Bexar Co., TX
(250, 252, 201 / 892 / 30 / 0, 0, 0, 16.2) [HDR]

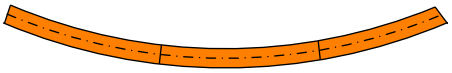

Three-span continuous, 4 girders,
Will not be buillt

(EICCS 30) LP1604 ES Connector, Bexar Co., TX
(171, 199, 201 / 647 / 30 / 0, 0, 0, 10) [HDR]

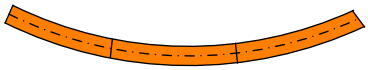

Three-span continuous, 4 girders,
Will not be buillt

(EICCS 31) LP1604 NW Connector - Unit1, Bexar Co., TX
(189, 222, 192 / 873 / 40 / -9.7, 0, 0, 0) [HDR]

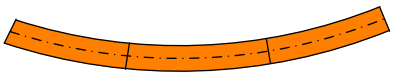

Three-span continuous, 5 girders,
Will not be buillt

(EICCS 32) LP1604 SW Connector, Bexar Co., TX
(232, 262, 217 / 869 / 30 / 0, 0, 0, 10.8) [HDR]

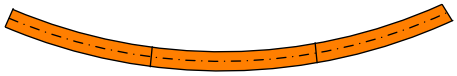

Three-span continuous, 4 girders,
Will not be buillt

Scale in feet
0 20 50 100

* Bridge has detailed erection plans.

Figure B.1.6. (continued). Existing I-girder bridges, Continuous-span, Curved with Skewed supports, (EICCS #) Description (LENGTH1, LENGTH2, … / RADIUS / WIDTH / θ_{Left}, …, θ_{Right}) [Source].

(EICCS 33) I-95 Southbound (Bridge B610) I95 / I-395 / I-495 Interchange, Fairfax Co., VA
(223, 273, 271 / 1308 / 59.5 / 0, -20.1, 0, 0)* [HSSI]

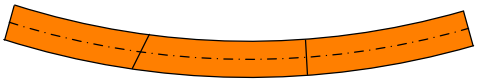

Three-span continuous, 6 girders

(EICCS 34) B-40-1111 Marquette Interchange - Unit 2, Milwaukee Co., WI
(116, 132, 144, 172, 170, 175, 110 / 1410, ∞, / 58.9 / -4.31, 0, 0, -10.7, -28.1, -28.1, -28.1, -28.1)* [WisDOT]

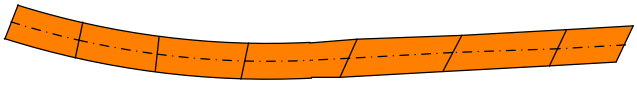

Seven span continuous, 5 I-girders

(EICCS 35) B-40-1211 Marquette Interchange - Unit 2, Milwaukee Co., WI
(119, 137, 188, 171, 195, 150 / 1450, ∞ / 58.9 / 8.54, 0, 0, -11.5, -27.5, -27.5, -27.5)* [WisDOT]

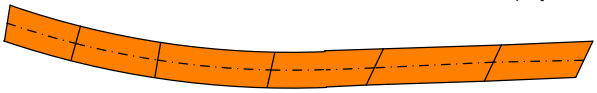

Six span continuous, 5 I-girders

* Bridge has detailed erection plans.

Figure B.1.6. (continued). Existing I-girder bridges, Continuous-span, Curved with Skewed supports, (EICCS #) Description (LENGTH1, LENGTH2, ... / RADIUS / WIDTH / θ_{Left}, ..., θ_{Right}) [Source].

APPENDIX C.

DESCRIPTION OF CASE STUDY BRIDGES FOR ANALYTICAL STUDIES

This appendix provides detailed information about the case study bridges that are used for the analytical studies. The framing plan, girder plate dimensions and lengths and cross-frame geometry information are presented for each case study. Camber profiles from line-girder and finite element analysis are also presented. Both of the camber profiles are obtained from the negative of the steel or dead load deflections from line-girder analysis and beam-shell finite element analysis.

C.1. EISSS6

EISSS6, is an existing straight simple-span I-girder bridge constructed with TDLF detailing with a 265 ft simple span and 62 degree skew at the bearing lines. A perspective and plan view of the bridge, which was constructed in New York State in 2003, is shown in Fig. C.1.1 with some key attributes. The girders are labeled from bottom toward top as Girder 1 to Girder 8 (G1-G8). Moreover, Fig. C.1.2 shows the framing plan of EISSS6. Girder plate dimensions are illustrated in Fig. C.1.3 and girder plate lengths are shown in Table C.1.1. The cross-frame member sizes are summarized in Table C.1.2. The intermediate cross-frames are X-type, and V-type cross-frames are used at abutments. Flange lateral bracing members with an area of 8.96 in^2 are used between girders G1 and G2, G4 and G5, and G7 and G8. Figure C.1.4 provides the steel dead load girder camber profile that is obtained from finite element analysis deflections. Also, Fig. C.1.5 provides total dead load camber profiles of EISSS6 obtained from finite element solutions.

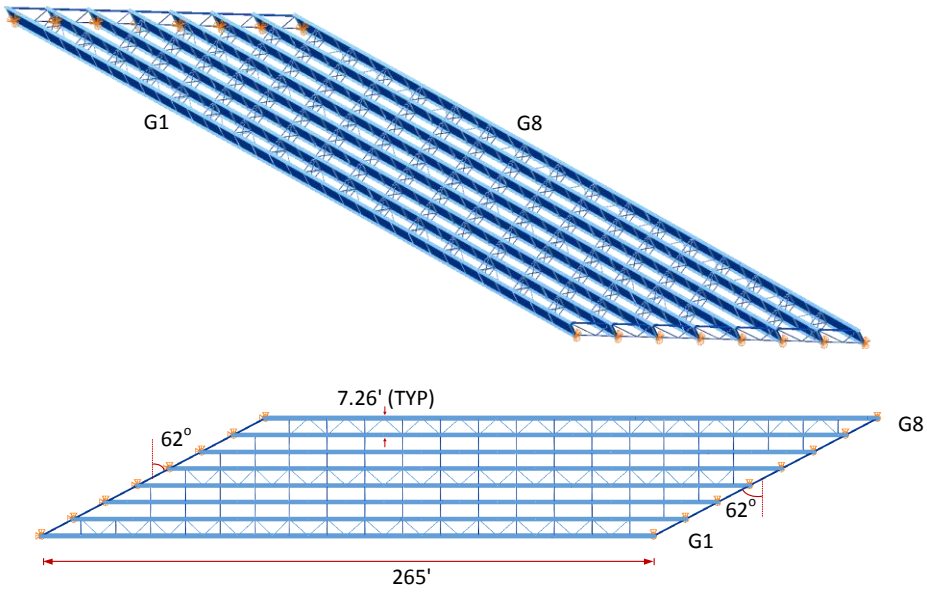

Figure C.1.1. EISSS6, Perspective and plan view.

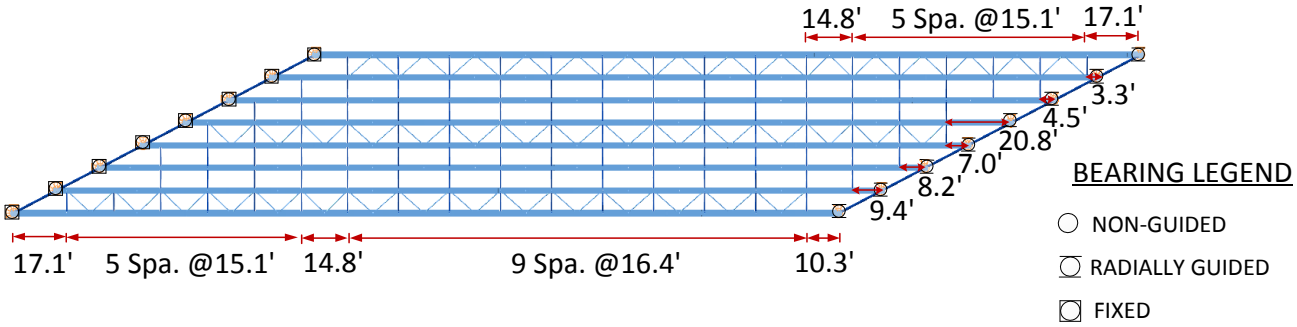

Figure C.1.2. EISSS6, Framing plan.

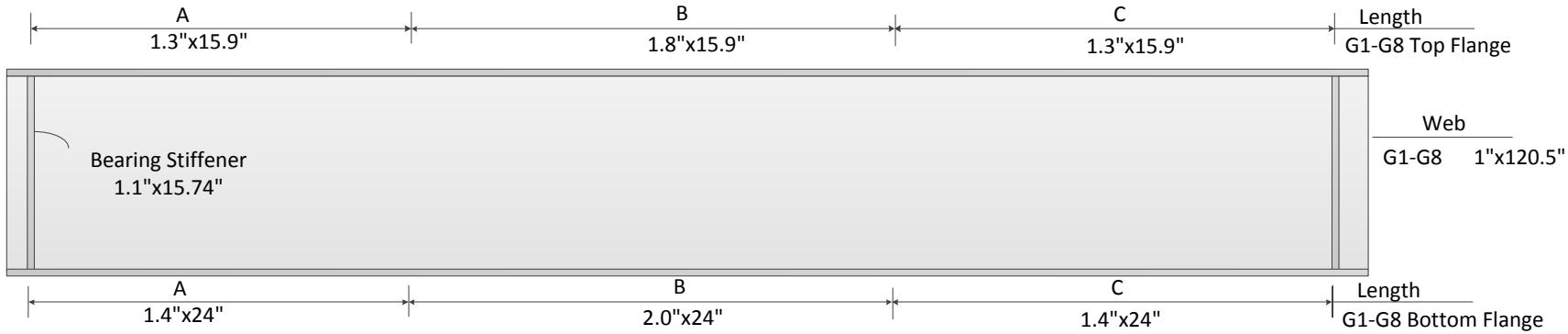

Figure C.1.3. EISSS6, Girder plate dimensions.

Table C.1.1. EISSS6, Girder plate lengths.

Girder	A	B	C
G1-G9	55’	155’	55’

Table C.1.2. EISSS6, Cross-frame member sizes.

Cross-Frame Type	Top Chord	Diagonals	Bottom Chord
Interior (X)	L6x6x1/2	L6x6x1/2	L6x6x1/2
End (V)	W16x89	L6x6x3/4	L6x6x3/4

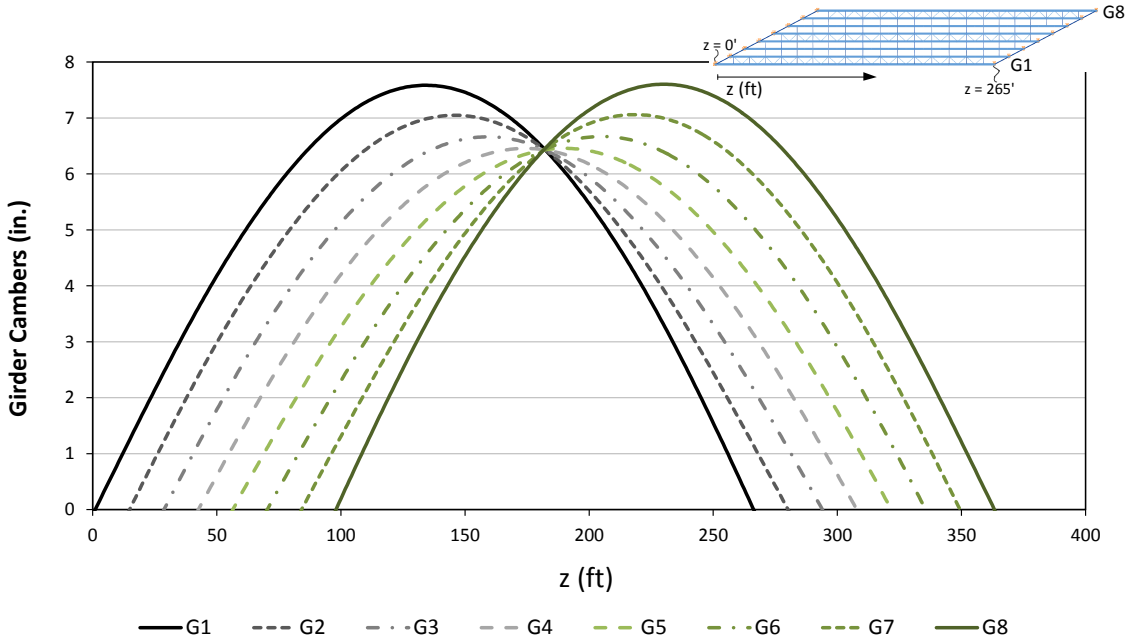

Figure C.1.4. EISSS6, Steel dead load cambers obtained from finite element analysis deflections.

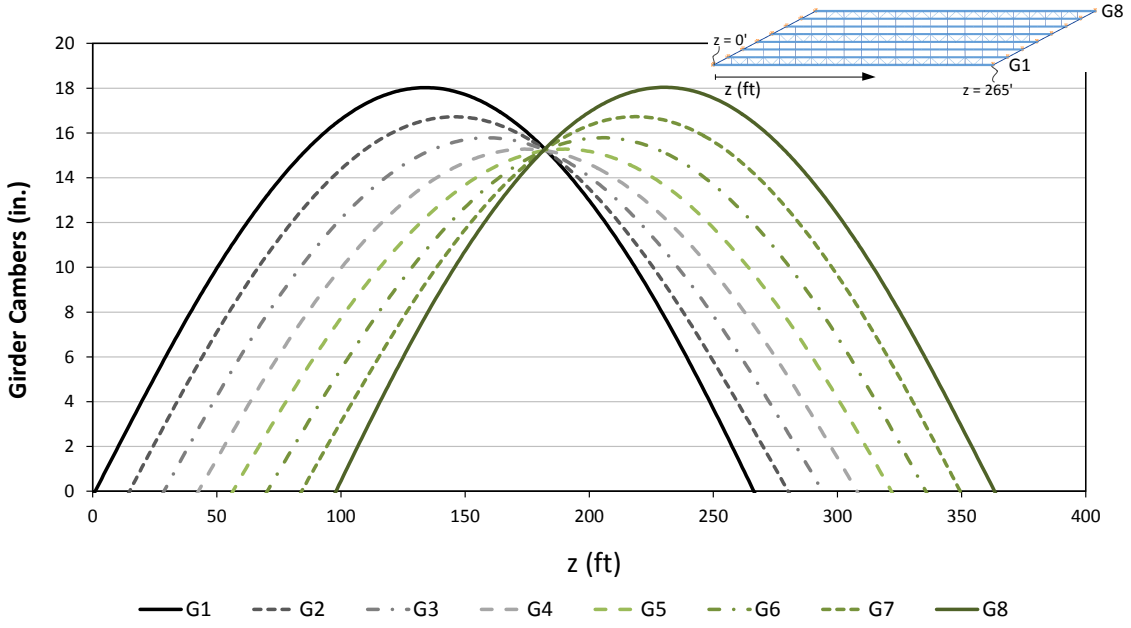

Figure C.1.5. EISSS6, Total dead load cambers obtained from finite element analysis deflections.

C.2. NISSS54

NISSS54 is a 300ft span simply-supported straight I-girder bridge with parallel abutments skewed at 70°. Figure C.2.1 shows the perspective and plan view of NISSS54 with some key attributes. The girders are labeled from bottom toward top as Girder 1 to Girder 9 (G1-G9). Moreover, Fig. C.2.2 shows the framing plan of NISSS54. Girder plate dimensions are summarized in Fig. C.2.3 and girder plate lengths are shown in Table C.2.1. The intermediate cross-frames are X-type, and inverted V-type cross-frames are used at abutments. The cross-frame member sizes are summarized in Table C.2.2. Figures C.2.4 and C.2.5 provides steel and total dead load girder camber profiles of NISSS54 obtained from line-girder and finite element solutions.

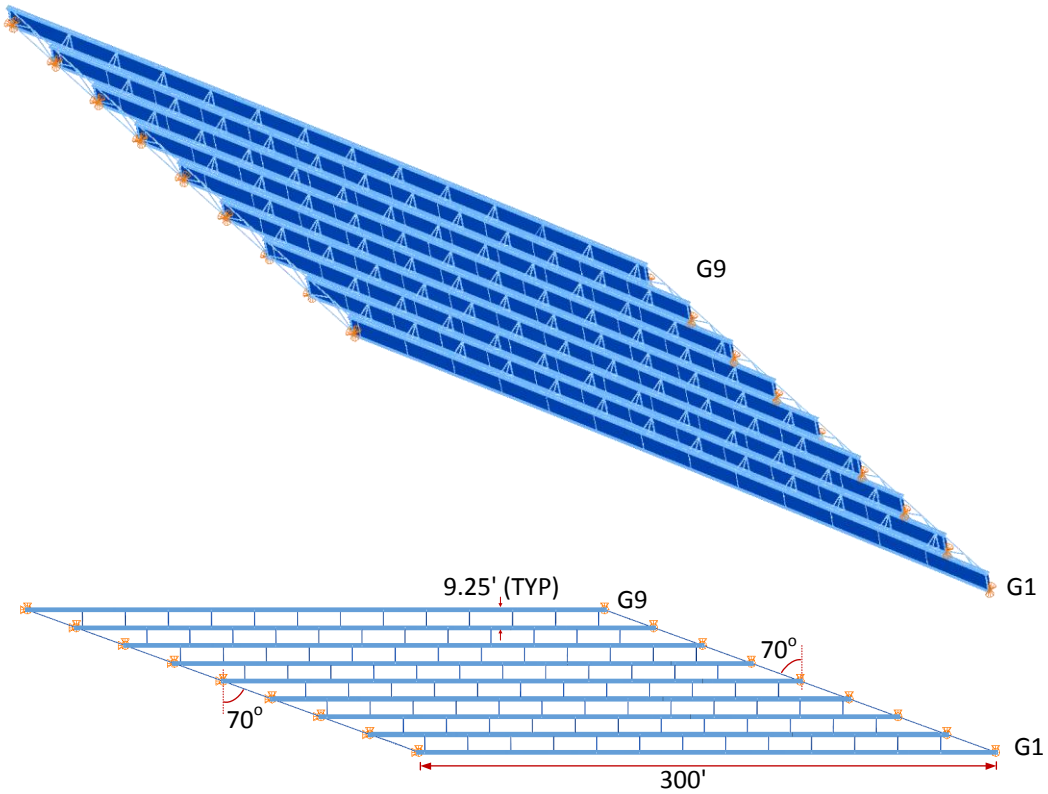

Figure C.2.1. NISSS54, Perspective and plan views.

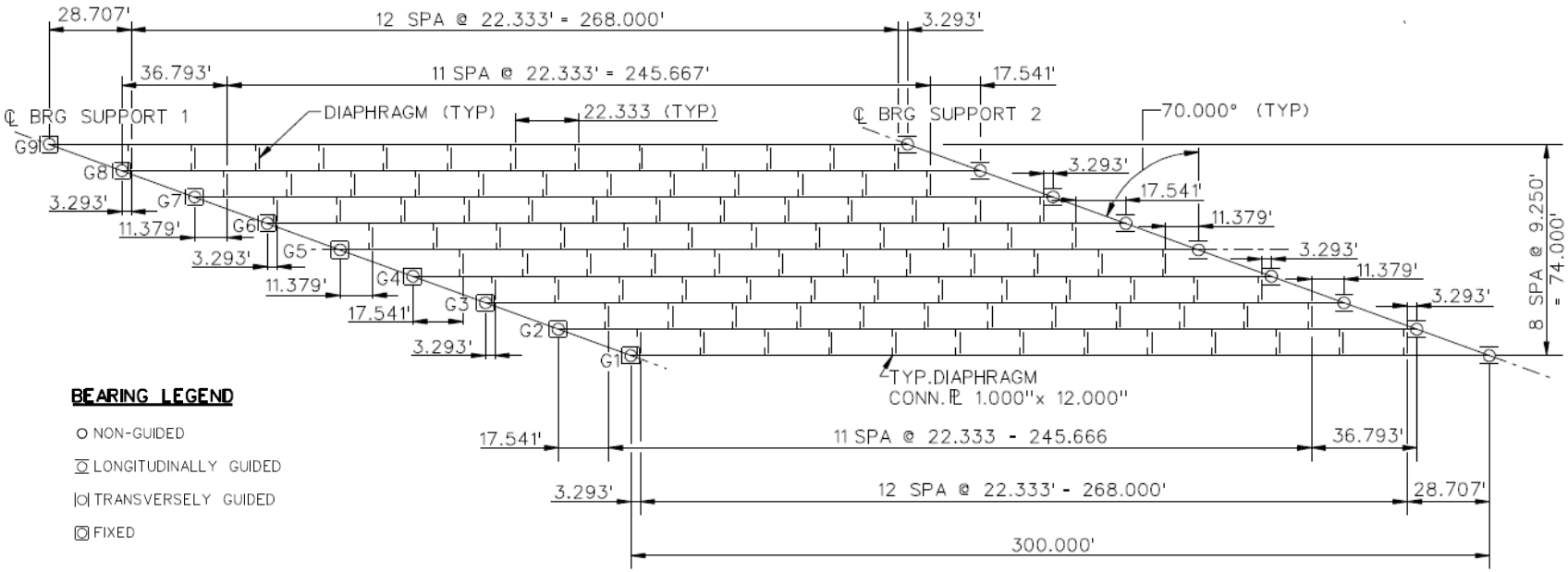

Figure C.2.2. NISSS54, Framing plan.

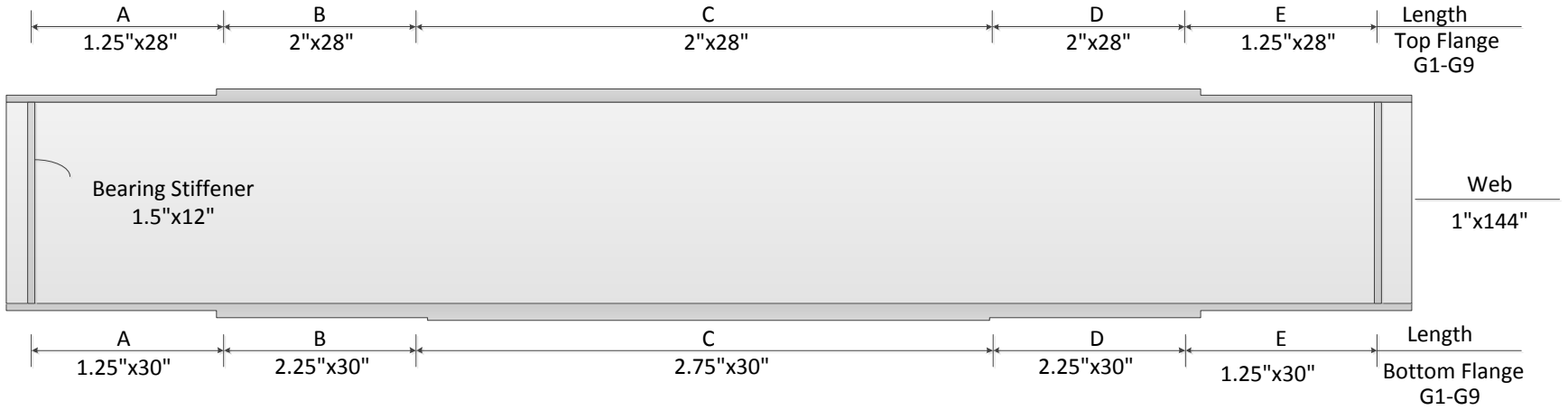

Figure C.2.3..NISSS54, Girder plate dimensions.

Table C.2.1. NISSS54, Girder plate lengths.

Girder	A	B	C	D	E
G1-G9	45’	45’	45’	45’	45’

Table C.2.2. NISSS54, Cross-frame member sizes.

Cross-Frame Type	Top Chord	Diagonals	Bottom Chord
Interior (X type)	L6x6x1	L6x6x1	L6x6x1
End (Inverted V)	WT6x53	WT6x60	WT9x38

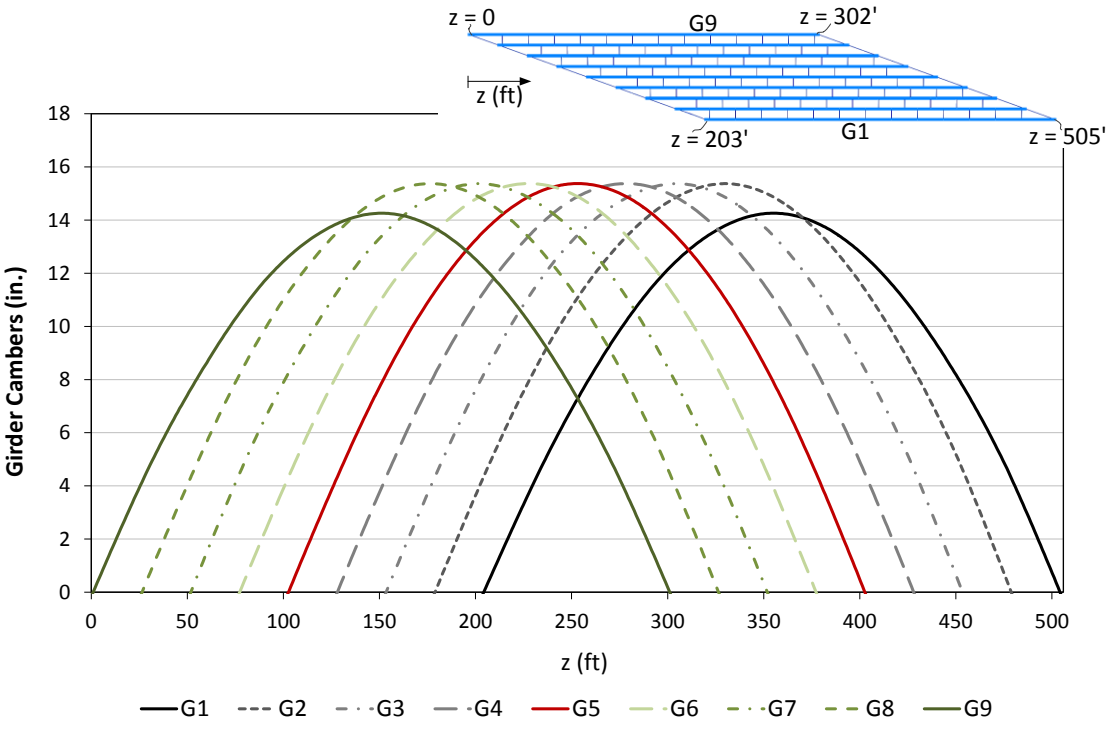

(i) Camber set based on line-girder analysis

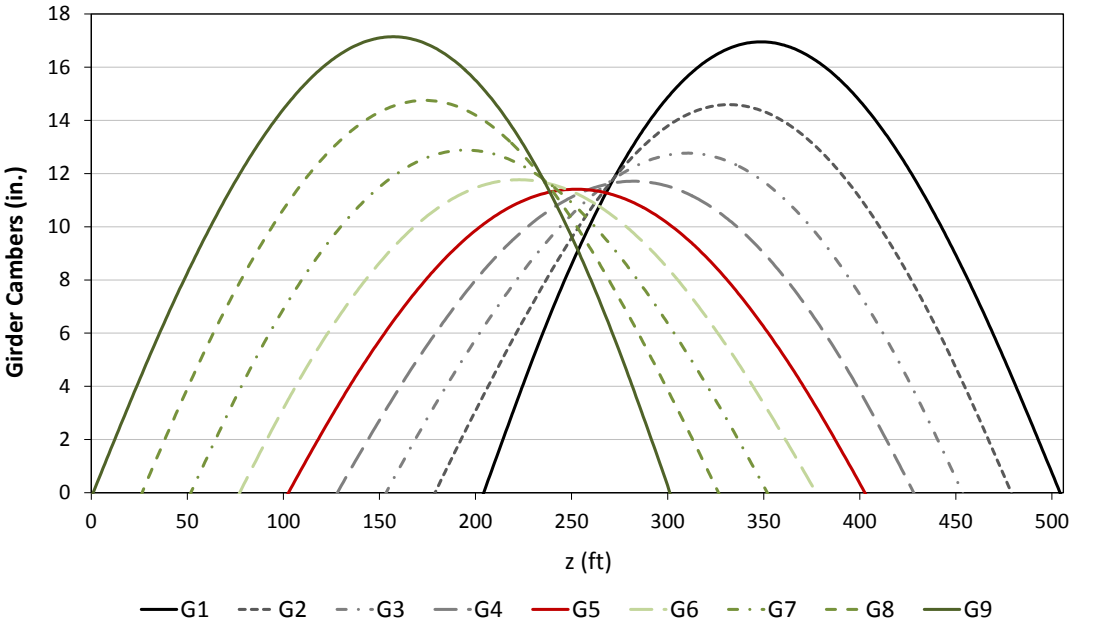

(ii) Camber set based on FEA deflections

Figure C.2.4. NISSS54, Steel dead load cambers obtained from line-girder and finite element analysis.

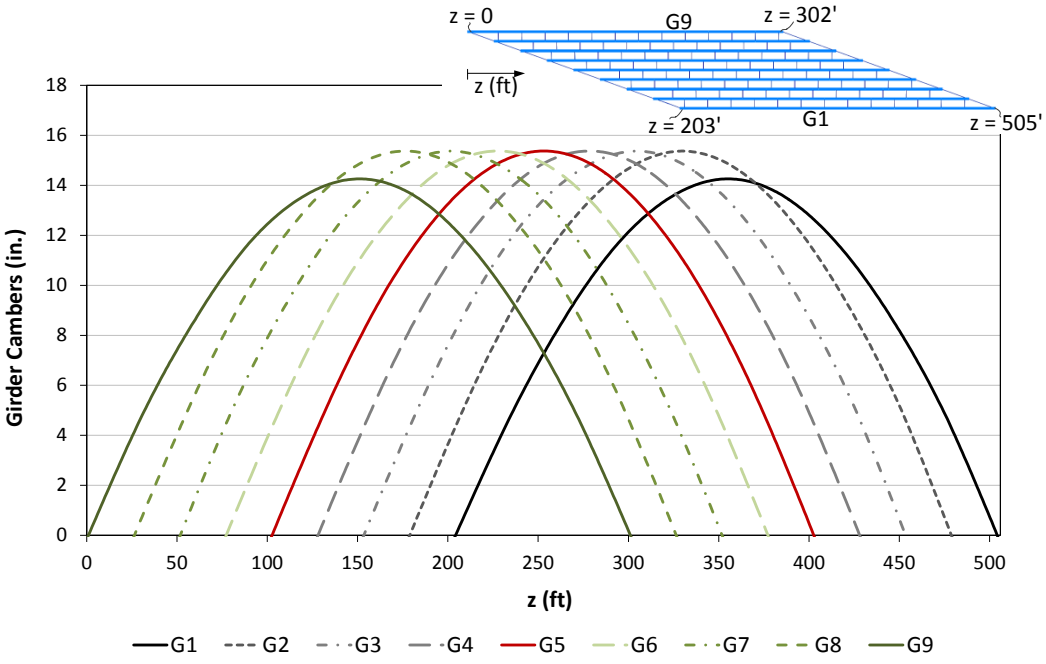

(i) Camber set based on line-girder analysis

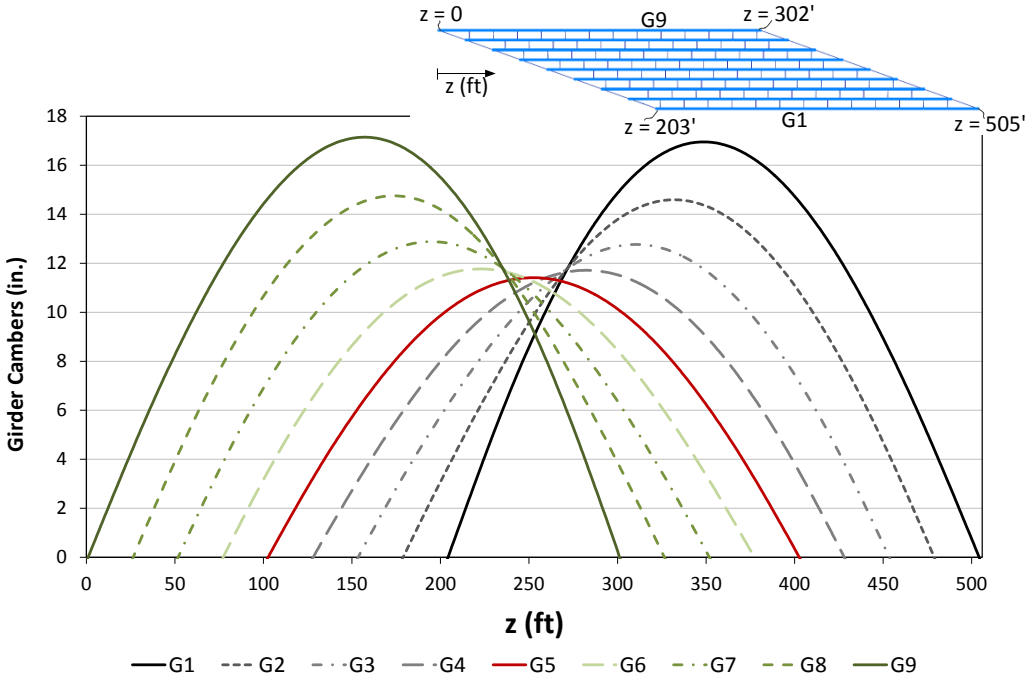

(ii) Camber set based on FEA deflections

Figure C.2.5. NISSS54, Total dead load cambers obtained from line-girder and finite element analysis.

C.3. XICSS5

XICSS5 is a three span continuous straight I-girder bridge with the span lengths of 140ft, 175ft and 140ft with parallel abutments skewed at 60°. This bridge is taken from the NHI Course No.130081A-D (NHI/FHWA, 2007). Figure C.3.1 shows the perspective and plan view of XICSS5 with some key attributes. The girders are labeled from bottom toward top as Girder 1 to Girder 4 (G1-G4). Moreover, Fig. C.3.2 shows the framing plan of XICSS5. Girder plate dimensions are illustrated in Fig. C.3.3. The intermediate cross-frames are V-type, and inverted V-type cross-frames are used at abutments. The cross-frame member sizes are summarized in Table C.3.1. Figure C.3.4 provides the steel dead load girder camber profile that is obtained from finite element analysis deflections. Also, Fig. C.3.5 provides total dead load camber profiles of XICSS5 obtained from line-girder and finite element solutions respectively.

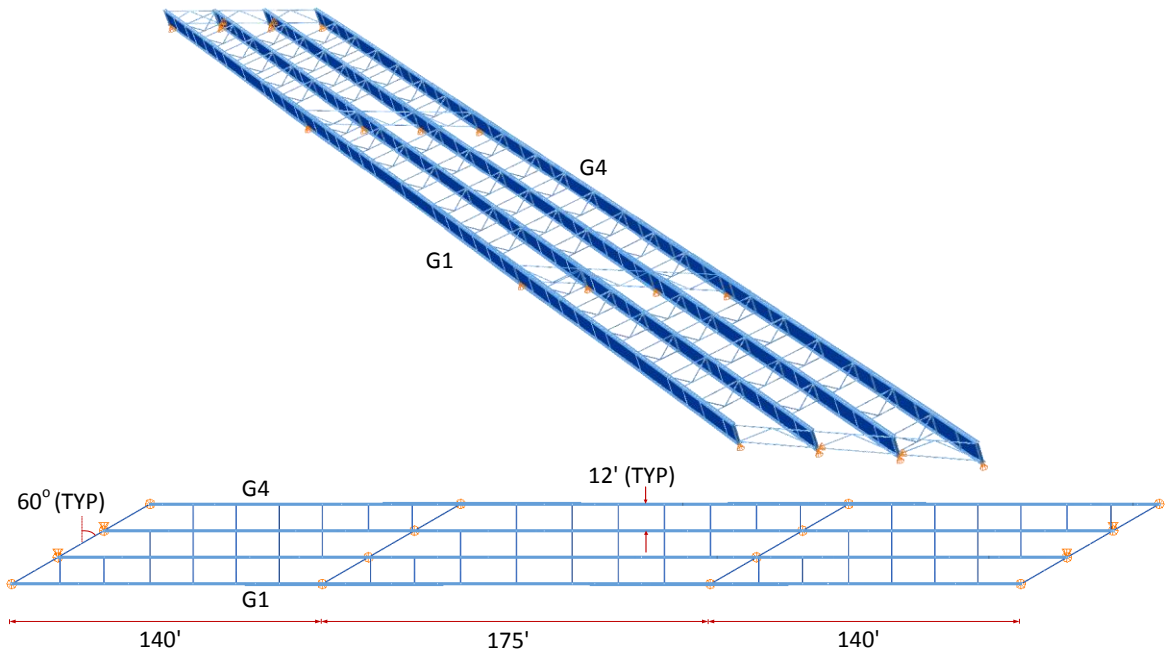

Figure C.3.1. XICSS5, Perspective and plan views.

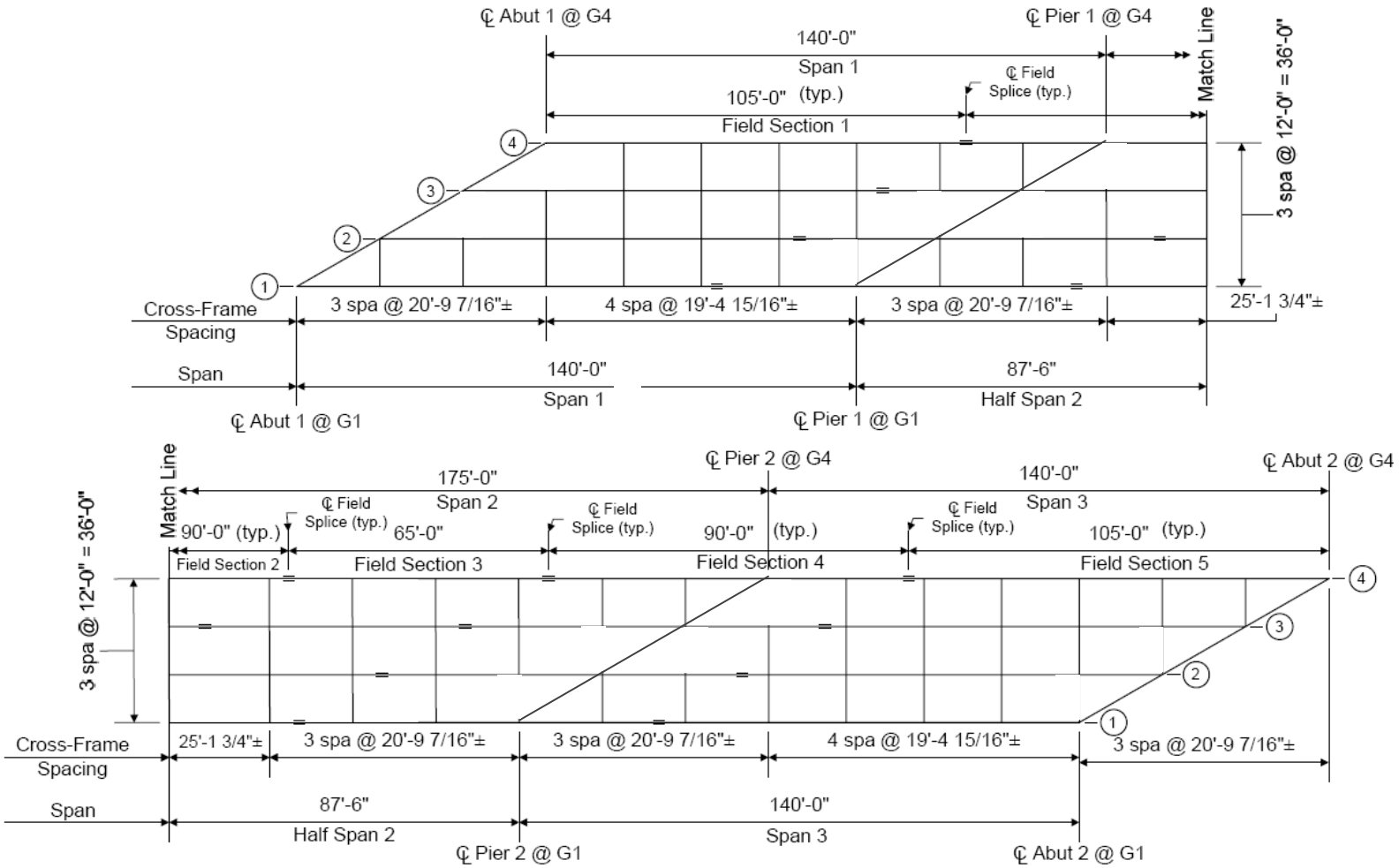

Figure C.3.2. XICSS5, Framing plan.

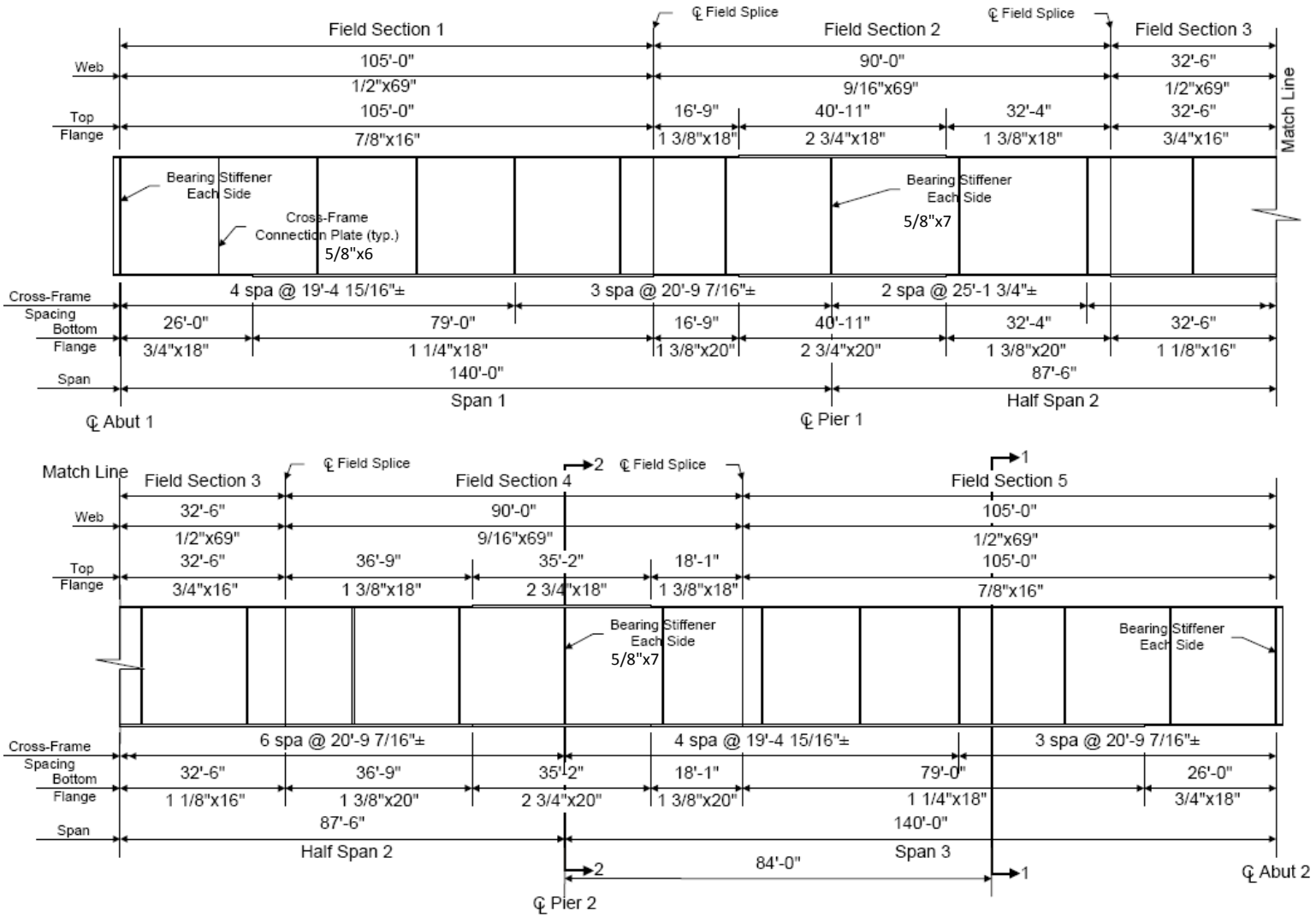

Figure C.3.3. XICSS5, Girder plate dimensions.

Table C.3.1. XICSS5, Cross-frame member sizes.

Cross-Frame Type	Top Chord	Diagonals	Bottom Chord
Interior (V)	L6x6x1/2	L6x6x5/8	L6x6x5/8
End (Inverted V)	L6x6x1/2	L6x6x5/8	L6x6x5/8

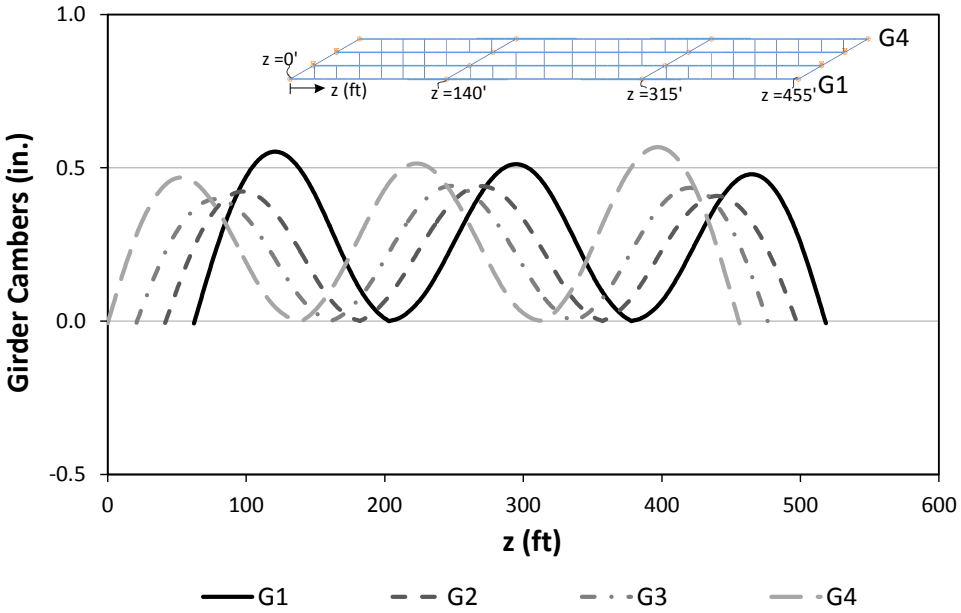

Figure C.3.4. XICSS5, Steel dead load cambers obtained from finite element analysis deflections.

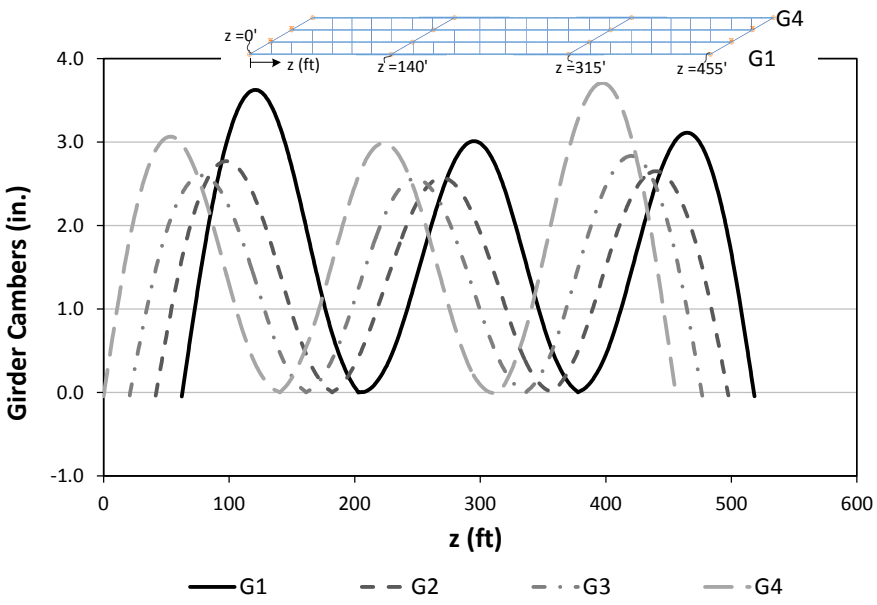

(i) Camber set based on line-girder analysis

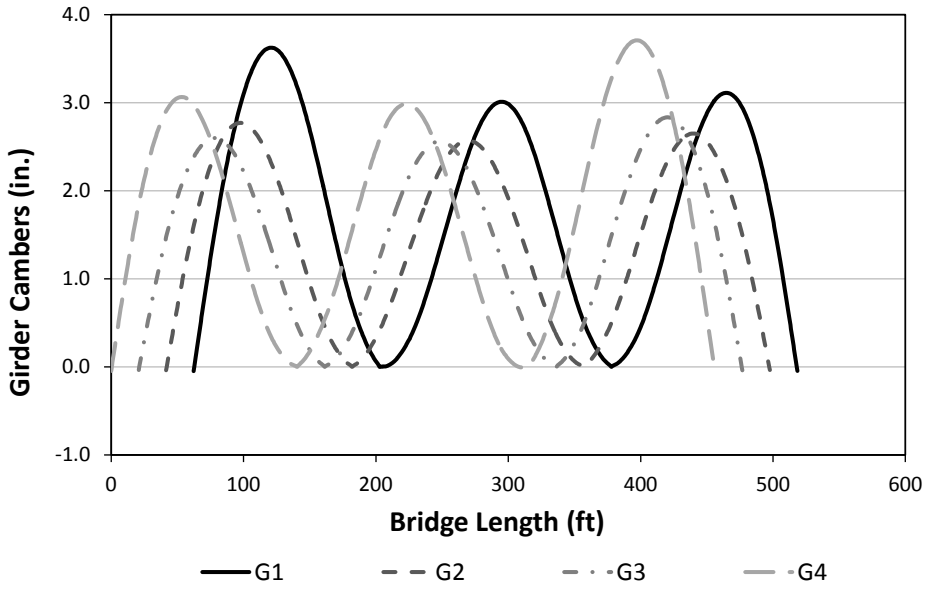

(i) Camber set based on FEA deflections

Figure C.3.5. XICSS5, Total dead load cambers obtained from line-girder and finite element analysis solutions.

C.4. EICSS12

EICSS12 is one of the existing straight simple-span I-girder bridges where a lean-on bracing system is applied. The bridge is named as the US 82 main lane underpass at 19th stress west bound bridge. This bridge is studied in detailed by Romage (2008). Figure C.4.1 shows the perspective and plan view of the bridge with some key attributes. EICSS12 has two spans with the span length of 150.5 ft and 139 ft. The bridge has a skew angle of approximately 60 degrees on all bearings Fig. C.4.2 shows the framing plan of EISSS6. The full bracing points are indicated with thicker lines in the framing plan, whereas the cross-frames with only top and bottom chords are indicated with relatively thinner lines. The girders are labeled from bottom toward top as Girder 1 to Girder 6 (G1-G6). Moreover, Girder plate dimensions are illustrated in Fig. C.4.3 and girder plate lengths are shown in Table C.4.1. The cross-frame member sizes are summarized in Table C.4.2. Figure C.4.4 provides the steel dead load girder camber profile that is obtained from finite element analysis deflections. Also, Fig. C.4.5 provides total dead load camber profiles of EISSS6 obtained from finite element solutions respectively.

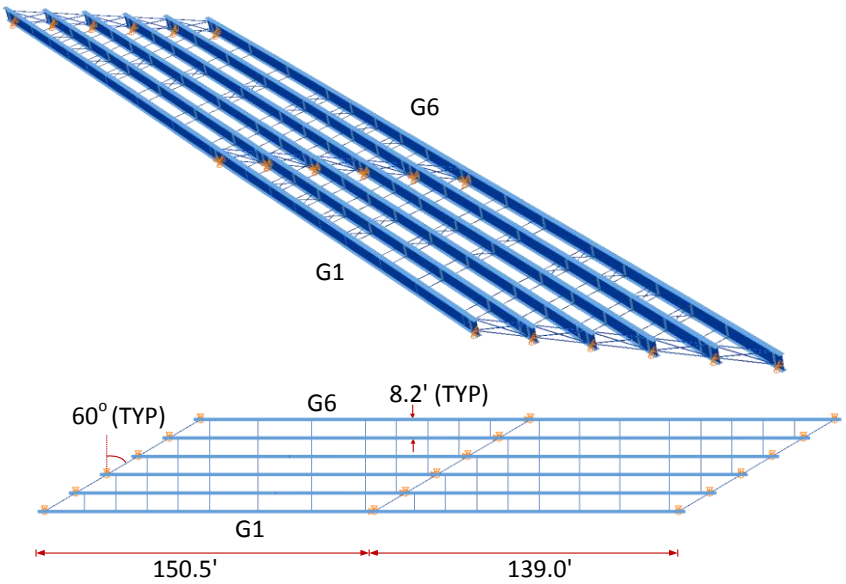

Figure C.4.1. EICSS12, Perspective and plan view.

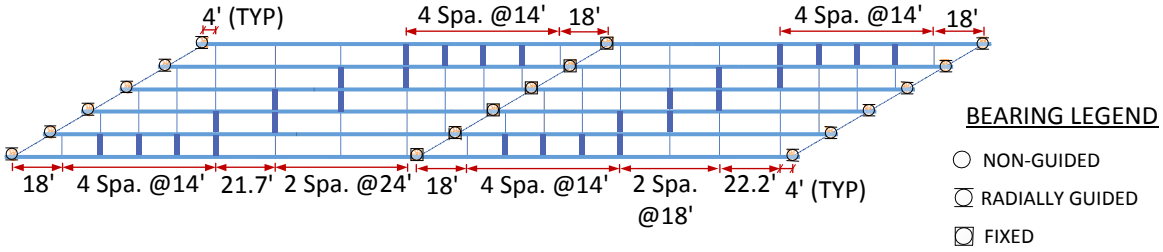

Figure C.4.2. EICSS12, Framing plan.

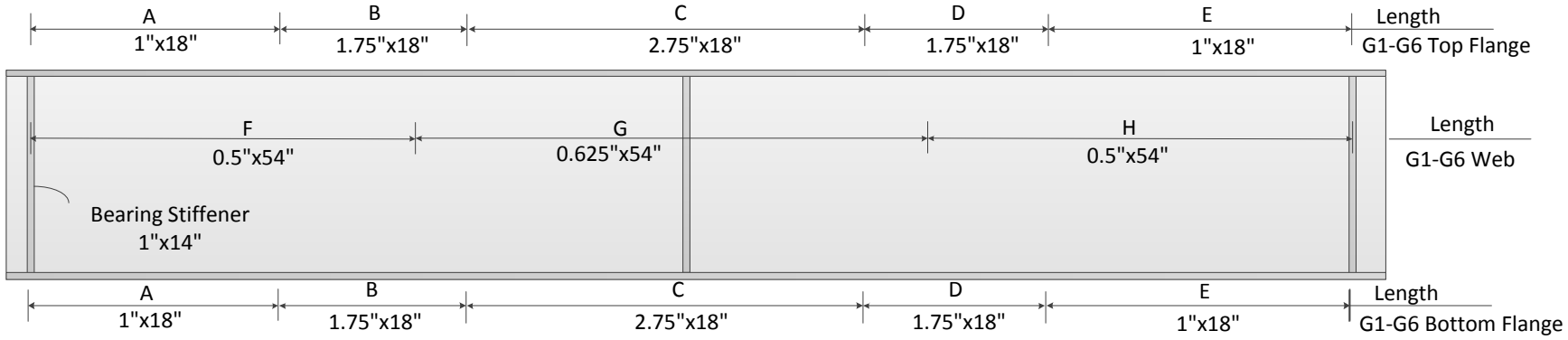

Figure C.4.3. EICSS12, Girder plate dimensions.

Table C.4.1. EICSS12, Girder plate lengths.

Girder	A	B	C	D	E	F	G	H
G1-G9	89’	30’	58.5’	31’	81’	107’	84.5’	92’

Table C.4.2. EICSS12, Cross-frame member sizes.

Cross-Frame Type	Top Chord	Diagonals	Bottom Chord
Interior (X)	L4x4x3/8	L4x4x3/8	L4x4x3/8
End (X)	L5x5x3/4	L5x5x3/4	L5x5x3/4

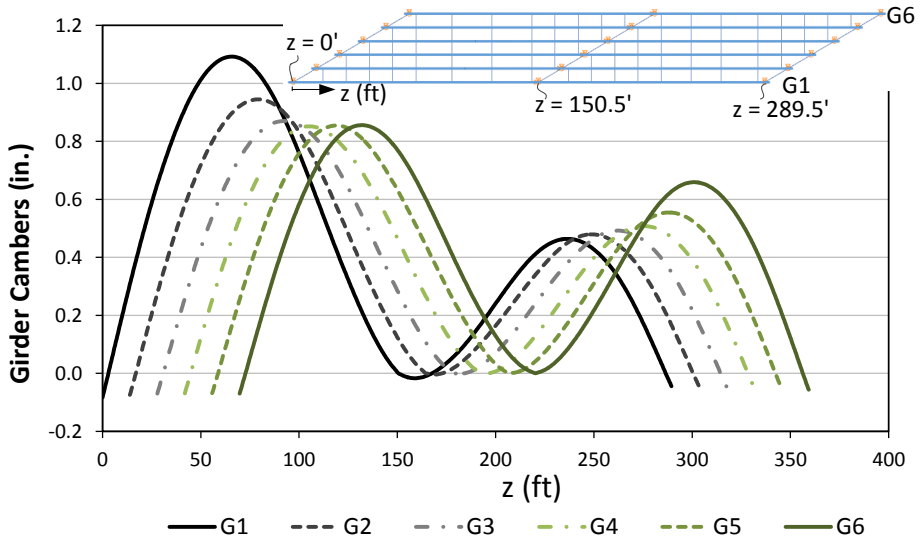

Figure C.4.4. EICSS12, Steel dead load cambers obtained from finite element analysis deflections.

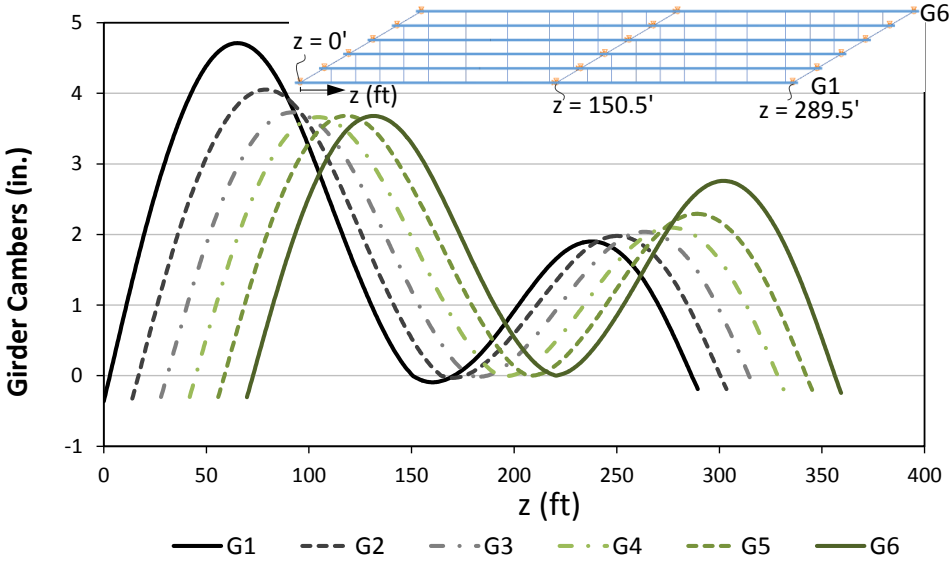

Figure C.4.5. EICSS12, Total dead load cambers obtained from finite element analysis deflections.

C.5. EISCR1

EISCR1, FHWA Test Bridge is a simple span horizontally curved I-girder bridge with radial abutments. Jung (2006) and Jung and White (2008) provide a detailed discussion of the characteristics and the behavior of this test bridge. Figure C.5.1 shows the perspective view of EISCR1 with some key attributes. The girders are labeled from outside toward inside as Girder 1 to Girder 3 (G1-G3). Moreover, Fig. C.5.2 shows the framing plan of EISCR1. Girder plate dimensions are summarized in Fig. C.5.3 and girder plate lengths are shown in Table C.5.1. The intermediate cross-frames are X-type, and inverted V-type cross-frames are used at abutments. The cross-frame member sizes are summarized in Table C.5.2. Figures C.5.4 and C.5.5 provide the steel and total dead load girder camber profiles of EISCR1 respectively. The girder cambers are obtained from finite element analysis deflections.

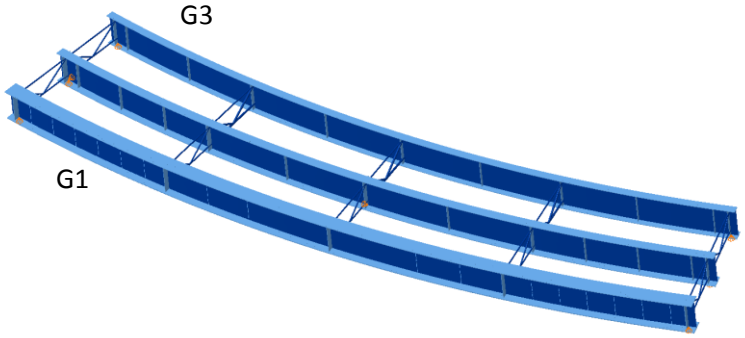

Figure C.5.1. EISCR1, Perspective view.

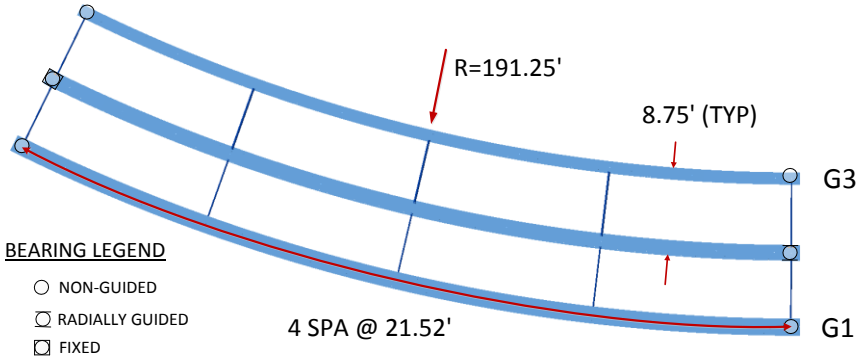

Figure C.5.2. EISCR1, Framing plan.

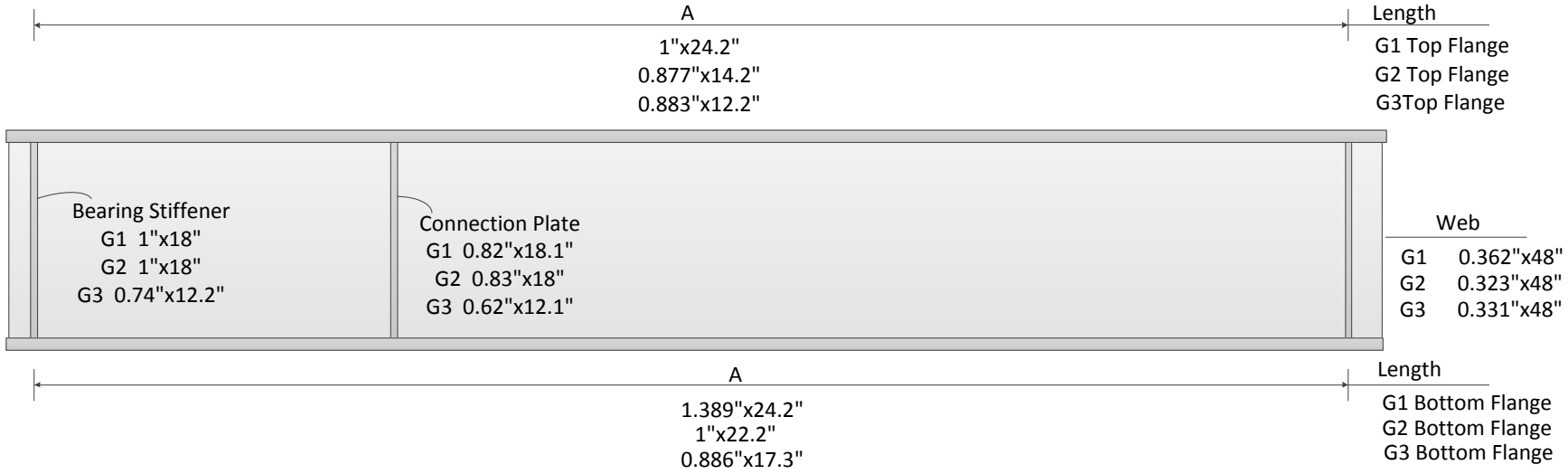

Figure C.5.3. EISCR1, Girder plate dimensions.

Table C.5.1. EISCR1, Girder plate lengths.

Girder	A
G1	96.025
G2	92
G3	87.975

Table C.5.2. EISCR1, Cross-frame member sizes.

Cross-Frame Type	Top Chord	Diagonals	Bottom Chord
Interior (V type)	HSS 5*x¼*	HSS 5*x¼*	HSS 5*x¼*
End (V type)	HSS 5*x¼*	HSS 5*x¼*	HSS 5*x¼*

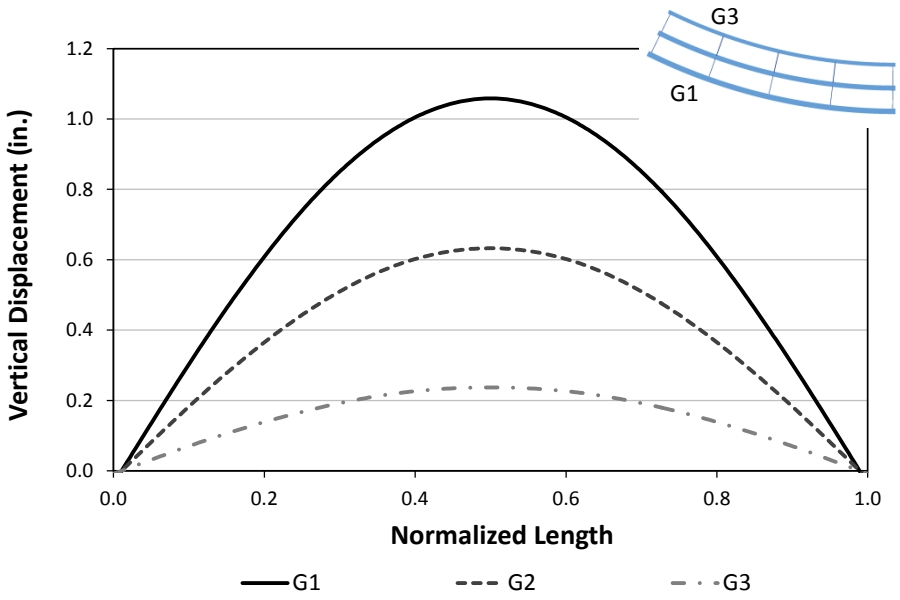

Figure C.5.4. EISCR1, Steel dead load cambers obtained from finite element analysis deflections.

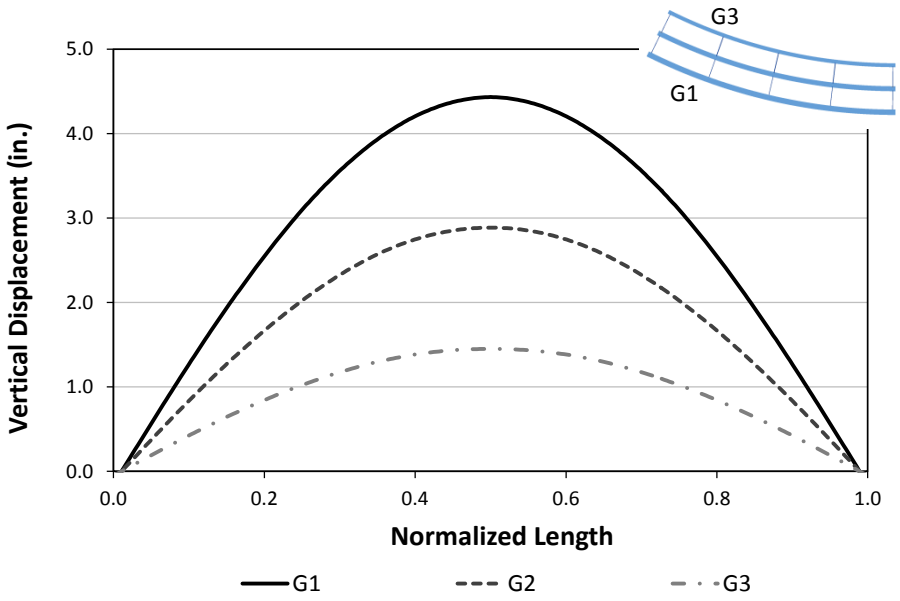

Figure C.5.5. EISCR1, Total dead load cambers obtained from finite element analysis solutions.

C.6. NISCR2

NISCR2 is a simple span horizontally curved I-girder bridge with radial abutments. Figure C.6.1 shows the perspective and plan views of NISCR2 with some key attributes. The girders are labeled from outside toward inside as Girder 1 to Girder 4 (G1-G4). Moreover, Fig. C.6.2 shows the framing plan of NISCR2. Girder plate dimensions are summarized in Fig. C.6.3 and girder plate lengths are shown in Table C.6.1. The intermediate cross-frames are X-type, and inverted V-type cross-frames are used at abutments. The cross-frame member sizes are summarized in Table C.6.2. Figure C.6.4 provides the steel dead load girder camber profile that is obtained from finite element analysis deflections. Also, Fig. C.6.5 provides total dead load girder camber profiles of NISCR2 obtained from line-girder and finite element solutions respectively.

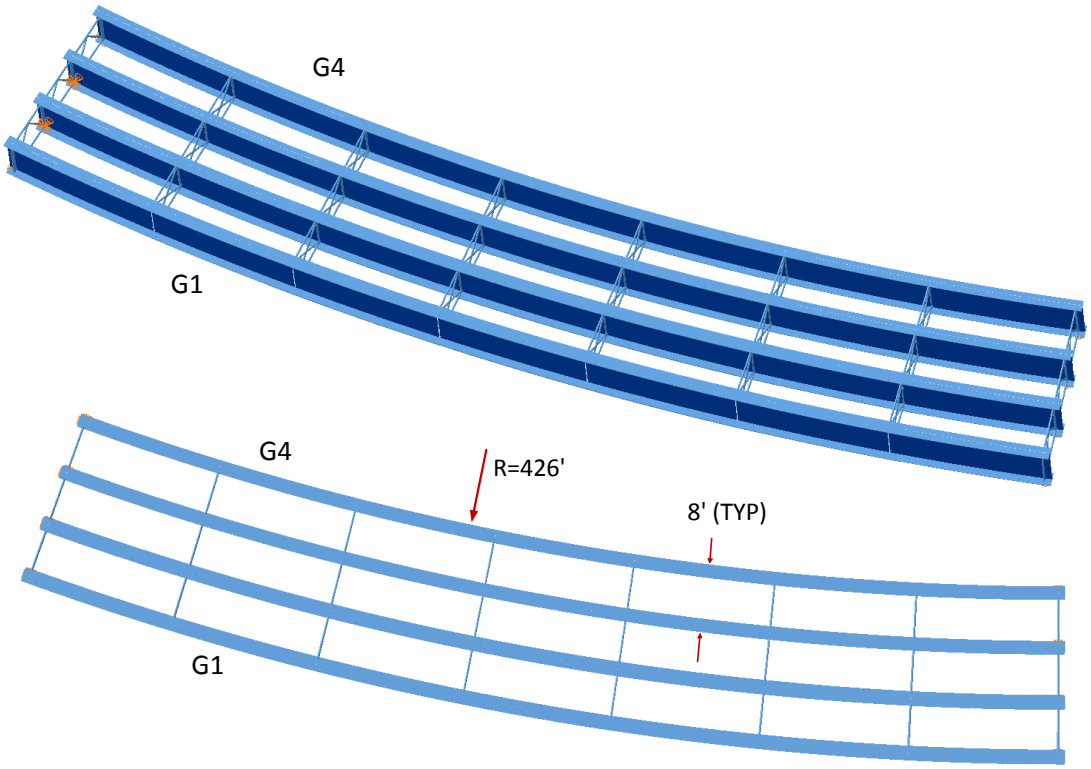

Figure C.6.1. NISCR2, Perspective and plan views.

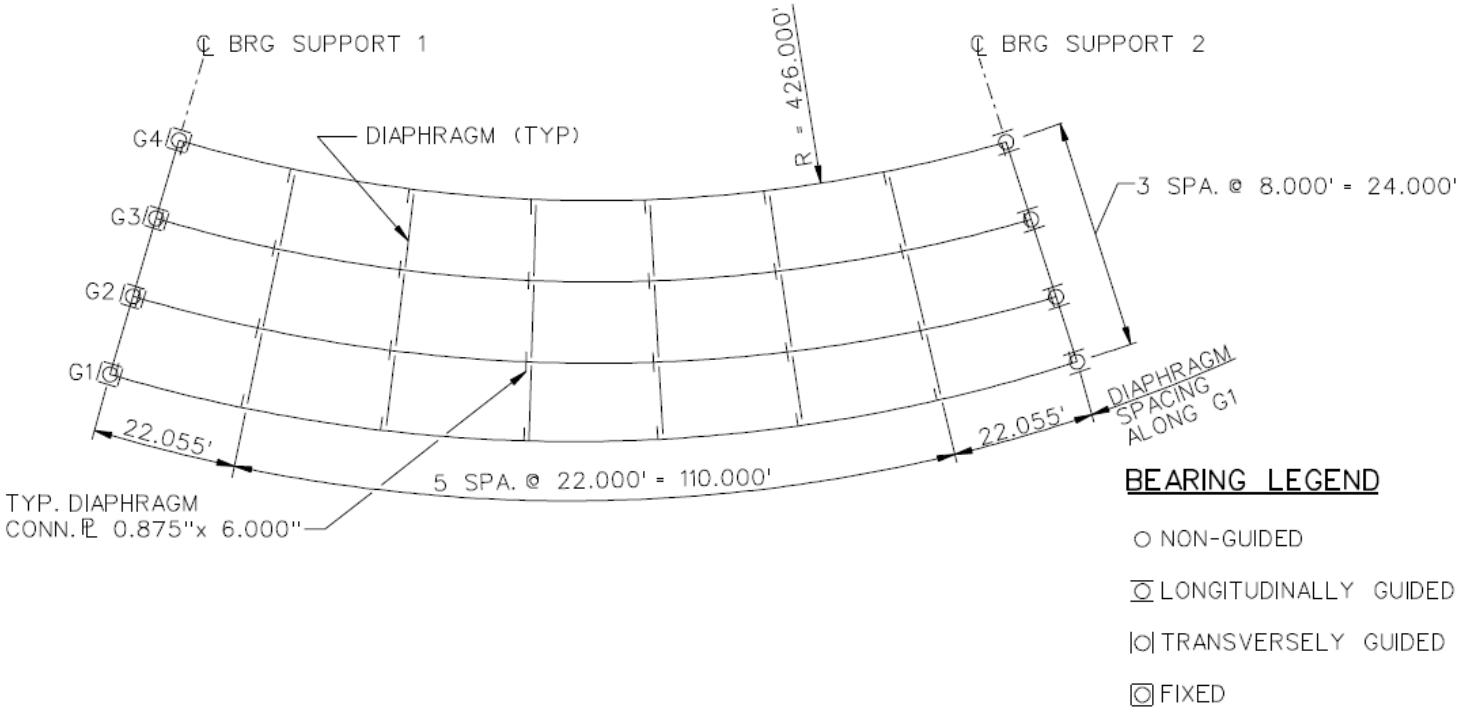

Figure C.6.2. NISCR2, Framing plan.

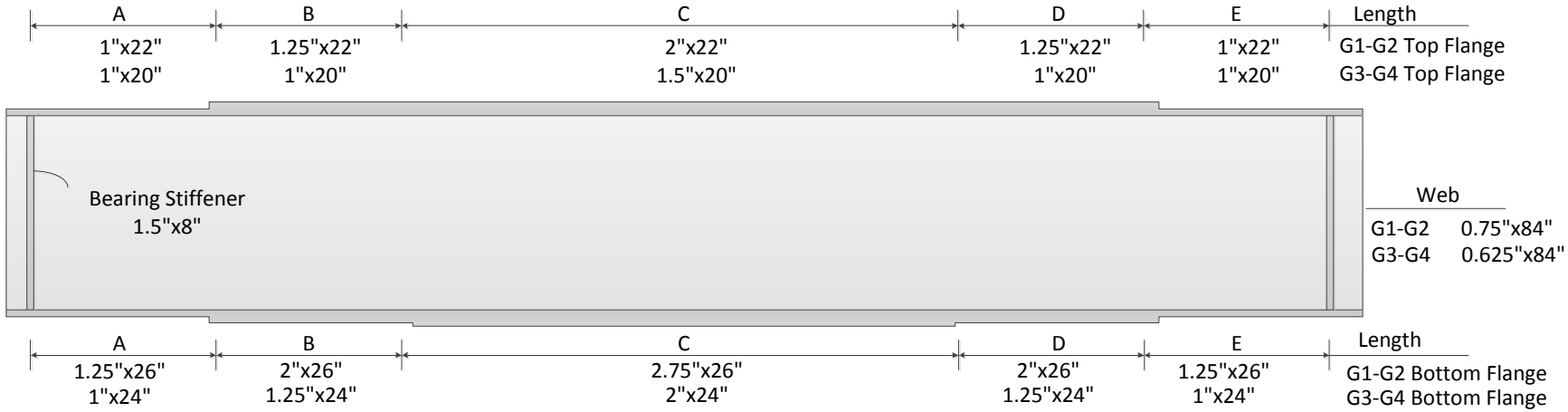

Figure C.6.3. NISCR2, Girder plate dimensions.

Table C.6.1. NISCR2, Girder plate lengths.

Girder	A	B	C	D	E
G1	20.0’	20.0’	74.1’	20.0’	20.0’
G2	19.6’	19.6’	72.8’	19.6’	19.6’
G3	19.3’	19.3’	71.5’	19.3’	19.3’
G4	18.9’	18.9’	70.2’	18.9’	18.9’

Table C.6.2. NISCR2, Cross-frame member sizes.

Cross-Frame Type	Top Chord	Diagonals	Bottom Chord
Interior (X type)	L6x6x0.75	L6x6x0.75	L6x6x0.75
End (Inverted V)	L6x6x0.75	L6x6x0.75	L6x6x0.75

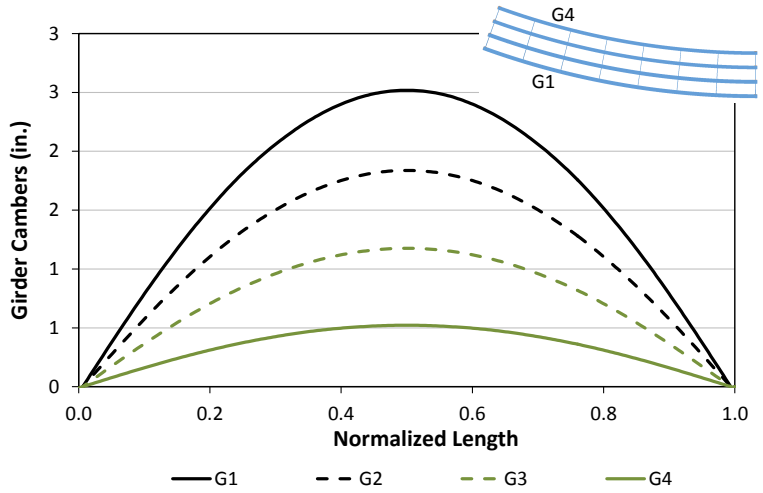

Figure C.6.4. NISCR2, Steel dead load cambers obtained from finite element analysis deflections.

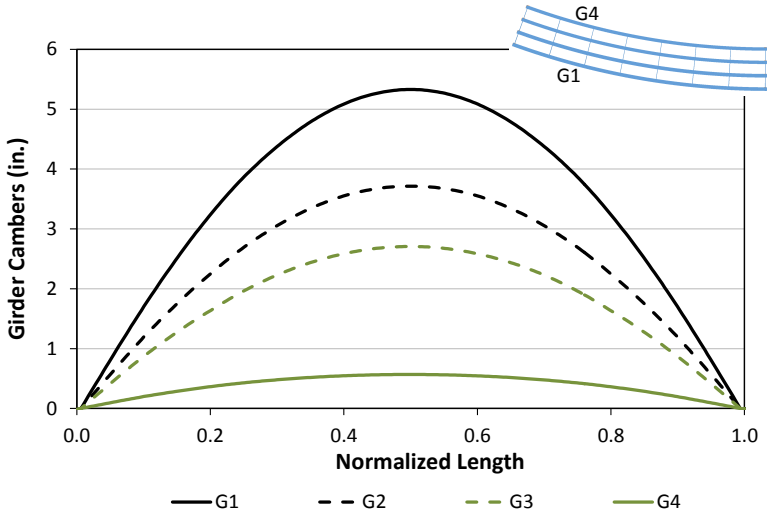

(i) Camber set based on line-girder analysis

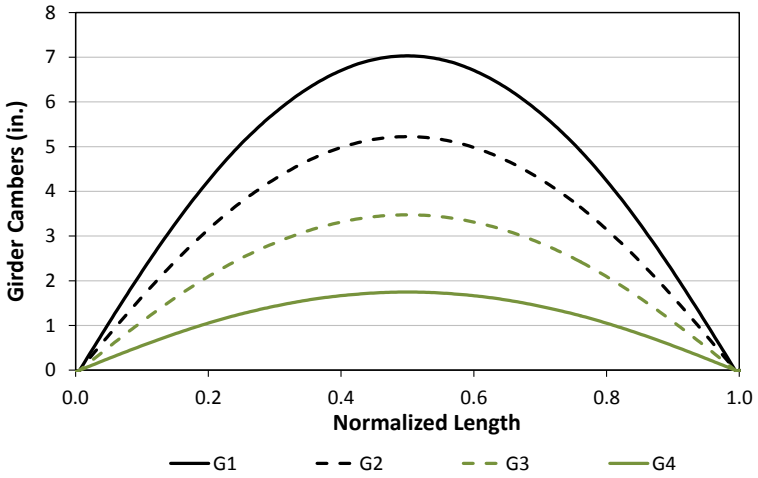

(ii) Camber set based on FEA deflections

Figure C.6.5. NISCR2, Total dead load cambers obtained from line-girder and finite element analysis solutions.

C.7. NISCR5

NISCR5 is a simple span horizontally curved I-girder bridge with radial abutments. Figure C.7.1 shows the perspective and plan view of NISCR5 with some key attributes. The girders are labeled from outside toward inside as Girder 1 to Girder 4 (G1-G4). Moreover, Fig. C.7.2 shows the framing plan of NISCR5. Girder plate dimensions are summarized in Fig. C.7.3 and girder plate lengths are shown in Table C.7.1. X-type cross-frames are used throughout the bridge. The cross-frame member sizes are summarized in Table C.7.2. Figures C.7.4 and C.7.5 provide the steel and total dead load girder camber profiles respectively. Girder cambers are obtained from finite element analysis deflections.

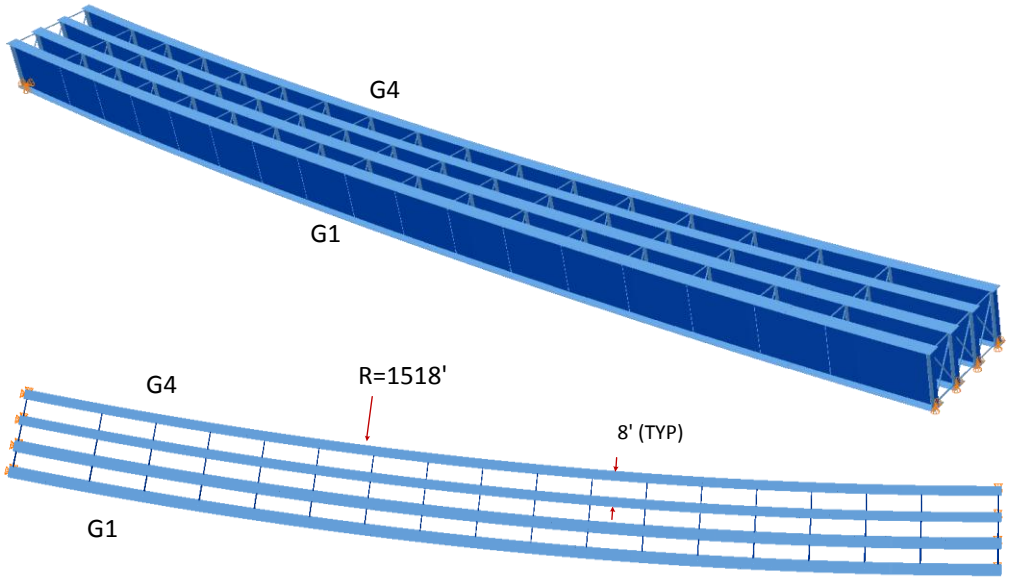

Figure C.7.1. NISCR5, Perspective and plan views.

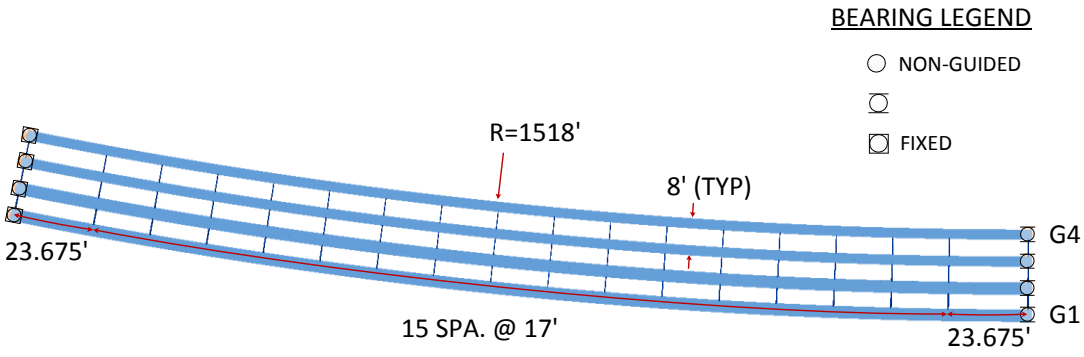

Figure C.7.2. NISCR5, Framing plan.

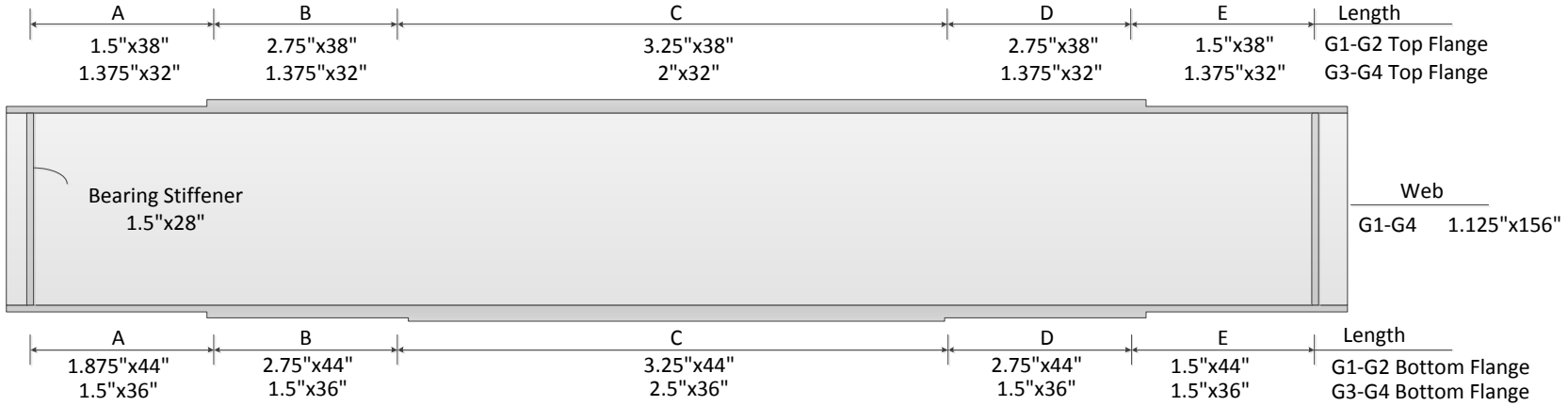

Figure C.7.3. NISCR5, Girder plate dimensions.

Table C.7.1. NISCR5, Girder plate lengths.

Girder	A	B	C	D	E
G1	32.175’	54.000’	130.000’	54.000’	32.175’
G2	32.008’	53.720’	129.326’	53.720’	32.008’
G3	31.841’	53.440’	128.651’	53.440’	31.841’
G4	31.674’	53.160’	127.977’	53.160’	31.674’

Table C.7.2. NISCR5, Cross-frame member sizes.

Cross-Frame Type	Top Chord	Diagonals	Bottom Chord
X	L6x6x1	L6x6x1	L6x6x1

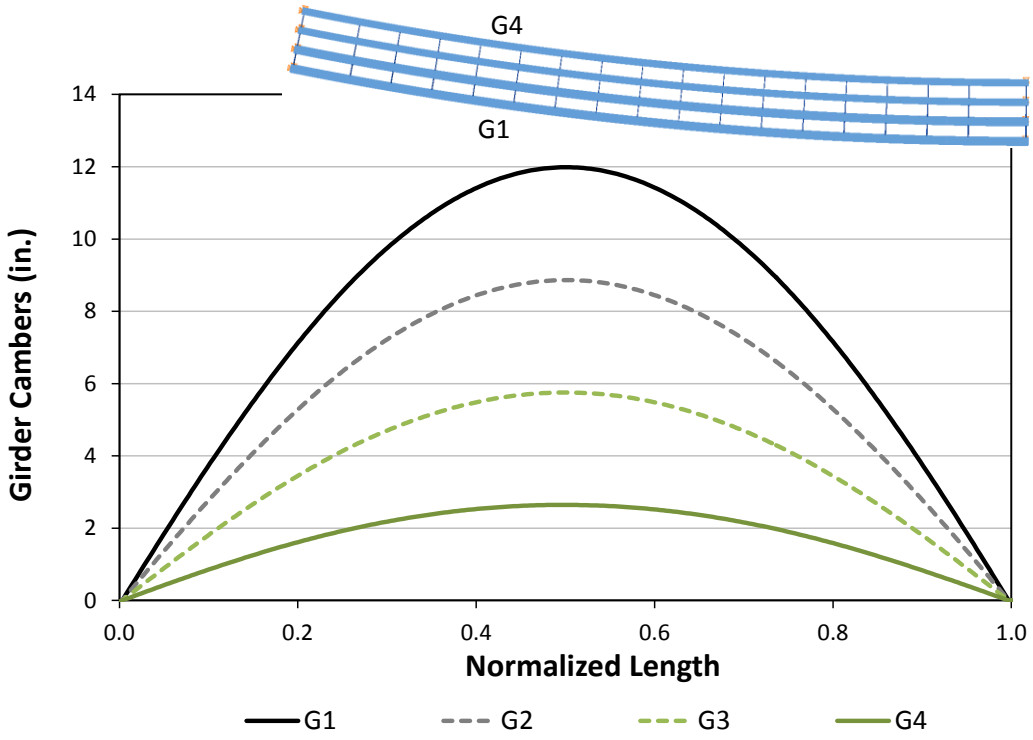

Figure C.7.4. NISCR5, Steel dead load cambers obtained from finite element analysis deflections.

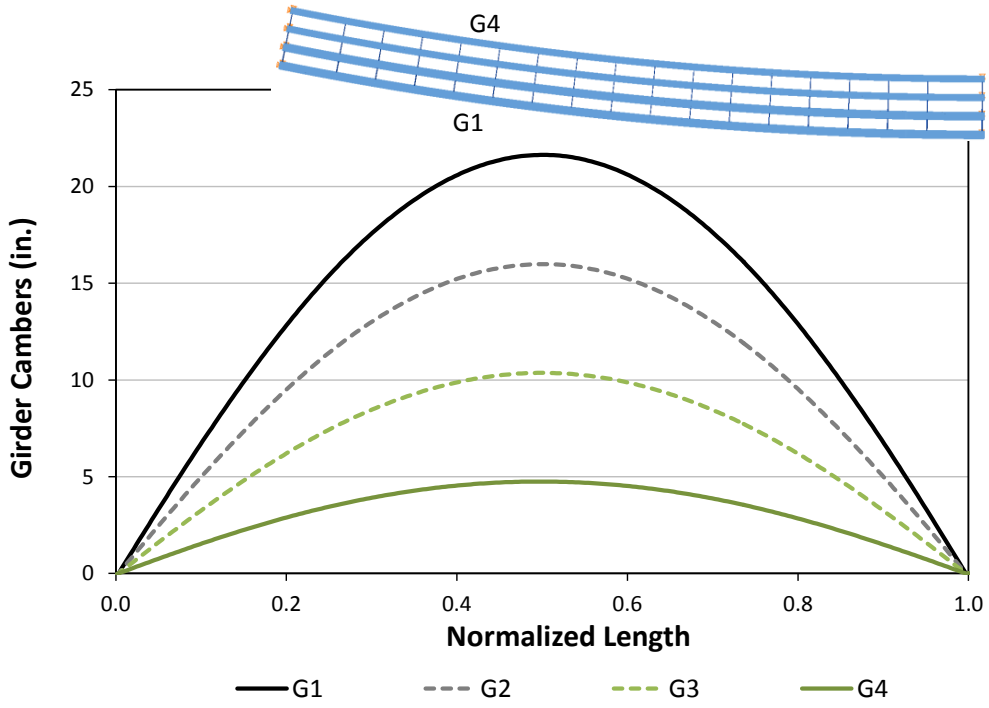

Figure C.7.5. NISCR5, Total dead load cambers obtained from finite element analysis solutions.

C.8. NISCS14

NISCS14 is a simple span curved bridge with 150ft span length with respect to its center line. Figure C.8.1 shows the perspective of NISCS14. The girders are labeled from outside toward inside as Girder 1 to Girder 9 (G1-G9). Moreover, Fig. C.8.2 provides the framing plan of NISCS14 with some key attributes. The left bearing has a skew angle of 53.7° whereas the right bearing is radial. Girder plate dimensions are illustrated in Fig. C.8.3 and girder plate lengths are shown in Table C.8.1. X-type cross-frames are used for NISCS14. The cross-frame member sizes are summarized in Table C.8.2. Figures C.8.4 and C.8.5 provide steel and total dead load girder camber profiles that are obtained from finite element analysis deflections.

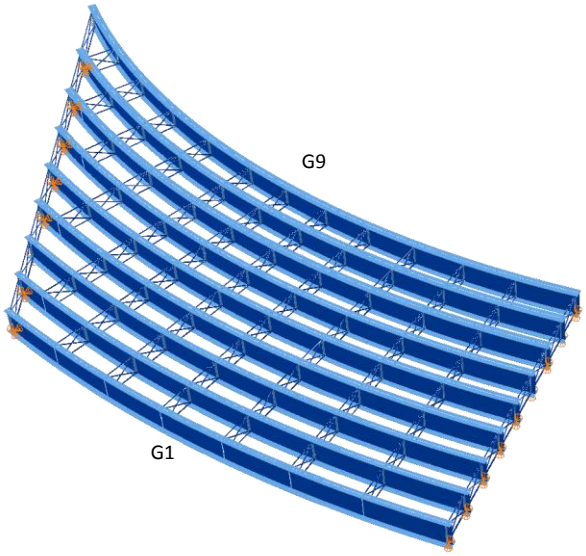

Figure C.8.1. NISCS14, Perspective view.

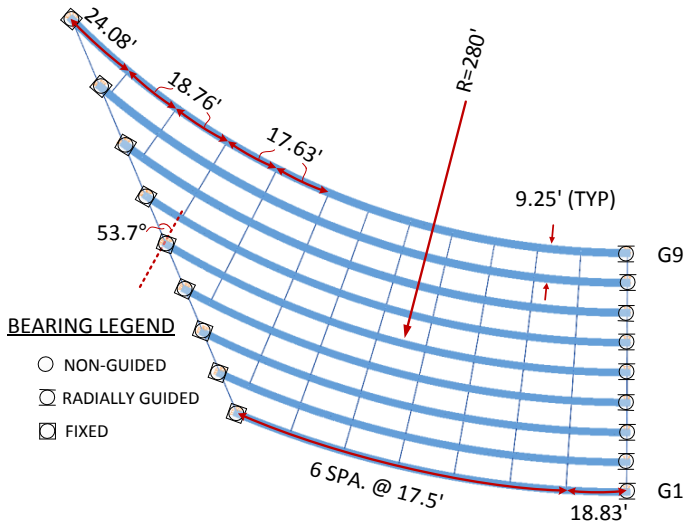

Figure C.8.2. NISCS14, Framing plan.

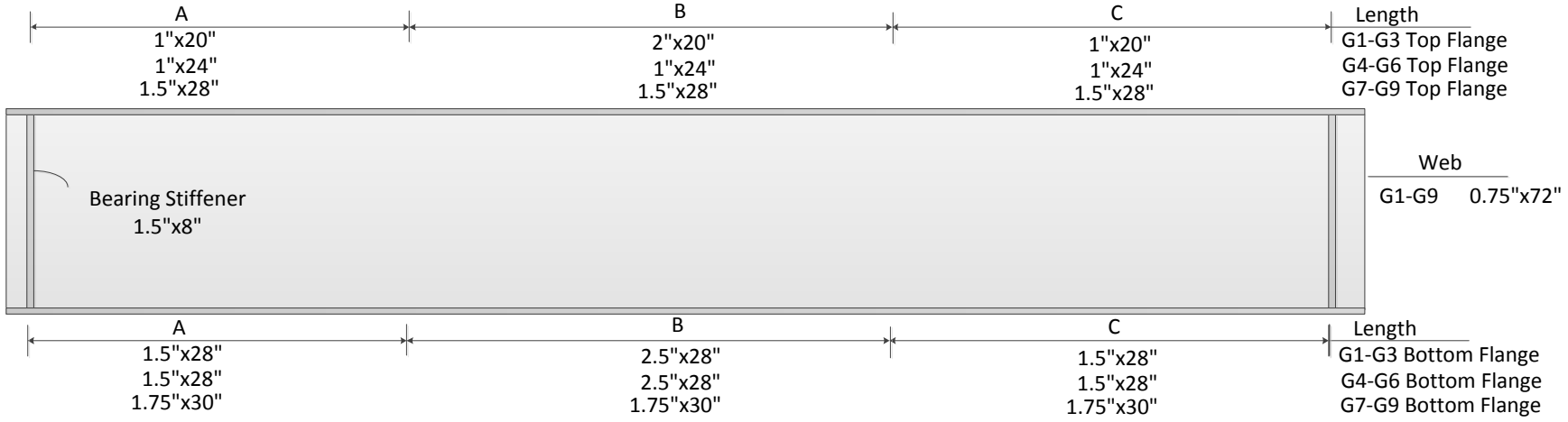

Figure C.8.3. NISCS14, Girder plate dimensions.

Table C.8.1. NISCS14, Girder plate lengths.

Girder Plate	Girder 1	Girder 2	Girder 3	Girder 4	Girder 5	Girder 6	Girder 7	Girder 8	Girder 9
A	30.0’	32.0’	30.0’	35.0’	35.0’	40.0’	40.0’	55.0’	70.0’
B	65.8’	69.7’	78.0’	67.7’	75.0’	78.1’	77.2’	73.1’	71.8’
C	28.0’	28.0’	28.0’	40.0’	40.0’	40.0’	50.0’	50.0’	50.0’

Table C.8.2. NISCS14, Cross-frame member sizes.

Cross-Frame Type	Top Chord	Diagonals	Bottom Chord
Interior (X)	WT6x29	WT6x29	WT6x29
End (X)	WT6x22.5	WT6x22.5	WT8x44.5

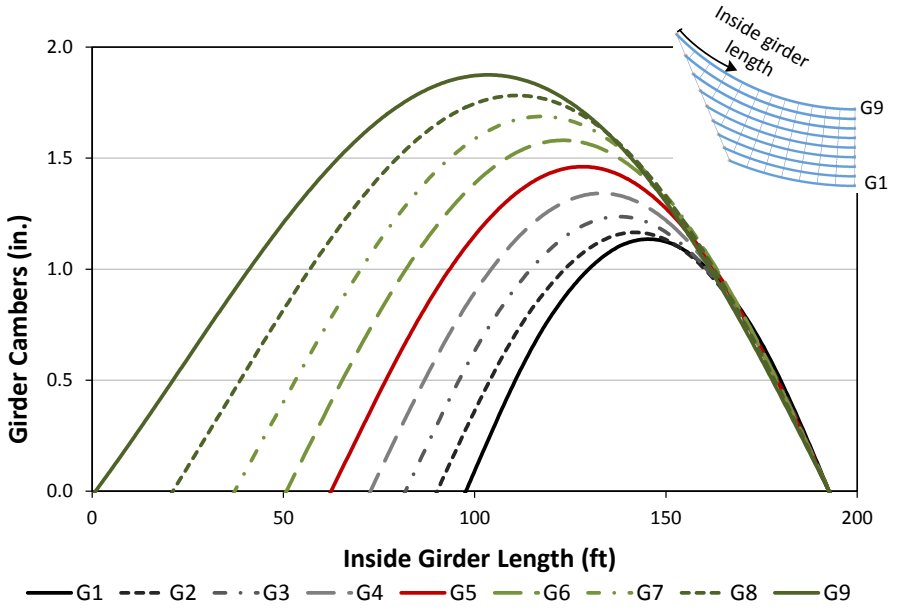

Figure C.8.4. NISCS14, Steel dead load cambers obtained from finite element analysis deflections.

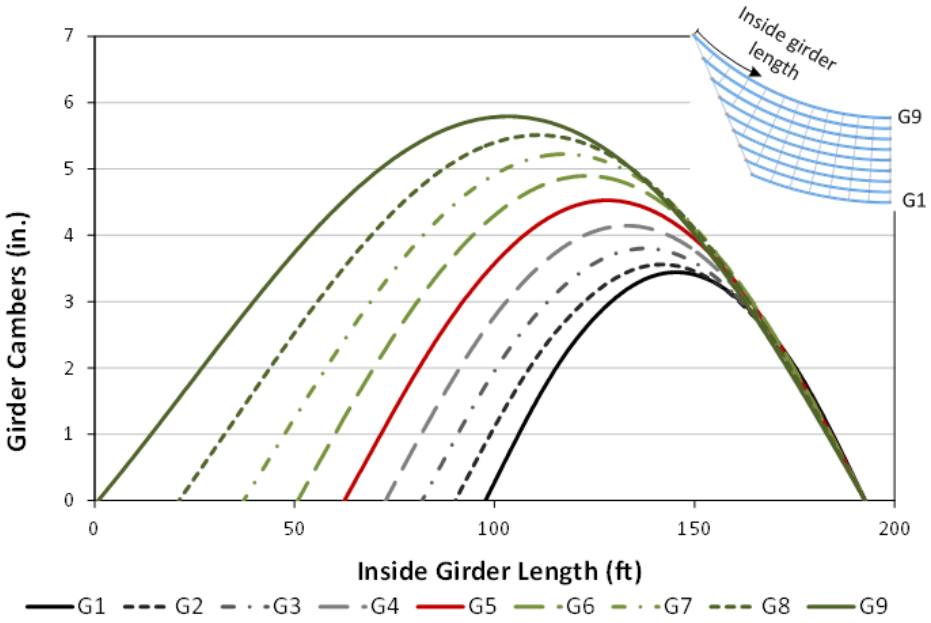

Figure C.8.5. NISCS14, Total dead load cambers obtained from finite element analysis deflections.

C.9. NISCS15

NISCS15 is a simple span curved bridge with 150ft span length with respect to its center line. Figure C.9.1 shows the perspective of NISCS15. The girders are labeled from outside toward inside as Girder 1 to Girder 9 (G1-G9). Moreover, Fig. C.9.2 provides the framing plan of NISCS15 with some key attributes. The left bearing has a skew angle of -35° whereas the right bearing is radial. Girder plate dimensions are illustrated in Fig. C.9.3 and girder plate lengths are shown in Table C.9.1. X-type cross-frames are used for NISCS15. The cross-frame member sizes are summarized in Table C.9.2. Figures C.9.4 and C.9.5 provide steel and total dead load girder camber profiles that are obtained from finite element analysis deflections.

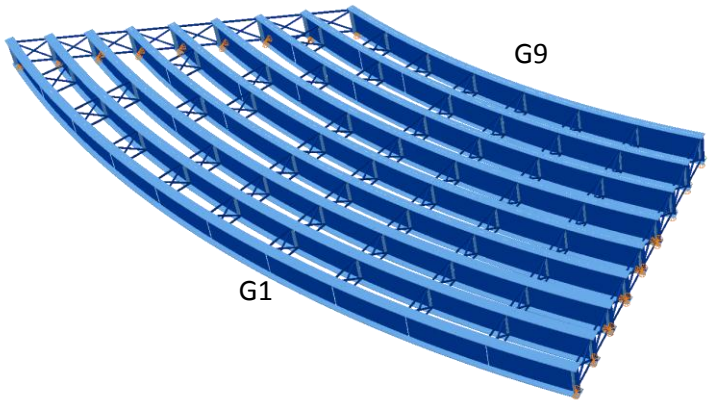

Figure C.9.1. NISCS15, Perspective view.

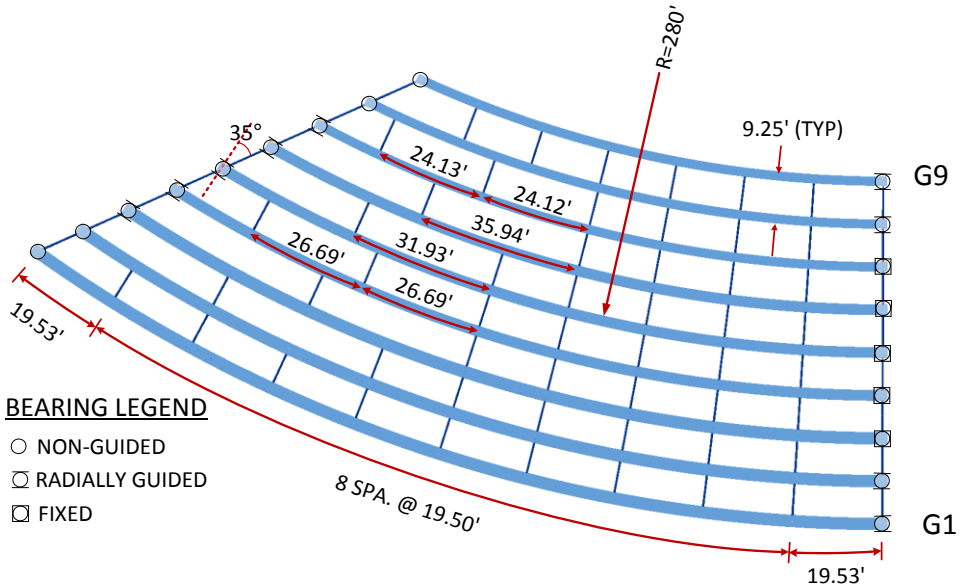

Figure C.9.2. NISCS15, Framing plan.

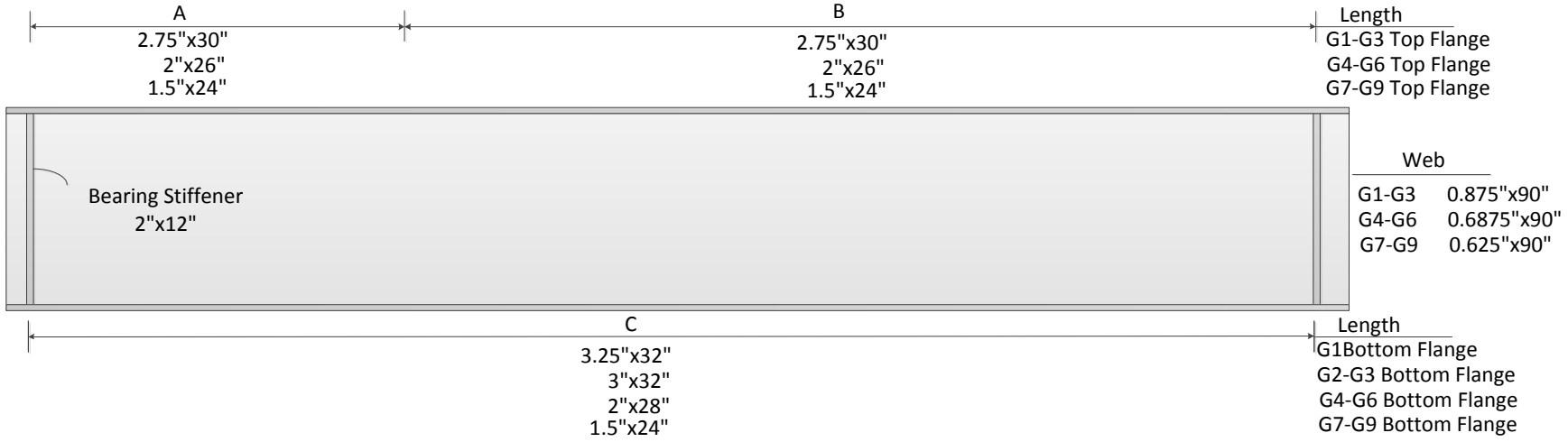

Figure C.9.3. NISCS15, Girder plate dimensions.

Table C.9.1. NISCS15, Girder plate lengths.

Girder Plate	Girder 1	Girder 2	Girder 3	Girder 4	Girder 5	Girder 6	Girder 7	Girder 8	Girder 9
A	65.1’	57.7’	50.3’	42.8’	35.2’	27.5’	-	-	-
B	130.0’	126.2’	122.4’	118.6’	114.8’	111.0’	-	-	-
C	195.1’	183.9’	172.7’	161.4’	150’	138.5’	126.9’	115.1’	103.2’

Table C.9.2. NISCS15, Cross-frame member sizes.

Cross-Frame Type	Top Chord	Diagonals	Bottom Chord
(X)	W12x87	WT9x79	W12x87

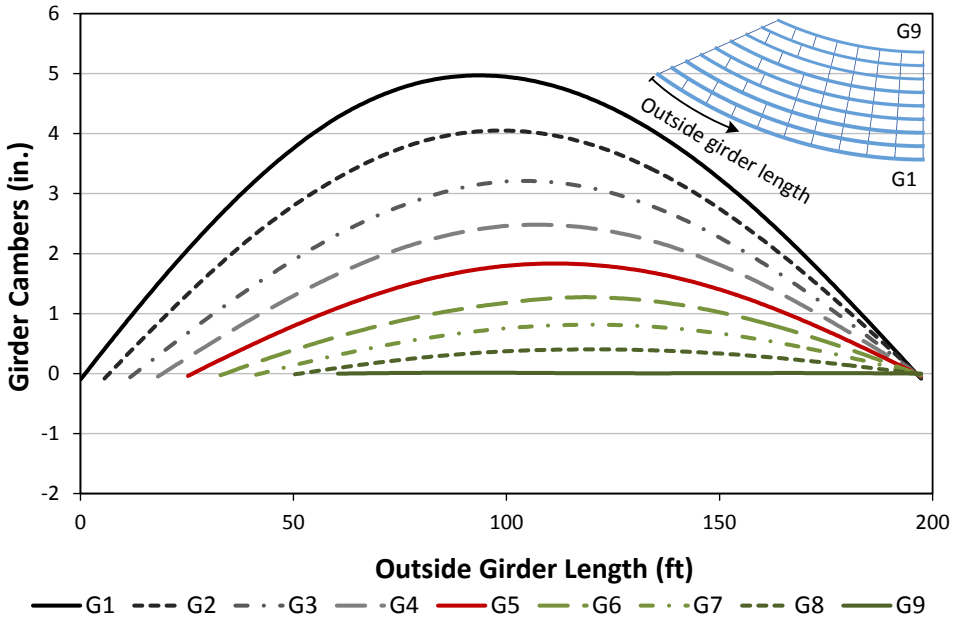

Figure C.9.4. NISCS15, Steel dead load cambers obtained from finite element analysis deflections.

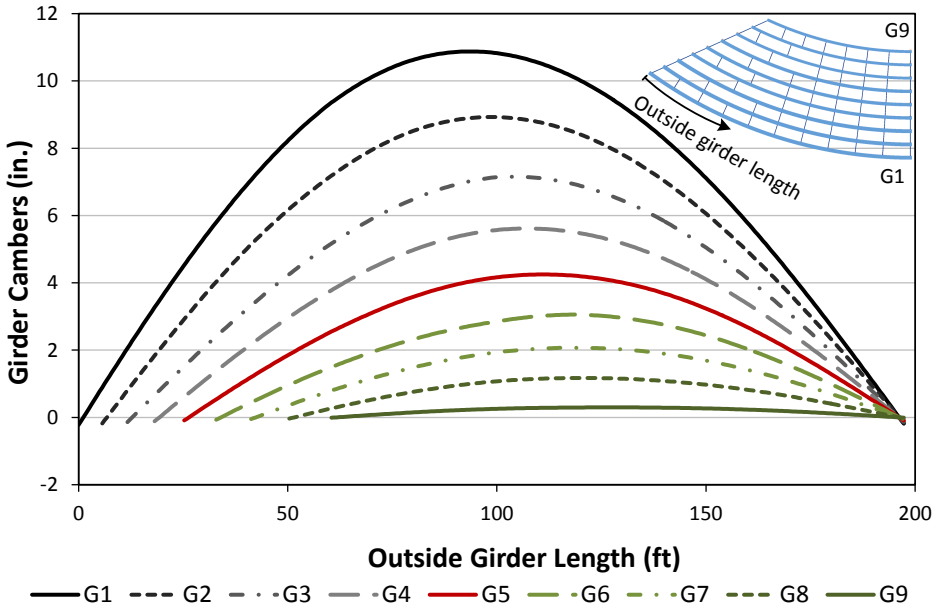

Figure C.9.5. NISCS15, Total dead load cambers obtained from finite element analysis deflections.

C.10. NISCS37

NISCS37 is a simple span curved bridge with 300ft span length with respect to its center line. Figure C.10.1 shows the perspective of NISCS37. The girders are labeled from outside toward inside as Girder 1 to Girder 9 (G1-G9). Moreover, Fig. C.10.2 provides the framing plan of NISCS37 with some key attributes. The left bearing has a skew angle of 35° whereas the right bearing is radial. Girder plate dimensions are illustrated in Fig. C.10.3 and girder plate lengths are shown in Table C.10.1. X-type cross-frames are used for NISCS37. The cross-frame member sizes are summarized in Table C.10.2. Figures C.10.4 and C.10.5 provide steel and total dead load girder camber profiles along the length of the inside girder. Girder cambers are obtained from finite element analysis deflections.

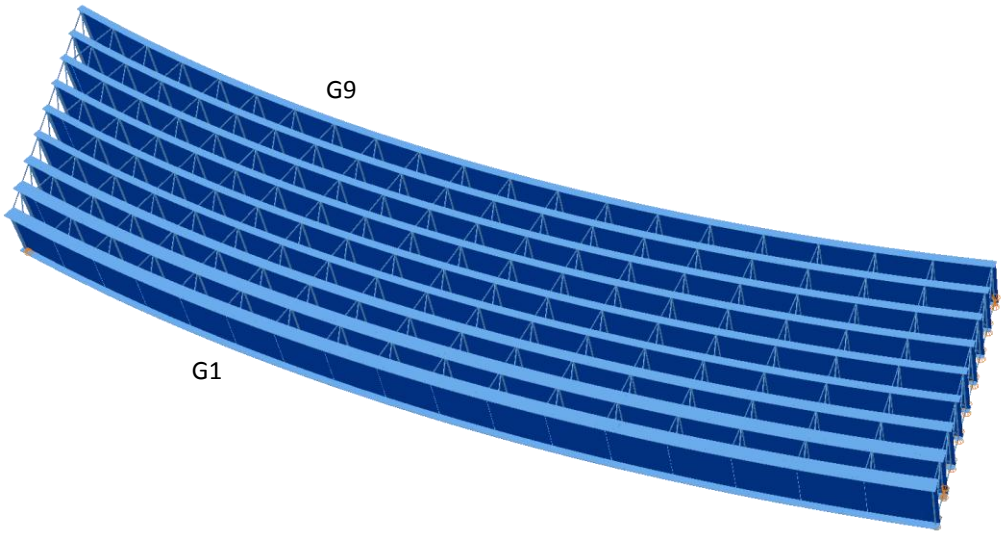

Figure C.10.1. NISCS37, Perspective view.

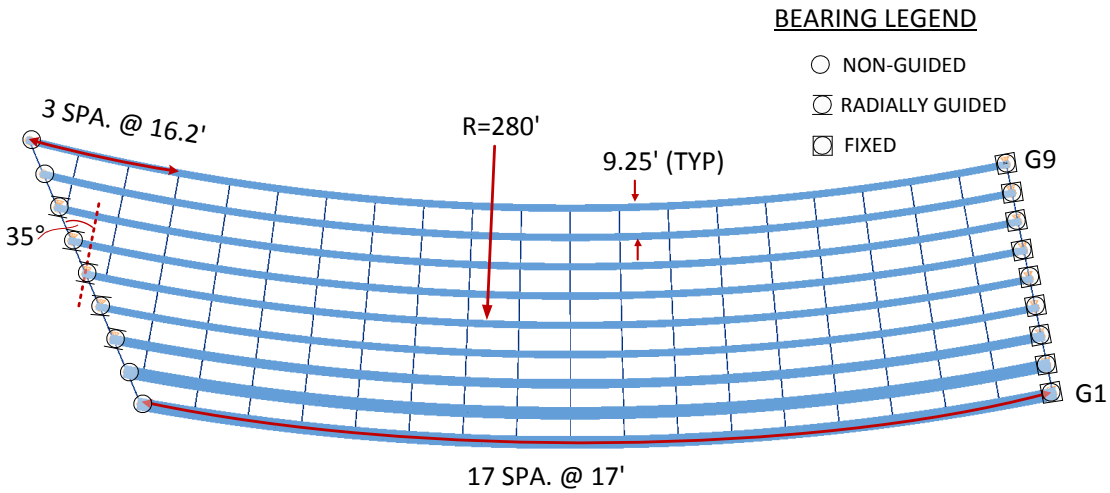

Figure C.10.2. NISCS37, Framing plan.

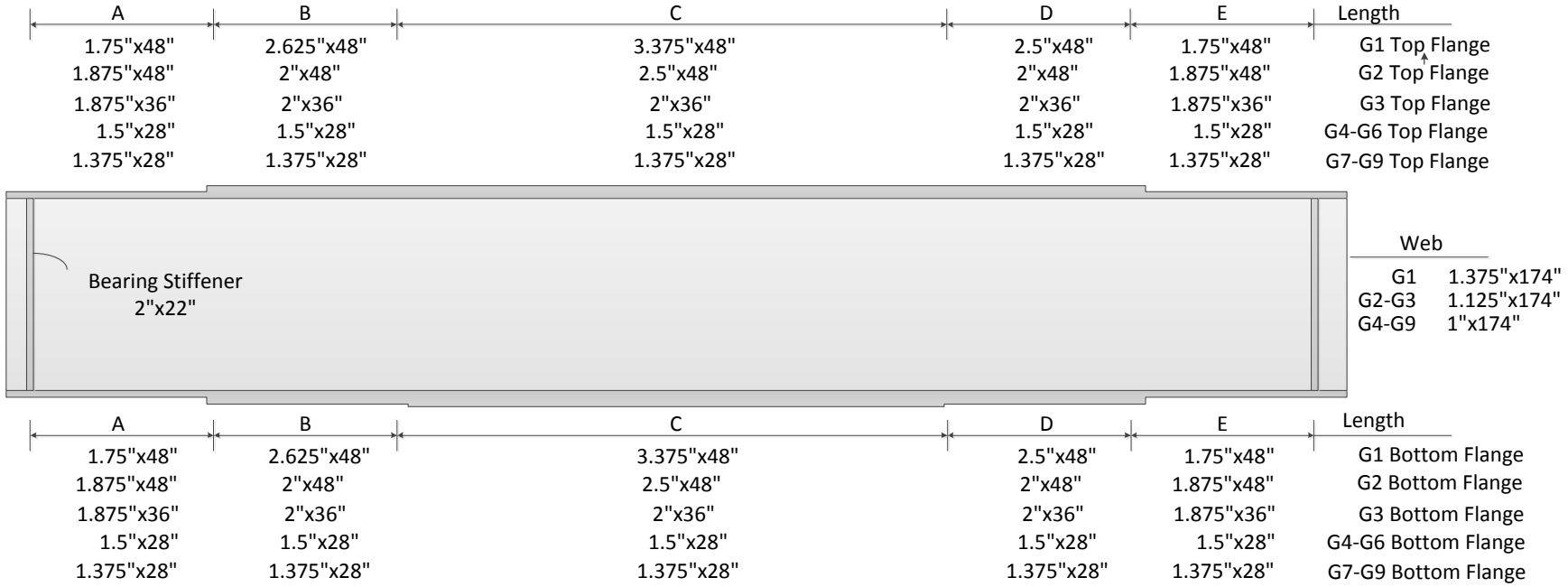

Figure C.10.3. NISCS37, Girder plate dimensions.

Table C.10.1. NISCS37, Girder plate lengths.

Girder Plate	Girder 1	Girder 2	Girder 3	Girder 4	Girder 5	Girder 6	Girder 7	Girder 8	Girder 9
A	35.0’	35.0’	35.0’	35.0’	35.0’	35.0’	35.0’	35.0’	35.0’
B	44.8’	46.1’	47.4’	48.7’	50.0’	51.3’	52.7’	54.1’	55.5’
C	130.0’	130.0’	130.0’	130.0’	130.0’	130.0’	130.0’	130.0’	130.0’
D	44.8’	46.1’	47.4’	48.7’	50.0’	51.3’	52.7’	54.1’	55.5’
E	35.0’	35.0’	35.0’	35.0’	35.0’	35.0’	35.0’	35.0’	35.0’

Table C.10.2. NISCS37, Cross-frame member sizes.

Cross-Frame Type	Top Chord	Diagonals	Bottom Chord
X	WT6x53	WT6x53	WT6x53

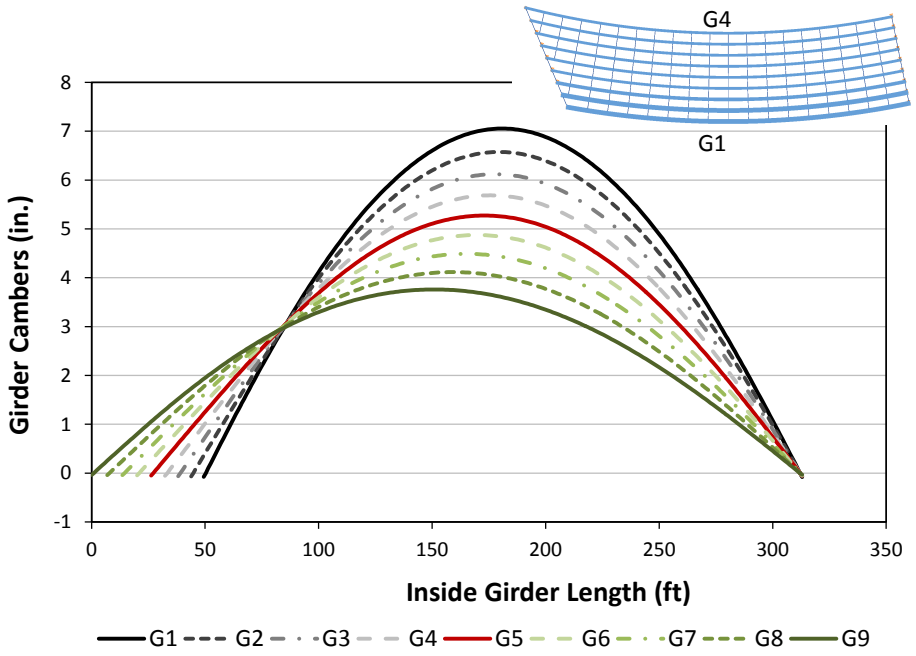

Figure C.10.4. NISCS37, Steel dead load cambers obtained from finite element analysis deflections.

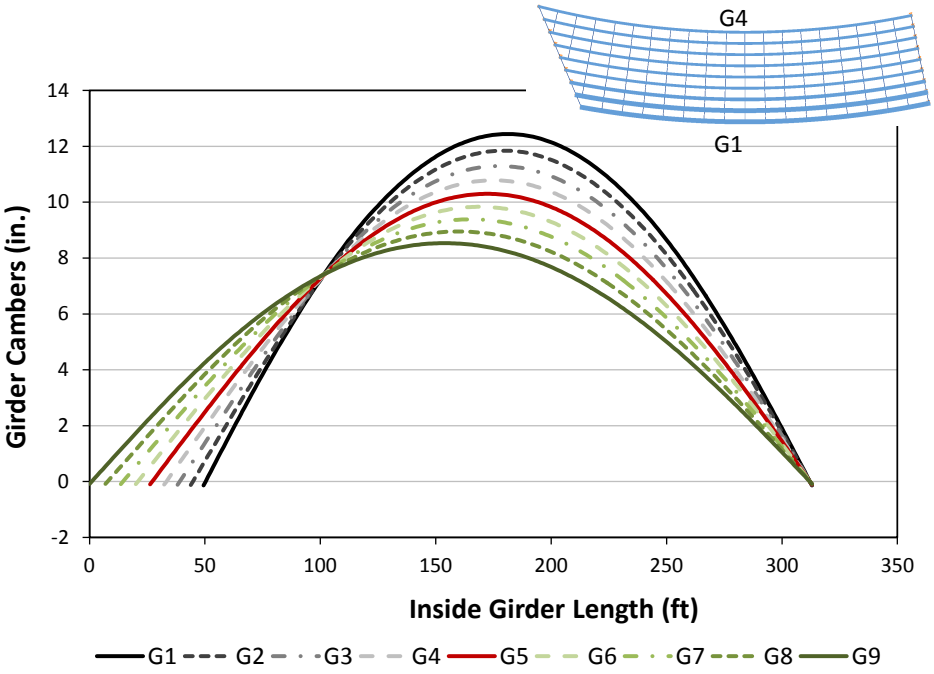

Figure C.10.5. NISCS37, Total dead load cambers obtained from finite element analysis deflections.

C.11. EICCR11

EICCR11, The Ford City bridge represents an important model case where due to combinations of long spans, deep girders with relatively close spacing compared to the girder depths, and relatively tight curvature, substantial erection challenges had to be addressed in the erection engineering of the structure. This bridge has been studied thoroughly in prior work by Chavel and Earls (2006a & b & 2001) and by Chang (2006). Figure C.11.1 shows the perspective and plan view of EICCR11 with some key attributes. EICCR11 is a three span continuous I-girder bridge with the span lengths of 321ft, 418ft and 324ft. The girders are labeled from bottom toward top as Girder 1 to Girder 4 (G1-G4). Although EICCR11 has flange lateral bracing system, they are removed for the purposes of investigating the effect of cross-frame detailing methods. Moreover, Fig. C.11.2 shows the framing plan of EICCR11. Girder plate dimensions and girder plate lengths are shown in Tables C.11.1 through C.11.3. X-type cross-frames are throughout the bridge. The cross-frame member sizes are summarized in Table C.11.4. Cross-frame #1 (CF1) is used between pier 2 and abutment 2, cross-frame #2 (CF2) is used between abutment 1 and pier 1 as well as between piers 1 and 2, cross-frame #3 (CF3) is used at abutments 1 and 2 and finally, cross-frame #4 (CF4) is used at piers 1 and 2. Figure C.11.3 provides the steel dead load girder camber profile that is obtained from finite element analysis deflections. Also, Fig. C.11.4 provides total dead load camber profiles of EICCR11 obtained from finite element solutions respectively.

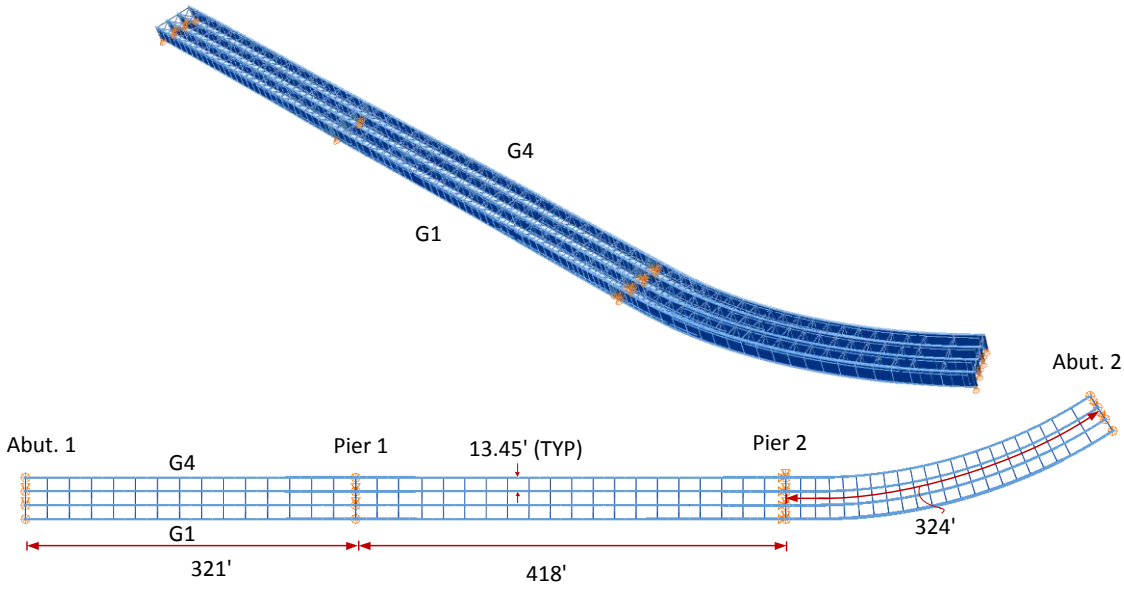

Figure C.11.1. EICCR11, Perspective view.

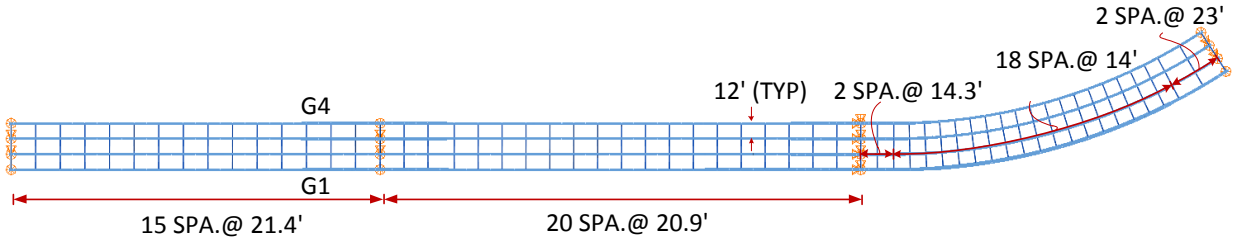

Figure C.11.2. EICCR11, Framing plan.

Table C.11.1. EICCR11, Girder dimensions and girder plate lengths for Girders 1 and 2.

Girder 1					Girder 2				
$b_{f.Top}$ (in)	$t_{f.Top}$ (in)	$b_{f.Bot}$ (in)	$t_{f.Bot}$ (in)	Length (ft)	$b_{f.Top}$ (in)	$t_{f.Top}$ (in)	$b_{f.Bot}$ (in)	$t_{f.Bot}$ (in)	Length (ft)
27.6	1.1	27.6	1.0	51.8	27.6	1.1	27.6	1.0	51.8
27.6	2.0	27.6	2.0	137.1	27.6	1.6	27.6	1.6	137.1
27.6	1.5	27.6	1.5	65.6	27.6	1.5	27.6	1.5	65.6
31.5	1.5	31.5	2.0	43.8	31.5	1.6	31.5	2.0	43.8
31.5	2.8	31.5	2.8	50.0	31.5	2.8	31.5	2.8	50.0
31.5	1.5	31.5	2.0	34.5	31.5	1.6	31.5	2.0	33.5
27.6	2.2	27.6	2.2	222.6	27.6	1.5	27.6	1.5	223.6
31.5	2.8	31.5	2.8	75.6	27.6	2.2	27.6	2.2	75.6
35.4	2.4	36.4	2.4	34.0	35.4	2.2	35.4	2.2	34.0
35.4	3.1	36.4	3.1	50.0	35.4	3.1	35.4	3.1	50.0
35.4	2.4	36.4	2.4	5.8	35.4	2.2	35.4	2.2	5.8
31.5	2.0	31.5	3.5	56.3	27.6	1.6	27.6	1.6	54.9
35.4	3.9	42.3	3.9	214.9	27.6	3.5	31.5	3.5	209.5
35.4	2.4	36.4	2.4	36.9	35.4	2.2	35.4	2.2	36.0

Table C.11.2. EICCR11, Girder dimensions and girder plate lengths for Girders 1 and 2.

Girder 3					Girder 4				
$b_{f.Top}$ (in)	$t_{f.Top}$ (in)	$b_{f.Bot}$ (in)	$t_{f.Bot}$ (in)	Length (ft)	$b_{f.Top}$ (in)	$t_{f.Top}$ (in)	$b_{f.Bot}$ (in)	$t_{f.Bot}$ (in)	Length (ft)
27.6	1.1	27.6	1.0	51.8	27.6	1.1	27.6	1.0	51.8
27.6	1.8	27.6	1.8	137.1	27.6	2.0	27.6	2.0	137.1
27.6	1.5	27.6	1.5	65.6	27.6	1.5	27.6	1.5	65.6
31.5	1.6	31.5	2.0	43.8	31.5	1.8	31.5	2.0	43.8
31.5	2.8	31.5	2.8	50.0	31.5	3.1	31.5	3.1	50.0
31.5	1.8	31.5	2.0	33.5	31.5	1.8	31.5	2.0	33.5
27.6	1.5	27.6	1.5	299.2	27.6	1.5	27.6	1.5	74.8
31.5	1.6	31.5	2.0	34.0	27.6	2.8	27.6	2.8	148.8
31.5	3.1	31.5	3.1	50.0	27.6	1.5	27.6	1.5	75.6
31.5	1.6	31.5	2.0	5.8	31.5	1.6	31.5	2.0	34.0
27.6	1.5	27.6	1.5	257.5	31.5	2.8	31.5	2.8	50.0
31.5	1.6	31.5	2.0	35.0	31.5	1.6	31.5	2.0	5.8
					27.6	1.5	27.6	1.5	176.1
					27.6	1.8	27.6	1.8	74.5
					31.5	1.6	31.5	2.0	34.1

Table C.11.3. EICCR11, Girder web dimensions and girder plate lengths.

Girder 1			Girder 2			Girder 3			Girder 4		
D (in)	t_w (in)	Length (ft)	D (in)	t_w (in)	Length (ft)	D (in)	t_w (in)	Length (ft)	D (in)	t_w (in)	Length (ft)
168.3	0.6	51.8	168.3	0.6	51.8	168.3	0.6	51.8	168.3	0.6	51.8
168.3	0.7	202.7	168.3	0.7	202.7	168.3	0.7	202.7	168.3	0.7	202.7
168.3	0.8	127.8	168.3	0.8	127.8	168.3	0.8	127.8	168.3	0.8	127.8
168.3	0.7	298.7	168.3	0.7	298.7	168.3	0.7	298.7	168.3	0.7	298.7
168.3	1.1	397.9	168.3	1.1	89.8	168.3	1.1	89.8	168.3	0.8	89.8
			168.3	1.0	264.3	168.3	1.0	257.5	168.3	0.7	250.6
			168.3	1.1	36.0	168.3	1.1	35.0	168.3	0.8	34.1

Table C.11.4. EICCR11, Cross-frame member sizes.

Cross-Frame #	Top Chord	Diagonals	Bottom Chord
1	W8x40	W8x40	W8x40
2	WT6x25	WT7x34	WT7x34
3	W16x50	WT7x34	W8x40
4	W12x50	W12x50	W12x50

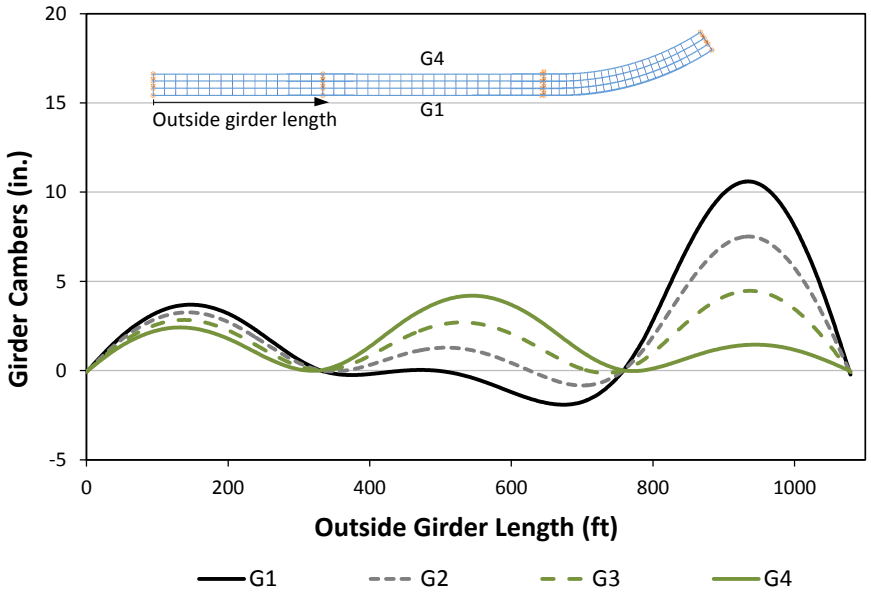

Figure C.11.3. EICCR11, Steel dead load cambers obtained from finite element analysis deflections.

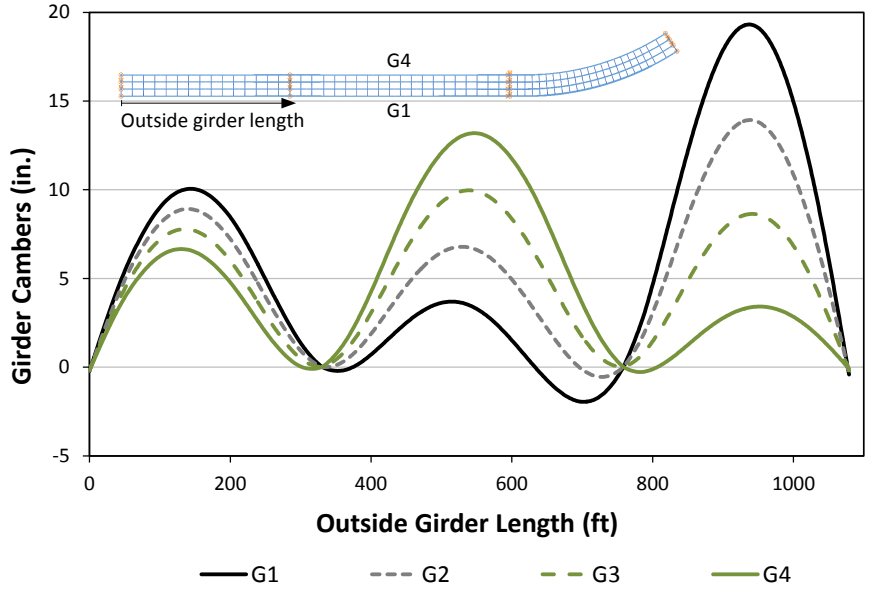

Figure C.11.4. EICCR11, Total dead load cambers obtained from finite element analysis deflections.

APPENDIX D.

DETAILED FEA RESULTS FOR SELECTED CASE STUDY BRIDGES

This appendix presents detailed steel and total dead load finite element analysis results of the selected bridges constructed with different types of cross-frame detailing, with focus on

- girder layovers
- girder vertical deflections
- maximum amplitude of the component axial forces in each of the cross-frames
- girder major-axis and flange lateral bending stresses

Selected bridges cover the range of different bridges categories. Differential steel and total dead load cambers between the girders are provided for each bridge

D.1. NISSS54

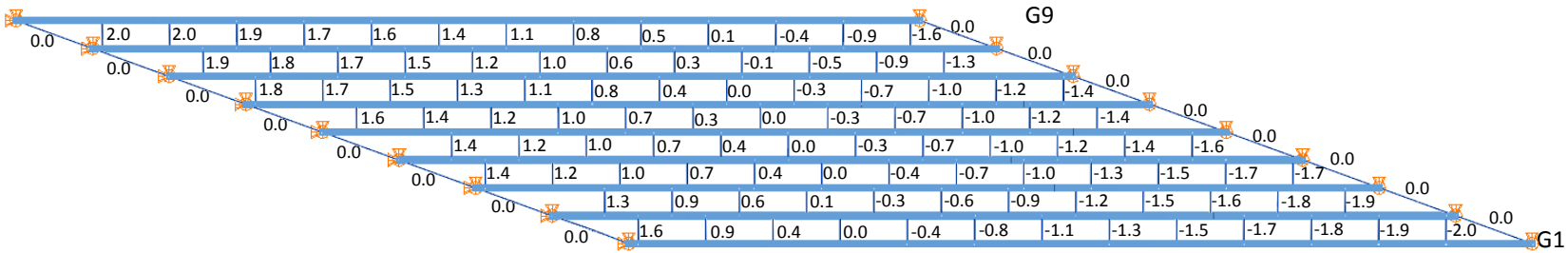

(i) Steel dead load

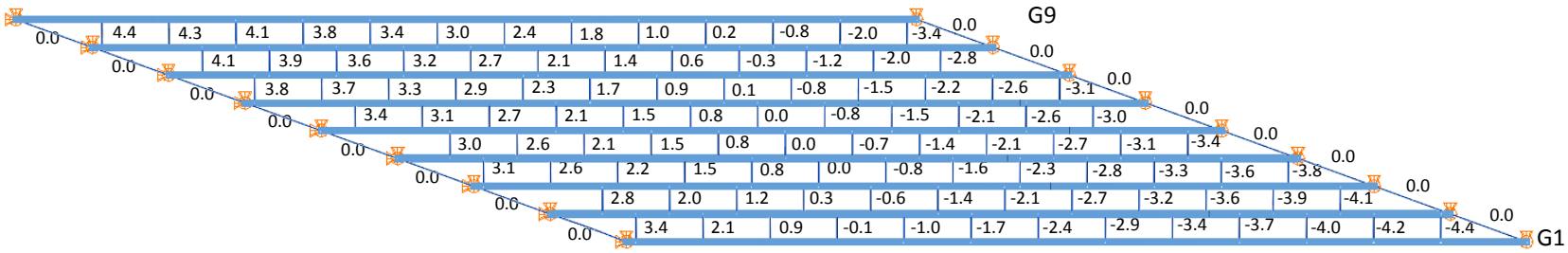

(ii) Total dead load

Figure D.1.1. NISSS54, Differential cambers between girders from steel and total dead load deflections.

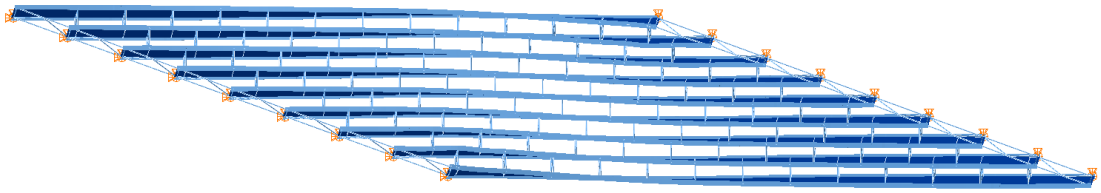

(i) NLF

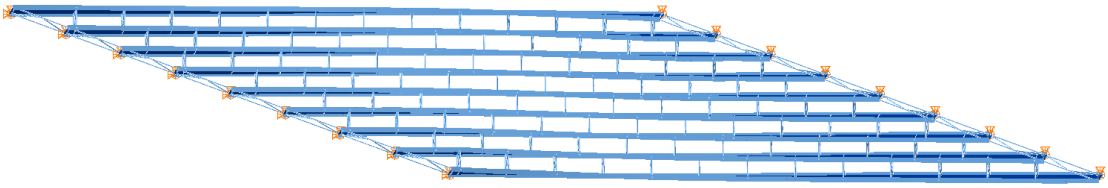

(ii) SDLF

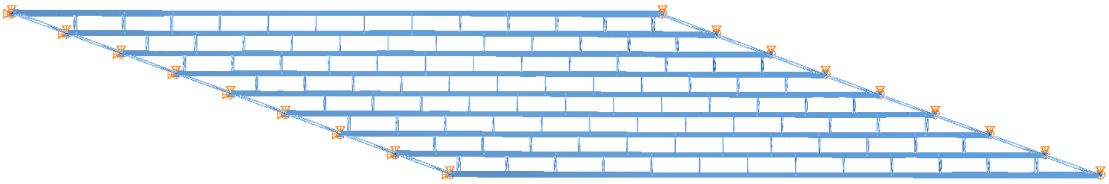

(iii) TDLF

Figure D.1.2. NISSS54, Deflected shape under total dead load for different detailing methods (magnified by 10x).

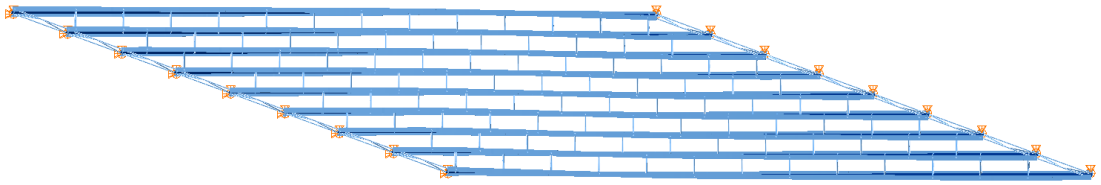

(i) NLF

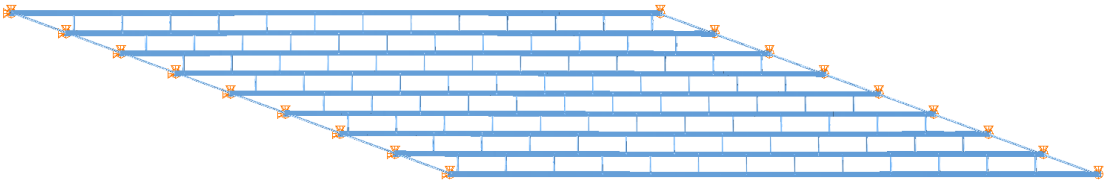

(ii) SDLF

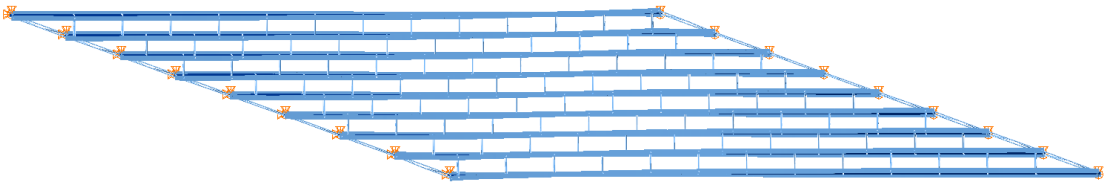

(iii) TDLF

Figure D.1.3. NISSS54, Deflected shape under steel dead load for different detailing methods (magnified by 10x).

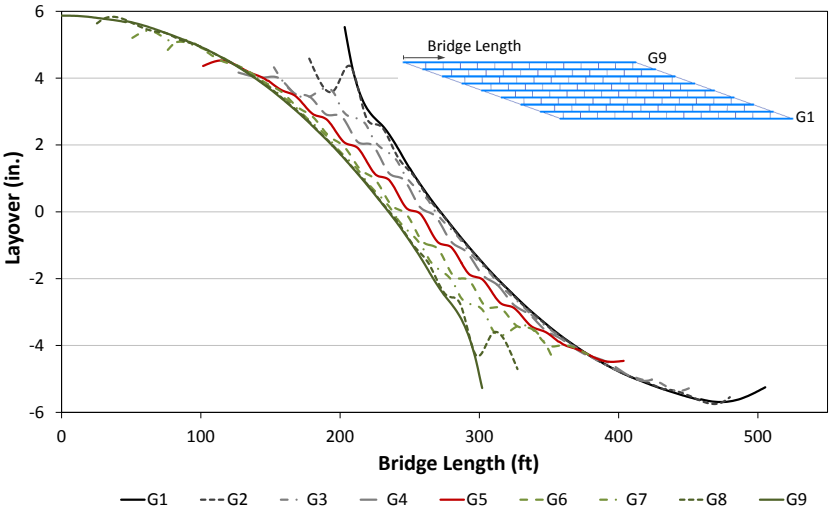

(i) NLF

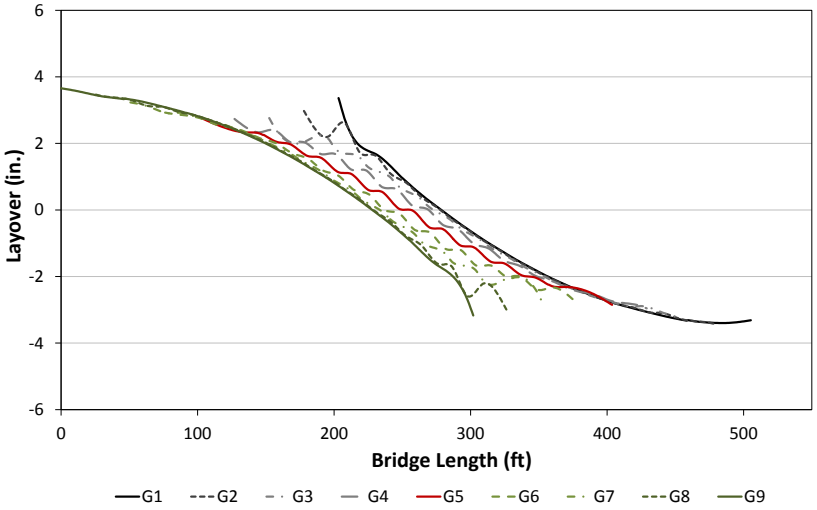

(ii) SDLF

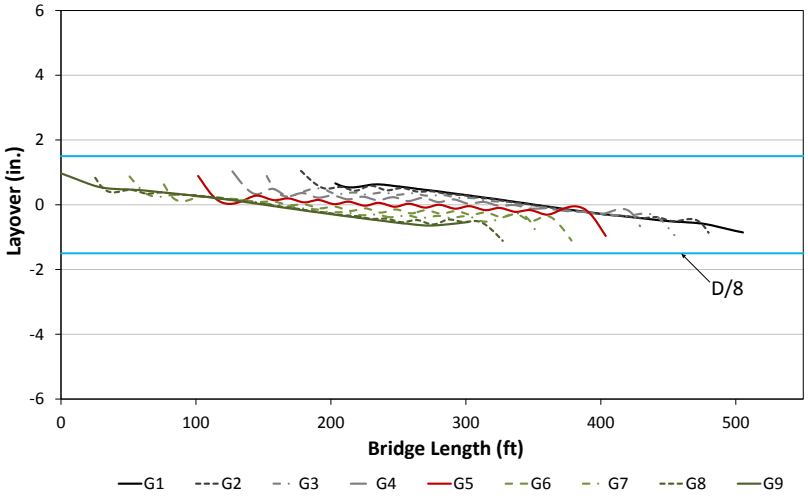

(iii) TDLF

Figure D.1.4. NISSS54, Layover of girders under total dead load for different detailing methods.

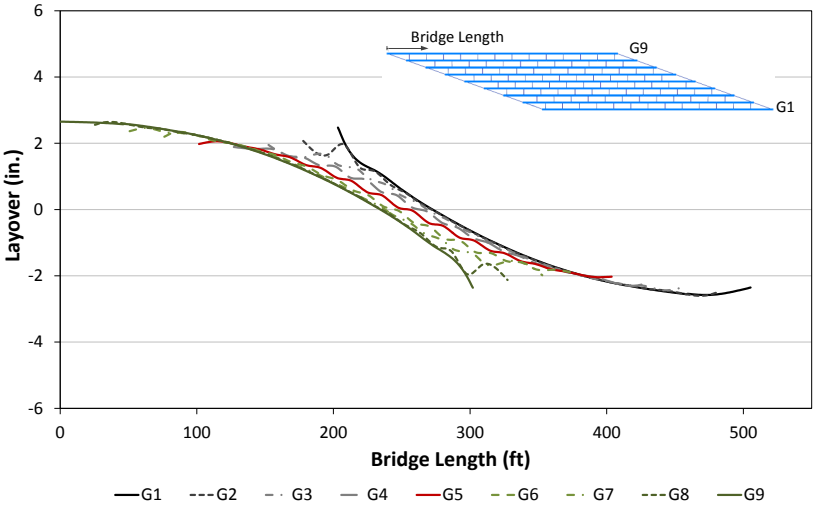

(i) NLF

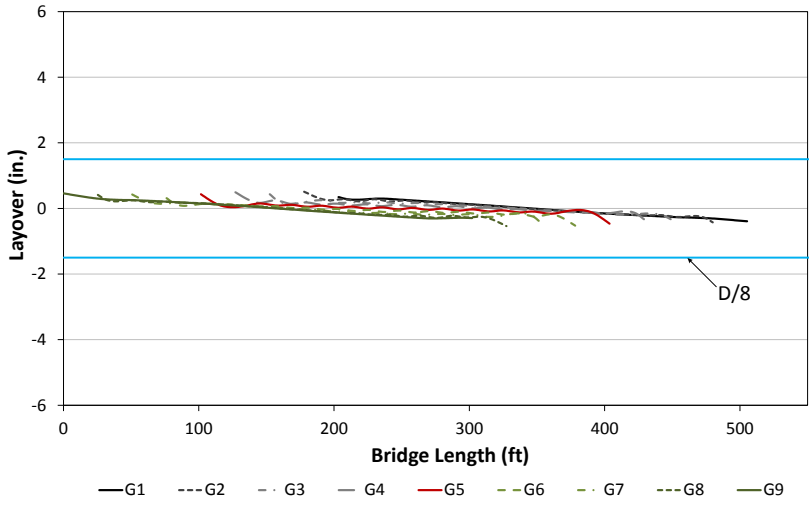

(ii) SDLF

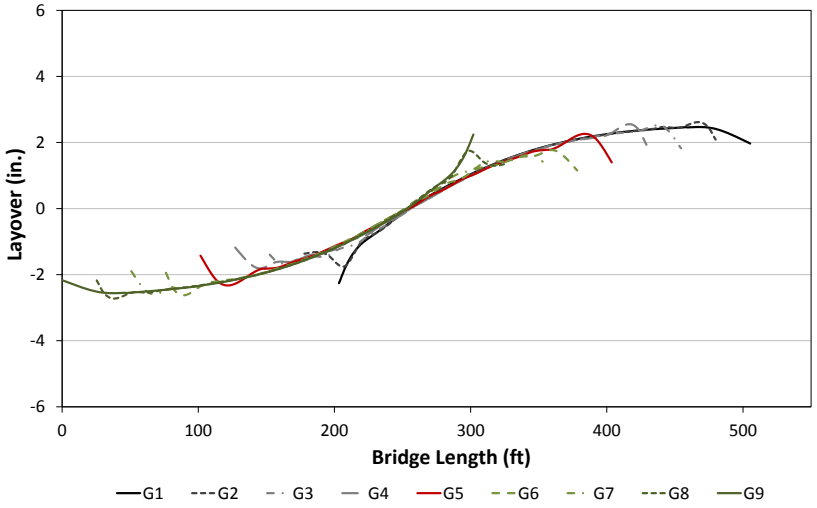

(iii) TDLF

Figure D.1.5. NISSS54, Layover of girders under steel dead load for different detailing methods.

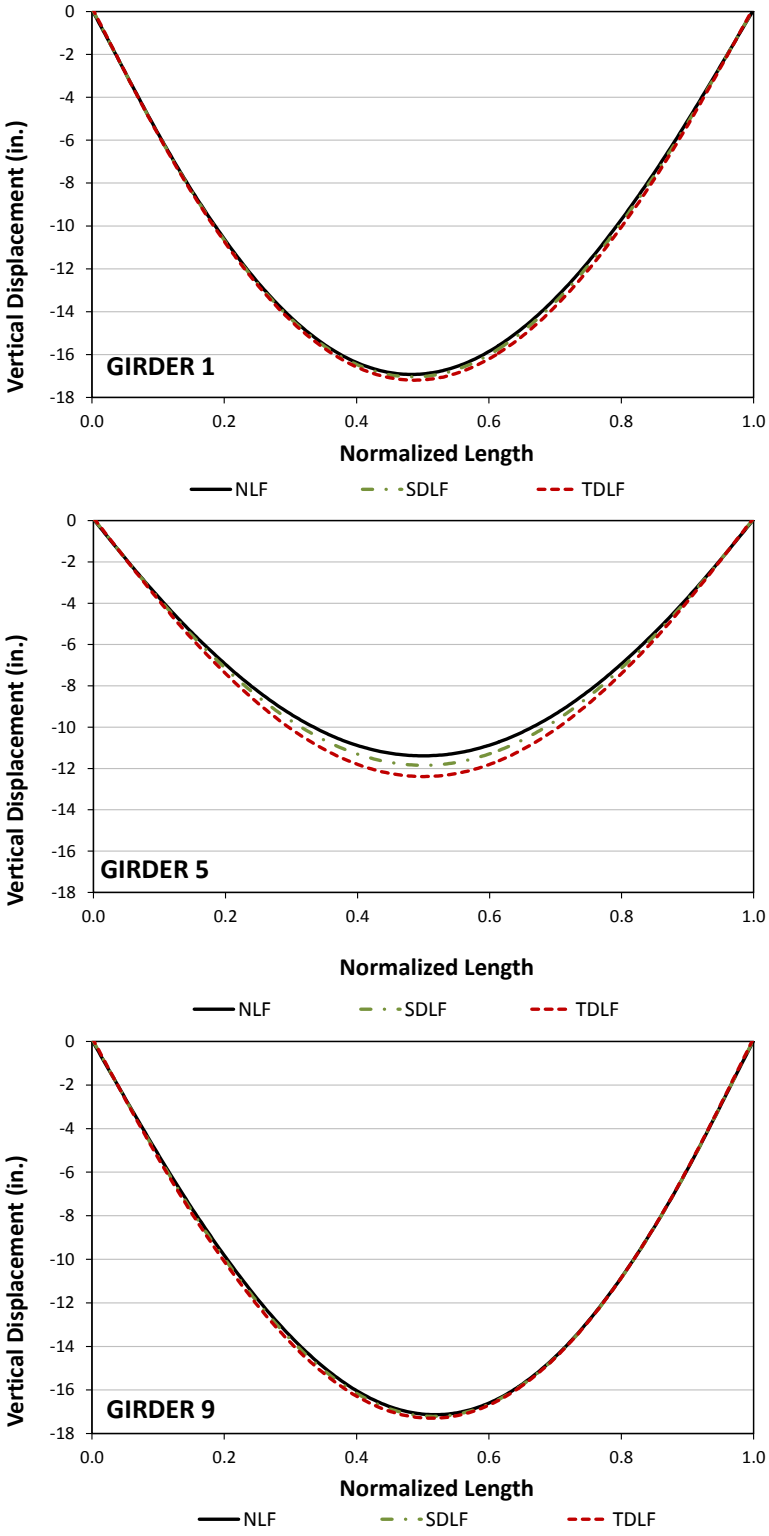

Figure D.1.6. NISSS54, Vertical deflections under total dead load for different detailing methods.

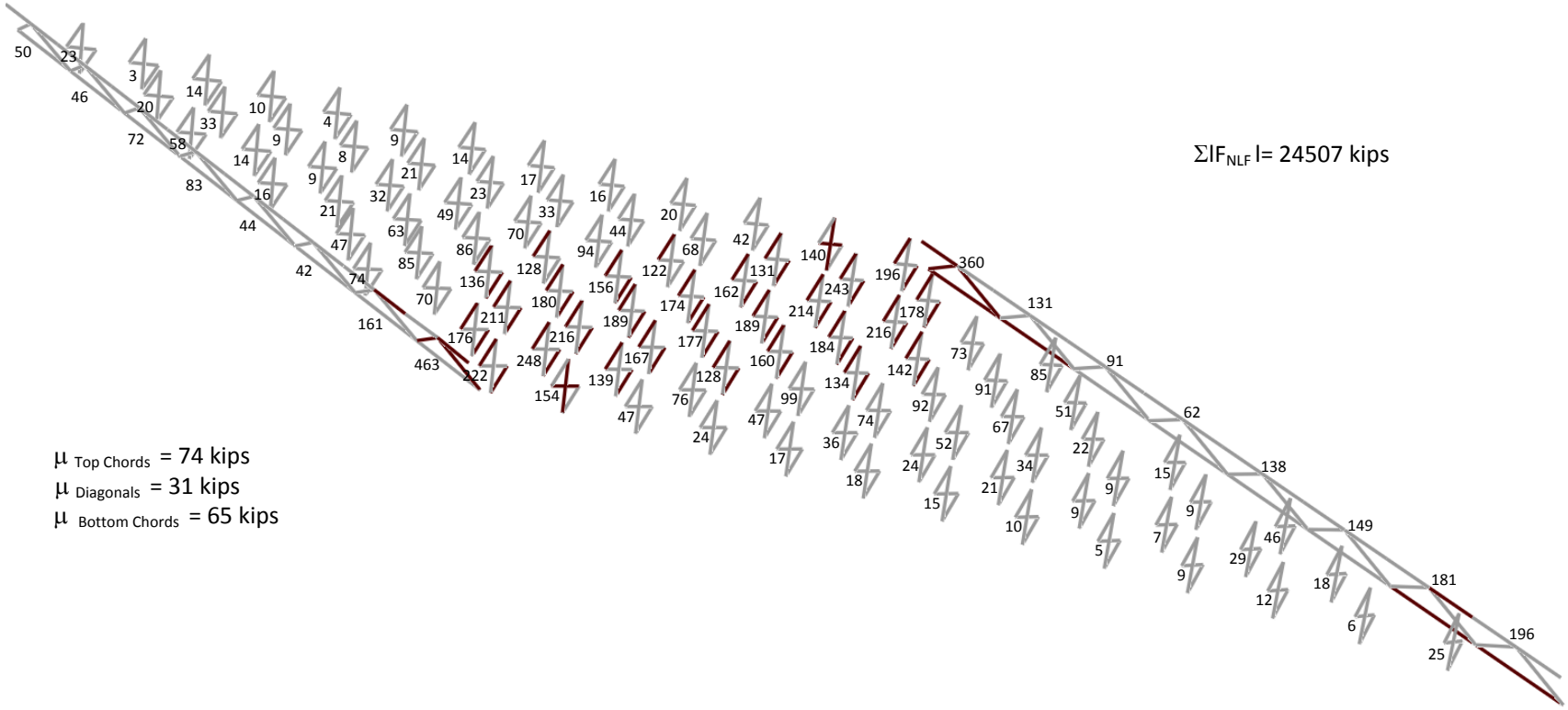

Figure D.1.7. NISSS54, maximum amplitude of the component axial forces in each of the cross-frames under total dead load (NLF detailing).

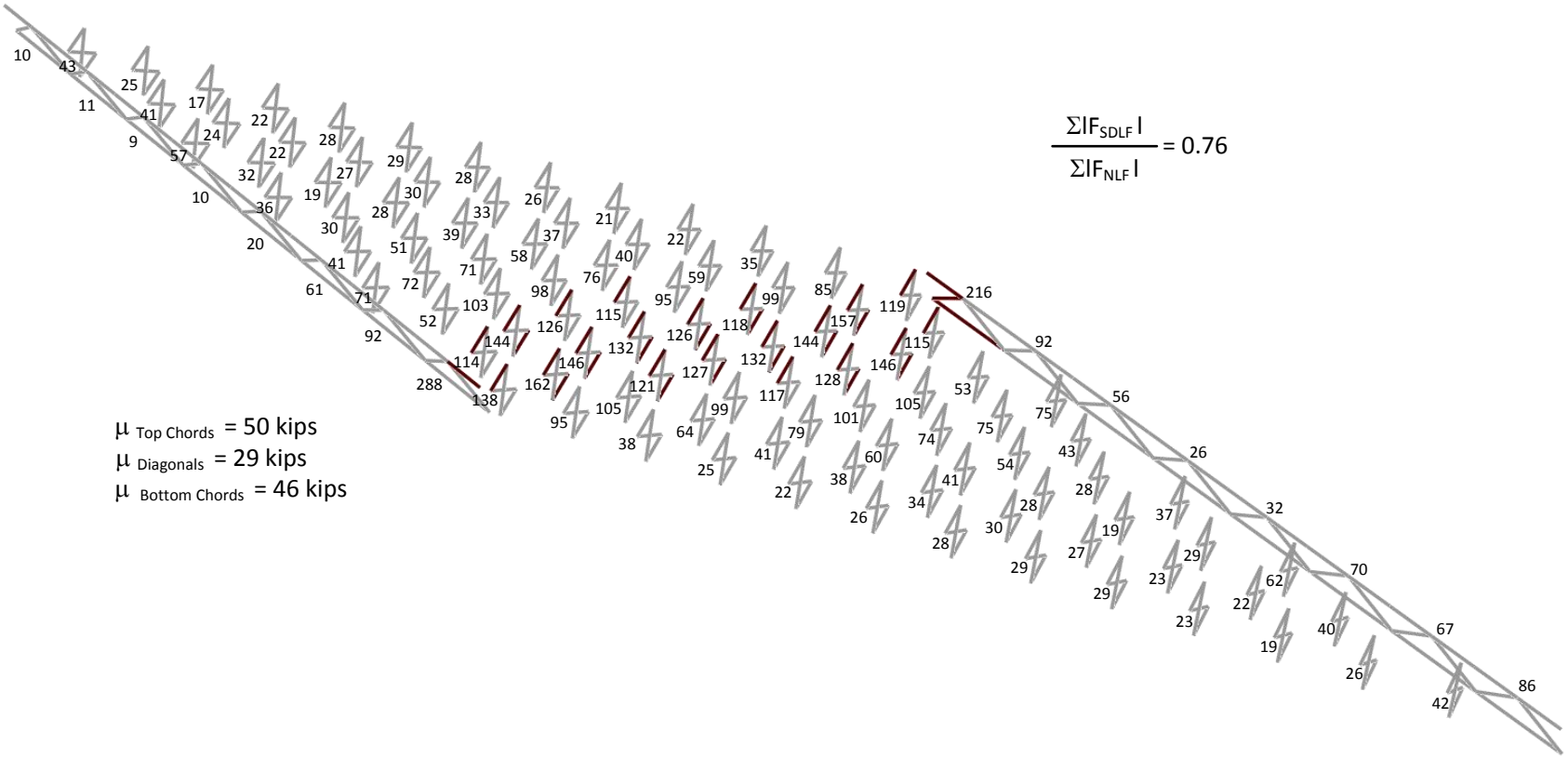

Figure D.1.8. NISSS54, maximum amplitude of the component axial forces in each of the cross-frames under total dead load (SDLF detailing).

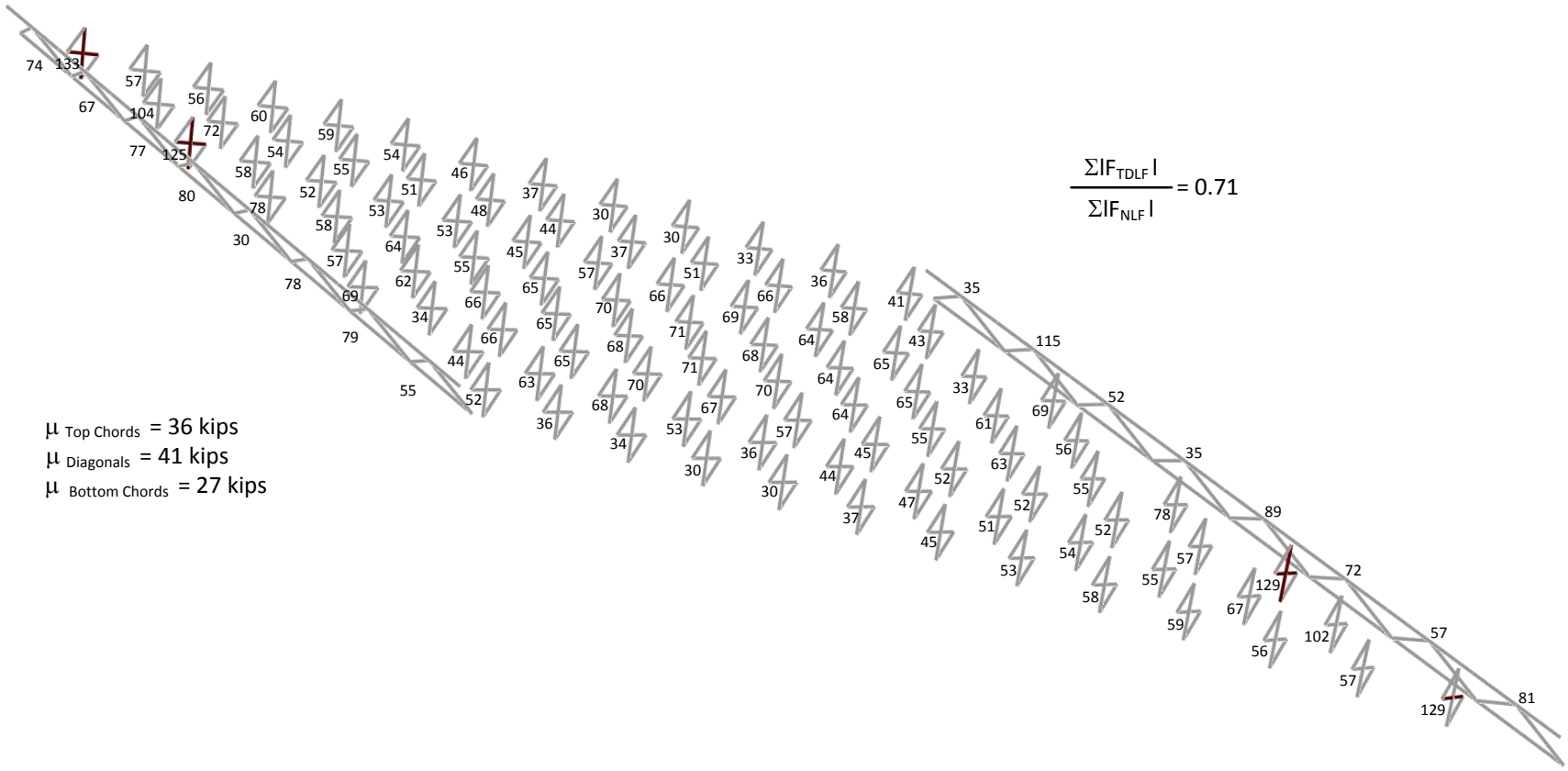

Figure D.1.9. NISSS54, maximum amplitude of the component axial forces in each of the cross-frames under total dead load (TDLF detailing).

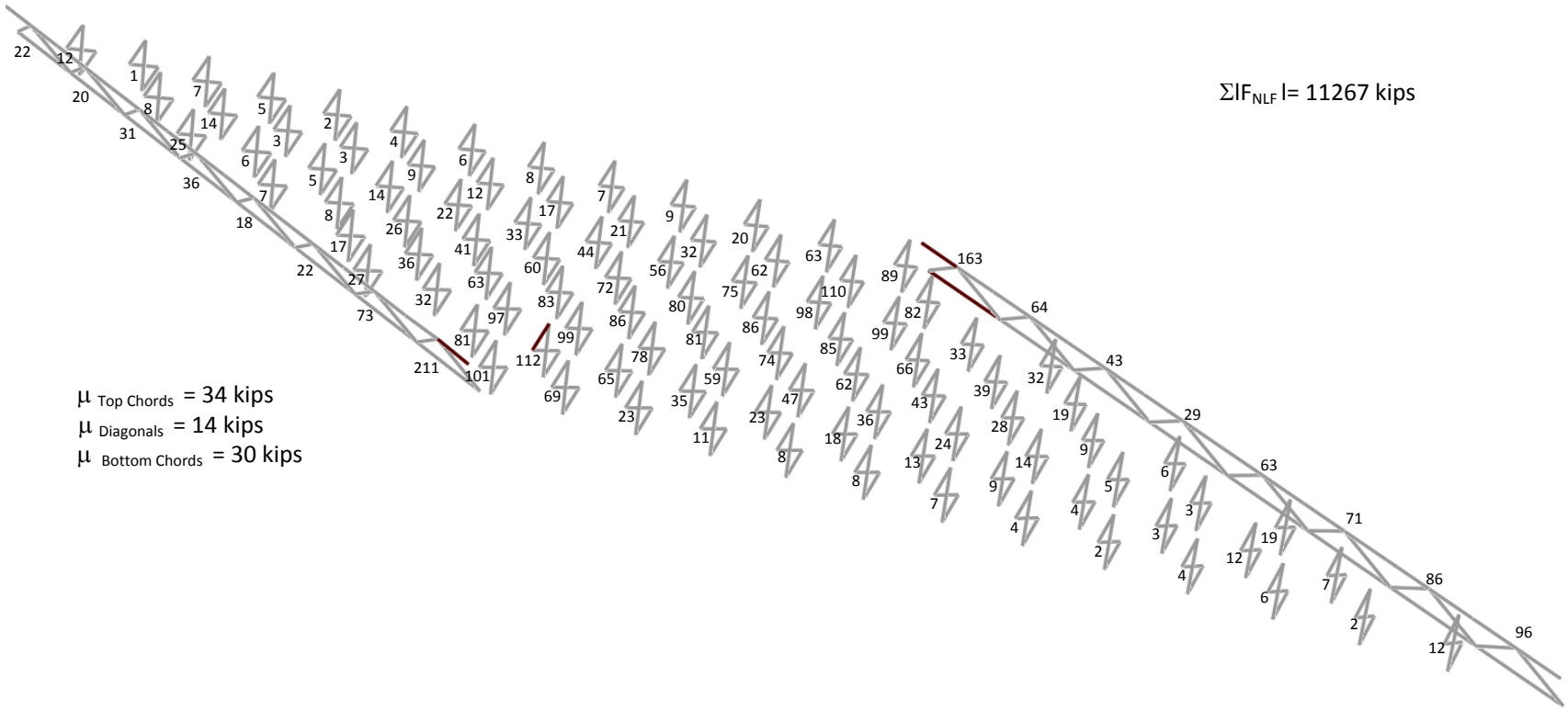

Figure D.1.10. NISSS54, maximum amplitude of the component axial forces in each of the cross-frames under steel dead load (NLF detailing).

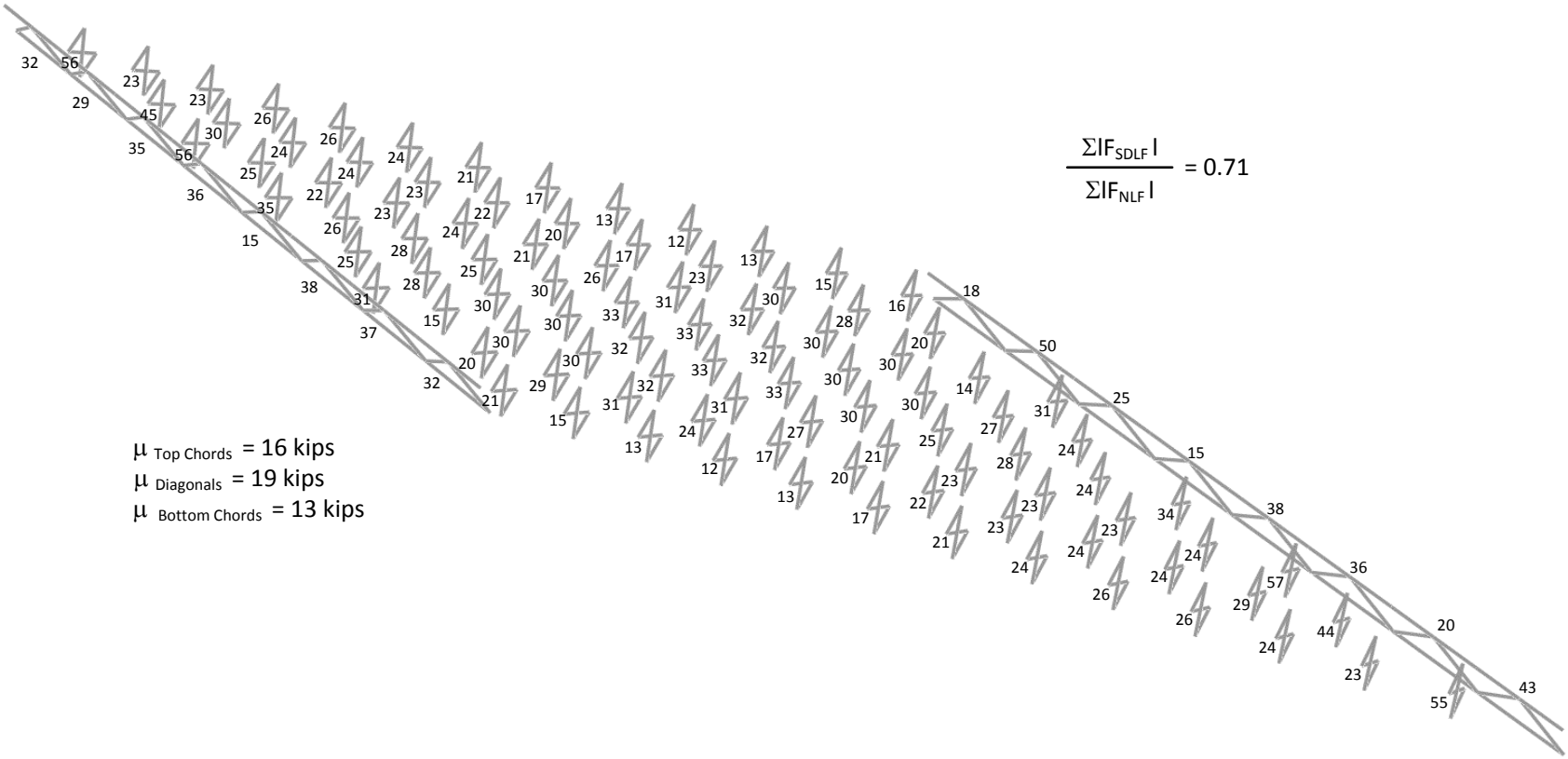

Figure D.1.11. NISSS54, maximum amplitude of the component axial forces in each of the cross-frames under steel dead load (SDLF detailing).

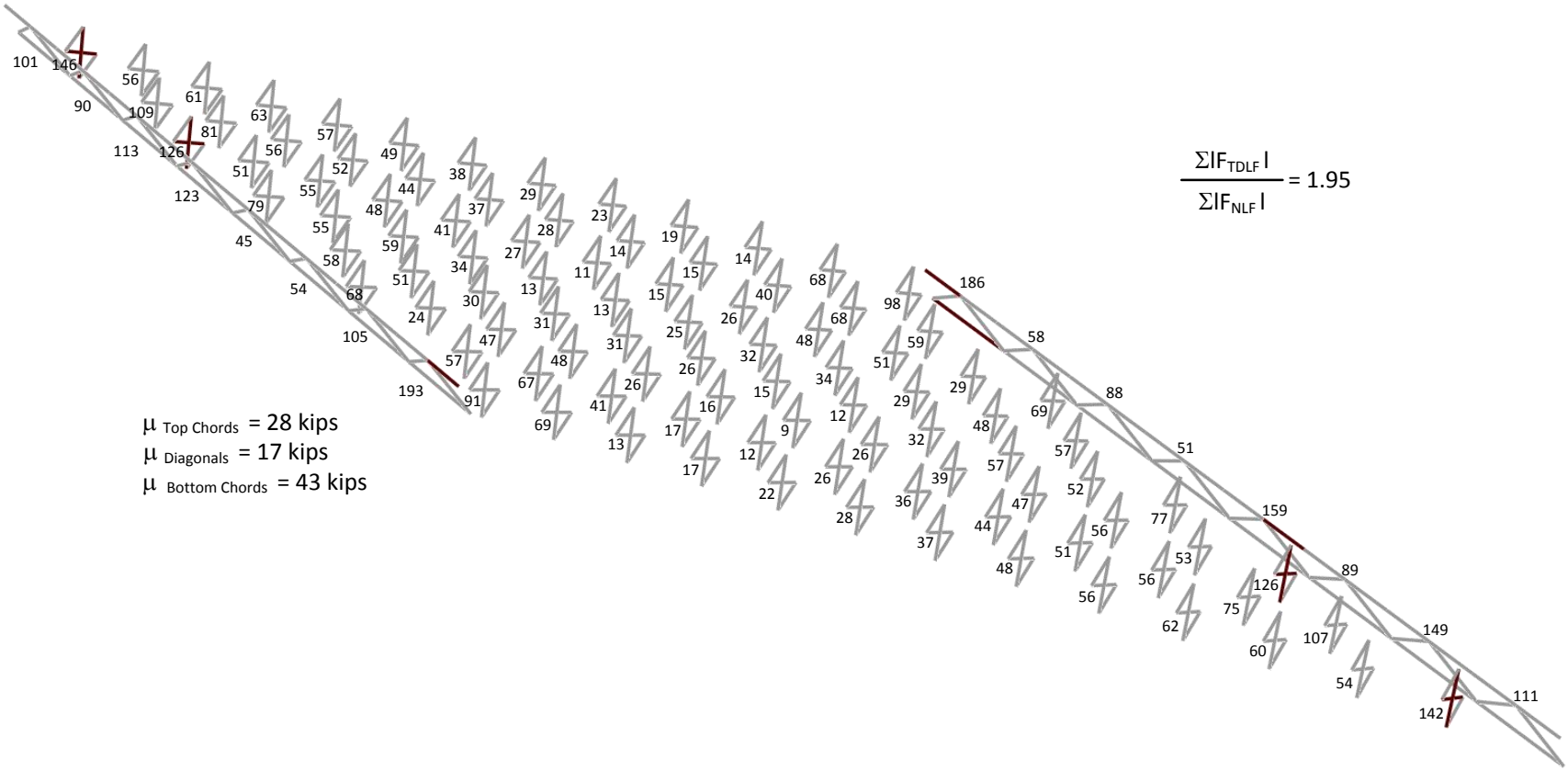

Figure D.1.12. NISSS54, maximum amplitude of the component axial forces in each of the cross-frames under steel dead load (TDLF detailing).

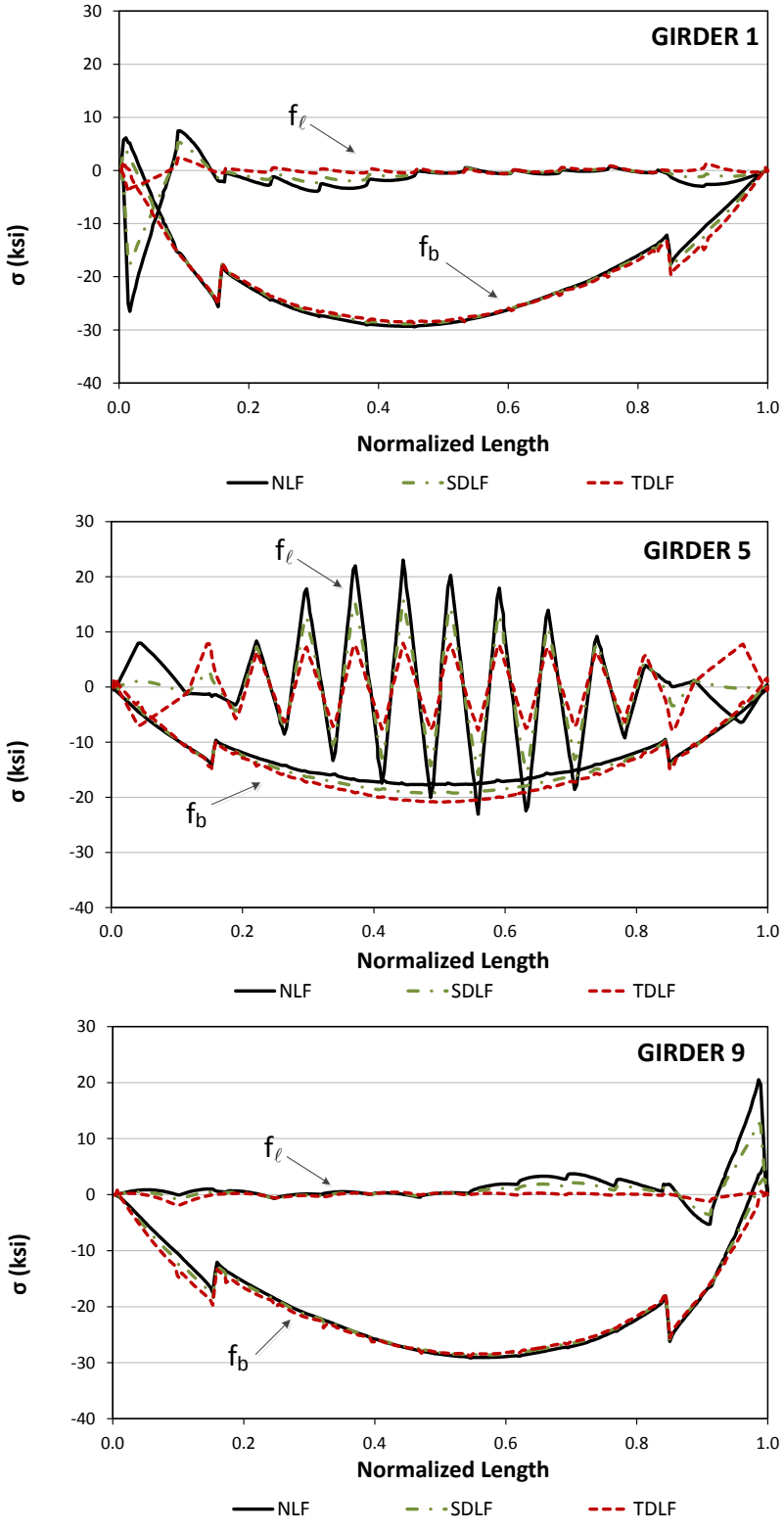

Figure D.1.13. NISSS54, Top flange stresses under total dead load for different detailing methods.

D.2. NISCR2

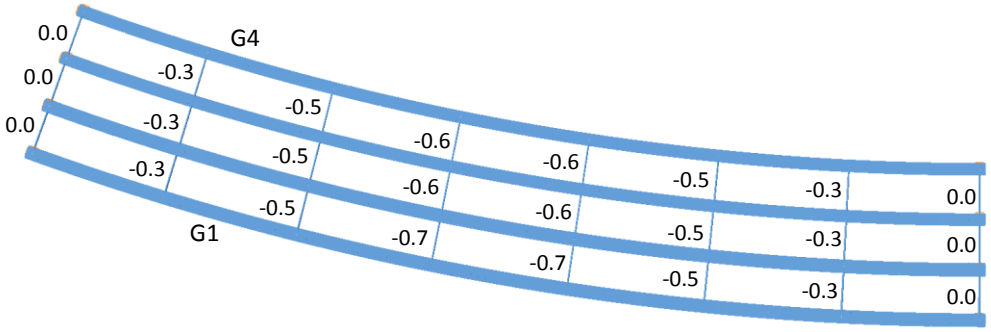

(i) Steel dead load

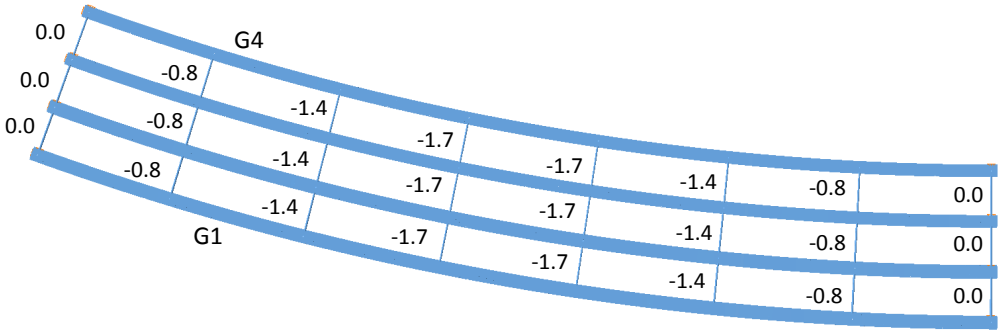

(ii) Total dead load

Figure D.2.1. NISCR2, Differential cambers between girders from steel and total dead load deflections.

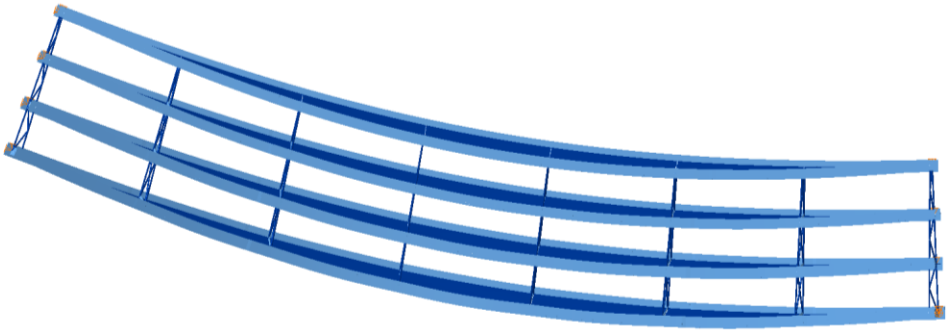

(i) NLF

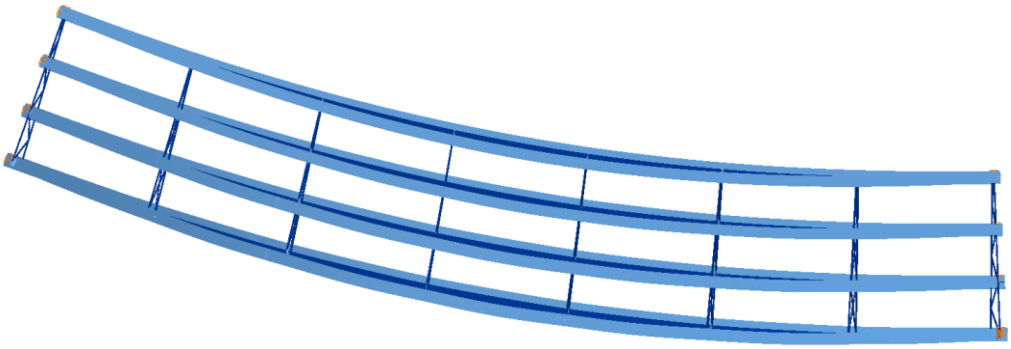

(ii) SDLF

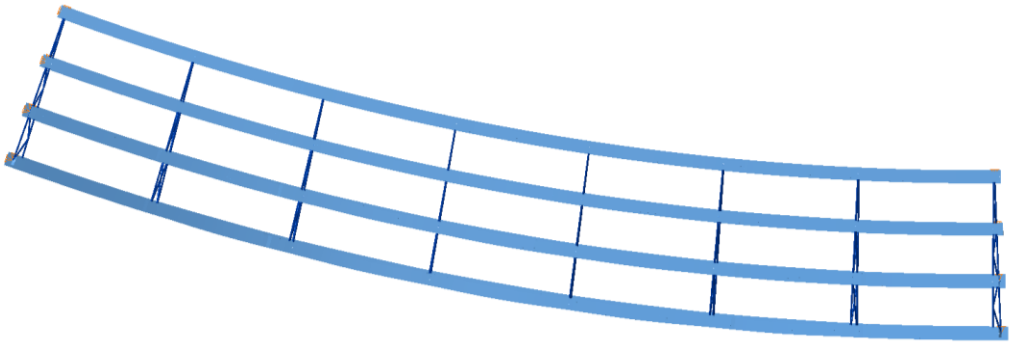

(iii) TDLF

Figure D.2.2. NISCR2, Deflected shape under total dead load for different detailing methods (magnified by 20x).

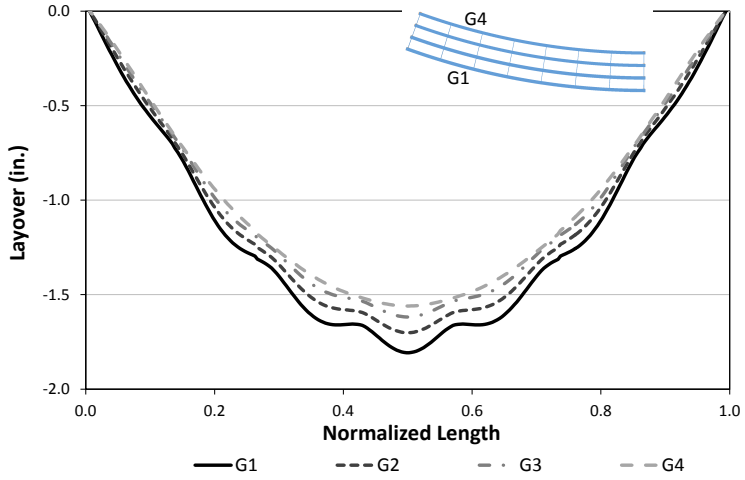

(i) NLF

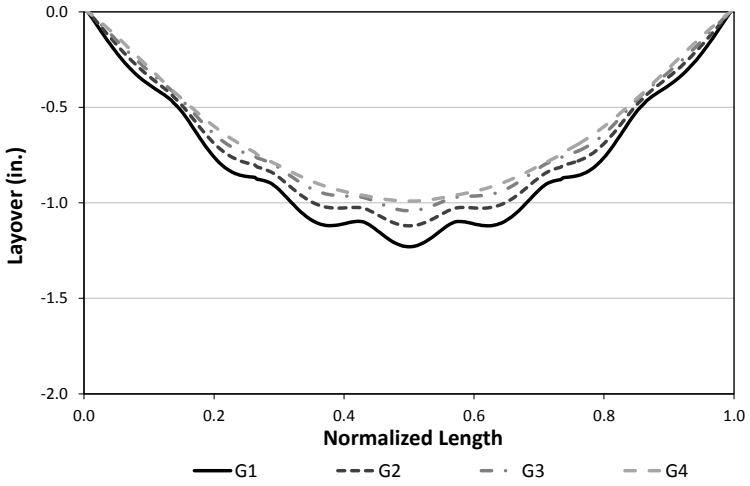

(ii) SDLF

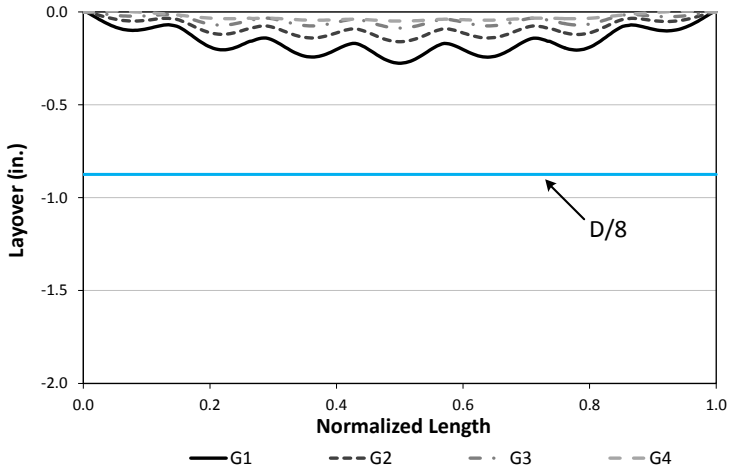

(iii) TDLF

Figure D.2.3. NISCR2, Girder layovers under total dead load for different detailing methods.

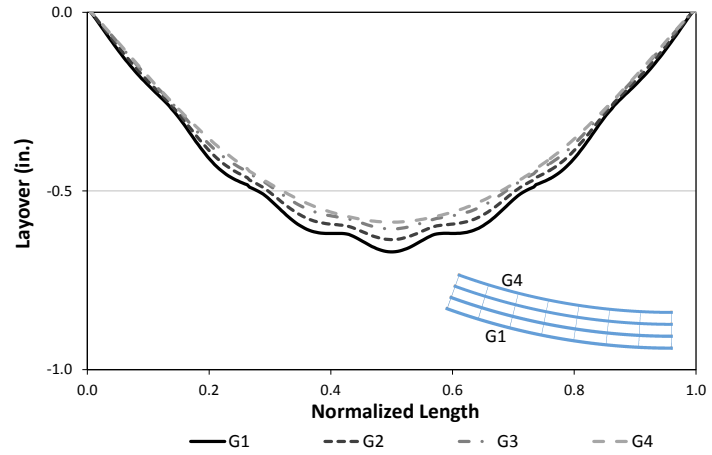

(i) NLF

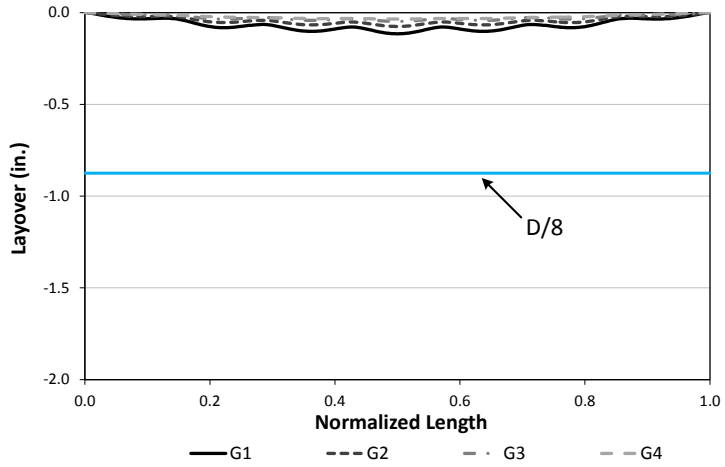

(ii) SDLF

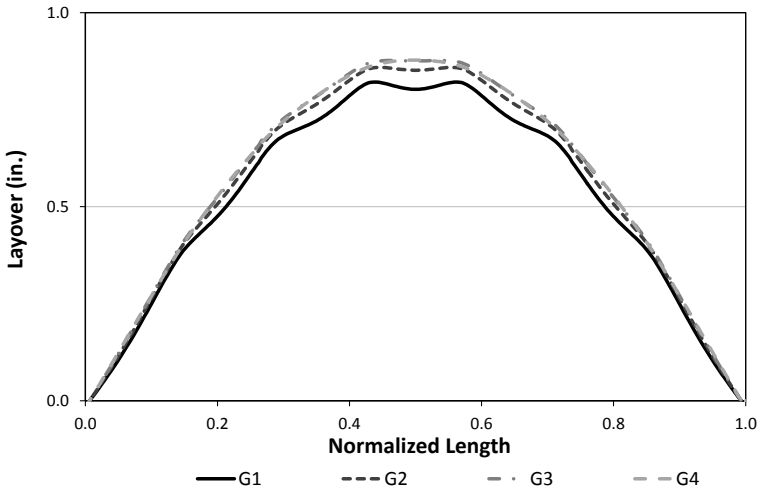

(iii) TDLF

Figure D.2.4. NISCR2, Girder layovers under steel dead load for different detailing methods.

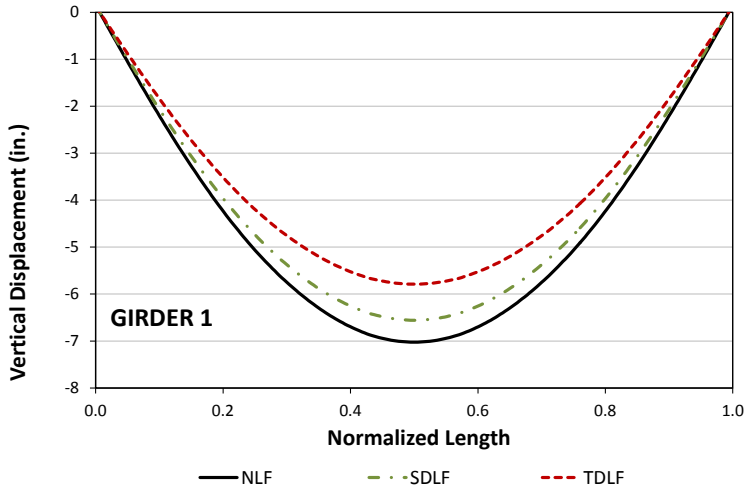

(i) Girder 1

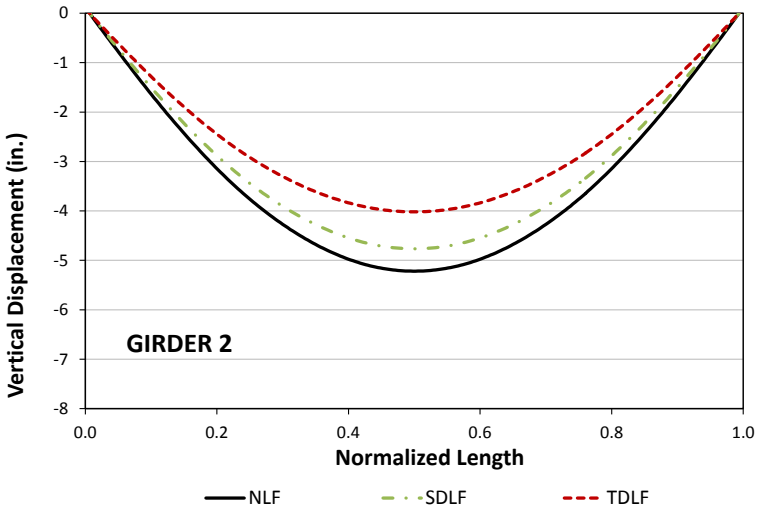

(ii) Girder 2

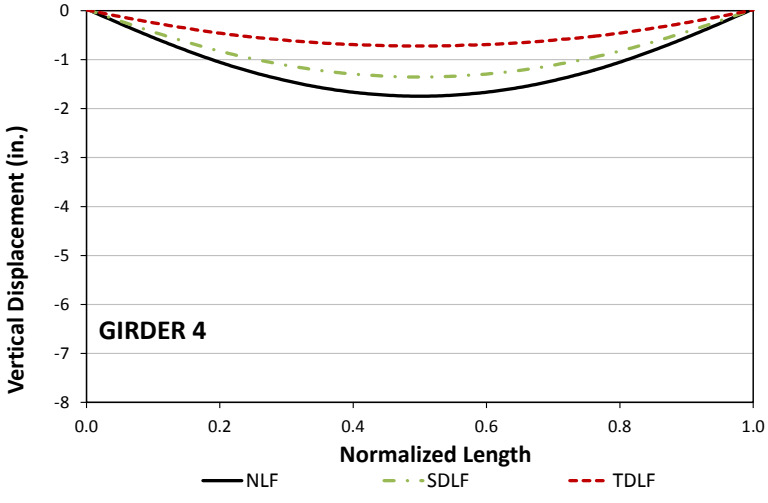

(iii) Girder 4

Figure D.2.5. NISCR2, Vertical deflections under total dead load for different detailing methods.

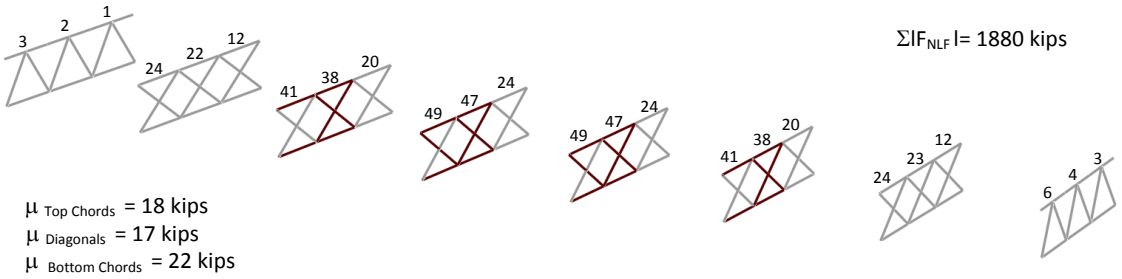

Figure D.2.6. NISCR2, maximum amplitude of the component axial forces in each of the cross-frames under total dead load (NLF detailing).

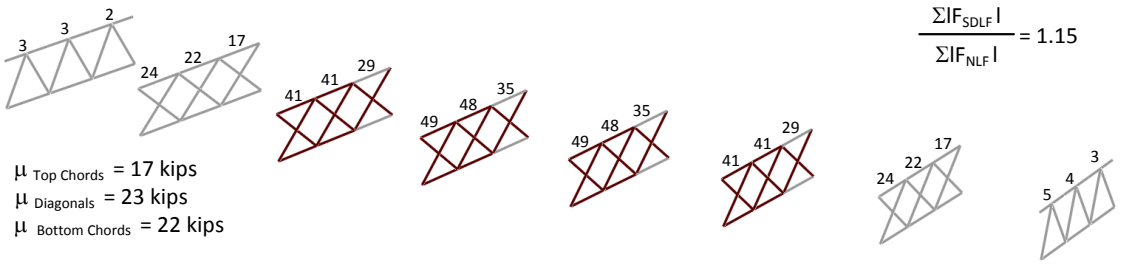

Figure D.2.7. NISCR2, maximum amplitude of the component axial forces in each of the cross-frames under total dead load (SDLF detailing).

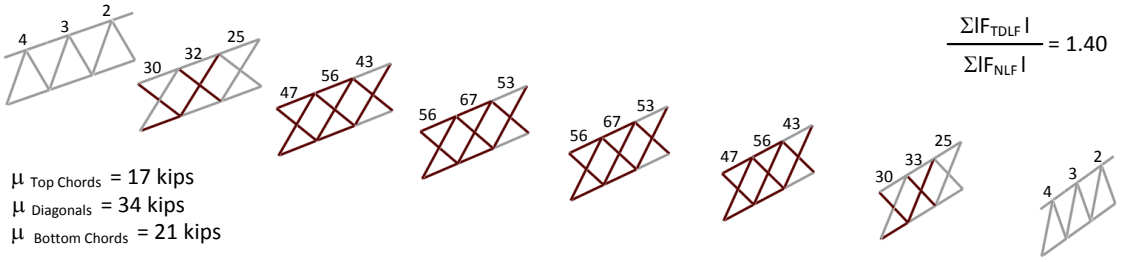

Figure D.2.8. NISCR2, maximum amplitude of the component axial forces in each of the cross-frames under total dead load (TDLF detailing).

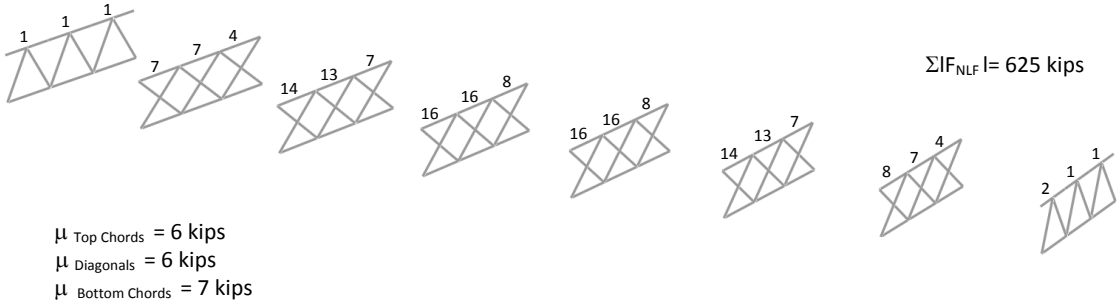

Figure D.2.9. NISCR2, maximum amplitude of the component axial forces in each of the cross-frames under steel dead load (NLF detailing).

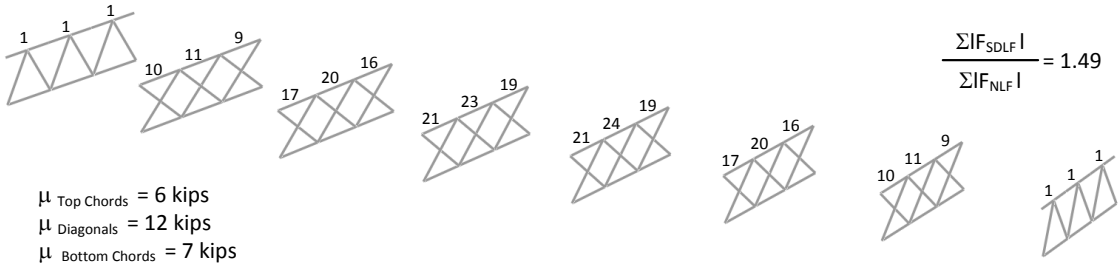

Figure D.2.10. NISCR2, maximum amplitude of the component axial forces in each of the cross-frames under steel dead load (SDLF detailing).

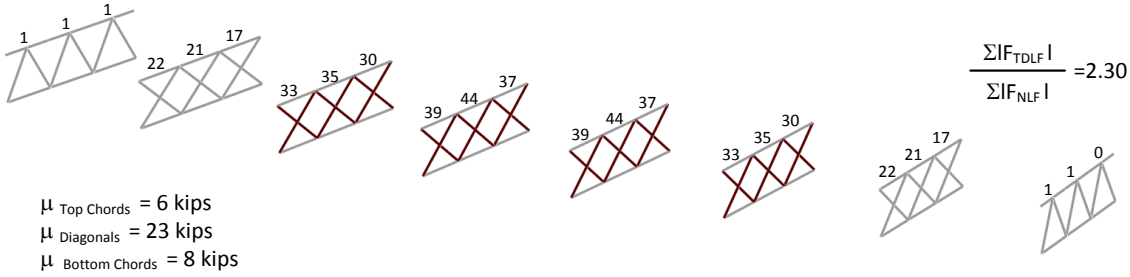

Figure D.2.11. NISCR2, maximum amplitude of the component axial forces in each of the cross-frames under steel dead load (TDLF detailing).

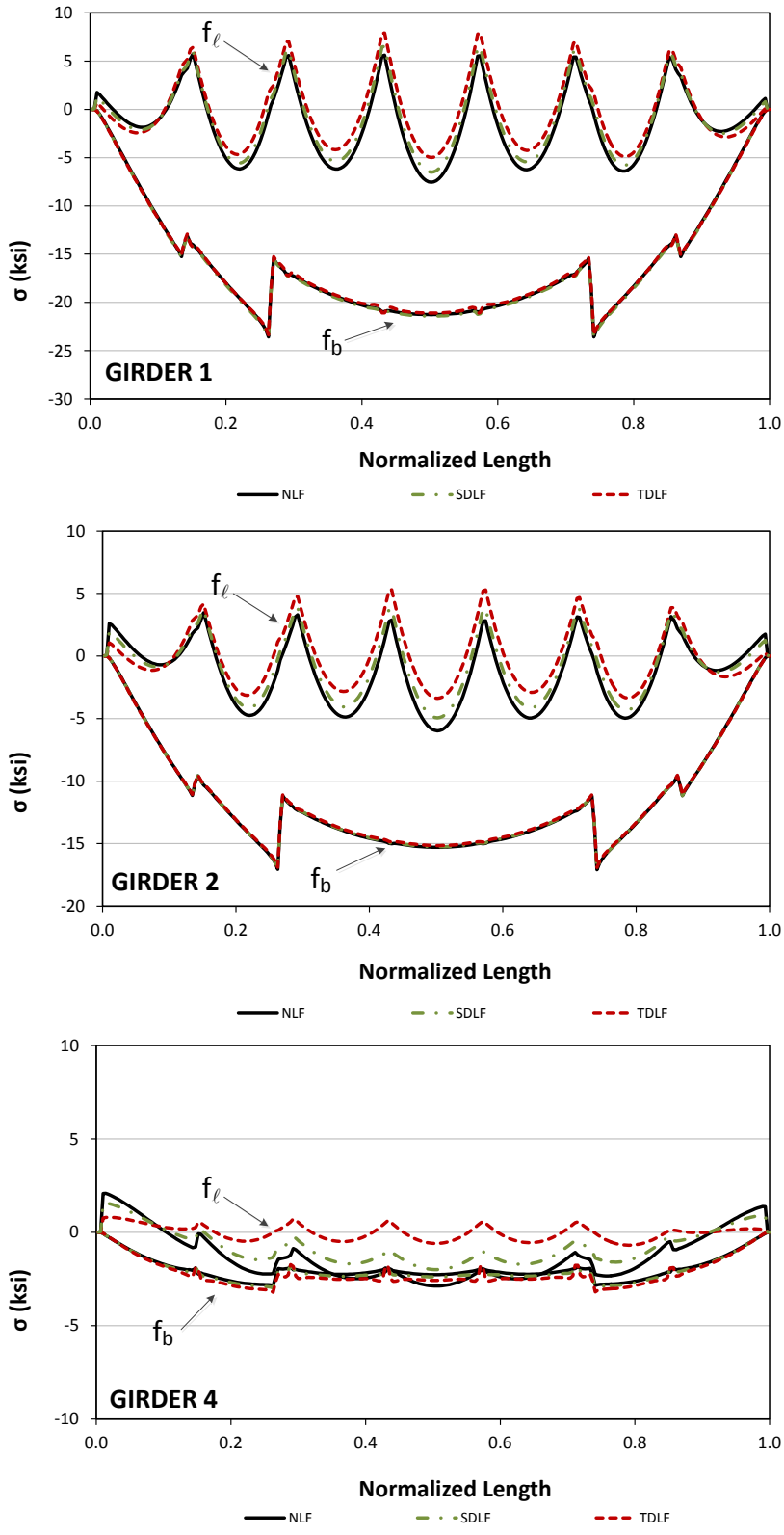

Figure D.2.12. NISCR2, Top flange stresses under total dead load for different detailing methods.

D.3. XICSN5

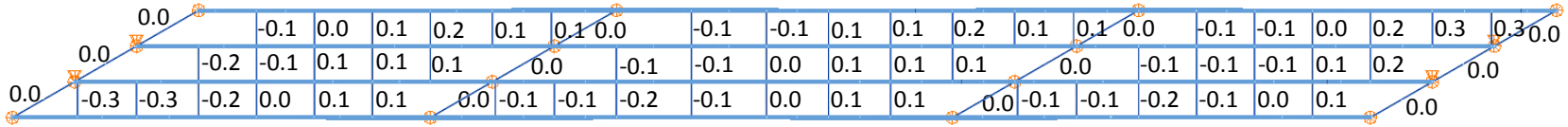

(i) Steel dead load

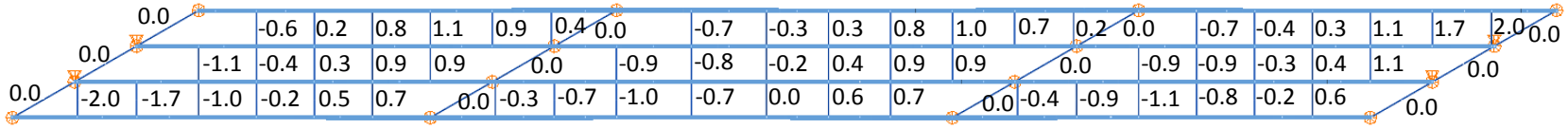

(ii) Total dead load

Figure D.3.1. XICSS5, Differential cambers between girders from steel and total dead load deflections.

(i) NLF

(ii) SDLF

(iii) TDLF

Figure D.3.2. XICSS5, Deflected shape under total dead load for different detailing methods (magnified by 30x).

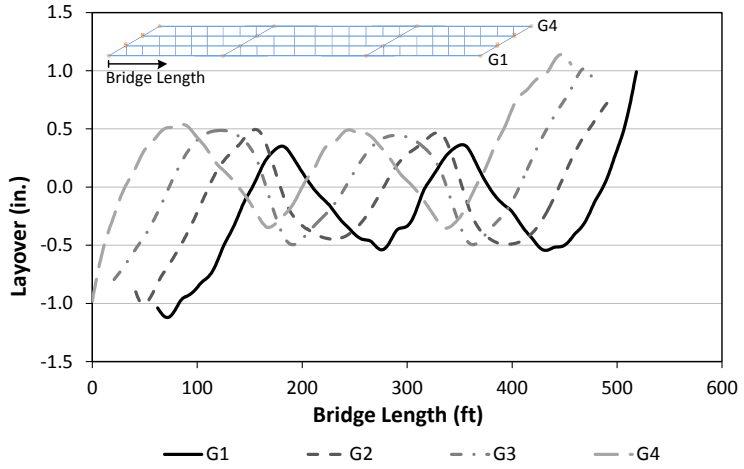

(i) NLF

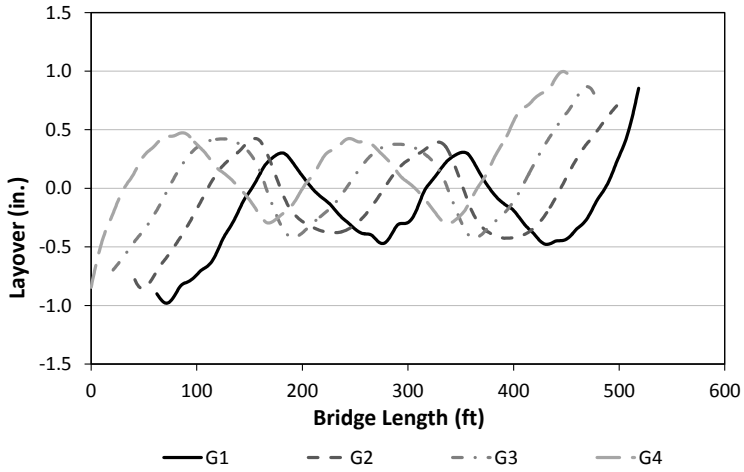

(ii) SDLF

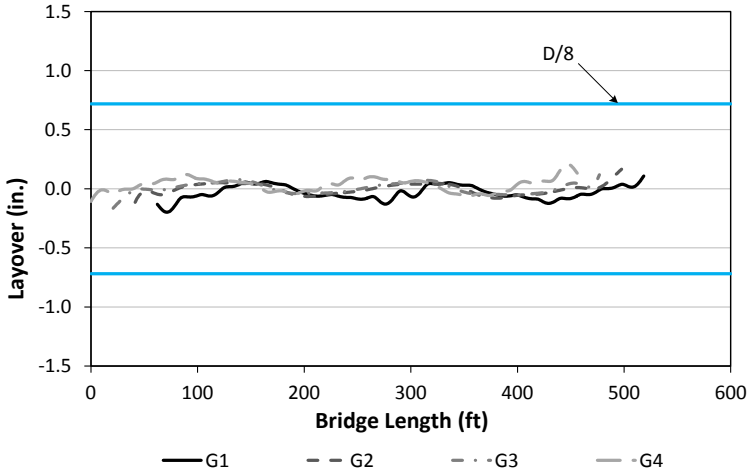

(iii) TDLF

Figure D.3.3. XICSS5, Relative lateral displacements under total dead load for different detailing methods.

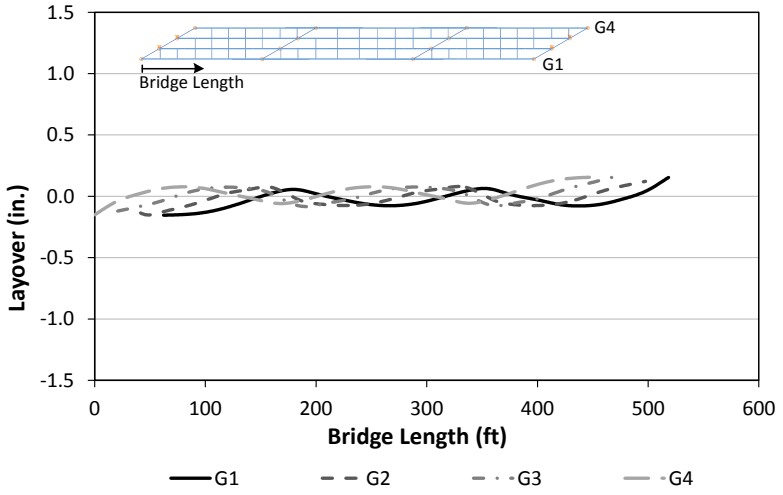

(i) NLF

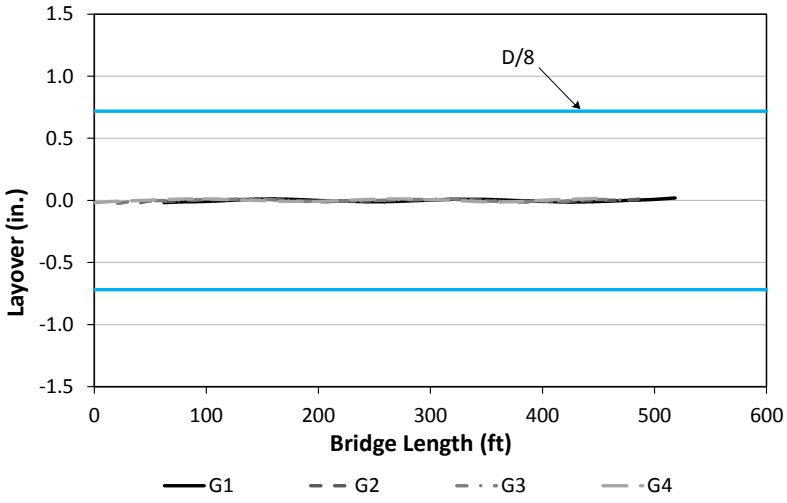

(ii) SDLF

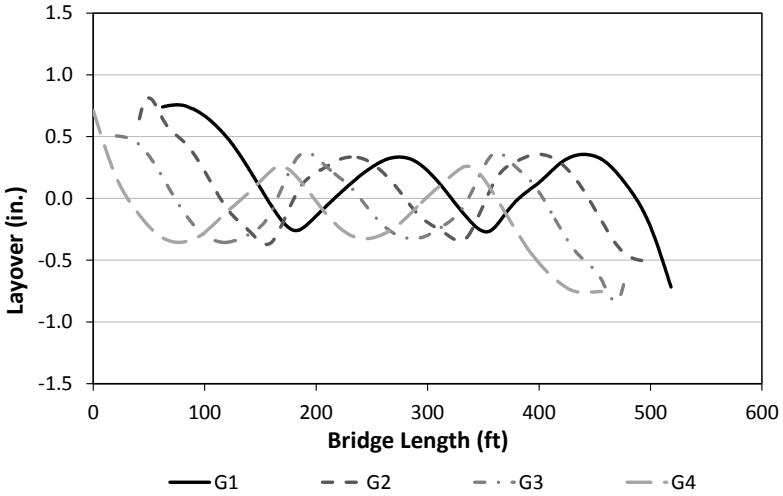

(iii) TDLF

Figure D.3.4. XICSS5, Relative lateral displacements under total dead load for different detailing methods.

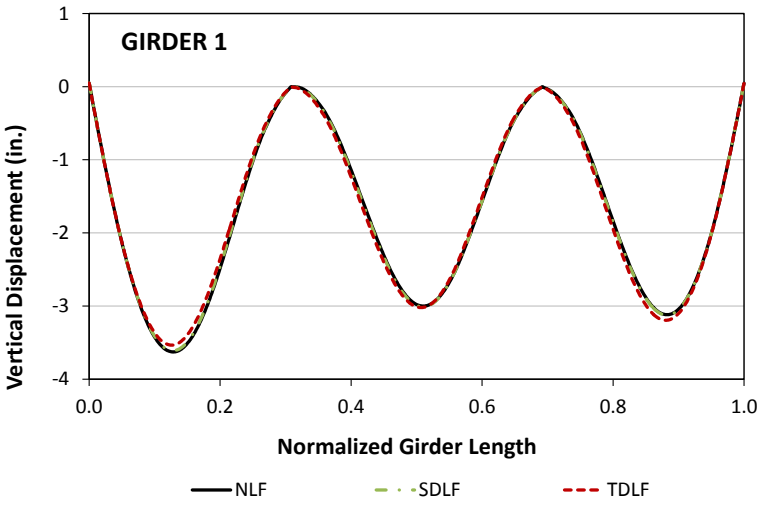

(i) Girder 1

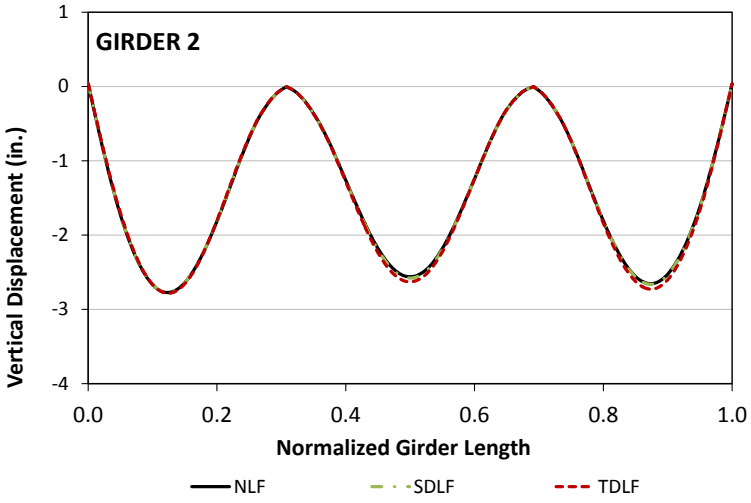

(ii) Girder 2

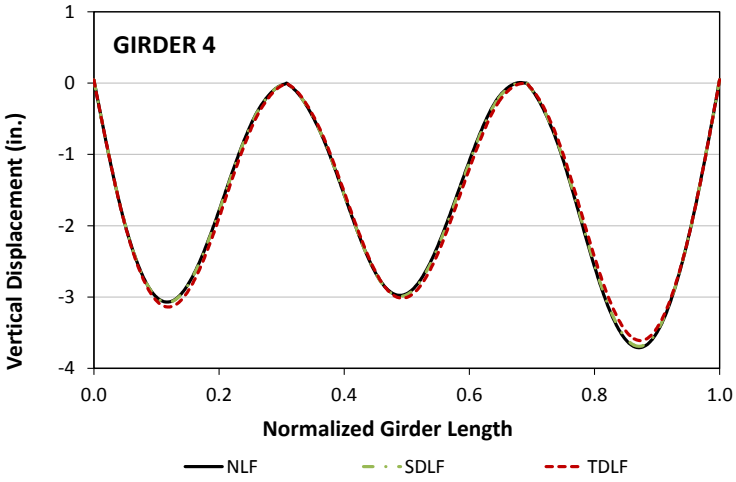

(iii) Girder 4

Figure D.3.5. XICSS5, Vertical deflections under total dead load for different detailing methods.

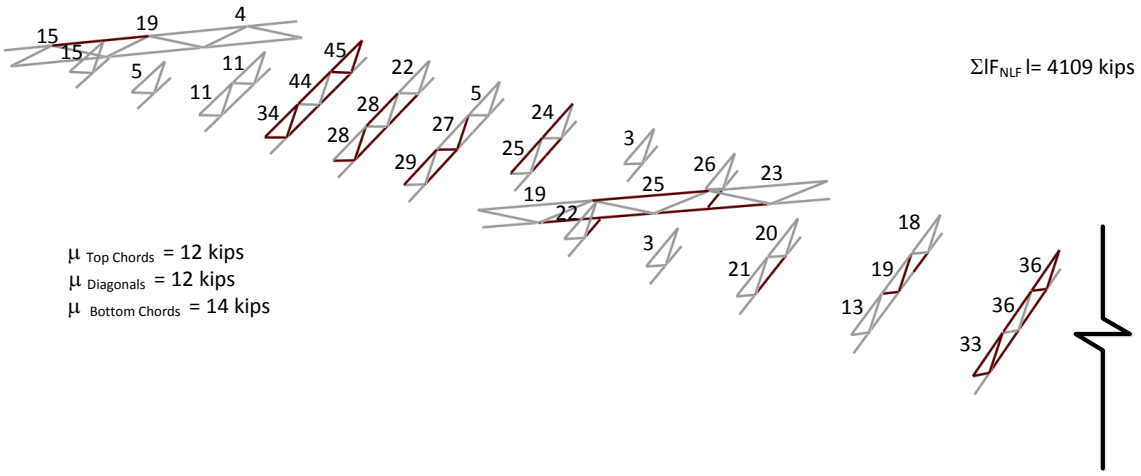

Figure D.3.6. XICSS5, maximum amplitude of the component axial forces in each of the cross-frames under total dead load (NLF detailing).

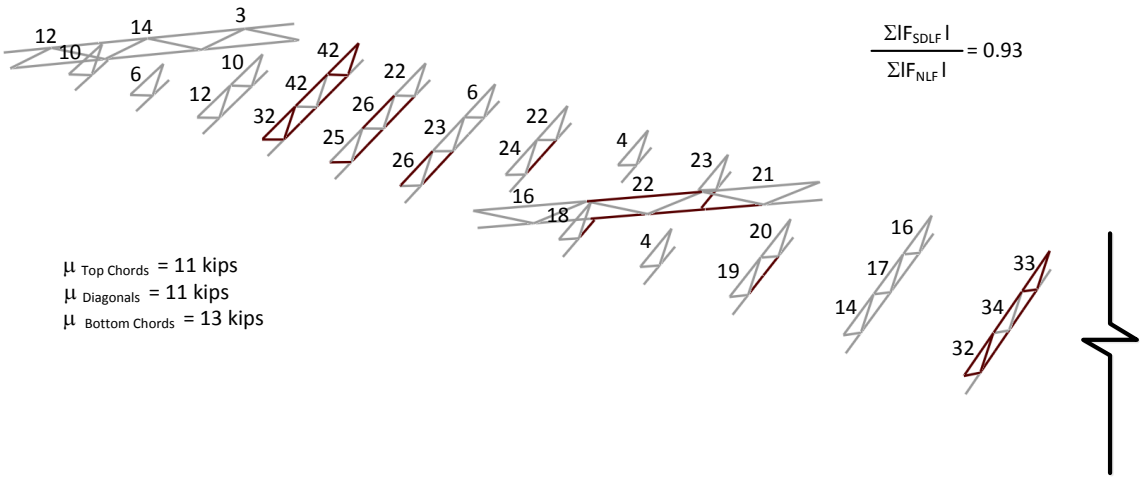

Figure D.3.7. XICSS5, maximum amplitude of the component axial forces in each of the cross-frames under total dead load (SDLF detailing).

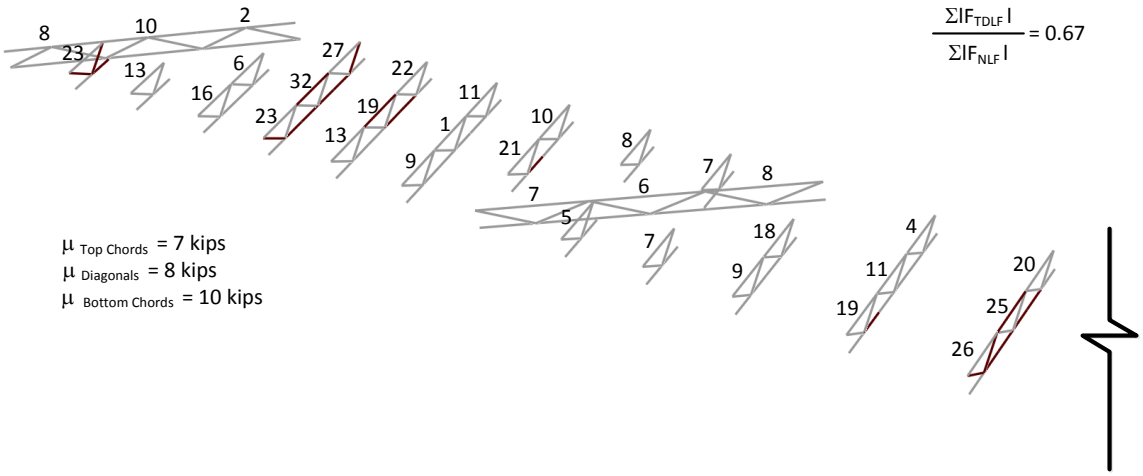

Figure D.3.8. XICSS5, maximum amplitude of the component axial forces in each of the cross-frames under total dead load (TDLF detailing).

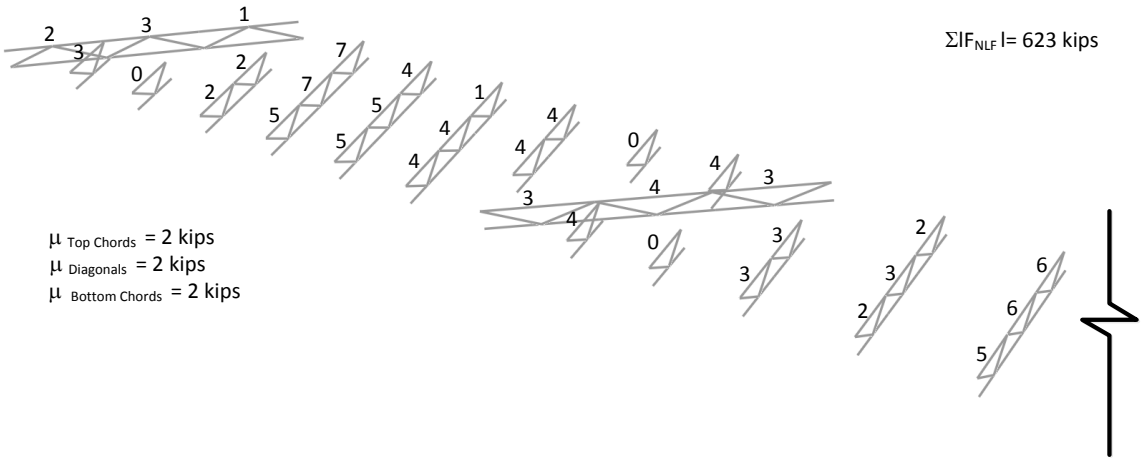

Figure D.3.9. XICSS5, maximum amplitude of the component axial forces in each of the cross-frames under steel dead load (NLF detailing).

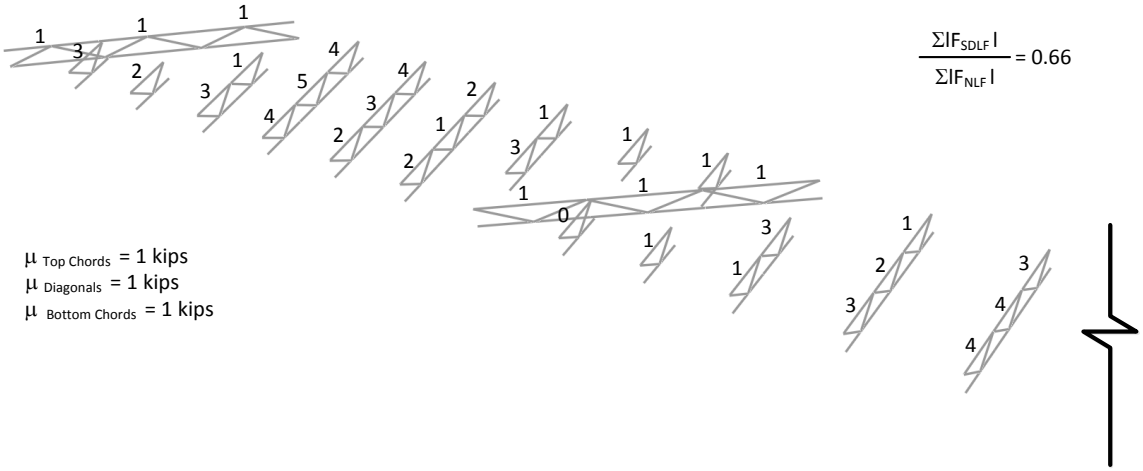

Figure D.3.10. XICSS5, maximum amplitude of the component axial forces in each of the cross-frames under steel dead load (SDLF detailing).

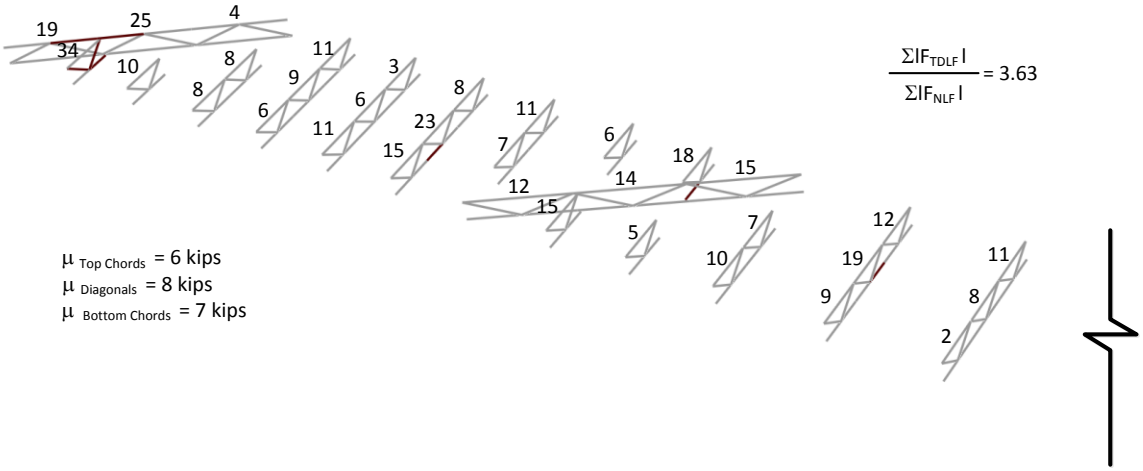

Figure D.3.11. XICSS5, maximum amplitude of the component axial forces in each of the cross-frames under steel dead load (TDLF detailing).

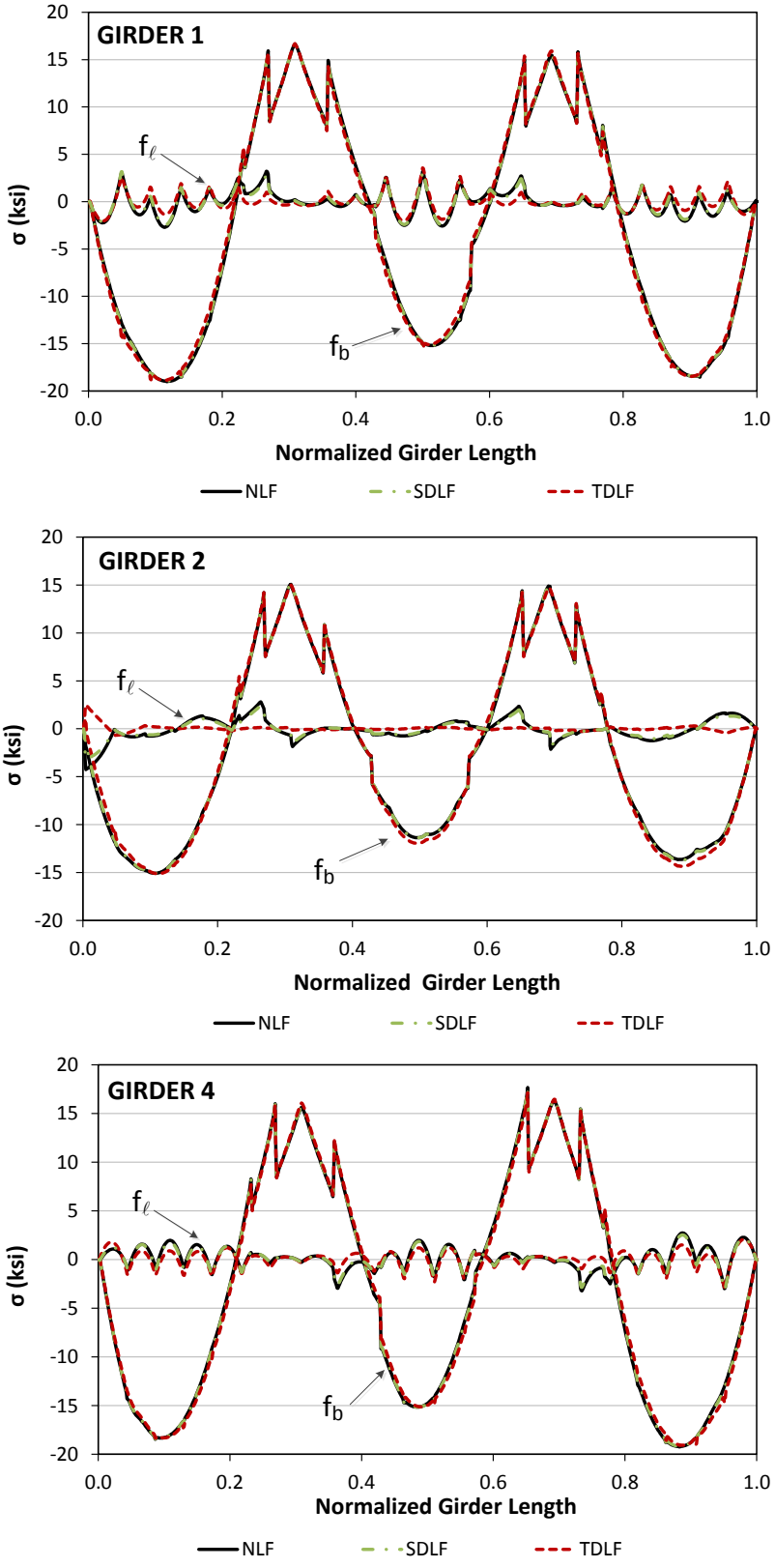

Figure D.3.12. XICSS5, Top flange stresses under total dead load for different detailing methods.

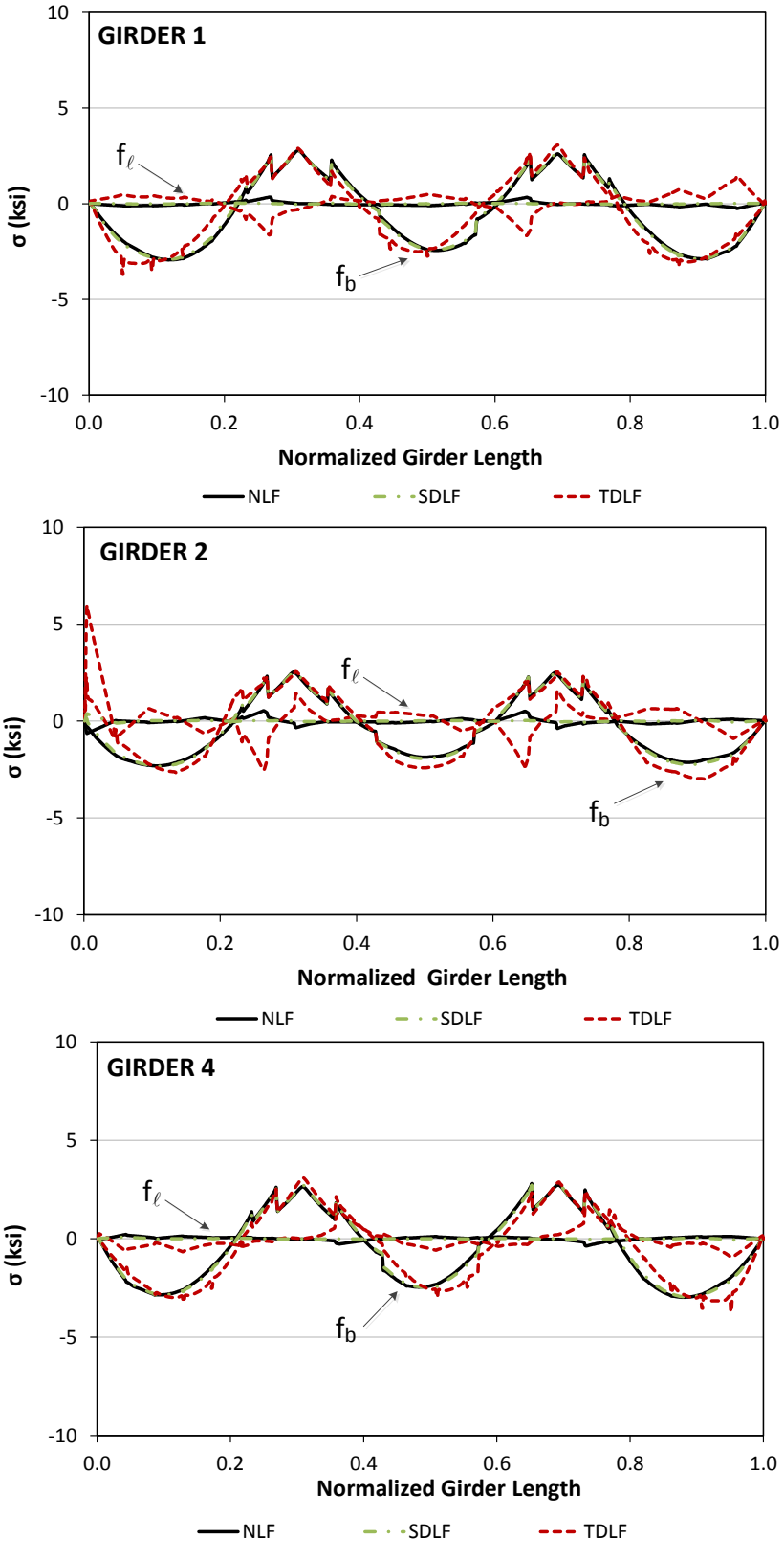

Figure D.3.13. XICSS5, Top flange stresses under steel dead load for different detailing methods.

D.4. NISCS14

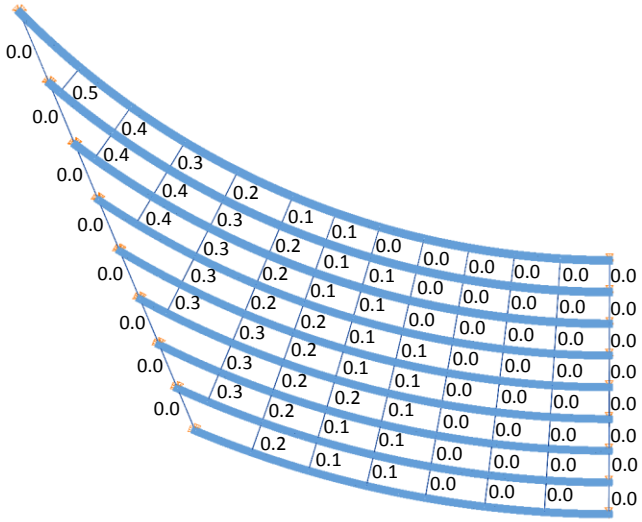

(i) Steel dead load

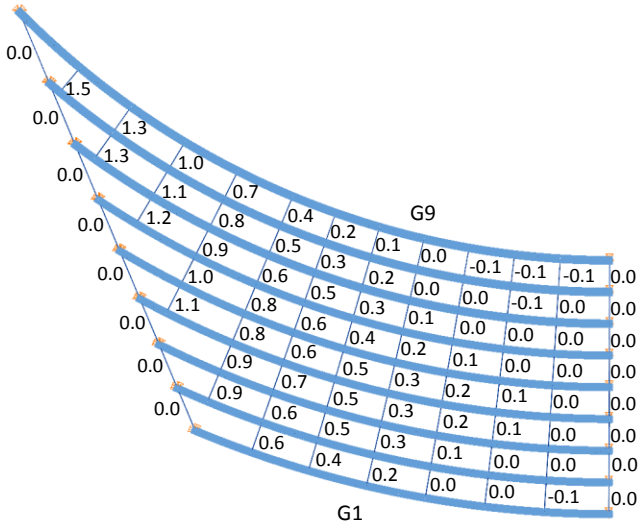

(ii) Total dead load

Figure D.4.1. NISCS14, Differential cambers between girders from steel and total dead load deflections.

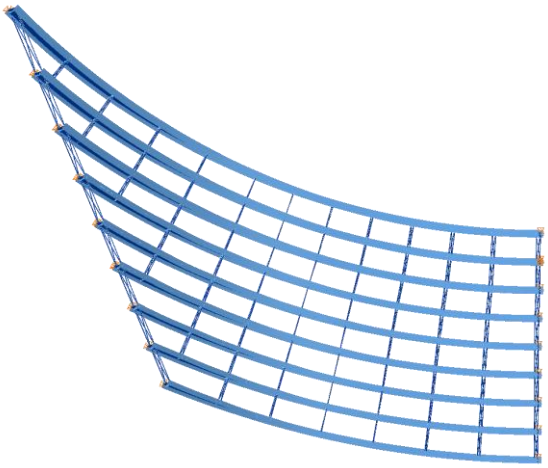

(i) NLF

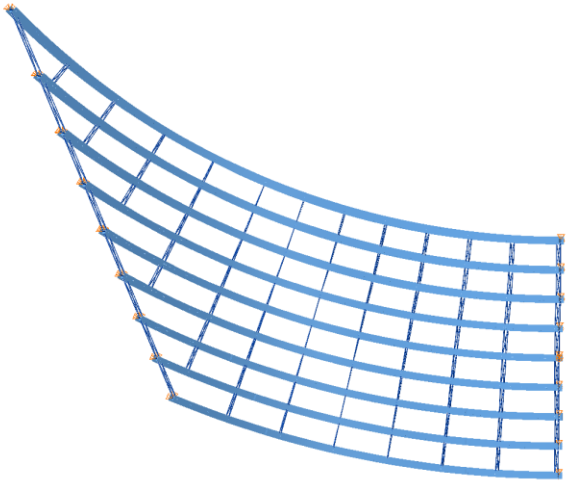

(ii) SDLF

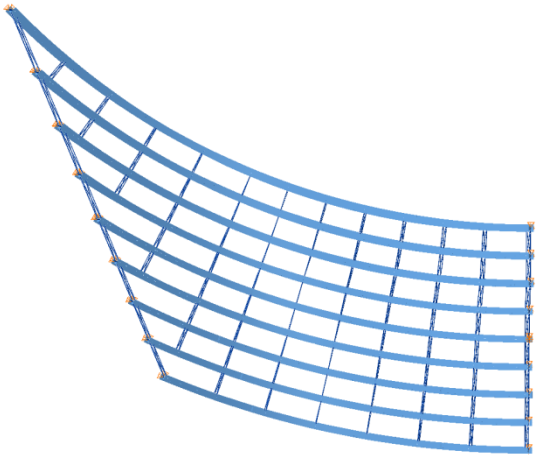

(iii) TDLF

Figure D.4.2. NISCS14, Deflected shape under total dead load for different detailing methods (magnified by 30x)

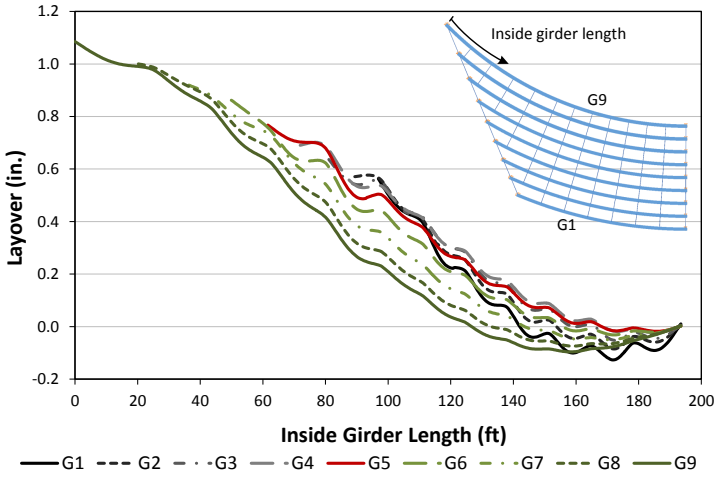

(i) NLF

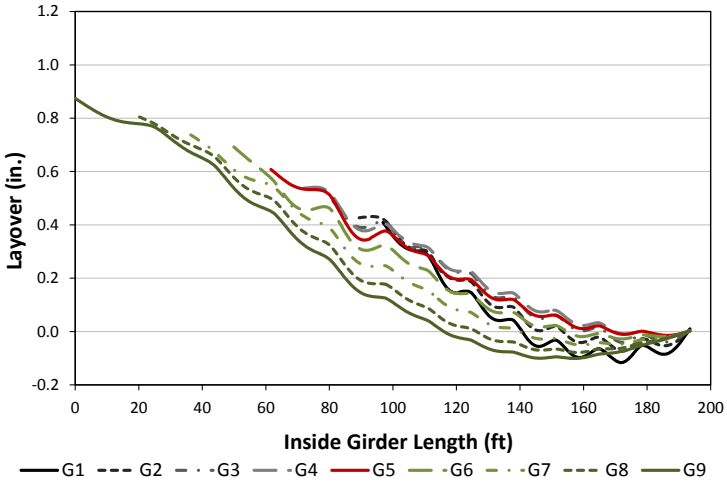

(ii) SDLF

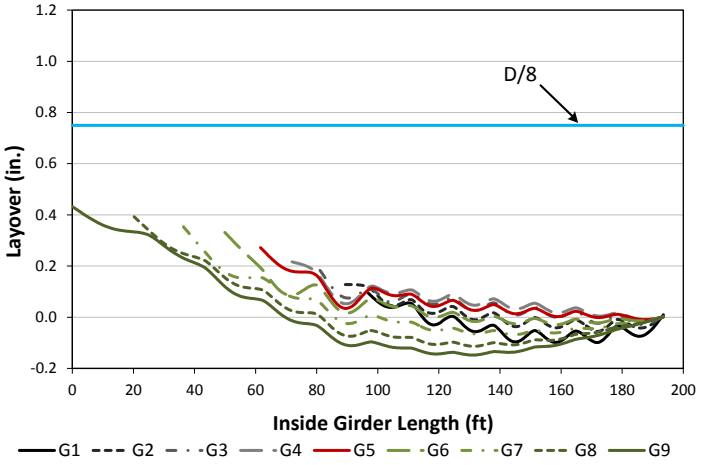

(iii) TDLF

Figure D.4.3. NISCS14, Girder layovers under total dead load for different detailing methods.

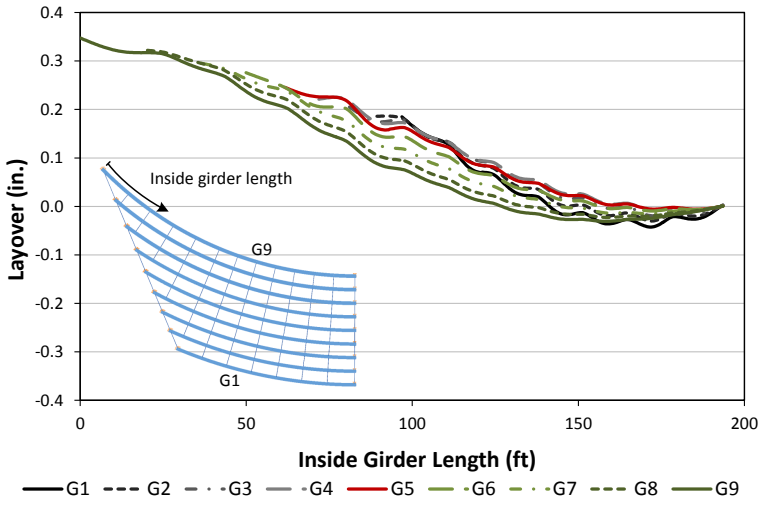

(i) NLF

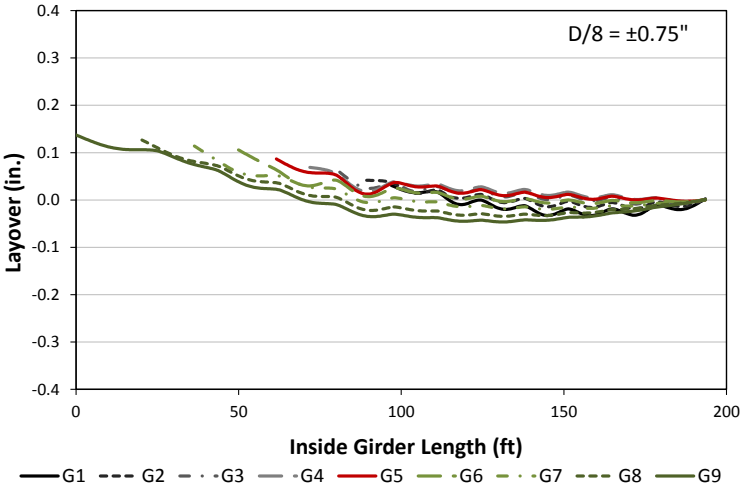

(ii) SDLF

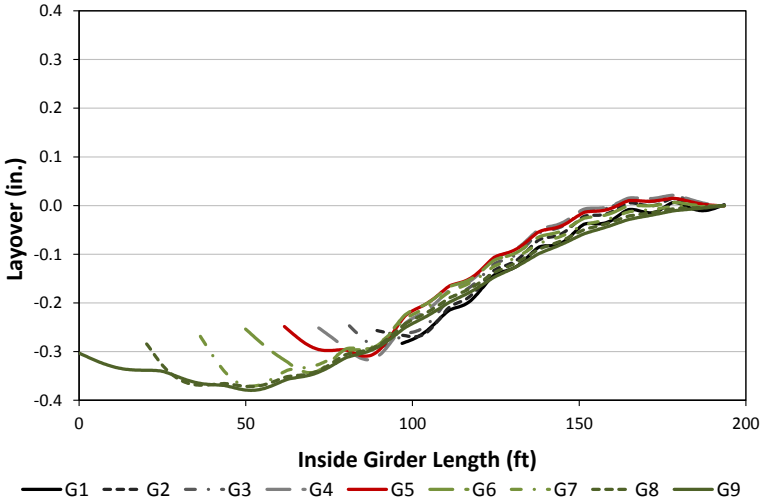

(iii) TDLF

Figure D.4.4. NISCS14, Girder layovers under total steel load for different detailing methods.

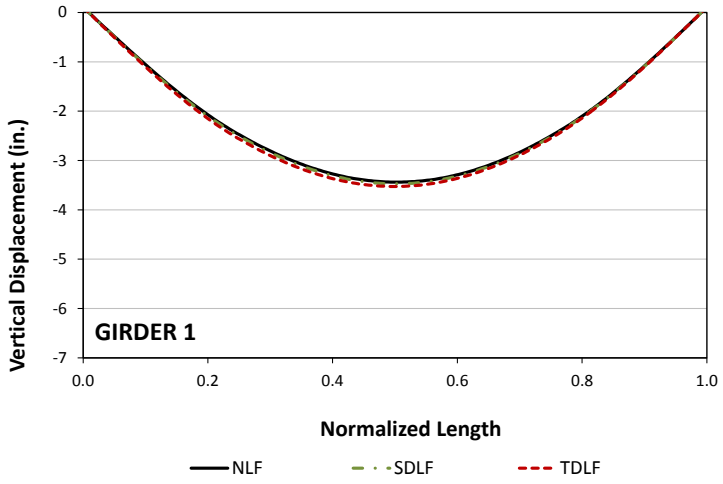

(i) Girder 1

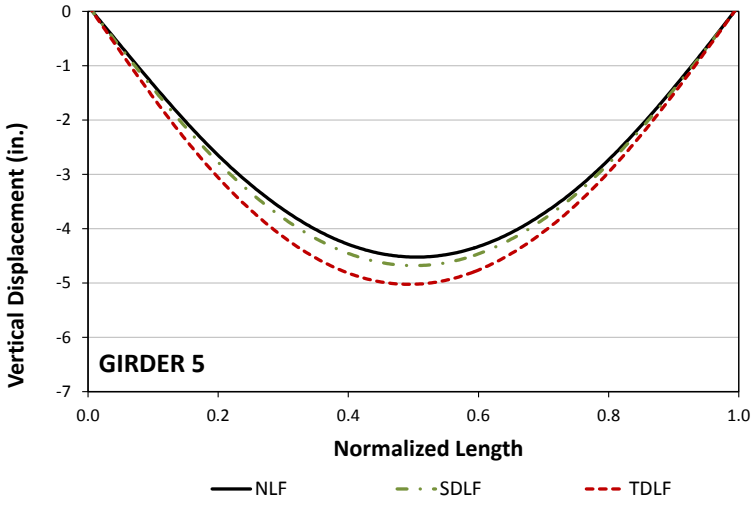

(ii) Girder 5

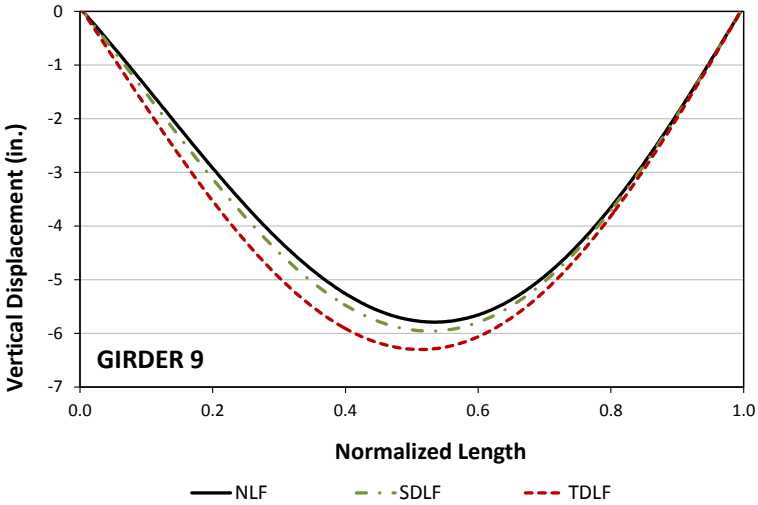

(iii) Girder 9

Figure D.4.5. NISCS14, Vertical deflections under total dead load for different detailing methods.

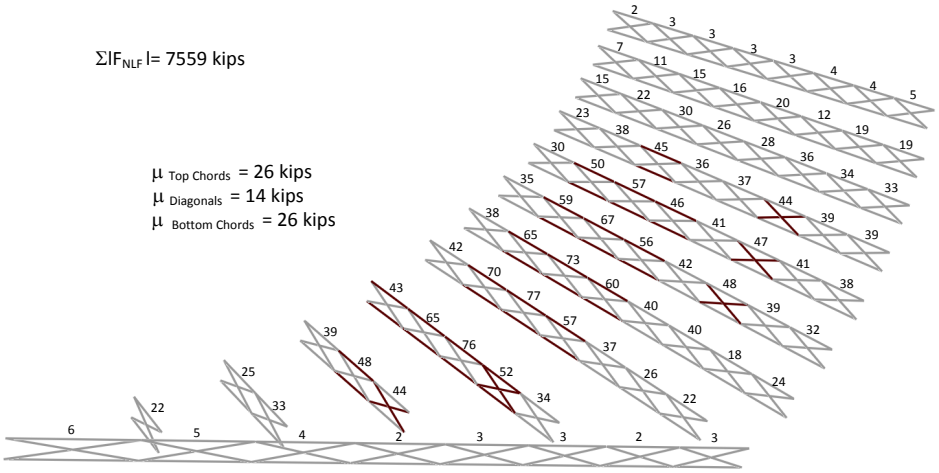

Figure D.4.6. NISCS14, maximum amplitude of the component axial forces in each of the cross-frames under total dead load (NLF detailing).

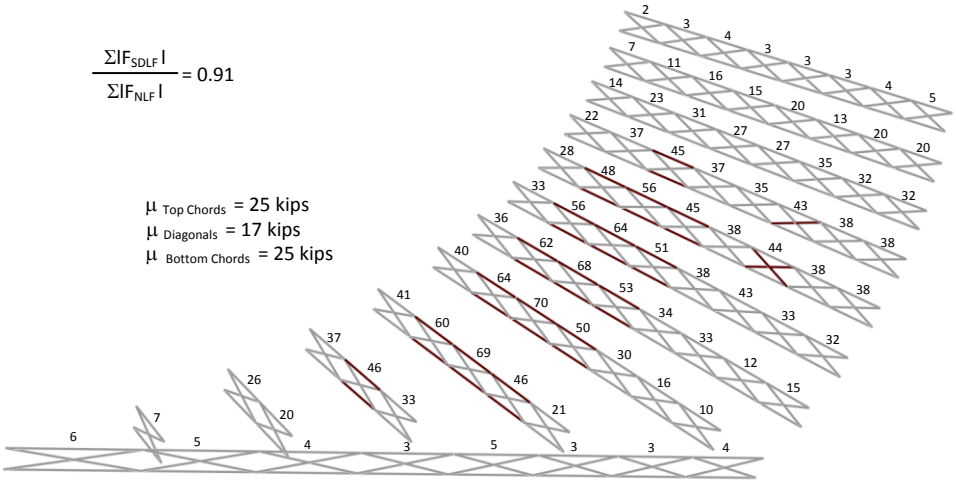

Figure D.4.7. NISCS14, maximum amplitude of the component axial forces in each of the cross-frames under total dead load (SDLF detailing).

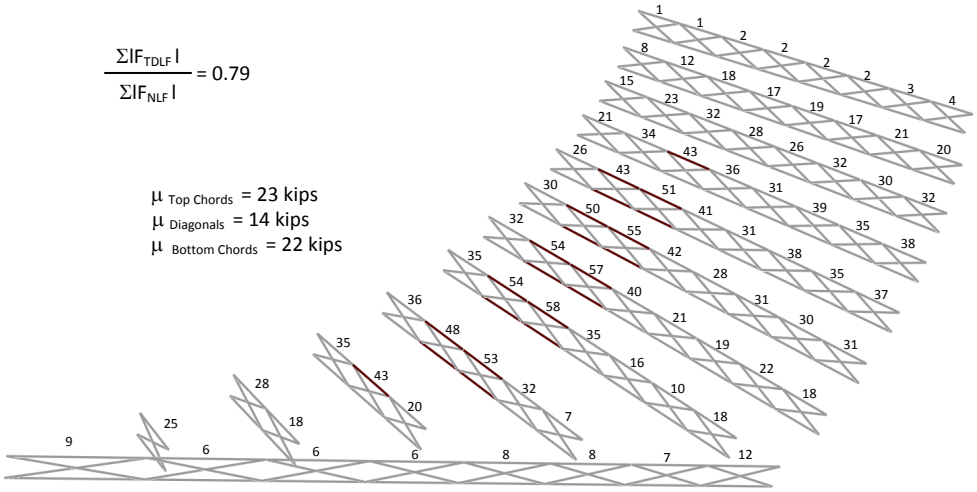

Figure D.4.8. NISCS14, maximum amplitude of the component axial forces in each of the cross-frames under total dead load (TDLF detailing).

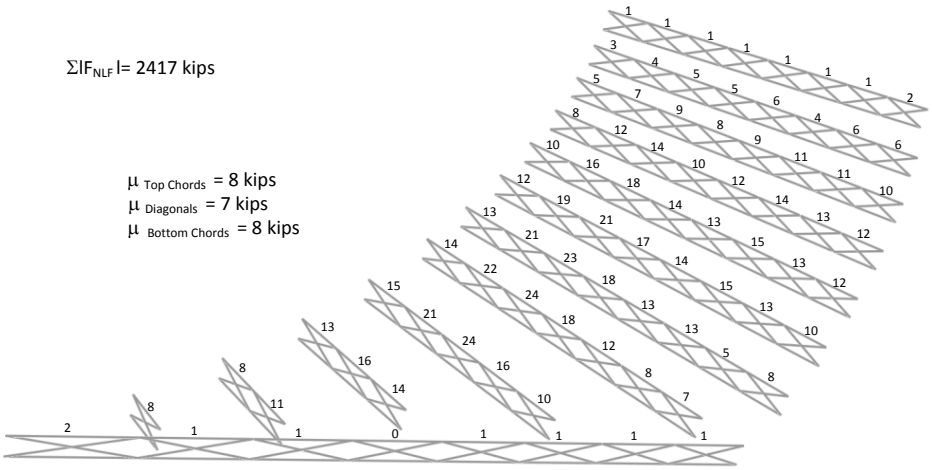

Figure D.4.9. NISCS14, maximum amplitude of the component axial forces in each of the cross-frames under steel dead load (NLF detailing).

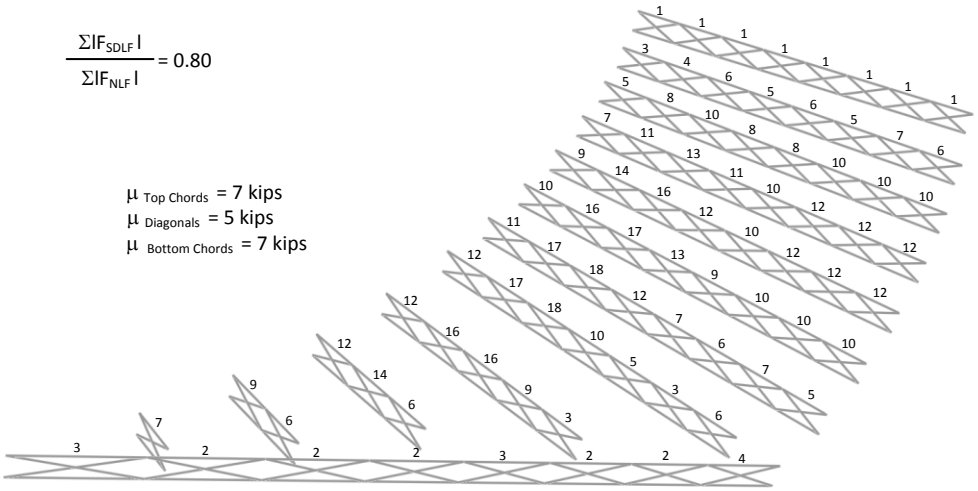

Figure D.4.10. NISCS14, maximum amplitude of the component axial forces in each of the cross-frames under steel dead load (SDLF detailing).

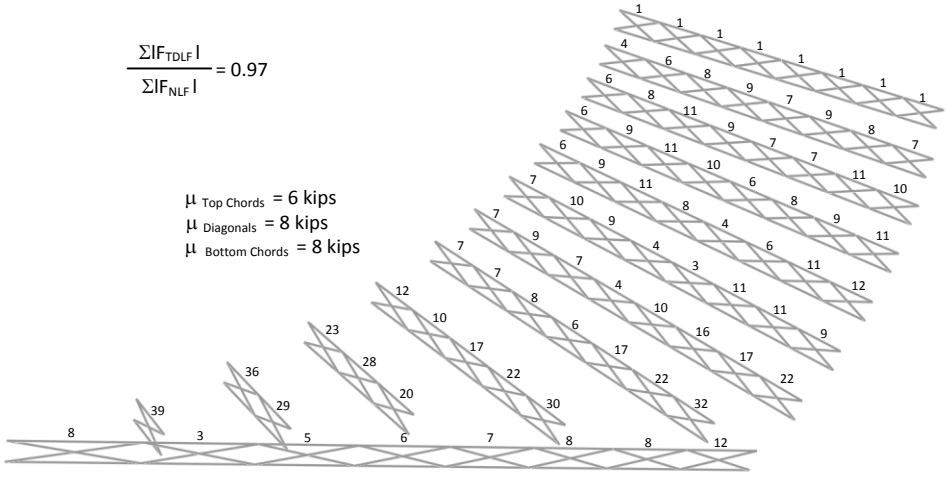

Figure D.4.11. NISCS14, maximum amplitude of the component axial forces in each of the cross-frames under steel dead load (TDLF detailing).

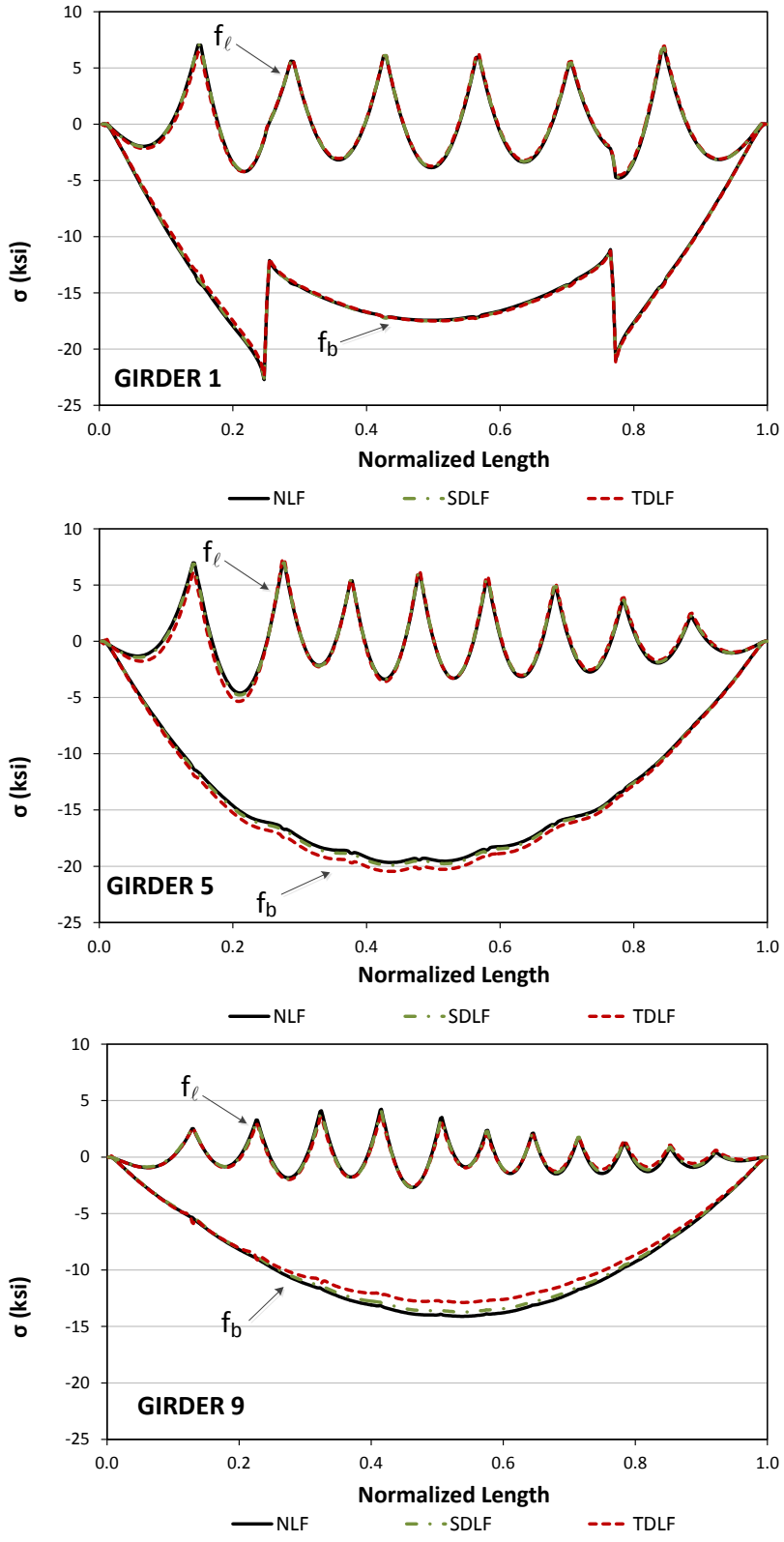

Figure D.4.12. NISCS14, Top flange stresses under total dead load for different detailing methods.

D.5. NISCS15

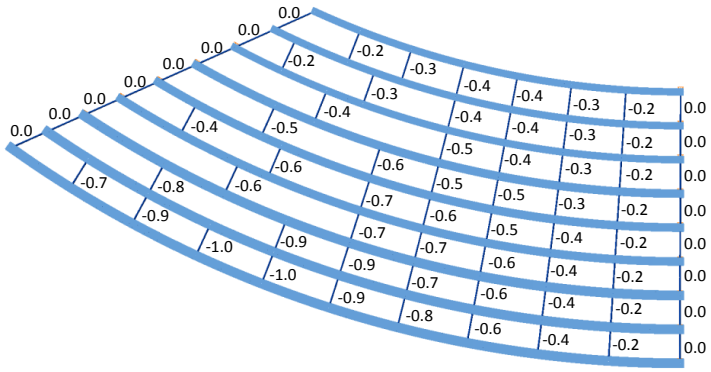

(i) Steel dead load

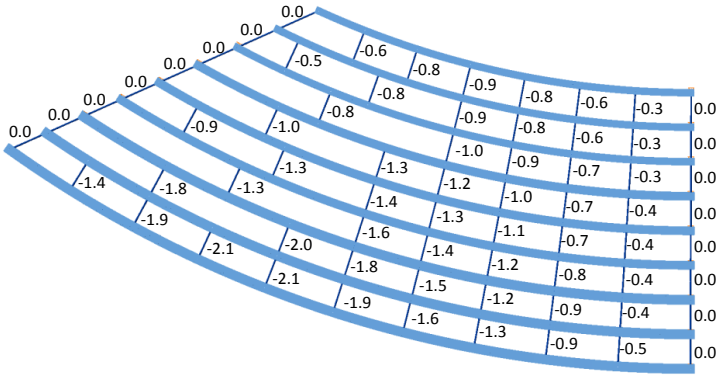

(ii) Total dead load

Figure D.5.1. NISCS15, Differential cambers between girders from steel and total dead load deflections.

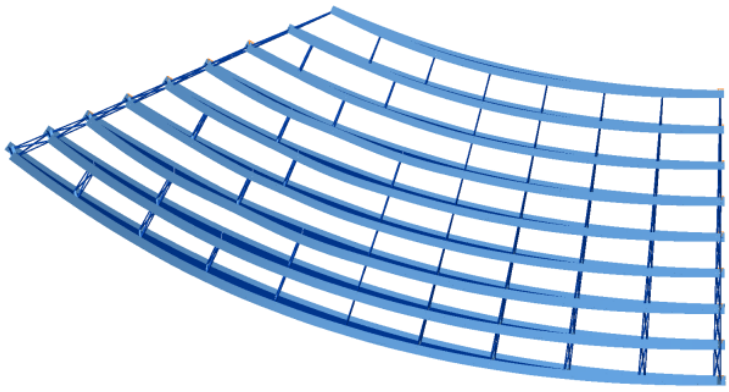

(i) NLF

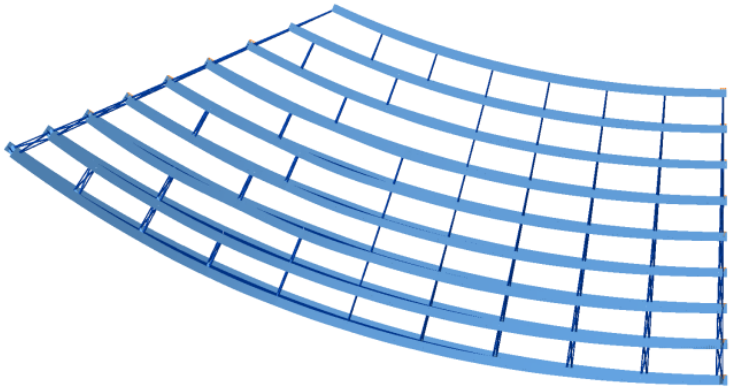

(ii) SDLF

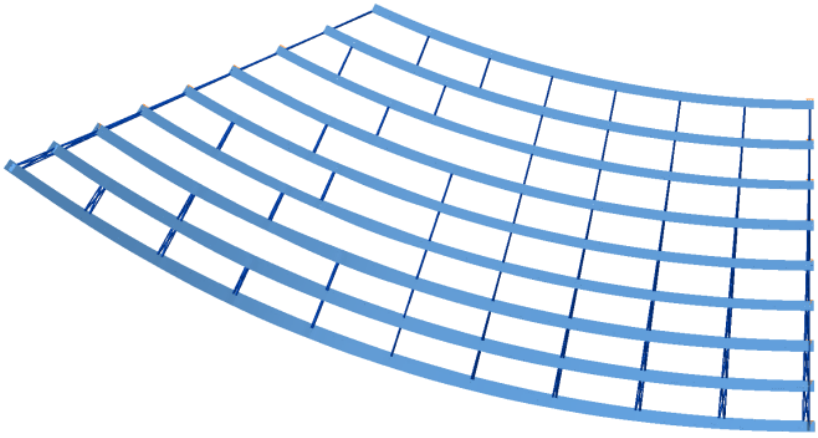

(iii) TDLF

Figure D.5.2. NISCS15, Deflected shape under total dead load for different detailing methods (magnified by 20x).

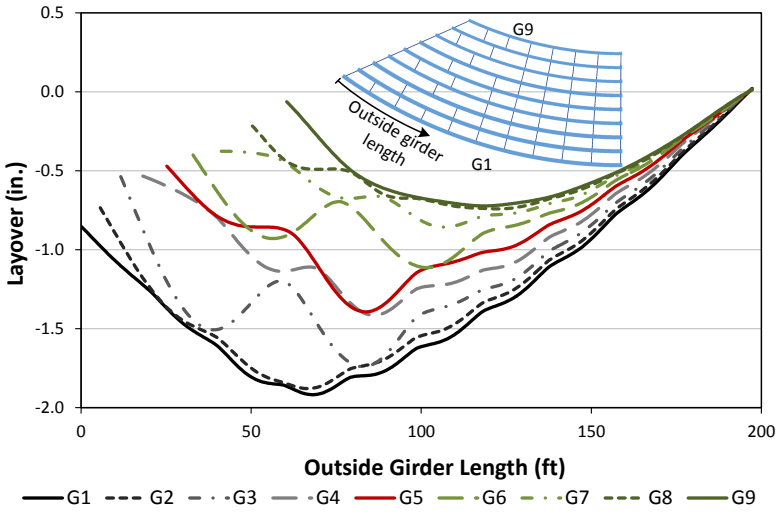

(i) NLF

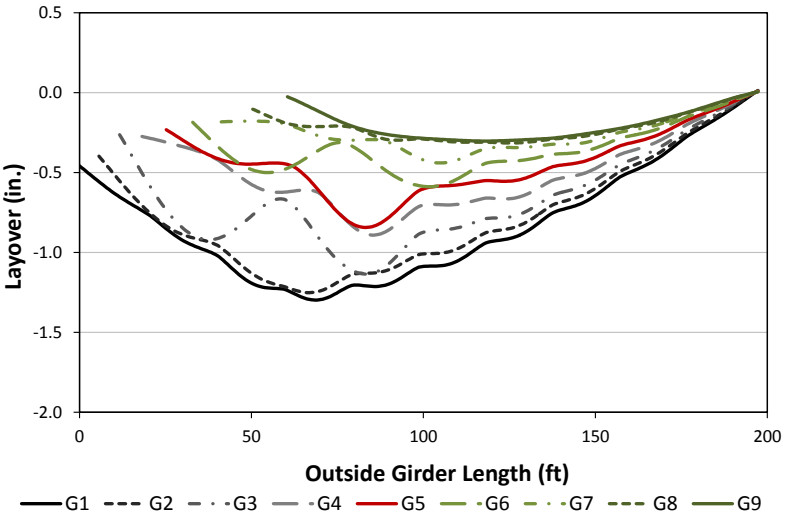

(ii) SDLF

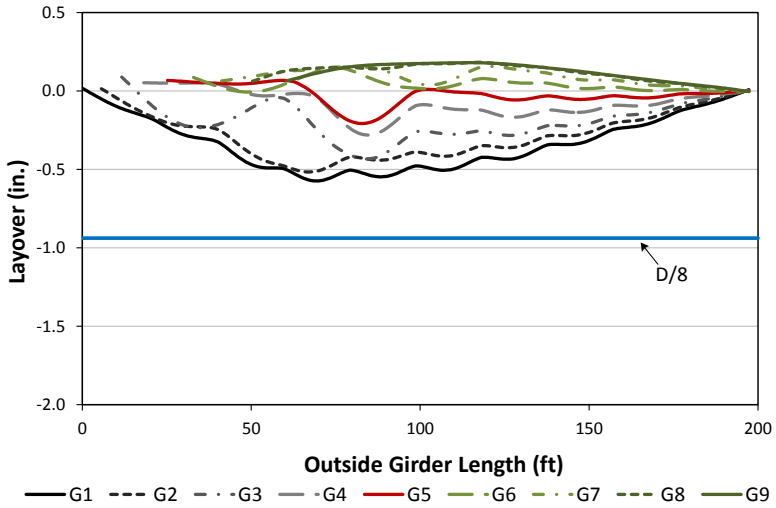

(iii) TDLF

Figure D.5.3. NISCS15, Girder layovers under total dead load for different detailing methods.

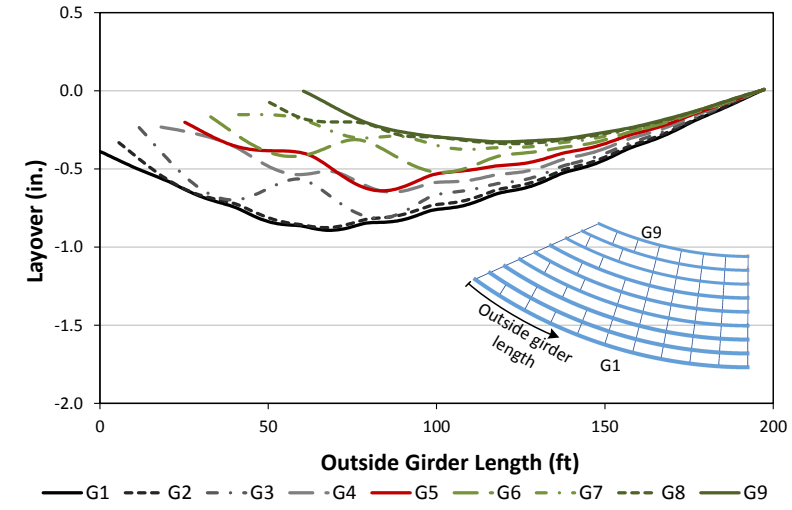

(i) NLF

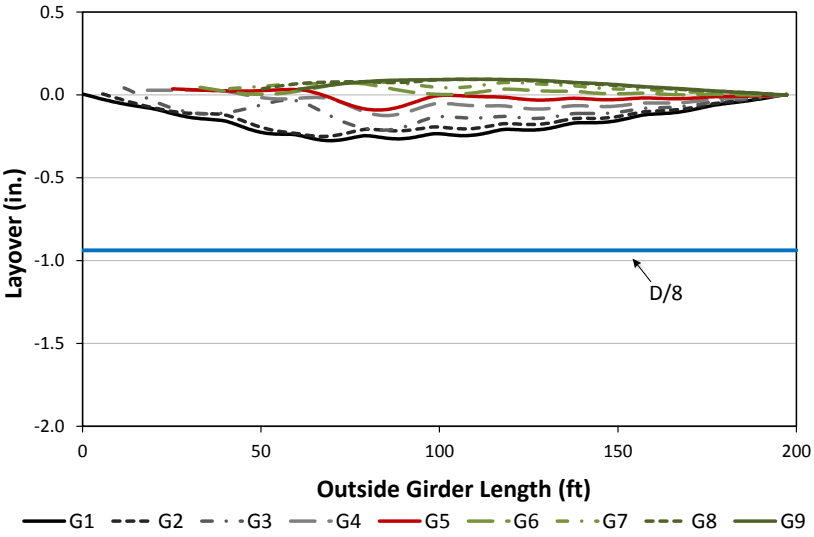

(ii) SDLF

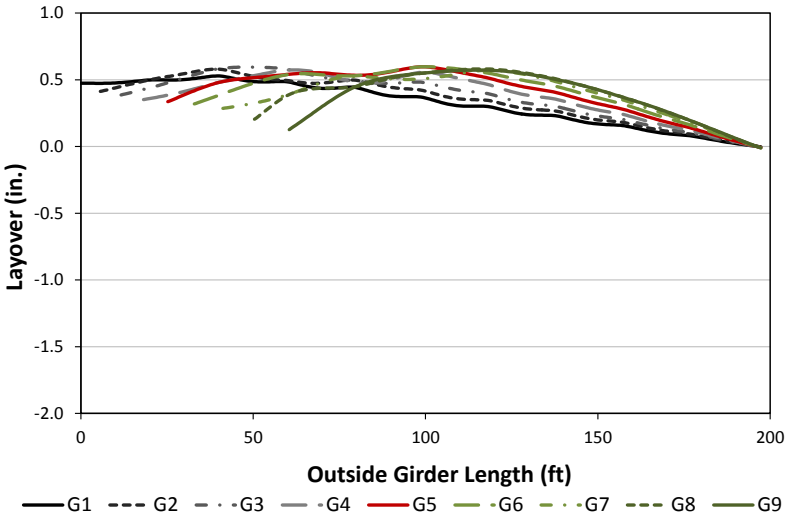

(iii) TDLF

Figure D.5.4. NISCS15, Girder layovers under steel dead load for different detailing methods.

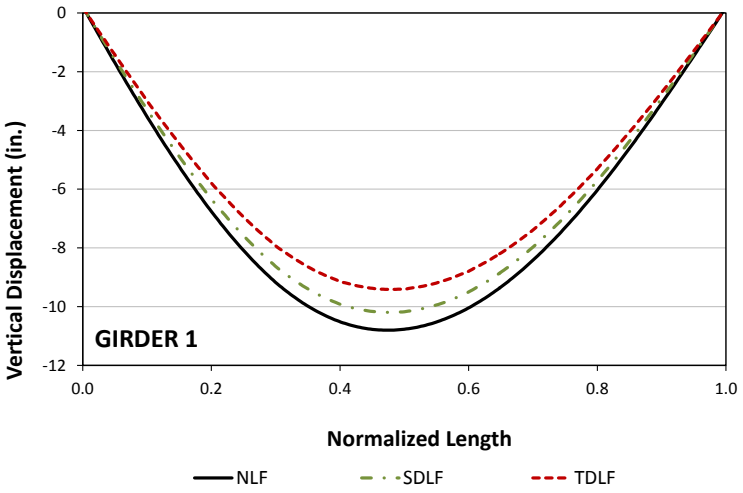

(i) Girder 1

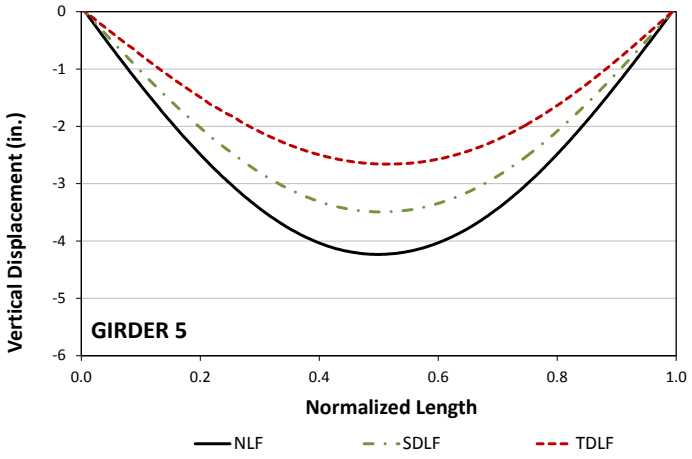

(ii) Girder 5

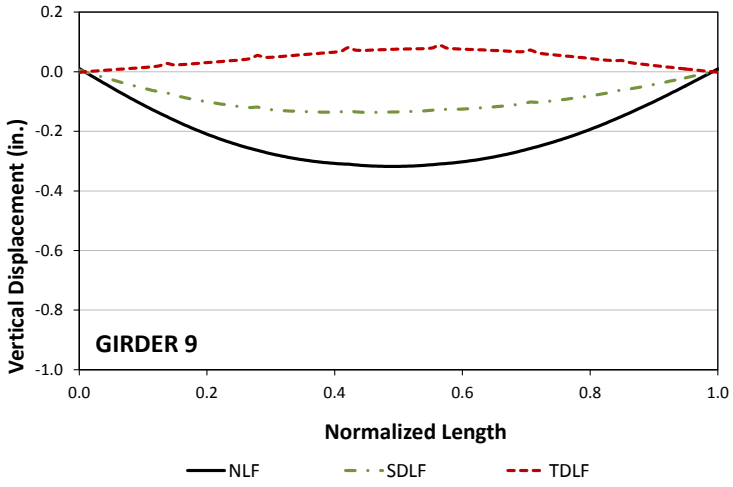

(iii) Girder 9

Figure D.5.5. NISCS15, Vertical deflections under total dead load for different detailing methods.

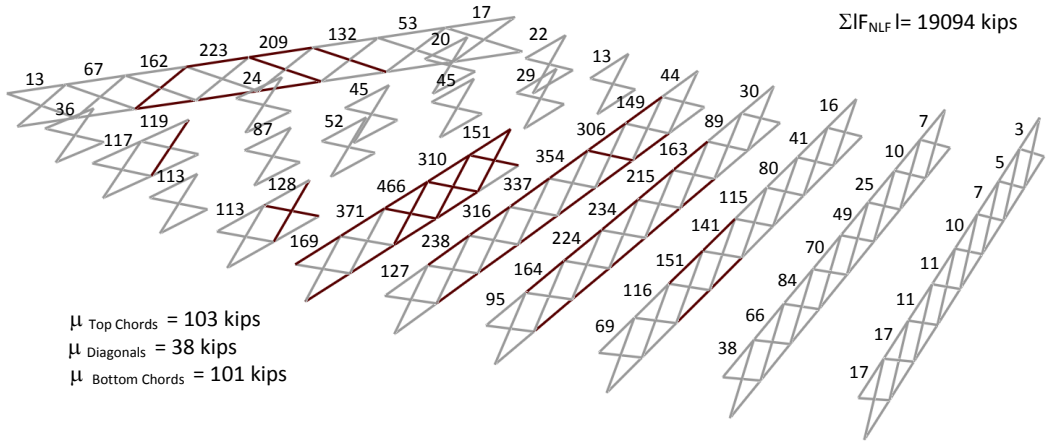

Figure D.5.6. NISCS15, maximum amplitude of the component axial forces in each of the cross-frames under total dead load (NLF detailing).

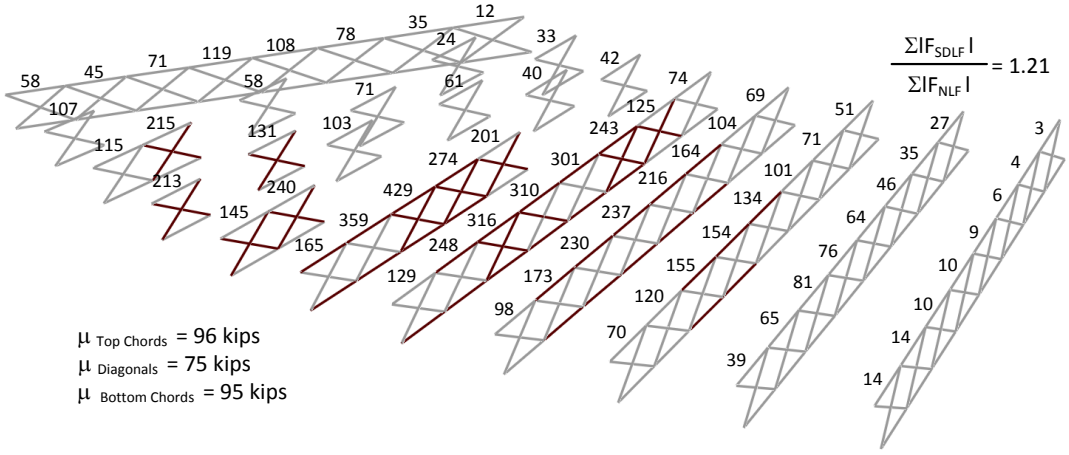

Figure D.5.7. NISCS15, maximum amplitude of the component axial forces in each of the cross-frames under total dead load (SDLF detailing).

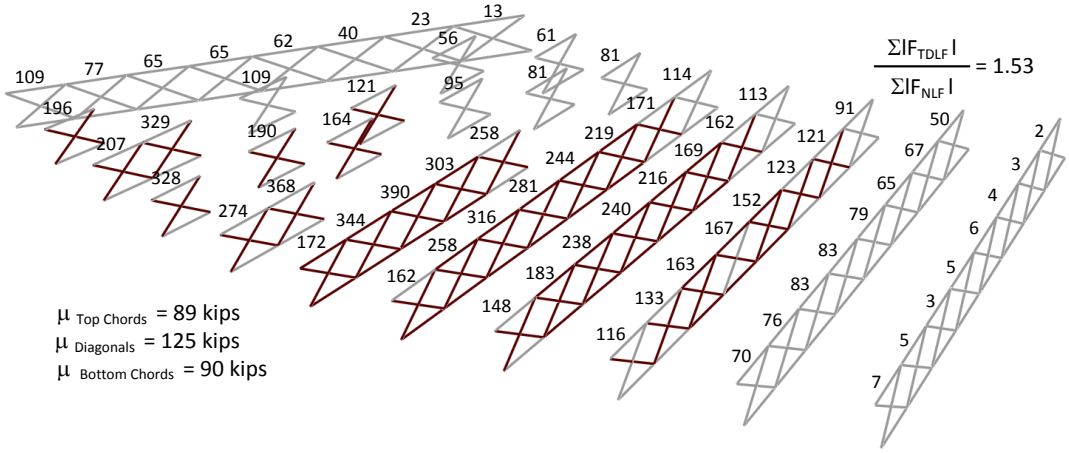

Figure D.5.8. NISCS15, maximum amplitude of the component axial forces in each of the cross-frames under total dead load (TDLF detailing).

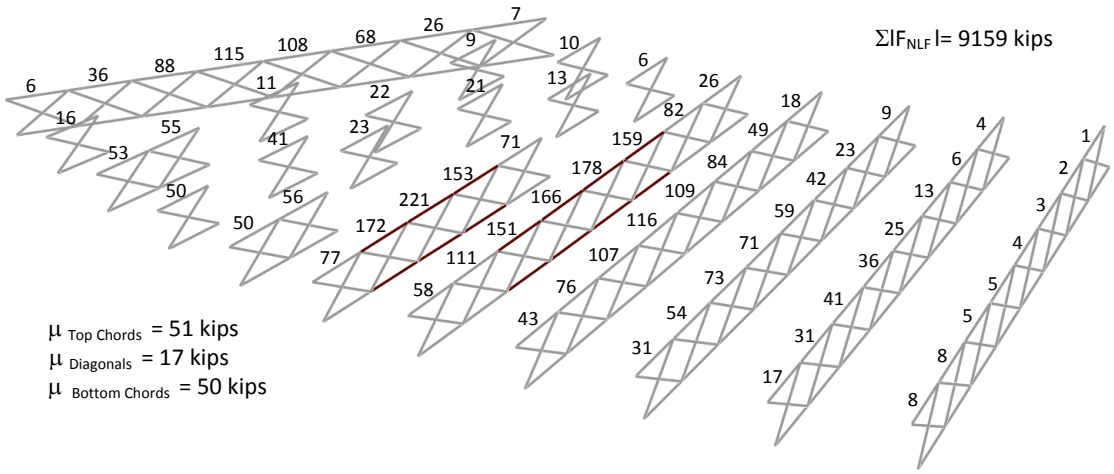

Figure D.5.9. NISCS15, maximum amplitude of the component axial forces in each of the cross-frames under steel dead load (NLF detailing).

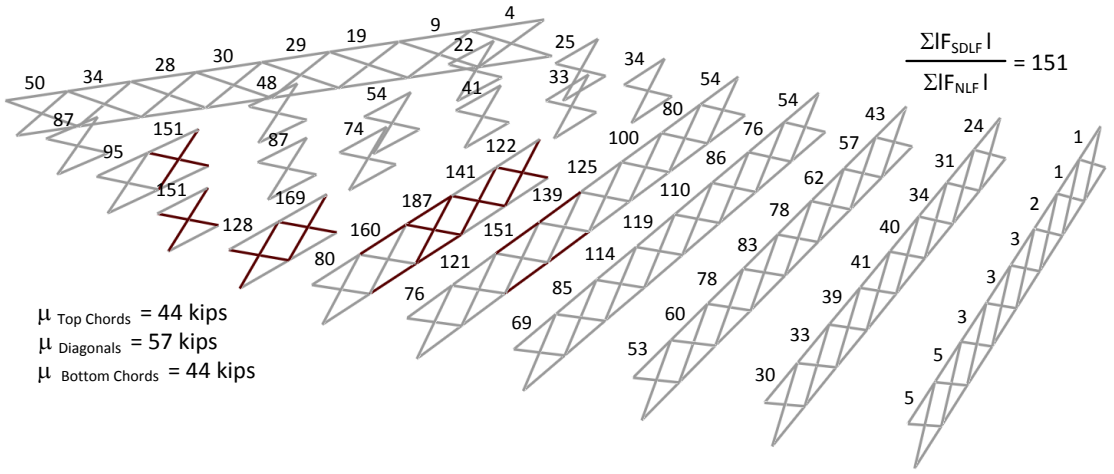

Figure D.5.10. NISCS15, maximum amplitude of the component axial forces in each of the cross-frames under steel dead load (SDLF detailing).

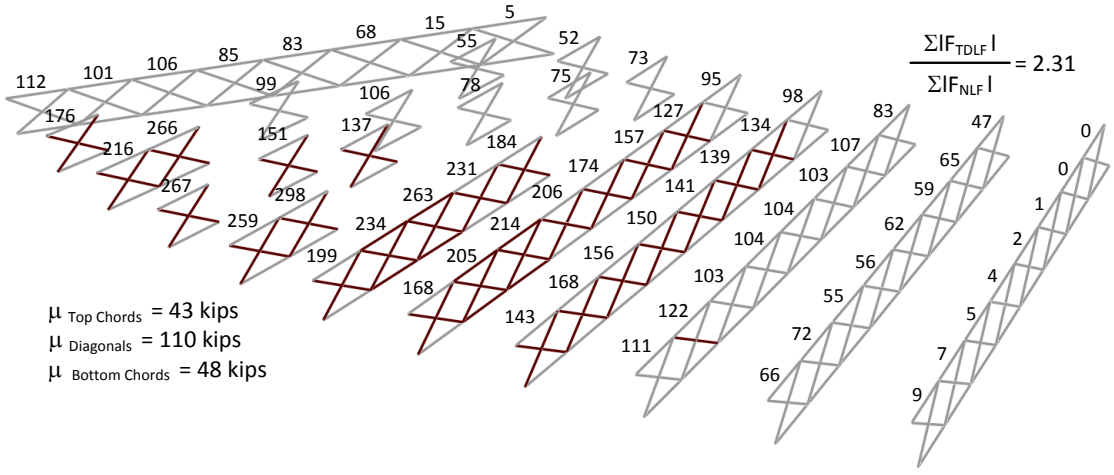

Figure D.5.11. NISCS15, maximum amplitude of the component axial forces in each of the cross-frames under steel dead load (TDLF detailing).

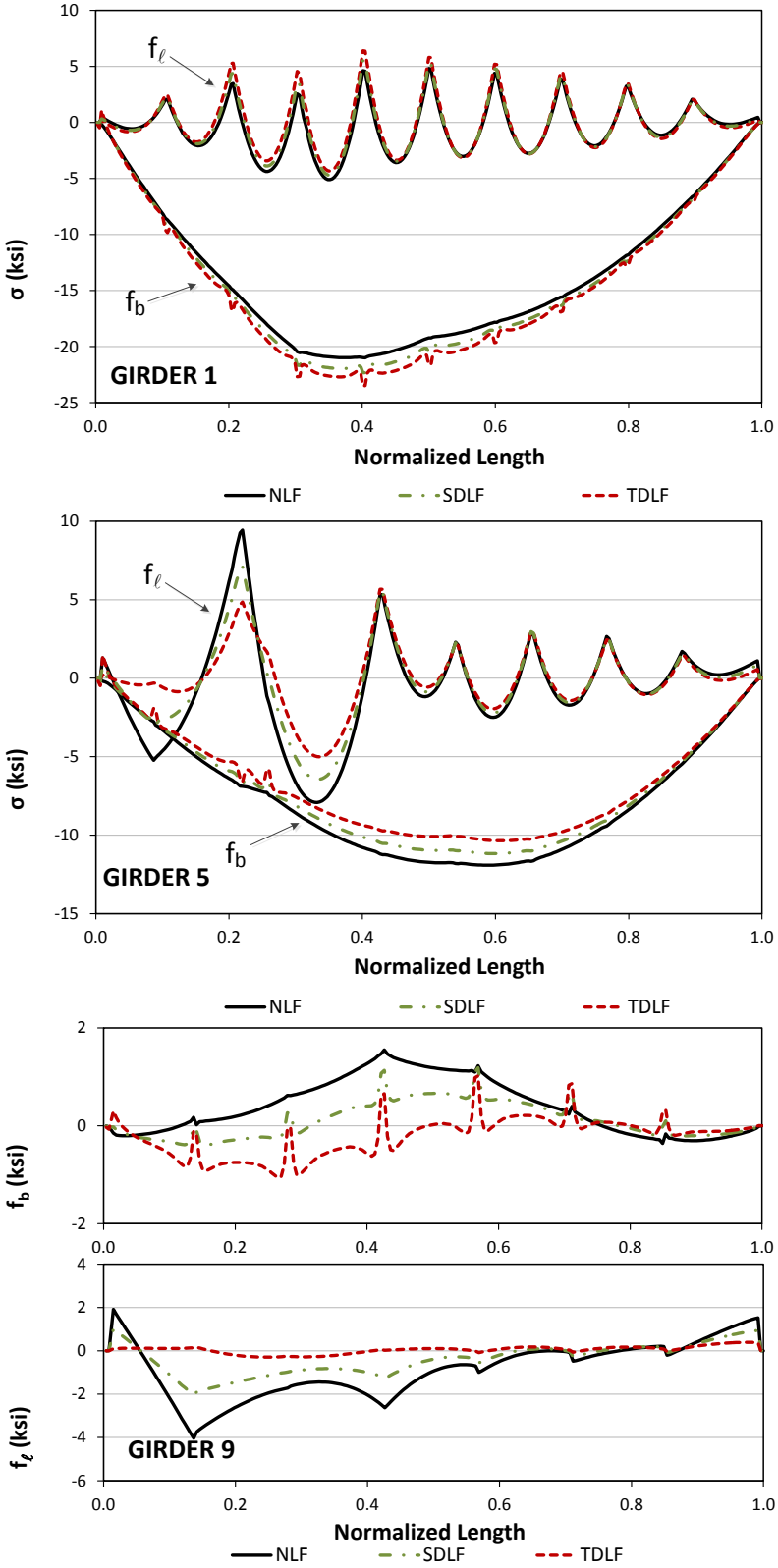

Figure D.5.12. NISCS15, Top flange stresses under total dead load for different detailing methods

D.6. EICCR11

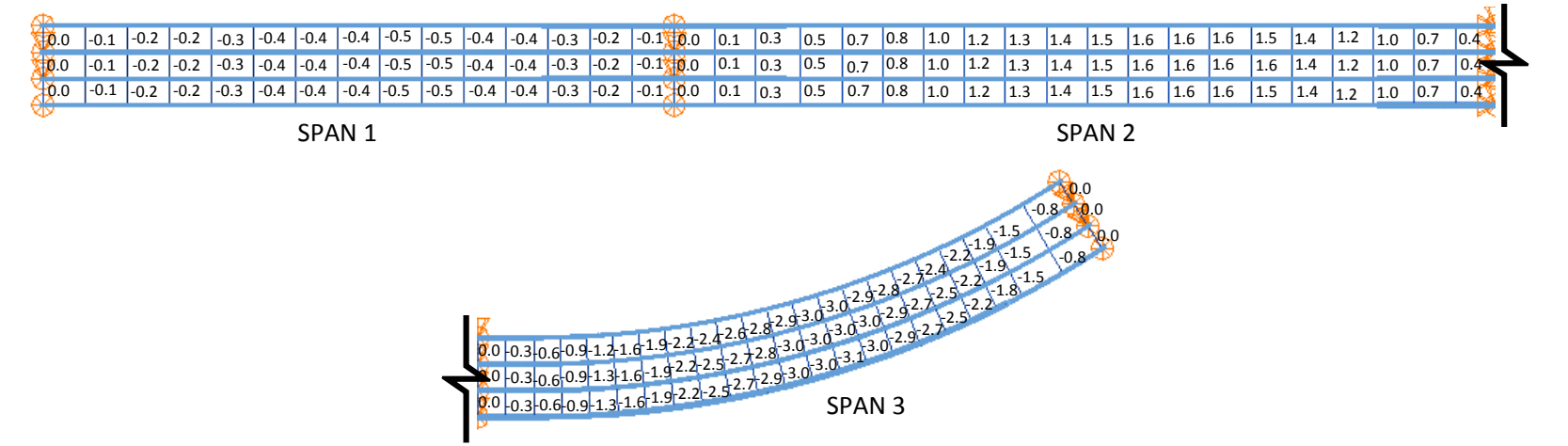

(i) Steel dead load

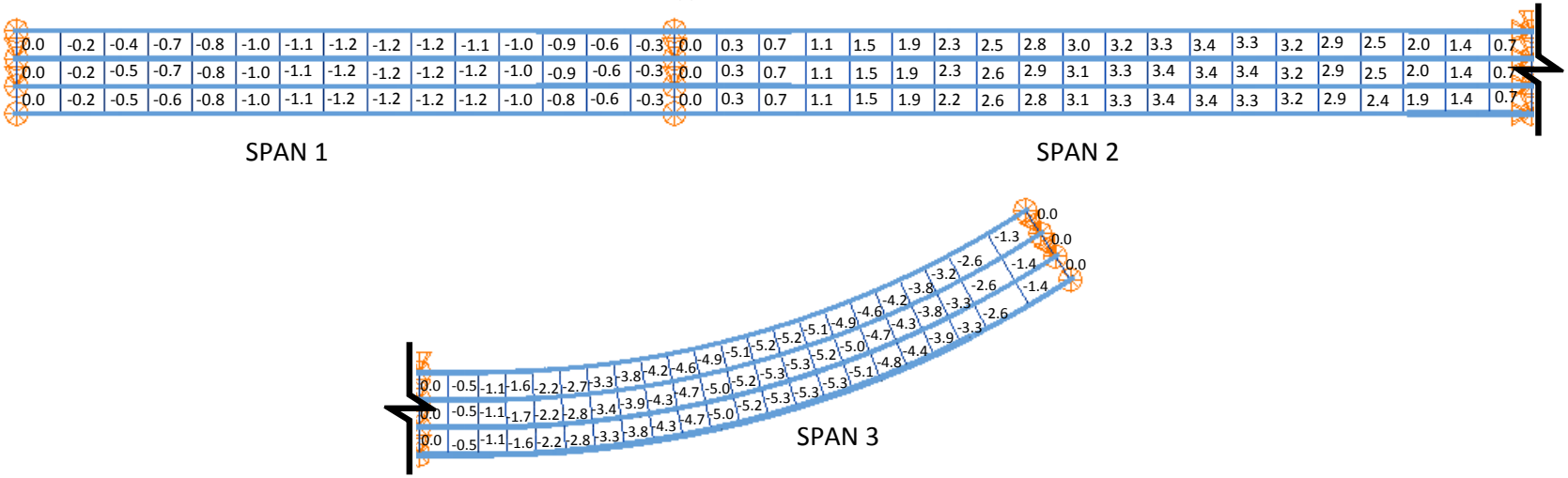

(ii) Total dead load

Figure D.6.1. EICCR11, Differential cambers between girders from steel and total dead load deflections.

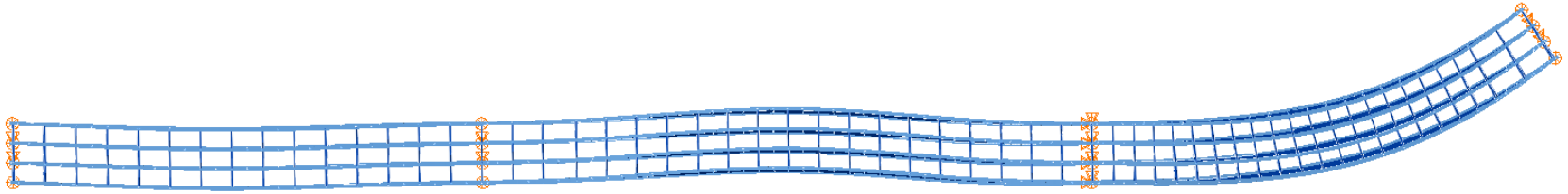

(i) NLF

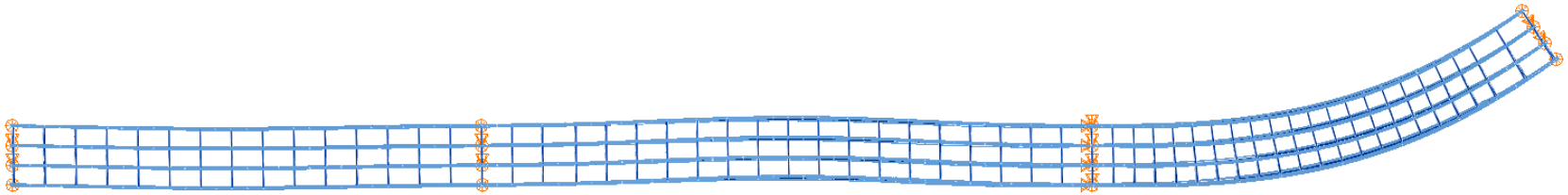

(ii) SDLF

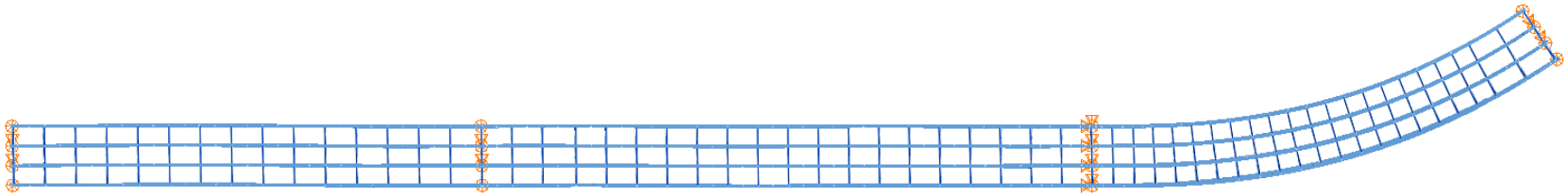

(iii) TDLF

Figure D.6.2. EICCR11, Deflected shape under total dead load for different detailing methods (magnified by 10x)

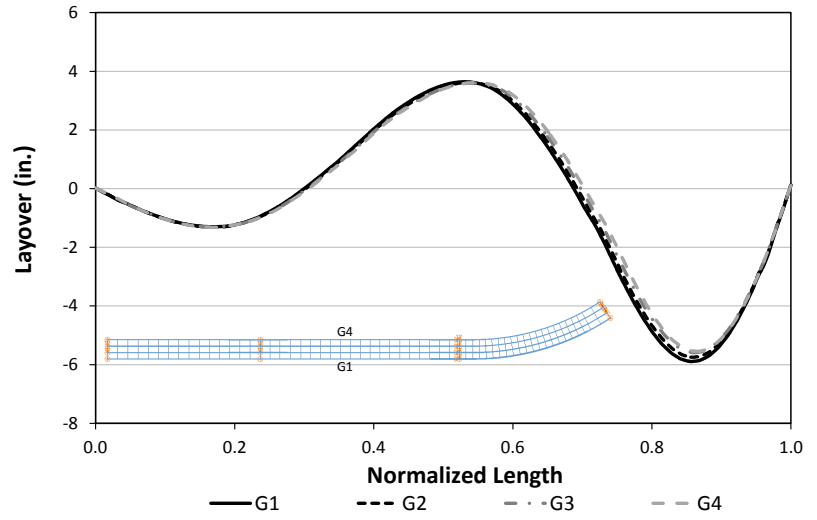

(i) NLF

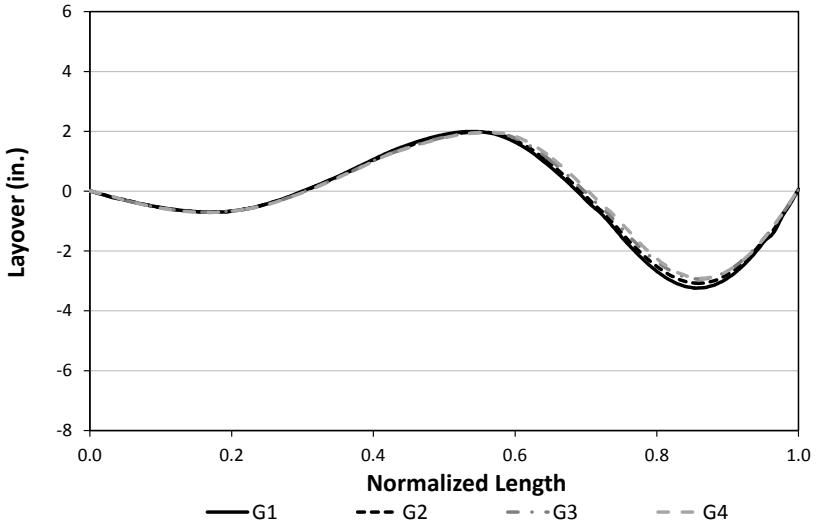

(ii) SDLF

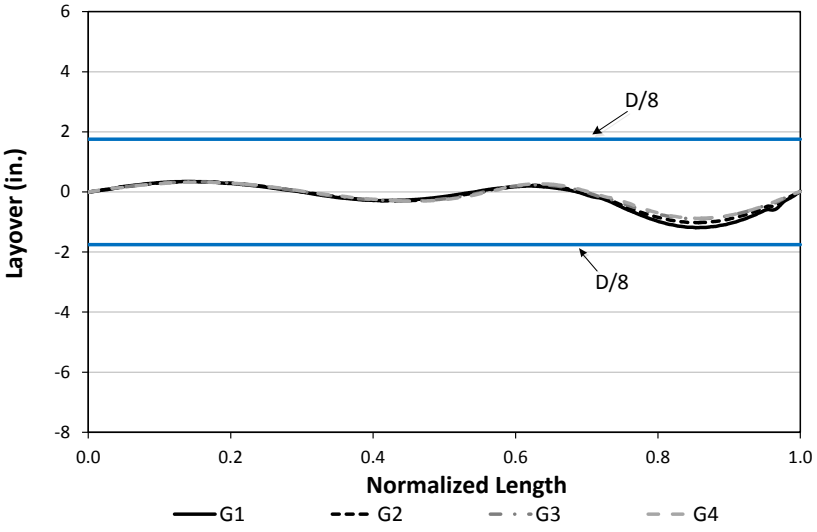

(iii) TDLF

Figure D.6.3. EICCR11, Girder layovers under total dead load for different detailing methods.

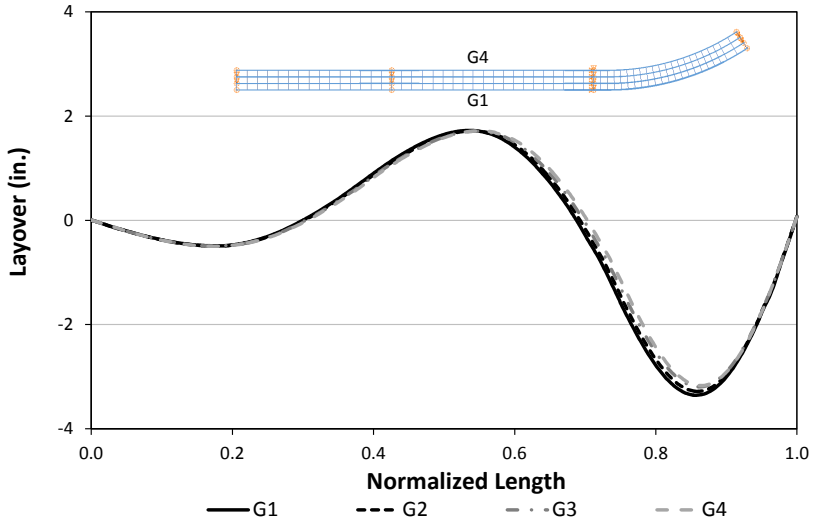

(i) NLF

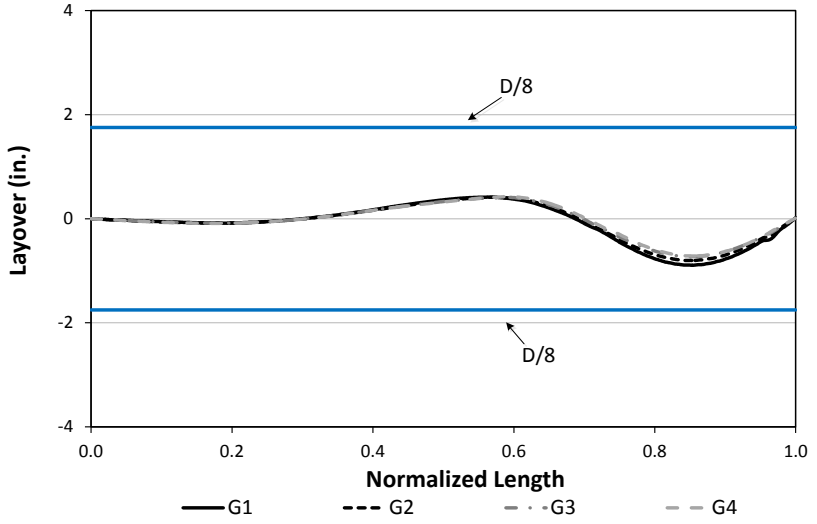

(ii) SDLF

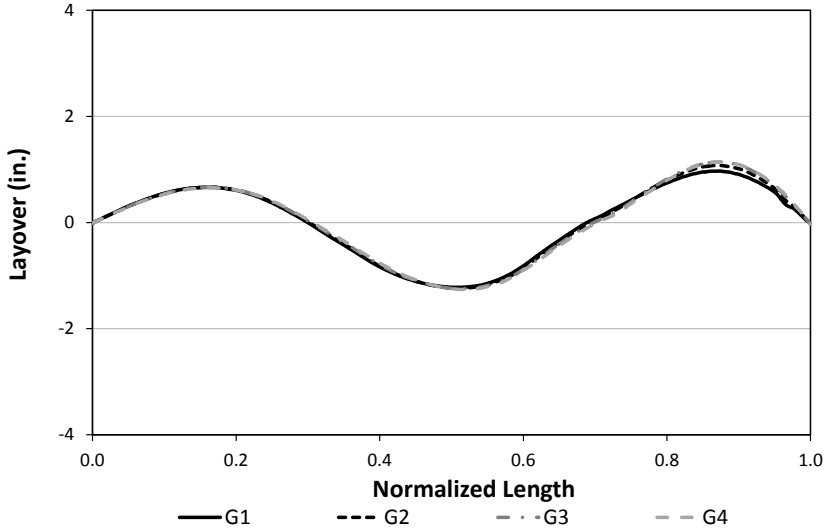

(iii) TDLF

Figure D.6.4. EICCR11, Girder layovers under steel dead load for different detailing methods.

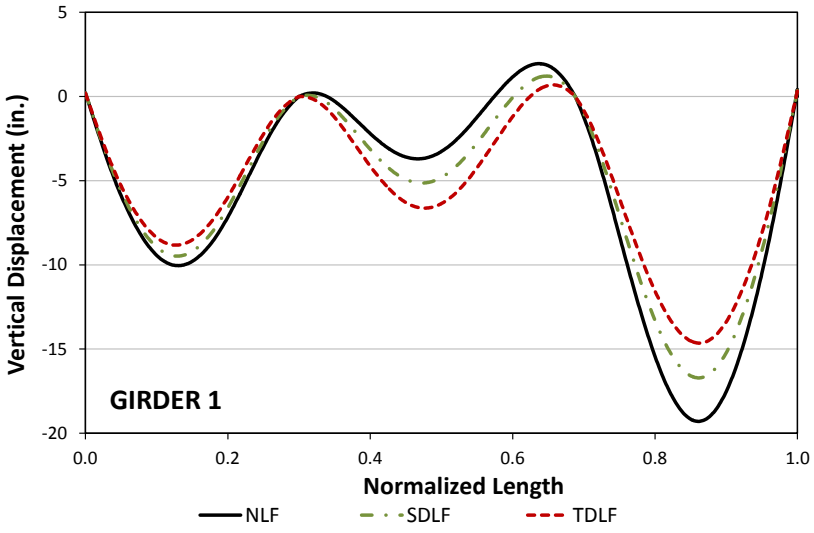

(i) Girder 1

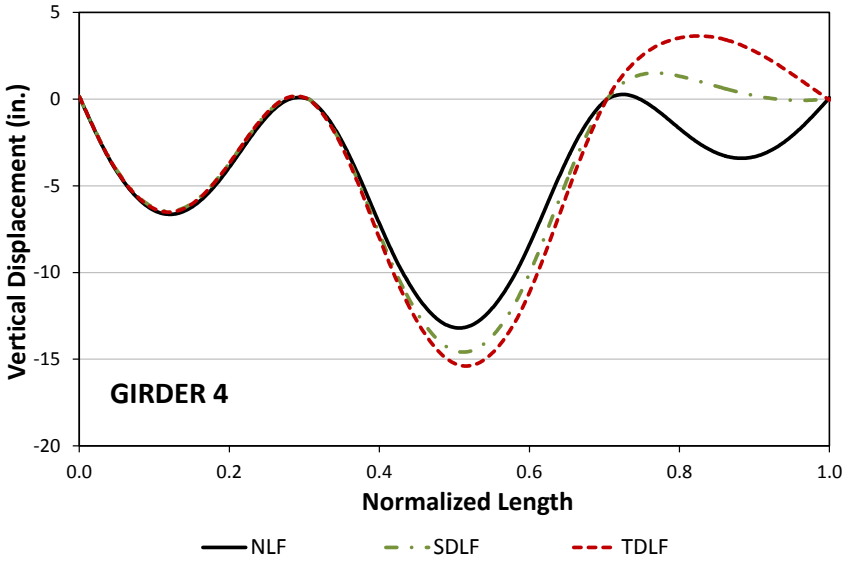

(ii) Girder 4

Figure D.6.5. EICCR11, Vertical deflections under total dead load for different detailing methods.

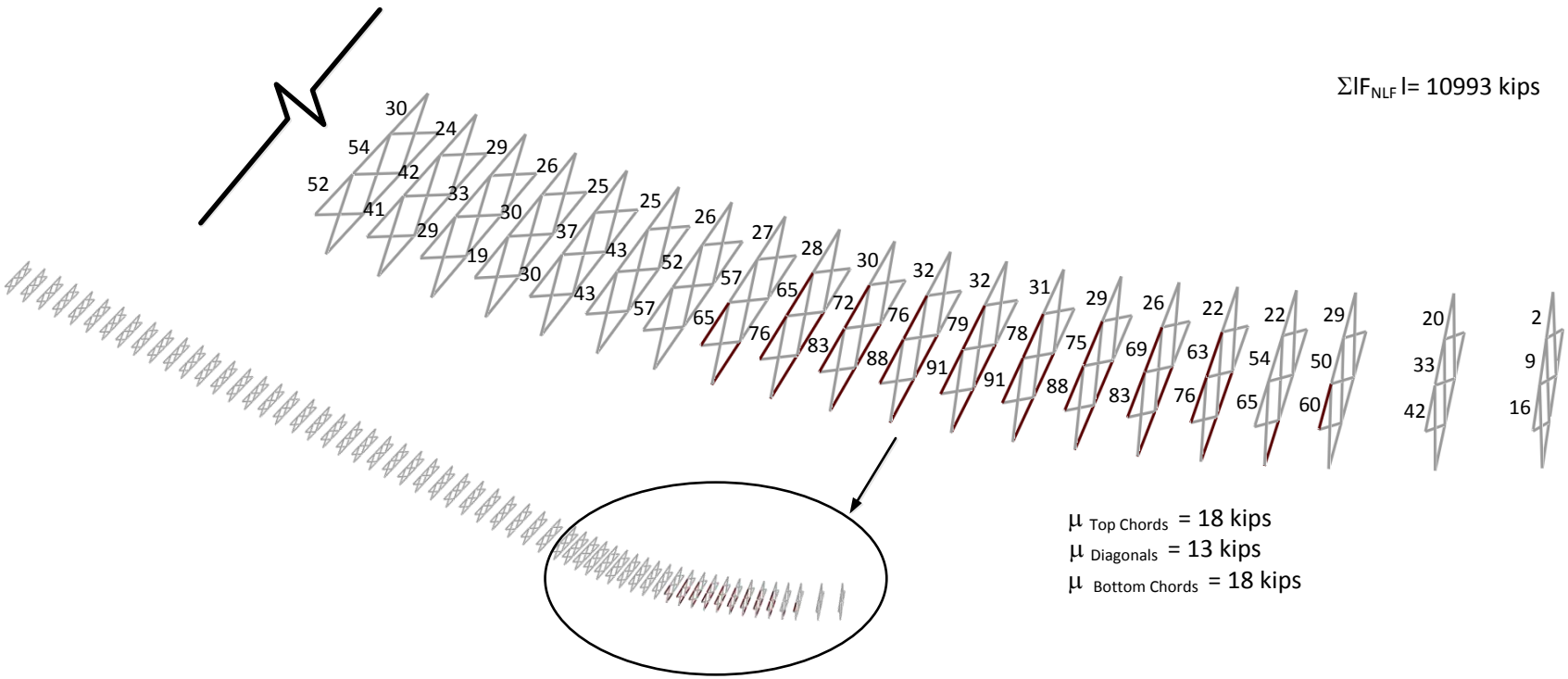

Figure D.6.6. EICCR11, maximum amplitude of the component axial forces in each of the cross-frames under total dead load (NLF detailing).

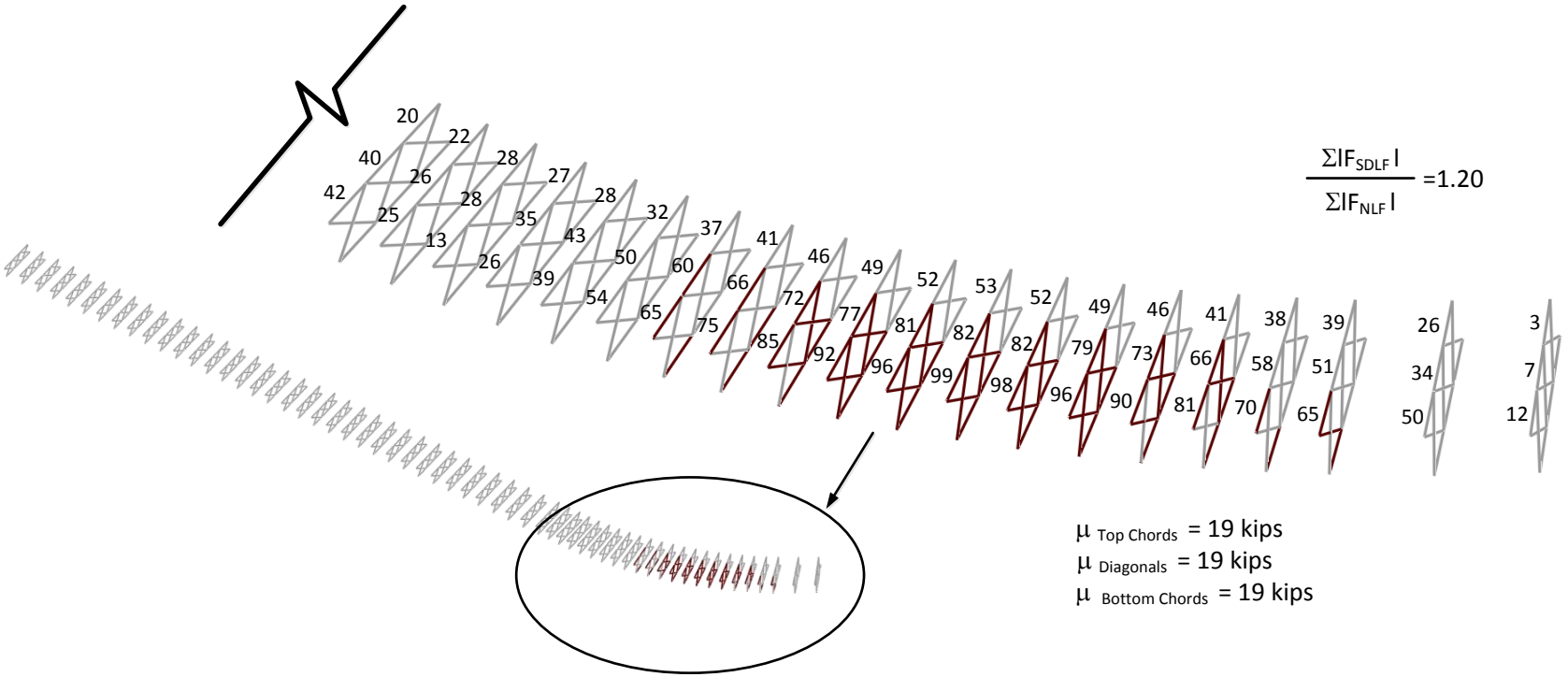

Figure D.6.7. EICCR11, maximum amplitude of the component axial forces in each of the cross-frames under total dead load (SDLF detailing).

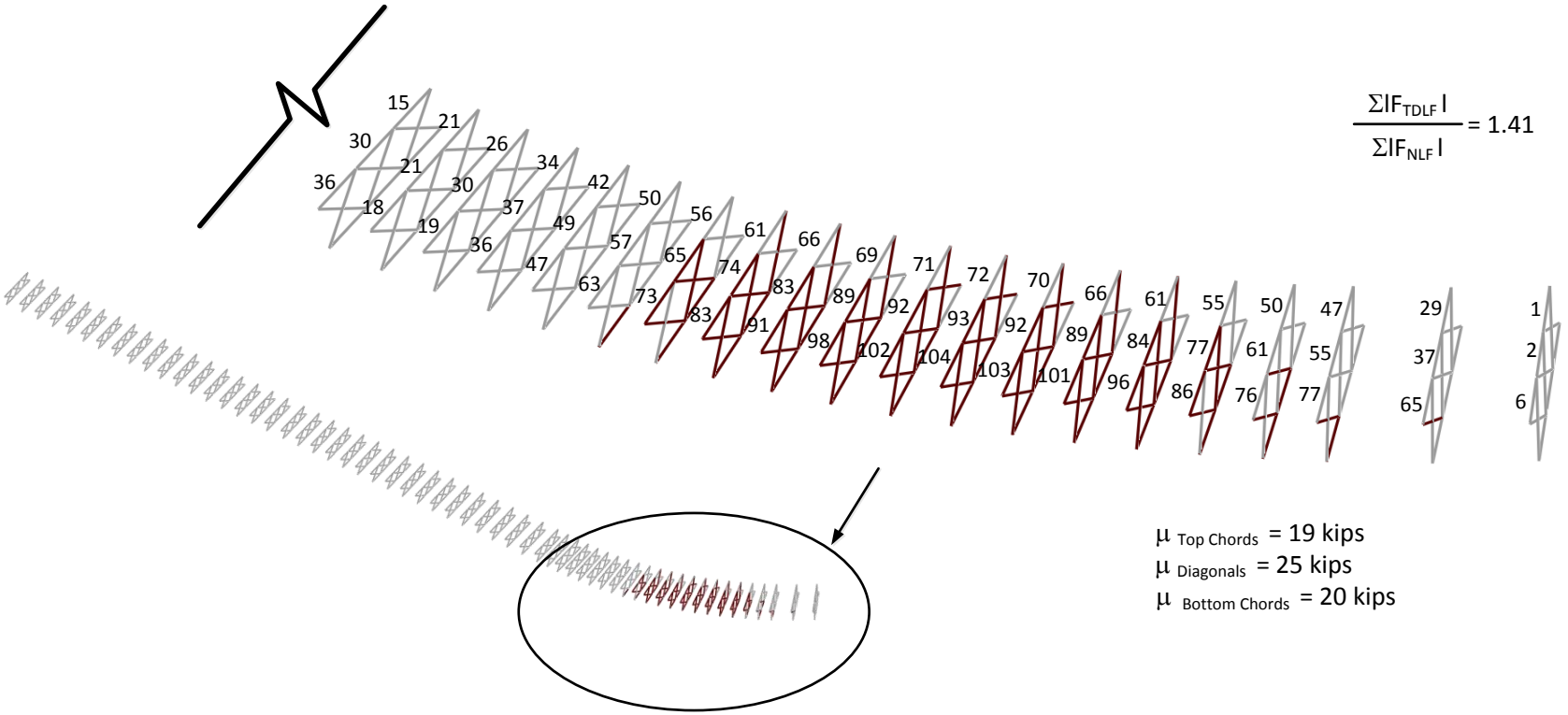

Figure D.6.8. EICCR11, maximum amplitude of the component axial forces in each of the cross-frames under total dead load (TDLF detailing).

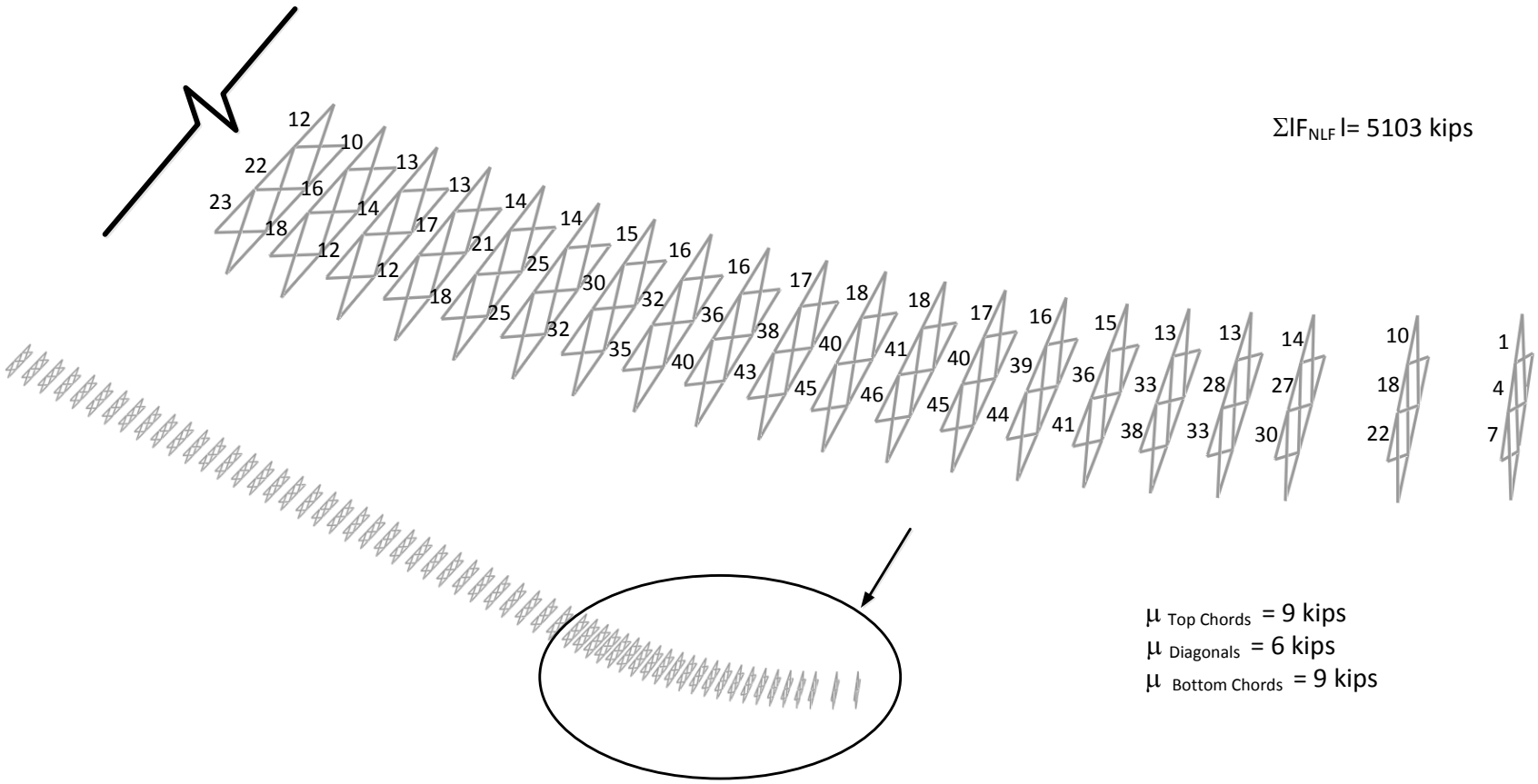

Figure D.6.9. EICCR11, maximum amplitude of the component axial forces in each of the cross-frames under steel dead load (NLF detailing).

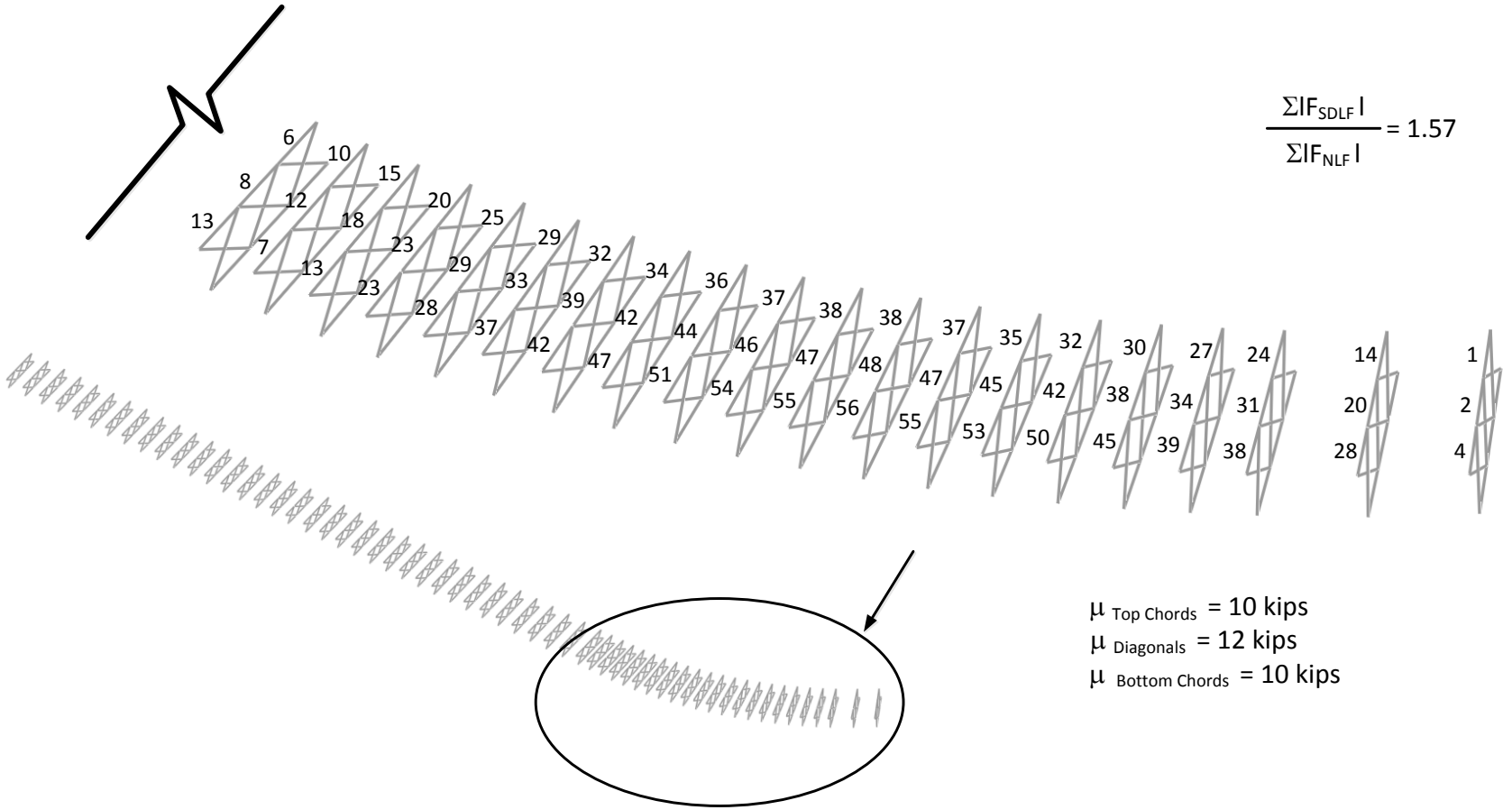

Figure D.6.10. EICCR11, maximum amplitude of the component axial forces in each of the cross-frames under steel dead load (SDLF detailing).

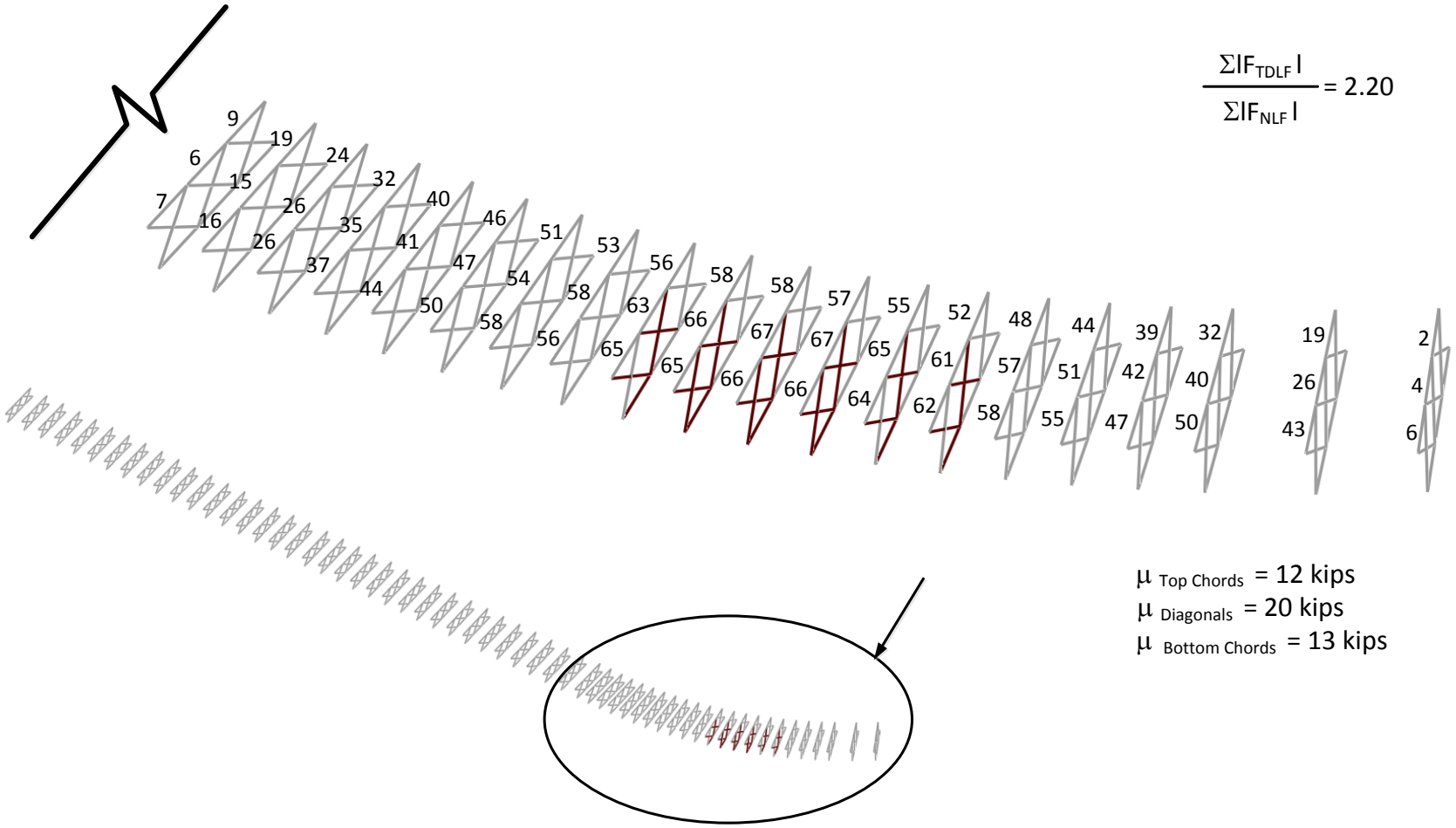

Figure D.6.11. EICCR11, maximum amplitude of the component axial forces in each of the cross-frames under steel dead load (TDLF detailing).

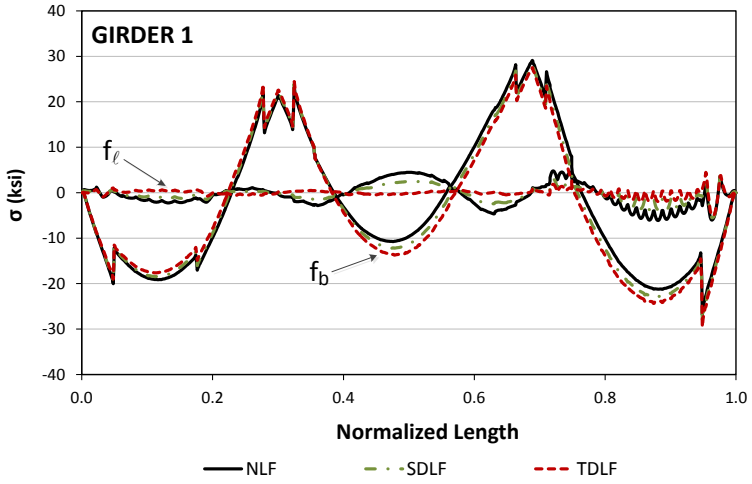

(i) Girder 1

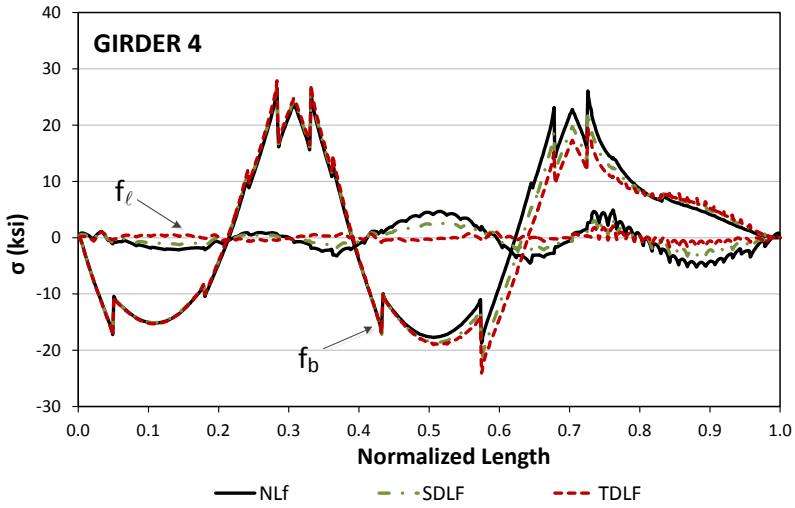

(ii) Girder 4

Figure D.6.12. EICCR11, Top flange stresses under total dead load for different detailing methods.

D.7. EICSS12

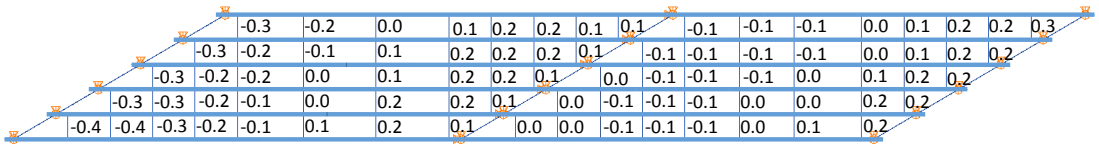

(i) Steel dead load

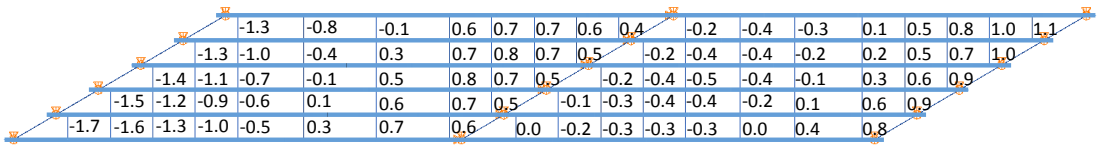

(ii) Total dead load

Figure D.7.1. EICSS12, Differential cambers between girders from steel and total dead load deflections.

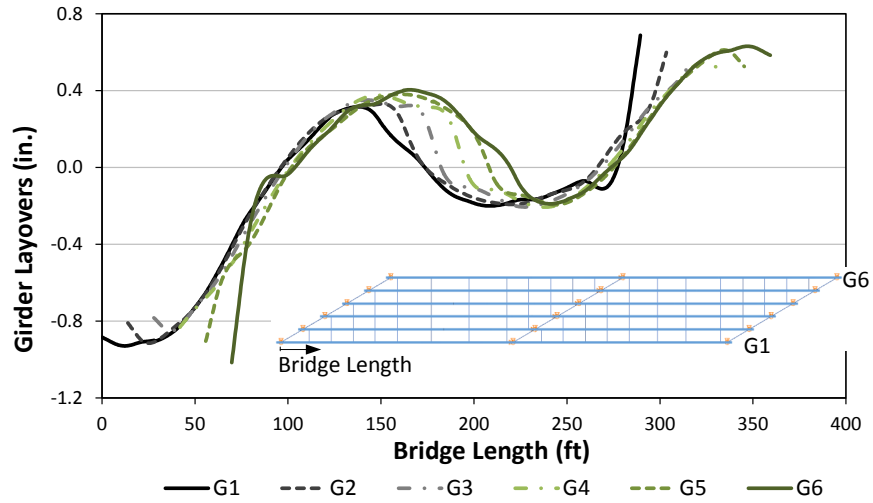

(i) NLF

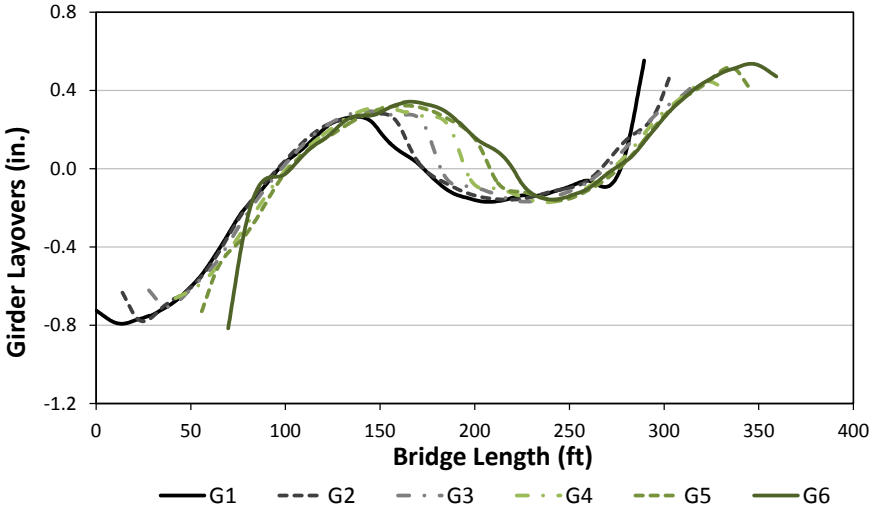

(ii) SDLF

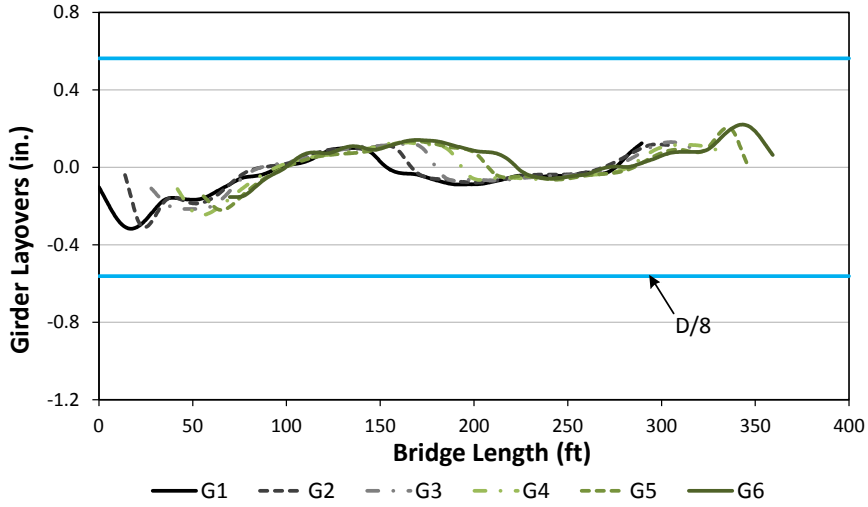

(iii) TDLF

Figure D.7.2. EICSS12, Girder layovers under total dead load for different types of detailing methods.

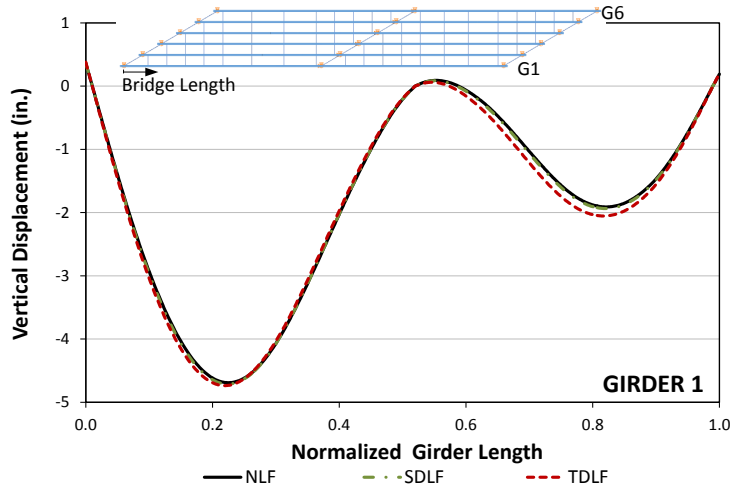

(i) Girder 1

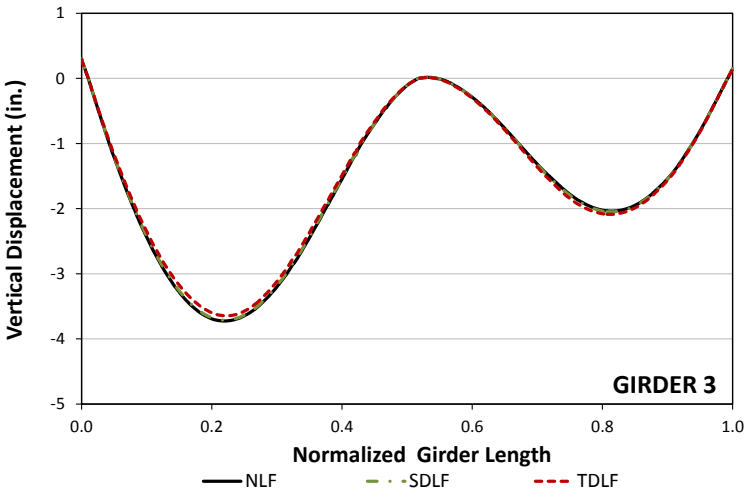

(ii) Girder 3

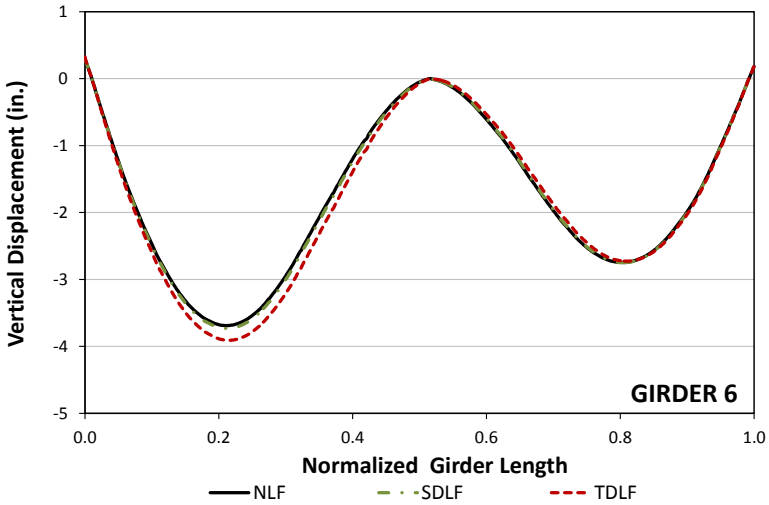

(iii) Girder 6

Figure D.7.3. EICSS12, Vertical deflections under total dead load for different types of detailing methods.

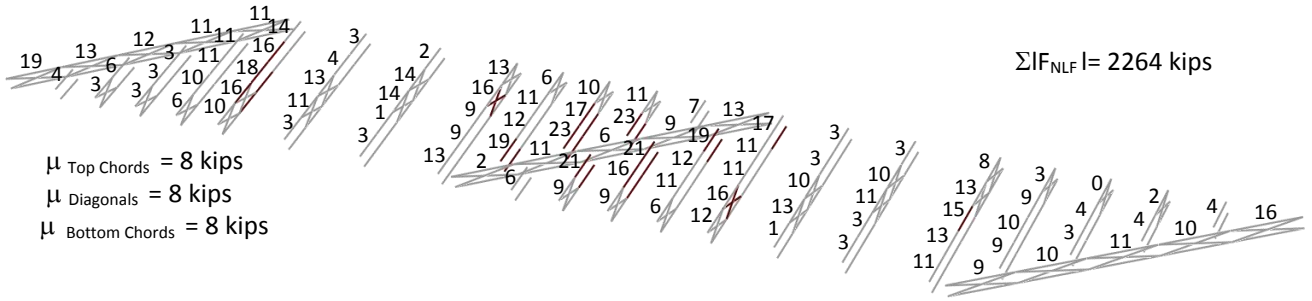

Figure D.7.4. EICSS12, maximum amplitude of the component axial forces in each of the cross-frames under total dead load (NLF detailing).

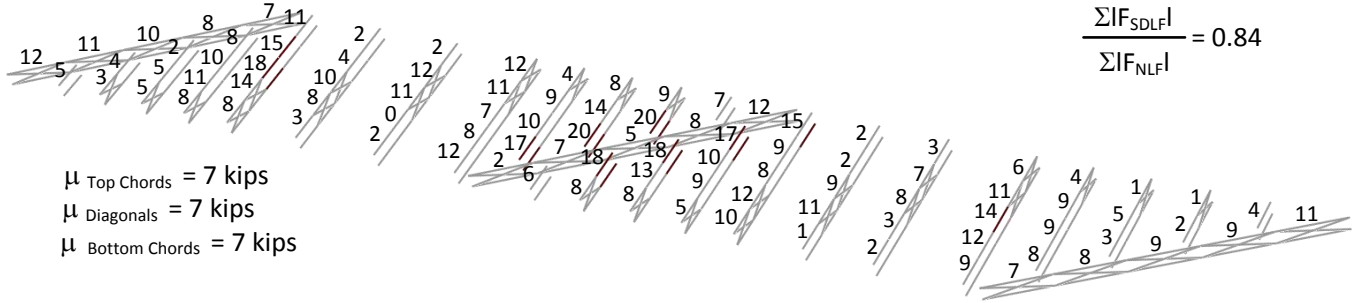

Figure D.7.5. EICSS12, maximum amplitude of the component axial forces in each of the cross-frames under total dead load (SDLF detailing).

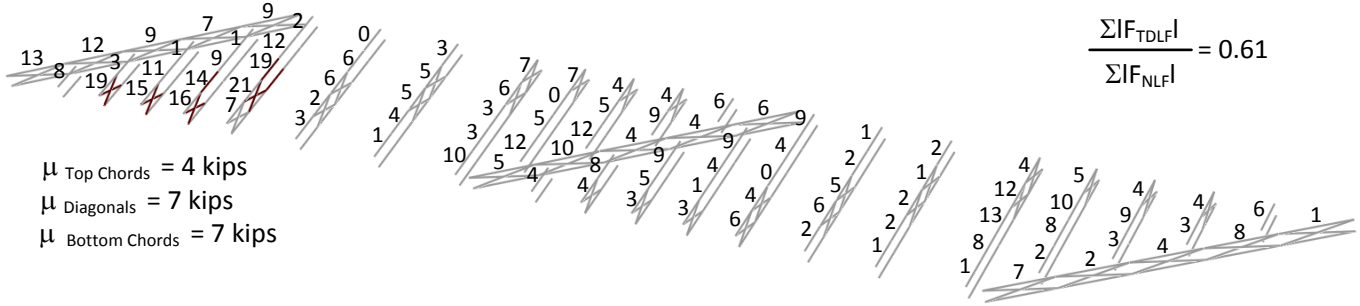

Figure D.7.6. EICSS12, maximum amplitude of the component axial forces in each of the cross-frames under total dead load (TDLF detailing).

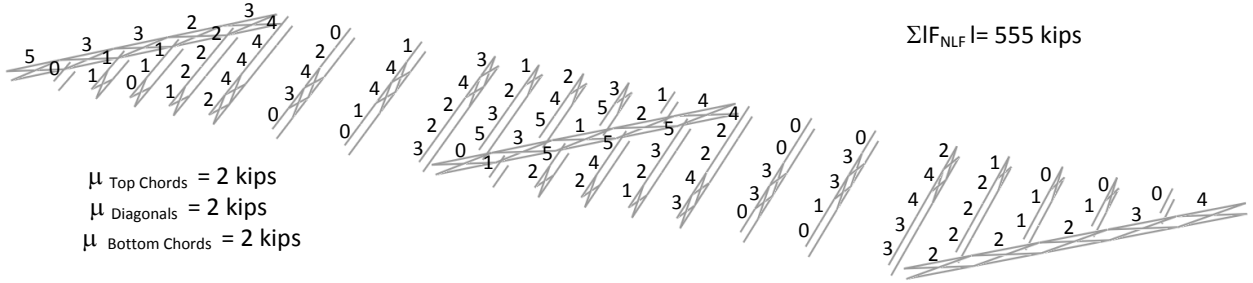

Figure D.7.7. EICSS12, maximum amplitude of the component axial forces in each of the cross-frames under steel dead load (NLF detailing).

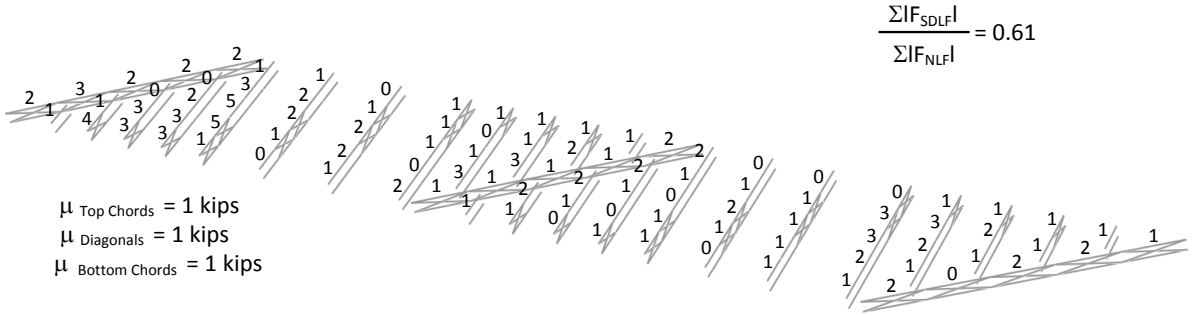

Figure D.7.8. EICSS12, maximum amplitude of the component axial forces in each of the cross-frames under steel dead load (SDLF detailing).

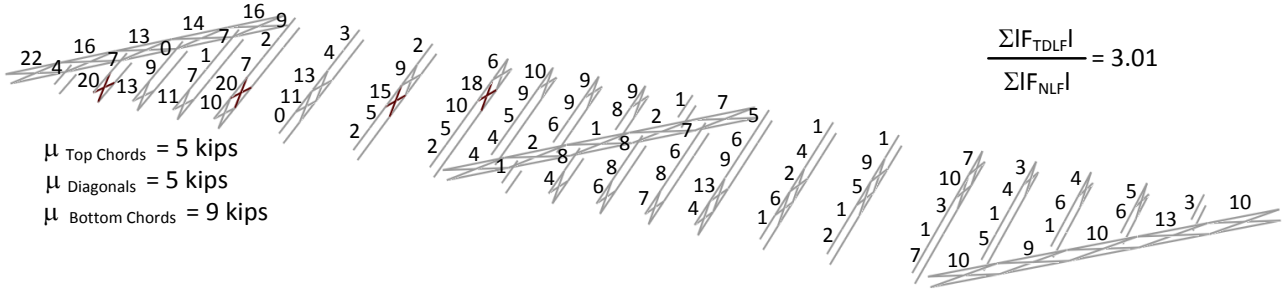

Figure D.7.9. EICSS12, maximum amplitude of the component axial forces in each of the cross-frames under steel dead load (TDLF detailing).

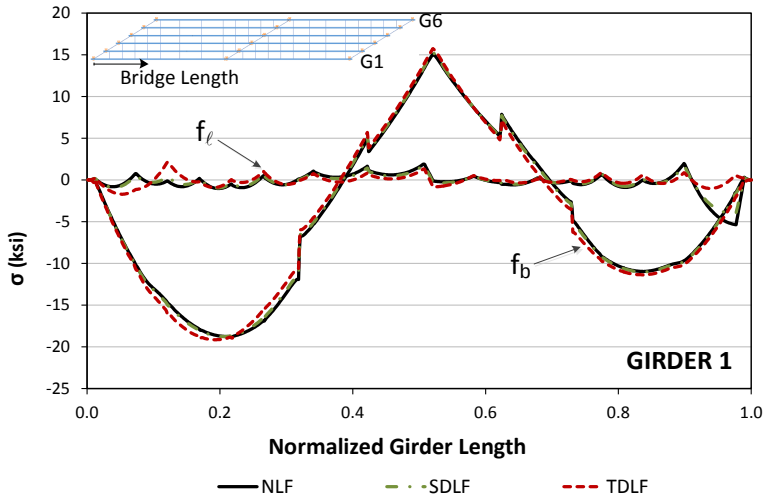

(i) Girder 1

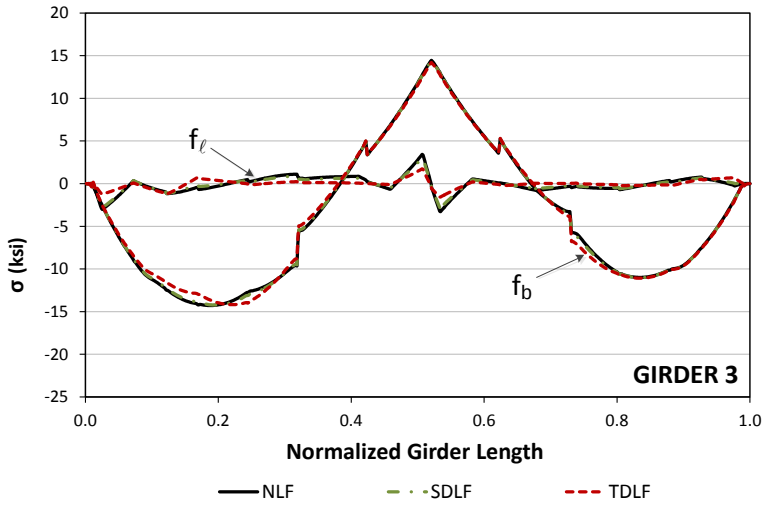

(ii) Girder 3

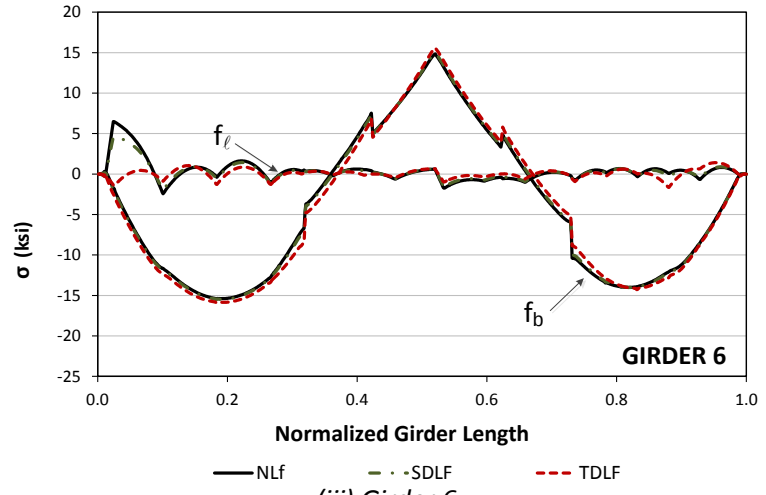

(iii) Girder 6

Figure D.7.10. EICSS12, Top flange stresses under total dead load for different detailing methods.

REFERENCES

AASHTO (2010). *AASHTO LRFD Bridge Design Specifications*, 5th Edition, American Association of State Highway and Transportation Officials, Washington, DC.

AASHTO (2007). *AASHTO LRFD Bridge Design Specifications*, 4th Edition, American Association of State Highway and Transportation Officials, Washington, DC.

AASHTO/NSBA (2011). *Guidelines for the Analysis of Steel Girder Bridges*, G13.1, AASHTO/NSBA Steel Bridge Collaboration, American Association of State Highway and Transportation Officials, Washington, DC and National Steel Bridge Alliance, Chicago, IL.

AASHTO/NSBA (2007). *Steel Bridge Erection Guide Specification*, S10.1, AASHTO/NSBA Steel Bridge Collaboration, American Association of State Highway and Transportation Officials, Washington, DC and National Steel Bridge Alliance, Chicago, IL.

AASHTO/NSBA (2006). *Guidelines for Design Details*, G1.4, AASHTO/NSBA Steel Bridge Collaboration, American Association of State Highway and Transportation Officials, Washington, DC and National Steel Bridge Alliance, Chicago, IL.

Bell, B.J. and Linzell, D.G. (2007). "Erection Procedure Effects on Deformations and Stresses in a Large-Radius, Horizontally Curved, I-Girder Bridge," Journal of Bridge Engineering, 12(4), 467-476.

Beshah, F. (2008). "Testing of Composite Bridge," Volume 9, Curved Steel Bridge Research Project, Federal Highway Administration, McLean, VA.

Chang C.-J. (2006). "Construction Simulation of Curved Steel I-Girder Bridges," Doctoral Dissertation, School of Civil and Environmental Engineering, Georgia Institute of Technology, Atlanta, GA, 340 pp.

Chang, C.-J., and White, D.W. (2006). "Construction Simulation of Curved I-Girder Bridge Systems," Annual Proceedings, Structural Stability Research Council, San Antonio, TX, 93-114.

Chang, C.-J., White, D.W., Beshah, F., and Wright, W. (2005). "Design Analysis of Curved I-Girder Bridge Systems – An Assessment of Modeling Strategies," Annual Proceedings, Structural Stability Research Council, Montreal, Quebec, 349-369.

Chavel, B.W. (2008). "Construction and Detailing Methods of Horizontally Curved Steel I-Girder Bridges," Ph.D. Dissertation, Swanson School of Engineering, University of Pittsburgh, Pittsburgh, PA, 357 pp.

Chavel, B.W., and Earls, C.J. (2006a). "Construction of a Horizontally Curved Steel I-Girder Bridge. Part I:Erection Sequence." Journal of Bridge Engineering, 11(1), ASCE, 81-90.

Chavel, B., and Earls, C. (2003). “Deflection of Horizontally Curved I-Girder Bridge Members Under Construction,” Report No. CE/ST 28, Department of Civil Engineering, University of Pittsburgh, Pittsburgh, PA, 261 pp.

Chavel, B. W and Earls, C. J. (2001). “Evaluation of Erection Procedures of the Horizontally Curved Steel I-Girder Ford City Bridge,” Research in Civil and Environmental Engineering, Research Report No. CE/ST18, Department of Civil and Environmental Engineering University of Pittsburgh, Pittsburgh, PA, 457 pp.

Coletti, D., and Yadlosky, J. (2007). “Analysis of Steel Girder Bridges – New Challenges,” Proceedings, World Steel Bridge Symposium, National Steel Bridge Alliance, New Orleans, LA, 21 pp.

Domalik, D.E., Linzell, G.D. and Shura, J.F.(2005). “Design and Field Monitoring of a Horizontally Curved Steel Plate Girder Bridge,” Bridgeline, HDR Enginieering, Inc., 14(1) , 1-3

Galambos, T.V., Hajjar, J.F., Leon, R.T., Huang, W.-H., Pulver, B.E., and Rudie, B.J. (1996). “Stresses in Steel Curved Girder Bridges,” Report MN/RC-96/28, University of Minnesota, Minneapolis, MN, 340 pp.

Helwig, T., and Wang, L. (2003). “Cross-Frame and Diaphragm Behavior for Steel Bridges with Skewed Supports,” The University of Houston, Research Report 1772-1.

Jung S.K. and White, D.W. (2008) “Inelastic Strength Behavior of Horizontally Curved Composite I-Girder Bridge Structural Systems,” Research Report FHWA-HRT-***, Federal Highway Administration, 731 pp.

Jung S.K. (2006) “Inelastic Strength Behavior of Horizontally Curved Composite I-Girder Bridge Structural Systems,” Doctoral Dissertation, School of Civil and Environmental Engineering, Georgia Institute of Technology, Atlanta, GA, 811 pp.

Kim, Y.K. (2010), “Behavior and Design of Metal Building Frames Using General Prismatic and Web-Tapered Steel I-Section Members,” Ph.D. Dissertation, Georgia Institute of Technology, Atlanta, GA

Krupicka, G., and Poellot, B. (1993). “Nuisance Stiffness,” Bridgeline, 4(1), HDR Engineering, Inc., 3 pp.

Leon, R., White, D., Dykas, J., Bhuiyan, M., Ozgur, C., Jimenez, J., Sanchez, A., (2011) “Field Monitoring and Computational Studies of a Horizontally Curved Steel Girder Bridge During Construction,” Report to Tennessee Department of Transportation, School of Civil and Environmental Engineering, Georgia Institute of Technology, Atlanta, GA, September (to appear).

MATLAB (2010). “MATLAB The Language of Technical Computing”, Version 7.11 (R2010b), The MathWorks Inc., Natick, MA, http://www.mathworks.com/

Montgomery, D. G. (2004). Design and Analysis of Experiments, 6th Edition, Wiley, New York, NY, 660 pp.

Morera F. (2010). “Lateral Flange Bending in Heavily Skewed Steel Bridges,” Doctoral Dissertation, Civil Engineering, North Carolina State University, Raleigh, NC, 408 pp.

NCHRP (2011). *Guidelines for Analytical Methods and Erection Engineering of Curved and Skewed Steel Deck-Girder Bridges*, NCHRP 12-79, National Cooperative Highway Research Program, Washington, DC, and Transportation Research Board, Washington, DC.

NHI/FHWA (2011a). *Load and Resistance Factored Design and Analysis of Skewed and Curved Steel Bridges*, Design Manual, NHI Course No. 130095, Publication No. FHWA-NHI-10-087, National Highway Institute, Federal Highway Administration, 1476 pp.

NHI/FHWA (2011b). *Load and Resistance Factored Design and Analysis of Skewed and Curved Steel Bridges*, Participant Workbook, NHI Course No. 130095, Publication No. FHWA-NHI-10-086, National Highway Institute, Federal Highway Administration, 1476 pp.

NHI/FHWA (2007). *Load and Resistance Factor Design (LRFD) for Highway Bridge Superstructures*, Design Manual, NHI Course No. 130081, 130081A-130081D, Publication No. FHWA-NHI-07-035, National Highway Institute, Federal Highway Administration, 1982 pp.

Nowak, A.S., Szwed, A., Podhorecki, P.J., Czarnecki, A., Laumet, P. and Galambos, T.V. (2006). “Calibration of LRFD Design Specifications for Steel Curved Girder Bridges,” Research Report NCHRP-563, Appendix C, Washington, DC, 94 pp.

Osborne, L. (2002). “Construction of Curved I-girder Bridges: Case Study of the I-459 Flyover,” Lance Osborne, MSCE student report and project presentation, April.

Ozgur, C., and White, D.W. (2007). “Behavior and Analysis of a Curved and Skewed I-Girder Bridge,” Proceedings, World Steel Bridge Symposium, National Steel Bridge Alliance, Chicago, IL, 18 pp

Richardson, G. and Associates (1963). Analysis and Design of Horizontally Curved Steel Bridge Girders, United States Steel Structural Report, ADUSS 88-6003-01

Prawel, S. P., Morrell, M.L. and Lee, G.C. (1974), “Bending and Buckling Strength of Tapered Structural Members,” Welding Research Supplement, Vol. 53, February, 75-84.

Romage, M. L. (2008), “Field Measurements on Lean-On-Bracing for Steel Girder Bridges with Skewed Supports,” Masters Thesis, University of Texas at Austin, Austin, TX

Sanchez, T. A. (2011), “Influence of Bracing Systems on the Behavior of Curved and Skewed Steel I-Girder Bridges during Construction,” Ph.D. Dissertation, Georgia Institute of Technology, Atlanta, GA, 350 pp.

Sanchez, T.A. and White, D.W. (2011). “Stability of Curved Steel I-Girder Bridge during Construction,” Structural Engineering, Mechanics, and Materials Report No. 77, School of Civil and Environmental Engineering, Georgia Institute of Technology, Atlanta, GA.

Schilling, C.G., and Morcos, S. S. (1988). “Moment-Rotation Tests of Steel Girders with Ultracompact Flanges", Project 188 Autostress design of Highway bridges, AISI, July.

Shah, D.M. (2007), “Effective Flange Width Evaluation for Prestressed Concrete Bulb-Tee Girder Bridges,” M.S. Thesis, Department of Civil Engineering, The State University of Buffalo, NY, 131 pp.

Shanmugam, N. E., Thevendran, V., Richard Liew, J.Y.,Tan, L.O. (1995). “Exoerimental Study on Steel Beams in Curved in Plan” Journal of Structural Engineering, ASCE, 115(9), September, 2145-2165.

Shura, J. F. (2004). “The Effects of Horizontal Curvature on Warping during Construction of a Steel Plate Girder Bridge with Large Radii,” M.S. Thesis, Department of Civil Engineering, The Pennsylvania State University, PA, 150 pp.

Simulia (2010). “Abaqus, Realistic Simulations” http://www.simulia.com/

Yura, J., Helwig, T., Herman, R. and Zhou, C. (2008). “Global Lateral Buckling of I-Shaped Girder Systems,” Journal of Structural Engineering, 134(9), 1487-1494.

Zureick, A.H., White, D.W., Phoawanich, N., and Park, J. (2002). “Shear Strength of Horizontally Curved Steel I-Girders – Experimental Tests, “Structural Engineering, Mechanics and Materials Report No. 02-4, Final Report to Professional Services Industries, Inc. and Federal Highway Administration, School of Civil and Environmental Engineering, Georgia Institute of Technology, Atlanta, Georgia, March, 157pp

VITA

Cagri Ozgur was born in Trabzon, Turkey on 10 February 1981, the son of Huri and Guner Kemal Ozgur. He received his Bachelor of Science in Civil Engineering from Middle East Technical University (METU) in Ankara, Turkey in February 2005 and completed the minor program in Architectural Culture at Middle East Technical University (METU) in February 2005. In August 2005, he moved to United States to attend the Graduate School of Civil and Environmental Engineering at Georgia Institute of Technology (Georgia Tech). Upon receiving her Master's degree in Structural Engineering from Georgia Tech. in 2007, Cagri continued his graduate study pursuing a Doctoral Degree in Structural Engineering at Georgia Institute of Technology.